GEO391 FIELD STRATIGRAPHY IN THE GUADALUPE MOUNTAINS

Spring 2012

Instructors: Peter Flemings, David Mohrig

Field Guide

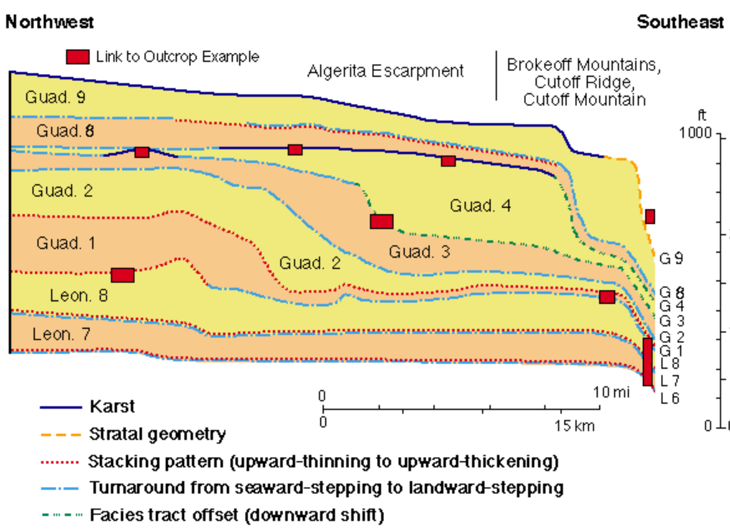

GEO 391 Field Trip

Wednesday 16 May:

6:30 AM	Depart Austin
	Drive to Washington Ranch (approx. 9 hour drive).
5:00 PM	Arrive Washington Ranch and check in
6:00 PM	Dinner
7:00 PM	Drive to Carlsbad for food shopping
10:00 PM	Bed

Thursday 17 May: Salt Flat Bench

6:30 AM	Breakfast
7:00 AM	Depart for day
	Salt Flat Bench
6:00 PM	Dinner/Bed

Friday 18 May: Salt Flat Bench

6:30 AM	Breakfast
7:00 AM	Depart for day
	Salt Flat Bench
6:00 PM	Dinner/Bed
7:30 PM	Graduation group departs for airport

Saturday 19 May: McKittrick Canyon

6:30 AM	Breakfast
7:00 AM	Depart for day
	McKittrick Canyon Reef Trail & Carlsbad Caverns
6:00 PM	Dinner/Bed

Sunday 20 May: Williams Ranch (Solar Eclipse)

6:30 AM	Breakfast
7:00 AM	Depart for day
	Bone Canyon & Schumard Canyon
9:00 AM	Graduation group back in New Mexico (drive to join group at Bone Canyon)
6:00 PM	Dinner/Bed

Monday 21 May: Williams Ranch

6:30 AM	Breakfast
7:00 AM	Depart for day
	Bone Canyon
6:00 PM	Dinner/Bed

Tuesday 22 May: McKittrick Canyon

6:30 AM	Breakfast
7:00 AM	Depart for day
	Basinal pinch out of sands against the carbonate foreslope
6:00 PM	Dinner/Bed

Wednesday 23 May: McKittrick Canyon

6:30 AM	Breakfast
7:00 AM	Depart for day
	Basinal pinch out of sands against the carbonate foreslope
6:00 PM	Dinner/Bed

Thursday 24 May:

6:30 AM	Breakfast
7:00 AM	Depart for Austin (approx. 9 hour drive)
6:00 PM	Arrive Austin, drop off rental cars

Table of Contents

1) Regional Stratigraphy

Yao You and John Shaw

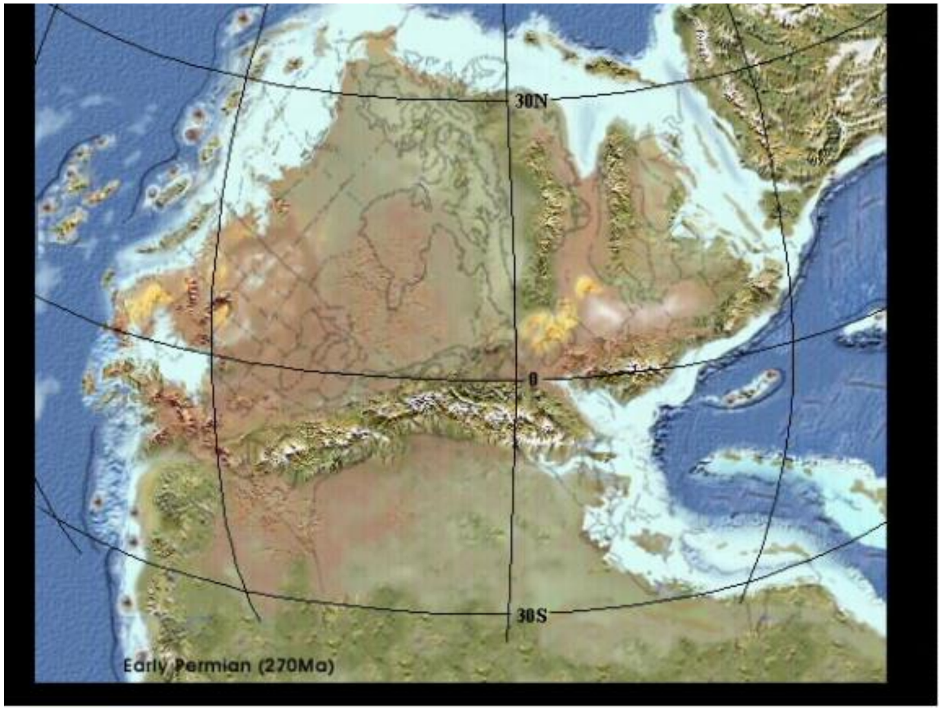

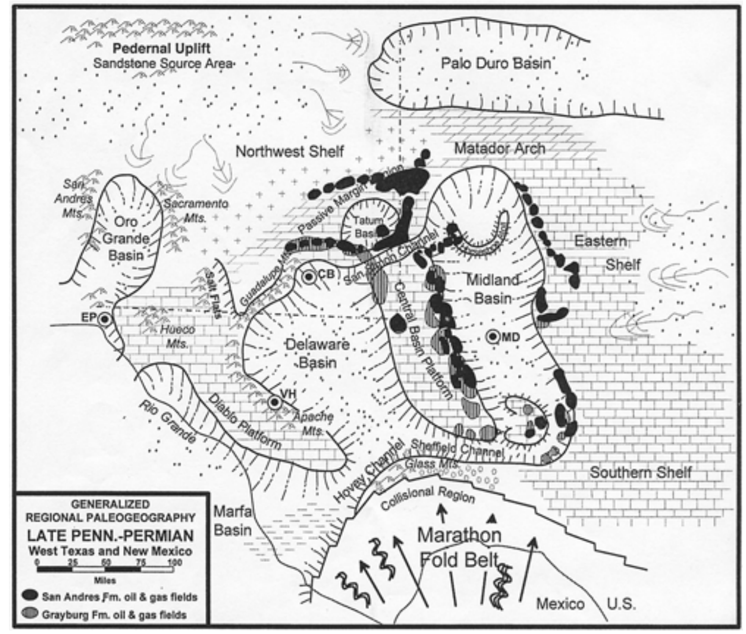

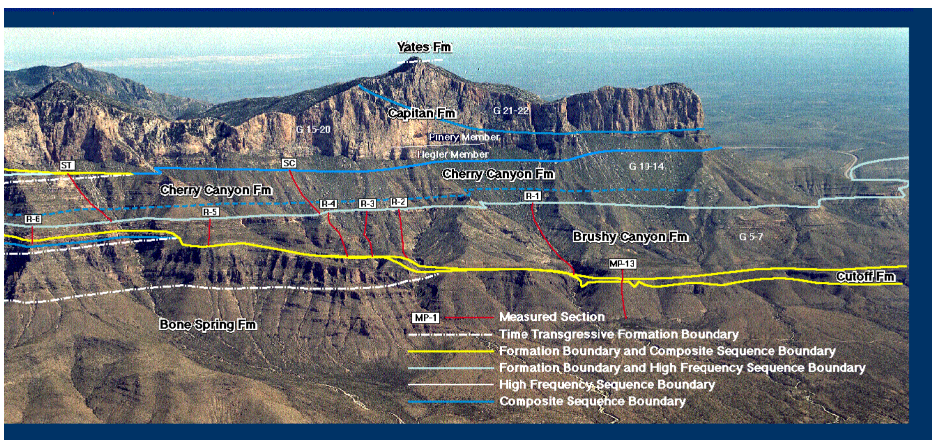

Figure 4—Mapped channel trends in the Delaware Mountain Group. Modified from Basham (1996).

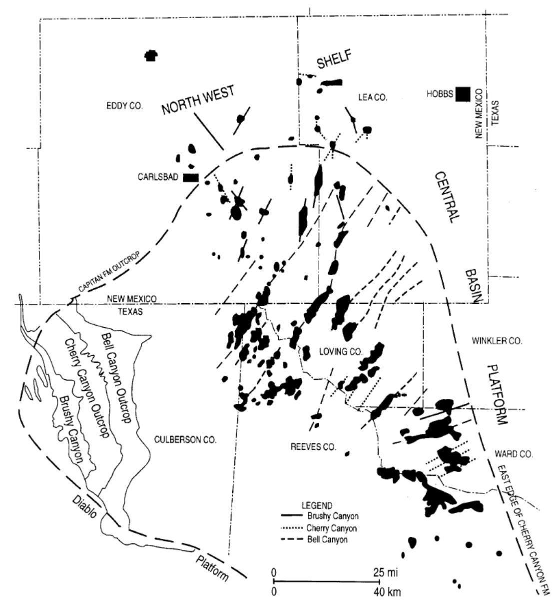

From Montgomery et al. 1999

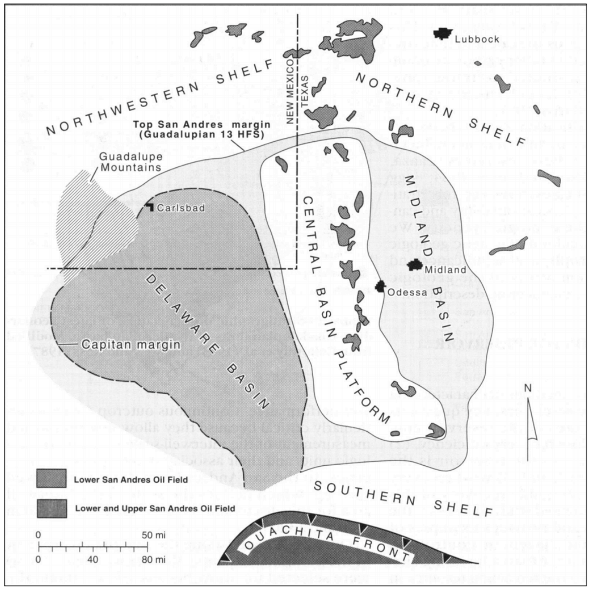

Karens, et al., 1994

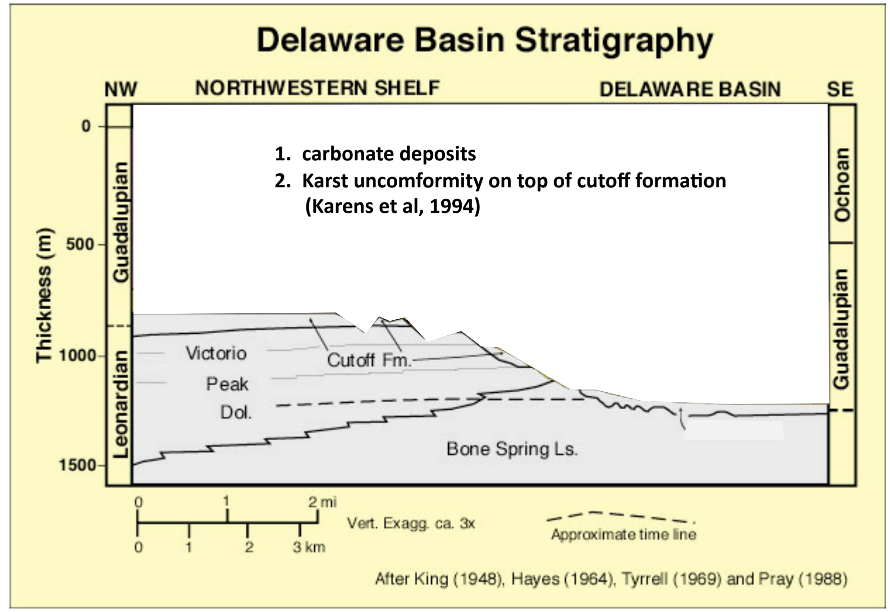

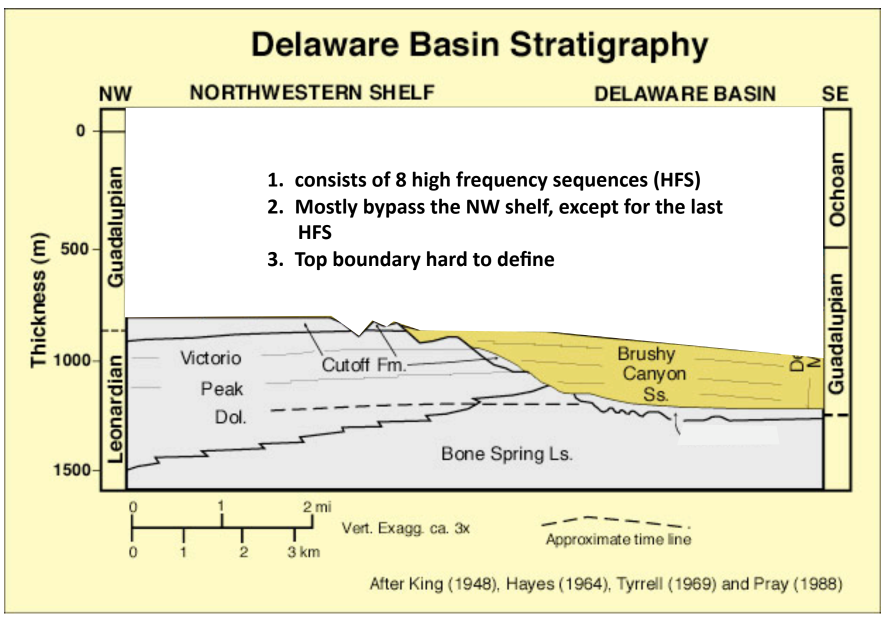

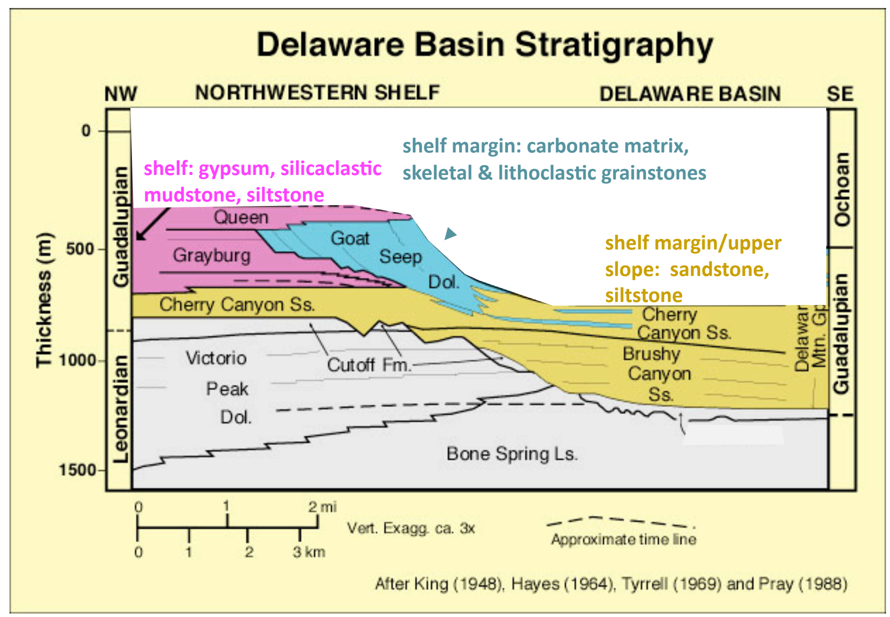

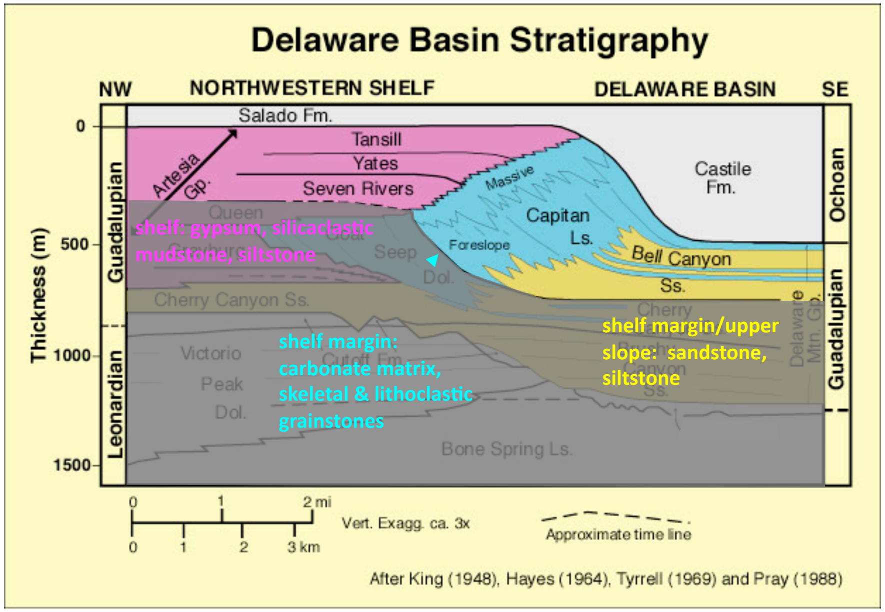

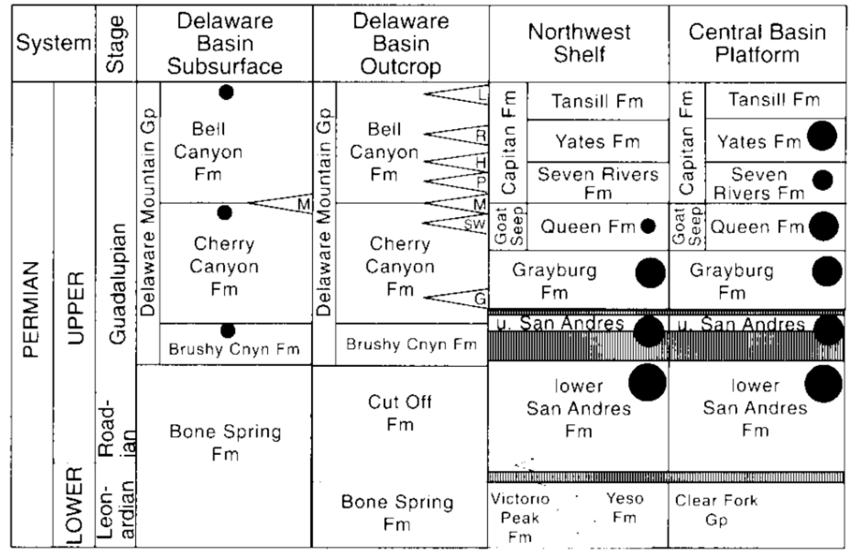

Carbonate tongues within the Delaware Mountain Gp: G = Getaway, SW = South Wells, M = Manzanita, P = Pinery, H = Hegler, R = Rader, L = Lamar

References for Field Guide

- Kerans, C., F. J. Lucia, and R. K. Senger (1994), Integrated characterization of carbonate ramp reservoirs using Permian San Andres Formation outcrop analogs, *AAPG bulletin*, *78*, 181–181.
- Montgomery, S., J. Worrall, and D. Hamilton (1999), E & P-Delaware Mountain Group, West Texas and Southeastern New Mexico, A Case of Refound Opportunity. Part 1–Brusby Canyon, *AAPG Bulletin*, *83*(12), 1901.

E & P Notes

Delaware Mountain Group, West Texas and Southeastern New Mexico, A Case of Refound Opportunity: Part 1—Brushy Canyon

Scott L. Montgomery,[1] John Worrall,[2] and Dean Hamilton[3]

ABSTRACT

Exploration in Permian (Guadalupian) deep-water sandstones of the Delaware Mountain Group, west Texas and southeast New Mexico, represents a success story of the 1990s derived from reevaluation of reservoirs previously deemed uneconomical. Recent discoveries have concentrated on the Brushy Canyon in New Mexico and, to a lesser extent, the Cherry Canyon in Texas. Brushy Canyon reservoirs in particular previously were overlooked due to indications of poor reservoir quality from log and well test data; however, oil shows observed on mud logs across the northern Delaware basin led to new completion efforts in the late 1980s and 1990s using gel-sand fracture stimulations. Productive reservoirs are very fine to fine-grained arkosic to subarkosic sandstones with porosities of 12–25% and permeabilities typically of 1–5 md. Better reservoir quality is concentrated in massive channel sandstones variably interpreted as deposited by turbidity or saline density currents. Significant clay content, lamination, and close interbedding between oil- and water-bearing units make log analysis and reserve estimates problematic. As a result, the mud log remains the cheapest, most practical indicator of pay. Reservoir sandstones can be divided into a series of major productive trends related to proximal/slope and more distal/basin-floor depositional settings. Well productivity is variable within each trend, but primary recovery rarely exceeds 10%. Options for enhanced recovery include pressure maintenance, waterflooding, and carbon dioxide flooding. Early indications suggest that carbon dioxide flooding may be most appropriate in these low-permeability, clay-bearing reservoirs.

INTRODUCTION

The history of hydrocarbon exploration in the Permian basin includes many episodes of refound opportunity. In recent years, such episodes have expanded reserves in a number of Permian reservoirs, such as the Bone Spring formation, Leonardian detrital carbonates, the San Andres-Grayburg interval, and Canyon (latest Pennsylvanian–Early Permian) sandstones. In the Delaware basin portion of the province, one of the most widespread reservoir-bearing intervals to be successfully reexplored in recent years is the Delaware Mountain Group, a relatively deep-water siliciclastic interval up to 4500 ft (1372 m) thick dominated by fine-grained sandstones and siltstones. In particular, new discoveries and field development in the lower portion of the interval, mainly in the Brushy Canyon and, to a lesser extent, the lower Cherry Canyon formations, have added more than 120 MMbbl oil and 200 bcf gas to Permian basin reserves.

The Delaware Mountain Group has been the target of three major periods of exploration and development effort. During the 1950s and 1960s, the uppermost portion of the interval, known as the Bell Canyon Formation, was a common, shallow

[1]Petroleum Consultant, 1511 18th Avenue East, Seattle, Washington 98112.
[2]Scott Exploration Inc., 200 W. First Street, Suite 648, Roswell, New Mexico 88201.
[3]Consulting Geologist, Midland, Texas.

target at depths of 5000 ft (1525 m) or less basinward of the Capitan Reef margin in Loving, Ward, and Reeves counties of west Texas, and in southernmost Eddy and Lea counties, New Mexico (Kosters et al., 1983). Reservoirs are mainly very fine grained, well-sorted sandstones in the upper Bell Canyon that were deposited in northeast-southwest lenses interpreted as channels within basin-floor submarine lobe and channel complexes (Gardner, 1997). Traps are mainly stratigraphic (lateral and updip pinch-out) and structural-stratigraphic in nature. Drilling and field development of Bell Canyon reservoirs resulted in production of more than 120 MMbbl oil and 500 bcf gas by 1985.

During the late 1970s and early 1980s, the upper and middle Cherry Canyon Formation was the focus of exploration within the Delaware Mountain Group. As with the Bell Canyon, production was primarily found in very fine to fine-grained sandstones, in which oil principally was trapped stratigraphically by lateral and vertical loss of porous sandstone into nonpermeable sandstone, siltstone, or carbonate. Key Cherry Canyon fields discovered during this period included the Rhoda Walker and Dimmitt fields of west Texas and the Indian Draw and Esperanza fields of southeast New Mexico. Several wells in these areas produced large volumes of oil, such as the Gulf Trace 1 in Esperanza, which has yielded more than 700,000 bbl of oil as of mid-1999.

A third major phase of activity, focused on the deeper Brushy Canyon and lower Cherry Canyon formations, has taken place only within the past 15 yr, with most field development occurring since 1990. Drilling has been centered in the New Mexico portion of the basin, where stratigraphic trapping is predominant, and in Ward and Winkler counties, Texas, where a significant structural component to entrapment exists. Prior to the mid-1980s, Brushy Canyon sandstones in particular were not an exploration target for three basic reasons: (1) they exhibited a low-resistivity log response and less permeability development than Bell Canyon reservoirs, (2) they lie at greater depths (generally >7000 ft; 2135 m), making them appear less economical, and (3) they yield unencouraging results on drill-stem tests (DST). The last of these reasons was especially influential. Brushy Canyon sandstones flow little or no oil on test (producing only oil-cut drilling fluid) and measure low pressures under standard 1 hr initial and final shut-in pressure runs.

During the late 1970s and early 1980s, hundreds of wells were drilled in the Delaware basin to Pennsylvanian targets (mainly Morrowan and Atokan intervals), providing a large new database for reexamining Permian formations. Mud logs from these wells commonly indicated good shows in the upper and lower Brushy Canyon. Sample analyses, moreover, suggested sufficient oil saturations for commercial recovery. Experimentation with well testing and reservoir stimulation approaches eventually indicated two vital pieces of information: (1) shut-in tests need to be run for 4–6 hr to obtain accurate pressure data and (2) artificial fracturing that employs cross-linked gel as a fluid and sand as a proppant could greatly improve production rates and per-well drainage areas. As a result of this information, the play developed rapidly in central and southern Lea and Eddy counties, New Mexico. As of early 1999, more than 75 MMbbl of oil and 175 bcf gas had been produced from Brushy Canyon and Cherry Canyon reservoirs in this area.

Although a significant number of published studies on the Brushy Canyon now exist (see, for example, articles and references in DeMis and Cole, 1996), few regional syntheses of productive trends and their relationships to lithologic, depositional, and petrophysical characteristics have been assembled. This paper is an attempt to help fill this gap. Our aim is to offer a brief synthesis of existing information and to augment such information with unpublished data mainly from Nash Draw field. Nash Draw has been the subject of a detailed reservoir characterization and simulation study intended specifically to address the issue of low recovery in the Delaware Mountain. This study has been performed as part of the U.S. Department of Energy Class III (Slope and Basin Clastic Reservoirs) Field Demonstration Program. Data related to this work can be found in Murphy et al. (1996), Martin et al. (1997), and Strata Production Company (1998).

SETTING

The Delaware basin is the westernmost portion of the Permian basin geologic province, located in west Texas and southeastern New Mexico (Figure 1A). The basin is bounded on three sides by major basement uplift features, including the Marathon fold and thrust belt to the south, the Diablo platform to the west, and the Central Basin platform (CBP) to the east. To the north, the border of the Delaware basin is marked by the Northwest shelf, a significant break in slope that proprietary seismic data suggest may overlie deep-seated basement faulting.

The Delaware basin is asymmetric in geometry with its axis adjacent and largely parallel to the fault-bounded margins of the CBP. Structures within the basin include local reverse faulting and graben development along the border of the CBP and minor anticlinal features along the northern slope in New Mexico. The western flank of the basin is monoclinal with small-scale normal faulting. Published and unpublished seismic and geologic information suggests that major deformation

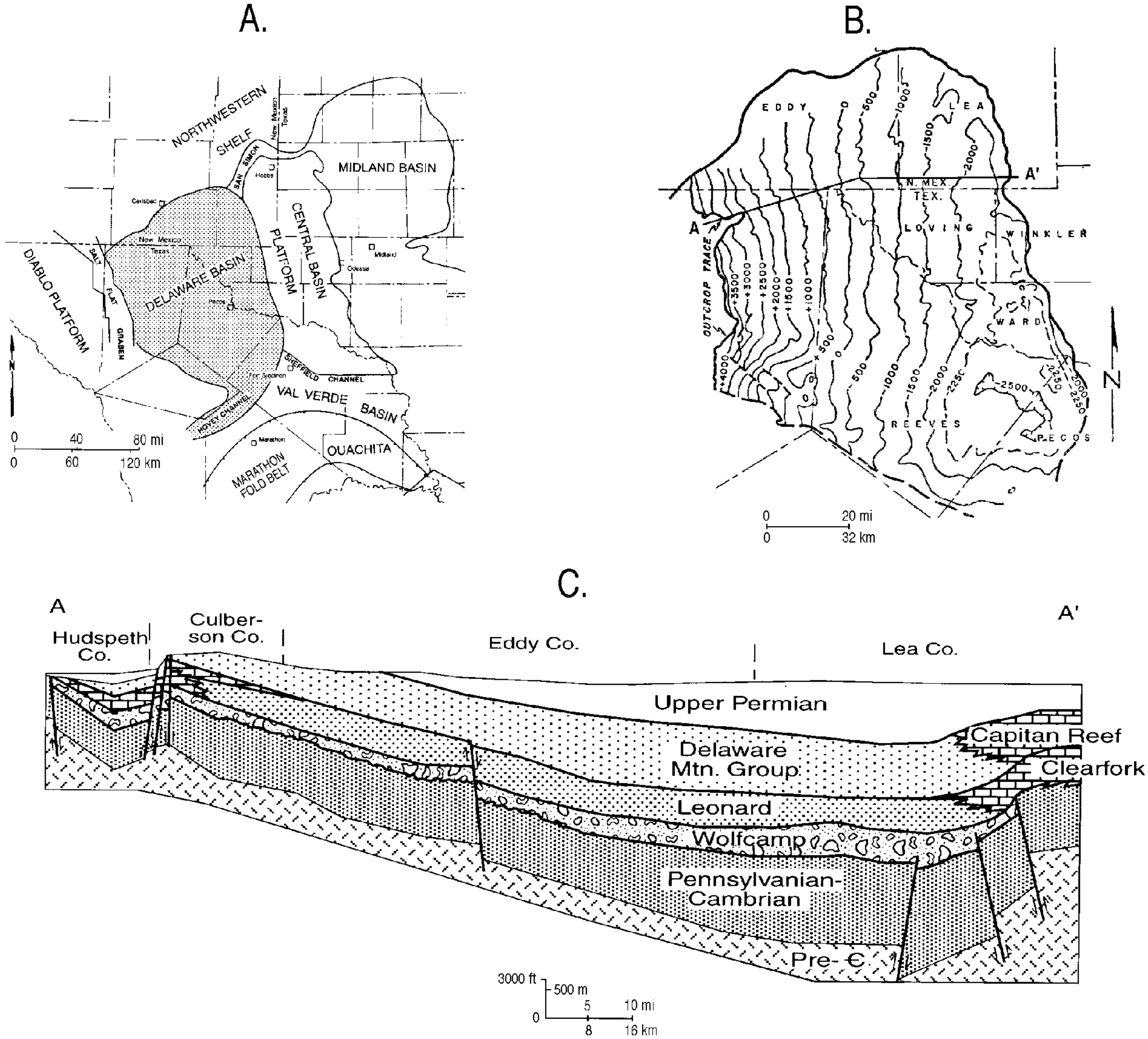

Figure 1—(A) Regional tectonic map, (B) structure contour map, and (C) simplified structural cross section of the Delaware basin, west Texas. Contours in (B) drawn on top of the Delaware Mountain Group (Guadalupian). (B) is modified from Grauten (1979); (C) is modified from Montgomery (1997).

within the basin and along its margins had ceased by the Wolfcampian–early Leonardian (Hills, 1984; Yang and Dorobek, 1995). An east-southeastern regional tilt was imposed during the Late Cretaceous–early Tertiary as a result of Laramide transpression in the Trans-Pecos region to the west (Dickerson, 1985). Permian strata dip at a rate of approximately 100 ft/mi (19 m/km) in western Eddy County, New Mexico, decreasing eastward to one-half this amount and finally flattening out in the basin center in eastern Lea County (Figure 1B).

Delaware Mountain Group sediments are draped over preexisting, mainly Pennsylvanian structures. Masking of these structures is not complete; a Pennsylvanian feature with as much as 300 ft (91 m) of relief may appear at the Brushy Canyon level as a subtle terrace, nose, or closure with 25 ft (8 m) of relief. Removal of Laramide tilt has been used to identify such structures in Delaware Mountain Group strata. Resulting maps have shown a consistent, although not absolute, relationship between structure and hydrocarbon production in the

Delaware Mountain. Oil entrapment, however, is observed to be stratigraphic, mainly related to pinch-out of reservoir-quality sandstones. The relationship between structure and production is thus subtle and indirect, possibly related to sand depositional patterns, diagenetic history, oil emplacement, or some combination of these factors.

As indicated on the cross section of Figure 1C, Permian deposits comprise the major proportion of basin fill. Leonardian strata, included within the Bone Spring formation, consist of interbedded debris-flow carbonate and sandstone with subsidiary siltstone and pelagic shale. This material represents the slope and basinal equivalent to thick carbonate platform and shelf-margin buildup sequences (Abo, Yeso intervals) that rimmed the Delaware basin. Although related basin-margin carbonate deposition continued into the Guadalupian with significant progradation in many areas (Goat Seep, Capitan intervals), deposition within the basin proper underwent a significant transition to sandstone and siltstone facies (Delaware Mountain Group). Carbonate strata exist within the Delaware Mountain section only as relatively local, proximal tongues. Lithologically, the Brushy Canyon, Cherry Canyon, and Bell Canyon intervals each are composed of more than 95% medium- to very fine grained sandstone and siltstone.

The considerable thickness of clastic material (3500–4500 ft; 1067–1372 m or more), deposited at a time when basin margins were the site of maximum carbonate platform and buildup development, has posed certain challenges to interpretation. Identifying paleocanyons as potential sediment conduits has been important to paleogeographic reconstructions and analyses of facies architecture (see, for example, Gardner and Sonnenfeld, 1996). At present, it is generally accepted that Delaware Mountain clastics represent a series of wedges deposited during episodes of sea level lowstand, with material having been mainly supplied by eolian processes and bypassing a karsted carbonate platform and shelf margin (Fischer and Sarnthein, 1988; Gardner, 1992; Basham, 1996). Sandstones have been mapped in channel-like trends that extend as much as 50 mi (80 km) along the basin floor (Harms and Williamson, 1988). The most highly contested aspect to these deposits remains their precise mode of deposition within the basinally restricted setting.

STRATIGRAPHY AND LITHOLOGY

The Delaware Mountain Group, consisting of the Brushy Canyon, Cherry Canyon, and Bell Canyon formations, is interpreted to encompass the entire Guadalupian interval in the Delaware basin. Regional stratigraphic relationships are shown in Figure 2. The base of the Delaware Mountain Group is marked by a persistent limestone used to delineate the top of the Bone Spring formation. The top of the interval is designated by another carbonate, the Lamar limestone, included in the Bell Canyon Formation. Delaware Mountain strata are replaced in a paleolandward direction by shelf-margin Goat Seep and Capitan carbonate, behind which partly restricted, platform deposits of the Artesia Group (Grayburg, Queen, Seven Rivers, Yates, and Tansill formations) occur (Figure 2).

Brushy Canyon sandstones are mainly equivalent to the San Andres Formation. The Brushy Canyon comprises a basinward-thickening wedge that onlaps an erosional surface in updip areas and overlies Cutoff formation sandstones and shales along the paleoslope or, where absent, the Bone Spring formation. This unconformity is interpreted to indicate an episode of sea level fall that terminated basinward progradation of shelf-margin carbonates (Yeso) and began major clastic influx. A tongue of the Cherry Canyon Formation extends landward from the Yeso shelf margin, marking the stratigraphic break between Leonardian and Guadalupian carbonate buildup (Figure 2) along the Northwest shelf. On the Central Basin platform, the Cherry Canyon is represented by sandstones of the Queen Formation (Hamilton, 1996).

Stratigraphic divisions within the Delaware Mountain Group are somewhat uncertain due to lithologic similarity and thus a lack of clear boundaries between the major formational intervals. Intragroup unconformities are absent; however, several significant marker horizons, such as the Manzanita bentonite bed located 100–150 ft (30–45 m) below the top of the Cherry Canyon, commonly are used to facilitate subsurface correlation. The top of the Brushy Canyon Formation remains the most difficult stratigraphic boundary to determine. Certain persistent radioactive siltstone markers are often employed to divide the Brushy Canyon informally into upper, middle, and lower intervals (Figure 3).

Figures 2 and 3 indicate that the Capitan reefal complex prograded several kilometers basinward and in places overlies the Cherry Canyon and Bell Canyon intervals. South and east of the Capitan limit, a full section of Delaware Mountain Group sediments is present. This includes up to 1800 ft (549 m) of Brushy Canyon, 1200 ft (366 m) of Cherry Canyon, and 1200 ft (366 m) of Bell Canyon deposits. Recent sequence stratigraphic studies have interpreted the Brushy Canyon interval as representing a third-order lowstand episode and consisting of four wedge-shape to tabular low-order cycles (Gardner, 1992, 1997). According to this model, the deposits of succeeding cycles demonstrate a general

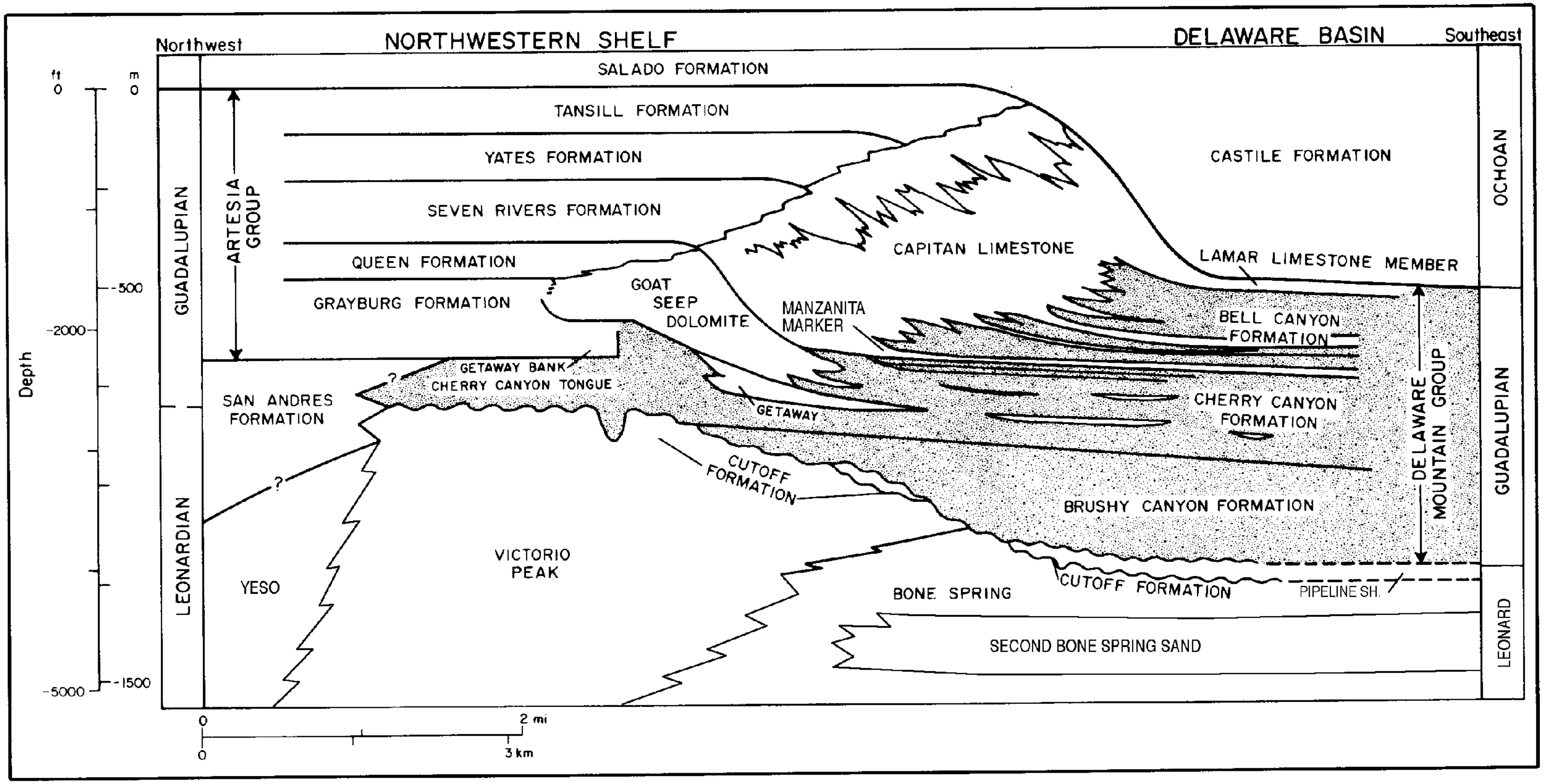

Figure 2—Simplified northwest-southeast cross section showing regional stratigraphic relationships between the Northwest shelf and Delaware basin, southeastern New Mexico. Modified from Harms and Williamson (1988).

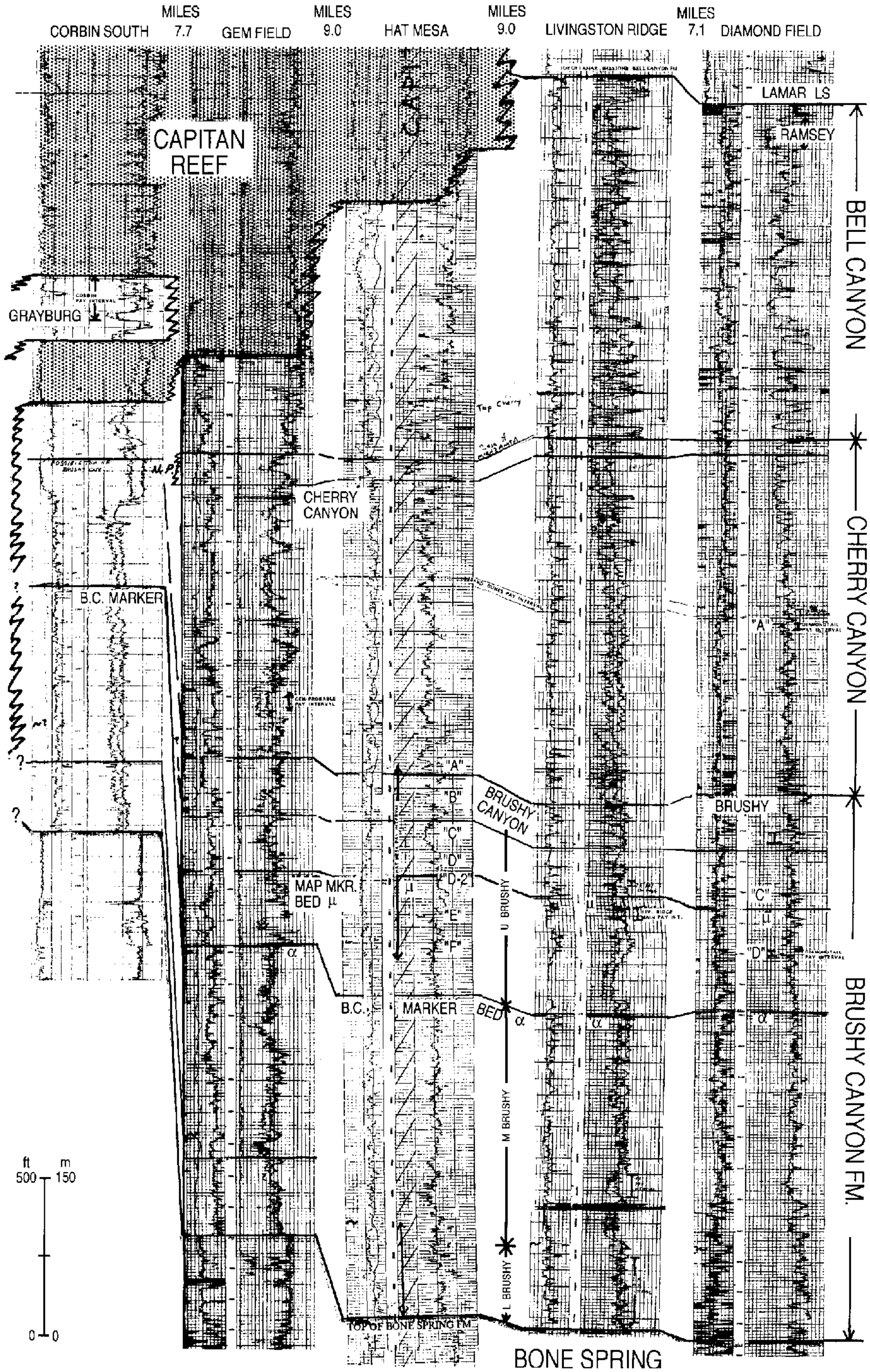

Figure 3—Regional north-south log cross section showing interpreted subsurface stratigraphic relationships of the Delaware Mountain Group.

upward increase in thickness and sandstone volume. Lowermost Brushy Canyon sandstones exhibit evidence of progradational relationships, whereas the uppermost Brushy Canyon cycle displays backstepping relationships with sandstone thicks closer to the basinal margins (Gardner, 1997). Cherry Canyon strata are interpreted to have been deposited during a continuation of the Brushy

Canyon lowstand, as well as the initial stages of a succeeding transgression, with stratigraphic turnaround identified in the upper portion of the formation (Gardner, 1997). An important implication of this model is that reservoir sealing should be least well developed in the middle portion of the Brushy Canyon. To date, few fields have been productive from the middle Brushy Canyon.

In order of importance, sediments of the Brushy Canyon and Cherry Canyon intervals consist of the following: (1) very fine to fine-grained arkosic to subarkosic sandstones, mostly massive in character, (2) very fine grained sandstones microlaminated with siltstones, (3) dark-colored organic siltstones (lutites), (4) carbonate beds (limestone or dolomite) more prevalent near shelf margins, and (5) black to dark gray, calcareous shales. Clay shale is notably rare in the section and is virtually absent from the Brushy Canyon Formation. Local cross-bedding exists in some sandstone units and bioturbation occurs in some siltstones. Sandstones exhibit a mixture of calcite and silica cement, with some evidence of framework grain dissolution (especially feldspars) and grain-coating illite clays. Carbonate units (mainly limestone) are present in the upper Cherry Canyon and, especially, Bell Canyon intervals. Bell Canyon limestones have been named, and include, from bottom to top the Hegler, Pinery, Rader, McCombs, and Lamar limestones. The Lamar Limestone Member, where present, typically is used to mark the top of the Bell Canyon Formation.

DEPOSITIONAL MODELS

Considerable, long-term debate has surrounded the interpretation of depositional models for the Delaware Mountain Group (Harms and Brady, 1996). In broad terms, consensus now exists that some form of gravity-flow mechanism, or mechanisms, should be considered responsible for these deposits. Discussion currently favors deposition either by turbidity currents, whether in deep-water conditions or during significant sea level fluctuations (Silver and Todd, 1969; Berg, 1979; Rossen and Sarg, 1988; Basu and Bouma, 1996; Gardner and Sonnenfeld, 1996), or by clastic-laden saline density currents (Harms, 1974; Harms and Williamson, 1988; Harms and Brady, 1996). Both hypotheses require sediment supply to the basin through narrow channels cut into the carbonate margin.

Several aspects to Delaware Mountain Group sandstones pose a challenge to standard models of slope and basinal deposition. Among these aspects are the conspicuous lack of sedimentary structures suggesting turbidity or contour-type currents and the notable absence of detrital clay. As discussed by workers such as Basham (1996), Harms and Brady (1996), and Wegner et al. (1998), contemporary study of both sandstone and siltstone character has not yet provided determining evidence in favor of a single depositional model; however, to account for the lack of clay and the presence of moderate-to-good sorting in Delaware Mountain sandstones, it has been postulated that sediment was supplied mainly by eolian processes. Dunes are thought to have migrated across the platform, either amassing sand at the shelf break (Fischer and Sarnthein, 1988), thereby giving rise to periodic slumping and turbidity currents, or providing sediment to evaporitic lagoons in which mobile saline water masses accumulated and flowed downslope to the shelf edge (Harms and Brady, 1996).

Both of these interpretive schemes highlight the importance of submarine channels beyond the shelf break as major sediment conduits and sites of cleaner sand deposition. A large number of these channels in Delaware Mountain deposits have been identified and mapped (Basham, 1996), as indicated by Figure 4. This figure shows that channels are commonly fairly linear and oriented perpendicular to basin margins. It is clear from the change in relative abundance, size, and orientation of these channels that principal sediment source areas underwent a significant shift between the times of Brushy Canyon and Bell Canyon deposition. The great majority of Brushy Canyon channels are concentrated in the northern portion of the Delaware basin and are oriented south-southeast, indicating sediment supply from the Northwest shelf. Cherry Canyon channels are located in this same area, as well as along the southern portion of the CBP, where their orientation is southwest, suggesting a transition in source areas. Finally, Bell Canyon channels extend for considerable distances in a southwest orientation, strongly implying a major shift in sediment provenance to the northern and central CBP. The considerable extent and relative linearity of channel trends, particularly in the Bell Canyon Formation, imply some degree of structural (fault?) control; however, the precise nature of such control is not well understood, even in areas of intensive drilling.

Changes in the location, scale, length, and sedimentary character of these channels between the times of Brushy Canyon and Bell Canyon deposition suggest that no single model may be able to account for all data. As suggested by Figure 4, channels in the Bell Canyon Formation are unique in terms of their remarkable length and linearity, as well as the lack of influence by basin axial trends on their orientation. Such factors continue to pose certain challenges to traditional turbidite models.

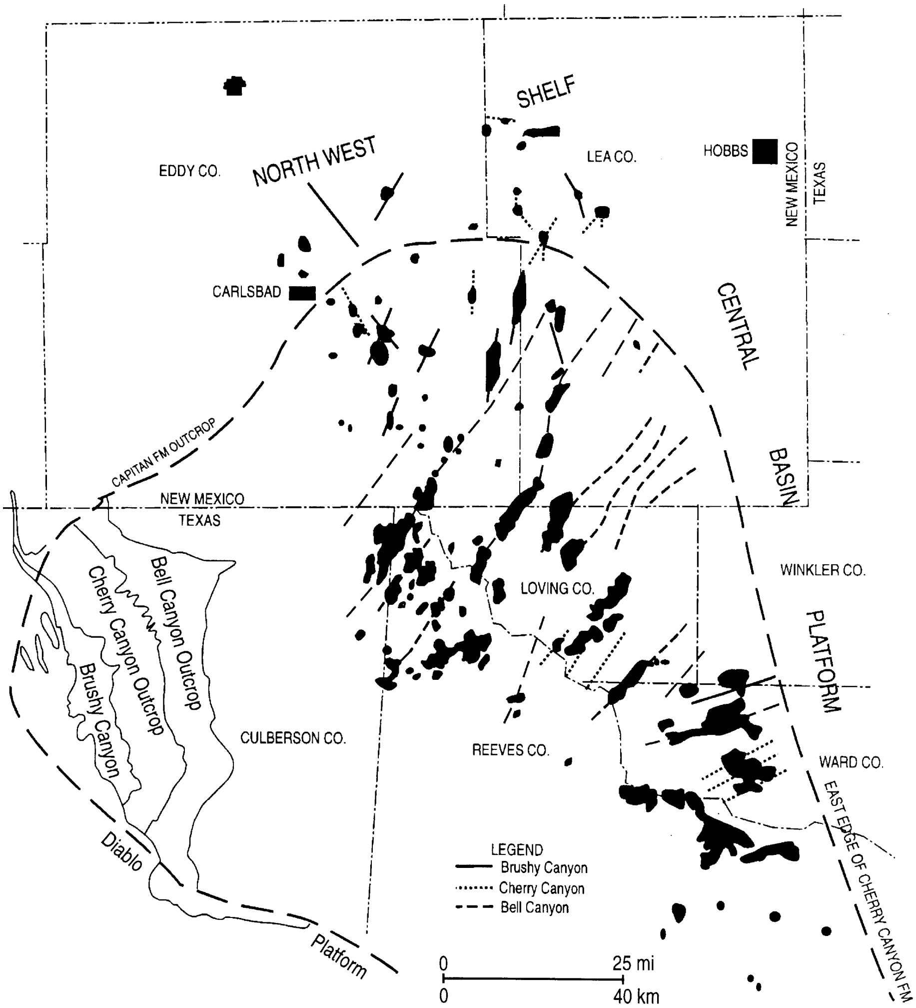

Figure 4—Mapped channel trends in the Delaware Mountain Group. Modified from Basham (1996).

SANDSTONE RESERVOIR CHARACTERISTICS

Composition

Reservoirs of the Brushy Canyon and Cherry Canyon typically consist of angular to subangular, moderate to well-sorted, fine- to very fine grained sandstones. These sandstones have an arkosic to subarkosic (feldspathic) composition, consisting of 60–80% quartz, 20–30% feldspar (K-spar and plagioclase), 5–12% rock fragments, and 2–12% authigenic clays. Authigenic clay species consist mainly of illite, mixed-layer illite/smectite, and Fe-rich chlorite, which occur as grain-coating and pore-lining material (Behnken, 1996; Green et al., 1996). Carbonate (calcite, dolomite, ankerite) cements are common, but variably developed between different sandstone units.

Figure 5 shows that mineralogic composition is often highly consistent over thick intervals (>150 ft; 45 m). Samples in which authigenic clays are less abundant exhibit an increased amount of secondary quartz in the form of epitaxial microcrystalline grain coatings and syntaxial overgrowths. Compositional analysis implies that the combination of small framework grain size, grain-coating chlorite and illite, and pore-occluding illite will significantly affect log calculations of porosity and water saturation. In particular, clay microporosity is known to result in high irreducible water saturations for these sandstones.

Core Descriptions and Petrophysical Character

Core description, petrographic study, and scanning electron micrograph (SEM) analysis have been performed on sidewall and whole-rock core samples from the Brushy Canyon and Cherry Canyon formations (see, for example, Spain, 1992; Thomerson

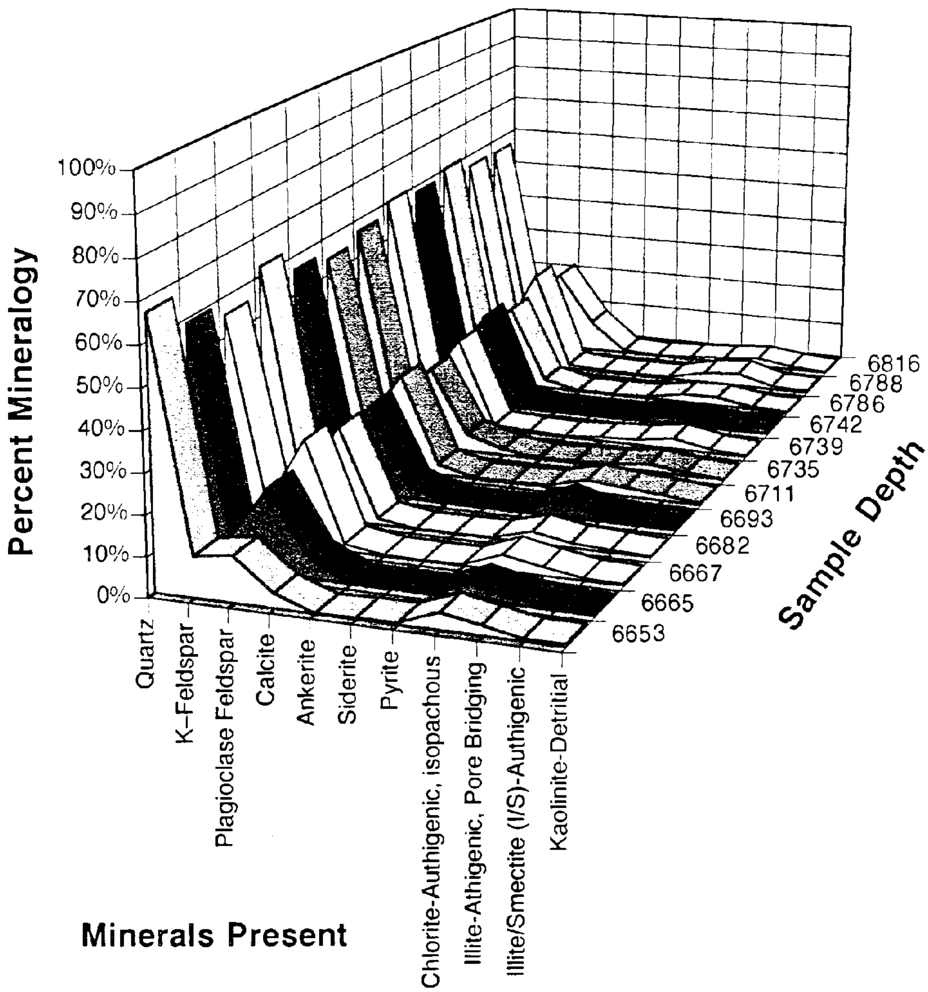

Figure 5—Mineralogic determinations by means of x-ray diffraction for 12 samples, Nash Unit 23, Nash Draw field, Eddy County, New Mexico.

and Asquith, 1992; Behnken, 1996). These analyses indicate grain size within productive zones ranges from 0.05 (silt) to 0.12 mm (very fine sand). Primary intergranular porosity is dominant in most samples, with secondary dissolution porosity also significant. Pore geometry is polygonal to highly variable due to the subrounded texture and small size of framework quartz and feldspar grains and presence of secondary quartz. In general, interparticle porosity is reduced in four ways: (1) by suturing along quartz grain boundaries due to pressure solution, (2) by grain-coating and pore-bridging clays, (3) by quartz overgrowths and epitaxial secondary grain-coating quartz, and (4) by pore-filling carbonate cements.

Porosities and permeabilities in productive intervals range from 12–25% and 1–5 md, respectively, but occasional "streaks" of permeability of up to 200 md are sometimes present. The best reservoir quality exists in relatively massive sandstones, such as those shown in Figure 6A. Sandstones containing wispy lamination, soft sediment deformation, or bioturbation also can be productive (Figure 6B). Nonreservoir zones include siltstones and highly laminated sandstone/siltstone units, the latter of which may contain significant oil in thin (<1 cm) sandstone layers but generally are water productive (Figure 6C). An important aspect to productive intervals is the close interbedding between oil-bearing, water-bearing zones and nonreservoir zones. As revealed by the core photographs of Figure 7, such interbedding results in significant vertical and possibly lateral reservoir discontinuity, with a lack of any single oil/water contact.

Thin section and scanning electron micrographs from productive Brushy Canyon sandstones in Nash Draw field (Eddy County, New Mexico) are shown in Figures 8 and 9, respectively. In Figure 8A, primary intergranular (dominant) and secondary dissolution pore types are evident. Pore and pore-throat geometries are enhanced by dissolution of quartz and feldspar grains but adversely affected by calcite cement, quartz overgrowths, local pressure solution, and authigenic clays. A magnified view (Figure 8B) exhibits considerable porosity but reduced permeability due to grain boundary suturing and pore throat plugging by clays. Solution along grain boundaries is observed in only a few locations (I-7). The sample also displays probable oil staining within clay microporosity. Scanning electron micrographs highlight the reduction of permeability as a result of grain suturing, cementation, and clay presence (Figure 9). In Figure 9B, the bridging of pore space by illite/smectite is especially apparent.

Log Analysis

The relatively low permeabilities, high clay content, and presence of iron in these very fine to fine-grained sandstones (Brushy Canyon and Cherry Canyon) have a number of important effects with regard to log analysis. Significant difficulty exists with respect to differentiating pay and nonpay (wet) zones, and thus performing reserve calculations, on the basis of standard calculations. Frequently, productive intervals calculate S_w at 40–70% due both to the presence of bound water in clays and to interbedding between oil-bearing and water zones; moreover, in a particular well, wet zones yield values of S_w only 10–20% higher than for pay zones (Figure 10). Other effects include high ("shalier") gamma-ray response (40–60 API units), due to the presence of K-feldspar, and an overestimation of porosity by the compensated neutron tool as a result of authigenic clays.

Operators have addressed these effects by relying on mud log data as a primary means for distinguishing pay and calibrating log response to core analysis based on sidewall sampling. For the Brushy Canyon, it has been found that the mud log provides the most reliable indication of pay in most instances; however, such is not universally the case for the Cherry Canyon. Some productive zones at War-Wink field yielded no shows on mud logs.

Figure 10 illustrates fairly typical log data for Brushy Canyon pay. Prospective zones have good oil shows (bright yellow to white fluorescence), significant gas increase above background levels, and a good drilling break with drill rates falling to 1.0 ft/min (0.305 m/min) or less. In addition, cutting samples through good reservoir zones typically appear as unconsolidated sand. Another approach to identifying pay zones at greater resolution has been attempted in Nash Draw field (Martin et al., 1997). The basic procedure is based on the premise that only zones with residual oil saturation have a good probability of being productive. Microlateral log data calibrated via core analysis are used to calculate residual oil saturations for each 0.5 ft (15 cm) of reservoir section. Calibration with other log data and use of porosity correction transforms provide a basis for net pay and volumetric calculations in uncored wells. Comparison between resulting volumetrics and those derived from decline-curve analysis has shown good agreement (Murphy et al., 1996).

The standard suite of electric logs run includes a gamma-ray, neutron/density, and dual-formation resistivity or dual-induction log. Core-based analysis in a number of fields has suggested that certain cross-plot relationships may be locally effective in helping identify pay and pay cutoff. For example, in East Livingston Ridge field (Brushy Canyon), cross-plots of core-measured porosity vs. bulk density indicate good correlation (R^2 = 0.9) and allow correction of density log porosities with high confidence (Thomerson and Catalano, 1996). In Hat Mesa field (Brushy Canyon) to the north, a plot of core porosity vs. absolute permeability provided a porosity cutoff of 15% for zones with permeability of less than 1 md and S_w of less than 60% (Thomerson and Asquith, 1992). For other fields, however, a 12% porosity cutoff is widely used. With regard to Cherry Canyon, Hamilton (1996) noted that in War-Wink field (Texas), reservoir log parameters have been determined as follows: porosity = 18%, R_w = 0.037–0.052, resistivities = 1.5–3.5 ohm-m, with some recent workovers successful at 1.0 ohm-m.

Simultaneously, however, the complex nature of these reservoirs may well render the use of single porosity cutoff values problematic. Given the low permeabilities involved, capillary pressure and relative permeability measurements, in some instances, may yield more useful results for explaining and

Figure 6—Sidewall core samples, Brushy Canyon Formation. (A) Massive, good-quality reservoir sandstone from productive interval. Permeability = 9.76 md; porosity = 16.7%. Oil saturation = 18.5%; water saturation = 54.1%. (B) Reservoir sandstone showing evidence of bioturbation(?). Permeability = 4.98 md; porosity = 14.0%. Oil saturation = 16.9%; water saturation = 59.1%. (C) Nonreservoir, oil-bearing laminated sandstone/siltstone. Such lithologies commonly have significant oil saturations (>15%) corresponding to sandstone layers with better porosity, but they also have high water saturations (>60%) and are water productive. Permeability = <0.01 md; porosity = 5.5%. Oil saturation = 19.2%; water saturation = 72.4%.

(A)

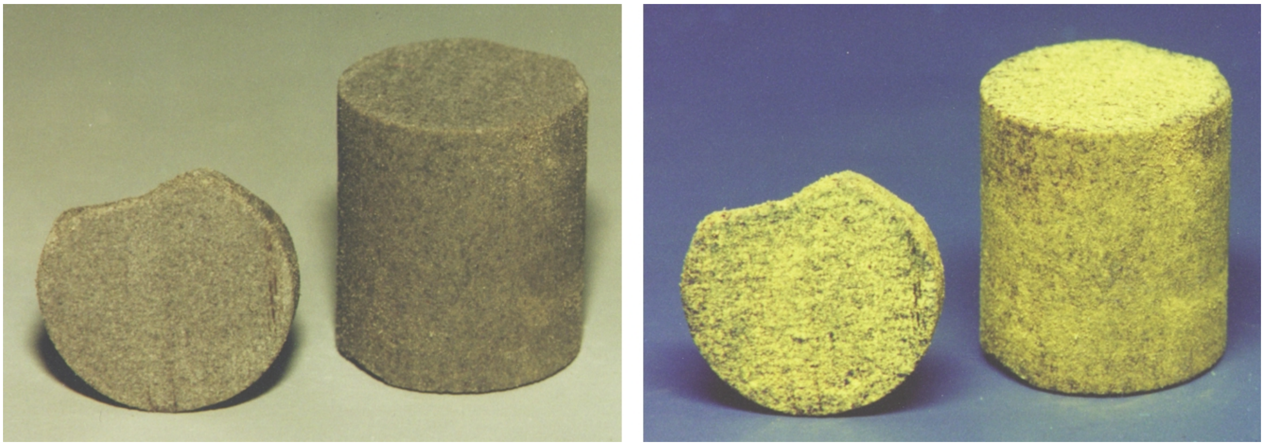

(B)

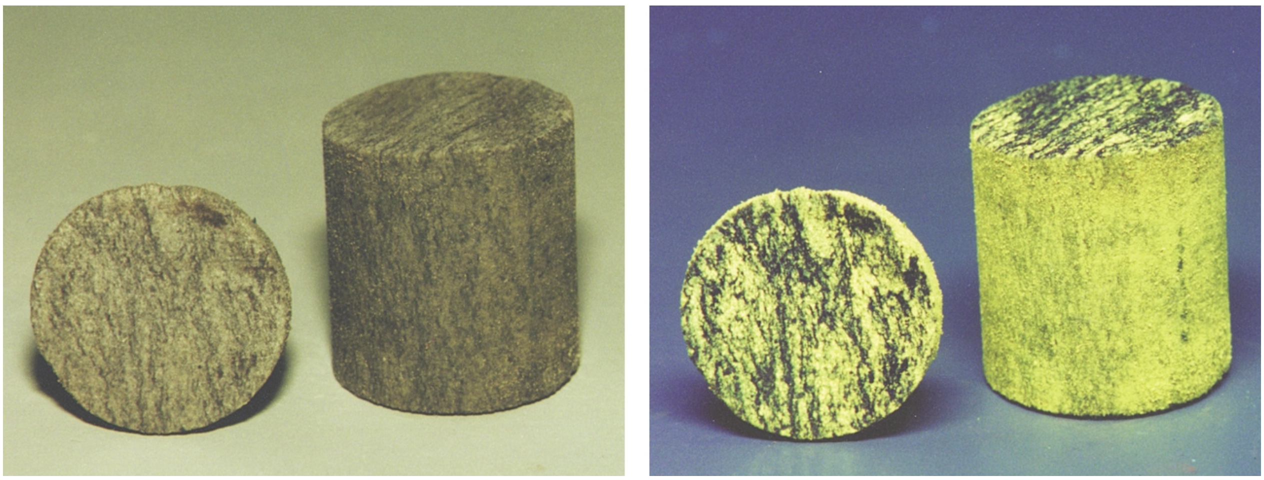

(C)

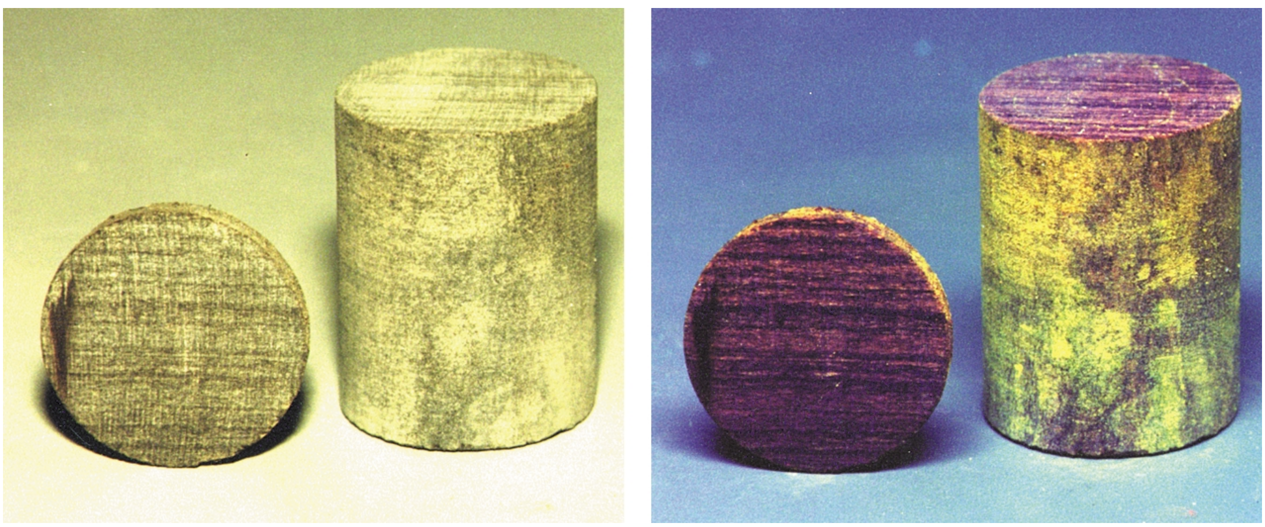

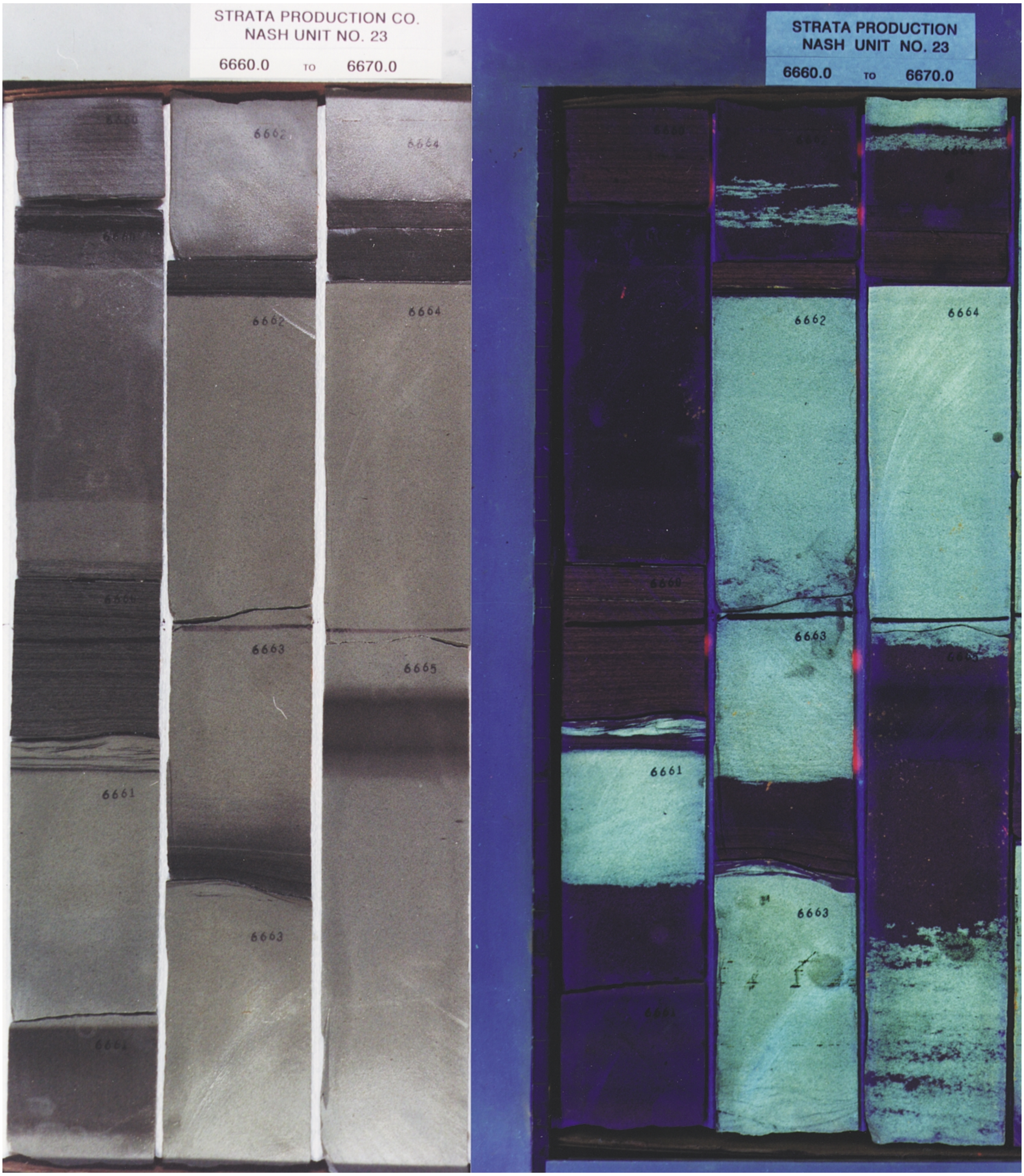

Figure 7—Whole-rock core samples from Nash Unit 23, Nash Draw field, revealing a high degree of interbedding between massive textured, oil-bearing sandstone and dark-colored laminated sandstone/siltstone. Samples on the left are shown under natural light; samples on the right are shown under ultraviolet light.

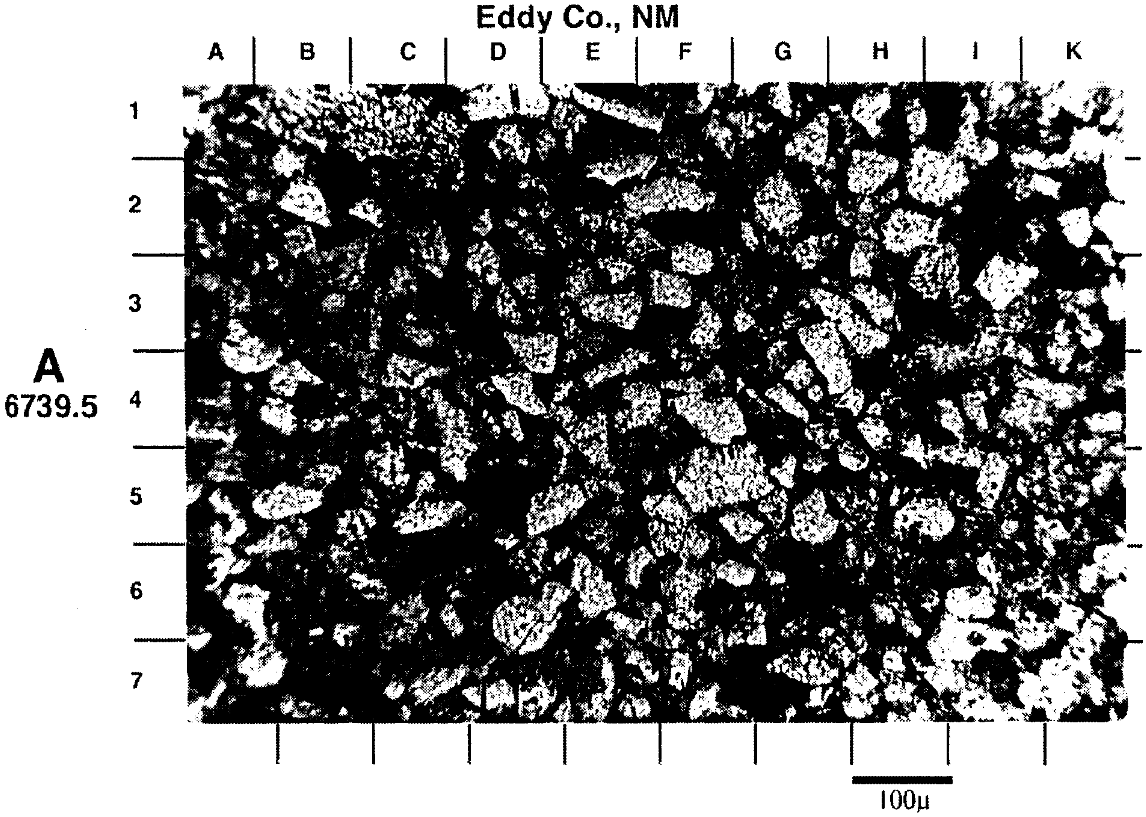

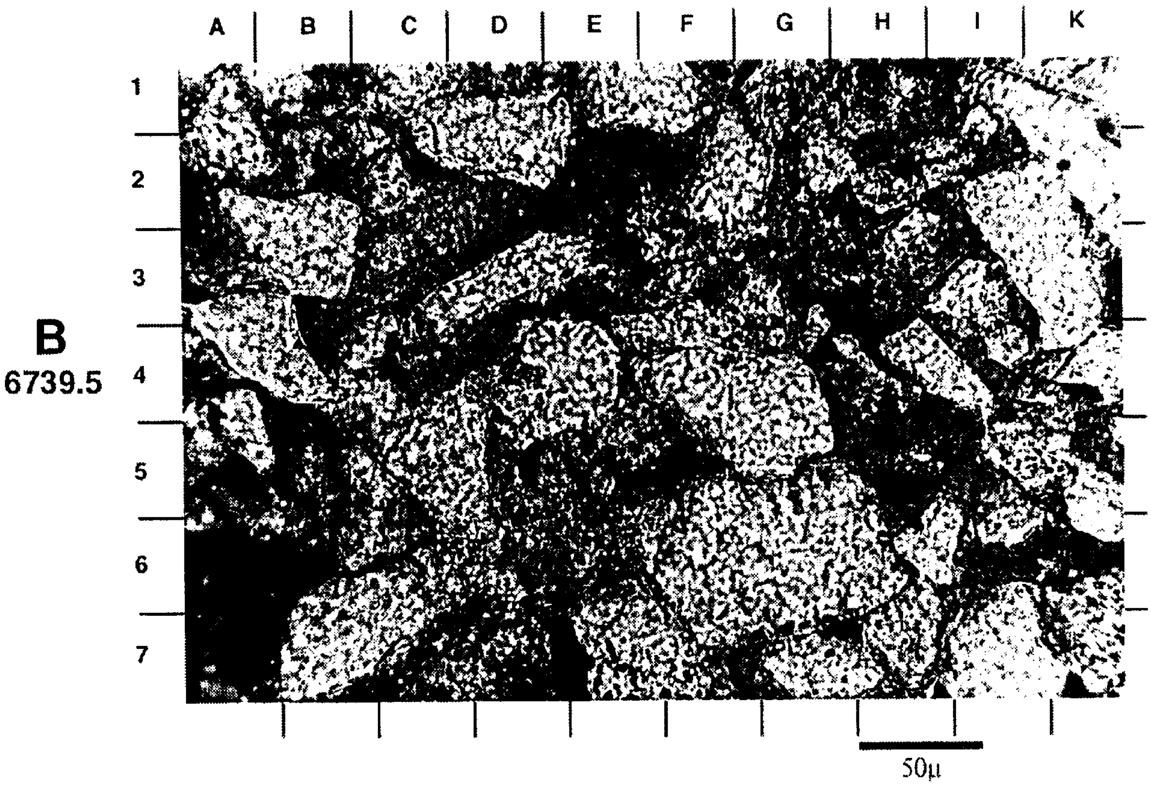

Figure 8—Thin section photomicrographs of productive Brushy Canyon sandstone, Nash Draw field (T23S, R29E), Eddy County, New Mexico, at (A) moderate and (B) high magnification. Samples are taken from the same well and depth (6739.5 ft; 2055.5 m) as that in Figure 6A. See text for discussion.

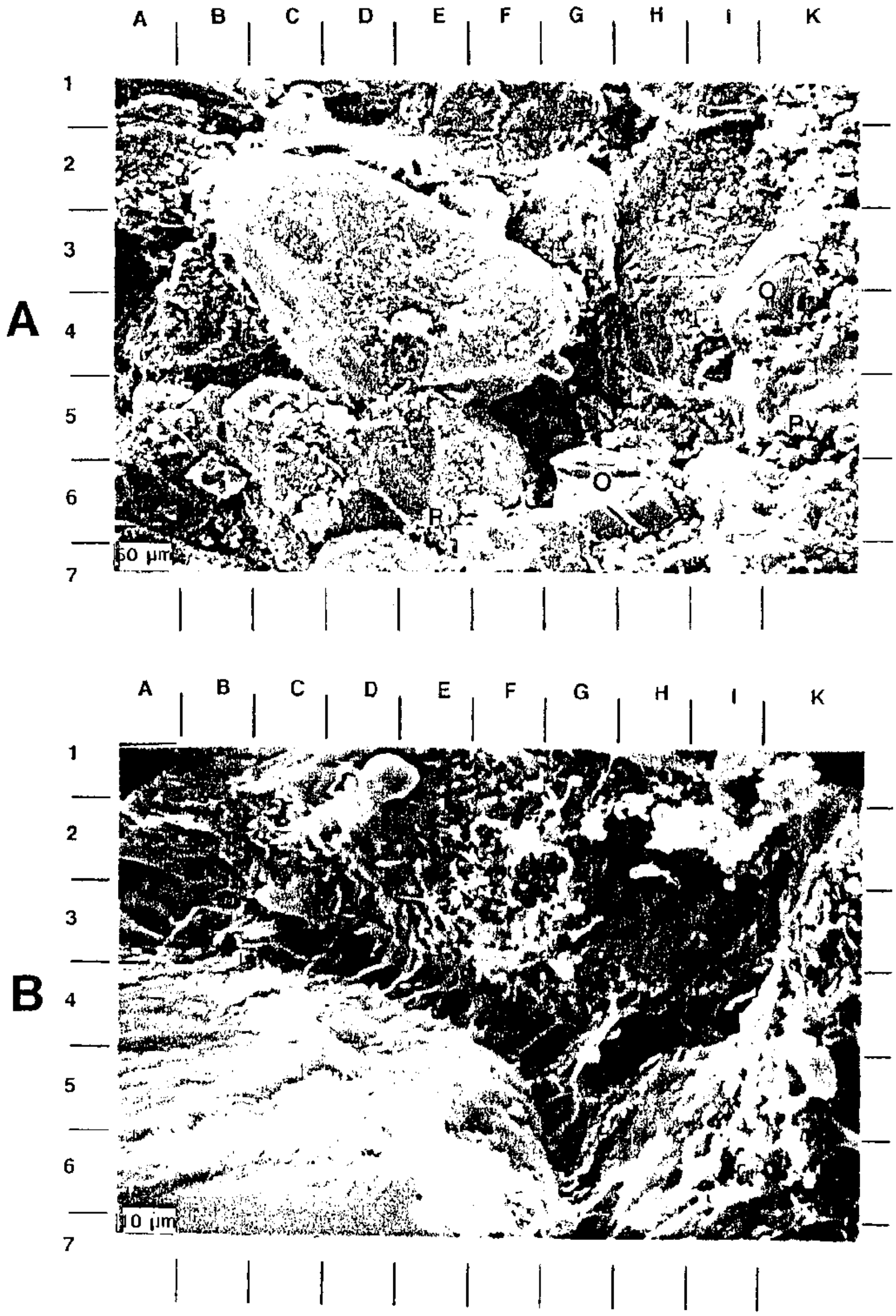

Figure 9—Scanning electron micrographs (SEM) of productive sandstones, Nash Draw field, Eddy County, New Mexico. (A) Example of primary intergranular pore system showing quartz overgrowths (O), pore-filling cement (P), and authigenic pyrite (Py). (B) Image showing fibrous authigenic illite/smectite partially occluding intergranual pore space.

predicting reservoir quality distribution. Detailed study in Nash Draw field, for example, has established that below 1 md, the relative permeability of water to oil in Brushy Canyon sandstones is too high for commercial production; moreover, different productive sandstone units exhibit different porosity cutoffs for a permeability of 1 md, with values ranging from 11.5 to 14% (Murphy et al., 1996).

Nuclear magnetic resonance (NMR) logs also have been used recently in Brushy Canyon. Experience indicates that these logs are able to distinguish oil-bearing vs. water-bearing reservoirs and to provide relatively accurate measurements of permeability. Such determinations are based on laboratory study using NMR measurements on core plugs; these measurements have accurately predicted pore-size distributions (Logan et al., 1995). NMR logs have been successfully used in Nash Draw field and a few other locations. Good correlations have been indicated with mud log shows, core-determined permeability, and vertical distribution of production. Generally, due to their added expense, NMR logs are considered especially helpful where mud log data is either absent or deemed to be of poor quality.

Reservoir Thickness, Geometry, and Continuity

Productive zones within the Brushy Canyon and Cherry Canyon range from a minimum of 8 ft (2 m) to 200 ft (61 m), with thicker intervals showing a significant degree of interbedding between oil-bearing and wet zones. Net pay within wells is commonly in the range of 30–90 ft (9–27 m). Productive zones are lenticular in geometry and can exhibit rapid lateral pinch-out between adjacent wells (Figure 11). These zones are commonly separated by thin, impermeable siltstone intervals that appear to mantle sandstone thicks (Figure 11). These siltstones act as top and lateral seals.

Lateral continuity and heterogeneity of reservoirs depend on specific depositional setting. Upper Brushy Canyon reservoirs in lower slope and basin-floor settings proximal to the shelf margin (e.g., Avalon field) display evidence of deposition by suspension and thus exhibit little overall heterogeneity (Cantrell and Kane, 1995). In contrast, lower Brushy Canyon and most Cherry Canyon reservoirs were deposited in more distal, submarine channel/fan settings with sandstones characteristically showing less continuity and more complexity.

A good example of the latter type of reservoir is found at Nash Draw field (Eddy County, New Mexico). Abundant core data in this field have indicated that individual productive sandstone zones with areal extent of several square miles or more actually are composed of a number of stacked units ranging from 1 to 6 ft (0.3 to 1.8 m) thick, each with lateral extent of 0.25 to 0.50 mi (0.4 to 0.8 km) (Martin et al., 1997). Little vertical permeability is observed to exist between these "microreservoirs." As a result, a significant degree of compartmentalization appears to characterize productive zones. This assumption is supported by capillary pressure data, which have been calculated for several cored wells. Maps of resulting values vs. structure suggest the existence of multiple sand pods with different characteristics (Murphy et al., 1996). In addition, seismic attribute analysis in this field, using a 3-D (three-dimensional) data set, also predicts a complex distribution of good-quality reservoir (Balch et al., 1998). Comparison with core data from other, nearby fields (e.g., Loving field) indicates strong similarity in terms of sandstone geometry and character.

Reservoir Facies

Recent studies of Brushy Canyon and Cherry Canyon sandstones in New Mexico and Texas have tentatively identified several main reservoir facies (Spain, 1992; Thomerson and Catalano, 1996; Gardner, 1997; Martin et al., 1997). These facies are based on a fine-grained turbidite depositional model for the subsurface Delaware basin and include (1) channel facies sandstones typified by more massive character and highly lenticular geometry (Figure 11), (2) levee/overbank sandstones exhibiting a more laminated, bioturbated character, and (3) basin-floor fan facies showing greater lateral continuity and bioturbation. Massive channel and levee/overbank sandstones are interpreted to reflect deposition in an inner or middle fan setting with basin-floor sandstones more indicative of distal, outer fan environments. Most productive are channel facies, which comprise the main reservoir sandstones in a majority of fields. Reservoir quality generally is highest in the thickest portions of channels, but porosity thicks also can occur outside and parallel to the central channel scour (May, 1996).

Reservoirs in the Brushy Canyon exist in the upper and lower portions of the formation. Lower Brushy Canyon reservoirs, occurring in multistory basin-floor submarine channel and lobe complexes, represent part of the initial, progradational phase of basin filling. In general, porosities and permeabilities are somewhat higher in these lower Brushy Canyon sandstones than in overlying intervals due to lesser amounts of carbonate cement. This fact is interpreted to reflect a highly efficient sediment bypass system, such that eolian- or fluvial-supplied clastics did not incorporate material from shelf-edge carbonates during transport to slope and basinal settings. Upper Brushy Canyon sandstones are considered part of a backstepping sequence (Gardner, 1997) that onlaps and extends landward of the Victorio Peak shelf margin. Reservoirs in this interval appear to consist of both slope and basin-floor fan deposits. Slope sandstones lie closer to the coeval shelf edge and exhibit less heterogeneity than lower Brushy Canyon channel/lobe deposits. They are overlain by a thinner Cherry Canyon–Bell Canyon section prograded by the Capitan reef system.

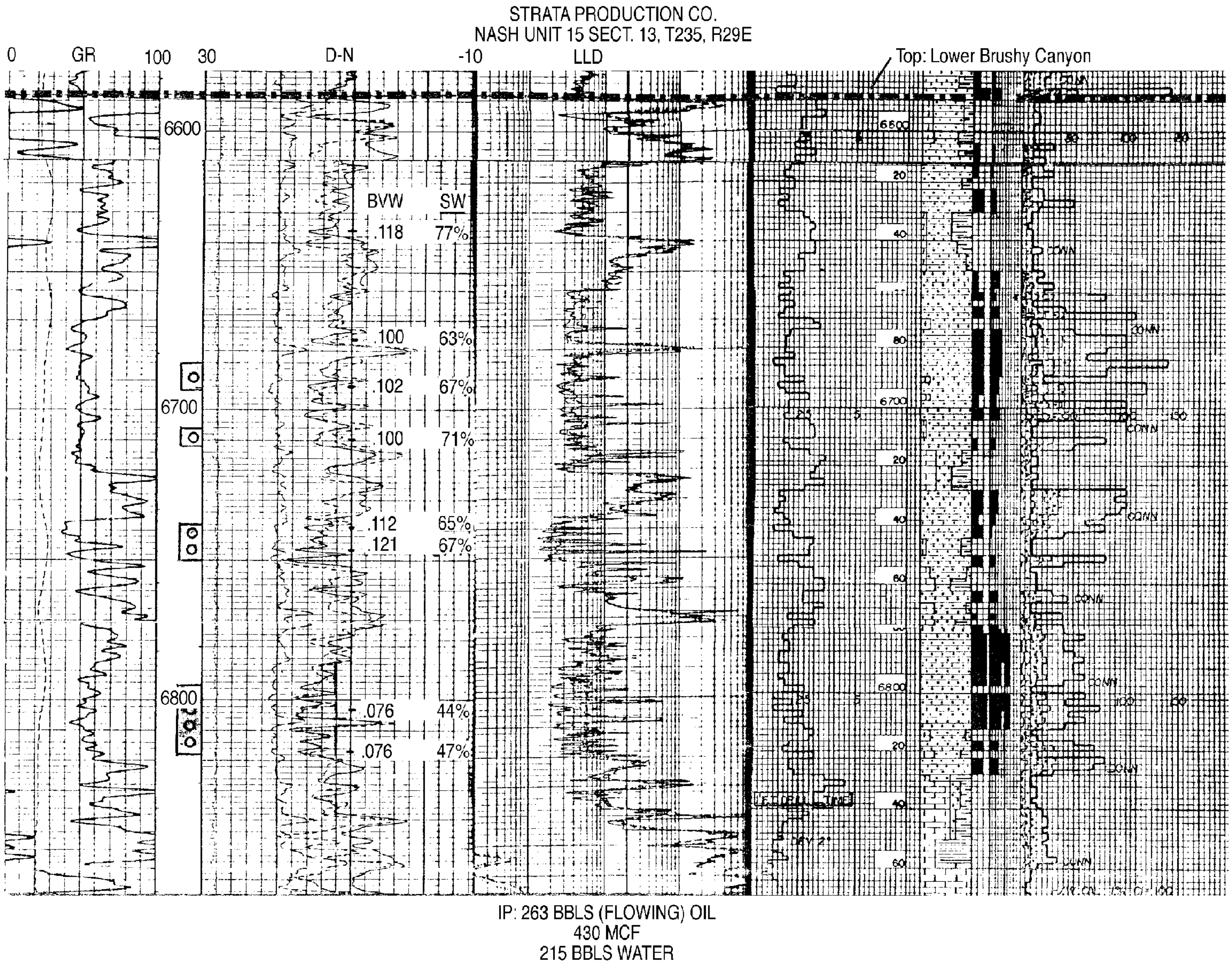

Figure 10—Log data, Nash Unit 15, Nash Draw field, Eddy County (New Mexico), showing typical response through pay and nonpay zones in the lower Brushy Canyon, including mud log shows and calculated water saturation for selected sandstones.

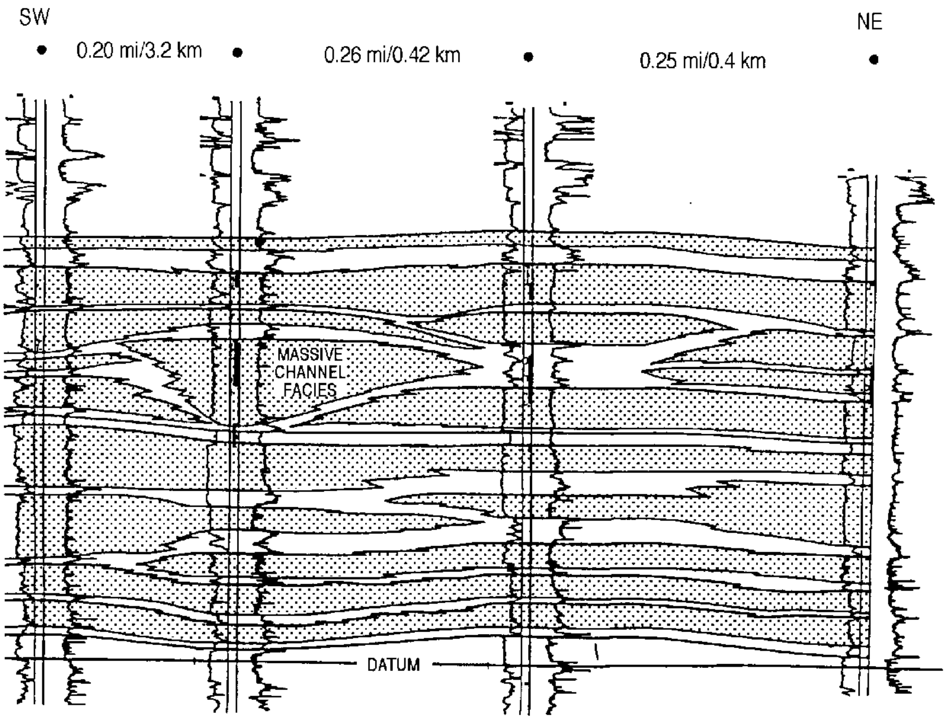

Figure 11—Northeast-southwest cross section, East Livingston Ridge field (Lea County, New Mexico), showing lenticular morphology of Brushy Canyon sandstone units. Cross section shows the upper portion of the Brushy Canyon, where "D" zone sandstones, including a massive channel facies, form the primary reservoir. Modified from Thomerson and Catalano (1996).

REGIONAL RESERVOIR TRENDS

A map distinguishing the principal reservoir trends in the Brushy Canyon and Cherry Canyon formations is given in Figure 12. A total of five trends are shown: (1) lower Brushy Canyon in distal, basin-floor settings (e.g., Loving, Nash Draw, Sand Dunes fields), (2) upper Brushy Canyon in basin-floor settings (Lost Tank, Livingston Ridge, East Livingston Ridge fields), (3) upper Brushy Canyon in slope turbidite channel/fan settings commonly within 5 mi (8 km) of the shelf margin (Catclaw Draw, Avalon, Parkway fields), (4) Cherry Canyon in lower slope and basin-floor settings, and (5) Cherry Canyon in upper/middle slope settings with updip pinch-out into shelf-margin carbonates.

Brushy Canyon fields are confined to the northern portion of the Delaware basin, in New Mexico. Fields in Cherry Canyon reservoirs, however, are more widely dispersed, existing in slope and basinal positions both in the northern and central parts of the basin. With the exception of War-Wink field in Texas, exploration and field development have concentrated on the newer Brushy Canyon plays, the majority of which have been discovered since 1985 (Table 1). These plays, and reservoir trends in general, have depended on the mapping of channel fairways. As previously noted, these fairways are oriented perpendicular to the shelf margin in more proximal areas (e.g., within 5–10 mi; 8–16 km) and more north-south within the deeper northern basin.

Trapping within Brushy Canyon and Cherry Canyon reservoirs is dominantly stratigraphic in nature, related to lateral and updip pinch-out of porous sandstone facies. In many cases, however, porosity pinch-out occurs in conjunction with low-relief structures, many of which have been mapped in the lower Brushy Canyon. A typical example, shown in Figure 13 for the Los Medanos and Sand Dunes producing area, suggests that related structures helped control channel development and thus deposition of higher quality sands. Data from certain fields productive in the lower Brushy Canyon strongly imply that channel deposition took place in paleobathymetric lows or along subtle ledges of the underlying Bone Spring formation (Murphy et al., 1996; Thomerson and Catalano, 1996). Such features may have been influenced by preexisting structure. In most cases, maximum reservoir thickness appears located along the flanks of a particular closure or structural nose (Figure 13B).

Alternately, present-day entrapment and reservoir development may reflect early charging of Delaware Mountain sandstones on structural highs. Oil migration into these sandstones would have inhibited subsequent cementation and quartz overgrowth development compared with downdip positions, thereby resulting in lateral pinch-out of porosity.

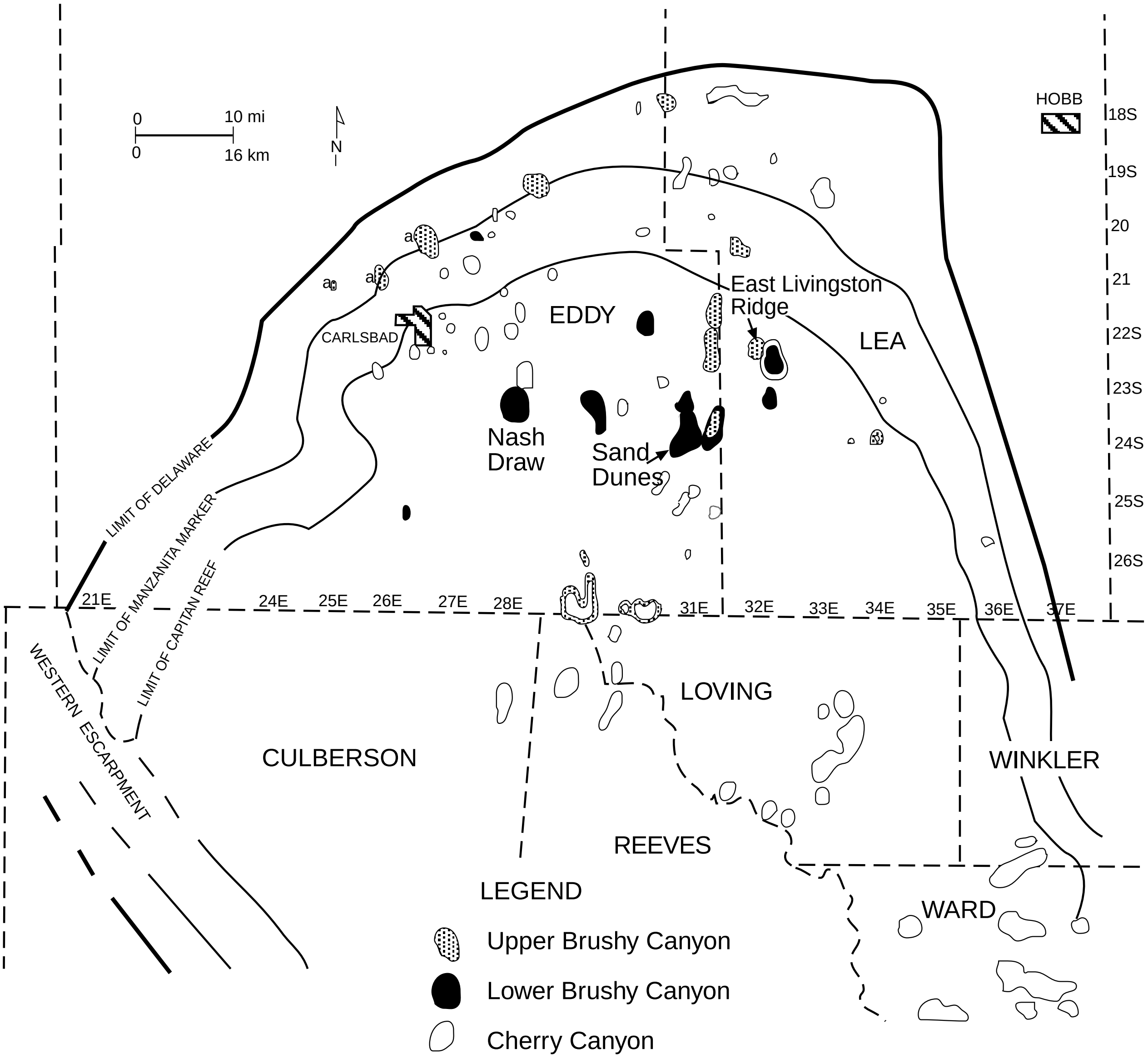

Figure 12—Principal reservoir trends in the Brushy Canyon and Cherry Canyon, northern Delaware basin.

Later tilting due to Laramide tectonism would not have affected entrapment, yet shifted the thickest reservoir section off-structure. More detailed study is clearly required to resolve the question of how structure, deposition, and oil occurrence are related.

PRODUCTION

Rates of production for individual wells completed in the Brushy Canyon and Cherry Canyon are on the order of 50–400 bbl oil, 100–1000 mcf gas, and 30–350 bbl water per day. Due to the highly interbedded nature of oil- and water-bearing zones, nearly all wells have significant water cuts, usually in the range of 40–65%. Estimated ultimate primary recovery for wells in most fields is 50,000–100,000 bbl oil and 40–200 mmcf gas (see, for example, Broadhead and Luo, 1996). These figures generally represent no more than 10% of the original oil in place (OOIP).

The oil is a sweet crude, 37–43° gravity (API), whereas gas is commonly 60–75% methane with a

Table 1. New Mexico Delaware Fields

Fields with cumulative production >500 MBO
Production through February 1998

	Field	Active Wells	MBO	MMCFG	MBW	ZONE	DISC
	Malaga	16	592	99	1,132	BELL	1951
	Mason N	59	4,347	8,284	6,487	BELL	1955
	El Mar	62	6,150	13,648	5,802	Bell	1956
	Brushy Draw	118	6,292	10,003	22,589	CC, BR	1959
	Shugart	6	1,585	1,540	346	BR	1959
	Corral Canyon	15	671	618	1,567	Bell	1960
	Double X	33	1,322	3,644	2,503	Bell	1961
	Paduca	61	12,936	14,623	14,232	Bell	1961
	Cruz	20	992	1,673	5,030	Bell	1962
	Mason, E	26	1,372	2,136	2,053	BELL	1962
	Salado Draw	11	762	1,394	850	BELL	1962
	Esperanza	8	1,193	352	1,280	CC	1969
•	Sand Dunes CC	13	908	462	1,183	CC	1970
	Indian Draw	22	3,131	163	4,675	CC	1974
•	Cedar Canyon	27	502	600	1,126	C, BR	1976
•	Corbin, West	46	2,410	3,401	4,120	CC	1976
	Indian Flats	13	561	196	1,233	CC	1976
	Herradura Bend	24	874	64	996	BELL	1977
•	Avalon	55	4,027	9,351	9,379	CC, BR	1984
•	Fenton NW	21	727	2,956	1,419	CC	1984
•	Herradura Bend E	52	1,236	8,207	4,608	BR	1986
•	Shugart E	18	2,114	4,698	1,908	BR	1986
•	Cabin Lake	36	3,267	3,675	9,038	CC, BR	1987
•	Loving, Brushy Canyon E	109	6,291	36,491	7,287	BR	1987
•	Lusk, West	34	2,287	4,666	2,023	BR	1987
•	Parkway	34	2,502	7,953	2,159	BR	1987
•	Ingle Wells	120	5,438	13,713	11,368	BR	1989
•	Lea, NE	66	3,028	3,365	2,964	CC	1989
•	Livingston Ridge	54	4,187	6,536	7,565	BR	1989
•	Hat Mesa	21	1,364	1,536	1,913	BR	1990
•	Sand Dunes W	82	4,872	19,571	4,243	BR	1990
•	Catclaw Draw, E	19	960	2,419	1,181	CI, BR	1991
•	Los Medanos	38	2,162	5,842	3,048	BR	1991
•	Lost Tank	44	2,162	3,991	5,035	BR	1991
•	Livingston Ridge, E	36	1,729	1,827	5,331	BR	1992
•	Nash Draw Brushy Canyon	38	1,108	5,702	2,085	BR	1992
•	Red Tank, W	85	3,432	5,626	6,869	B, CC, BR	1992
•	Triste Draw W	17	513	828	1,022	BR	1992
•	Happy Valley	24	602	510	1,277	CC, BR	1993
•	Mesa Verde	19	645	1,135	1,104	BR	1993
•	Poker Lake SW	24	648	1,787	1,729	BR	1996
	41 Fields	1,626	101,901	215,285	171,759		

• = Discovered or primarily developed since 1985

heat content of 1100–1470 btu/ft^3. Reservoirs produce by solution-gas drive; a great majority yield oil and associated gas with only a few producing nonassociated gas. Initial pressures in many reservoirs are only slightly (several hundred psi) above bubble-point pressure. As a result, early decline rates are steep, and gas/oil ratios, which begin relatively high, typically 600–5000 scf/bbl, increase rapidly. Fields are generally developed on 40 ac (16 ha) spacing with a few on 80 ac (32 ha). Detailed analysis of producing wells in Nash Draw field suggests that actual drainage areas range from 19–66 ac (7–26 ha) (average 34 ac; 13 ha) with significant interference occurring in certain areas (Strata Production Company, 1998).

Figure 13—Maps comparing (A) structure and (B) reservoir sandstone thickness (porosity >14%), lower Brushy Canyon main pay interval, Sand Dunes field, Eddy County, New Mexico. Modified from Hoose and Dillman (1995).

(A)

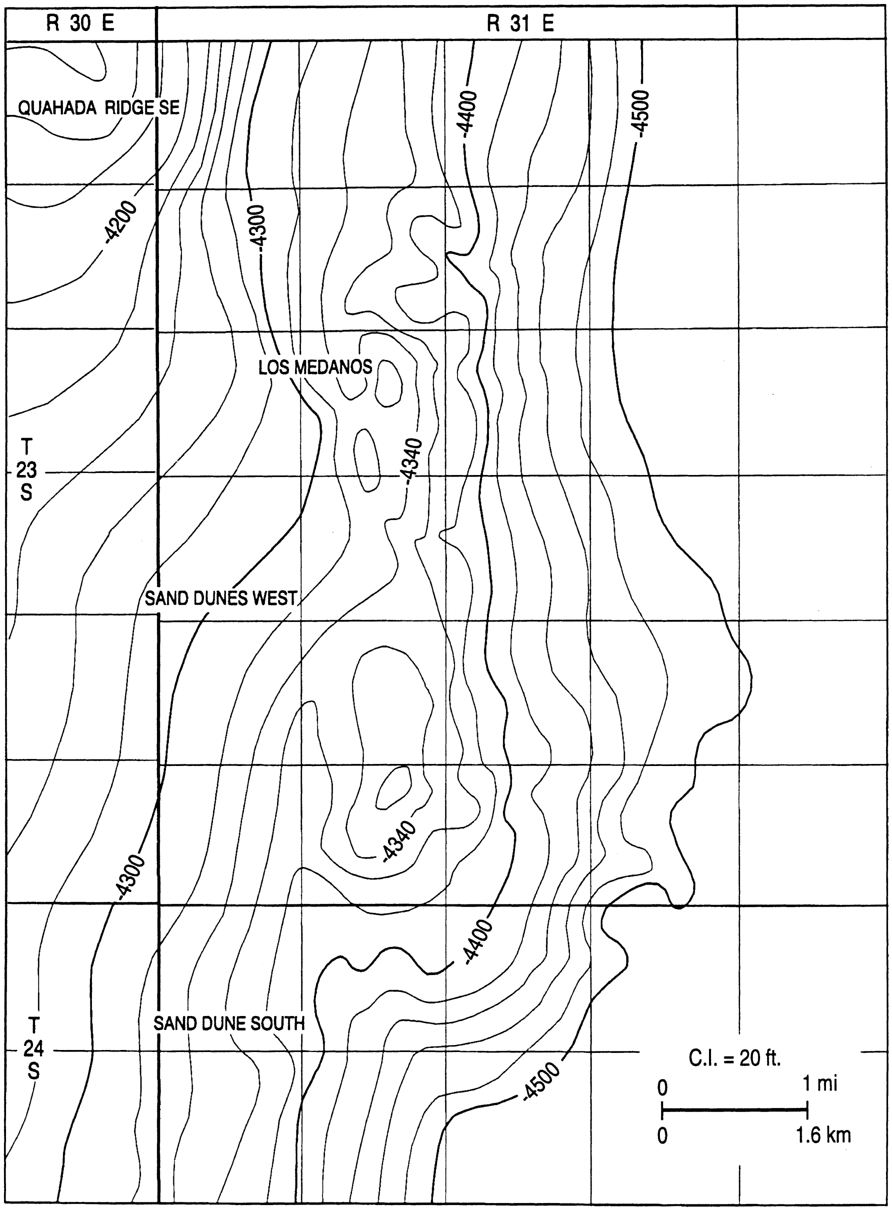

Figure 14 is a plot of per-well calculated flow capacity (k_h/μ), computed from core data for the main pay zone (lower Brushy Canyon "L" zone) in Nash Draw field. Given that most wells in this field have been completed in a similar manner, this histogram suggests a considerable variety in reservoir quality and well performance. Decline curves for three of the wells are given in Figure 15 and confirm significant differences in performance over time. For example, the Nash 15 shows a more rapid decline in oil production and rise in water production than either of the other two wells, especially during the first 2 yr. Gas production remains relatively flat for wells 13 and 15, but declines significantly in well 19, which, however, displays a fairly constant oil/water ratio in contrast to the other wells. Such differences point to changes in reservoir character among these locations, which are all 0.25-0.5 mi (0.4-0.8 km) of each other. Figure 15 also indicates typical hyberbolic decline for these fracture-stimulated wells.

(B)

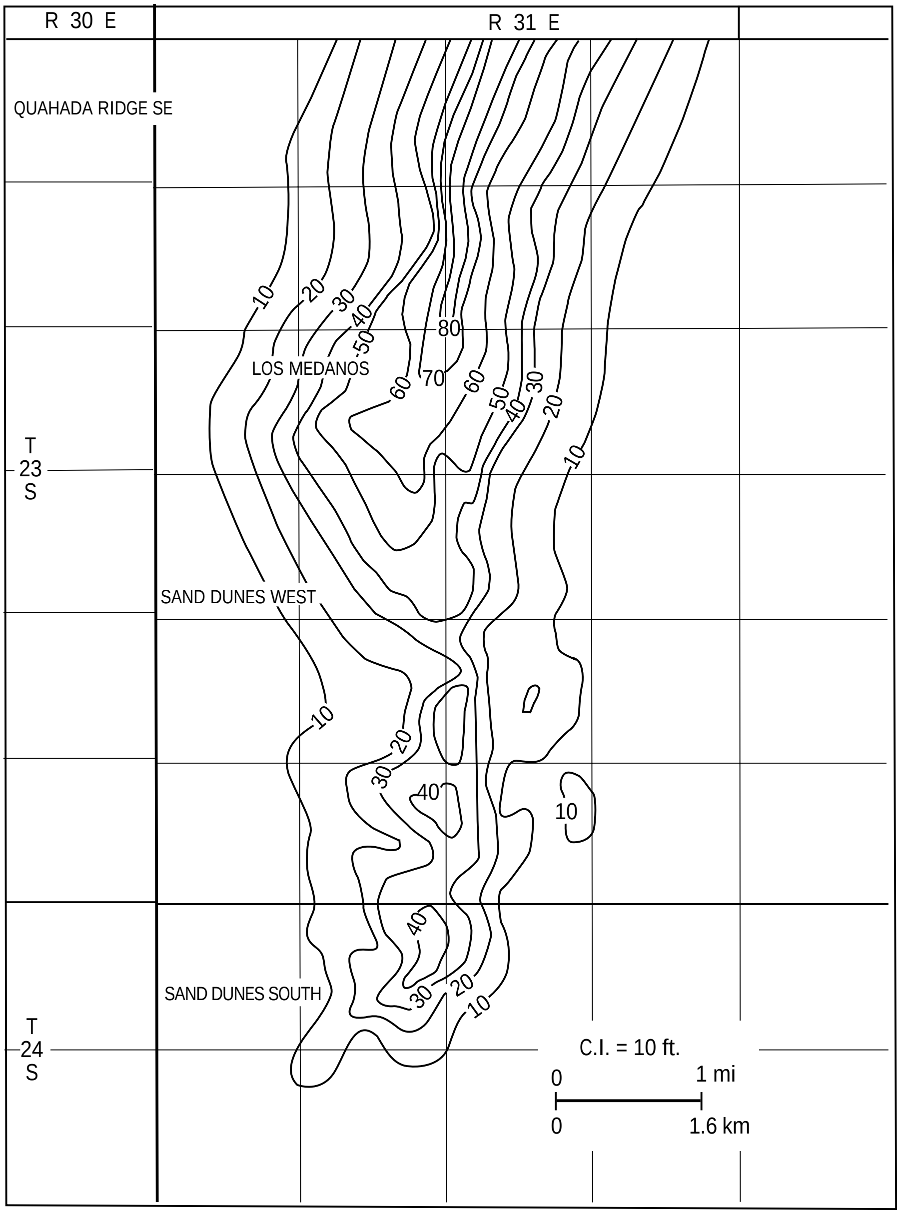

Figure 13—Continued.

Many operators consider secondary recovery essential to future development (Broadhead and Luo, 1996); their thinking is based on three main reasons: (1) relatively low primary recoveries (7–10%), (2) steep oil production decline, which can be up to 50% in the first year, and (3) rapidly increasing gas/oil ratios. A few fields, such as Indian Draw (Eddy County, New Mexico), which produces from the Cherry Canyon, have successfully doubled primary production through long-term waterflooding. Waterfloods have been initiated recently in several upper Brushy Canyon and lower Cherry Canyon fields (Avalon, Parkway, and Lusk West), along the proximal lower slope/basin floor trend. Reservoirs in these fields show less lateral heterogeneity than in other trends and thus may be more appropriate targets of waterflooding. Related efforts have employed as injectors both existing wells and new wells drilled on 20-ac (8-ha) spacing.

In more complex heterogeneous reservoirs, a combination of early pressure maintenance (gas injection) and secondary carbon dioxide flooding

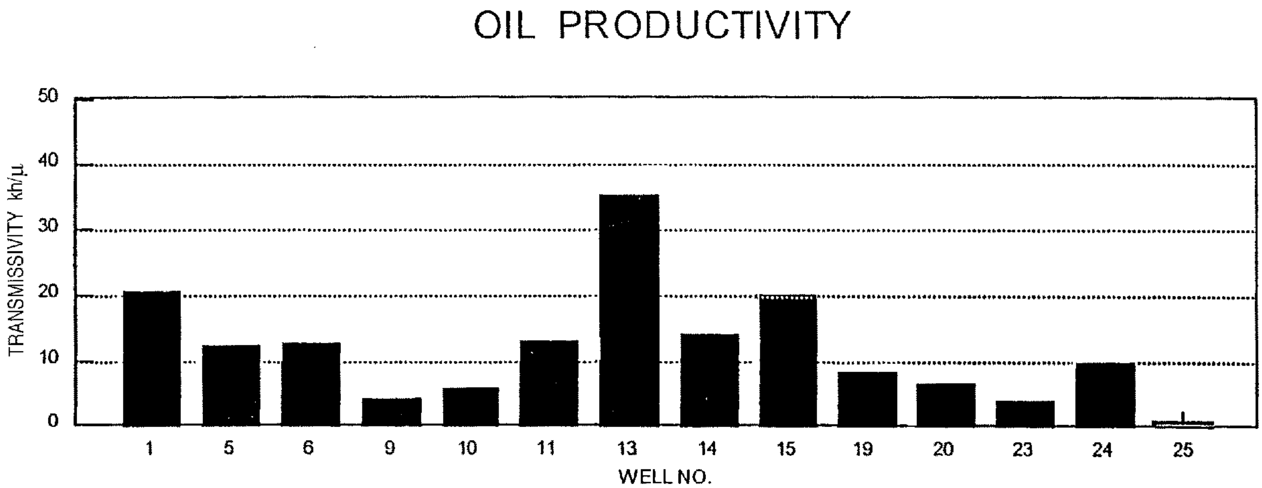

Figure 14—Flow capacity (k_h/μ) calculated on a per-well basis for the main productive zone (lower Brushy Canyon) in Nash Draw field. Modified from Murphy et al. (1996).

Figure 15—Decline curve data for three wells in Nash Draw field. Wells are chosen to illustrate the significant variation observed in field production over short distances. Wells 13 and 19 are 0.25 mi (0.4 km) apart and approximately 0.5 mi (0.8 km) from well 15.

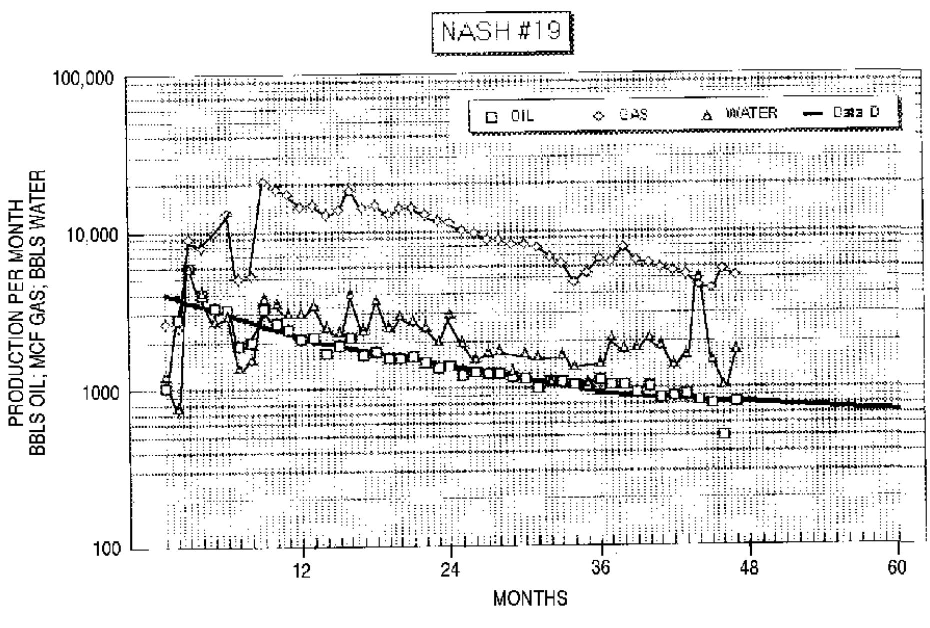

may be able to maximize production. Use of gas instead of water as an oil-mobilizing agent is suggested as preferable due to the low permeabilities involved and high water-to-oil relative permeabilities (Strata Production Company, 1998). Carbon dioxide floods have been performed in several Bell Canyon fields; in one case, Two Freds field (Ward and Loving counties, Texas), the volumes of oil recovered have exceeded those from primary and earlier waterflooding combined. Whether similar results might be attained for Brushy Canyon and Cherry Canyon reservoirs in New Mexico is not known.

DRILLING AND COMPLETION

The nature of Brushy Canyon and Cherry Canyon reservoirs requires that drilling and completion techniques be adjusted to minimize formation damage and ensure good fracture stimulation. In particular, the presence of clays, K-feldspar, and Fe-rich chlorite make these reservoirs susceptible to damage as a result of swelling, fines migration, and acid sensitivity (iron chelation) (Behnken, 1996; Green et al., 1996). As a result, operators have employed appropriate additives, mud salinities, and KCl-based fluids to reduce damage.

Figure 15—Continued.

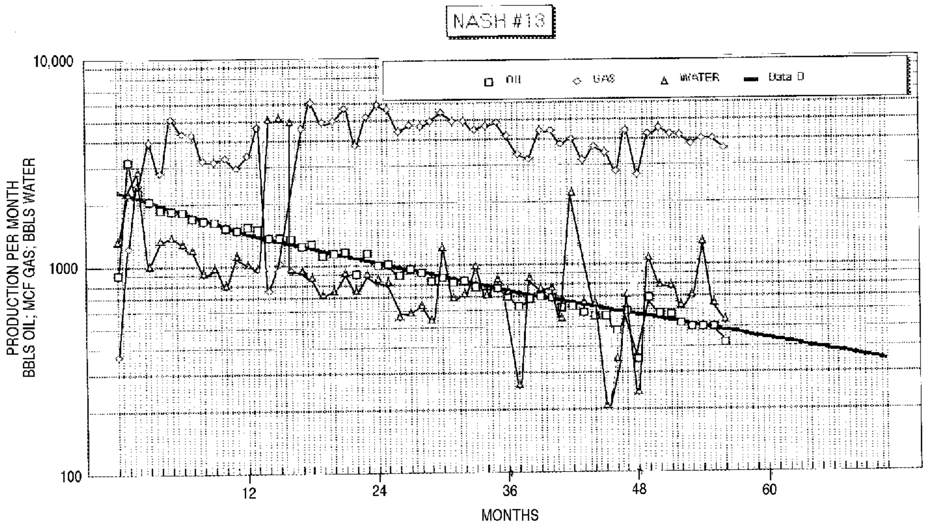

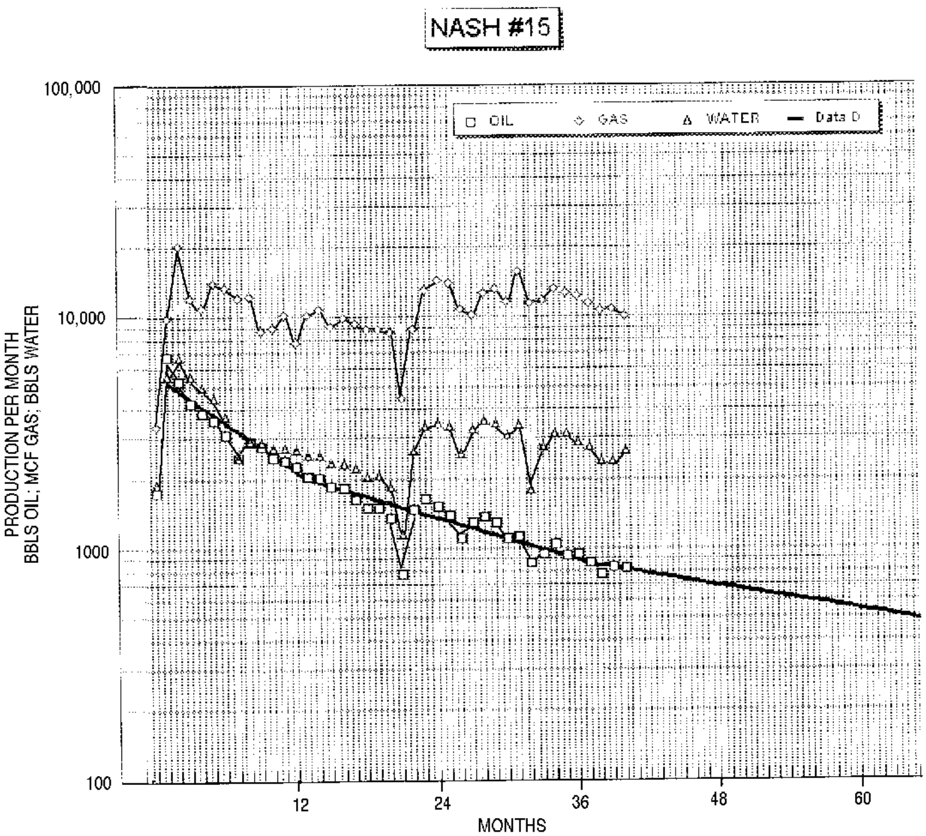

Extensive acidization is generally avoided; a typical treatment involves 100 gal (378 L) per perforation (one shot per foot), injected at a rate of 3 bbl per minute.

Fracture stimulation commonly is rendered problematic in these reservoirs due to their multilayered, thin-bedded character, the vertical interbedding or proximity of water-bearing zones, and the general lack of stratal fracture barriers (Scott and Carrasco, 1996). Adjustments to standard stimulation techniques have been required to adequately address these factors. Earlier treatments often were quite large, ranging up to 300,000 lb (136,200 kg) or more of sand pumped at rates of 15–40 bbl/min with high proppant concentrations of 6–12 lb/gal (Scott and Carrasco, 1996). This type of stimulation had trouble controlling vertical fracture propagation and usually yielded fracture heights equal to, or even greater than, fracture length. Larger treatments at high pumping rates also resulted in screenout.

To control fracture growth and avoid screenout, operators now design stimulations for smaller fracture lengths (e.g., 400 ft; 122 m) and lower pump injection rates. A common size for these stimulations is 75,000–100,000 lb (34,050–45,400 kg) of resin-coated sand with 50,000 gal (189,250 L) of cross-linked gel as the transport fluid. Smaller stimulations (e.g., 10,000 lb; 4540 kg) or acidization alone are used in cases of thinner sandstones located in vertical proximity to water zones. Full stimulations employ a fairly low proppant concentration of up to 6 lb/gal, pumped at a rate of 6–15 bbl per minute. As discussed by Scott and Carrasco (1996), improved results have come from continuous, progressive ramping of the pump rate in combination with an increase in sand concentration (e.g., from 1 to 10 lb/gal). This technique works well to prevent premature screenout while achieving good placement of the proppant.

In most field settings, design of fracture treatments will need to evolve as a result of experience and increased information on reservoir character as development progresses. The lateral heterogeneity and reservoir compartmentalization observed in many Brushy Canyon reservoirs, moreover, also may demand design reevaluation and adjustment for different portions of a specific field.

CONCLUSIONS

Exploration and development of basin-restricted sandstone reservoirs in the lower Delaware Mountain Group during the past 10–15 yr represent a significant addition to hydrocarbon plays of the Permian basin. These low-permeability, high-porosity oil and gas reservoirs of the Brushy Canyon and Cherry Canyon formations can be divided into several main productive trends, each reflecting a specific depositional style and setting. Slope and basin-floor submarine channel/fan systems exist proximal to the coeval carbonate shelf margin and in more distal trends. Reservoir sandstones do not show typical turbidite sedimentary features but are very fine grained, commonly massive, highly laminated, and interbedded with thin, organic siltstones lacking in detrital clay. Reservoir character commonly is complex with significant lateral heterogeneity. Productive sandstone intervals tend to be multilayered with considerable interbedding between oil-bearing and water-bearing zones. These characteristics continue to present challenges for interpreting depositional history, predicting reservoir quality, and achieving maximum recovery.

REFERENCES CITED

Balch, R. S., W. W. Weiss, and S. Wo, 1998, Correlating seismic attributes to reservoir properties using multi-variate non-linear regression: available online at http://baervan.nmt.edu/REACT/Links/nash-wtgs/Nash-wtgs.html.

Basham, W. L., 1996, Delaware Mountain Group sandstone channel orientations: implications for sediment source and deposition, *in* W. D. DeMis and A. G. Cole, eds., The Brushy Canyon play in outcrop and subsurface: concepts and examples: Permian Basin Section SEPM, Publication 96-38, p. 91–102.

Basu, D., and A. H. Bouma, 1996, New method to determine the depositional mechanisms in a submarine fan channel-levee complex, Brushy Canyon Formation, west Texas, *in* W. D. DeMis and A. G. Cole, eds., The Brushy Canyon play in outcrop and subsurface: concepts and examples: Permian Basin Section SEPM, Publication 96-38, p. 85–90.

Behnken, F. H., 1996, Reservoir characterization of the Brushy Canyon Formation Sandstone (Late Permian), Strata Production Nash Unit 15, Nash Draw Delaware field, Eddy County, New Mexico, *in* W. D. DeMis and A. G. Cole, eds., The Brushy Canyon play in outcrop and subsurface: concepts and examples: Permian Basin Section SEPM, Publication 96-38, p. 173–182.

Berg, R. R., 1979, Reservoir sandstones of the Delaware Mountain Group, southeast New Mexico, *in* N. M. Sullivan, ed., Guadalupian Delaware Mountain Group of west Texas and southeast New Mexico: Permian Basin Section SEPM, Publication 79-18, p. 75–94.

Broadhead, R. F., and F. Luo, 1996, Oil and gas resources in the Delaware Mountain Group at the WIPP site, Eddy County, New Mexico, *in* W. D. DeMis and A. G. Cole, eds., The Brushy Canyon play in outcrop and subsurface: concepts and examples: Permian Basin Section SEPM, Publication 96-38, p. 119–130.

Cantrell, D. L., and T. V. Kane, 1995, Production history and geology, Avalon (Delaware) field, *in* J. Worrall, general chairman, Symposium of the oil and gas fields of southeastern New Mexico, 1995 supplement: Roswell Geological Society, p. 50–54.

DeMis, W. D., and A. G. Cole, eds., 1996, The Brushy Canyon play in outcrop and subsurface: concepts and examples: Permian Basin Section SEPM, Publication 96-38, 277 p.

Dickerson, P. W., 1985, Evidence for Late Cretaceous–early Tertiary transpression in Trans-Pecos Texas and adjacent Mexico, *in* P. W. Dickerson and W. R. Muehlberger, eds., Structure and tectonics of Trans-Pecos Texas: West Texas Geological Society, Publication 85-81, p. 185–194.

Fischer, A. G., and M. Sarnthein, 1988, Airborne silts and dune-derived sands in the Permian of the Delaware basin: AAPG Bulletin, v. 72, p. 637–643.

Gardner, M. H., 1992, Sequence stratigraphy of eolian-derived turbidites: deep water sedimentation patterns along an arid carbonate platform and their impact on hydrocarbon recovery in Delaware Mountain Group reservoirs, west Texas, *in* D. H. Mruk and B. C. Curran, eds., Permian basin exploration and production strategies: applications of sequence stratigraphic and reservoir characterization concepts: West Texas Geological Society, Publication 92-91, p. 7–11.

Gardner, M. H., 1997, Sequence stratigraphy and hydrocarbon habitat of the Permian (Guadalupian) Delaware Mountain

Group, Delaware basin, west Texas, *in* R. P. Major, ed., Oil and gas on Texas state lands: an assessment of the resource and characterization of type reservoirs: University of Texas at Austin, Bureau of Economic Geology, Report of Investigations 241, p. 147–157.

Gardner, M. H., and M. D. Sonnenfeld, 1996, Stratigraphic changes in facies architecture of the Permian Brushy Canyon Formation in Guadalupe Mountains National Park, west Texas, *in* W. D. DeMis and A. G. Cole, eds., The Brushy Canyon play in outcrop and subsurface: concepts and examples: Permian Basin Section SEPM, Publication 96-38, p. 17–40.

Grauten, W. F., 1979, Fluid relations in Delaware Mountain sandstone, *in* N. M. Sullivan, ed., Guadalupian Delaware Mountain Group of west Texas and southeast New Mexico: Permian Basin Section SEPM, Publication 79-18, p. 191–204.

Green, K. M., S. M. Frailey, and G. B. Asquith, 1996, Laboratory analysis of the clays within the Brushy Canyon Formation and their reservoir and petrophysical implications: Red Tank field, Lea County, New Mexico, *in* W. D. DeMis and A. G. Cole, eds., The Brushy Canyon play in outcrop and subsurface: concepts and examples: Permian Basin Section SEPM, Publication 96-38, p. 165–172.

Hamilton, D. C., 1996, Mid-lower Cherry Canyon play in War-Wink area of the Delaware basin, Ward and Winkler counties, Texas, *in* W. D. DeMis and A. G. Cole, eds., The Brushy Canyon play in outcrop and subsurface: concepts and examples: Permian Basin Section SEPM, Publication 96-38, p. 131–136.

Hamilton, D. C., and T. Hunt, 1996, War-Wink Cherry Canyon trend, serendipity in spades, *in* R. L. Martin, ed., Permian basin oil and gas fields: keys to success that unlock future reserves: West Texas Geological Society, Publication 96-101, p. 107–116.

Harms, J. C., 1974, Brushy Canyon Formation, Texas: a deep-water density current deposit: Geological Society of America Bulletin, v. 85, p. 1763–1784.

Harms, J. C., and M. J. Brady, 1996, Deposition of the Brushy Canyon Formation: 30 years of conflicting hypotheses, *in* W. D. DeMis and A. G. Cole, eds., The Brushy Canyon play in outcrop and subsurface: concepts and examples: Permian Basin Section SEPM, Publication 96-38, p. 51–60.

Harms, J. C., and C. R. Williamson, 1988, Deep-water density current deposits of Delaware Mountain Group (Permian), Delaware basin, Texas and New Mexico: AAPG Bulletin, v. 72, p. 299–317.

Hills, J. M., 1984, Sedimentation, tectonism, and hydrocarbon generation in Delaware basin, west Texas and southeastern New Mexico: AAPG Bulletin, v. 68, no. 3, p. 250–267.

Hoose, G., and G. Dillman, 1995, Sand Dunes Delaware, W.; Sand Dunes Delaware, S., *in* J. Worrall, general chairman, Symposium of the oil and gas fields of southeastern New Mexico, 1995 supplement: Roswell Geological Society, p. 325–328.

Kosters, E. C., et al., 1983, Atlas of major Texas oil reservoirs: Gas Research Institute and Bureau of Economic Geology, University of Texas at Austin, 150 p.

Logan, D., C. Morriss, and R. Williams, 1995, Comparison of nuclear magnetic resonance techniques in the Delaware, *in* J. Worrall, general chairman, Symposium of the oil and gas fields of southeastern New Mexico, 1995 supplement: Roswell Geological Society, p. 112–136.

Martin, D. F., B. A. Hardage, M. B. Murphy, R. P. Kendall, B. A. Stubbs, B. J. Uszynski, W. W. Weiss, and E. M. Whitney, 1997, Reservoir characterization as a risk reduction tool at the Nash Draw pool: Society of Petroleum Engineers Paper 38916, 14 p.

May, B. A., 1996, Geology and development history of the Livingston Ridge and Lost Tank Delaware pools, southeastern New Mexico, *in* W. D. DeMis and A. G. Cole, eds., The Brushy Canyon play in outcrop and subsurface: concepts and examples: Permian Basin Section SEPM, Publication 96-38, p. 113–118.

Montgomery, S. L., 1997, Permian Bone Spring Formation: sandstone play in the Delaware basin part I—slope: AAPG Bulletin, v. 81, no. 8, p. 1239–1258.

Murphy, M. B., B. A. Hardage, D. F. Martin, R. P. Kendall, B. A. Stubbs, B. J. Uszynski, W. W. Weiss, and E. M. Whitney, 1996, Advanced oil recovery technologies for improved recovery from slope basin clastic reservoirs, Nash Draw Brushy Canyon pool, Eddy County, N. M.: U.S. Department of Energy Cooperative Agreement DE-FC-95BC14941, First Annual Report, 80 p.

Rossen, C., and J. F. Sarg, 1988, Sedimentology and regional correlation of a basinally restricted deep-water siliciclastic wedge: Brushy Canyon Formation, Cherry Canyon tongue (lower Guadalupian), Delaware basin, *in* S. T. Reid, R. O. Bass, and P. Welch, eds., Guadalupe Mountains revisited, Texas and New Mexico: West Texas Geological Society, Publication 88-84, p. 127–132.

Scott, G. L., and A. Carrasco, 1996, Delaware sandstone reservoir completions and real-time monitoring of hydraulic fractures, *in* W. D. DeMis and A. G. Cole, eds., The Brushy Canyon play in outcrop and subsurface: concepts and examples: Permian Basin Section SEPM, Publication 96-38, p. 183–188.

Silver, B. A., and R. G. Todd, 1969, Permian cyclic strata, northern Midland and Delaware basin, west Texas and southeastern New Mexico: AAPG Bulletin, v. 53, no. 11, p. 2233–2251.

Spain, D. R., 1992, Petrophysical evaluation of a slope fan/basin-floor fan complex: Cherry Canyon Formation, Ward County, Texas: AAPG Bulletin, v. 76, p. 805–827.

Strata Production Company, 1998, Advanced oil recovery technologies for improved recovery from slope basin clastic reservoirs, Nash Draw Brushy Canyon pool, Eddy County, N. M.: U.S. Department of Energy Cooperative Agreement DE-FC-95BC14941, Second Annual Report, 83 p.

Thomerson, M. D., and G. B. Asquith, 1992, Petrophysical analysis of the Brushy Canyon Formation, Hat Mesa Delaware field, Lea County, New Mexico, *in* D. H. Mruk and B. C. Curran, eds., Permian basin exploration and production strategies: applications of sequence stratigraphic and reservoir characterization concepts: West Texas Geological Society, Publication 92-91, p. 80–90.

Thomerson, M. D., and L. E. Catalano, 1996, Depositional regimes and reservoir characteristics of the Brushy Canyon sandstones, East Livingston Delaware field, Lea County, New Mexico, *in* W. D. DeMis and A. G. Cole, eds., The Brushy Canyon play in outcrop and subsurface: concepts and examples: Permian Basin Section SEPM, Publication 96-38, p. 103–112.

Wegner, M., K. M. Bohacs, J. A. Simo, A. R. Carroll, and D. Pevear, 1998, Siltstone facies of the upper Brushy Canyon and lower Cherry Canyon formations (Guadalupian), Delaware basin, west Texas: depositional processes and stratigraphic distribution, *in* W. D. DeMis and M. K. Nelis, eds., The search continues into the 21st century: West Texas Geological Society, Publication 98-105, p. 59–66.

Yang, K-M., and S. L. Dorobek, 1995, The Permian basin of west Texas and New Mexico: tectonic history of a "composite" foreland basin and its effects on stratigraphic development, *in* S. L. Dorobek and G. M. Ross, eds., Stratigraphic evolution of foreland basins, SEPM, Special Publication 52, p. 149–174.

ABOUT THE AUTHORS

Scott L. Montgomery

Scott L. Montgomery is a petroleum consultant and author residing in Seattle, Washington. He received his B.A. degree in English from Knox College in 1973 and his M.S. degree in geological sciences from Cornell University in 1978. He is widely published in the geosciences, and since 1996 he has been principal author of the E&P Notes series in the *Bulletin*. His other publications include seven books on topics in petroleum geology, science education, and the history of science, plus articles and monographs related to frontier plays, new technologies, field studies, and reservoir characterization.

John G. Worrall

John G. Worrall is a consulting geologist residing since 1988 in Roswell, New Mexico. He received his B.A. degree in geology from Rice University in 1984, and his M.A. degree in geology from the University of Texas in 1987. His career has focused on various exploration plays in the Permian Basin and, most recently, coalbed methane and carbon dioxide exploitation in the Raton Basin.

Dean Hamilton

Dean Hamilton is an independent geologist in Midland, Texas. He earned a B.A. degree from Baylor University in 1955. During his career, he worked for Amoco (Stanolind/Pan American) and Texas Pacific Oil Company. An independent since 1980, he has concentrated on the Delaware sands. He received the A.I. Levorsen Award in 1984 for best paper at the Southwest Section AAPG. He is a member of AAPG, SIPES, and the West Texas Geological Society.

2) Basin Subsidence and Paleography
Travis Swanson and Dallas Dunlap

Subsidence and Paleogeography

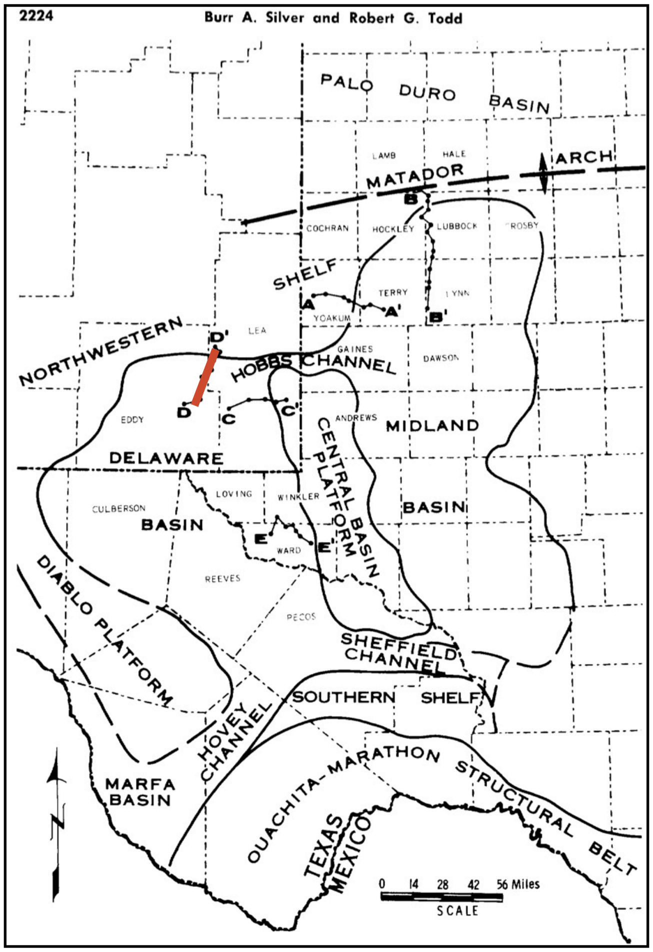

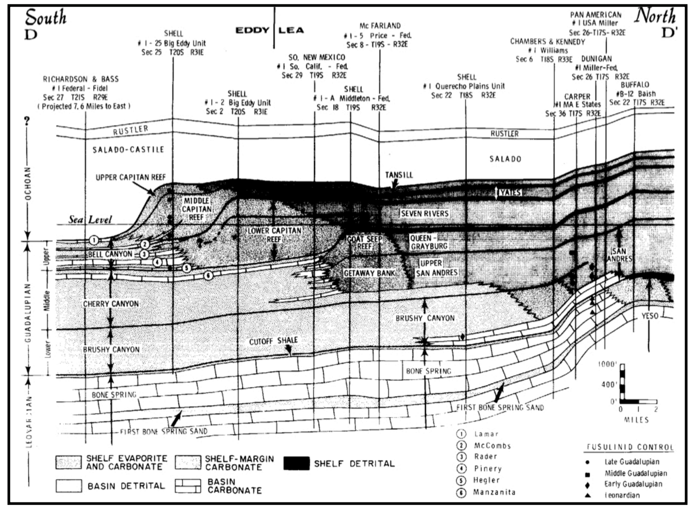

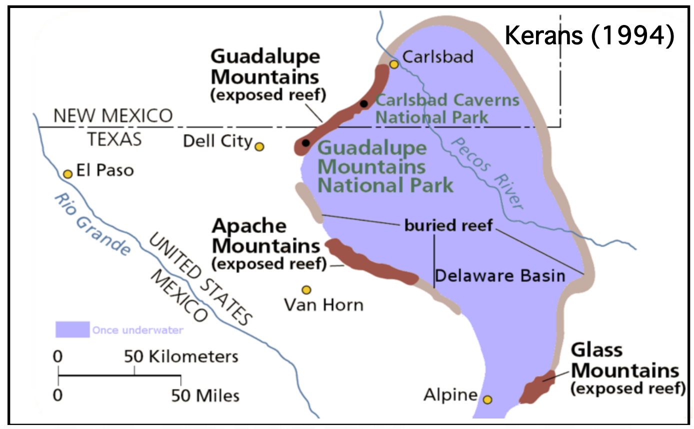

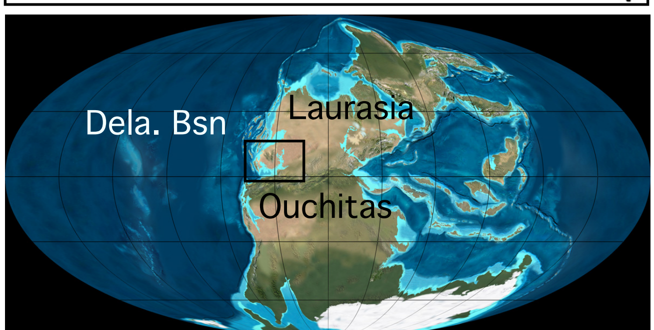

Blakey

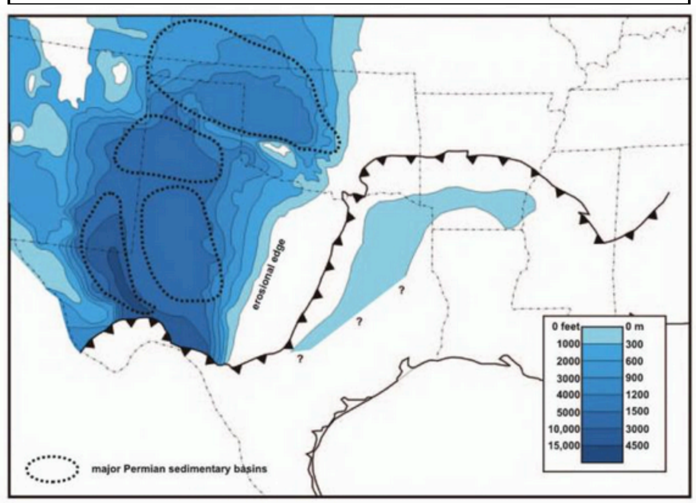

ure 25 Permian isopachs (after Cook and Bally, 1975).

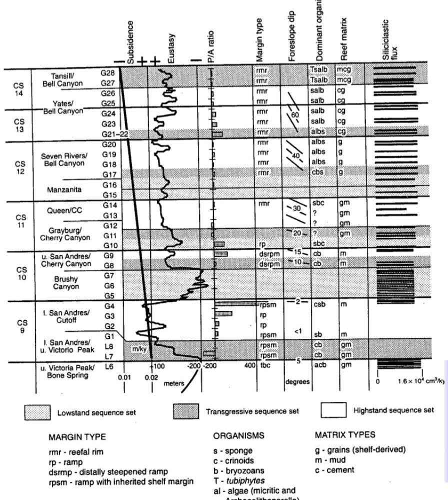

Kerans and Tinker (1999)

Blakey

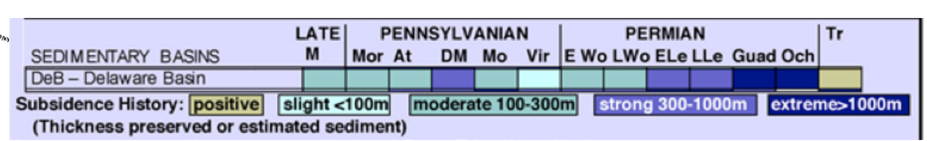

The American Association of Petroleum Geologists Bulletin
V. 53, No. 11 (November, 1969) P. 2223-2251, 13 Figs., 1 Table

Permian Cyclic Strata, Northern Midland and Delaware Basins, West Texas and Southeastern New Mexico[1]

BURR A. SILVER[2] and ROBERT G. TODD[3]
Kingsville, Texas 78363, and Houston, Texas 77001

Abstract Permian cyclic rocks of Wolfcampian-Guadalupian age in the northern Permian Basin, West Texas and southeast New Mexico, are grouped into five regionally extensive lithofacies: (1) shelf evaporite-carbonate, (2) shelf detritus, (3) shelf-margin carbonate, (4) basin carbonate, and (5) basin detritus.

Recognition of these lithofacies within an unconformity-bounded sequence suggests the following sedimentary model. During normal sea-level conditions, Wolfcampian-Guadalupian shelf-margin reefs and banks formed near sea level. The resultant backreef lagoon was shallow but very broad; therefore little terrigenous sand reached the distant basin. Deposition of shelf-margin carbonate was at a maximum and the sediments accumulating in the basin were chiefly pelagic mud and micrite. Relative lowering of sea level, possibly eustatic-epeirogenic, initiated regression, causing continental and nearshore sand and mud to prograde across the lagoon. Continued progradation enabled shelf detritus to enter the basin through numerous reentrants and submarine canyons dissecting the shelf margin; additional regression subaerially exposed the shelf clastic beds, providing an unconformity-delimited datum surface. Flooding of the shelf by transgression restricted the supply of detritus and reactivated normal carbonate deposition. Correlation of a shelf-detritus top with a coeval basin-detritus top provides the framework for Wolfcampian-Guadalupian shelf-to-basin correlations.

Introduction

Among the many difficult problems facing geologists is the formulation of a valid time-stratigraphic framework for an area of complex lithosomal patterns and relatively steep depositional topography. Pennsylvanian and Permian strata in the Permian Basin of West Texas and southeast New Mexico (Fig. 1) exemplify this problem. Many geologists have recognized shelf, shelf-margin, and basin deposits in this area (Adams *et al.*, 1951; Galley, 1958; King, 1948; Van Siclen, 1958; Wright, 1962). However, because depositional topography has been accentuated by differential compaction along shelf margins, many of the consequent time-stratigraphic problems are unsolved. Correlation of anachronous lithosomes has resulted in erroneous facies, structural, and paleotopographic interpretations.

The concept of depositional topography is not new. Rich (1951) recognized the importance of differentiating among horizontally bedded rocks deposited above wave base (undaform), those laid down on the slope (clinoform), and those deposited in deeper water on the sea floor (fondoform). Van Siclen (1958) later applied Rich's concepts to Late Pennsylvanian and Early Permian (Wolfcampian) strata on the Eastern shelf of the Midland Basin. Meissner (1967) and Jacka and St. Germain (1967) described sea-level changes in Middle Permian (Guadalupian) strata of the Delaware Basin and speculated on how these changes affected depositional topography and lithofacies. Meissner's approach to Guadalupian shelf-to-basin correlations is similar to ours, but many of his correlations are different, particularly in the early Guadalupian beds.

This paper is the outgrowth of a detailed stratigraphic study in the northern part of the Midland and Delaware Basins (Fig. 1). The study comprised six phases: (1) sample description of key wells including those on cross-sections A-E (Figs. 9-13), (2) use of commercial and Humble sample descriptions of additional wells to fill in data, (3) determination of depositional environments for lithic types, (4) systematic integration of biostratigraphic data (primarily fusulinid control) with physical stratigraphic data, (5) development of shelf-to-basin correlations based on these data, and (6) formulation of a sedimentary model which best explains the physical correlations and delineated environments, thus facilitating interpretation of areas where subsurface control was sparse.

[1] Manuscript received, June 19, 1968; revised and accepted, February 2, 1969.

[2] Geologist, Humble Oil & Refining Company.

[3] Esso Production Research Company.

Sincere thanks are extended to the Humble Oil & Refining Company for permission to publish this paper. Fusulinid identifications are by J. W. Skinner and G. L. Wilde, Humble Oil & Refining Company; timely discussions with them regarding fusulinid biostratigraphic interpretations have contributed greatly to this study. R. M. Jeffords, F. A. Johnson, Jr., F. L. Peirce, and H. W. Praetorius, Humble Oil & Refining Company, and Mrs. R. G. Todd, and H. W. Wheeler, University of Washington, critically read the manuscript. Appreciation is extended to B. J. Walker, Humble Oil & Refining Company, draftsman, and Mrs. B. A. Silver, typist.

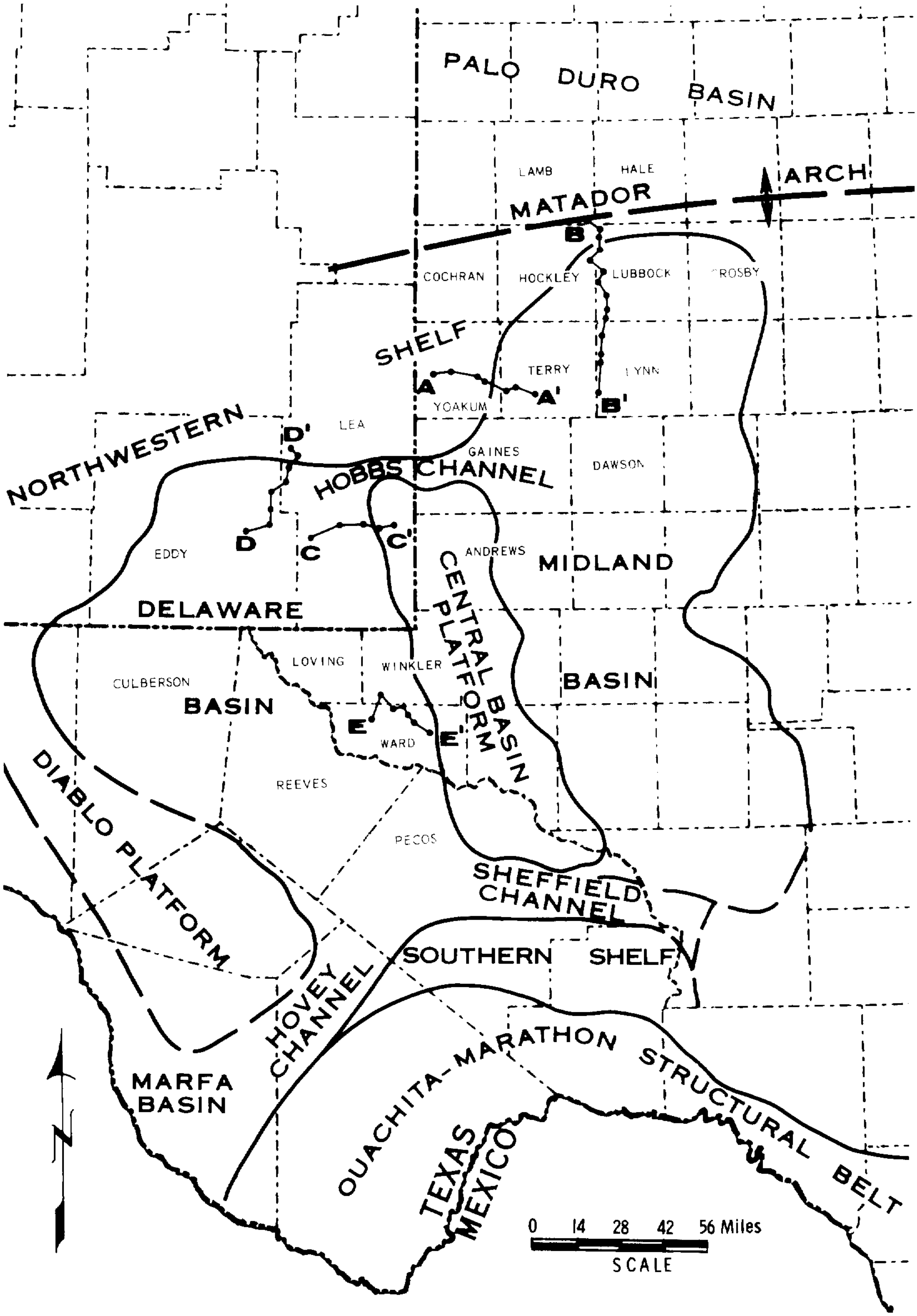

FIG. 1.—Major Permian geologic features, including location of cross sections, West Texas and southeastern New Mexico. Modified after McKee *et al.* (1967). Sections A-A′ through E-E′ are Figures 9–13.

34

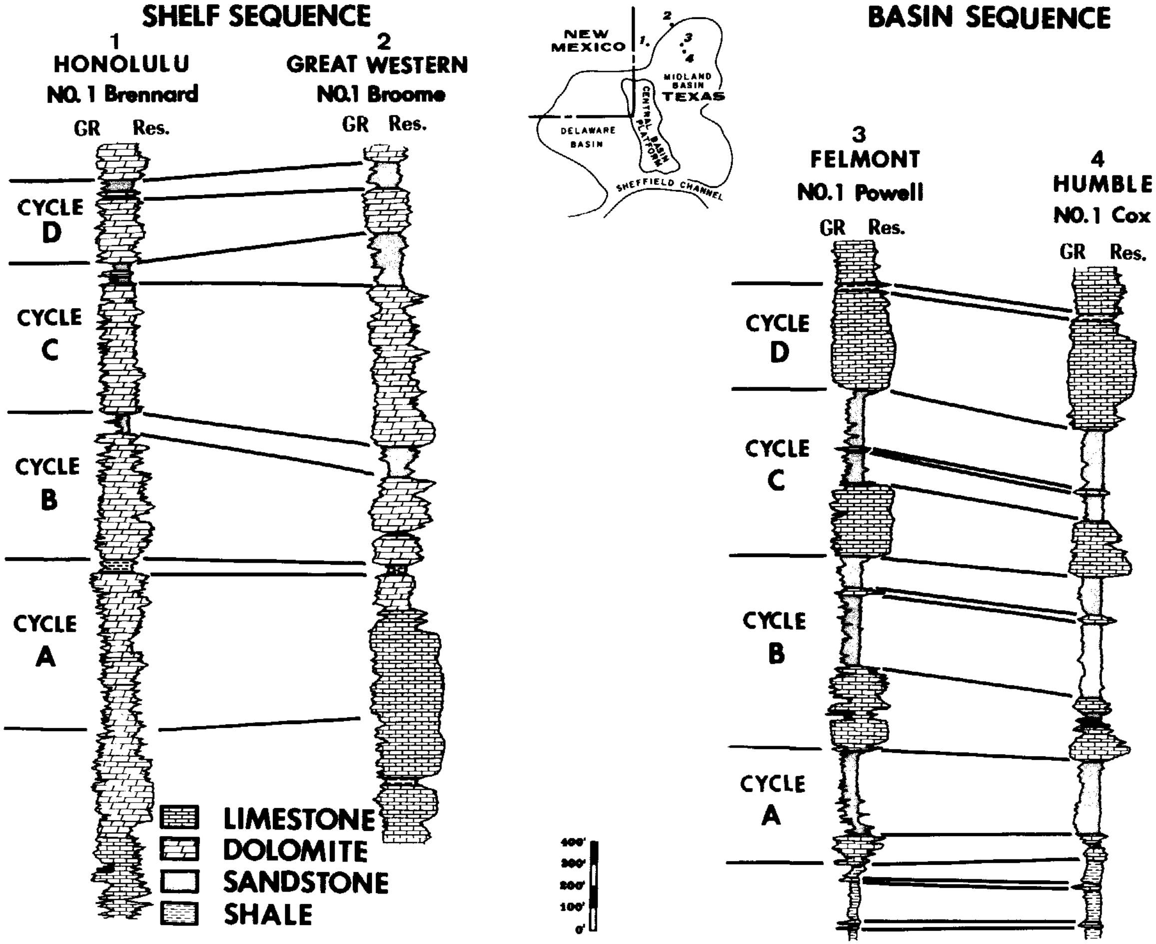

FIG. 2.—Leonardian sedimentary cycles, Midland Basin, West Texas. Vertical scale in feet.

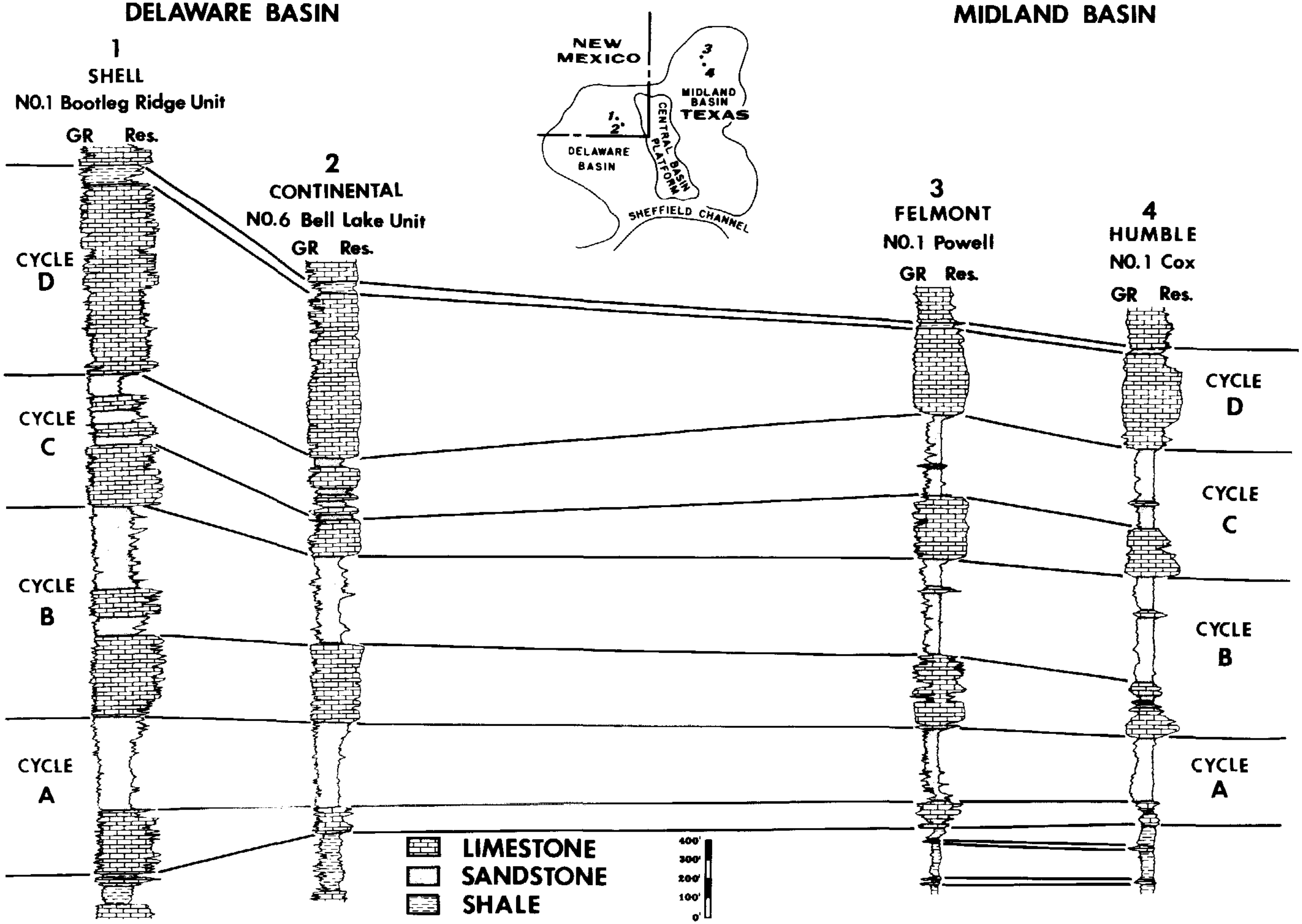

FIG. 3.—Comparison of Delaware Basin and Midland Basin Leonardian sedimentary cycles, West Texas and southeastern New Mexico. Vertical scale in feet.

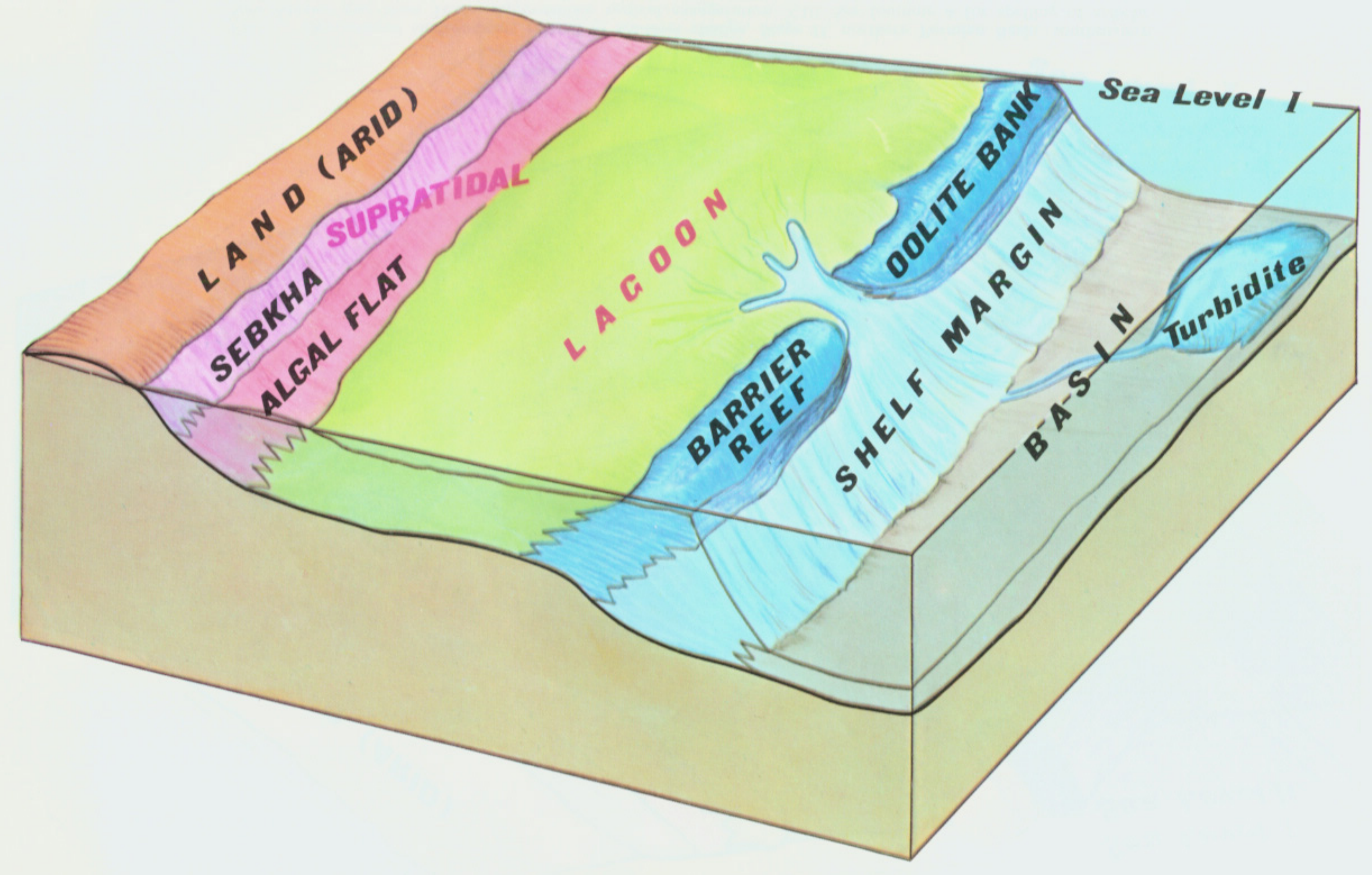

FIG. 4.—Depositional environments related to normal sea level, Stage I, northern Permian Basin, southeastern New Mexico and West Texas. Approximate vertical exaggeration ×10. See footnote 4 for spelling of *sebkha*.

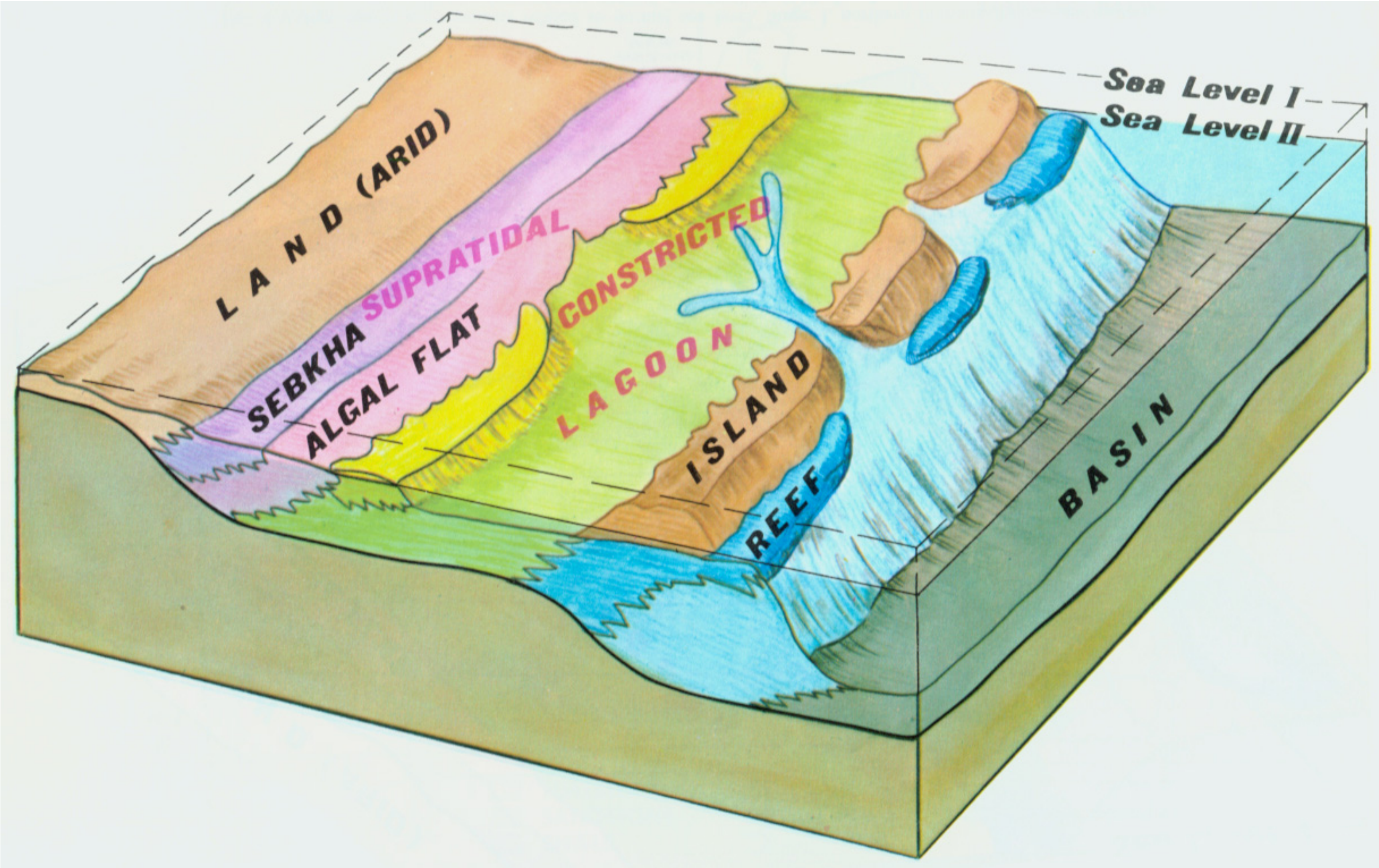

FIG. 5.—Depositional environments related to sea-level change, Stage II, northern Permian Basin, southeastern New Mexico and West Texas. Approximate vertical exaggeration ×10. See footnote 4 for spelling of *sebkha*.

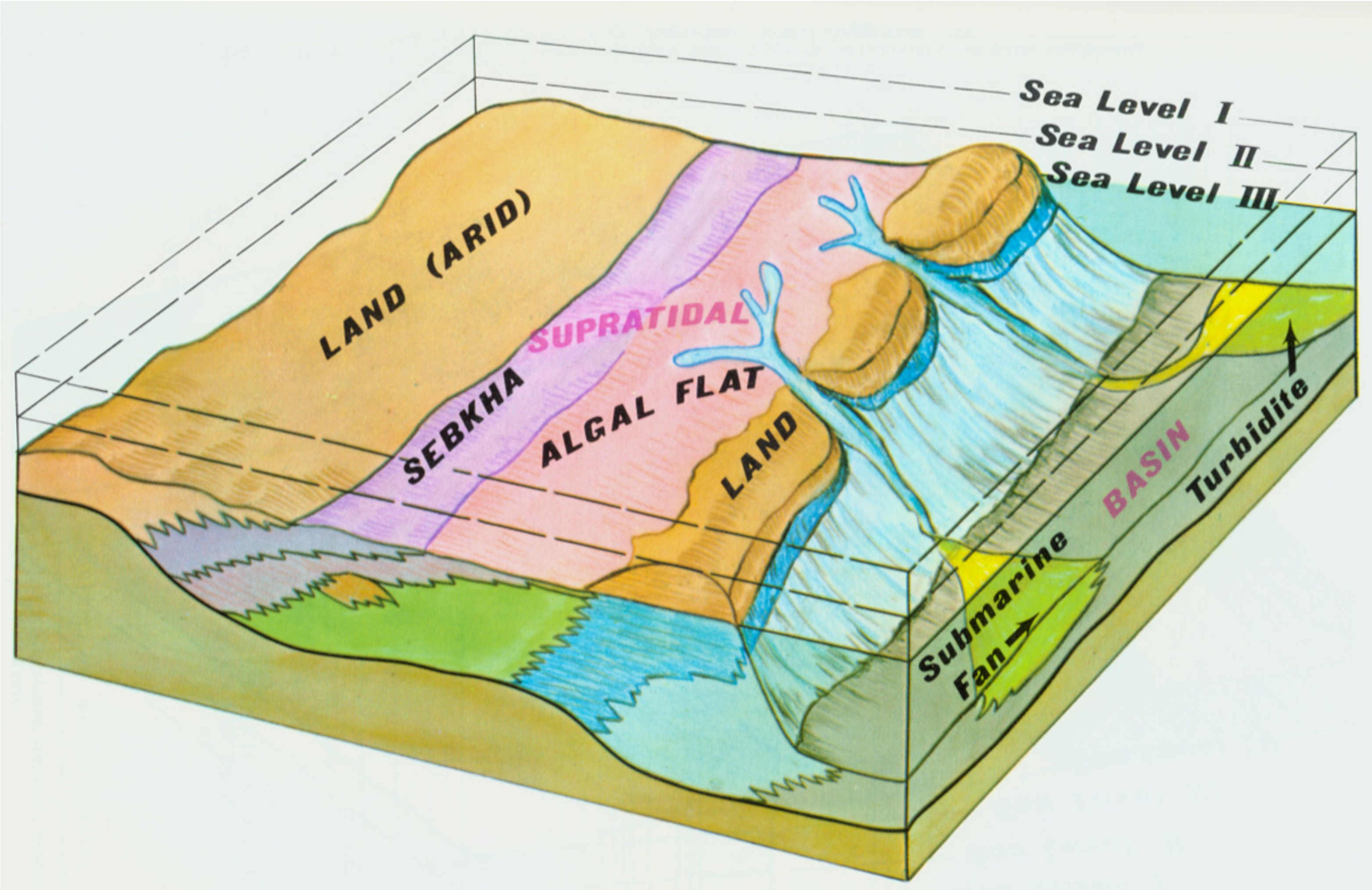

FIG. 6.—Depositional environments related to sea-level change, Stage III, northern Permian Basin, southeastern New Mexico and West Texas. Approximate vertical exaggeration ×10. See footnote 4 for spelling of *sebkha*.

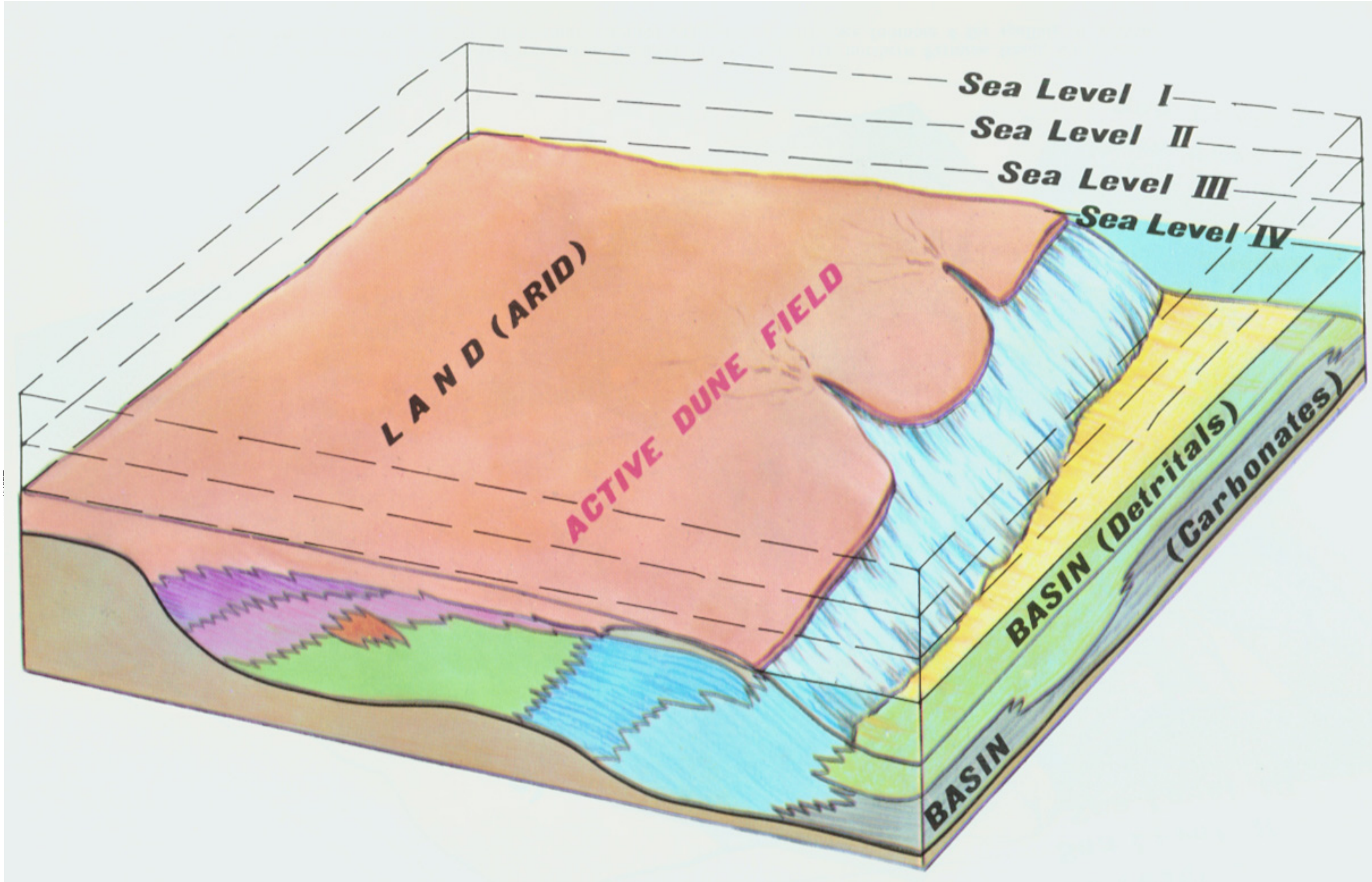

FIG. 7.—Depositional environments related to sea-level change, Stage IV, northern Permian Basin, southeastern New Mexico and West Texas. Approximate vertical exaggeration ×10.

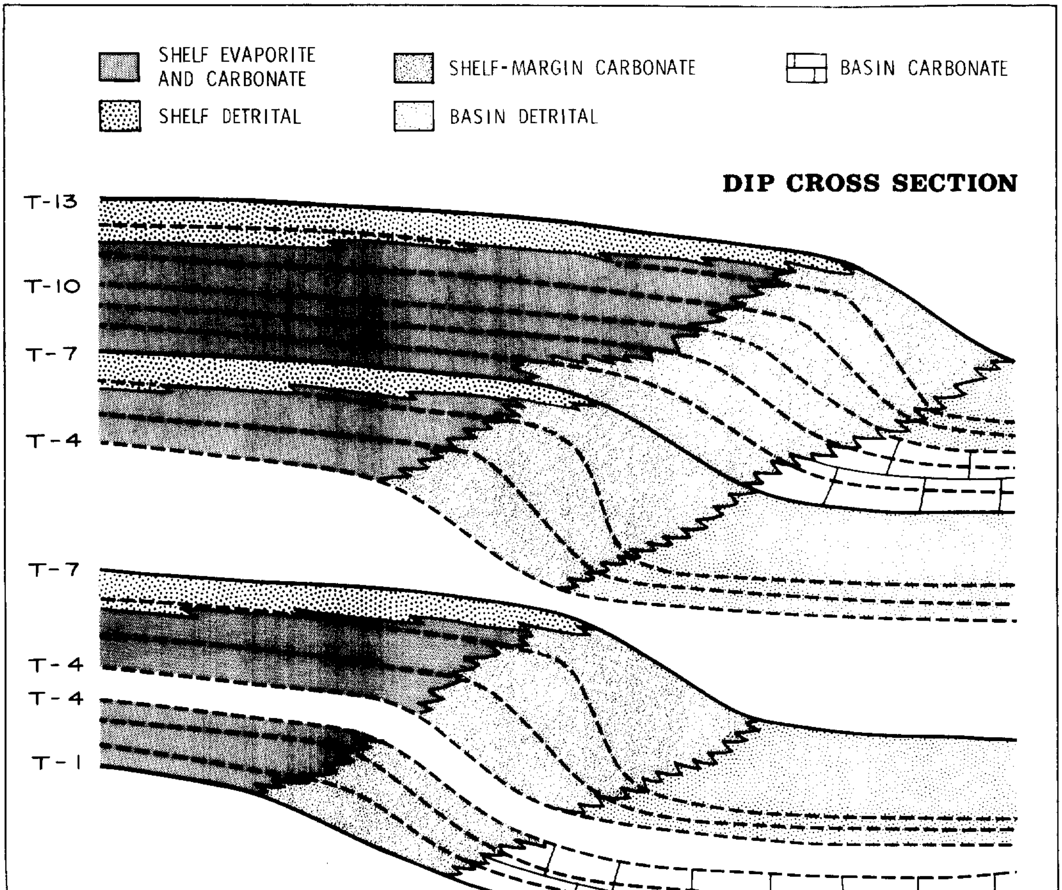

FIG. 8 TIME-STRATIGRAPHIC SEDIMENTARY MODEL, WOLFCAMPIAN - GUADALUPIAN.

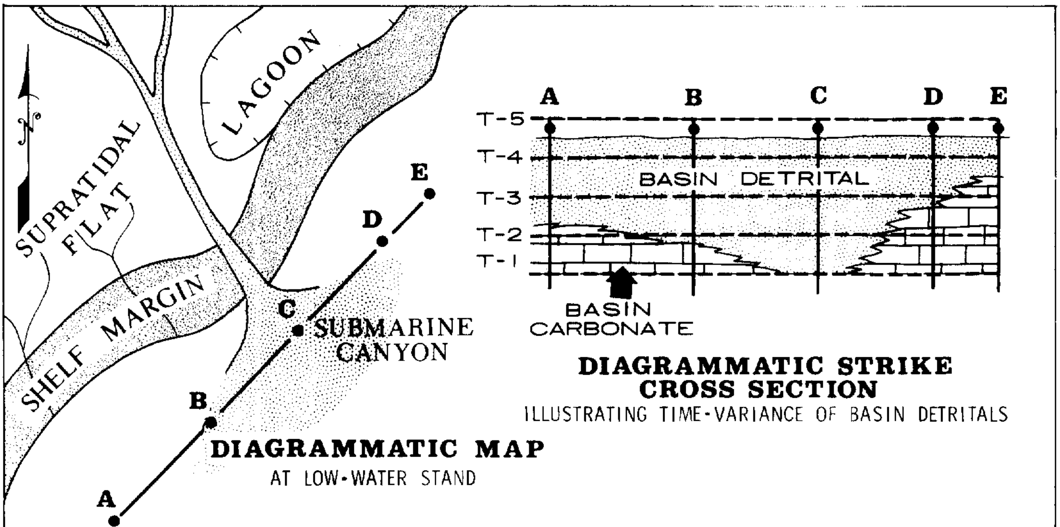

FIG. 8 EXAMPLE OF TIME-DATUM VARIANCE OF BASIN DETRITAL.

FIG. 8.—Detailed time-stratigraphic relations of Wolfcampian through Guadalupian lithofacies, northern Permian Basin, southeastern New Mexico and West Texas.

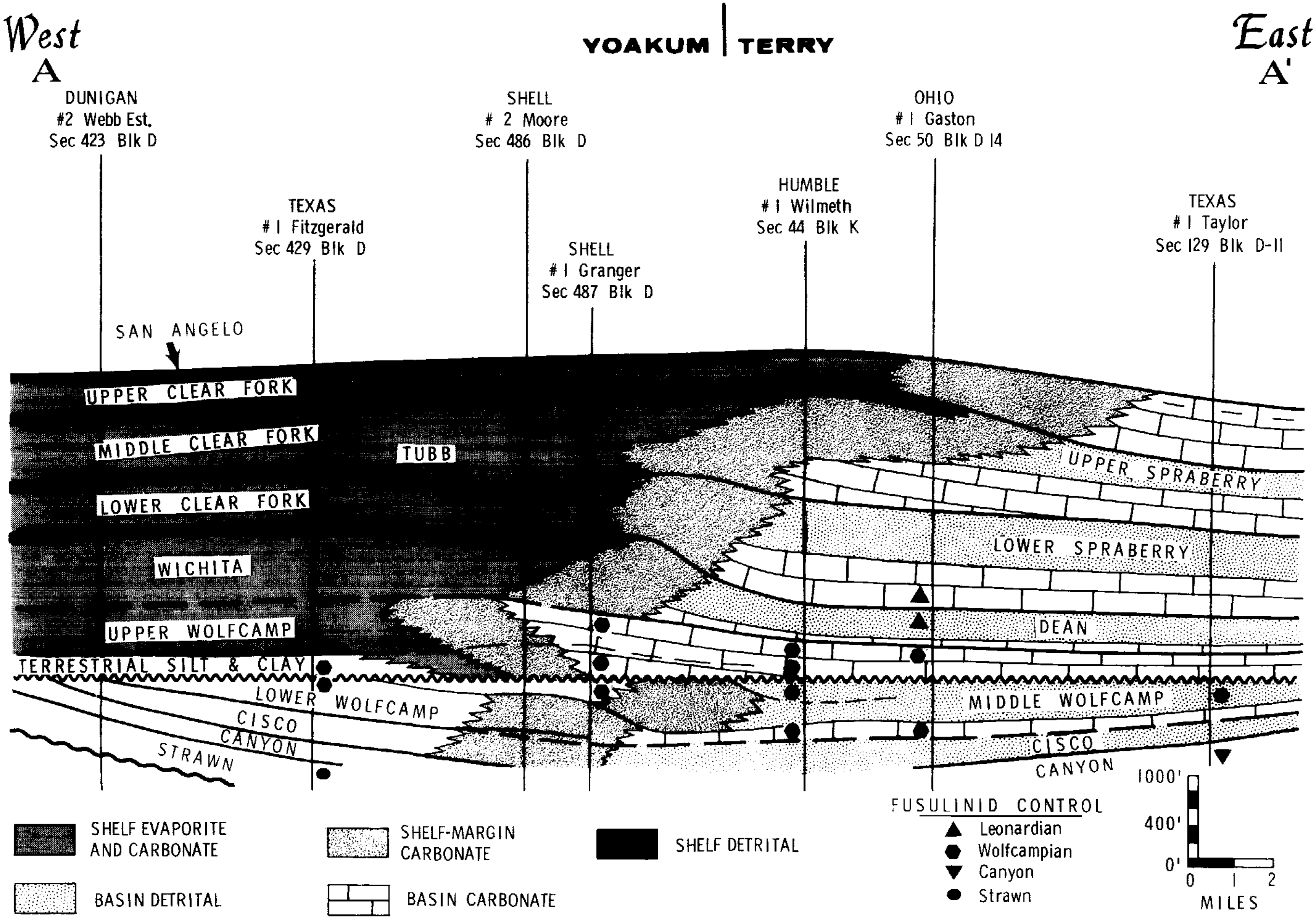

FIG. 9.—West-east cross-section A-A', Wolfcampian through Leonardian physical stratigraphic framework, northern Permian Basin, Yoakum and Terry Counties, Texas. Location shown in Figure 1. Vertical scale in feet.

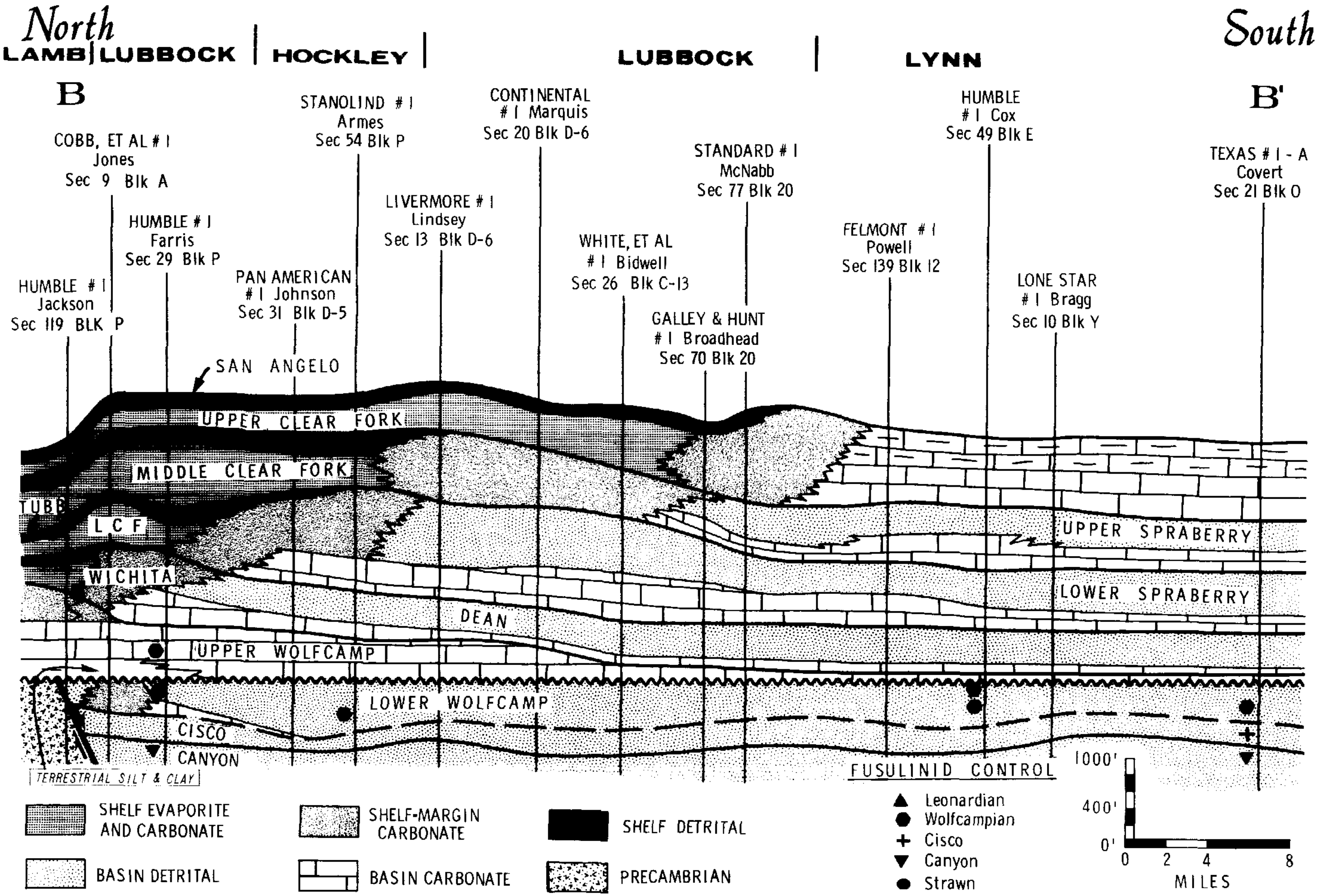

FIG. 10.—North-south cross-section B-B′, Wolfcampian through Leonardian physical stratigraphic framework, northern Permian Basin, Lamb, Lubbock, Hockley, and Lynn Counties, Texas. Location shown in Figure 1. Vertical scale in feet.

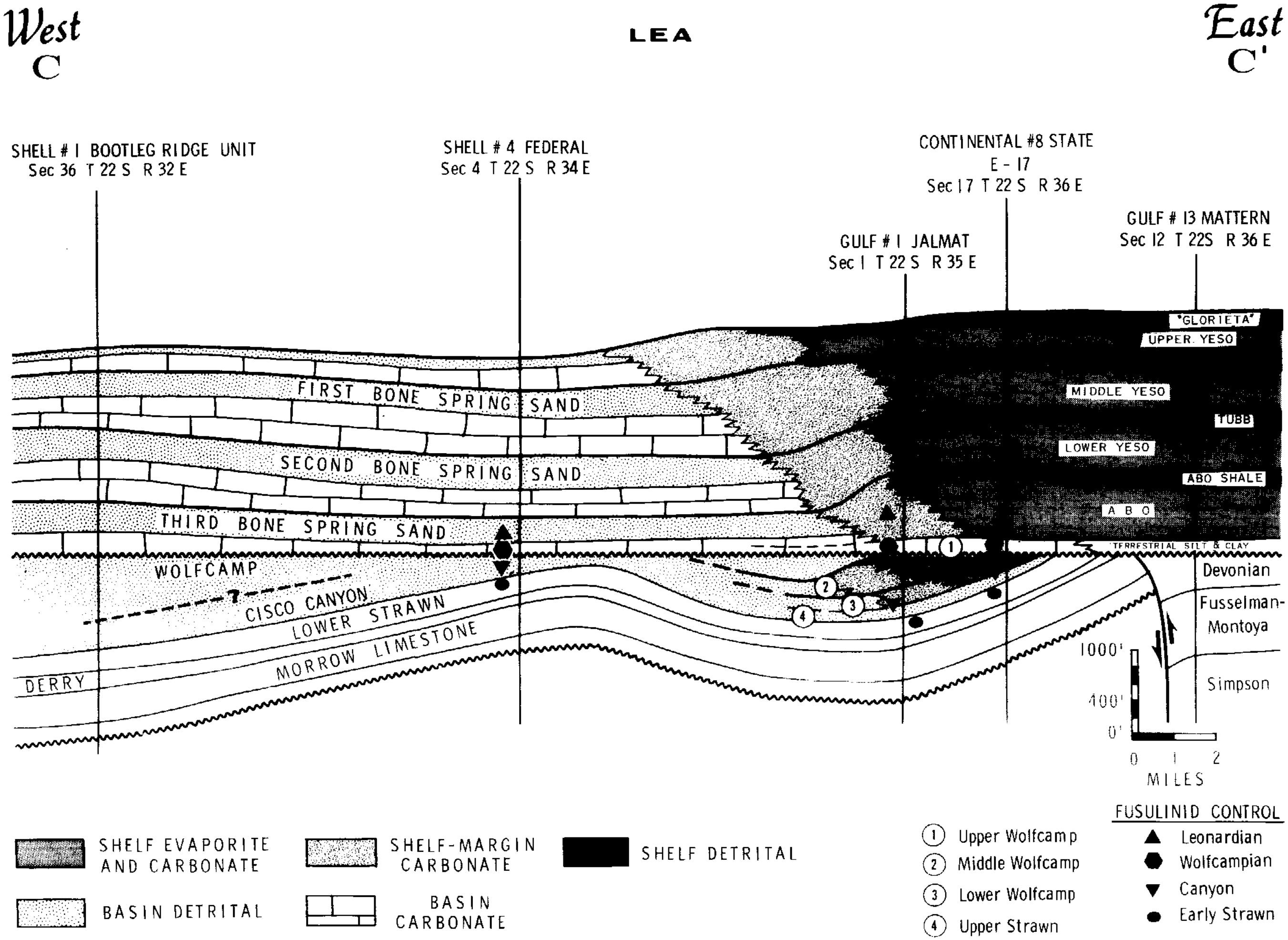

FIG. 11.—West-east cross-section C-C', Wolfcampian through Leonardian physical stratigraphic framework, northern Permian Basin, Lea County, New Mexico. Location shown in Figure 1. Vertical scale in feet.

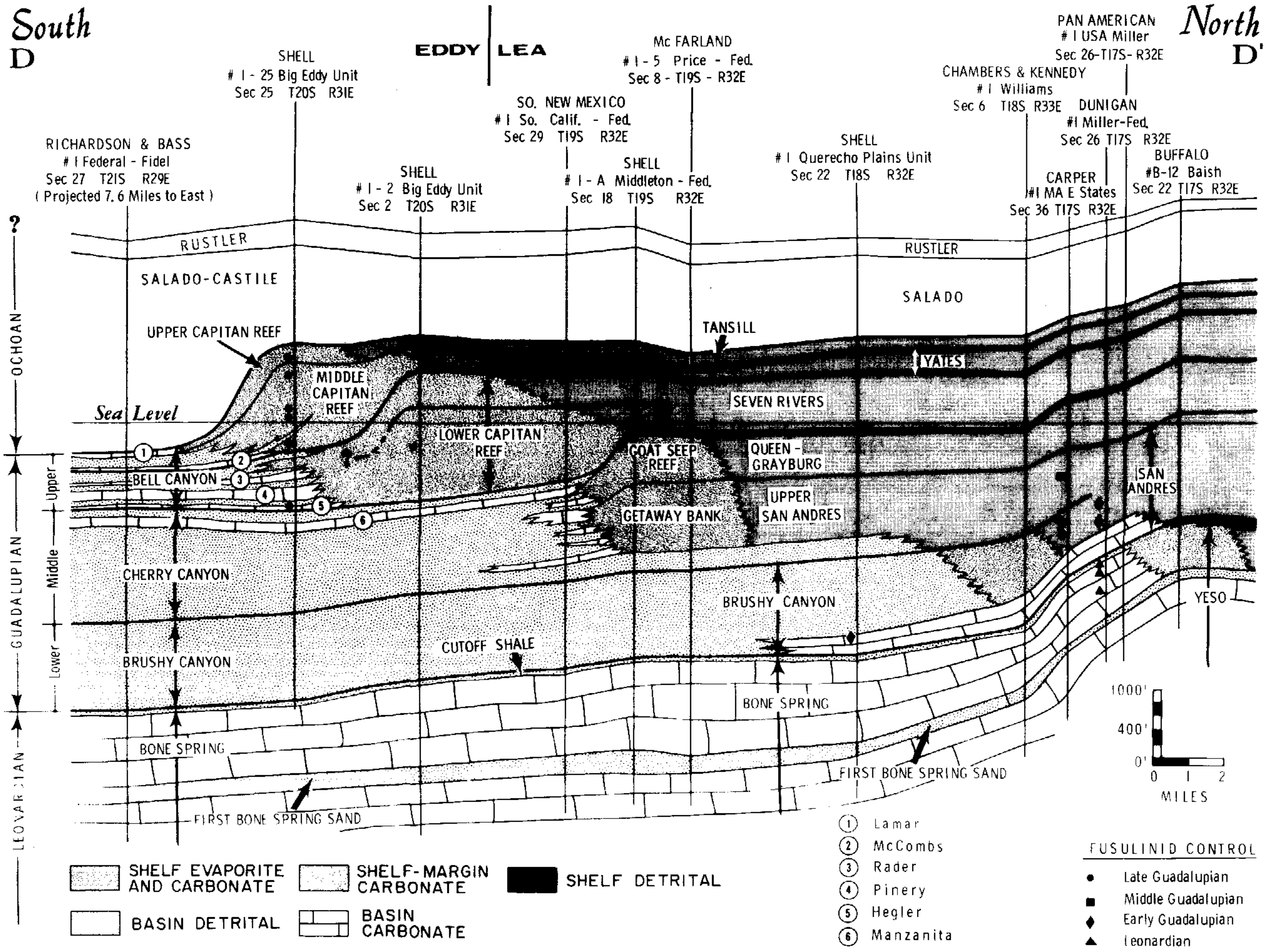

FIG. 12.—South-north cross-section D-D′, Guadalupian physical stratigraphic framework, northern Permian Basin, Eddy and Lea Counties, New Mexico. Location shown in Figure 1. Vertical scale in feet.

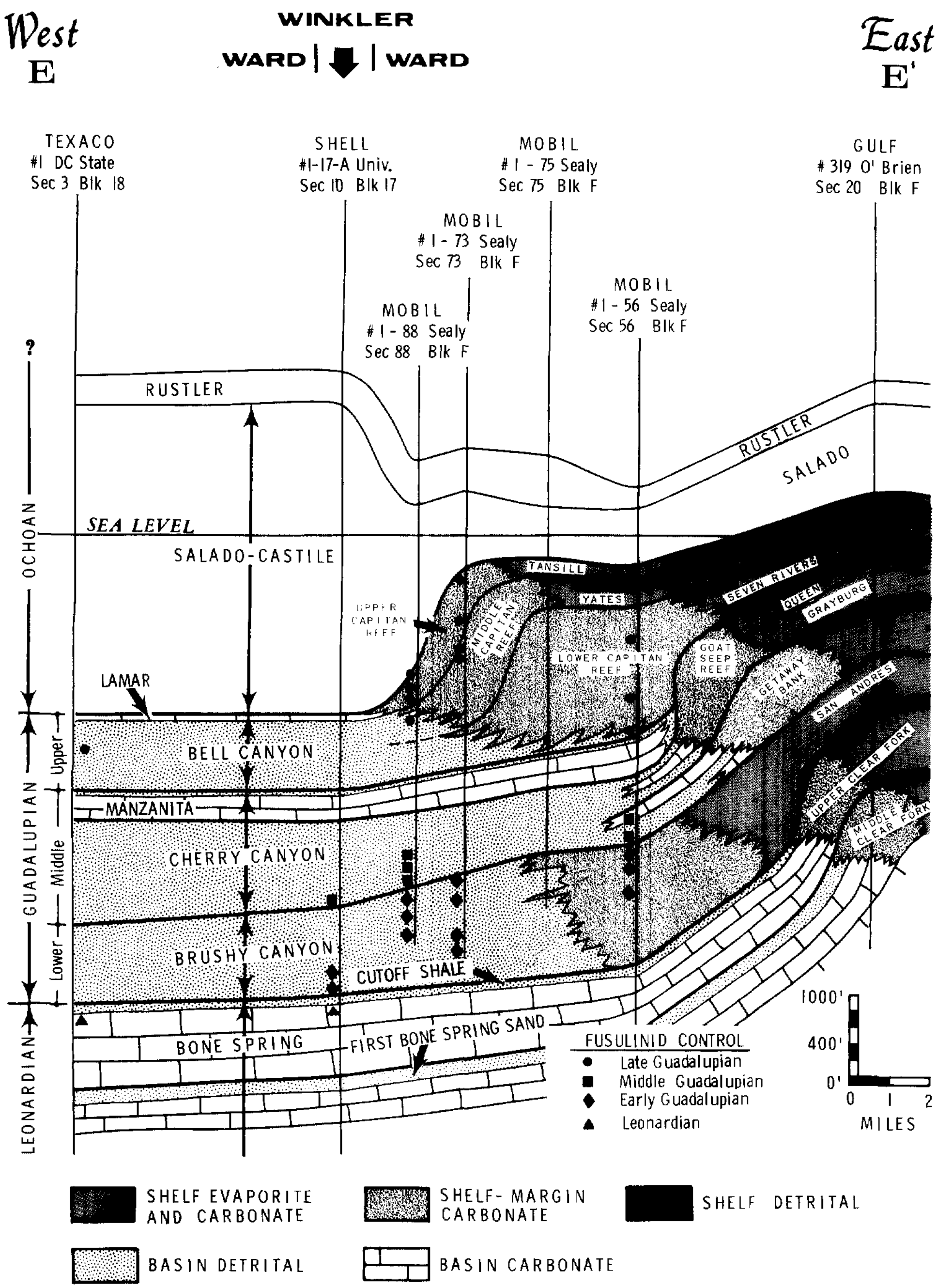

FIG. 13.—West-east cross-section E-E', Guadalupian physical stratigraphic framework, northern Permian Basin, Ward and Winkler Counties, Texas. Location shown in Figure 1. Vertical scale in feet.

It is the intent of this study to place the Permian Basin into a regional framework characterized by cyclic changes in sea level during Early and Middle Permian time. A sedimentary model is used to show how it may explain the origin of the cyclic lithofacies and permit interpretation of their synchronous patterns. The stratigraphic intervals discussed include the late Wolfcampian, Leonardian, and Guadalupian Series. A complex stratigraphic nomenclature has evolved to differentiate among shelf, shelf-margin, and basin beds; where possible, however, this nomenclature is avoided in order to emphasize the gross stratigraphic relations.

Geologists generally employ two suites of terms to refer to depositional topography—shelf, shelf margin, and basin; or undaform, clinoform, and fondoform (Rich, 1951). Although both suites have certain fundamental limitations, the use of shelf, shelf margin, and basin most accurately describes environment and site of accumulation of late Wolfcampian-Guadalupian strata in the northern Permian Basin. Most objectionable is the term *basin*. Unfortunately it has been applied to a site of sediment accumulation irrespective of original depositional environments and/or preservational patterns. To avoid confusion the term *Basin* is used with a capitalized proper name to refer to a preserved thick sedimentary section regardless of its depositional environment (*e.g.*, Midland Basin, Delaware Basin); however, when *basin* remains in lower case letters, it denotes an environment of deposition seaward of a shelf margin and below normal wave base.

Sedimentary Model

Late Wolfcampian, Leonardian, and Guadalupian rocks are characterized by large-scale cyclic lithosomes. For example, Leonardian shelf rocks (Fig. 2) are typified by alternating carbonate and terrigenous clastic beds. Shelf and shelf-margin carbonates commonly are light-colored, dolomitized micritic and micritic-skeletal limestone. Vugs filled with anhydrite are perhaps the most striking characteristic of these shallow-water carbonate rocks. Varicolored shale, siltstone, and sandstone beds commonly intercalated with evaporite beds constitute shelf clastic rocks. Basin carbonate lithofacies (Fig. 2) are characteristically dark micritic and micritic-skeletal limestone. Dark claystone, siltstone, and sandstone typify basin terrigenous rocks. Four complete cycles of carbonate and clastic beds are recognized in the Midland Basin both on the shelf and in the basin. Similar cycles are present in the Delaware Basin (Fig. 3). For example, two wells in the Delaware Basin, the Shell No. 1 Bootleg Ridge Unit and the Continental No. 6 Bell Lake Unit, are correlated with the Felmont No. 1 Powell and the Humble No. 1 Cox wells in the Midland Basin (Fig. 3). The following sedimentary model is an attempt to explain the lithic cyclicity and juxtaposition of depositional environments observed in upper Wolfcampian, Leonardian, and Guadalupian strata of the northern Midland and Delaware Basins.

Depositional Environments

Continental.—Lithologic and biotic data suggest an arid to semiarid climate during Early Permian time (Walker, 1967, p. 364). Fluvial sediment transport, therefore, was not regionally important and is considered subordinate to eolian sediment transport, much like that in the modern environmental setting described by Illing *et al.* (1965) for the Persian Gulf. Early and Middle Permian continental strata consist of a redbed sequence of terrigenous sand and shale. Generally, shale lithic types are red and green quartzose clayite (Clark, 1954, p. 4) and siltite with interbeds of gray to brown mudrock.

Shelf.—Continental sediments were bordered by broad supratidal and intertidal flats composed of sabkha[4] (salt flat) and laminated algal deposits. The tidal-flat beds are composed generally of irregularly laminated, dolomitized micritic limestone with interbeds of quartzitic clayrock and siltrock. Nodular anhydrite commonly is associated with dolomite. Stromatolitic algae produce most of the characteristic laminae.

Supratidal and intertidal flats were bordered by extremely wide lagoons which, during normal sea level, probably extended 10–150 mi shelfward. Lagoonal beds consist of thinly laminated, medium-crystalline, dolomitized micritic-skeletal limestone. Laminations have been destroyed locally by burrowing animals and soft-sediment deformation.

Shelf margin.—Shelf-margin beds are subdivided into three main groups, each reflecting the influence of sea-floor topography, relation to effective wave base, and relative change in

[4] Editor's footnote: Because writers have used a variety of spellings, Kinsman (1969, p. 832) proposed that *sabkha* be used as a standard spelling. Illustrations for this paper were drafted prior to that proposal, and the form *sebkha* is used on them.

sea level. These beds are characterized by bank, reef, and forebank or forereef debris. In general, bank environments were dominant during Wolfcampian and Leonardian time, whereas reefs were characteristic of the Guadalupian. Banks consist of oölite bars and non-wave-resistant skeletal buildups which are distinctly bedded. Biota is dominated by crinoid remains, fusulinids, and calcareous algae; brachiopods, corals, bryozoans, and sponges are common. Guadalupian reef facies are characterized by calcareous sponges, numerous types of calcareous algae, bryozoans, and specialized brachiopods all incorporated into a massive wave-resistant framework. Both banks and reefs bordered foreslopes of moderately steep depositional topography. Foreslope deposits are distinguished from shallow-water bank and reef beds by their darker color, common presence of silicified fossils, and by numerous shelf-derived lithoclasts. Deposition was the result of several mass-transport processes such as slow creep and suspension, and turbidity currents.

Basin.—Two lithic types, carbonate and terrigenous detritus, constitute basin deposits. The carbonate type is dark, laminated micrite. The sparse fossils include fusulinids and other foraminifers, crinoid columns, siliceous sponge spicules, and ammonoids. Most of the micrite in the basin probably was derived from the shelf and shelf margin by transport in suspension. Mass transport of coarse carbonate detritus through submarine canyons as subaqueous slides or turbidite flows resulted in extensive redeposition of shallow-water carbonates in deeper water. These beds are characterized by a displaced shallow-water biota, clasts of both shelf and basin origin, graded bedding, and silicification of fossils. Terrigenous detritus consists of quartzose clayrock and siltrock, with intercalated beds of dark micritic limestone that are regionally extensive. Generally these rocks lack fossils except where they interfinger with shelf-margin strata. Base level shifted frequently during low-water stands, resulting in reworking of sediment.

Cyclic Depositional Environments

A series of block diagrams (Figs. 4–7) diagrammatically depicts a falling sea level and its control of sedimentary patterns. Major cyclic fluctuation of base level with intermittent still-stands contemporaneous with subsidence are the major controlling processes of this environmental model. It is suggested that cyclic changes in sea level caused cyclic depositional patterns.

Sea-level stage I.—During normal sea-level stand (Fig. 4), shelf-margin reefs and banks formed near sea level. The resultant lagoon was shallow but very broad; therefore little terrigenous sand reached the distant basin. Deposition of shelf-margin carbonates was at a maximum and the main sediments in the basin were pelagic mud and micrite.

Sea-level stage II.—At sea-level stage II (Fig. 5), shelf-margin strata were partly subaerially exposed but still were forming actively at a lower elevation. Islands developed along the topographically highest parts of the shelf margin. The lagoon was constricted and was bordered landward by an extensive algal flat. Locally, barrier islands developed during this sea-level stage. Continental and sabkha environments prograded basinward from their location at normal sea-level stand. Pelagic mud and micrite were the dominant lithic types deposited in the basin.

Sea-level stage III.—At this substantially lower sea level (Fig. 6), continental and near-shore clastic beds continued to prograde seaward. Sabkha and algal-flat deposits replaced previous lagoonal sediments. Reefs and/or banks ceased to develop and were replaced by an extensive stable land surface dissected by canyons and tidal channels. Tidal and near-shore currents and local rivers swept land detritus into canyon heads which were formed most commonly near salient features on the shelf margin. This clastic material was transported down the canyons by traction, slow creep, or turbulent flow. Channel and overbank systems distributed clastic material in the form of prograding submarine fans along the basin floor.

Sea-level stage IV.—At maximum low-water stand (Fig. 7), land-derived detritus, at least locally, prograded completely across the shelf. Sediment transport was at maximum, so that sheetlike sands, perhaps more correctly described as coalescing eolian and fluvial sands, prograded over the supratidal flat to the shelf edge. Lagoonal and shelf-margin environments were exposed subaerially before being covered by prograding continental-derived sediments. Base level shifted frequently during maximum low-water stand; major degradation prior to burial beneath prograding continental sedi-
scale, but was a locally important process. De-
ments probably did not occur on a regional
trital sediment was carried across the shelf
margin by suspension or through submarine

canyons by a combination of mass transport, slow creep, and tidal and nearshore currents.

Interpretation of Time Surfaces

Time-surface configuration.—The depositional environments are represented by five major lithofacies: (1) shelf detritus (continental and nearshore terrigenous clastic material), (2) shelf evaporite-dolomite (supratidal-flat and lagoonal strata), (3) shelf margin (oölite banks, reefs, *etc.*), (4) basin carbonate (pelagic micrite), and (5) basin detritus (submarine fan, turbidite, and bypass terrigenous clastic material).

If topography is assumed to have been monoclinal at time-surface T_1 (Fig. 8), the sedimentary evolution as suggested in Figures 4 and 5 occurred from T_1 through T_4. Time-surfaces T_2 and T_3 indicate that sedimentation rates were greater at the shelf margin than on the shelf or in the basin and that sedimentation was progradational. Time-surfaces T_5 and T_6 are interpreted from the sedimentary model and suggest that sedimentary rates were greater at the shelf margin than on the shelf, and were slowest in the basin. Figure 7 is not depicted precisely in upper Figure 8, but is approximated by the interval between T_6 and T_7. Transport of sediment in suspension over the shelf margin was probably a more important process during Wolfcampian and Leonardian time than during the Guadalupian. If additional time surfaces were added between T_6 and T_7, they would converge on the shelf and diverge in the basin and, because of local variability in the aggradational and degradational processes, exact time equivalents of specific basin strata may not be present on the shelf. Time surfaces may or may not be preserved on the shelf or shelf margin because nondeposition and local degradation were probably more active processes than sedimentation.

A relative rise in sea level in an area characterized by a broad, topographically featureless platform would initiate extensive lagoonal and supratidal environments on a newly formed shelf. Reestablishment of extensive lagoons and supratidal flats would then prevent detritus from being transported across the shelf, thus allowing carbonate sedimentation to recur. In other words, after initial rapid transgression, progradational patterns from T_7 through T_{10} were similar to that described for T_1 through T_4. Each time-rock unit (*i.e.*, sediments deposited during T_1-T_4 and T_4-T_7) is cyclic and reflects periodic changes in base level.

Time-datum variance.—Initial sedimentation of a given lithosome within the sedimentary model discussed depends upon (1) topographic relief on land, (2) evolution rate of the landward geomorphic cycle, (3) extent and kind of environments established on the shelf, (4) seafloor topography, (5) lithic type and rate of sedimentation for the shelf margin and basin, (6) rate of change in sea level, and (7) efficiency of sediment distribution by marine processes. Assume a situation at approximately T_4 (Fig. 8, upper) in an area resembling that illustrated in Figure 8 (lower). Land-derived detritus is transported along the floor of the submarine canyon forming a prograding submarine fan. Submarine currents may transport some of this sediment a limited distance northeast and southwest. Thus at T_1 (strike cross section, Fig. 8, lower) sedimentation of detritus at locality C is contemporaneous with sedimentation of micrite in the basin. With lowering sea level, shelf detritus is permitted to prograde over the supratidal flats southwest of the canyon and "spill" over the shelf margin, so that at T_3 land-derived detritus is being deposited at localities A, B, C, and D contemporaneously with sedimentation of micritic limestone at locality E. Furthermore, at T_3 land-derived detritus is deposited on the shelf, shelf margin, and basin throughout the map area except in the lagoon and downdip of the lagoon at locality E. Not until the lagoon is filled is clastic material deposited at locality E. This simplified example shows that the base of a basin detrital lithofacies is not a reliable time datum, but the top of each detrital lithofacies approximates a regional time surface and provides the basis for shelf-to-basin correlations for upper Wolfcampian through Guadalupian rocks of the northern Permian Basin.

Geologic Processes

Geologic processes required for the model include (1) subsidence, (2) compaction, (3) progradational sedimentation, (4) large supply of terrigenous sediment, and (5) cyclic change in sea level characterized by long periods of stillstand. Critical study of Figures 4–7 shows that subsidence is depicted schematically as contemporaneous with a falling sea level. Subsidence is thought to be a result of regional downwarping, possibly epeirogenic rather than compactional. Differential compaction, however, was important in influencing upper Wolfcampian through Guadalupian sedimentary patterns. Shelf and shelf-margin carbonate sediments compact only slightly, whereas very fine-grained basin clastic material compacts as much as 65 percent upon burial under 100 ft of sediment (Weller, 1959, p. 289). Thus differential compaction enhanced shelf-to-basin relief and therefore influenced the distribution of carbonate sedimentation. It is suggested that depositional topography mapped today may be due partly to differential compaction. Weller (1959, p. 289) demonstrated that very fine-grained sediment buried 10,000 ft may be compacted nearly 80 percent. Detailed compaction studies of basin clastic sediments of the Midland and Delaware Basins may help interpretation of basin water depths during late Wolfcampian through Guadalupian time.

Figure 8 (upper) schematically illustrates theoretical time-surface configuration. The time surfaces represent basinward sediment accretion. The terms marine *transgression* and *regression* as geologic processes apply to major advances and retreats of the strandline over a large area, with no reference to sedimentary patterns. It may be useful to use the term *progradation* to describe area-time relations of sedimentary accretionary patterns in a seaward direction. Progradation may occur during sea-level transgression, stillstand, or regression.

A large supply of quartzose sediments is indicated by the presence of thick shelf and basin clastic beds in upper Wolfcampian through Guadalupian strata. The source area was probably positive throughout Early Permian time. Cyclic deposition of clastic sediment was a function of cyclic degrees in efficiency of sediment transport and periodic presence of broad lagoons which kept clastic material from entering the basin. Broad lagoonal and supratidal environments were formed during regional rises in sea level which may have been caused by rapid regional subsidence or by eustasy.

Cause of Sea-Level Change

Postulation of sea-level changes leads to speculation as to their cause. Cyclic sedimentary patterns caused eustatically are compared with those caused tectonically in Table 1. Evidence suggests that eustatic change was the controlling factor in the formation of Wolfcampian-Guadalupian cyclic patterns in the northern Permian Basin.

Rock thicknesses are interdependent. For example, each cyclic detrital lithosome reflects depositional topography and kind and extent of depositional environment on the shelf and shelf margin. Shelf-margin facies are extremely homogenous in lithic and biologic composition and can be mapped around the periphery of the Permian Basin. The base and top of each shelf or basin lithosome are regionally subparallel and these units are correlative between the Midland and Delaware Basins (Figs. 3, 9, 11). Perhaps the most significant evidence supporting eustatic control of sea level is the presence of cyclic lithofacies in the Lower Permian of the Paradox Basin, the Denver Basin, and the Perm Basin of Russia.

Table 1. Characteristics of Eustatic-Epeirogenic and Tectonic Controls of Sea Level

Eustasy-Epeirogeny	*Orogeny*
1. Shelf, shelf-margin, and basin strata thickness interdependent	1. Shelf, shelf-margin, and basin strata thickness dependent on direction of regional tilt
2. Shelf-margin lithofacies development around basin relatively constant	2. Shelf-margin lithofacies significantly different around basin
3. Lithofacies relatively homogenous	3. Lithofacies significantly nonhomogenous, reflecting tectonically active areas
4. Base and top of lithofacies boundaries subparallel to parallel	4. Base and top of lithofacies boundaries nonparallel
5. Reasonably good correlations between basins	5. Different sedimentary patterns between basins, making accurate correlations difficult

Evidence for late Paleozoic glaciation is abundant in the southern hemisphere (Hamilton and Krinsley, 1967; Teichert, 1941), and has led many workers to assume that the sea-level changes in the Pennsylvanian (Wanless and Cannon, 1966) and Permian (Jacka, 1967; Meissner, 1967) of North America were eustatically controlled. Paleontologic and paleobotanic data from the Gondwana Beds of the southern hemisphere suggest that the glaciation is no younger than Permian Wolfcampian (Hamilton and Krinsley, 1967). The dating of these deposits was based solely on faunal and floral elements which are present only in the Gondwana Beds; therefore their exact time relations to other biotas are not accurately known.

Wilson (1967) described numerous cyclothems in Cisco (Virgilian) and Wolfcamp rocks of the Sacramento Mountains of New Mexico. He concluded that available evidence supported a tectonic control, although he did not rule out a glacial origin for the cycles. Bott and Johnson (1967) have argued that varying rates of crustal subsidence are sufficient to produce eustatic rise in sea level and produce the cyclic sedimentation observed in the Carboniferous.

Sedimentary evidence as compiled in Table 1 suggests that eustatic sea-level change contemporaneous with subsidence is the major control for the cyclic nature of Wolfcampian-Guadalupian strata, although local tectonics certainly influenced these patterns. Glacially controlled eustatic sea-level changes are favored as the cause of cyclic deposition for the Permian Basin.

Stratigraphic Framework

Most of the rock types discussed in the environmental model are in upper Wolfcampian-Guadalupian strata of the northern Permian Basin. Based on the sedimentary model, a physical stratigraphic framework is proposed which relates the delineated lithosomes in time and space. Because of cyclic lithosomes, depositional topography, and sparse subsurface control, no "positive" lithologic or biologic entity is mappable from the shelf across the shelf margin into the basin. Thus several interpretations of temporal relations are possible. It is necessary to delimit a mappable stratigraphic datum throughout the study area to which the cyclic rock units may be related. The sedimentary model suggests that subsidence and relative changes in sea level are the principal processes which control cyclic rock units and that lithosomes for the shelf, shelf margin, and basin are genetically related. Thus, a physical datum upon which cyclic sedimentation began would provide a means of correlating superimposed lithogenetic strata within the sedimentary framework.

Sloss (1963, p. 94), Wheeler (1963, p. 1498), and Schleh (1966, p. 269), among others, have demonstrated the usefulness of regional unconformities as valid, mappable stratigraphic datums. Several geologists (Cooper and Grant, 1964, p. 1584; Meyer, 1966, p. 69; Ross, 1963, pl. 1; Wilde, 1962, p. 71) have noted an unconformity below upper Wolfcamp strata in the Permian Basin, and that upper Wolfcamp rocks are in unconformable contact with strata ranging in age from middle Wolfcampian through Precambrian. At Wasson field, Yoakum County, Texas, upper Wolfcamp strata progressively overlie rocks of middle Wolfcampian through Desmoinesian (Strawn) age (Fig. 9). Upper Wolfcamp rocks unconformably overlie Precambrian granite along the Matador arch (Fig. 10) and Devonian strata on the Central Basin platform (Fig. 11). Regional sedimentary patterns of shelf-margin deposits further demonstrate the extensiveness of this pre-upper Wolfcamp unconformity.

In the northern Permian Basin, upper Strawn through middle Wolfcamp shelf margins are parallel. Except where tectonic processes have modified regional patterns, each Strawn (Desmoinesian), Canyon (Missourian), and Cisco (Virgilian) shelf margin is situated progressively landward from the preceding one. This pattern is opposite that on the eastern shelf. Incipient regression of shelf-margin patterns began in early Wolfcampian time; therefore, middle Wolfcamp shelf-margin rocks are basinward of lower Wolfcamp shelf-margin beds (Fig. 9). Strawn (Desmoinesian) through middle Wolfcamp strata thus are a sedimentary and preservational unit; that is, these rocks were deposited within an overall transgressive-regressive cyclic phase and are bounded by unconformities. These strata, as well as pre-Desmoinesian rocks, underwent a pre-late Wolfcampian deformation and therefore were preserved differentially under upper Wolfcamp strata. Late Wolfcampian through Guadalupian rocks likewise are a related sequence, but whereas the pre-upper Wolfcamp shelf rocks were deposited in a transgressive sea, the post-upper Wolfcamp rocks are regressive. Therefore, on the basis of both degradational and sedimentary patterns, the pre-upper Wolfcamp unconformity is a valid regional stratigraphic datum.

A series of physical stratigraphic cross sections with supporting paleontologic data have been constructed by using the pre-upper Wolfcamp unconformity as a stratigraphic datum. Shelf-to-basin correlations are based on principles discussed for the environmental model (Figs. 4–8). In Figures 9–11 the pre-upper Wolfcamp unconformity has been flattened arbitrarily, even though there was considerable local topographic relief on this surface. Pre-upper Wolfcamp strata plotted beneath the unconformity show degradational patterns and structure relative to it; post-unconformity rocks, plotted above the unconformity, reflect depositional topography.

Monoclinal depositional topography in the northern Permian Basin was initiated once during Middle Pennsylvanian and once during Early Permian time. Pennsylvanian depositional topography has been documented by Van Siclen (1958, p. 1899). Development of late Wolfcampian depositional topography was governed partly by residual relief on the unconformity, differential accumulation of skeletal carbonate sediments near effective wave base, and prevailing wind and water-current directions.

Late Wolfcampian

A threefold physical division of Wolfcamp strata is proposed which allows delineation of three distinct shelf-margin developments in the northern Permian Basin. This division can be recognized partly by precise fusulinid zonation; accurate mapping of the middle and lower Wolfcamp boundary, however, is possible only in shelf and shelf-margin strata. A twofold division of the Wolfcamp is more practical in basinal facies.

Topographic relief on the pre-upper Wolfcamp unconformity was apparently slight in the northern Midland and Delaware Basins, because (1) the upper Wolfcamp is characterized by a regionally extensive micritic limestone, (2) the thickness of the interval between the top of the Dean or Third Bone Spring sand to the base of the upper Wolfcamp limestone is characterized by regional thinning rather than by local anomalies, and (3) the upper Wolfcamp rocks lie just above the unconformity surface except locally on the northern part of the Central Basin platform, where early Leonardian strata lap onto this erosion surface. Minor residual topography, however, was present in places throughout the area, as suggested by the presence of isolated mounds of upper Wolfcamp skeletal limestone in Terry, Lynn, and Garza Counties, Texas, and Lea County, New Mexico. Distinct monoclinal residual topography was present in southwestern Yoakum County, Texas, where a well-developed late Wolfcampian shelf margin is present (Fig. 9). There is no distinct, regionally extensive late Wolfcampian shelf margin in the northern Permian Basin, but discontinuous margins were developed locally, as in northern Lubbock County, Texas (Fig. 10). Transgression of upper Wolfcamp strata over the pre-upper Wolfcamp erosion surface is demonstrated in the Shell No. 1 Granger (Fig. 9), where basin carbonate beds overlie shelf-margin carbonate beds.

Upper Wolfcamp strata in the northern Delaware Basin are characterized by interbedded shale and micritic limestone. True shelf-margin beds are restricted to the northwest section of the Delaware Basin and were formed during the latest Wolfcampian; they are generally associated genetically with incipient Abo Formation shelf-margin development. Skeletal-limestone beds, characteristic of a shoaling environment, have been recognized along the western flank of the Central Basin platform.

Leonardian

Wichita deposition.—During early Leonardian time, the northern Permian Basin was characterized by a continued rise in sea level which resulted in the basinward progradation of shelf-margin sediments. This is demonstrated by the lack of an upper Wolfcamp basinal detrital lithofacies and the basinward position of the Wichita shelf-margin strata in relation to the upper Wolfcamp shelf-margin rocks. For example, if upper Wolfcamp shelf-margin rocks had been deposited in a regressive sea, a constriction of the lagoon would have permitted land-derived sediments to enter the basin (Fig. 6). Wichita sedimentation was not affected uniformly by rising sea level because of the influence of late Wolfcampian depositional topography. Depending on sea-floor topography, shelf-margin facies may "stack" (Cobb *et al.* No. 1 Jones, Fig. 10) or migrate seaward (Gulf No. 1 Jalmat, Fig. 11). Maximum depositional topography (maximum sea-floor relief) during Wichita deposition was in the northern Midland Basin in areas where late Wolfcampian shelf margins were developed best (Fig. 9). Depositional topography across the shelf margin was greater along the northwest shelf area of the Permian Basin (Fig. 1) than along the Central Basin platform. Broad lagoonal and supratidal environments are evidenced by evaporite and dolomitized limestone beds in the Palo Duro Basin (Fig. 1).

In general, depositional patterns during late Wichita sedimentation represent regression, which continued throughout the Leonardian, interrupted only by comparatively small transgressions. A discontinuous bank was contemporaneous with widespread development of the shelf evaporite and dolomite facies and basin carbonate facies. Physical stratigraphic correlations based on the sedimentary model (Figs. 4–7) suggest that the green and red quartzose clayrock and siltrock composing the shelf detritus facies are partly coeval with the basin detritus facies. In the Permian Basin there is no satisfactory formal name for the shelf evaporite-dolomite, shelf detritus, or basin carbonate facies. It is unfortunate that the terms "Abo" and "Wichita" have been applied to shelf evaporite-dolomite and shelf-margin carbonate lithofacies of early Leonardian age in the Midland and Delaware Basins (Jones, 1953, p. 29–33). Lee (1909, p. 17) described the Abo sandstone as ". . . coarse-grained sandstone, dark red to purple, usually conglomeratic at base; with subordinate amount of shale, which attains prominence in some places." Like the Abo sandstone, the Wichita Formation is varicolored sandstone, claystone, and conglomerate with no limestone (Cummins, 1891, p. 400). Thus, in order to apply these terms it is necessary to demonstrate the equivalency of the terrigenous sand, shale, and conglomerate beds of the Abo and Wichita on the surface with the dolomitized limestone and evaporite beds of the subsurface. Furthermore, this facies change is not within a time-stratigraphic unit, in that the lower Abo sandstone at the type section includes late Wolfcampian and early Leonardian fusulinids, whereas the Wichita Formation at the type locality is probably entirely of Leonardian age (Skinner, oral commun.). It is suggested that the terms "Abo" and "Wichita" be restricted to the shelf clastic lithofacies and that a nomenclatural framework be proposed for the Leonardian that is similar to the one developed for the Guadalupian Series (King, 1948, p. 12), using the principle of arbitrary cutoff (Wheeler and Mallory, 1953, p. 2412) for designation of stratigraphic units.

The terms "Dean" and "Third Bone Spring sand" (Fig. 11) are most commonly applied to the basin detritus facies in the northern Midland and Delaware Basins, respectively. It is suggested that most of the sediments composing the Dean sand (Third Bone Spring sand) were transported primarily through submarine canyons similar to those in Figure 4. Canyons 1–2 mi wide filled with as much as 1,500 ft of early Leonardian sand have been delimited in the northern Permian Basin. One such canyon in north-central Hockley County, Texas, extended at least 5 mi landward of the Wichita shelf margin. Because shelf detritus is finer grained than basin detritus, it is concluded that sediment transport by suspension was not an important process for distributing detritus into the basin during early Leonardian time.

Schubertella melonica, Schwagerina crassitectoria, and *S. hawkinsi* are present in the 100–150-ft limestone bed just below the Dean sand and Third Bone Spring sand. Thus, by either biostratigraphic or physical stratigraphic criteria, the Dean sand (Third Bone Spring sand) in the Permian Basin is of early Leonardian age (J. Skinner and G. Wilde, oral commun.). No regional degradational patterns have been observed below Leonardian strata in the study area, although the limestone with *Schubertella melonica* and *Schwagerina hawkinsi* varies inversely in thickness with the Dean sand. Local absence of the lowermost Leonardian limestone in the vicinity of submarine fans or turbidity-flow deposits is thought to be due to submarine scouring.

Lower Clear Fork deposition.—The Wichita-Clear Fork boundary is characterized by landward migration of shelf and shelf-margin lithofacies, and deposition of carbonate rather than detritus in the basin. Though transgression may have resulted in tens of miles of landward migration of shoreline, it may reflect only a few tens of feet increase of water depth. This is suggested by shallow-water, supratidal, and lagoonal environments which persisted just behind the higher energy shelf-margin lithofacies of the lower Clear Fork (Figs. 9–11).

Inherited depositional topography greatly affected the distribution of lower Clear Fork lithofacies. In Yoakum County, Texas, lower Clear Fork shelf-margin beds are "stacked" on those of Wichita age (Fig. 9); in contrast, a distinct seaward migration of shelf-margin strata is evident in northern Lubbock County, Texas (Fig. 10). If the relative sea-level rise was uniform in the two areas, the "stacking" in Yoakum County is probably due to the relatively steep pre-lower Clear Fork depositional topography. "Stacking" of Abo and lower Yeso shelf-margin sediments occurred also in the northern Delaware Basin. Stratigraphic relations along the Central Basin platform (Fig. 1) are difficult to generalize because of lack of data; however, preliminary seismic interpretations suggest that in Lea County, New Mexico, the lower Yeso shelf margin migrated seaward.

Broad, shallow-water shelf environments were present during lower Clear Fork deposition as evidenced by extensive evaporite and dolomite beds in the Palo Duro Basin (Fig. 1). During maximum low-water stand (Fig. 7) the northern Permian Basin was typified by extensive salt "pans." Eolian processes were responsible for most sediment transport on land.

Physical stratigraphic correlations suggest that the red and gray quartzose siltrock and sandstone beds of the Tubb Formation are coeval with the siltstone and sandstone beds of the lower Spraberry sand (Second Bone Spring sand) in the basin. An alternate interpretation by some geologists is that the Tubb Formation is equivalent to the Dean (Third Bone Spring sand). However, this conclusion is difficult to justify in such wells as the Sun Oil Company No. 1 Harper (Sec. 26, T25S, R35E, Lea County, New Mexico) and the Pan American No. 1 Johnson (Fig. 10), where normal sections of the Tubb and Dean (Third Bone Spring sand) are present in the same borehole. Shelf evaporite and dolomite beds of the lower Clear Fork Formation are partly equivalent to the micritic limestone beneath the lower Spraberry sand and above the Dean (Third Bone Spring sand) in the basin. Most lower Clear Fork shelf-margin beds are coeval with shelf evaporite and dolomite beds and basin limestone beds.

Because lower Clear Fork depositional topography across the shelf margin was not as pronounced, submarine canyons were not as well developed as those of Wichita age. Several Wichita submarine canyons are thought to have been partly filled with sand during lower Clear Fork sedimentation. Sediment bypass over the shelf margin by traction, slow creep, and suspension at low-water stand was an important process during late lower Clear Fork deposition (Figs. 6–9).

Middle Clear Fork deposition.—Early middle Clear Fork deposition in the northern Permian Basin was characterized by migration of the middle Clear Fork shelf margin basinward from the lower Clear Fork shelf margin. A sea-level rise smaller than that in the two preceding Leonardian cycles is suggested by a small landward migration of facies, coupled with a less distinct inherited depositional topography (Figs. 9, 10).

Landward or seaward migration of facies with a given change in sea level is dependent upon local difference in sea-floor topography and rate of sedimentation. Thus locally, in Hockley and Lubbock Counties, middle Clear Fork shelf-margin beds migrated farther landward than lower Clear Fork shelf-margin beds, and in south-central Yoakum County, Texas (Fig. 9), lower middle Clear Fork shelf-margin beds are in contact with lower Clear Fork shelf-margin rocks of the same lithic type. These local deviations from the regional framework result from topographic differences on the pre-middle Clear Fork sea floor.

Middle Clear Fork shelf rocks are regionally extensive. For the first time in the Leonardian, "salt pans" were present south of the Matador arch (Fig. 1), as exemplified in the Humble No. 1 Farris (Fig. 10). Middle Clear Fork (Yeso) varicolored siltstone beds are intercalated with thin beds of dolomitized micritic limestone. No validated formation name has been applied to the middle Clear Fork or middle Yeso shelf detrital rocks.

Physical stratigraphic correlations based on the sedimentary model (Figs. 4–7) suggest that the varicolored shelf detritus at the top of the middle Clear Fork (middle Yeso) Formation is partly coeval with the upper Spraberry sand (First Bone Spring sand). Middle Clear Fork (middle Yeso) shelf evaporite and dolomite beds are correlative with the upper Spraberry sand (First Bone Spring sand) and with basin limestone beds below the upper Spraberry (First Bone Spring sand) and lower Spraberry (Second Bone Spring sand) in the basin.

In general upper Spraberry sand of the northern Midland Basin and the correlative First Bone Spring sand of the northern Delaware Basin are finer grained than the lower Spraberry (Second Bone Spring) sand. This is attributed to the presence of fewer submarine canyons during middle Clear Fork deposition than during lower Clear Fork deposition.

Upper Clear Fork deposition.—The youngest Leonardian cyclic rock unit is characterized by even less monoclinal topography than older cycles. Mapping of upper Clear Fork and upper Yeso rocks is difficult because of vertical gradation and "interfingering" of rock types. Transgression at the beginning of lower Clear Fork (Yeso) deposition was more widespread than the preceding Leonardian ones, even though actual rise in sea level may have been less, because of the very slight pre-upper Clear Fork relief in the northern part of the Permian Basin, except in southern Yoakum (Fig. 10) and northern Gaines Counties, Texas. McDaniel and Pray (1967, p. 474) report similar low monoclinal topography for contemporaneous shelf-margin rocks in the Guadalupe Mountains, Texas. Upper Clear Fork shelf margins are most commonly 3–5 mi wide and locally, in north-central Lubbock County, Texas, reach a maximum width of 10 mi.

Poor preservation of shelf evaporite and dolomite beds in the Palo Duro Basin probably is due to the combined effects of erosion, nondeposition, and solution. Salt and anhydrite are very common in upper Clear Fork shelf strata in the vicinity of the Matador arch.

Physical stratigraphic relations suggest that the San Angelo Formation of the northern Midland Basin is partly correlative with the argillaceous micritic limestone in the basin and that the Glorieta Formation is coeval with the Cutoff Shale[5] in the northern Delaware Basin. King (1945, p. 10) and Lloyd (1949, p. 22), among others, concluded that the Glorieta (Rich, 1921, p. 225) and San Angelo (Cummins and Lerch, 1891, p. 73) are coeval. Meissner (1967, p. 38) has suggested that the Glorieta Formation is correlative with the First Bone Spring sand. This conclusion is incompatible with the sedimentary model, as initiated on the pre-upper Wolfcamp erosion surface; moreover, the presence of a normal section of Glorieta in the same borehole with a normal section of First Bone Spring sand in both the Odessa Natural Gas No. 1 El Paso State (Sec. 36, T17S, R30E, Eddy County, New Mexico), and the Standard No. 1 McNabb (Fig. 10) precludes it. A well-developed basin detrital unit commonly was lacking in the northern Permian Basin during late Clear Fork (Yeso) sedimentation; there are several exceptions, however, such as at Reeves field, Yoakum County, Texas. There local basin detritus is present at the top of the Leonard and probably represents a submarine fan. General lack of upper Clear Fork (Yeso) basin detritus is attributed to (1) a very slight gradient along the shelf margin, minimizing landslide or slow-creep transport of fine detritus downslope, (2) a very broad upper Clear Fork (Yeso) shelf margin which inhibited sediment bypassing, (3) a lack of source of detritus, and (4) eolian and fluvial processes that were less active than those of early Leonardian time.

The upper Clear Fork shelf detritus facies, furthermore, is predominantly an evaporitic, dolomitic unit interbedded with quartzose siltstone and sandstone in the northern Permian Basin. This shelf facies is unique in that it generally can be traced farther seaward than any of its predecessors. Shelf evaporite and dolomite facies are coeval with basinal micritic limestone. Faunal and textural characteristics, such as increased foraminiferal content and the churned nature of matrix material, suggest that upper Clear Fork (Yeso) basin rocks were deposited in shallower water than middle Clear Fork (Yeso) basin strata.

[5] Wilde and Todd (1968, p. 12) have suggested that the Cutoff Shale is a regionally extensive but discontinuous unit of early Guadalupian age. Problems yet to be completely resolved are (1) the Cutoff Shale of the surface may not be the same physical unit as that in the subsurface and (2) fusulinid and ammonoid specialists are not in complete agreement as to the age of the Cutoff Shale. It is believed that the shaly interval at the top of the Bone Spring Limestone in the Delaware Basin is regionally extensive, continuous, and represents maximum low-water stand at the end of upper Clear Fork deposition. Whether the unit is earliest Guadalupian or latest Leonardian does not affect the physical stratigraphic correlations presented.

Guadalupian

Guadalupian strata differ from upper Wolfcampian-Leonardian rocks in several important aspects. In contrast to the Leonardian, terrigenous clastic rocks are more abundant on the shelf and dominate in the basin. Repetitious interbedding of terrigenous clastic strata with carbonate and/or evaporite units is more common in the Guadalupian, suggesting more frequent relative sea-level changes. Biotic content of middle and upper Guadalupian shelf-margin beds differs significantly from that of underlying Leonard beds in that both the upper Goat Seep and Capitan Formations represent true organic reefs, whereas skeletal and oölitic banks characterize Leonard rocks.

Carbonate sediments were deposited mostly during "normal" sea-level stands (Fig. 4). Most of the carbonate rocks in the basin are distributed around its periphery; relatively few beds extend into the center and thus a comparatively thin "starved-basin" sequence is equivalent to a considerably thicker sequence of shelf-margin beds. The Lamar Member of the Bell Canyon Formation and the Manzanita Member of the Cherry Canyon Formation (Figs. 12, 13) are the only two carbonate units which can be traced across the basin. Carbonate sediment in the basin is generally silt or clay size, but markedly coarser materials are present in turbidite and submarine-slide deposits. Newell *et al.* (1953, p. 71) described shelf-derived limestone blocks up to 14 ft across as far as 10 mi in front of the Capitan reef.

The terrigenous clastic rocks of the Guadalupian are generally of much finer texture than detrital carbonate beds deposited as turbidites or submarine slides. Only during early Guadalupian (Brushy Canyon) deposition did quartz grains reach coarse size and they mainly are "floating" in a fine- to very fine-grained matrix. The coarser grained deposits, moreover, seem to be limited to the western part of the Delaware Basin near the Guadalupe Mountains (King, 1948; Wilde and Todd, 1968, p. 29) and do not extend far into the basin. Younger beds (Cherry Canyon and Bell Canyon) are characterized by very fine- to fine-grained sand with comparatively few medium-size grains.

The marked difference in grain size between terrigenous and carbonate clastic rocks is explained by the fact that terrigenous material originated far beyond the limits of the Delaware Basin, whereas carbonate grains were being produced continually within the immediate area.

As has been discussed, terrigenous clastic material was introduced into the Delaware basin during low sea-level stands (Figs. 6, 7). A significant drop in sea level would have exposed the shelf margin and resulted in subaerial exposure of the topographically higher points of the reef or bank as a series of island chains similar to the Florida Keys. Evidence of such exposure of reef and backreef facies includes caliche pisolites (Dunham, 1965; Thomas, 1965, 1968), vadose silt (Dunham, 1963), sandstone dikes (Newell *et al.,* 1953, p. 130), and laminated calcite that lines vugs.

Reefs on the shelf margin probably kept pace with initial regression but grew at a topographically lower elevation determined by a continually lowering sea level. Several geographically separated mounds of algal-encrusted sponges, apparently in growth position, are present far down the forereef slope of the Capitan reef in the Guadalupe Mountains. If the reef crest is assumed to represent minimum sea level, these organisms would have been living in several hundred feet of water. A main contributor to these mounds, however, is the red alga *Archaeolithoporella,* which is presumed to have lived in rather shallow water and probably represents *in situ* reef growth during a lowered sea-level stage. Continued reef growth during lowering of sea level may partly explain how the Capitan reef was able to build basinward 6–10 mi. Maximum low-water stand and regression probably eliminated all carbonate development (Fig. 7). At that time, terrigenous clastic material was carried mainly through submarine canyons into the basin, but at least locally was transported over the exposed reef crest as well.

Cyclic deposition in the Guadalupian has been described by several workers (Hull, 1957, p. 301; Jacka, 1967; King, 1948, p. 32; Meissner, 1967; Newell *et al.,* 1953, p. 44). Although repetitious interbedding of carbonate and terrigenous clastic units is present both on the shelf and in the basin, basin cycles understandably represent a more complete sedimentary record.

Both the Cherry Canyon and Bell Canyon Formations show well-developed cyclothems; King (1948, p. 31) described sedimentary cycles from the Brushy Canyon Formation, but they probably were produced by shifting submarine fans (Jacka *et al.* 1968) rather than by relative sea-level changes.

Hull (1957, Fig. 15, p. 301) described a typical cyclothem for the Delaware Mountain Group. Individual cyclothems are about 140 ft thick and consist of a lower clastic member, overlain by a laminated quartz sandstone member, which is capped by a 50- to 100-ft massive sandstone member. Cyclothems of this type are well displayed in the upper Cherry Canyon and Bell Canyon Formations.

Hull (1957, p. 303) attributed the cyclothems to differing rates of subsidence. Initial subsidence created conditions favorable for carbonate development both on the shelf and in the basin. A slower rate of subsidence produced an influx of terrigenous sand moving across the shelf and subsequent deposition of laminated sandstone in the basin. Cessation of subsidence permitted abundant silt and sand to be transported across the shelf and to accumulate as massive beds in the basin. The King and Hull explanations both require relative sea-level changes to account for the repetitive interbedding of carbonate and terrigenous clastic units. The possible cause or causes of the postulated sea-level changes have been discussed.

Although the Guadalupian Series traditionally is divided into early (Capitanian), based on the zone of *Polydiexodina,* and late (Wordian), based on the zone of *Parafusulina* (Dunbar *et al.,* 1960), a threefold division is recognizable (King, 1948, p. 28) and proves more useful. Wilde and Todd (1968, Fig. 4) readily recognize this threefold division from fusulinid zonation.

Early Guadalupian.—Early Guadalupian rocks in the northern Delaware Basin consist of the Brushy Canyon Formation deposited in the basin and the lower San Andres Formation representing shelf and shelf-margin deposits. King (1948) and Newell *et al.* (1953) did not find a shelf equivalent to the Brushy Canyon Formation in the Guadalupe Mountains, but found middle Guadalupian Cherry Canyon beds unconformably overlying rocks of Leonardian age. Numerous subsurface data, however, suggest that this is a local unconformity controlled by the Bone Spring flexure, and that the lower part of the San Andres Formation is also of early Guadalupian age and thus is partly equivalent to the Brushy Canyon Formation. Fusulinid control (Figs. 12, 13) supports these conclusions. Hayes (1959) reported a similar relation in Big Dog Canyon, 42 mi southwest of Carlsbad, New Mexico. He believed the San Andres at this locality represents continuous deposition from latest Leonardian or earliest Guadalupian through early middle Guadalupian (Cherry Canyon) time. Accordingly, the Brushy Canyon Formation does have a shelf equivalent in this area.

Meissner (1967) considered the entire San Andres Formation around the periphery of the Delaware Basin to be of Leonardian age. This conclusion is contradicted by abundant paleontologic evidence presented herein (Figs. 12, 13) and elsewhere (Skinner, 1946, p. 1865; Wilde and Todd, 1968) that the San Andres Formation is of Guadalupian age in the Permian Basin.

Because of insufficient well control, the exact geometric configuration of the lower San Andres bank is not well understood; accordingly, in Figures 12 and 13 the bank is presented schematically. The basinward position of the lower San Andres bank relative to the Leonardian shelf margins, however, suggests that shelf-to-basin relief was not great.

Middle Guadalupian.—The Cherry Canyon Formation of the basin is correlative with the Goat Seep reef and Getaway (upper San Andres) bank of the shelf margin (Figs. 12, 13). The Queen and Grayburg Formations are the shelf equivalents of the Goat Seep reef, and the upper San Andres is the shelf equivalent of the Getaway bank.

The suggested relation of terrigenous clastic to carbonate units set forth here is well supported by the facies changes in the Queen-Grayburg, Goat Seep reef, and upper Cherry Canyon Formations (Figs. 12, 13). The upper sandstone of the Queen Formation, Shattuck Member (Newell *et al.*, 1953), was traced to the very edge of the Goat Seep reef. Subjacent to the Shattuck Member is the Goat Seep reef and superjacent to it are the backreef deposits of the Capitan reef. The fusulinid *Parafusulina* found in the upper part of the Queen (Newell *et al.*, 1953, p. 41) indicates a middle Guadalupian age, whereas overlying beds contain *Polydiexodina*, an index fossil for late Guadalupian strata. Just in front of the Goat Seep reef and about 1,000 ft topographically lower than its crest is an equivalent sandstone (Figs. 12, 13) which marks the top of the middle Guadalupian Cherry Canyon Formation (King, 1948). *Parafusulina* is present below this sandstone, and *Polydiexodina* is present just above it in the Hegler Member of the late Guadalupian Bell Canyon Formation. Tracing the top of the Queen (Shattuck Member) across the shelf margin and equating it with the top of this basinal sandstone provided the basis for the Guadalupian shelf-to-basin correlations. This particular example is supported by surface correlations of King (1948) and Newell *et al.* (1953, p. 45) and by paleontologic data. Application of this framework in the subsurface, where comparable lithologic and paleontologic data are less clear, permits interpretation of stratigraphic form lines for lower and middle Guadalupian beds

Although King (1948) and Newell *et al.* (1953) substantiated the equivalence of the Queen-Grayburg with the Goat Seep reef in the Guadalupe Mountains, considerable doubt remained about its stratigraphic position in the subsurface (Frenzel, 1955, 1962). The problem is created by the "masking" effect of the Capitan reef, which began growing in front of the Goat Seep reef (Fig. 12). Consequently, only in an area of dense well control can the true relation of the Capitan and Goat Seep reefs be interpreted. Figure 12 extends across the Pennsylvanian (Desmoinesian) Lusk field of Eddy and Lea Counties, New Mexico, an area of relatively deep well control, in which the Capitan-Goat Seep contact was accurately mapped. Scale does not permit all the wells originally used during the study to be included in Figure 12; however, well spacing of approximately 2,000 ft fully supports all correlations.

Subsurface data indicate 700–900 ft of relief from shelf to basin at the end of Goat Seep reef growth (Figs. 12, 13). These figures agree reasonably well with the estimate of 900 ft made by Newell *et al.* (1953, p. 190) in the Guadalupe Mountains.

Of particular interest is the relation of the Manzanita Member of the Cherry Canyon Formation to the Goat Seep reef. Whereas the other basin limestone members of the Delaware Mountain Group (Getaway, South Wells, Hegler, *etc.*) pass into a shelf-margin facies, the Manzanita does not, but laps out against the Goat Seep reef (King, 1942, p. 588; Newell *et al.*, 1953, p. 27, Fig. 16). Another characteristic of the Manzanita is its widespread distribution virtually throughout the Delaware Basin as a light-colored dolomite or dolomitic limestone. Only one other Guadalupian carbonate unit, the Lamar Member, is comparably widespread, but in contrast to the Manzanita it changes rather abruptly basinward into dark, calcareous shale. It is suggested that a relatively great drop in sea level after Goat Seep deposition was responsible for deposition of the Manzanita throughout the basin; it is thought that the light color and dolomitic nature also is attributable to this exceptionally low stand of sea level. The faunal change from *Parafusulina* to *Polydiexodina* is at this horizon, and further suggests that the sea-level drop near the end of middle Guadalupian time was particularly pronounced.

Late Guadalupian.—More published data are available on late Guadalupian shelf-to-basin relations than on any others discussed. Excellent exposures in the Guadalupe Mountains and the detailed surface geologic work of King (1948), Newell *et al.* (1953), and Hayes (1964) add greatly to the understanding of late Guadalupian history. Many features described by these workers are documented also in the northern Permian Basin.

Newell *et al.* (1953, p. 190) suggested that the Delaware Basin was about 1,800 ft deep at the end of late Guadalupian deposition. Figure 13, in which the crest and slope of the upper Capitan (Tansill) reef are adequately controlled by three wells, Mobil's No. 1–75, 1–73, and 1–88 Sealy, indicates 1,800 ft of depth for the Delaware Basin. Figure 12, which is nearly as well controlled, indicates 1,400 ft of water. The difference in depth seems due to greater tectonic activity along the Central Basin platform and in the Guadalupe Mountains than in the north end of the Delaware Basin.

Upper Guadalupian terrigenous clastic rocks provide a key to differentiating the several shelf-margin sedimentary cycles. The lower Yates sandstone marks the end of lower Capitan (Seven Rivers) reef development. Conditions seem to have been rather stable during this interval, as indicated by the great amount of basinward reef growth. On the west side of the Central Basin platform, the lower Capitan reef prograded 5 mi into the basin (Fig. 13), and on the north (Fig. 12) nearly 7 mi. Clastic interbeds indicate minor interruptions in this pattern, but they are minimal in comparison with those in the overlying Yates Formation. During this rather stable period significant carbonate submarine slides and turbidites accumulated in the Hegler, Pinery, and Rader Members of the Bell Canyon Formation.

Growth of the middle Capitan (Yates) reef took place during a less stable period. Relative sea-level changes were more common, with the result that the Yates Formation contains nearly equal amounts of interbedded sandstone and carbonate. The upper Yates sandstone marks the end of middle Capitan deposition. Relative sea-level change which produced the widespread distribution of this sandstone also created another significant faunal break. The zone of *Polydiexodina* is not present above the Yates Formation on the shelf or the McCombs Member in the basin.

The upper Capitan (Tansill) reef is the least well developed of the late Guadalupian reefs. Its growth evidently was of rather brief duration and signified the end of prolific carbonate development in the Permian of West Texas and southeastern New Mexico. Fusulinid evidence supports the correlations. A rather distinct assemblage characterized by *Yabeina texana*, *Paraboultonia splendens*, and *Reichelina lamarensis* is present in both the Lamar Member of the basin and Tansill Formation on the shelf and proves their equivalency (Skinner and Wilde, 1955; Tyrrell, 1962). The presence of *Yabeina* is particularly noteworthy in that it represents mixing of "Tethyan" fusulinids with those of the Permian Basin area. A siltstone unit in the upper part of the Tansill Formation, the Ocotillo Member, signifies a brief relative drop in sea level. The Ocotillo siltstone is equivalent to the post-Lamar clastic beds of the Delaware Basin. These correlations are consistent with the stratigraphic model presented herein and have been supported by the surface work of Tyrrell (1962, p. 68).

The Castile Formation of Ochoan age transitionally overlies post-Lamar beds in the basin (Hayes, 1959; Wilde and Todd, 1968, p. 23). Core information from shelf beds in the Fort Stockton field of Pecos County, Texas, indicates similarly continuous deposition from the Tansill Formation into the overlying Salado Formation of Ochoan age. Jones (1954) also concluded that the Tansill and Salado are conformable, based on numerous potash test cores and radioactivity logs from southeast New Mexico. King (1948) reported an unconformity between the Tansill and Salado in the Guadalupe Mountains, and postulated that the Castile has no shelf equivalent. Subsurface data, however, suggest that this may have been a local discontinuity and that the basal part of the Castile grades laterally into the post-Ocotillo siltstone part of the Capitan reef. Jones (1954) believed the rest of the Castile to be coeval with the lower part of the Salado. Numerous unconformities undoubtedly are present in the Salado, but they probably are only local and represent a rather short time span, although local degradation may have been severe.

Conclusions

More than 15 major environmental rock types are recognized in the Wolfcampian-Guadalupian strata of the northern Permian Basin. They are grouped into five lithofacies (lithosomes): (1) shelf evaporite-carbonate, (2) shelf detritus, (3) shelf-margin carbonate, (4) basin carbonate, and (5) basin detritus. Recognition of these lithofacies within unconformity-bounded sequences suggests the following conclusions.

1. Under stable conditions, Permian shelf-margin reefs and banks formed near sea level. The resultant lagoon was very shallow but very broad, and therefore little terrigenous sand reached the distant basin. Shelf-margin carbonate bodies were at maximum development and the main sediments deposited in the basin were pelagic mud and micrite; locally submarine slides and turbidites composed of carbonate grains accumulated. Regression caused by a drop in sea level, probably eustatic-epeirogenic, permitted continental and nearshore sands to prograde across the lagoon. Continued progradation enabled shelf detritus to enter the basin through numerous reentrants and submarine canyons dissecting the shelf margin. Prograding submarine fans aided by well-developed overbank systems distributed detritus along the basin floor. At maximum low-water stand the shelf detritus was exposed subaerially.

Later flooding of the shelf by a rising sea restricted the sand supply and reactivated normal carbonate deposition. Correlation of a shelf detritus top with a coeval basin detritus top provides the framework for Wolfcampian-Guadalupian shelf-to-basin correlations.

2. A Wolfcampian-Leonardian physical stratigraphic framework is proposed which suggests: (1) the green quartzose clayrock and siltrock at the top of the Wichita Formation (Abo Formation of New Mexico) is coeval with the Dean sand of the Midland Basin and the Third Bone Spring sand of the Delaware Basin; (2) the Tubb Formation is correlative with the lower Spraberry sand of the Midland Basin and the Second Bone Spring sand of the Delaware Basin; (3) the red and green quartzose siltrock and evaporitic unit at the top of the middle Clear Fork Formation (middle Yeso Formation of New Mexico) is coeval with the upper Spraberry sand of the Midland Basin and First Bone Spring sand of the Delaware Basin; and (4) the San Angelo Formation is equivalent to a brown argillaceous micritic limestone at the top of the Bone Spring Formation. The Glorieta Formation of the Northwestern Shelf is correlative with the Cutoff Shale of the Delaware Basin.

3. Physical and biostratigraphic data support a threefold division of Guadalupe rocks in the northern Delaware Basin. A Guadalupian framework is proposed which suggests that (1) the lower San Andres Formation is partly coeval with the early Guadalupian Brushy Canyon Formation; (2) the sandstone (Shattuck Member) at the top of the Queen Formation is coeval with the sandstone at the top of the middle Guadalupian Cherry Canyon Formation between the Manzanita Member and overlying Hegler Member; (3) the sandstone directly overlying the late Guadalupian Seven Rivers Formation is coeval in part with the sandstone above the Rader Member of the Bell Canyon Formation; (4) the sandstone at the top of the late Guadalupian Yates Formation is correlative with the sandstone between the McCombs and Lamar Members of the Bell Canyon Formation; and (5) the late Guadalupian lower Tansill Formation below the Ocotillo Siltstone is coeval with the Lamar Member, whereas the Ocotillo is correlative with the post-Lamar beds. Upper Tansill beds are partly coeval with the basal Castile Formation of Ochoan age.

4. Cyclic sedimentation is characteristic of upper Wolfcampian through Guadalupian shelf and basin facies. Ease of correlation between the Midland and Delaware Basins and laterally along the shelves suggests this cyclicity was caused by eustatic-epeirogenic sea-level changes. Periodic glaciation and deglaciation in the southern hemisphere contemporaneous with subsidence are favored as the cause of cyclicity during Wolfcampian-Guadalupian time in the northern Permian Basin.

5. Recognition of the late Wolfcampian through Guadalupian unconformity-bounded sequence and the depositional model permit (1) rapid regional mapping of shelf-margin strata, (2) definition of valid structural horizons, (3) delineation of regional potential source and reservoir rocks both on the shelf margin and in the basin, and (4) recognition of similar relations in Early Permian basins characterized by shelf-to-basin topography.

References Cited

Adams, J. E., H. N. Frenzel, M. L. Rhodes, and D. P. Johnson, 1951, Starved Pennsylvanian Midland basin: Am. Assoc. Petroleum Geologists Bull., v. 35, no. 12, p. 2600–2607.

Bott, M. H. P., and G. A. L. Johnson, 1967, The controlling mechanism of Carboniferous cyclic sedimentation: Geol. Soc. London Quart. Jour., v. 122, p. 421–441.

Clark, T. H., 1954, Shale—a study in nomenclature: Royal Soc. Canada Trans., ser. 3, v. 48, sec. 4, p. 1–7.

Cooper, G. A., and R. E. Grant, 1964, New Permian stratigraphic units in Glass Mountains, West Texas: Am. Assoc. Petroleum Geologists Bull., v. 48, no. 9, p. 1581–1588.

Cummins, W. F., and O. Lerch, 1890, Concho County, a geological survey: Am. Geologist, v. 7, p. 73–75, 321–325.

——— 1891, Report on the geology of northwestern Texas: Texas Geol. Survey 2d Ann. Rept., p. 359–554.

Dunbar, C. O., chm., *et al.*, 1960, Correlation of the Permian formations of North America: Geol. Soc. America Bull., v. 71, p. 1763–1806.

Dunham, R. J., 1963, Early vadose silt in Townsend mound (reef), New Mexico (abs.): Am. Assoc. Petroleum Geologists Bull., v. 47, no. 2, p. 356.

——— 1965, Vadose pisolite in the Capitan reef (abs.): Am. Assoc. Petroleum Geologists Bull., v. 49, no. 3, pt. 1, p. 338.

Frenzel, H. N., 1955, The Queen-Grayburg problem: Soc. Econ. Paleontologists and Mineralogists Permian Basin Sec. Field Conf. Guidebook, p. 52–58.

——— 1962, The Queen-Grayburg-San Andres problem solved, *in* Permian of the central Guadalupe Mountains, Eddy County, New Mexico: West Texas Geol. Soc. Pub. 62–48, p. 87–90.

Galley, J. E., 1958, Oil and geology in the Permian basin of Texas and New Mexico, *in* L. G. Weeks, ed., Habitat of oil, a symposium: Am. Assoc. Petroleum Geologists, p. 395–446.

Hamilton, W., and D. Krinsley, 1967, Upper Paleozoic glacial deposits of South Africa and southern Australia: Geol. Soc. America Bull., v. 78, p. 783–800.

Hayes, P. T., 1959, San Andres Limestone and related Permian rocks in Last Chance Canyon and vicinity, southeastern New Mexico: Am. Assoc. Petroleum Geologists Bull., v. 43, no. 9, p. 2197–2213.

——— 1964, Geology of the Guadalupe Mountains, New Mexico: U.S. Geol. Survey Prof. Paper 446, 69 p.

Hull, J. P. D., Jr., 1957, Petrogenesis of Permian Delaware Mountain sandstone, Texas and New Mexico: Am. Assoc. Petroleum Geologists Bull., v. 41, no. 2, p. 278–307.

Illing, L. V., A. J. Wells, and J. C. M. Taylor, 1965, Penecontemporary dolomite in the Persian Gulf, *in* L. C. Pray and R. C. Murray, eds., Dolomitization and limestone diagenesis, a symposium: Soc. Econ. Paleontologists and Mineralogists Spec. Pub. 13, p. 89–111.

Jacka, A. D., 1967, Guadalupian depositional cycles of the Delaware basin and Northwest Shelf (abs.), *in* Cyclical sedimentation in the Permian basin: West Texas Geol. Soc. Symposium, p. 49–50.

——— R. H. Beck, L. C. St. Germain, and S. C. Harrison, 1968, Permian deep-sea fans of the Delaware Mountain Group (Guadalupian), Delaware basin, *in* B. A. Silver (ed.), Guadalupian facies, Apache Mountains area, West Texas: Soc. Econ. Paleontologists and Mineralogists Permian Basin Sec. Guidebook Pub. 68–11, p. 49–90.

——— and L. C. St. Germain, 1967, Deep-sea fans in the Permian Delaware Mountain Group, Delaware basin, West Texas and New Mexico (abs.): Am. Assoc. Petroleum Geologists Bull., v. 51, no. 3, pt. 1, p. 471–472.

Jones, C. L., 1954, The occurrence and distribution of potassium minerals in southeastern New Mexico: New Mexico Geol. Soc. 5th Field Conf. Guidebook, p. 107–112.

Jones, T. S., 1953, Stratigraphy of the Permian basin of West Texas: West Texas Geol. Soc., 63 p.

King, P. B., 1942, Permian of West Texas and southeastern New Mexico: Am. Assoc. Petroleum Geologists Bull., v. 26, no. 4, p. 535–763.

——— 1948, Geology of the southern Guadalupe Mountains, Texas: U.S. Geol. Survey Prof. Paper 215, 183 p.

King, R. E., 1945, Stratigraphy and oil-producing zones of the pre-San Andres formations of southeastern New Mexico: New Mexico School Mines Bull. 23, 31 p.

Kinsman, D. J. J., 1969, Modes of formation, sedimentary associations, and diagnostic features of shallow-water and supratidal evaporites: Am. Assoc. Petroleum Geologists Bull., v. 53, no. 4, p. 830–840.

Lee, W. T., 1909, Stratigraphy of the Manzano Group of the Rio Grande Valley, New Mexico: U.S. Geol. Survey Bull. 389, 141 p.

Lloyd, E. R., 1949, Pre-San Andres stratigraphy and oil-producing zones in southeastern New Mexico: New Mexico School Mines Bull. 29, 79 p.

McDaniel, P. N., and L. C. Pray, 1967, Bank to basin transition in Permian (Leonardian) carbonates, Guadalupe Mountains, Texas (abs.): Am. Assoc. Petroleum Geologists Bull., v. 51, no. 3, pt. 1, p. 474.

McKee, E. D., *et al.*, 1967, Paleotectonic investigation of the Permian System in the United States: U.S. Geol. Survey Prof. Paper 515, 271 p.

Meissner, F. F., 1967, Cyclical sedimentation in mid-Permian strata of the Permian basin (abs.), *in* Cyclical sedimentation in the Permian basin: West Texas Geol. Soc. Symposium, p. 37–38.

Meyer, R. F., 1966, Geology of Pennsylvanian and Wolfcampian rocks in southeast New Mexico: New Mexico Inst. Mining and Technology, Bur. Mines and Mineral Resources Mem. 17, 123 p.

Newell, N. D., J. K. Rigby, A. G. Fischer, A. J. Whiteman, J. E. Hickox, and J. S. Bradley, 1953, The Permian reef complex of the Guadalupe Mountains region, Texas and New Mexico: San Francisco, W. F. Freeman, 236 p.

Rich, J. L., 1921, The stratigraphy of eastern New Mexico—a correction: Am. Jour. Sci., 5th ser., v. 2, p. 295–296.

——— 1951, Three critical environments of deposition, and criteria for recognition of rocks deposited in each of them: Geol. Soc. America Bull., v. 62, p. 1–20.

Ross, C. A., 1963, Standard Wolfcampian Series (Permian), Glass Mountains, Texas: Geol. Soc. America Mem. 88, 205 p.

Schleh, E. E., 1966, Review of sub-Tamaroa unconformity in Cordilleran region: Am. Assoc. Petroleum Geologists Bull., v. 50, no. 2, p. 269–282.

Skinner, J. W., 1946, Correlation of Permian of West Texas and southeast New Mexico: Am. Assoc. Petroleum Geologists Bull., v. 30, no. 11, p. 1857–1874.

——— and G. L. Wilde, 1955, New fusulinids from the Permian of West Texas: Jour. Paleontology, v. 29, p. 927–940.

Sloss, L. L., 1963, Sequences in the cratonic interior of North America: Geol. Soc. America Bull., v. 74, p. 93–114.

Teichert, Curt, 1941, Upper Paleozoic of western Australia, correlation and paleogeography: Am. Assoc. Petroleum Geologists Bull., v. 25, no. 3, p. 371–415.

Thomas, C. M., 1965, Origin of pisolites (abs.): Am. Assoc. Petroleum Geologists Bull., v. 49, no. 3, pt. 1, p. 360.

——— 1968, Vadose pisolites in the Guadalupe and Apache Mountains, West Texas, *in* B. A. Silver, ed., Guadalupian facies, Apache Mountain area, West Texas: Soc. Econ. Paleontologists and Mineralogists Permian Basin Sec. Guidebook Pub. 68-11, p. 32–35.

Tyrrell, W. W., Jr., 1962, Petrology and stratigraphy of near-reef Tansill-Lamar strata, Guadalupe Mountains, Texas and New Mexico, *in* Permian of the central Guadalupe Mountains, Eddy County, New Mexico: West Texas Geol. Soc. Pub. 62–48, p. 59–69.

Van Siclen, D. C., 1958, Depositional topography—examples and theory: Am. Assoc. Petroleum Geologists Bull., v. 42, no. 8, p. 1897–1913.

Walker, T. R., 1967, Formation of red beds in modern and ancient deserts: Geol. Soc. America Bull., v. 78, p. 353–368.

Wanless, H. R., and J. R. Cannon, 1966, Late Paleozoic glaciation: Earth-Sci. Rev., v. 1, p. 247–286.

Weller, J. M., 1959, Compaction in sediments: Am. Assoc. Petroleum Geologists Bull., v. 43, no. 2, p. 273–311.

Wheeler, H. E., and V. S. Mallory, 1953, Designation of stratigraphic units: Am. Assoc. Petroleum Geologists Bull., v. 37, no. 10, p. 2407–2421.

——— 1963, Post-Sauk and pre-Absaroka Paleozoic stratigraphic patterns in North America: Am. Assoc. Petroleum Geologists Bull., v. 47, no. 8, p. 1497–1526.

Wilde, G. L., 1962, Lower Permian biostratigraphic relationships and sedimentation, *in* A. Thomason, ed., Leonardian facies of the Sierra Diablo region, West Texas: Soc. Econ. Paleontologists and Mineralogists Permian Basin Sec. Guidebook Pub. 62-5, p. 68–77.

——— and R. G. Todd, 1968, Guadalupian biostratigraphic relationships and sedimentation in the Apache Mountain region, West Texas, *in* B. A. Silver, ed., Guadalupian facies, Apache Mountains area, West Texas: Soc. Econ. Paleontologists and Mineralogists Permian Basin Sec Guidebook Pub. 68–11, p. 10–31.

Wilson, J. L., 1967, Cyclic and reciprocal sedimentation in Virgilian strata of southern New Mexico: Geol. Soc. America Bull., v. 78, p. 805–818.

Wright, W. F., 1962, Fundamentals of oil exploration, Permian Basin, West Texas: Midland, Texas, Midland Reporter-Telegram Ser., Sept. 2, 1962–Dec. 22, 1963.

3) Sea Level Change
Andrew Smith and Isaac Smith

Glossary of Terms:

Regression: Shoreline advance basin-ward. This is sometimes associated with sea-level fall of basin uplift.

Transgression: Shoreline retreat landward. This is sometimes associated with sea-level rise or basin subsidence.

Parasequence: Relatively conformable, genetically related succession of beds bounded by marine flooding.

Retrogradation: Landward trend in the position of the foreslope of deposits with time. Volume of incoming sediment < accommodation due to subsidence, sea-level rise, and/or erosion. Interspersed with parasequences.

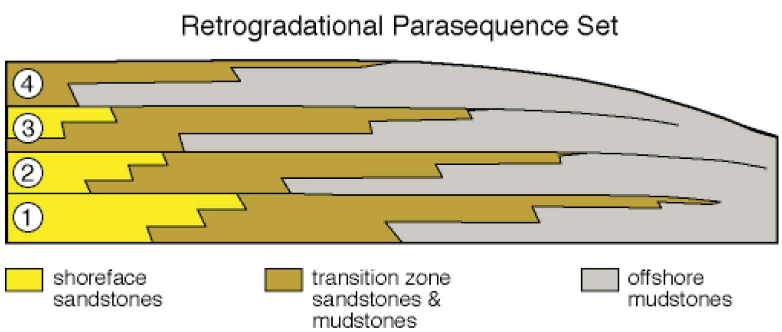

Adapted from Van Wagoner et al. (1990)

Aggradation: No overall trend in shoreline position through time. Supply of sediment ~ accommodation.

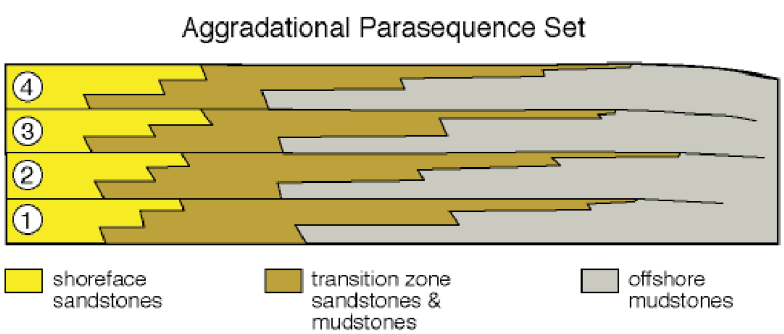

Adapted from Van Wagoner et al. (1990)

Progradation: Basinward trend in the position of the foreslope of deposits with time. Volume of incoming sediment is greater than accommodation due to uplift or sea-level fall. Interspersed with parasequences.

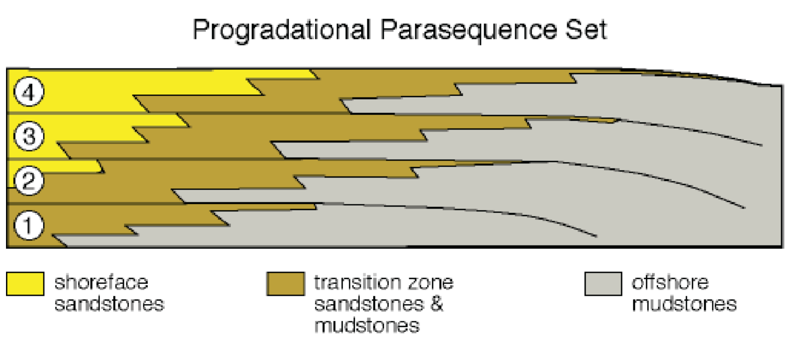

Adapted from Van Wagoner et al. (1990)

Exxon Sea-level Curve showing changes in sea level above present day (PD) (Haq et al., 1987; Haq and Schutter, 2008):

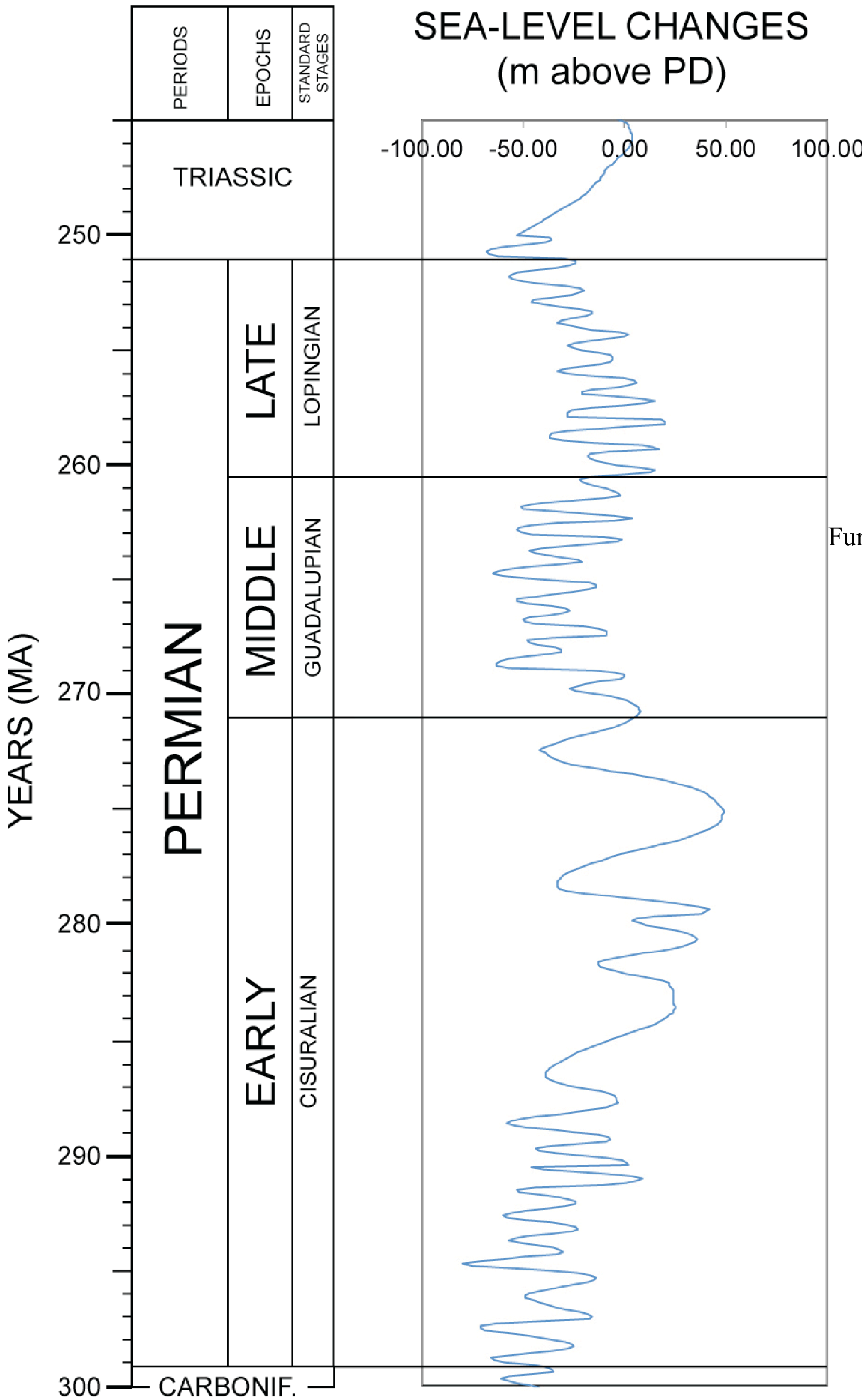

Further reading:

1) Haq, B. U., and S. R. Schutter (2008), A Chronology of Paleozoic Sea-Level Changes, *Science*, *322*(5898), 64-68.

2) Exerpt from: Osleger, D. A. (1998), Sequence architecture and sea-level dynamics of Upper Permian shelfal facies, Guadalupe Mountains, southern New Mexico, *Journal of Sedimentary Research*, *68*(2), 327-346.

A Chronology of Paleozoic Sea-Level Changes

Bilal U. Haq[1]* and Stephen R. Schutter[2]

Sea levels have been determined for most of the Paleozoic Era (542 to 251 million years ago), but an integrated history of sea levels has remained unrealized. We reconstructed a history of sea-level fluctuations for the entire Paleozoic by using stratigraphic sections from pericratonic and cratonic basins. Evaluation of the timing and amplitude of individual sea-level events reveals that the magnitude of change is the most problematic to estimate accurately. The long-term sea level shows a gradual rise through the Cambrian, reaching a zenith in the Late Ordovician, then a short-lived but prominent withdrawal in response to Hirnantian glaciation. Subsequent but decreasingly substantial eustatic highs occurred in the mid-Silurian, near the Middle/Late Devonian boundary, and in the latest Carboniferous. Eustatic lows are recorded in the early Devonian, near the Mississippian/Pennsylvanian boundary, and in the Late Permian. One hundred and seventy-two eustatic events are documented for the Paleozoic, varying in magnitude from a few tens of meters to ~125 meters.

Although there has been substantial progress in recent years in integrating the record of Mesozoic and Cenozoic eustatic fluctuations (*1*, *2*), relatively little attention has been paid to reevaluating or synthesizing Paleozoic sea-level data, the coverage of which has been largely piecemeal. The Paleozoic Era encompasses more than half of the Phanerozoic Eon, featuring some of the most intriguing unanswered questions in Earth history. Unexplored Paleozoic strata also are believed to contain important unrecovered hydrocarbons. A reevaluation of the eustatic history of this Era therefore would not only serve as a tool for exploration geology but hopefully also revive interest in Paleozoic Earth science.

Sea-level curves provide utilitarian predictive models of sedimentation and thus are invaluable in geologic exploration. These curves offer a working representation of the long-term trends of the base level along continental margins and the individual inundations and drainings/desiccations of interior seaways, and thus the migration of hydrocarbon reservoirs and source facies. Where local tectonic influences are minimal and have not deformed the stratigraphic record (or where tectonics can be corrected for), these curves also can aid in first-order correlations. The relative magnitude and frequency of sea-level highs and lows, the extent and nature of the transgressive condensed intervals on the shelf (when organic-rich sediments accumulate), and the duration of subaerial exposure and incision of the shelf are also important exploration criteria (*3*). Here we present an integrated semiquantitative model of the Paleozoic sea-level history. It is based on widely distributed sequence-stratigraphic data within the biochronostratigraphic constraints of varying quality and reliability for various Paleozoic periods.

Although previous reconstructions of regional sea-level histories have been limited to discrete slices of time, they provide a wealth of information on the long- and short-term trends and have been an invaluable resource for this synthesis [see the supporting online material (SOM) text]. Particularly, the studies from relatively stable pericratonic and cratonic basins of North American and Australian cratons have been indispensable. As discussed later, we have designated reference districts (RDs) for various time segments (largely from North America and Australia, but also from northern and southern Africa, northwestern Europe, and China). We interpret the sedimentary record in these districts as representing the modal mean of change in sea level during intervals of relative tectonic quiescence. The RDs were also compared with sections elsewhere around the world to ascertain the broad transgressive/regressive trends and individual variations of sea levels and provide corroborative data. Because of spatial constraints, in this article we only report a brief account of our main findings (see also SOM text).

Timing and magnitude of sea-level events in the Paleozoic. Obstacles encountered in resolving the timing and magnitude of individual sea level events based on a synthesis of worldwide data of varying quality and utility are not specific to the Paleozoic; they are also applicable to the younger eras. The Paleozoic, however, has a special suite of constraints that sets it apart. For example, most Paleozoic oceanic crust has been subducted (with the exception of a few obducted ophiolite mélanges), making it unfeasible to directly estimate the mean age of the oceanic crust for deciphering long-term eustatic trends. Paleozoic stratigraphy is also strongly biased toward epi- and pericratonic basins, characterized by their plentiful unconformities and endemic faunas. Nevertheless, these attributes make these basins natural places for the study of "unconformity-bounded" units (depositional sequences). The unconformity-bounded subdivision also makes the existing Paleozoic literature, spanning over a century of research, relevant and useful.

An accurate time scale is of crucial first-order importance for any global synthesis. Geological time scales have been improving and becoming better integrated in recent years. The Paleozoic time scale in particular has been in a considerable state of flux, with major recent changes to the ages of period and stage boundaries. The most up-to-date published time scale is that compiled by Gradstein *et al*. (*4*). Some parts of this chronostratigraphy have been updated recently (*5*), which we have adopted here. Ongoing attempts at astronomical tuning and recalibration of $^{40}Ar/^{39}Ar$ ages will probably lead to further refinements of the boundary ages (*6*). However, with the exception of a few radiometrically determined boundaries, all of the Paleozoic correlations are actually based on fossil biozonations. Thus, the duration of a biozone in question provides a minimum measure of uncertainty in the correlations of sequence boundaries.

The degree of precision of correlations from one basin to another depends on the biostratigraphic fossil assemblage used for such purposes. For the Paleozoic, biochronostratigraphy is traditionally based on several groups of commonly occurring fossils, the majority of which tend to be endemic and/or facies-controlled (*7*). This underscores the need to use multiple overlapping criteria (biozonal assignments based on several groups) where possible, to enhance the chronostratigraphic signal-to-noise ratio.

The second issue of importance for a reconstruction such as this concerns the uncertainty in estimating the magnitude of rises and falls in sea level. In the Paleozoic, the general lack of data on ice-volume proxies, such as oxygen isotopes (because of severe diagenetic alterations), limits us to relying on physical measures of sea-level changes from stratigraphic data. A fundamental limitation for accurate physical estimates stems from the lack of a universal reference point against which sea level changes can be computed. For convenience, we often compare past eustatic fluctuations with present-day (PD) shorelines, but over the longer periods this comparative reference point becomes less meaningful because continents have changed both by horizontal accretion/destruction and vertical motions. It is often possible to determine when the sea withdrew below the extant shelf edge, but it is challenging to accurately gauge the amount of

[1]National Science Foundation, Arlington, VA 22230, USA. [2]Murphy Oil International, Houston, TX 77094, USA.

*To whom correspondence should be addressed. E-mail: bhaq@nsf.gov

sea-level fall from stratigraphic data because of the unknown amount of erosion on the shelf. A rise in sea level is even more difficult to measure meaningfully because of the potentially less-than-complete filling of the accommodation space during the highstand or because of a subsequent fall in sea level that may erode part or much of the highstand systems tract. Thus, for practical purposes, all amplitude assessments from physical data must be considered relative rather than absolute.

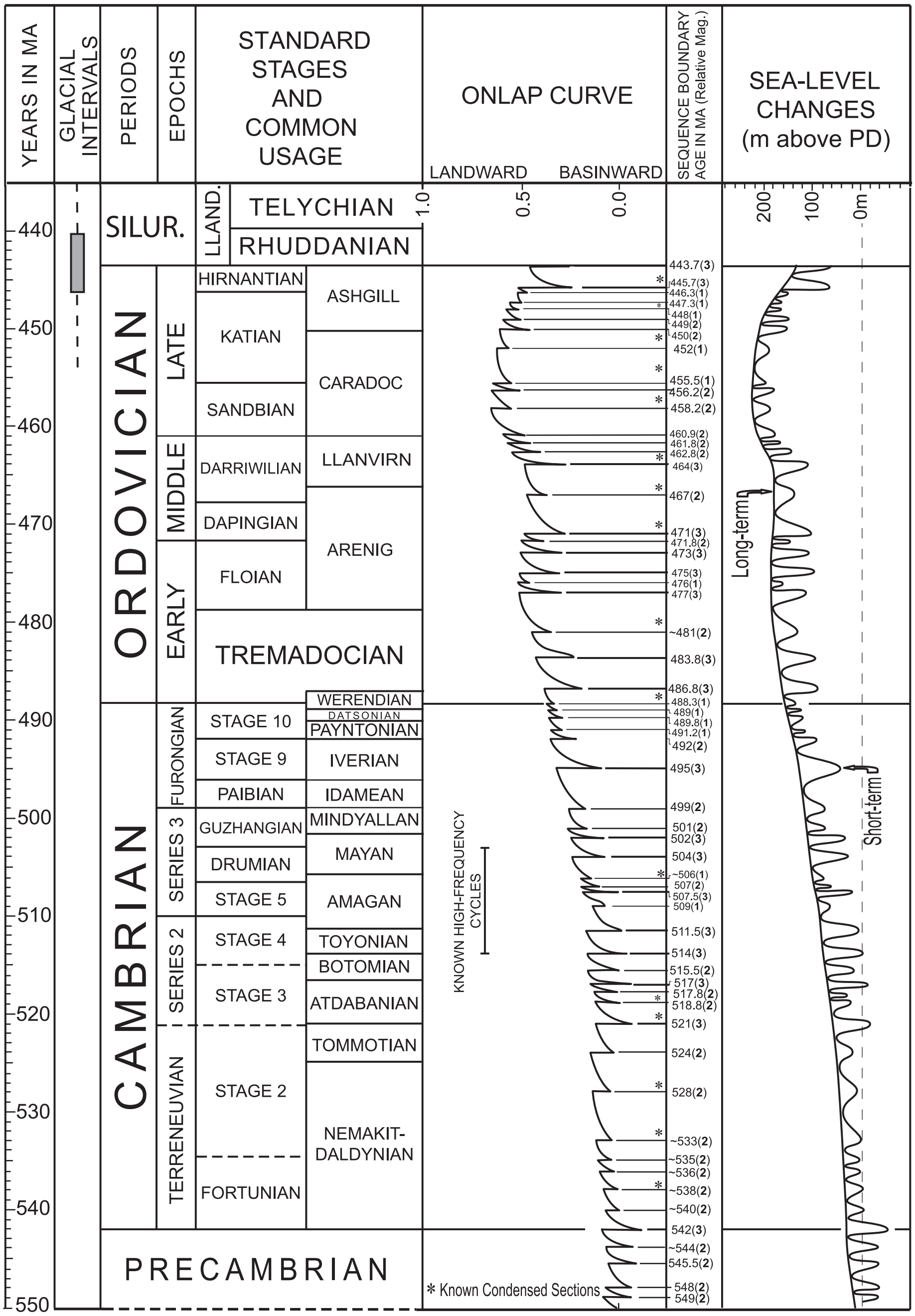

Fig. 1. Cambrian-Ordovician sea-level changes. The time scale and standard and regional stages are modeled after Gradstein *et al*. and Ogg *et al*. (*4*, *5*). The left half of Figs. 1 to 3 shows the stratigraphic subdivisions calibrated to the absolute time scale. Known intervals of continental glaciation (*26–28*) are indicated alongside the numerical time scale. The right half of each figure starts with an onlap curve, which is a measure of relative landward or basinward movement of the regional baseline as estimated in the RD sections. Sequences that are associated with known prominent condensed sections (indicated by asterisks) are also shown in this column. The biochronological ages of the sequence boundaries (estimated in the RDs and ancillary sections) are indicated in the next column. A semiquantitative measure of the relative magnitude of each short-term event is shown in parentheses [minor, **1** (<25 m); medium, **2** (25 to 75 m); and major, **3** (>75 m)]. Periods with known higher-frequency eustatic cycles and documented condensed sections are also indicated in this column, by vertical bars. This is followed to the right by the sea level curves, both the long-term envelope and the short-term curve of (third-order) fluctuations in the sea level (those suspected to be of fourth order are shown by dashed lines). The dashed vertical line in this column represents an approximation of the PD sea level. Long-term and short-term sea-level curves are calibrated to the PD sea level.

Backstripping can potentially refine such estimates through corrections for sediment loading and compaction and basin-floor subsidence (*8*, *9*). Nevertheless, considerable uncertainties remain in this approach because of long-ranging paleobathymetric indicators and the potential for differential subsidence. Corrections for the flexural response of a margin to the loading and unloading of water/ice and sediments are also not straightforward or precise and can bias the measurements in either direction. During this synthesis, the only meaningful approach we could adopt was to reproduce the magnitude estimates of rises and falls in sea level as gleaned from the RDs and ancillary sections (based variously on stratigraphic measures such as thickness of system tracts, bio- and lithofacies depth assessments, the depth of incision on shelves, and partial backstripping). We classified each event semiquantitatively (measured as a magnitude of fall from the previous highstand) as minor (<25 m), medium (25 to 75 m), or major (>75 m). From the worldwide data, it is apparent that although the overall long-term (cumulative) rise in sea level could be as much as 250 m, the individual third-order changes in sea level [that is, those occurring over ~0.5 to 6 million years (My)] rarely exceeded 150 m. Many of the higher-frequency (<0.5 My) variations are within the minor to medium range. These estimates will be subject to refinement in the future once various basins (in the RDs and elsewhere) have been effectively backstripped and when better paleobathymetric assessments are available.

Reconstruction of the Paleozoic sea-level history. Though Earth scientists have been interpreting changes in sea level based on stratigraphic data for over a century, the first attempt at an integrated history of the Paleozoic sea level was embedded in the broader presentation of seismic-stratigraphic methodology by Vail *et al*. (*10*). Hallam (*11*) also reviewed much of the Paleozoic sea level data accumulated up to the 1980s. More recently, Haq and Al-Qahtani (*12*) presented a regional history of the sea level in the Phanerozoic Arabian Platform and compared it with an updated eustatic sea level curve based on previous syntheses. However, the Paleozoic portions of those curves largely depicted second-order events, mostly cycles of >5 My duration.

The stratigraphic record is a composite of several orders of superimposed sedimentary cycles, depending on their causal mechanisms. They range from the high-frequency Milankovitch-scale climatic cycles (often 1 m to a few meters in thickness) to third-order (mostly 1 to 2 My in duration) and fourth-order (<0.5 My in duration)

66

eustatic cycles, and larger (several million years in duration) tectonic cycles. In practice, it is difficult to consistently separate third- and fourth-order cycles. Our ability to resolve the record chronostratigraphically in any given section depends on the thickness of the preserved section, the quality of the outcrop, the position of the section along the shelf-slope-basin profile, and the quality of biochronostratigraphic data. Here we have attempted to identify sequences at third-order resolution; however, a few fourth-order sedimentary cycles inevitably were also incorporated. Although the existence of higher-frequency cycles may be more widespread in the Paleozoic, some intervals more visibly preserve fourth-order (~400,000 years) cycles, such as the mid-Cambrian, mid-Devonian, mid- to late Carboniferous, and Permian (Figs. 1 to 3).

The Paleozoic sequence-stratigraphic data are derived entirely from public-domain outcrop sections (seismic data are generally lacking or spotty except for the late Paleozoic). The criteria for interpreting regional rises and falls in sea level from sequence-stratigraphic data and seismic data have been summarized elsewhere (*3*, *10*, *13*) and are not repeated here. In addition, several lithological features (condensed section deposits, transgressive coals, evaporites, carbonate megabreccias, and exposure-related and forced-regressive deposits) and paleontological attributes have also aided our interpretations in placing outcrop features within sequence-stratigraphic framework (see the description in the SOM text).

Reconstruction of the long-term envelope and the short-term history of changes in sea level requires differing approaches. The long-term changes are believed to be mostly driven by the slow tectonic processes that change the volumetric capacity of the ocean basins. Individually, each data set on which the long-term envelope can be based must be considered relative rather than absolute measures of eustatic trends. However, a long-term curve based on global continental flooding estimates (*14*–*17*), stacked regional sea-level data (evaluated by us), and modeling results for the mean age of the oceanic crust yields consistent results. Algeo and Seslavinsky (*17*) have presented an analysis of the flooding history and hypsometry of 13 Paleozoic landmasses and estimate that the long-term eustatic highs were 100 to 225 m above PD sea level. They also conclude that Paleozoic continents experienced an additional change of ±100 m in vertical movements because of epeirogeny. The upper limits of our estimates of long-term highs are influenced by this analysis.

More-recent modeling results of the Mesozoic-Cenozoic sea floor (*18*–*20*), although based on differing assumptions, consistently point to the mean age of the oceanic crust, rather than sea-floor spreading rates or ridge volume, as potential forcing for the long-term eustatic change. Cogné and Humler (*20*) have extrapolated their modeling results back to the Paleozoic, for which direct measurements of sea-floor isochrons are not possible because of subduction. Instead, they estimate land-ocean distributions from measurements of areas of continental landmasses based on paleomagnetic reconstructions. Their results show a credible agreement between periods of high fragmentation of the continents and high global sea levels through much of the Paleozoic. One recent aspect of the modeling efforts is the conclusion that continental margins could be subjected to a substantial degree of mantle flow–related vertical motions over relatively short geological intervals. This process causes changes in local dynamic topography, which may have led to an underestimation of changes in sea level from physical data in the past (*21*).

The shorter-term changes in sea level (third- and higher-order events) were more likely mostly driven by changes in the volume of water in the world ocean through glacial (and as yet unknown) processes. The short-term Paleozoic curve as portrayed here (Figs. 1 to 3) is based on the best of several sections in an area designated the RD, in which, according to our interpretations, tectonic influences were minimal and the eustatic signal is more likely to have been preserved. Sea level–change events identified in the RDs were then sought elsewhere worldwide (in the existing stratigraphic data) and documented in designated ancillary sections (SOM text).

The previous physically estimated magnitude of the shorter-term (third- and fourth-order) sea-

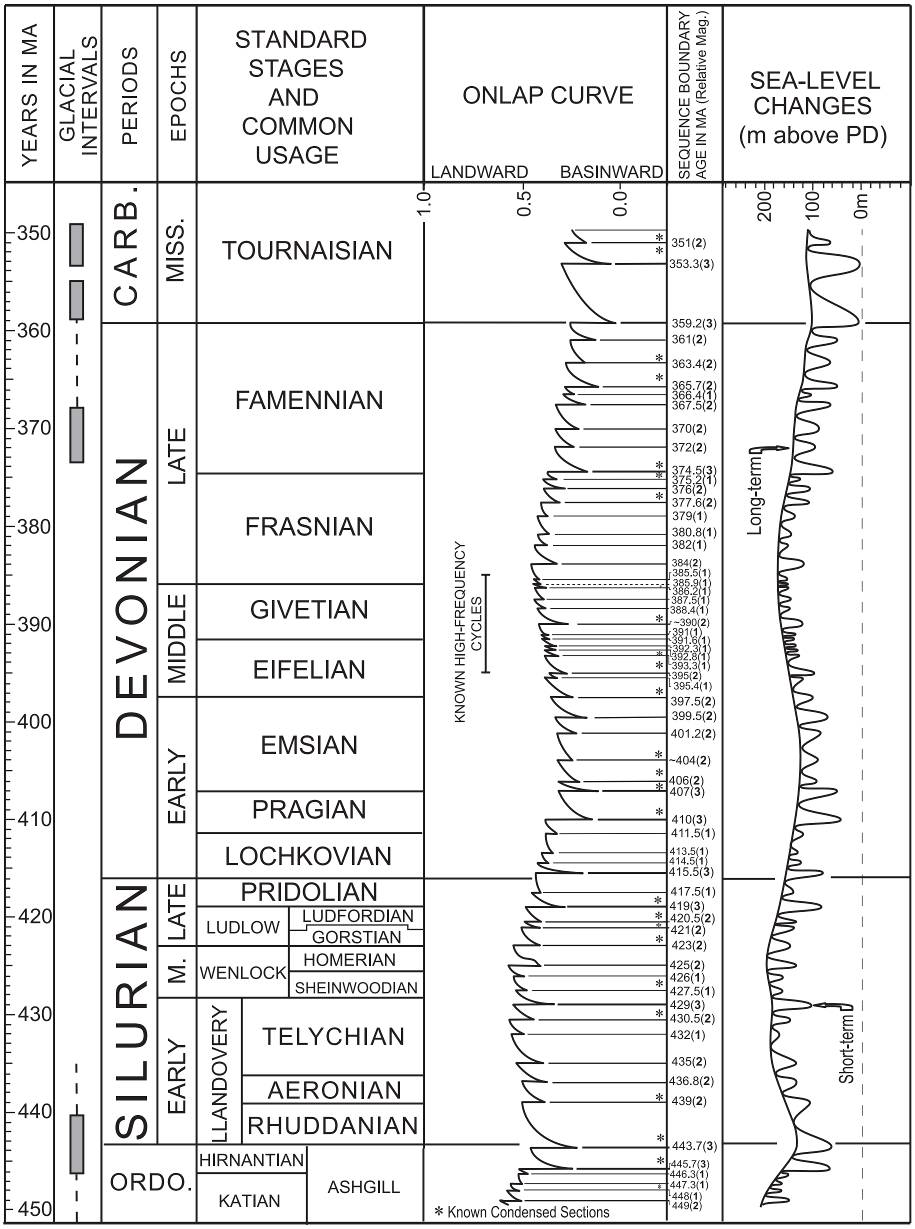

Fig. 2. Silurian-Devonian sea-level changes. See the caption of Fig. 1 for details.

level events in the Paleozoic range from a few tens of meters to ~250 m (*22*). A recent synthesis of the Carboniferous-Permian yielded fluctuations of a few tens of meters in the nonglacial intervals and changes of up to 120 m in the glacially dominated periods (*23*). Many of these regional estimates will be subject to refinement in the future, once the sections in question are rigorously backstripped.

Although we deem the long-term trends to be real, the difficulties in estimating meaningful measures of the magnitude of eustatic changes discussed above imply that the absolute global amplitude of both the long-term envelope and the short-term changes remain elusive. All such measures must be currently considered as approximate. These observations also caution us about the futility of generalizing the magnitude of individual sea-level events from one continental margin to represent worldwide eustatic values.

The concept of RDs [first proposed by M. E. Johnson (*24*)] implies that we consider the sections therein to be currently the best available representation of the modal mean for the time segment under consideration. Our criteria for inclusion of an area as a RD are as follows: (i) the time segment in question is represented by a period of tectonic quiescence locally (or is correctable for tectonic influences) and has suffered relatively little postdepositional deformation and is thus interpretable with sequence-stratigraphic methodologies; (ii) sections are relatively well-dated, preferably with multiple biostratigraphies (to enhance the chronostratigraphic signal-to-noise ratio); (iii) outcrops in the area have open public access; and (iv) the area will easily lend itself to geohistory analysis so that the relevant sections can be eventually backstripped (as well as corrected for local dynamic topographic changes over time) for more-refined estimates of the magnitude of changes in sea level. We list the selected RDs and ancillary sections in the SOM, along with background literature and ages assigned by us to the interpreted sequence boundaries.

Results and conclusions. Here we offer (in our view) a robust working model of the history of the Paleozoic sea level that is, nevertheless, subject to refinement with better chonostratigraphies and when the sections are subjected to backstripping analyses. Our results show a long-term sea level curve, including a rising sea level during the Cambrian–through–Early Ordovician interval [see fig. S1 and explanation in (*25*)], a marked dip during the Middle Ordovician (the Dapingian to early Darriwilian) preceding a substantial rise entering the early Late Ordovician, and the highest sea levels of the Paleozoic during the early Katian (when the sea level is estimated to be ~225 m higher than at the PD). This was followed by a sharp fall during the latest Ordovician (late Katian to the Hirnantian) that continued into the earliest Silurian. The remainder of the Early Silurian saw the beginning of another long-term rise that culminated in a mid-Silurian (mid-Wenlock) high, followed by a decline that lasted from Late Silurian (Ludlow) through Early Devonian (Emsian). The Middle Devonian saw the beginning of yet another long-term rise, which reached its acme in the early Late Devonian (Frasnian). After a slight dip at the Frasnian/Famennian boundary and a recovery in the early Famennian, the long-term curve shows a gradual sea-level decline in the later Devonian (late Famennian) with a punctuated fall near the Devonian/Carboniferous boundary. After a short recovery, subsequent long-term decline began in the mid-Mississippian (mid Visean), reaching a low in the late Mississippian (near the Mississippian/Pennsylvanian boundary). The next long-term rise (though less pronounced than all previous rises) began in the mid-Pennsylvanian (Moscovian) and lasted only until the end of the Pennsylvanian (Gzhelian), followed by a slight fall thereafter in the earliest Permian (Asselian). The sea level stabilized at that level for the remainder

68

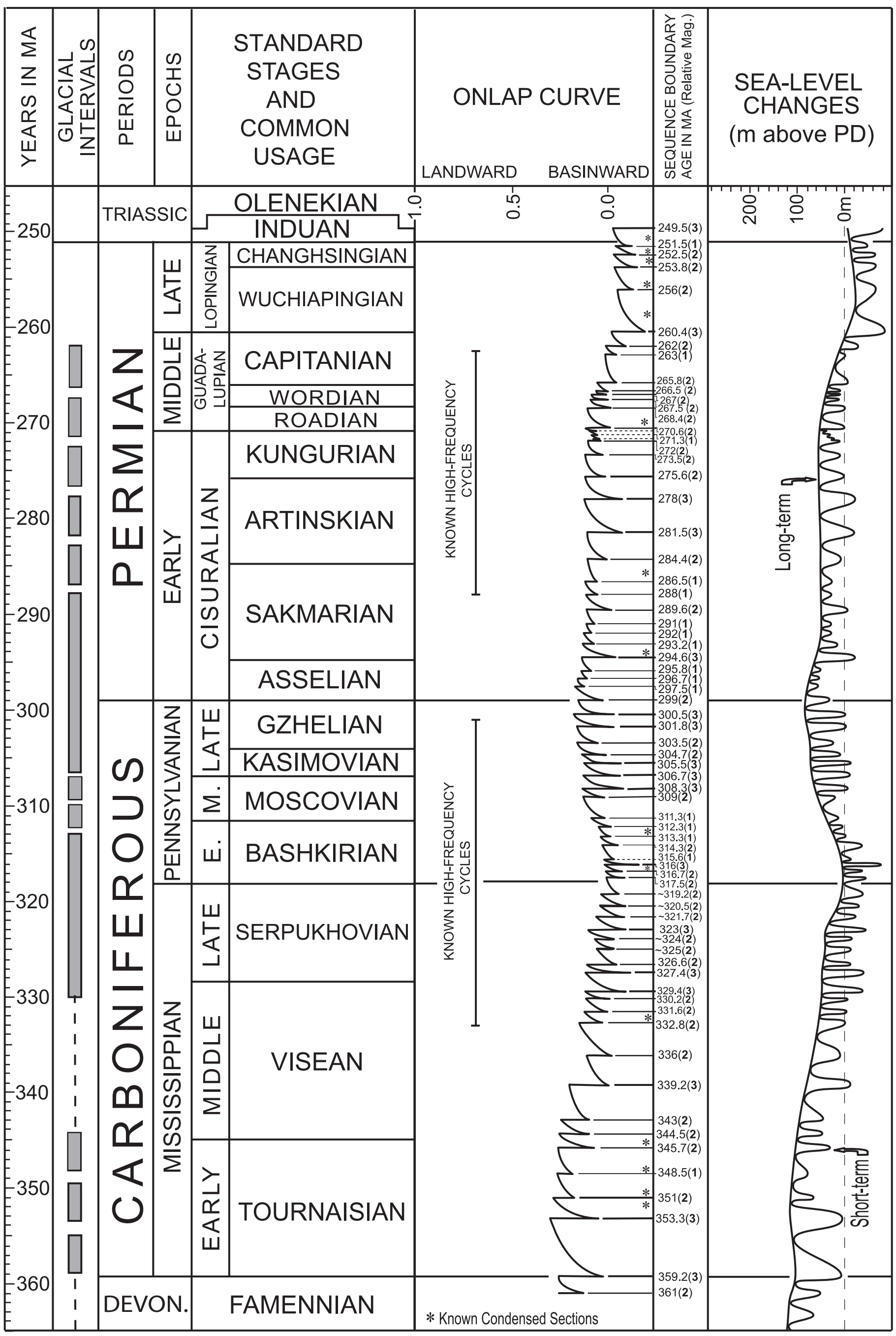

Fig. 3. Carboniferous-Permian sea-level changes. See the caption of Fig. 1 for details.

of the Early Permian. A sharp trend toward a declining sea level started in the mid-Permian (Roadian), culminating in the nadir of the sea level for the Paleozoic in the early Late Permian (Wuchiapingian). It began to recover in the latest Permian (Changhsingian), but the general low extended into the Early Triassic.

The shorter-term (third-order) base-level changes generally vary in duration from ~0.5 to 3.0 My (with the exception of Early-to-Middle Mississippian). One hundred seventy-two discrete third-order events (cycles) have been identified, with an average duration of ~1.7 My per cycle. In some intervals, the sections preferentially preserve fourth-order cycles, indicating a possible long-period orbital eccentricity control. Four such intervals have been identified so far: in the middle Cambrian (Toyonian to Mayan), middle Devonian (late Eifelian to Givetian), middle to late Carboniferous (late Visean to Kasimovian), and early to Middle Permian (Artinskian to Capitanian); however, fourth-order cycles may exist more widely. Whether this higher frequency is entirely due to higher sedimentation (a preservational effect) or the underlying signal (that is, long-term orbital forcing) is not always clear. The two younger intervals of higher-frequency cycles (in the Carboniferous and Permian) also coincide with periods of known glaciation, but for the two older intervals (the middle Cambrian and middle Devonian) no glaciation has been documented (*26–28*).

It should be noted that for the Early to middle Mississippian, the duration of most of the third-order cycles seem inordinately long (up to ~6.0 My). Although occasional long cycles (3 to 5 My) also occur at other times (for example, in the Cambrian through early Silurian), the consistent occurrence of long cycles in the Early to middle Mississippian may point to time-scale problems for this interval (the Tournaisian and Visean stages are also inordinately long, probably for the same reason).

We are unable to comment on all of the causes for shorter-term (third-order and fourth-order) eustatic changes in the Paleozoic. Although glaciation has been attributed to ~28% of the Paleozoic time (and suspected for another 10%), it has not been documented for the remainder of this era (*26–28*). Thus, waxing and waning ice sheets cannot be considered to be the only underlying cause for fluctuations in the Paleozoic sea level. Nevertheless, because the Paleozoic glacial record remains fragmentary, the question remains open. Conversely, there may be other, nonclimatic, causal mechanisms for short-term changes in sea level that still remain to be discovered.

References and Notes

1. J. Hardenbol *et al.*, *Soc. Econ. Paleontol. Mineral. Spec. Publ.* **60**, 3 (1998).
2. K. G. Miller *et al.*, *Science* **310**, 1293 (2005).
3. J. C. Van Wagoner, R. M. Mitchum, K. M. Campion, V. D. Rahmanian, *Am. Assoc. Petrol. Geol. Methods Explor. Ser.* **7**, 55 (1990).
4. *A Geologic Time Scale, 2004*, F. M. Gradstein, J. G. Ogg, A. G. Smith, Eds. (Cambridge Univ. Press, Cambridge, 2004), pp. 1–589.
5. J. G. Ogg, G. M. Ogg, F. M. Gradstein, *The Concise Geologic Time Scale* (Cambridge Univ. Press, Cambridge, 2008), pp. 1–178.
6. K. F. Kuiper *et al.*, *Science* **320**, 500 (2008).
7. Common Paleozoic biostratigraphic indicators include brachiopods, graptolites, chitinozoans, ammonoids, fusulinids, and conodonts. Brachiopods appear in the Early Cambrian and are common throughout the Paleozoic but tend to be provincial and facies-dependent, preferring shallow-water environments. Planktonic graptolites appear in the late Cambrian and persist through the early Devonian. They are particularly useful as index fossils in the Ordovician and Silurian, but they are more likely to occur in the basinal facies. Chitinozoa occur from Ordovician through Devonian and have been used successfully for the subdivision of this interval. Paleozoic ammonoids in general are common from the Devonian through the Permian and, although relatively widespread, they also show a considerable degree of provincialism or facies-dependence for some intervals. For example, the ammonoid *Goniatites,* preserved in Devonian-to-Permian strata, are strongly facies-controlled, preferring mostly the basinal environments of inland seas. Fusulinids have been used for biochronologic subdivision with varying degrees of success from the Late Mississippian through the Permian. Conodonts first appeared in the Cambrian and range through the Triassic. Their shallowest-water biofacies tend to be eurytopic, opportunistic, and long-ranging and thus only marginally useful for biostratigraphic resolution. But toward deeper waters they become more cosmopolitan and biostratigraphically meaningful. When deeper-water biofacies are present, conodonts are well suited for higher-resolution correlations from the Ordovician through the Permian interval.
8. W. A. van Sickel, M. A. Kominz, K. G. Miller, J. V. Browning, *Basin Res.* **16**, 451 (2004).
9. M. A. Kominz *et al.*, *Basin Res.* **20**, 211 (2008).
10. P. R. Vail, R. M. Mitchum, S. Thompson III, *Am. Assoc. Pet. Geol. Mem.* **26**, 63 (1977).
11. A. Hallam, in *Phanerozoic Sea-Level Changes* (Columbia Univ. Press, New York, 1992), p. 266.
12. B. U. Haq, A. M. Al-Qahtani, *GeoArabia* **10**, 127 (2005).
13. B. U. Haq, J. Hardenbol, P. R. Vail, *Soc. Econ. Paleontol. Mineral Spec. Publ.* **42**, 71 (1988).
14. D. U. Wise, in *The Geology of Continental Margin,* C. A. Burke, C. L. Drake, Eds. (Springer Verlag, New York, 1974), pp. 45–58.
15. *Phanerozoic History of Australia*, J. J. Veevers, Ed. (Clarendon Press, Oxford, 1984), pp. 1–418.
16. A. B. Ronov, *Am. J. Sci.* **294**, 777 (1994).
17. T. J. Algeo, K. B. Seslavinsky, in *Sequence Stratigraphy and Depositional Response to Eustatic, Tectonic and Climatic Forcing*, B. U. Haq, Ed. (Kluwer Academic, Dordrecht, The Netherlands, 1995), pp. 209–246.
18. M. Gurnis, *Nature* **344**, 754 (1990).
19. J. P. Cogné, E. Humler, V. Courtillot, *Earth Planet. Sci. Lett.* **245**, 115 (2006).
20. J. P. Cogné, E. Humler, *Earth Planet. Sci. Lett.* **273**, 251 (2008).
21. D. Müller, M. Sdrollias, C. Gaina, B. Steinberger, C. Heine, *Science* **319**, 1357 (2008).
22. For example, in the Middle and Late Cambrian, backstripped estimates from the Canadian Rockies yielded values of up to 250 m of change, whereas in Utah for strata of the same age, only ~100 m of change was estimated (*29*). In Iowa, nonbackstripped measurements from the Ordovician through Mississippian sequences provided estimates of a few tens of meters to ~100 m of change (*30*). Estimates from topographic relief of incised valleys in the Silurian yielded values of ~30 to >70 m of change worldwide (*24, 31, 32*). In the British Isles, a cumulative rise of 227 m in the Early Carboniferous and ~200 m in the mid-Carboniferous was indicated after partial backstripping, with the magnitude of individual third-order events ranging between 5 and 56 m (*33*). Estimates from the Late Mississippian yield magnitudes of 30 to 100 m of change in the Illinois Basin (*34*). Other estimates from North America in this glacially dominated interval imply minimum amplitudes of 80 m, reaching >100 m of change from preserved relief on subaerial exposure surfaces of large algal bioherms (*35*).
23. M. Rygel, C. R. Fielding, T. D. Frank, L. P. Birgenheier, *J. Sed. Res.* **78**, 500 (2008).
24. M. E. Johnson, J. Y. Rong, S. Kershaw, *N.Y. State Mus. Bull.* **491**, 3 (1998).
25. Because of scalar limitations, the Paleozoic cycle chart of sea level fluctuations is presented in three separate figures, each comprising two of the periods of the Paleozoic Era (Figs. 1 to 3). The SOM also includes a complete downloadable color PDF version (fig. S1) of the cycle chart with more details [for example, major orogenic and anoxic events, regional stratigraphic subdivisions and biozonations, and sequence nomenclature (*36*) and known carbonate megabreccias as they have been synthesized from the worldwide data. The latter tend to occur in the carbonate systems at major drawdowns of sea level].
26. M. V. Caputo, J. C. Crowell, *Geol. Soc. Am. Bull.* **96**, 1020 (1985).
27. N. Eyles, G. M. Young, in *Earth's Glacial Record,* M. Deynoux *et al.*, Eds. (Cambridge Univ. Press, Cambridge, 1994), p. 1.
28. J. L. Isbell, M. F. Miller, K. L. Wolfe, P. A. Lenaker, *Geol. Soc. Am. Spec. Pap.* **370**, 5 (2003).
29. G. C. Bond, M. A. Kominz, *Geol. Soc. Am. Bull.* **95**, 155 (1984).
30. B. J. Witzke, B. J. Bunker, *Geol. Soc. Am. Spec. Pap.* **306**, 307 (1996).
31. H. A. McClure, *Palaeogeogr. Palaeoclimatol. Palaeoecol.* **25**, 315 (1978).
32. D. Vaslet, *Episodes* **13**, 147 (1990).
33. W. H. C. Ramsbottom, *Proc. Yorkshire Geol. Soc.* **43**, 473 (1981).
34. L. A. Smith Jr., J. F. Read, *J. Sed. Res.* **71**, 985 (2001).
35. G. S. Soreghan, K. A. Giles, *Geology* **27**, 255 (1999).
36. L. L. Sloss, *Geol. Soc. Am. Bull.* **74**, 93 (1963).
37. Many regional experts, too numerous to name, both in the United States and abroad discussed the Paleozoic stratigraphic issues with us. Their insights were indispensable for our synthesis. B.U.H. acknowledges his release by NSF for a sabbatical during 2007 to complete this work. Much of that time was spent at the Institut Français de Recherche pour l'exploitation de la Mer, Brest, France. Their Marine Geosciences Department's (particularly S. Berne's) help in organizing the stay is gratefully acknowledged. S.R.S. in particular acknowledges P. Heckel for many valuable leads into Paleozoic eustasy and the state of Iowa for its amazing Paleozoic record. The authors also thank T. Algeo, A. Hallam, W. Hay, J. Ogg, and another anonymous reviewer for their comments and suggestions. We dedicate this work to our friends and colleagues Peter Vail, Jan Hardenbol, and Tony Hallam, pioneers in the study of sea-level changes of the past.

Supporting Online Material

www.sciencemag.org/cgi/content/full/322/5898/64/DC1
SOM Text
Fig. S1
References

11 June 2008; accepted 29 August 2008
10.1126/science.1161648

4) Brushy Canyon Formation

Trevor Hutton

Depositional Setting

- Deep water sand and siltstones
- Permian basin Complex of the Delaware Basin
  - Early Guadalupian (Permian) time
- During Deposition
  - 400-600m water depth
  - Surrounded by shallow marine shelfs
    - Diablo Platform
    - Central Basin Platform
- Paleocurrent direction NW>SE

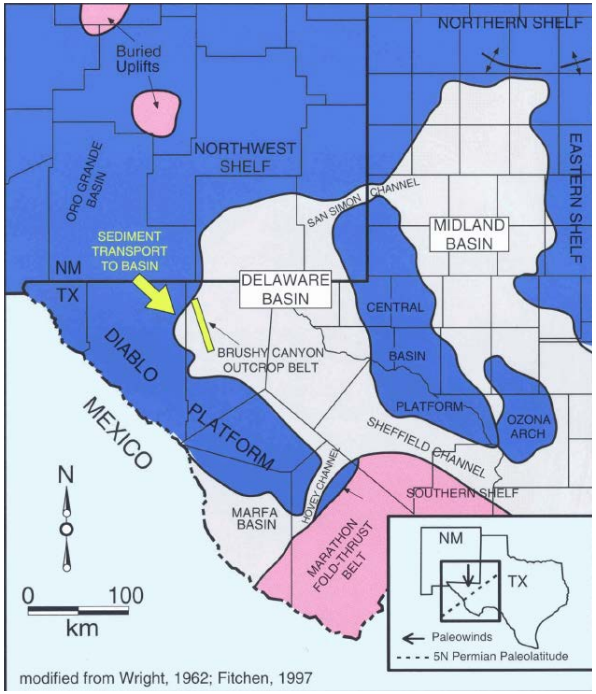

modified from Wright, 1962; Fitchen, 1997

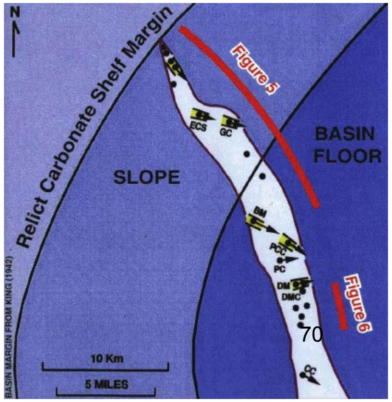

Brushy Canyon Sequence Stratigraphic Framework

- Basinally restricted marine sediments
- Third order lowstand sequence sets (110,000)
  - 3 laterally persistent sand units
    - Lower, Middle, Upper
    - Seperated by thin siltstones
      - 4th order (40,000 years)

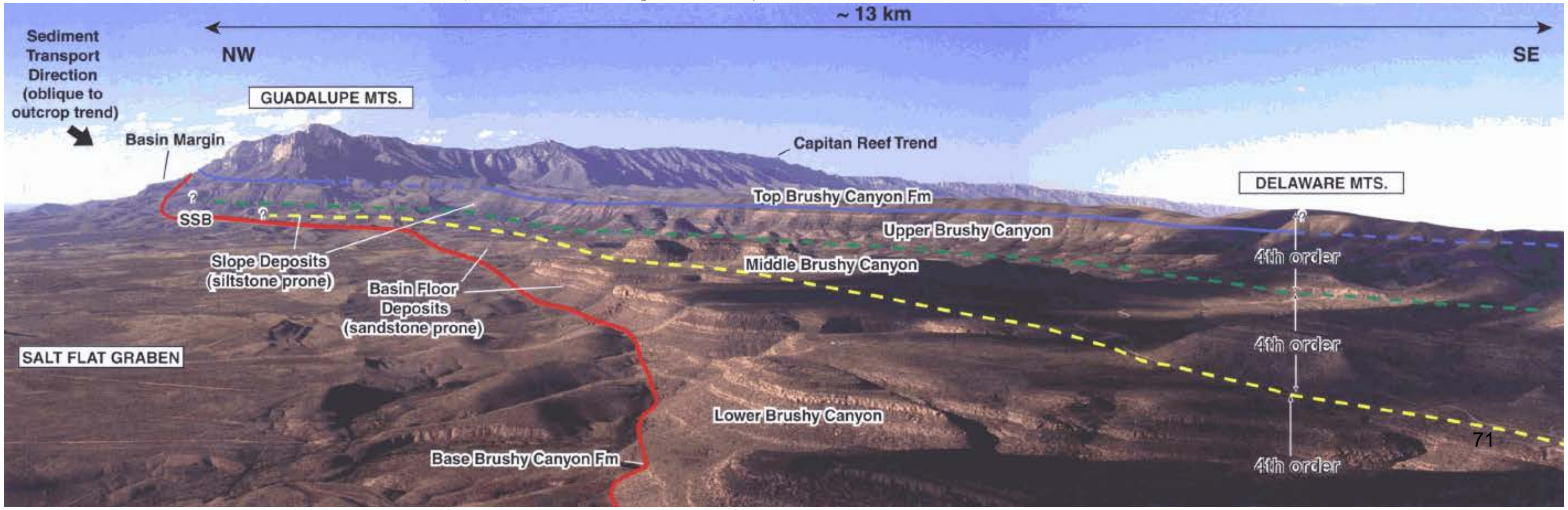

4th ordered units

- Upper
  - Very large, deeply incised multi story channel complexes
    - 1000 meters wide
  - Middle-lower slope
- Middle
  - Mix of laterally extensive sandstones
  - Large channels
    - Filled by massive sands
  - Proximal medial fan
- Lower
  - Sheet like tabular sandstone bodies
  - Medial outer fan

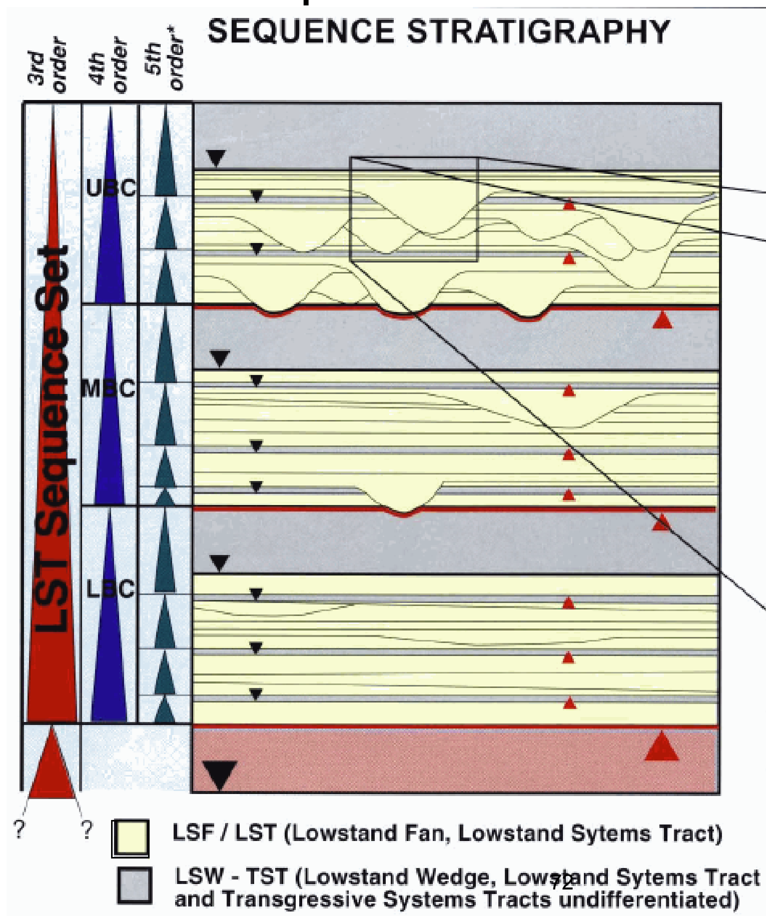

Brushy Canyon Deposits -Turbidites 90%

- Bedload Deposits
  - Grain size
    - >Coarse Sand
  - Stratification
    - Parallel lamination
    - Tabular and trough cross bedding
- Suspension Depostis
  - Grain size
    - <Medium Sand
  - Stratification
    - Structureless beds
    - Climbing dunes and trough cross bedding
    - Ripple and Parallel laminatinon
  - Sandy turbidites
    - 3m of transport per suspended load
      - Produce climbing ripples and duneforms
  - Silty turbidites
    - Thin bedded
    - Basin ward deposition resulting in wedge shaped packages

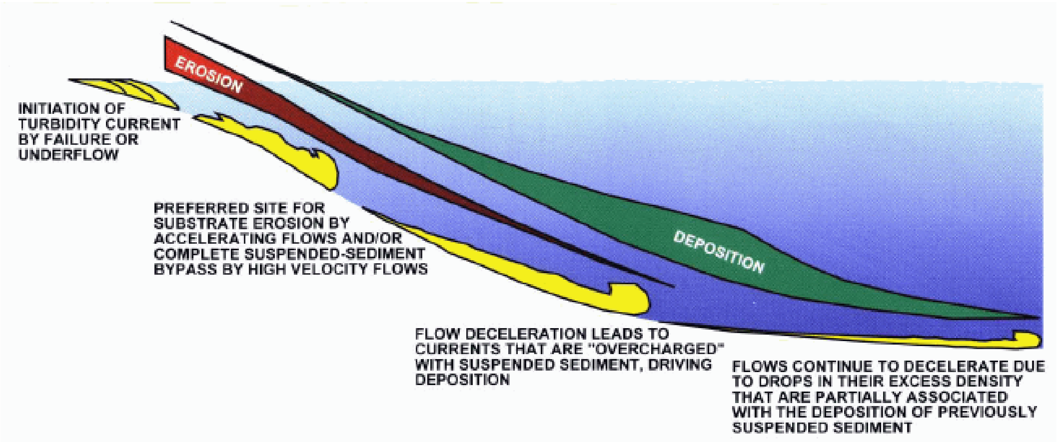

Brushy Canyon Deposits

- Debrites 5%
  - Gravels with sand filled pore space
  - Sandstones with small amounts of out-sized clasts as a result of underlying formations or intraformational rip-up clasts.
    - Pebbles
    - Cobbles
    - Boulders
- -Hemipelagites 5%
  - Mudstones from hypopycnal plumes
  - High Total Organic Content
  - Centimeter thick volcanic ash

Brushy Canyon Reservoir Quality

- Net porosity thickness maps illustrate reservoir quality sandstones came from Northwest shelf (turbidites).
- Depositional sandstone units seperated by 5ft-20ft thick layers of organic rich siltstones.
- Act as a seal for reservoir sandstones, and partly as source rocks.

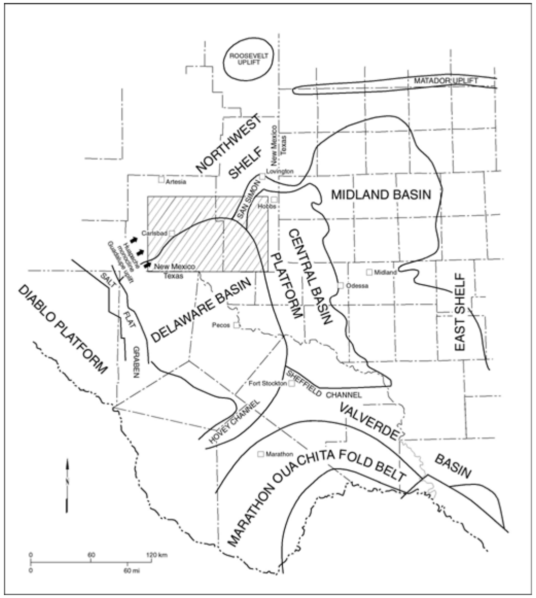

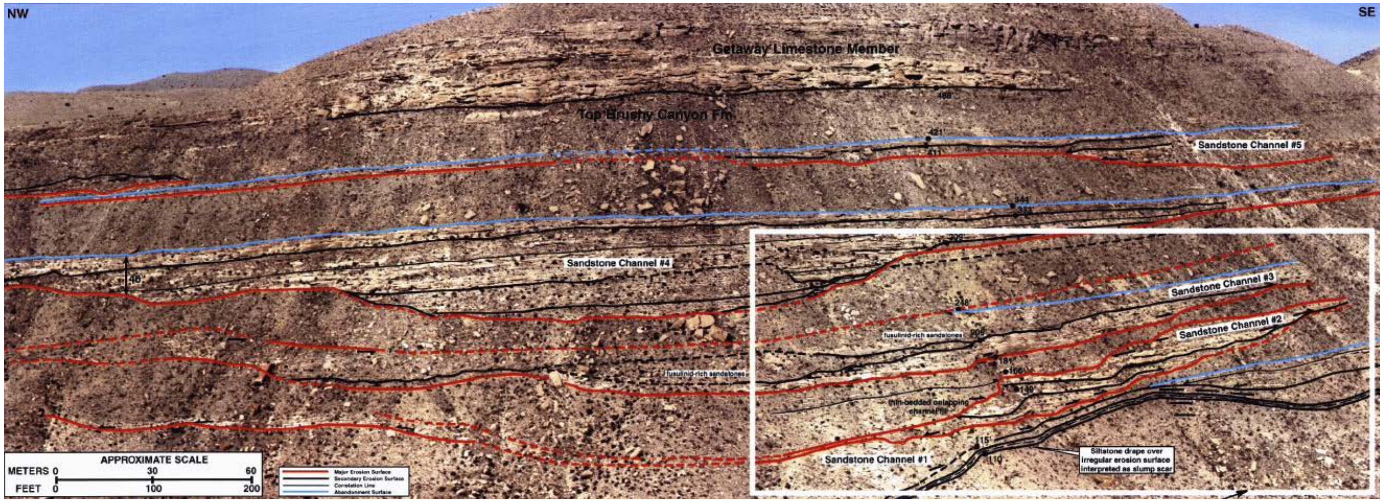

Brushy Canyon Formation, Texas: A Deep-Water Density Current Deposit

J. C. HARMS *Marathon Oil Company, Denver Research Center, P. O. Box 269, Littleton, Colorado 80120*

ABSTRACT

In mid-Permian time, the Delaware basin was a nearly circular deep, about 160 km in diameter. It was ringed by banks or reefs, which were surrounded in turn by very broad shallow shelves, lagoons, sabkhas, and alluvial plains. Broad tectonic downwarping caused deposition of about 1,000 m of sediment in the basin and neighboring shelves in both the Leonardian and Guadalupian Series (an average of 75 m/m.y.), whereas distant areas received only a fraction of those thicknesses. Although the basin and adjacent shelves accumulated nearly equal sediment thicknesses, appreciable slopes existed at the basin margins throughout mid-Permian time. Thus, the basin waters are estimated to have been more than 100 m deep in Leonardian time and as much as 600 m in late Guadalupian time. Simultaneously, bordering banks were very shallow or even emergent, and they prograded basinward several kilometers.

The basin margin is spectacularly revealed by a transverse fault in the Guadalupe Mountains. Here the relations of basin, slope, and shelf beds can be clearly seen.

The quartzose siltstone and sandstone of the Brushy Canyon Formation (the lower one-third of the Guadalupian Series), where they wedge out at the basin margin, are the topic of this study. These beds have been variously interpreted as shallow marine or deep turbidity current deposits. In my estimation, they are neither. Rather, they have unusual features that suggest deposition in relatively deep water by saline and cold density currents. Surrounding shelves provided these dense water masses.

Numerous basinward-trending channels are one product of these density currents. The channels are commonly 20 to 30 m deep, a kilometer or more wide, and extend far into the basin. Channel floors are flat, and the sides commonly slope 20° to 30°. The channels are filled in a special, though unordered, way. Finely laminated coarse- or medium-grained siltstone beds mantle channel floors, walls, and interchannel areas. Fine-grained, locally conglomeratic sandstone beds are confined to channel floors and abut the walls. Chaotic debris beds locally fill channels near the steepest basin slopes.

The basin waters were apparently density stratified. Dense shelf water, spilling through channels in surrounding banks, flowed down marginal slopes and along the basin floor. These denser flows cut channels or deposited sandstone beds confined to channels. At other times, less dense shelf water spread over more dense, stagnant basin layers, raining suspended silt over the irregular basin floor.

Characteristics that distinguish these density current deposits from the more common turbidity current deposits include (1) less evident proximal-distal changes (the same rock types and channel relations exist near the basin center as in outcrops 50 km away), (2) coarser porous sandstones confined entirely to channels (some channels have much sand and others little), (3) no levees or overbank deposits that would serve as channel proximity indicators, and (4) mostly ungraded sandstone beds that contain little finer matrix.

Similar density current deposits have not yet been recognized in other areas or geologic systems. However, they may be anticipated wherever basin waters were restricted sufficiently to become density stratified and where broad evaporitic shelves or lagoons bordered such basins.

Key words: stratigraphic geology, sedimentation, sedimentary structures, Permian, turbidity currents.

SUMMARY OF PROBLEMS AND INTERPRETATIONS

Permian strata exposed in the Guadalupe Mountains of Texas provide a basin-margin facies model that is widely known to sedimentologists. The relations between shelf, marginal, and basin sediments were first comprehensively clarified by King (1942, 1948). Newell and others (1953) added data to interpret the environmental conditions under which the celebrated reefs and associated deposits were formed. Although these studies are outstanding examples of regional facies interpretations and studies in adjacent areas (Boyd, 1958; Hayes, 1964; King, 1965) have substantiated most major conclusions, some

Geological Society of America Bulletin, v. 85, p. 1763–1784, 15 figs., November 1974

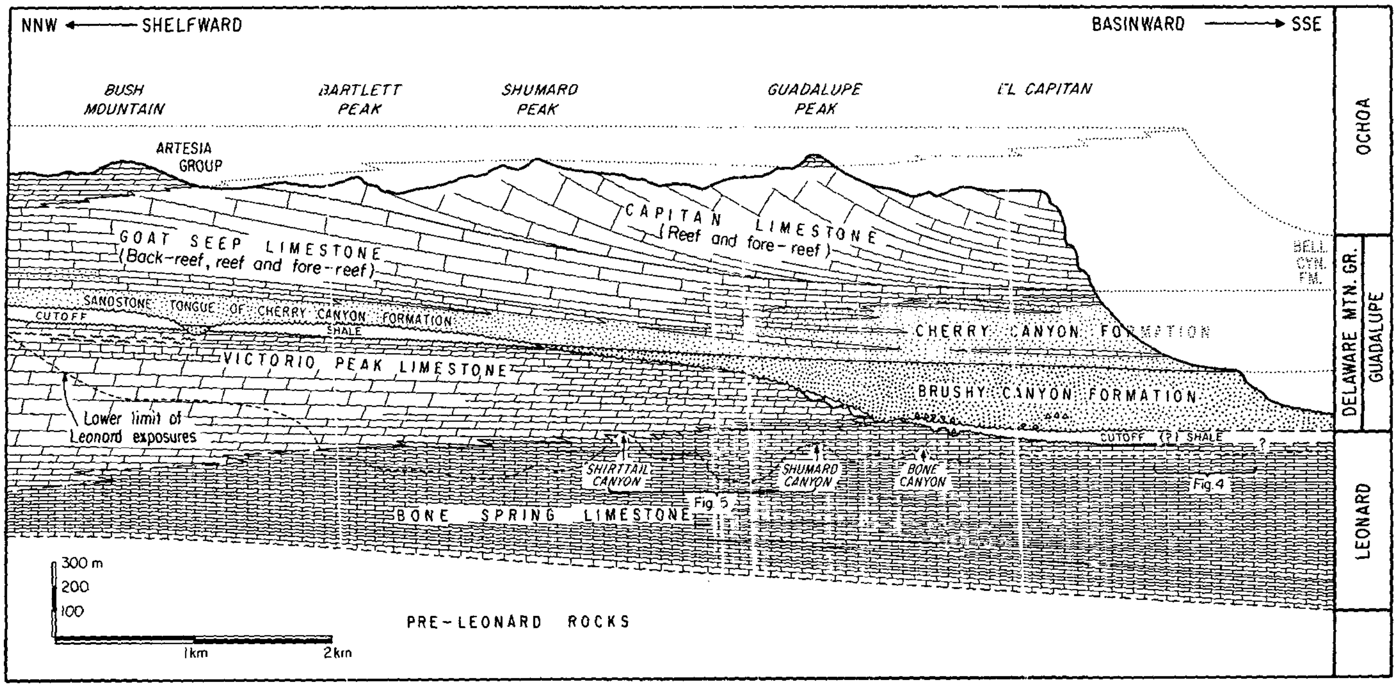

Figure 1. Cross section of west face of Guadalupe Mountains (adapted from King, 1948, and unpub. data of Pray and McDaniel). Location of topographic features shown in Figure 3.

troublesome problems remain. The depositional environments of some units are not thoroughly understood; the influence of tectonic adjustments or sea-level changes on sedimentation has been interpreted in various ways; and correlations between shelf, marginal, and basin facies have remained controversial for some parts of the section.

This paper summarizes studies of the Brushy Canyon Formation along the west face of the Guadalupe Mountains, where this siltstone and sandstone unit thins from 300 m and disappears in a distance of scarcely 3.5 km by onlap against a sloping surface of older basin and marginal carbonate rocks (Fig. 1). The Brushy Canyon Formation in this area allows study of some of the remaining important problems referred to above. For example, although Brushy Canyon rocks occupy a basin position, they had been interpreted as marine deposits laid down in shoal water by King (1948) and Newell and others (1953). In contrast, Hayes (1964, p. 52) and Jacka and others (1968) suggested a turbidity current origin on deep-sea fans. Because the Brushy Canyon Formation is enclosed between deeper basin sediments below and above, a shallow-water interpretation suggests an interruption of the evolution of the Delaware basin in early Guadalupian time (King, 1967, p. 44). Crustal movements or sea-level changes of at least local, and possibly regional, significance are implied. Neither an interruption of subsidence nor a greatly lowered sea level would be required if basin waters remained deep in early Guadalupian time. The Brushy Canyon Formation cannot be traced on outcrop to shelf equivalents, and correlation has been controversial. If water in the basin were shallow and surrounding shelves were widely emergent, this time interval would be represented by an unconformity of regional extent. However, equivalent shelf deposits would likely exist if the basin waters were deep and shelves were partly or wholly inundated.

These problems cannot be entirely resolved at this time because the Brushy Canyon Formation is not closely comparable to either agitated shallow marine deposits or deep-water turbidity current deposits as they are now understood. There is no compelling evidence that Brushy Canyon beds were deposited in shoal water or that the sloping surface against which these beds abut was ever subaerially exposed. But neither do most beds resemble turbidite units, and many characteristics suggest that sedimentation did not result from currents propelled by suspended fine material.

The outstanding features of the Brushy Canyon wedge exposed on the west face of the Guadalupe Mountains are numerous erosional channels of substantial dimensions. Typical characteristics of these channels and their filling sediments are summarized in Figure 2, along with inferred processes. Channel margins can commonly be traced cutting through 30 m or more of slightly older strata, in some places at angles exceeding 30°, and channel widths must exceed a kilometer in many cases. Channel trends, determined from strikes of channel margins and dips of cross-strata within channel-confined sandstones, point southeastward toward the center of the Delaware basin. Strong currents apparently flowed basinward approximately perpendicular to the local margin.

These channels are filled in an unusual way. Tabular beds of very fine to fine-grained quartzose sandstone, commonly containing pebbles and cobbles of Leonardian limestone or dolomite, can be traced extensively within channels, but they taper abruptly at sloping channel margins. Bedding surfaces are spaced at several centimeters to 2 m, most beds are ungraded, and stratification is horizontal or, less commonly, inclined. Interspersed between groups of these tabular sandstone beds are finely laminated medium- or coarse-grained siltstone beds that mantle channel floors, slopes, and interchannel areas without marked lateral thickness changes. These beds range in thickness from a few centimeters to many meters; their contacts with sandstone beds are sharp. There appears to be no preferred abundance of sandstone or siltstone within channels. Some are nearly entirely filled by sandstone and some by siltstone. Neither does there appear to be a systematic order to the fill; silt was deposited first in some channels, sand first in others.

The large volume of sediment removed suggests that channels were cut by powerfully erosive currents flowing basinward. They were filled partly by currents that transported sand and coarser debris tractionally in thin layers confined to channel floors and partly by other currents that flowed some substantial distance above basin floor irregularities and dropped suspended silt uniformly over existing bottom features (Fig. 2). Density currents, either hugging the bottom or moving over denser stagnant basin water, appear to have been the erosive and transport agent. These density currents are thought to be unlike most turbidity currents because graded beds are rare, sandstone and siltstone beds are sharply separated at their contacts, orderly vertical repetitions of lithologies or sedimentary structures are absent, and fine silt and clay form a negligible part of the basin-filling sediment. I believe that the higher density moving these currents basinward may have been gained largely by increased salinity or seasonally lowered temperature of shelf waters (Harms, 1968). If this analysis is correct, these currents may have flowed rather steadily and been less catastrophic or episodic than turbidity currents.

Density currents may have dominated sedimentary processes in the Delaware basin during all of Guadalupian and part of Leonardian time. Channels similar to those of the Brushy Canyon Formation are found scattered throughout the overlying Bell Canyon and Cherry Canyon Formations in outcrop areas near the Guadalupe Mountains, although the channels are less numerous and contain only very fine grained sandstone. Similar channels, some containing oil, can be inferred in the subsurface in the upper part of the Delaware Mountain Group throughout much of the Delaware basin, based on studies of cores and mechanical logs. These sedimentary layers are known to have been deposited in water depths ranging from 300 to 600 m because of relations to reef-talus tongues (King, 1948; Newell and others, 1953). A turbidity current origin for these channels was suggested by Nottingham (1960) and Meissner (1972, Figs. 12 and 13), but Motts (1972) invoked basinward-flowing brines during later Guadalupian time from studies of the northern shelf.

The striking angular discordances noted in the Bone Spring Limestone and the Cutoff Shale around Bone Canyon (King, 1948; Newell and others, 1953) — variously interpreted as unconformities or slides — also resemble in most important respects the Brushy Canyon channels. They differ because they occur in carbonate-dominated sequences and have fills that are largely thin, mantling beds of lime mud (Fig. 6F). However, I believe that they reflect a density current process like that of the Delaware Mountain Group.

The Brushy Canyon Formation was probably deposited while relatively deep water covered the Delaware basin. Because no shoal-water facies have been positively indentified over a 300-m interval where the formation abuts against older Leonardian rocks and because similar sedimentary features occur in younger Delaware Mountain Group rocks deposited in depths of several hundred meters, I believe that maximum water depth must have exceeded 300 m in early Guadalupian time. Perhaps some local areas within the Guadalupe Mountains and the Sierra Diablo were emergent from time to time, but I cannot point to positive evidence. Therefore, water depth in the basin exceeded 300 m by an unknown amount. If water depths were great, then there was no interruption in the evolution of the Delaware basin. Basinal environments persisted from Leonardian, through Guadalupian, and into Ochoan time. The shelf areas to the west and northwest were at least partly inundated in early Guadalupian time and were sites where dense (saline or cold) water masses developed before flowing basinward. The spawning ground of these water masses would likely be represented by sediments ranging from the middle San Andres Limestone to the lower Artesia Group interval, but somewhat limited exposures, intraformational unconformities, and rather general paleontologic age determinations make positive identification of strata equivalent to Brushy Canyon difficult.

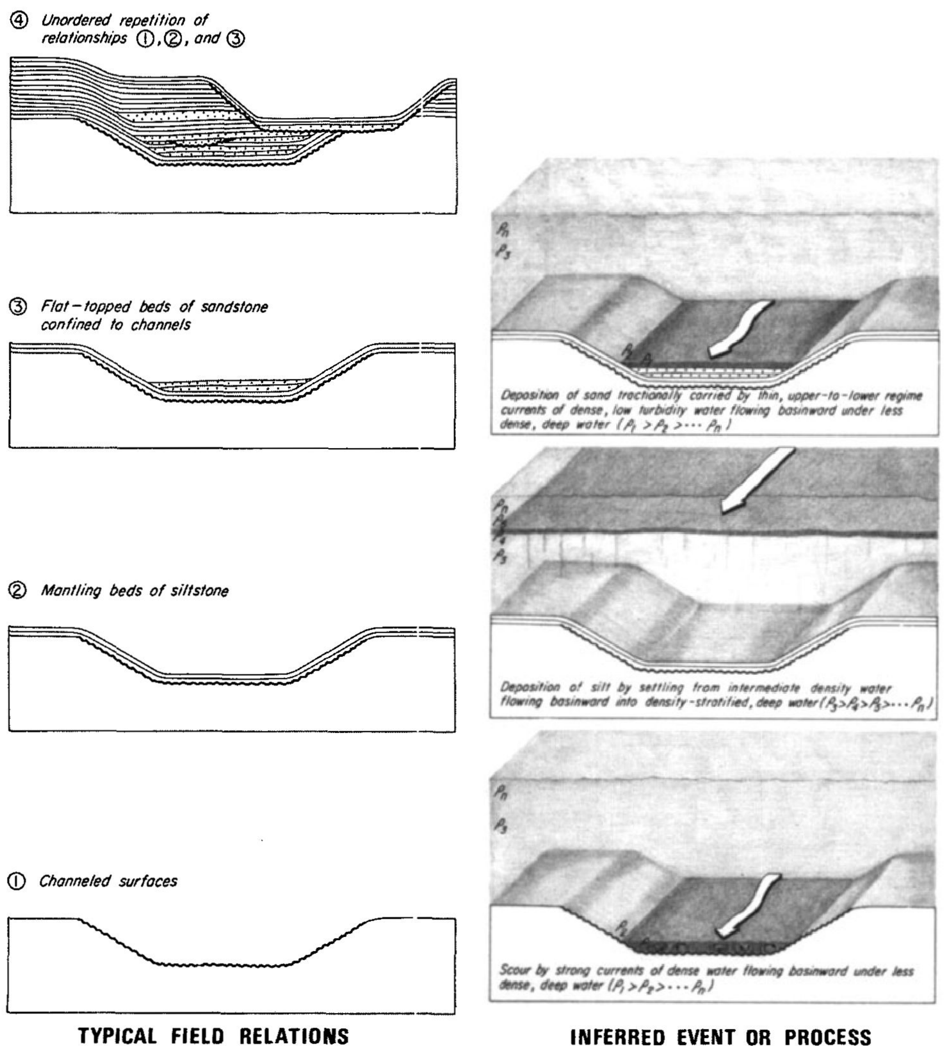

Figure 2. Typical bedding relations in Brushy Canyon Formation and their interpretations.

SUMMARY OF PERMIAN HISTORY

Geologic events in west Texas and southeastern New Mexico have been studied extensively by many workers. The history of the Guadalupe Mountains area has been summarized by King (1942, 1948), Adams and Frenzel (1950), Newell and others (1953), Boyd (1958), and Hayes (1964). Permian tectonic history and sedimentation in surrounding areas were reviewed by Oriel and others (1967), and regional correlations, lithofacies maps, cross sections and interpretive maps of sources, barriers, and basins for each of the Permian series were

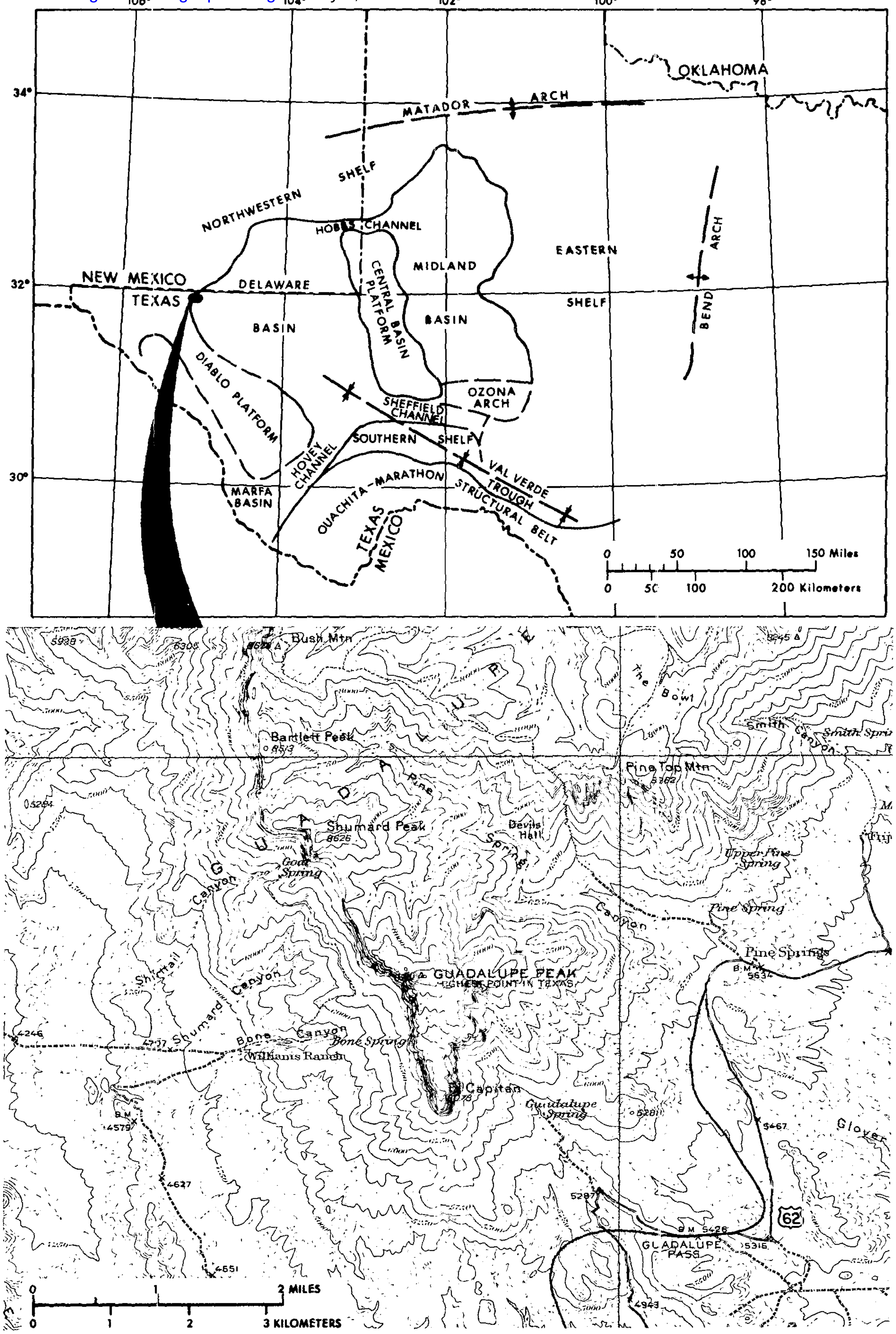

Figure 3. Regional structural setting (after Oriel and others, 1967) and topographic map of Guadalupe Mountains area.

presented by McKee and Oriel (1967). Meissner (1972) presented regional correlations and facies relations for the Middle Permian for a large area within the Western Interior.

Major tectonic elements, shown in Figure 3, were defined in Pennsylvanian time and persisted as relatively positive or negative features through all of Permian time (Oriel and others, 1967). The negative features, such as the Delaware basin, received basinal deposits through most of Permian time, whereas positive features received shelf facies. Carbonate reefs or banks developed in marginal zones between basins and shelves or platforms in the Leonardian and Guadalupian Series, when they accentuated and perpetuated tectonic boundaries (King, 1967).

Events in Leonardian, Guadalupian, and Ochoan time in the Guadalupe Mountains of Texas are summarized in Figure 1. Within the Delaware basin, the Leonardian Series is a mass nearly 1,000 m thick of black, thin-bedded limestone with some argillaceous or siliceous beds, the Bone Spring Limestone. The dark lime mud lithology apparently formed in a stagnant basin with deep water. The upper part of the Leonardian Series changes shelfward to the Victorio Peak Limestone, which is calcitic or dolomitic, light gray, thickly bedded, and fossiliferous. The Victorio Peak is interpreted as a bank deposit because frame-building organisms are sparse (King, 1948, p. 27). The bank margin migrated basinward a distance of nearly 5 km during later Leonardian time and about 450 m of Victorio Peak limestone layers were deposited. Water depths in the Delaware basin near the margin were estimated as more than 100 m by Newell and others (1953, p. 190) and McDaniel and Pray (1967) and as 300 m by King (1948). Shelfward, the Victorio Peak interval changes to thin-bedded limestone and dolomite with fewer fossils and evaporite beds composing the Yeso Formation and the lowest part of the San Andres Limestone (Boyd, 1958, Pl. 6E; Hayes, 1964, p. 24).

Rocks older than the Leonardian Series are not exposed in the Guadalupe Mountains, but in the nearby Sierra Diablo, persistent flexing at the basin margin late in Pennsylvanian and in Wolfcampian time is evident (King, 1965). This flexing, and a resulting unconformity between the Wolfcampian and Leonardian Series that probably fades out in the basin, formed the site upon which Victorio Peak and Bone Spring facies changes were superposed. The pre-Leonardian substrate in the Guadalupe Mountains is probably similar to that of the Sierra Diablo. Recurrent flexing occurred through Leonardian time along the Bone Spring flexure in King's (1948) opinion because stratigraphic complexities and folds are evident in Bone Spring limestone along the west side of the Guadalupe Mountains.

The sea deepened near the end of Leonardian time, and dark-gray siltstones and thin-bedded limestones about 70 m thick (Cutoff Shale) were deposited over Victorio Peak bank facies. Cutoff lithologies have distinctly basinal characteristics that can be traced about 20 km northwest from the earlier Leonardian basin margin, where these fine-grained, dark-colored rocks interfinger with typical shelf facies of the lower part of the San Andres (Boyd, 1958, Pl. 6E). Deeper basinal equivalents to the Cutoff Shale are undoubtedly present in the Delaware basin, but assignment of correlative strata has been varied (as reviewed by King, 1965, p. 78).

Cutoff beds cannot be traced continuously across the confusing rocks of the Bone Spring flexure. Pray (1971) suggested that the Cutoff in that area is bounded by two unconformities that locally intersect. The lower unconformity truncates more than 200 m of Victorio Peak beds and may extend shelfward as a disconformity, accounting for the lack of interfingering between the Victorio Peak Limestone and the Cutoff Shale observed by Boyd (1958). The upper of these two unconformities forms the base of the Brushy Canyon Formation and extends shelfward as a disconformity between the Cutoff Shale and the sandstone tongue of the Cherry Canyon Formation (Fig. 1). The confused relations in the Cutoff interval across the Bone Spring flexure probably reflect the influence of steep slopes inherited from the Victorio Peak bank and perhaps structural flexing during latest Leonardian time. Numerous angular relations and bodies of coarse debris indicate that erosion and mass transport occurred repeatedly in this area during deposition of the Cutoff shale. Carbonate masses interpreted by Newell and others (1953, p. 97) as patch reefs have been reinterpreted as allochthonous blocks by Pray and Stehli (1962). These blocks are thought to occur between unconformities of Cutoff age (Pray, 1971).

During the first part of Guadalupian time, the basin area received the quartzose siltstones and very fine to fine-grained sandstone of the Brushy Canyon Formation described in the first part of this paper. The Brushy Canyon Formation cannot be traced in outcrop to shelf equivalents (King, 1948; Newell and others, 1953). Because the Brushy Canyon Formation rests in places on beds mapped as Cutoff and contains pebbles and cobbles lithologically like the Cutoff, it appears to be entirely younger than Cutoff Shale. The time span of Brushy Canyon deposition is represented by a disconformity between the sandstone tongue of the Cherry Canyon Formation and the Cutoff Shale over a shelf barrier including much of the Guadalupe Mountains and the Sierra Diablo. In other parts of the shelf, the middle part of the San Andres Limestone may have been deposited at the same time as the Brushy Canyon Formation (Hayes, 1964, p. 28). Correlations by Boyd (1958, Pl. 6E) support this possibility. The Brushy Canyon Formation was correlated with the lower or middle part of the San Andres Limestone by Vertrees and others (1964) and Silver and Todd (1969, Fig. 12) from subsurface data in the northern part of the Delaware basin, where basin, marginal, and shelf facies may be continuous. However, correlations based on paleontologic and stratigraphic evidence remain controversial; Meissner (1972, Fig. 2) correlated the Brushy Canyon Formation with only the uppermost San Andres, as well as the lower part of the Artesia Group.

In mid-Guadalupian time, siltstone and sandstone of the Cherry Canyon Formation extended about 15 km shelfward from the margin of the Victorio Peak bank (Boyd, 1958, Pl. 6E). There the sandstone tongue of the Cherry Canyon Formation passes into patch reefs and detrital limestone banks of the San Andres Limestone (Boyd, 1958, p. 24–27; Hayes, 1964, Fig. 14).

The least certain portion of Leonardian and Guadalupian history is recorded in the Brushy Canyon Formation and the disconformity between the Cutoff Shale and the sandstone tongue of the Cherry Canyon Formation. If the Brushy Canyon Formation was deposited in shallow water and broad parts of the shelf to the northwest were emergent, then there was certainly a pause in subsidence and the evolution of the Delaware basin (King, 1967, p. 44). If, on the other hand, the Brushy Canyon Formation was deposited in deep water, as I believe, and the Cutoff unconformities developed in deep water (Pray, 1971), then the Cutoff Shale and the sandstone tongue of the Cherry Canyon Formation, both basinal in aspect, record the maximum incursion of basin environments across the shelf.

Development of the spectacular Goat Seep and Capitan limestone reefs or banks followed the Cherry Canyon sandstone tongue. The Goat Seep reef grew from a foundation approximately above the older Victorio Peak bank, and it built mainly upward, but the Capitan reef built significantly basinward (for a review of these basin-margin deposits, see Dunham, 1972). By the end of Guadalupian time, the reef front had advanced nearly 5 km basinward (Fig. 1). The reefs interfinger dramatically with the siltstone and sandstone of the Cherry Canyon and Bell Canyon Formations in the Delaware basin. Tongues of reef talus can be traced down steep slopes and in some cases extend many kilometers into the Delaware basin as flat-lying carbonate turbidites; they provide valuable marker beds in the otherwise monotonous basin sequence (King, 1948; Newell and others, 1953). All of the carbonate rocks were derived from the reef or reef slopes, although the lowest of the units (lower Getaway) was interpreted as containing patch reefs by Newell and others (1953, Fig. 50). These masses are reinterpreted as allochthonous blocks derived from the Goat Seep reef.

Shelfward, the Goat Seep and Capitan limestones interfinger with deposits known collectively as the Artesia Group. Facies boundaries strike northeast-southwest (Hayes, 1964, Fig. 9). The lithologies include dolomite, dolomitic limestone, sandstone, gypsum, and red siltstone and are interpreted as restricted lagoonal deposits (Newell and others, 1953; Boyd, 1958) or, in part, as dominantly supratidal flats or sabkha deposits (Kerr and Thomson, 1963; Meissner, 1972). The Artesia Group of the shelf has been correlated with the Delaware Mountain Group of the basin by invoking cyclic changes in sea level (Meissner, 1969, 1972; Silver and Todd, 1969). Their hypothesis states that during periods of raised sea level, carbonate was deposited over both shelf and basin, whereas during lowered sea level, terrigeneous clastics were spread across the shelf and into the basin. Frequent exposure of marginal facies by sea-level changes of a few meters or a few tens of meters is supported by the occurrence of vadose solution breccia and pisolite beds (Dunham, 1965, 1969, 1972; Thomas, 1968). However, large variations in sea level like those implied by Silver and Todd (1969, Fig. 6) have not been proven as numerous. Silt-filled cracks extending downward at least 150 m into marginal talus beds have been reported by Dunham (1972) and interpreted as evidence of some low sea-level stands. But correlative shallow-water deposits of later Guadalupian age have not been recognized in the Delaware basin as yet.

Growth of reefs along the Delaware basin was apparently terminated at about the beginning of Ochoan time. Evaporite deposition beginning in early Ochoan time was confined mainly to the Delaware basin (McKee and Oriel, 1967, Pl. 6B). Most evidence indicates that these varved evaporite units formed in fairly deep, unagitated water (Anderson and others, 1972). Although the changes causing this radical shift in style of sedimentation are largely speculative, it seems likely that an effective barrier to free circulation developed at the southern oceanward end of the basin (King, 1967, p. 44).

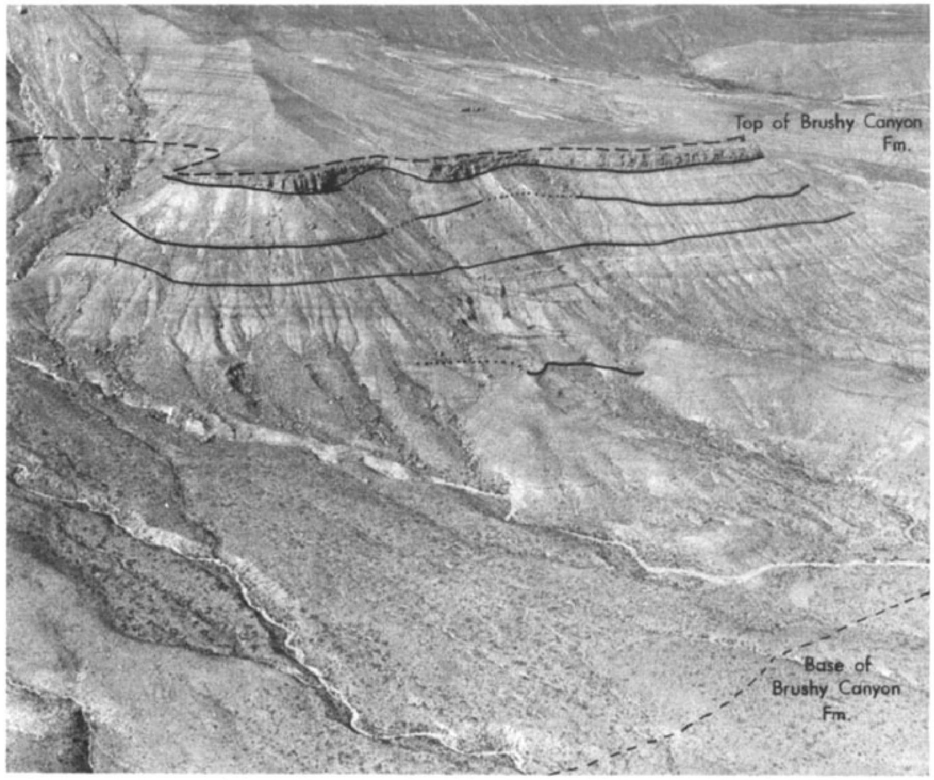

Figure 4. Oblique aerial view of west face of Guadalupe Mountains near southern foot of El Capitan. Area covered indicated on Figure 1. Solid and dotted lines mark positions or inferred positions of prominent erosion surfaces.

FEATURES OF BRUSHY CANYON FORMATION AND INTERPRETATION

Erosion Surfaces and Channel Fills

The Brushy Canyon wedge thins from 300 m and disappears in a distance of 3.5 km along the west face of the Guadalupe Mountains, shown diagrammatically in Figure 1 and by oblique aerial photographs in Figures 4 and 5. Within this wedge of siltstone and sandstone, erosion surfaces are common and exert an important control on local distribution and attitude of beds. These surfaces form flat-floored, steep-walled channels; very fine to fine-grained, conglomeratic sandstone beds are restricted to channel floors and abut against the steep channel walls, whereas laminated siltstone beds extend across channel floors, slopes, and interchannel areas without appreciable thickness changes.

Typical characteristics of the channeled surfaces and underlying and overlying beds are sketched in Figure 2 and illustrated with photographs in Figure 6. The channels formed by these erosion surfaces appear to have fairly flat floors and steep walls dipping commonly between 10° and 30°. Locally narrower channels are cut into the broader flat floors (Fig. 6D). No coarser lag deposit or erosional steps are consistently formed at these erosion surfaces, so that the exact position of such diastems are difficult to identify along channel floors or in interchannel areas where overlying and underlying beds are nearly parallel. The position of the erosion surfaces is easy to see at channel margins where sandstone beds taper abruptly or siltstone beds diverge dramatically from underlying bed attitudes (Fig. 6).

The scale of channels observed in the Delaware Group ranges from large to small. The largest amount of local scour observed within Brushy Canyon beds was 30 m of erosional relief along the west front of the Guadalupe Mountains, but 20- to 30-m deep channels are quite common. Evidence of channeling on a small scale has been reported broadly throughout the Delaware Group (King, 1948, p. 29; Newell and others, 1953, Fig. 47). Channels of large size are most easily identified along the mountain front where topographic relief is large, whereas smaller channels can be recognized in even the poorer outcrops in the rolling hills east of the mountain front.

The channels trend generally southeastward, and channel margins slope as steeply as 35°. The attitudes of channel margins are summarized as poles plotted on an equal-area projection in Figure 7, indicating trends range from east to south. These

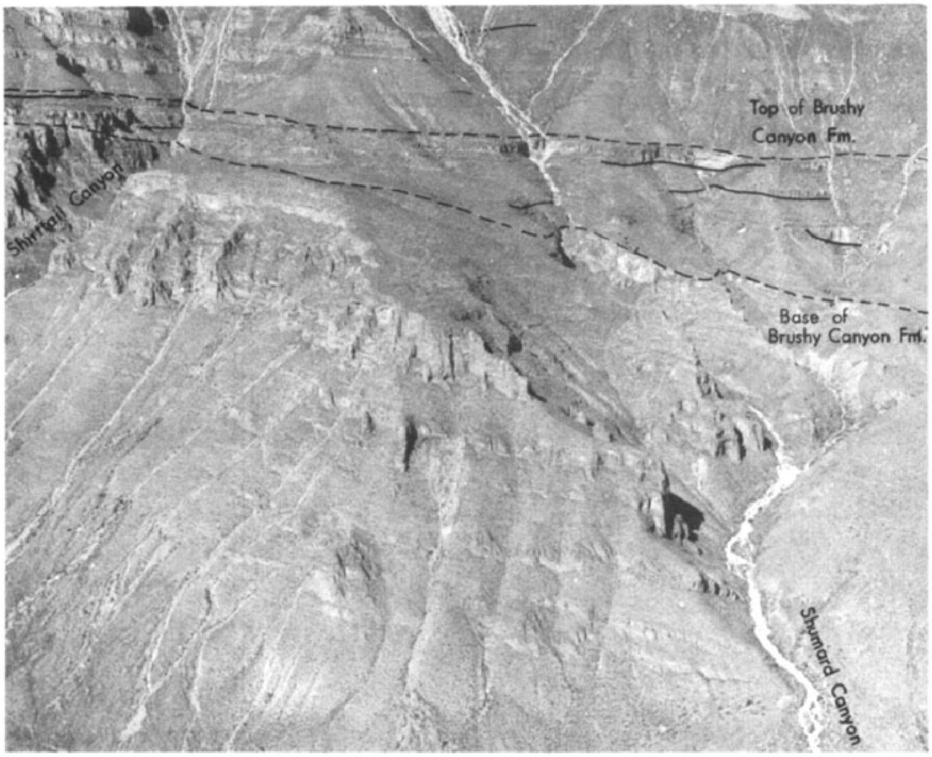

Figure 5. Oblique aerial view of west face of Guadalupe Mountains between Guadalupe and Shumard Peaks. Area covered indicated on Figure 1. Solid lines mark positions of prominent erosion surfaces.

orientation data were derived from nearly equally spaced stratigraphic sections along the west face of the Guadalupe Mountains and are thought to be quite representative for that area. Currents causing erosion and transport appear to have flowed basinward, based on the dip of cross-strata observed in channel-filling sandstone or the asymmetry of rare flute marks observed on the erosional surfaces.

The sequence of lithologies filling these channels is not orderly. The fill begins with siltstone in some cases and sandstone in others. Neither is the proportion of these two lithologies uniform among channels; some are filled mainly by siltstone and some by sandstone. I do not agree with the contention of Hull (1957, p. 301) that the Brushy Canyon Formation is cyclic and orderly.

Major Lithologies

The common lithologies in the Brushy Canyon wedge along the west face of the Guadalupe Mountains are finely laminated siltstone, coarsely laminated to massive sandstone, and massive boulder or cobble conglomerate. In the area from the pinchout of the Brushy Canyon Formation to a distance 7 km southward (Fig. 1), laminated siltstone composes about 65 percent of the section, sandstone about 35 percent, and coarse conglomerate less than 1 percent.

Mineralogy. Brushy Canyon sedimentary rocks are composed of quartz, feldspar, and carbonate clasts (Fig. 8). Hull (1957) presented a summary of petrologic data. Quartz is commonly the most abundant constituent. Most grains are single crystals showing undulatory extinction; maximum diameters range up to 0.5 mm. Feldspar is also common in the coarse silt to very fine sand size range. Potassium feldspar is somewhat more abundant than sodium plagioclase. Carbonate is a common constituent of most Brushy Canyon beds and occurs as both cement and clasts. Laminated siltstone beds (Fig. 8A, B) have the lowest average total carbonate content; carbonate determined by acid leaching averages 15 percent by weight and is rarely less than 5 percent or more than 25 percent. Sandstone samples (Fig. 8C, D, E, F) have a 25 percent average carbonate content, but the range is large; some individual samples contain only a few percent carbonate, whereas other thin beds would be classified as quartzose calcarenite (Fig. 8F).

Carbonate clasts are of four types. Very finely crystalline dolomite grains of silt-to-sand size are common throughout the Brushy Canyon sedimentary rocks. These dolomite grains have approximately the same size range as the quartz grains that they accompany; they were apparently derived from lithified dolomite beds to the west or north, and their abundance suggests significant erosion in the shelf area during Brushy Canyon deposition. Other dolomite grains are euhedral or subhedral single crystals (Fig. 8C). This second type of dolomite grain is restricted to very fine sand or silt-size sediments; although an authigenic origin could be argued for some grains of this type, most of the rhombs are approximately the same size as the quartz grains with which they are associated, are much larger than open pore spaces, and appear from petrographic details to have a clastic rather than a diagenetic (replacement) origin. Fossil fragments are abundant in some sandstone beds; entire or slightly worn fusilinids are the most abundant fossil constituent (Fig. 8D), but fragmented brachiopods, bryozoans, and crinoids are also fairly common (Fig. 8E, F). Carbonate clasts of pebble, cobble, or boulder size are observed either as pebbles scattered in sandstone beds throughout the Brushy Canyon interval or within massive conglomerate beds concentrated near the base of the formation. A wide variety of carbonate lithologies is represented in these larger clasts, but all varieties are similar to those observed in the Victorio Peak Limestone and the Cutoff Shale near the pinchout of the Brushy Canyon Formation.

Clay minerals and mica form a very small fraction of the total volume of the Brushy Canyon sediments. In even the finest grained beds, with median diameters of 10 to 15 μm, quartz and feldspar form the bulk of the detrital constituents (Fig. 8B). Organic detritus composes most of the fine material that marks lamination in these siltstones.

Diagenetic alterations of Brushy Canyon sediment are commonly extensive and complex, but this aspect of lithology was not studied in detail. Quartz overgrowths on grains are quite common in most sandstone; evidence of carbonate replacement of quartz grains is also common, suggesting that the redistribution of silica may be rather local. Calcite is an abundant cement in sandstone and in coarser laminae of siltstone (Fig. 8A, F). Calcite cement is less abundant in the upper part of the Brushy Canyon interval in sections south of Bone Canyon. Calcite stains show subtle tonal variations that suggest variable iron content on a small scale and in complex patterns. Dolomite commonly cements or replaces grains in both sandstone and siltstone (Fig. 8E). Dolomite of certain authigenic origin occurs as rhombs a few microns in size; other larger rhombs may be either authigenic or transported. Iron content of the dolomite varies from crystal to crystal in the same sample, based on differences in color when stained. Pyrite is a common authigenic constituent in organic-rich layers.

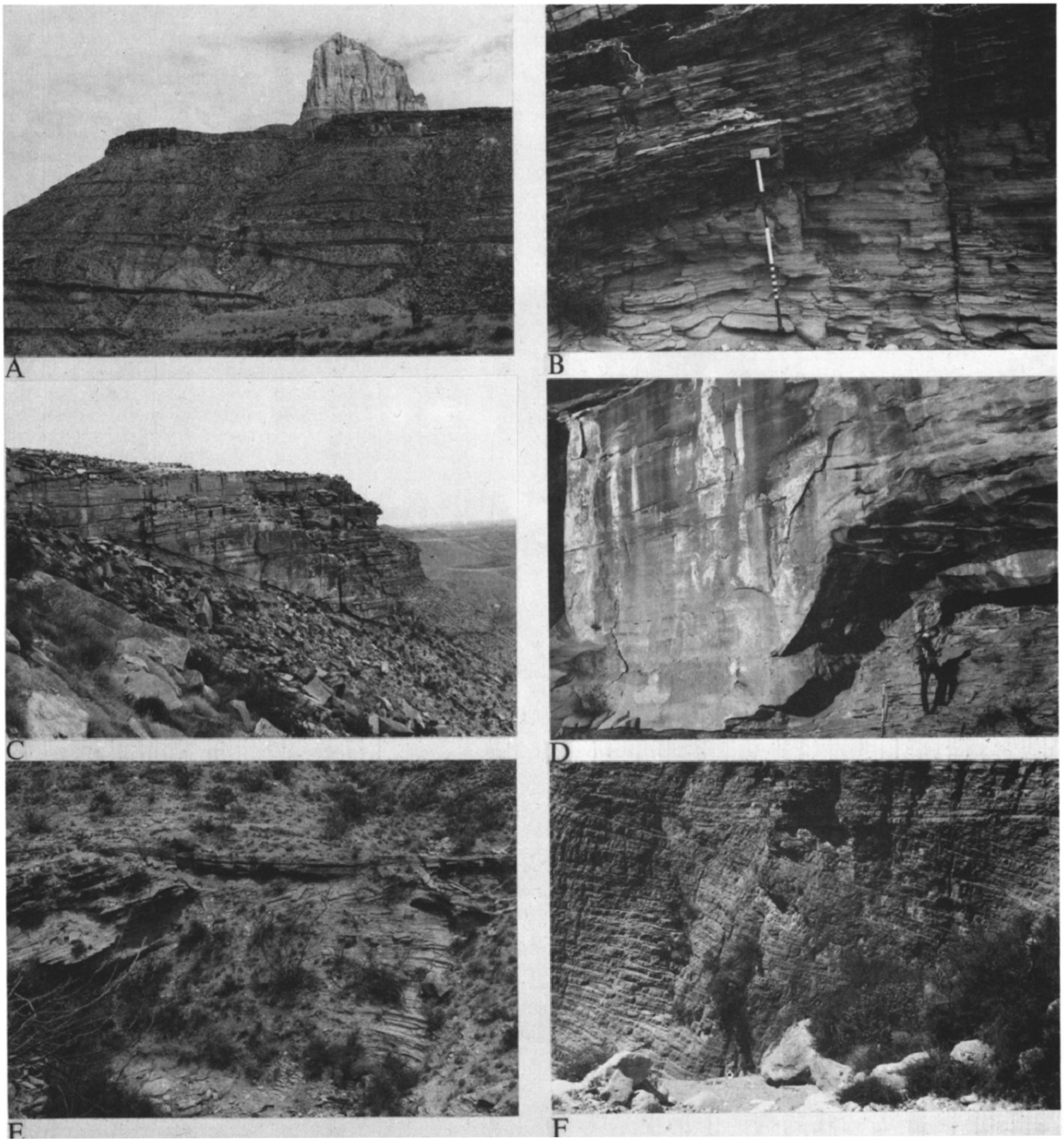

Figure 6. Channel margins and bedding relations. A. Mantling beds of dark-gray siltstone diverge about abutting beds of sandstone. Erosion surface controlling slope of mantling beds lies just below level of foreground. B. Medium-grained siltstone mantling an erosion surface (staff is 1.5 m). C. Flat-topped beds of sandstone abutting against steep channel wall. D. Local scour within channel-fill complex. E. Two intersecting erosion surfaces and their mantling siltstone beds. F. Two intersecting erosion surfaces and their mantling lime silt beds (Bone Spring Limestone, Bone Canyon).

Small phosphatic nodules occur in some of the finest siltstone beds with abundant organic material.

Dickite, a clay of the kaolin group, and hematite occur in small amounts as authigenic fillings of fossil chambers or vugs in carbonate clasts. I have noticed these minerals only in conglomerate and sandstone of the lower part of the Brushy Canyon Formation in the vicinity of Bone Canyon. The dickite, identified by x-ray diffraction using powder mounts by J. B. Hayes (1970, personal commun.), forms plates as broad as 10 μm arranged in vermiform stacks. Commonly thought of as an authigenic mineral that indicates somewhat elevated temperatures, dickite in the Brushy Canyon Formation is puzzling because other evidence of deep burial or hydrothermal activity is lacking. Hematite occurs as infill of angular vugs; individual crystals range in size up to 1 mm and radiate from vug margins.

Laminated Siltstone. Laminated siltstone is the most common lithology in the Brushy Canyon Formation along the west face of the Guadalupe Mountains, comprising about 65 percent of the exposed beds. Median diameters of these siltstone bodies range from 50 μm to 10 μm. The preponderant sedimentary structure is even, parallel laminae a fraction of a millimeter to 2 mm thick, marked by contrasting hue (Fig. 9A, C). Relatively coarser silt laminae are light gray, and finer laminae are dark gray; the darker laminae contain more abundant carbonaceous debris but not much mica, clay minerals, or clay-sized carbonate. Laminae are not conspicuously graded (Fig. 8A, B). Color is a reliable indicator of the grain size of bulk samples. Light-gray beds have median diameters in the coarse silt range.

Laminae and beds are remarkably parallel to the surface upon which they rest (Figs. 6B, 9D). Laminae that rest on erosional surfaces with slight relief or on ripples mantle these small irregularities and change in thickness only very slightly. Small irregularities such as ripples with a height of only 1 cm are reflected upward as curved laminae for several centimeters (Fig. 9C). Features with greater relief are reflected proportionately farther above the irregularity. Siltstone beds resting on steep channel margins with several meters of relief change very little in thickness upslope or downslope (Fig. 6A). These relations suggest that laminae formed as grains dropped to the sea floor along nearly vertical paths unaffected by currents. The average grain

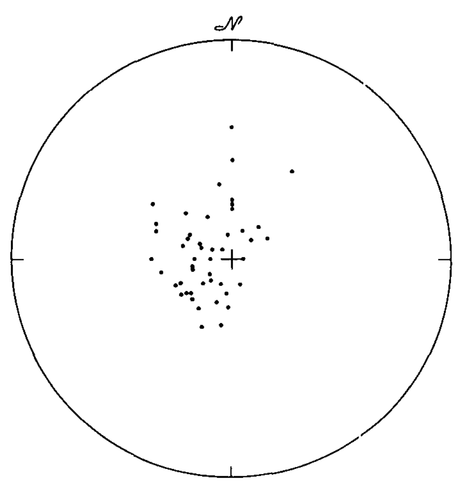

Figure 7. Orientation of channel margins shown as poles on equal-area plot (lower hemisphere).

size ranged from coarse silt to fine silt over millimeter-thick increments. I believe that the silt was transported into a density-stratified basin by flows of intermediate density water (Fig. 2). I dismiss an alternative hypothesis that the silt is wind transported, because the very fine sand grains commonly present in small proportions could not be transported very far in suspension by winds of reasonable velocities (Bagnold, 1941), and atmospheric dust samples taken near the modern Sahara coast contain few particles as coarse as 32 μm (Chester and Johnson, 1971).

Ripples are the second common primary sedimentary structure in siltstone (Fig. 9B, C). Most ripples occur within layers that are only one ripple thick and that parallel underlying laminations. The ripples are asymmetric, have rounded profiles, average spacing of 8 to 10 cm, heights of less than 1 cm, and long, straight to slightly sinuous crests. Average transport direction is to the southeast (basinward), as indicated by asymmetry and internal lamination. Transport directions for individual zones can range between eastward and southward, but no ripples have been observed that show northwestward transport. The rippled zones are composed of well-sorted quartz silt that generally resembles the coarser fraction of underlying laminated units. These relations suggest that ripples formed by reworking and winnowing of unconsolidated laminated silt by basinward-flowing currents. These currents likely flowed with velocities greater than 20 to 30 cm/sec near the bed, based on flume experiments by Southard and Harms (1972).

Laminated beds have sharp lower or upper contacts where episodes of erosion caused a hiatus in deposition. Within laminated sequences uninterrupted by erosional events, contacts between beds of finer, darker siltstone and lighter, coarser siltstone are commonly gradational (Fig. 9A, B). The thickness of such beds is measured in decimeters or meters. Apparently the average caliber of material reaching an area persisted through significant increments of deposition and changed only gradually. Rippled zones interspersed with laminated units are spaced only a few centimeters apart in some places but are many meters apart in other areas. I have discerned no order in the frequency of rippled zones relative to other features such as larger scale erosion surfaces, stratigraphic position, or geographic position.

Evidence of organic activity is sparse in laminated siltstone sequences. In some thin intervals, laminae are disturbed, causing a finely textured, flecked appearance. The small scale of the disturbance suggests tiny organisms. Some bedding surfaces bear trails, but these are rare. However, large bedding surfaces in siltstone lithologies are seldom exposed. The burrows and trails that have been observed are commonly closely associated with rippled layers, as though the currents that tractionally transported sediments improved bottom conditions for life. Remains of shelled organisms must be rare in siltstone, because I have not observed any shells even in several thousand meters of section. Rare occurrences of impressions of plants or soft-bodied animals have been seen (Fig. 13F).

Deformation structures developed shortly after deposition are quite rare, even in laminated siltstone beds that had large initial dips. For example, channel margins with slopes as steep as 30° are commonly mantled by siltstone beds with parallel planar laminae. Deposited on slopes estimated to be initially steeper than 35°, laminated siltstone apparently failed and moved downslope as small rotated blocks on curved slip surfaces. These observations indicate that laminated silt was mechanically stable on slopes of at least 30°. The implied coherence and high shear strength may result from good sorting, angular grains, and lack of lubricating clay minerals. Some beds of siltstone are cast into folds with amplitudes of decimeters or meters (Fig. 9E, F). These folds were of early origin because they are truncated by erosion surfaces and overlain by undeformed beds. Such beds have textures similar to undeformed siltstone and rest on beds with low dips, so that neither lithology nor slope appear to control the deformation. Elevated fluid pressure in pores may allow deformation on low slopes of sediments that otherwise have high shear strength, but in this case, no cause for such pressure has been determined.

Sandstone. Sandstone composes about 35 percent of the Brushy Canyon Formation along the west face of the Guadalupe Mountains. Individual sandstone beds are confined to channels cut into slightly older Brushy Canyon sediment or into underlying Leonardian carbonate. The percentage of sandstone is high in sections measured along the floors of Shumard and Shirttail Canyons (Fig. 5), giving the impression that this wedge of sediment is sandier where it thins. However, these sandstone-rich sections lie within a large channel cut into the Victorio Peak Limestone, as illustrated by King (1948, Pl. 9). I believe that sandstone abundance is mainly controlled by channel positions and is much less dependent on proximity to the basin margin. The following are arguments supporting this belief: (1) sections on the channel shoulder north of Shirttail Canyon contain a fairly low proportion of sandstone; (2) the Brushy Canyon interval transected by Bone Canyon (Fig. 1) is nearly entirely laminated siltstone in the upper 200 m; and (3) sections on slopes below El Capitan and southward along the Delaware Mountain front contain significant percentages of sandstone scattered at various positions in the interval (Fig. 4).

The sandstone bodies are commonly thickly bedded to massive and weather to shades of tan. Many beds contain scattered pebbles or cobbles of limestone or dolomite. Acid-insoluble fractions have median diameters in the very fine to fine sand range (0.062 to 0.25 mm). Samples with coarser median diameters are commonly better sorted than finer samples.

Crude horizontal lamination is the most common primary sedimentary structure in sandstone beds. Where such beds contain carbonate cobbles or fusilinid tests, the long axes of the clasts lie parallel to bedding surfaces (Fig. 10A, B). Alignment of long axes viewed on bedding surfaces is locally excellent, especially among fusilinid tests, but average orientation can change dramatically from patch to patch on the same bedding surface or from bed to bed.

Trough-shaped cross-stratification is common but not nearly so abundant as horizontal stratification. Sets range in thickness from a few centimeters to one meter. Many of the troughs are open in form and contain cross-laminae that dip at angles of a few degrees to 15° (Fig. 10C); other troughs are relatively deep compared to their plan-view size, have very steep northwestern margins, and imply scour of small pockets that must have been almost instantly filled with sediment (Fig. 10D). The asymmetry of these pockets and the inclination of cross-laminae indicate southeast (basinward) transport. Sets of cross-strata contain numerous fusilinid tests or scattered carbonate pebbles smaller than 3 cm in diameter in some places.

Ripples and small-scale cross-stratification are common in some sandstone beds in some areas, as pointed out by King (1948). These ripples are asymmetric (indicating southeast transport in general), are spaced at 12 to 15 cm, are 1 to 2 cm high, and have either fairly long sinuous crest lines or are strongly curved lunate or linguoid forms (Fig. 11A, B). They resemble current ripples formed on fine sand by unidirectional flow except that the profiles at the crest lines are consistently rounded rather than angular (Fig. 11D, E). These forms suggest that the ripples developed under current-dominated processes, but the flow also contained an oscillatory component (Harms, 1969, Figs. 7, 14). Paper-thin laminae of dark-gray, fine or medium silt lie on the steep downcurrent slopes of many ripples, which also suggests that flow slowed sufficiently for suspended load to settle on the bed (Fig. 11D, E).

The stratification observed in Brushy Canyon sandstone indicates that flows ranged from upper regime (horizontal stratification in cobble-bearing conglomeratic sandstone) transitionally to the upper part of the lower flow regime (sets of trough cross-strata with low- to high-angle cross-laminae), and to the lowest part of the lower flow regime (current-dominated ripples), as indicated by studies relating stratification, bed forms, and flow regime (Simons and others, 1965; Harms and Fahnestock, 1965). These currents consistently transported sand basinward — based on the inclination of cross-strata, the trend of small scours (Fig. 11F), and the rare occurrences of grooves on beds or flute casts on channel margins (Fig. 10E, 13B). The powerful currents moving sand, pebbles, and cobbles were apparently interrupted from time to time by conditions of much lower energy, because finely laminated siltstone beds commonly separate horizontally stratified, conglomeratic sandstone; in other places, rippled beds of appreciable thickness are interspersed with horizontally stratified sandstone (Fig. 11C). These fluctuations in current intensity may have been of rather long duration in cases where the laminated siltstone beds are thick. Variations in flow — of short duration — are suggested by ripple forms. The rounded profiles imply current reversals, as stated above, but these reversals must have been for short times and relatively weak, because northwest-dipping cross-laminae are never

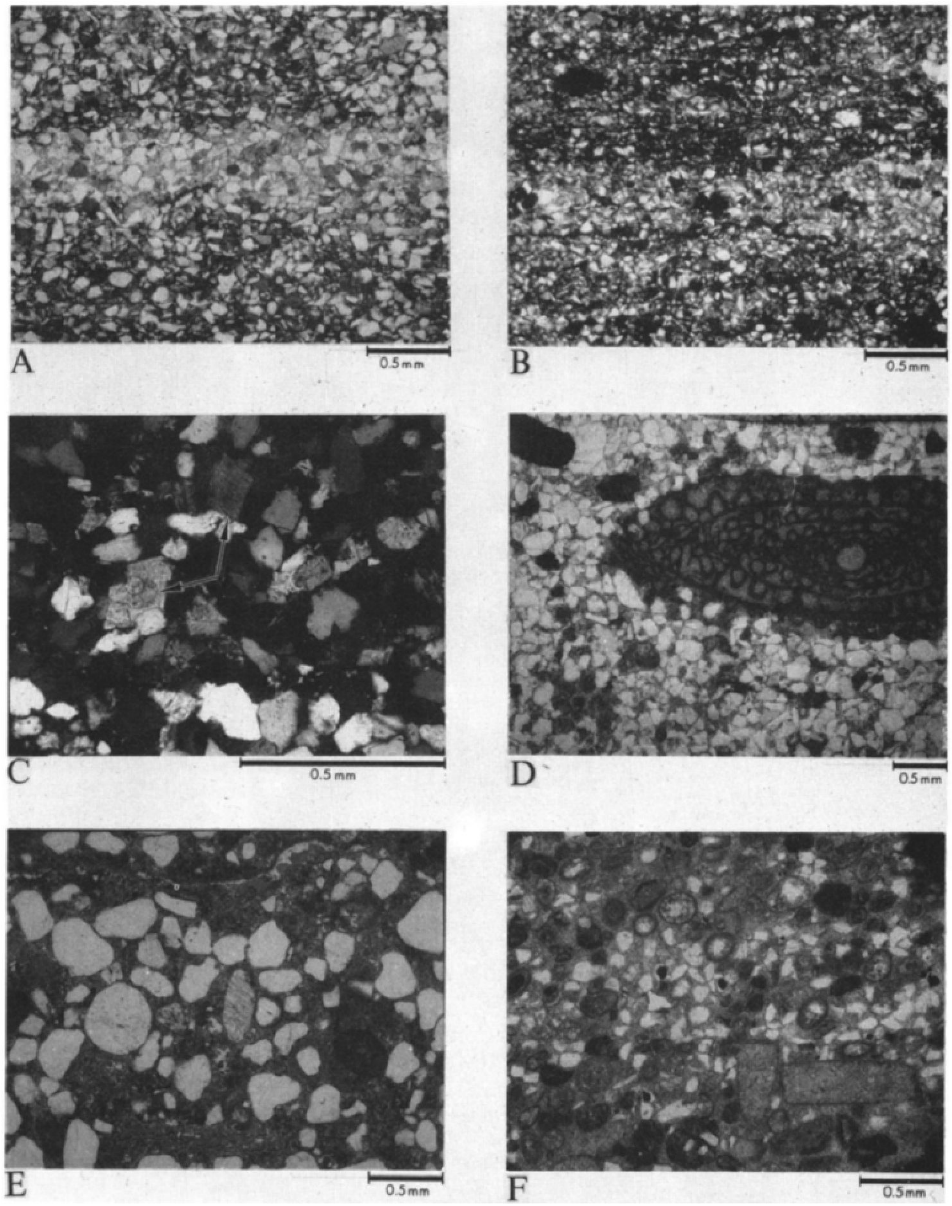

Figure 8. Photomicrographs of Brushy Canyon sediments. A. Coarse-grained siltstone laminations marked by variations in carbonaceous content. B. Laminated medium-grained siltstone. C. Very fine grained sandstone with subhedral dolomite clasts indicated by arrows. D. Fine-grained sandstone with fusilinid test. E. Fine-grained sandstone with brachiopod fragments and dolomite cement. F. Fine-grained sandy, oolitic calcarenite with calcite cement.

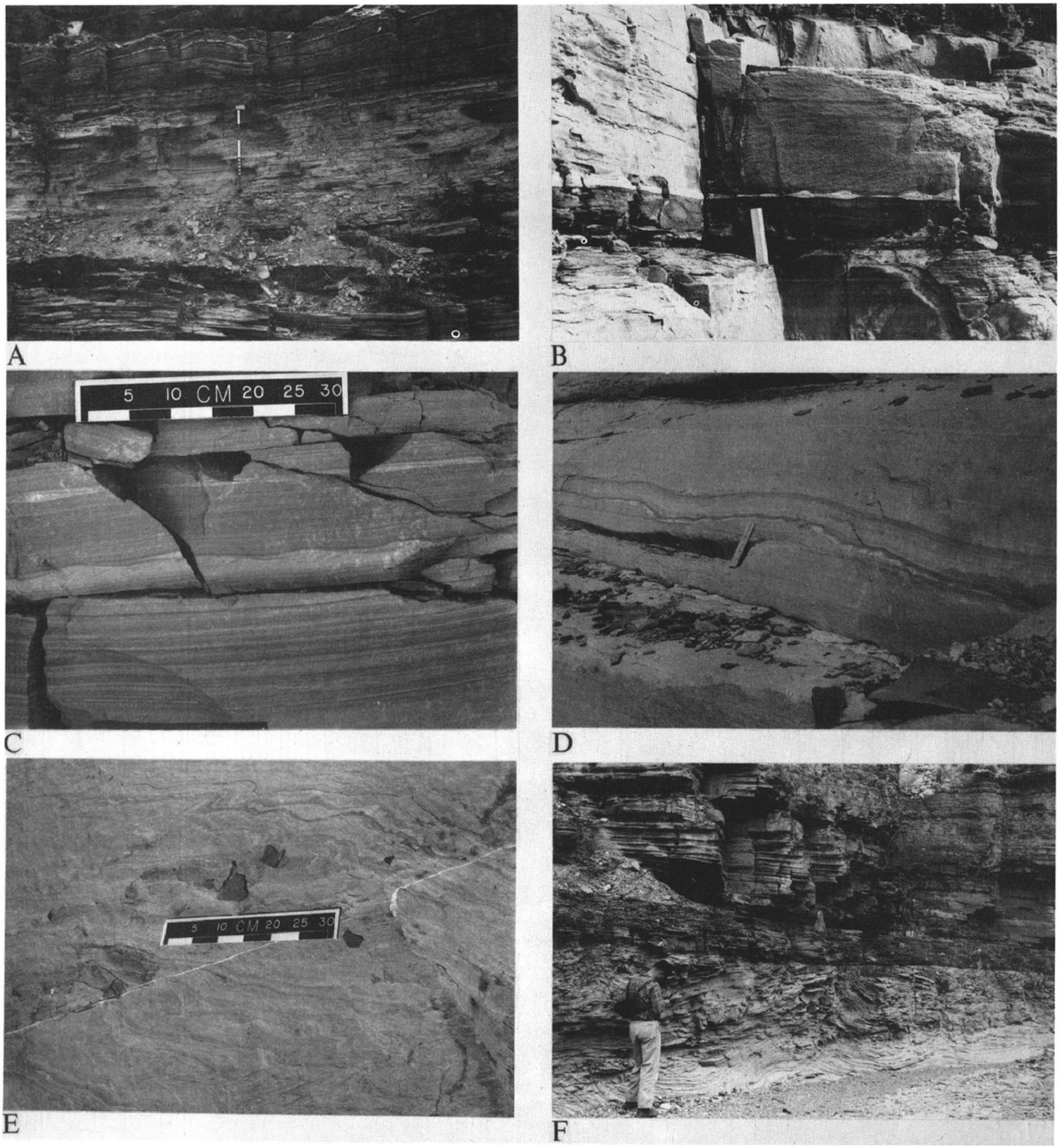

Figure 9. Features in siltstones. A. Appearance of bedding on weathered slopes (staff is 1.5 m). B. Light-gray coarse-grained siltstone, dark-gray medium-grained siltstone, and white, well-sorted coarse-grained silt ripples (scale is 15 cm). Horizontal lamination above rippled layer is obscured by plumose markings of joint surface. C. Laminations and ripples in typical coarse-grained siltstone. D. Low relief on scoured surface mantled by laminated siltstone (ruler is 15 cm). E. Small-scale chevron folding in laminated siltstone. F. Folds in laminated siltstone truncated by erosion surface and capped by undeformed layers.

observed. I envision weak currents flowing shelfward for periods of minutes or at most a few hours, generated by mechanisms such as internal waves or tides.

The stratification types described above do not occur in well-ordered or cyclic sequences. A bed containing any of these stratification types may rest upon or be overlain by sediments of any lithology in the section, including laminated siltstone and massive conglomerate. The bedding contacts of sandstone are sharp, either planar or irregular and erosional. The lateral termination of sandstone beds is almost invariably best interpreted as a depositional

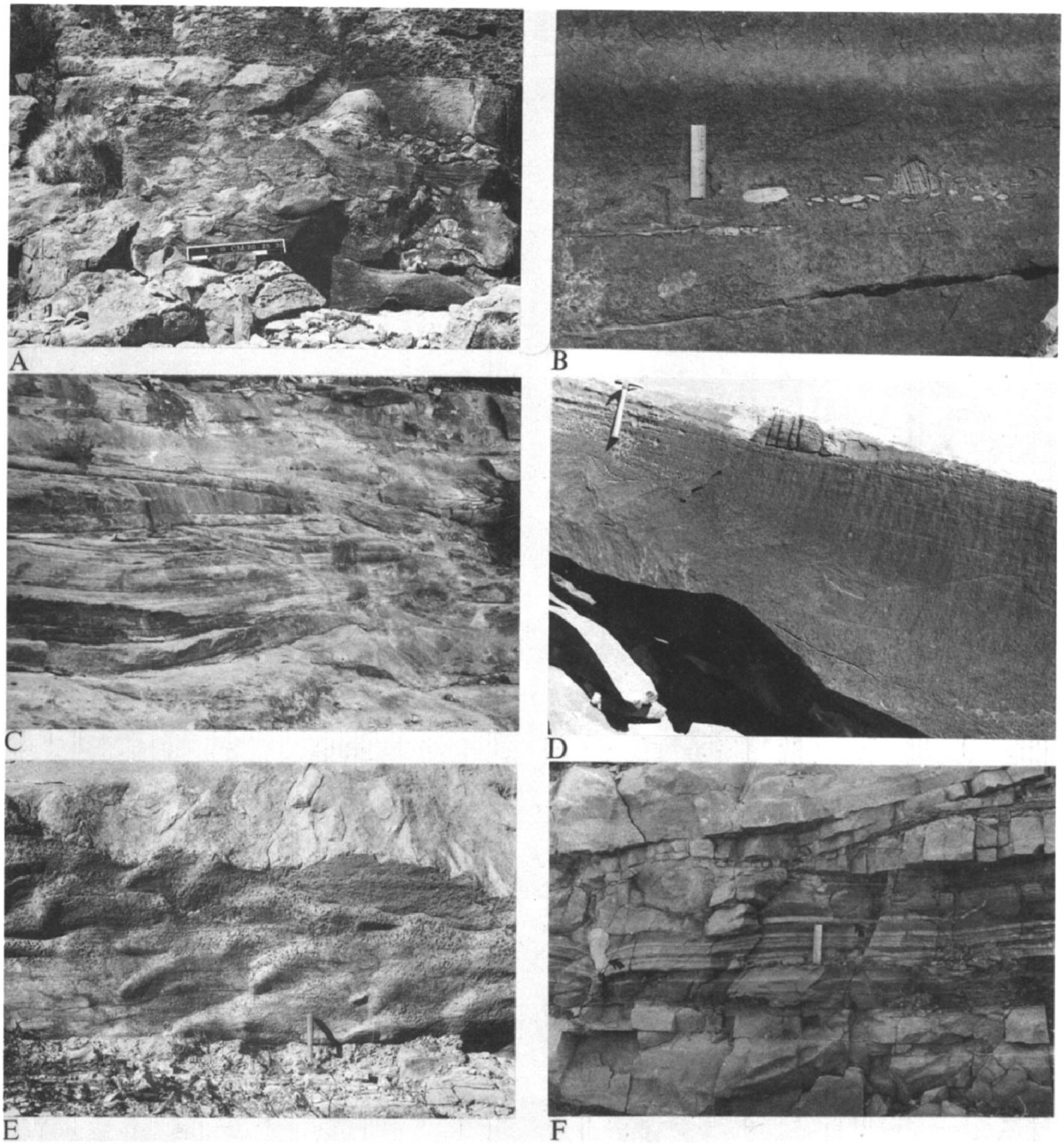

Figure 10. Features in sandstones. A. Horizontally stratified, fine-grained sandstone with scattered cobbles (scale is 30 cm). B. Horizontally stratified fine-grained sandstone with scattered carbonate pebbles and cobbles aligned in bedding (scale is 15 cm). C. Broad, shallow-trough cross-strata viewed in upcurrent direction. D. Small, deep scours associated with horizontal stratification, northwest to left (hammer is 30 cm). E. Exhumed flute casts on channel margin showing flow to southeast (hammer is 30 cm). F. Dikes and sills (arrows) of sandstone along channel margin (ruler is 15 cm).

contact against a sloping surface (Fig. 6A, C, D). Beds are flat topped where they taper against channel margins; no levees or textural variations have been observed at these margins. However, the lateral termination of some sandstone beds is complicated (notably in some U.S. Highway 62 roadcuts, Fig. 3) and can be interpreted in various ways. For most such examples, I believe that intrusive sandstone dikes or sills are responsible for the complex relations (Fig. 10F).

Textural grading within individual sandstone beds is rare and occurs in less than 1 percent of the units. These graded sand-

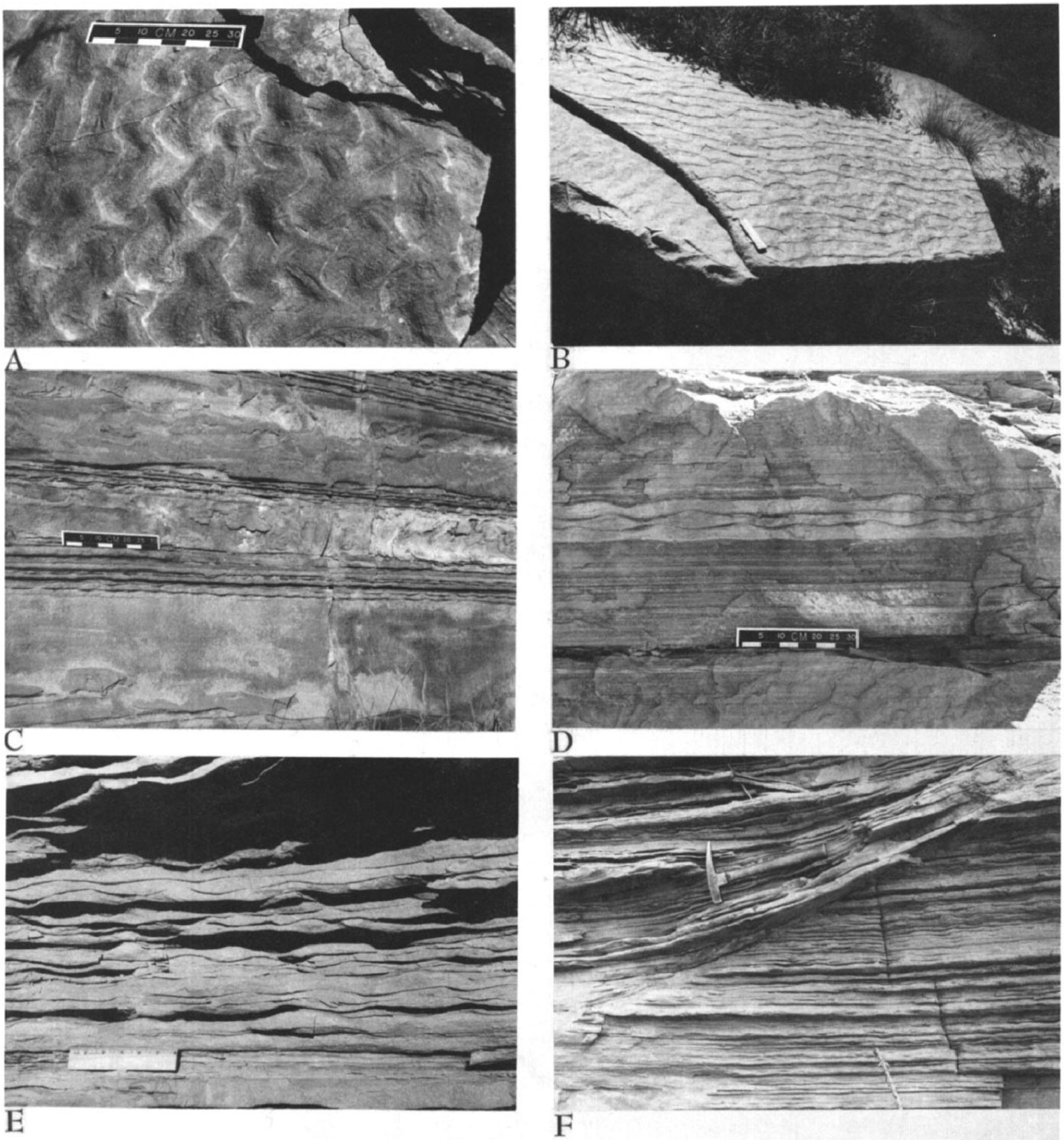

Figure 11. **Ripples. A. Cuspate ripples in very fine grained sandstone. B. Long-crested ripples in very fine grained sandstone (ruler is 15 cm). C. Beds of rippled, very fine grained sandstone alternating with beds of horizontally stratified sandstone. D. Rounded asymmetric ripples of coarse silt with intervening lenses of dark siltstone, transport from right to left. E. Rounded asymmetric ripples of very fine grained sand with siltstone lenses, transport from left to right (ruler is 15 cm). F. Small scour surface in very fine grained rippled sandstone (hammer is 30 cm).**

stones are mostly 10 to 30 cm thick (Fig. 12A, B, C). Median grain size in the lower part of such beds is very fine sand and grades upward to coarse or medium silt; larger clasts are uncommon in these beds, but some examples contain laminated siltstone pebbles or, very rarely, carbonate pebbles in their lower part. These graded beds appear massive or, toward their tops, horizontally stratified, and they therefore contain only the "a" and "b" intervals defined by Bouma (1962). Groove or flute casts are present on the undersurfaces of only a few beds.

Graded beds or sequences of

stratification types that might be attributed to turbidity current processes are very rare in the Brushy Canyon Formation or in the remainder of the Delaware Group (as determined by outcrop reconnaissance and examination of oil well cores). Although turbidity currents have been invoked as an important mechanism for transporting sediment into the Delaware basin, the textures, structures, and organization of beds differ greatly from the characteristics of modern and ancient turbidites so well documented by studies spanning the last two decades. Based on these differences, the proportion of sediments transported into the Delaware basin by turbid flows must be considered small.

Prelithification deformation structures are relatively rare in sandstone beds. The most dramatic examples of deformation are found where massive conglomerate rests on sandstone, as though quick loading deformed recently deposited sands with high water content (Fig. 15B). However, in most areas conglomerates did not deform underlying sandstones. Dikes and sills formed by injection of sand into adjacent beds have been observed in a few areas (Fig. 10F). These features are small, and dike or sill widths rarely exceed a few centimeters. In two examples, tiny dikes of sandstone extend for as much as 1 m downward into Leonardian carbonate rocks (Fig. 15F).

Structures formed by organisms are extremely rare in sandstone. The most common and distinct organic markings are S-shaped depressions 10 to 15 cm long on sandstone beds (Fig. 13A, B). These marks resemble the impressions left by the tails of startled hagfish observed in some deep-sea photographs. The markings on the Brushy Canyon beds may have been made in a similar fashion by an appendage of some swimming organism. Cylindrical burrows, ranging from 2 to 5 mm in diameter, cutting or parallel to bedding are locally abundant in some sandstone beds (Fig. 13B, C, D). These burrows have so little detail and are of such a general type that interpretation is difficult. Apparently the conditions under which most sandstone was deposited were not favorable for organisms, either because of strong currents or other environmental factors. However, burrowing faunas did develop locally from time to time, or the bottom was occasionally marked by swimming organisms.

Massive Conglomerate. Massive conglomerate forms a small fraction (less than 1 percent) of the Brushy Canyon Formation. These massive conglomeratic beds are distinguished from conglomeratic sandstone by lack of internal stratification within beds, extreme heterogeneity of clast size, occurrence of scattered large boulders ranging from 1 to 30 m in maximum dimensions, and random fabric. The massive conglomerate beds are also limited in their stratigraphic and geographic distribution; they are most common within 50 m of the base of the formation and in outcrops between Bone Canyon and the south side of El Capitan.

Beds of massive conglomerate are tabular and range in thickness from 1 to 10 m. These beds, like the Brushy Canyon sandstone, occupy erosional depressions and terminate laterally by onlap against sloping boundaries (Fig. 12D). No levees or zones of textural variation are evident at lateral margins. This relation is particularly clear in Bone Canyon, where conglomerate occupies a scour cut in Cutoff rocks, and individual beds can be traced to where they wedge out against the western margin of this channel. Debris lenses within the Cutoff interval in this same area (Pray and Stehli, 1962) are much less tabular in form and occupy narrow and relatively deeper channels.

Where several beds of massive conglomerate occur one above the other, they are commonly separated by beds of gray laminated siltstone a few centimeters thick or by beds of horizontally stratified, fine-grained sandstone several centimeters to a few meters thick (Fig. 14A, B). These separating beds are discontinuous in many places, as though they were eroded by events that preceded or accompanied the emplacement of the overlying conglomerate bed. When traced laterally, apparently single, thick conglomerate beds are seen to be a composite of thinner units separated by other lithologies. Sandstone beds beneath conglomerates are contorted in some places, suggesting that emplacement exerted considerable shear (Fig. 15B). However, in most areas the stratification in underlying sandstone is undeformed. Relatively gentle emplacement of conglomerate beds is suggested by another interesting feature. Larger boulders in some beds rise above the general level of the upper surface, and in some cases, this surface is mantled by a thin layer of laminated siltstone. Where this siltstone layer is overlain by a conglomerate unit, the layer is continuous and intact even over the protruding boulder, which presumably might act as a buttress and experience high shear (Fig. 14B).

Lithologies of pebble-sized or larger clasts are similar to carbonates found in the Victorio Peak and Cutoff intervals a few kilometers to the north. Cobble- and boulder-sized clasts are most commonly light-gray to gray dolomitic grainstone or packstone similar to the Victorio Peak Limestone; pebble-sized clasts are commonly dark-gray calcitic micrite, resembling the carbonate beds of the Cutoff Shale (Fig. 14B, C, D). Nearly all of these carbonate clasts are rounded. Most are also quite spherical, although the largest boulders are commonly slabs with length-to-thickness ratios exceeding 3, and some beds contain numerous flat clasts (Fig. 12E). Plastic deformation of clasts by compaction or the anvil effect of adjacent cobbles or boulders has not been observed, but a few have been split and intruded by adjacent finer matrix (Fig. 14D). These shape characteristics, along with disoriented geopetal infill of fossil voids (Fig. 14F), indicate that Leonardian rocks of the shelf were thoroughly lithified before erosion and transport to the basin and that transport mechanisms caused significant rounding.

The size composition of the massive conglomerate beds covers a broad spectrum. Scattered boulders with longest dimensions on the order of 30 m are the largest particles (Fig. 15A), and silt- or sand-sized quartz or carbonate grains are the smallest. The proportions of various size fractions resemble those of a well-designed concrete mix; the amount of finer material is sufficient to fill all interstices between larger particles, so that no void space or large patches of sparry cement exist, and larger particles are so abundant that they are not separated appreciably by significantly finer matrix (Fig. 14D, E).

The fabric is jumbled. Elongate clasts lie in all orientations relative to bedding, and even 3- to 4-m boulders that stick up above the general level of a bed may have their long axes oriented at large angles to bedding (Fig. 12E, F; Fig. 14B, C). No bed has been observed that has good grading of clast size throughout its thickness, but a few beds are capped by graded layers of coarse to very fine sand a few centimeters thick (Fig. 15C), suggesting that conglomerate emplacement was sometimes followed by turbidity currents.

The bulk density of conglomerate masses during final movement can be estimated from compaction effects around large boulders enclosed in single beds. Bulk density appears to have ranged between 1.8 and 1.9. This estimate is based on a present bulk density of about 2.15 and compaction to approximately 0.85 of the original bed thickness. Large boulders like that shown in Figure 14C were well lithified and presumably nearly uncompactable at the time of emplacement, based upon their well-rounded shapes, the lack of squeezing at contacts with other clasts, and evidence of cementation preceding transport (geopetal fabrics). Considerable strength in the moving conglomerate slurry is also implied by similar large dense blocks rising significantly above the tops of the beds with which they moved.

The mechanism(s) by which these massive conglomerates were transported and deposited is conjectural. Three possible mechanisms could be invoked: (1) flow by dispersive pressures generated by grain col-

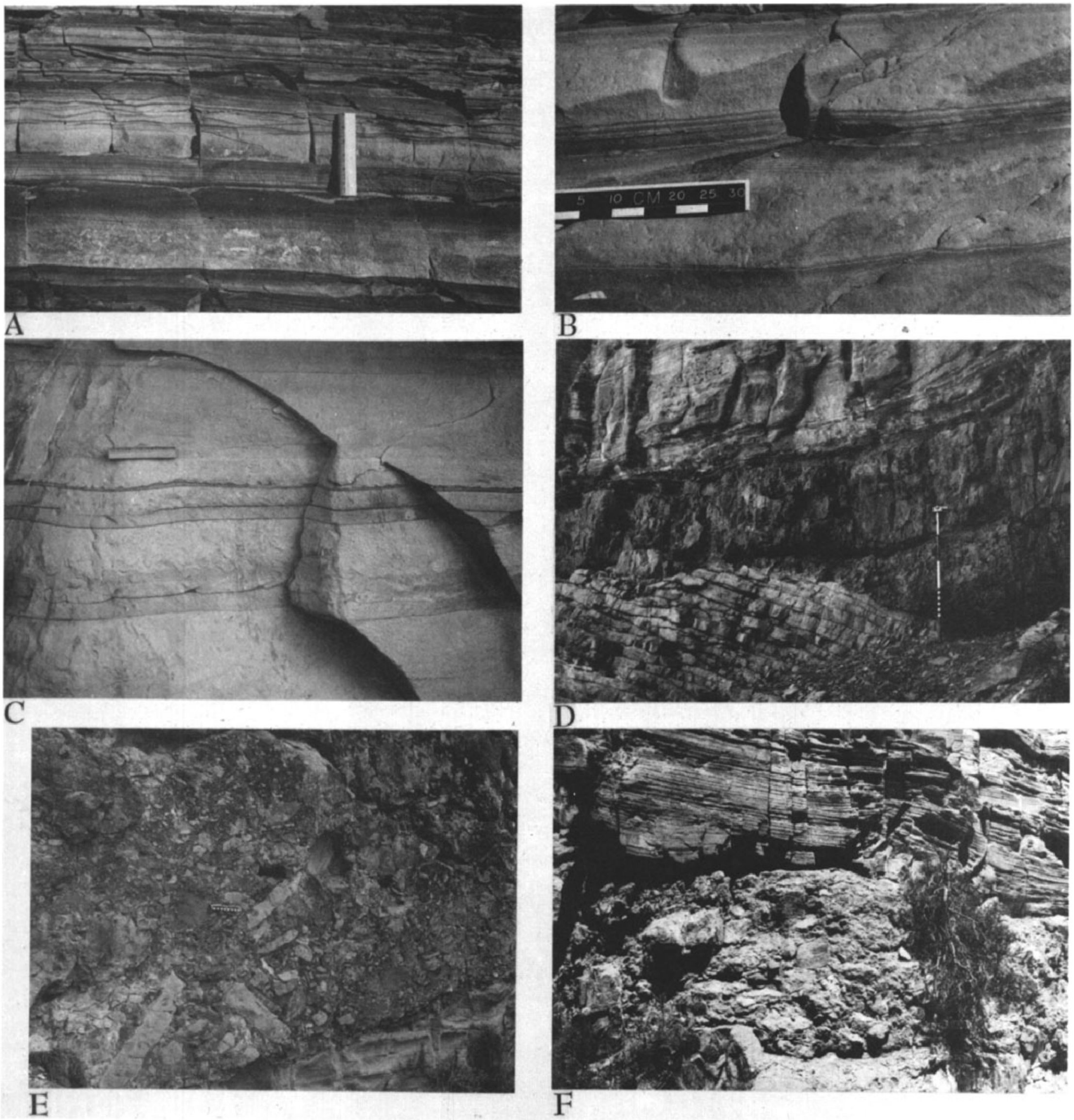

Figure 12. Graded beds and chaotic conglomerates. A. Sharp-based beds grading from very fine sand to coarse silt (ruler is 15 cm). B. Slightly thicker graded beds than in A. C. Graded beds with small load structures at their bases (ruler is 15 cm). D. Conglomerate beds at base of Brushy Canyon Formation abutting against erosion surface on Cutoff Limestone (staff is 1.5 m). E. Conglomerate bed containing many slabs in various orientations; erosion surface on undeformed sandstone toward lower right (ruler is 15 cm). F. Chaotic fabric in conglomerate with boulder rising above top of unit (arrow near bush) onlapped by horizontally stratified fine-grained sandstone (ruler is 30 cm).

lisons (Bagnold, 1954), (2) flow of a viscous slurry, and (3) slippage of a rigid plug over a shearing substrate (Johnson, 1970). However, none of these satisfactorily accounts for all the features in the Brushy Canyon conglomerate beds.

A dispersive pressure mechanism should cause a concentration of larger clasts toward the tops of beds, but it should not cause large boulders to protrude significantly above the bed tops. If dispersion is fairly large and concentration of clasts is low, drape of beds should be obvious at rigid channel margins. The lack of grading, boulders riding well above the beds, and lack of drape are all evidence that Brushy Canyon conglomerate did not move in a dispersed state.

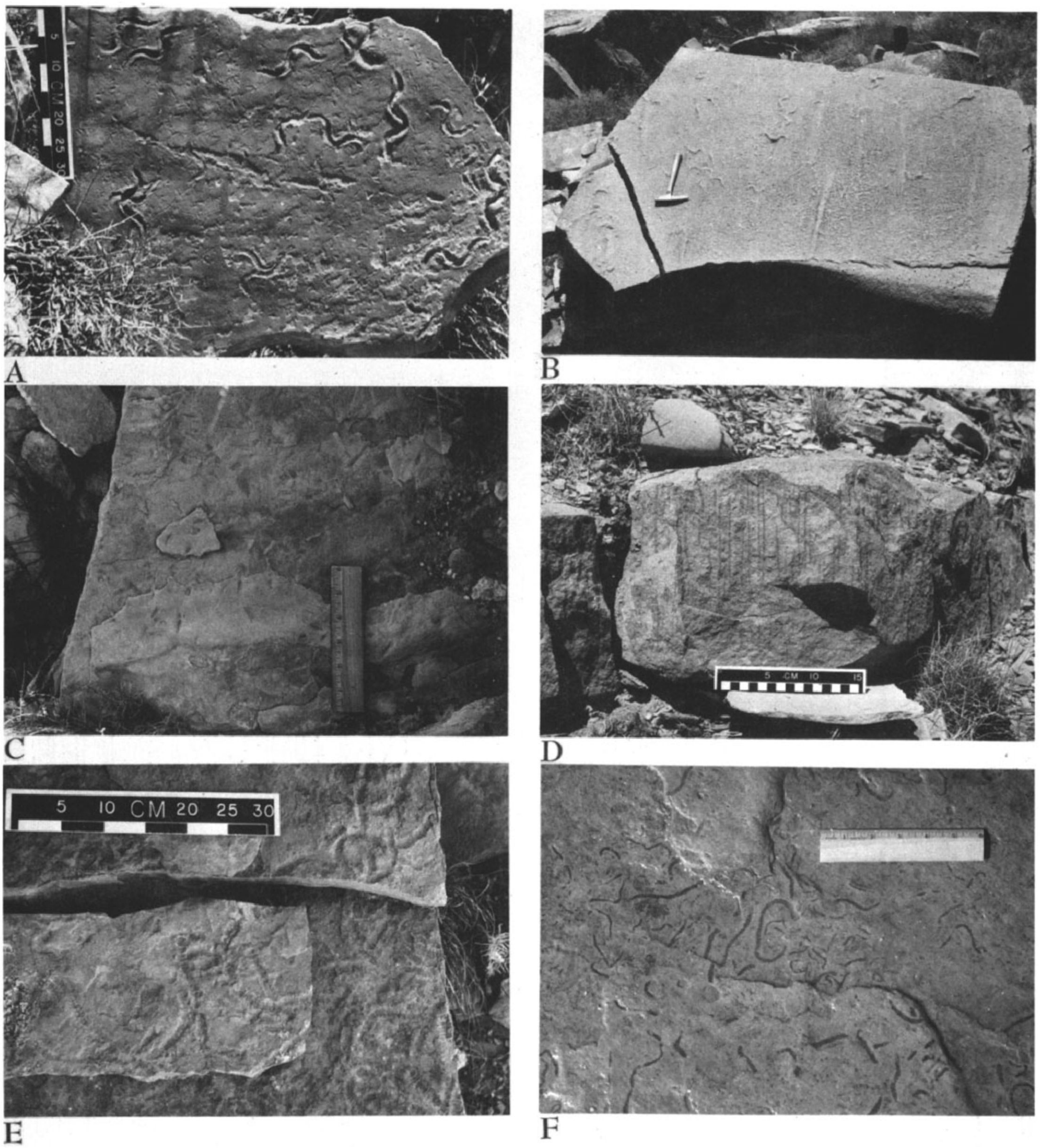

Figure 13. Trace fossils. A. S-shaped markings on upper surface of sandstone bed. B. Lower surfaces of sandstone bed with S-shaped markings and grooves (hammer is 30 cm). C. Cylindrical, low-angle burrows cutting ripples (ruler is 15 cm). D. Slender, vertical burrows in very fine grained sandstone, possibly occurring as pairs. E. Poorly preserved trails on bedding surfaces of calcarenite showing transverse internal markings. F. Segmented carbonaceous impressions on siltstone bedding surface, Cherry Canyon Formation (ruler is 15 cm).

If transport was accomplished by truly viscous flow, the fabric of conglomerate should be well oriented but ungraded. Beds should be flat-topped where they meet channel margins. Clasts should arrange themselves by density, and only clasts lighter than the moving slurry would float and rise above the bed top. The lack of a well-aligned fabric and large, dense boulders perched on the conglomerate beds suggest that these slurries did not behave viscously.

Plastic flow of a fairly rigid sheet or plug over a zone of shear suggests dual behavior of the moving mass. In the upper rigid sheet

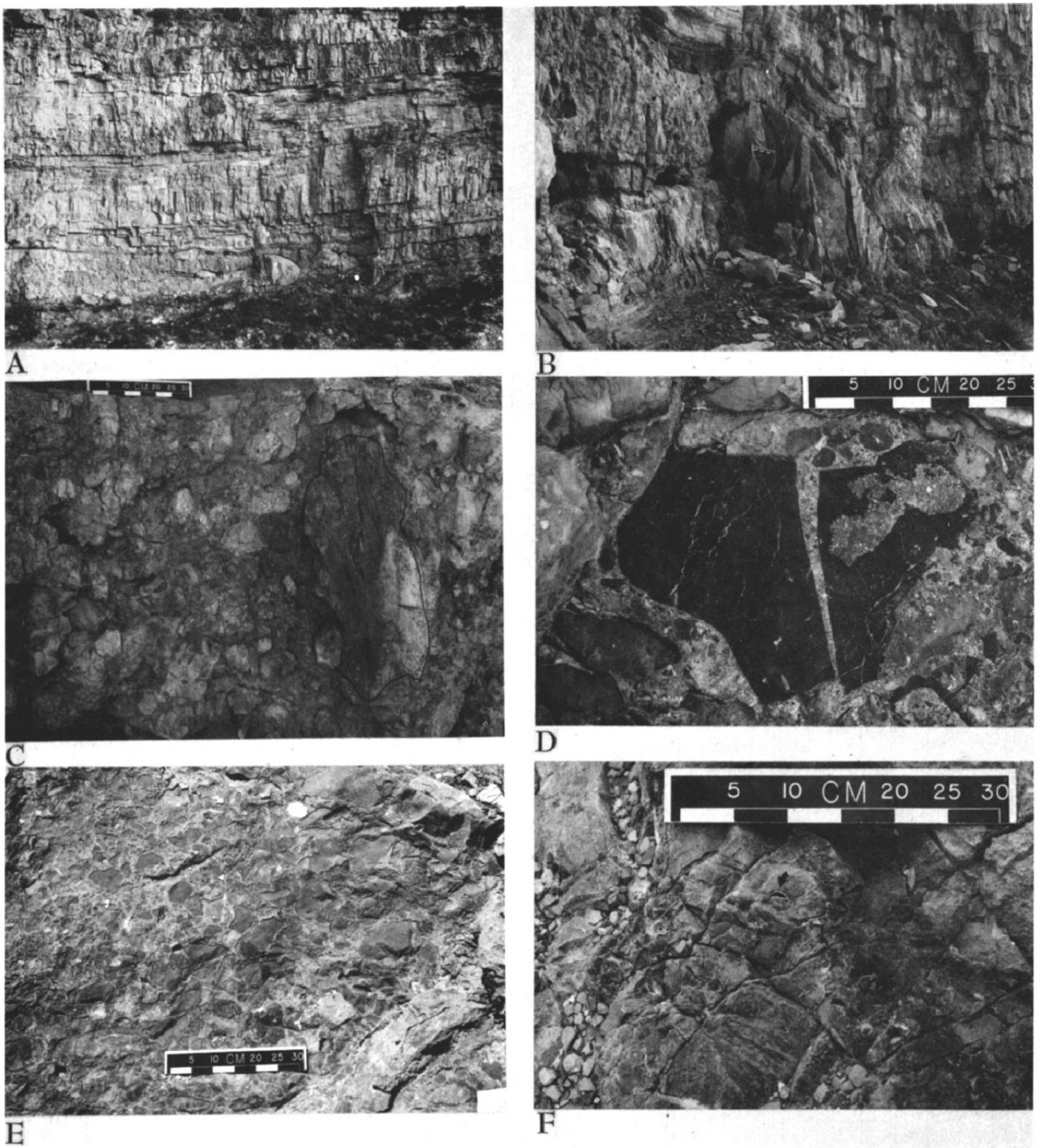

Figure 14. Features in massive conglomerate beds. A. Conglomerate with large boulders near base of Brushy Canyon Formation showing discontinuous preservation of separating siltstone beds. B. Large boulder shown in A with preserved mantling siltstone bed (ruler is 30 cm). C. Compaction effect around large boulder standing on end (outlined for clarity). D. Broken, small boulder viewed from above. E. Closely packed fabric in a cobble conglomerate. F. Geopetal fabric (arrow) in a small boulder viewed from above.

or plug, a plastic strength exists and large clasts can be held above the bed top, restricted internal movement inhibits a well-developed fabric or grading, and lateral and terminal margins should be steep. In the lower portion undergoing laminar shear, a subhorizontal aligned fabric should develop. Brushy Canyon conglomerate beds lack steep marginal slopes and aligned fabrics near the basal contact.

No single theory seems to explain all of the features of these conglomerate beds. Slopes ranging from a few degrees to perhaps 15° appear to be a requisite because massive conglomerate beds occur mainly on, or a few kilometers basinward of, the steepest slope at the base of the Brushy Canyon Formation. However, much steeper slopes existed on the Goat Seep and Capitan forereef talus, yet similar massive conglomerate beds at the foot of these slopes are rather uncommon. Environmental conditions or lithologic characteristics of Cutoff and Victorio Peak rocks must somehow have been different and contributed to the development of massive conglomerate layers. However, the exact nature of these conditions or characteristics remains uncertain.

Formation Contacts

The Brushy Canyon wedge along the west face of the Guadalupe Mountains rests on Leonardian rocks along a surface of complex origin. Toward the thin edge of this wedge, the contact is certainly erosional, the Cutoff Shale is truncated, and the Victorio Peak Limestone is deeply entrenched (Figs. 1, 5). Where the wedge thickens from 150 m to more than 300 m between Shumard Canyon and Bone Canyon, the Brushy Canyon Formation rests unconformably upon Victorio Peak and lenses of Cutoff, intersecting an older surface of unconformity (Pray, 1971). South of Bone Canyon, the Brushy Canyon overlies beds with lithologies very similar to those of the Cutoff, although stratigraphic assignment is disputed. There, direct evidence of unconformable relations, such as channeling or disparate dips, is lacking. The contact is conformable, but a hiatus is implied by most investigators.

The first-deposited Brushy Canyon sedimentary rocks are variable in character and include all of the types of lithologies represented within the formation. In some places, finely laminated siltstone rests on the basal contact, but in other places, sandstone or massive conglomerate are the lowest beds. I see no geographic trend in the lithologic character of beds resting on the contact. There are no sandstone or conglomerate beds with beach characteristics, such as might be anticipated if a shallow sea transgressed the sloping Leonardian surface. The contact with Leonardian rocks is everywhere sharp and smooth. Where the wedge thins dramatically northward from Bone Canyon, the contact is undulating and channeled on a broad scale. Locally, I have not observed small irregularities such as benches or terraces, solution depressions, or animal borings, but some small sand-filled dikes exist (Fig. 15F).

The lithologic contrast between the carbonate rocks of the Leonardian Series and the detrital rocks in the basinal sequence of the Guadalupian Series has commonly been emphasized. The contrast exists to be sure, but perhaps its abruptness has been overemphasized. Although consisting predominantly of carbonate, some beds within the Victorio Peak Limestone contain quartz sand, and some beds in the Bone Spring Limestone contain abundant quartz silt. Terrigenous detritus composes a significant proportion of the Cutoff Shale. Although the bulk of the Brushy Canyon Formation is detrital, some carbonate-rich beds occur in the lower part. Viewed in this way, the change in dominant lithology across this stratigraphic boundary is somewhat less abrupt than previously expected.

The subaerial origin of the Leonardian-Guadalupian unconformity, implied in most interpretations of Permian history in this area, is not required by any compelling evidence. Indeed, the lack of solution features, weathered zones, stream debris, wave-cut cliffs, beaches, or transgressive lag deposits points to a different, perhaps submarine, origin for this surface.

The top of the Brushy Canyon Formation was defined by King (1948) as a prominent brown weathering sandstone ledge about 300 m above the base of the formation in the Delaware Mountains and on the slopes below El Capitan (Figs. 4, 5, 6A, C). This sandstone is conglomeratic and contains quartz grains ranging in size up to 0.5 mm. It occupies erosional channels and is absent in some outcrop localities, but it does provide the best formation boundary available in the outcrop area because it is nearly continuous and texturally distinct from the coarse siltstone or very fine grained sandstone of the conformably overlying Cherry Canyon. Although the base of this uppermost Brushy Canyon sandstone is erosional, these channels are thought to be no more significant than the numerous channels recognized both higher and lower stratigraphically. Medium-sized quartz grains did not reach the basin in significant quantities during Cherry Canyon or Bell Canyon deposition, but this textural difference is thought to reflect processes and transport on the northwestern shelf, rather than a hiatus or alteration of process in the basin.

The wedge of Brushy Canyon sediment disappears in outcrop about 1,200 m north of Shirttail Canyon. Beyond this point, finely laminated siltstone of the sandstone tongue of the Cherry Canyon Formation rests on the Cutoff Shale. The disconformity represented by this contact is equivalent to the time required for 300 m of sedimentation in the basin. This relation, typical of the outcrop area south of the Texas–New Mexico border, is interrupted in one place between Bush Mountain and Bartlett Peak. A previously unrecognized channel, which was first pointed out to me by Pray (1967, personal commun.), cuts through 70 m of the Cutoff Shale and an additional 30 m into the Victorio Peak Limestone (Figs. 1, 15D, E). This channel is nearly 700 m wide in the Cutoff interval but narrows to about 175 m at the top of the Victorio Peak. It is filled largely with laminated siltstone, but it contains fine-grained sandstone beds and massive conglomerate with large carbonate blocks in the lower part. The age of the channeling and fill is uncertain, but the position below the general level of the Cherry Canyon tongue and the coarseness of part of the fill suggest that the feature may be correlative with the Brushy Canyon Formation. This channel may be the sole outcrop representative of the type of conduit that fed sediment into the basin in early Guadalupian time.

REVIEW OF INTERPRETATION

The Brushy Canyon Formation is an extraordinary assemblage of detrital beds, unusual in its association of textures, sedimentary structures, and large-scale erosion and fill features. No similar example has been reported in the literature to my knowledge, although some aspects resemble other deep-water deposits. I believe that its unusual characteristics can best be attributed to nonturbid density currents that at times scoured the sea floor or flowed confined in channels cut by earlier currents. At other times these currents must have traveled into the basin above denser water masses as intrastratal flows losing sediment slowly into underlying stagnant water (Fig. 2). I reached this conclusion because energetic processes and substantial deposition are required in a basin containing relatively deep water, but in a style not compatible with our understanding of turbidity currents.

Evidence Suggesting Deep Water During Brushy Canyon Deposition

The Brushy Canyon Formation has been interpreted in the past as a shoal-water deposit. One vital step in interpretation is to evaluate this contention and estimate the depth of water that prevailed during deposition. Several kinds of evidence are negative, in that they emphasize features that are absent in the Brushy Canyon Formation. However, I believe that the following arguments narrow the range of plausible hypotheses:

1. There are no shoreline deposits, sea cliffs, or marine terraces formed on the sloping unconformity underlain by Leonardian rocks. The stratification sequences, textural gradients, and sedimentary structures that have become well known in recent years from both modern and ancient examples of shoreline and nearshore deposits have not been recognized in any part of the Brushy Canyon Formation. If the water had been shallow during any fraction of Brushy Canyon time, evidence of shoreline processes should be found on the unconformity where it rises 300 m in 3.5 km.

2. There are no systematic facies changes in the Brushy Canyon wedge that would

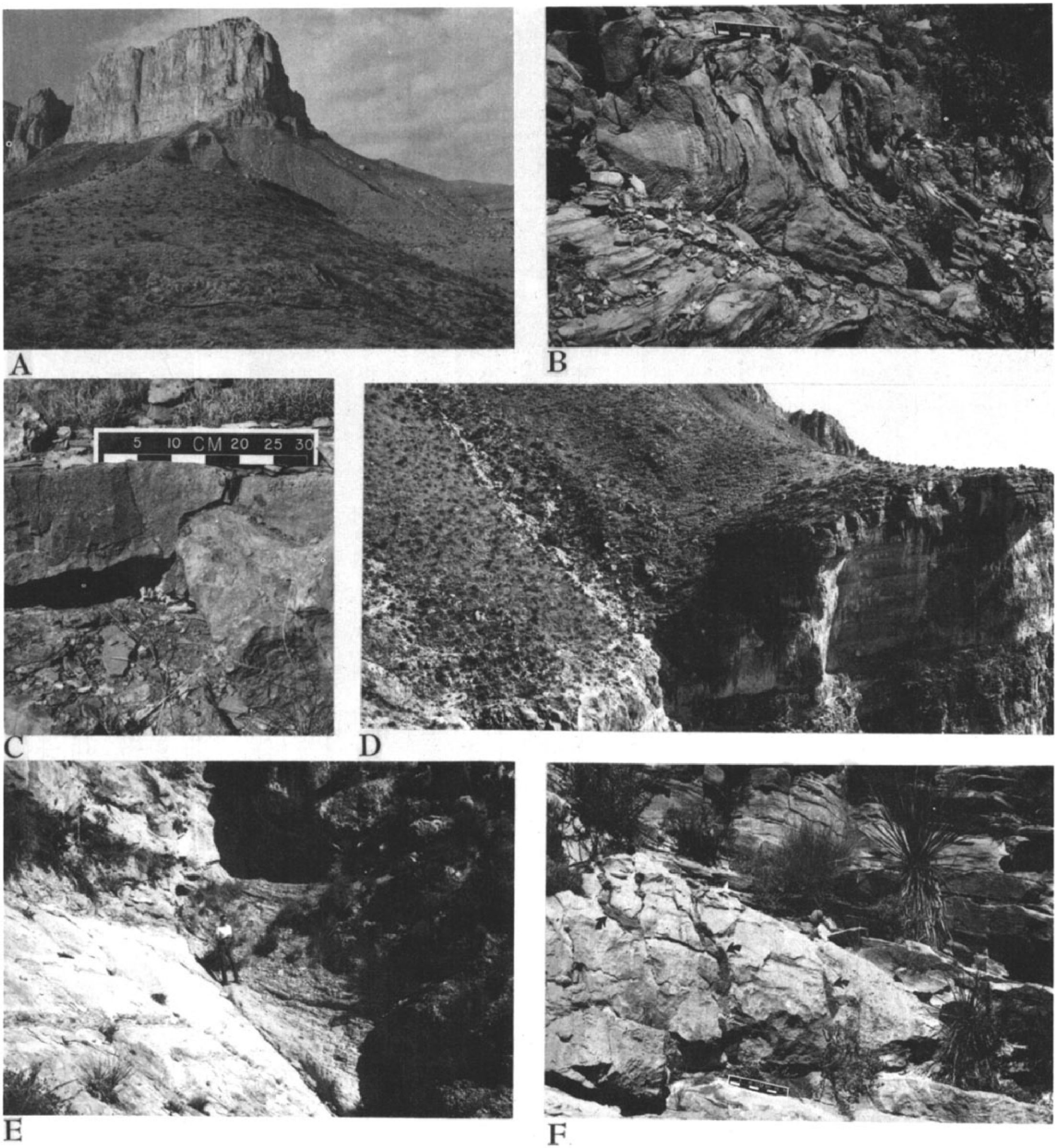

Figure 15. Features in conglomerate beds and at basal Brushy Canyon Formation contact. A. Large carbonate slab 30 m long (above bracket) near base of Brushy Canyon Formation southwest of El Capitan. B. Deformed sandstone just beneath conglomerate zone shown in A and short distance to southeast (ruler is 30 cm). C. Graded granule-bearing sandstone capping massive conglomerate layer. D. South wall of channel cut in Victorio Peak Limestone near Bush Mountain. E. North wall of channel cut in Victorio Peak Limestone near Bush Mountain has slope of 35° at man's foot. F. Sandstone dikes (arrows) extending from base of Brushy Canyon sandstone into Victorio Peak Limestone in Shumard Canyon (ruler is 30 cm).

support an interpretation of shallow to deep or shoreline to offshore processes. On the contrary, the types of lithologies, their proportions, and the style of sedimentation are generally similar regardless of geographic or stratigraphic position. Only the massive conglomerate beds are concentrated within the lower 50 m of the formation where the post-Leonardian unconformity is steepest. However, these conglomerate beds do not have characteristics that necessarily link them to a shallow-water or shoreline origin.

3. There is no certain evidence of a post-Leonardian, pre-Guadalupian emer-

gence anywhere in the outcrop area, as would be required if the lower part of the Brushy Canyon Formation was deposited in shallow water. Weathered zones, soils, solution features, and stream debris are all absent along the Leonardian-Guadalupian contact.

4. Fossils that indicate shallow-water environments, as do the fusilinids during Capitan deposition (Newell and others, 1953, Fig. 79), have been transported; their presence in Brushy Canyon channel fills implies strongly that suitable shallow-water environments existed somewhere to the west or northwest during parts of early Guadalupian time. There are few biogenic structures in Brushy Canyon sediment; in contrast, such spoors are common in sandy or muddy shallow marine environments of normal salinity.

5. The Brushy Canyon siltstone and sandstone interval changes transitionally to marginal carbonate facies and shelf facies along the northern and eastern rim of the Delaware basin, according to interpretations of subsurface data. Although correlations are imprecise, it is unlikely that the Brushy Canyon abuts against a slope of Leonardian rocks in the subsurface as in the outcrop. Therefore, subsurface data imply that the Brushy Canyon was deposited in deeper basinal waters that were partly surrounded by contemporaneously building shoals, a pattern similar to that of later Guadalupian time.

6. Many of the lithologies and sedimentary features of the Brushy Canyon Formation resemble those of the Cherry Canyon and Bell Canyon Formations where these units intertongue with reef talus and were almost certainly deposited in water depths ranging from 300 to 600 m. Although the Brushy Canyon Formation contains some beds that are coarser grained or conglomeratic, the bulk of sediment throughout the 1,000-m-thick Delaware Group is remarkably uniform.

Considering these six points, I believe that the Brushy Canyon sea must have stood at or above the level of the Cutoff and Victorio Peak Formations in the outcrop area (Fig. 1). This interpretation requires water depths greater than 300 m a short distance basinward early in Guadalupian time.

Evidence Suggesting Nonturbid Density Flows

1. Incised channels and sandstone beds restricted to channel floors indicate that erosion and some deposition were accomplished by bottom-hugging currents. Because the orientation of the channels and directional features within channels indicate flow downslope and perpendicular to the basin margin, gravitationally propelled density flows appear to be required.

2. Textural grading and well-organized stratification sequences that have been so widely recognized in turbidite units, both modern and ancient, are lacking in all but a small fraction of Brushy Canyon sandstone beds. The absence of these well-established characteristics suggests that the mechanisms of transport and deposition were substantially different from turbidity current processes.

3. Clay-sized material is rare in outcrop or in subsurface material representing the Delaware Mountain Group throughout the basin. Clay, either dispersed within sandstone or segregated as beds, is too sparse to have caused repeated, large turbid flows. Silt-sized material is extremely abundant throughout the Delaware basin but is commonly segregated from sandstone beds. Turbidity currents, generated by suspended silt, could not be the primary mechanism that eroded and filled channels because siltstone beds mantle the large-scale erosional features without regard to topography and do not consistently overlie erosion surfaces. Currents propelled by suspended silt should relate to topographic features and move through channels; the small number of graded, sandy to silty beds noted in outcrop studies probably did originate as turbidity currents.

4. Configuration of beds illustrated in Figure 2 is not similar to sediment found in and along channels on modern deep-sea fans built by turbidity currents (for a summary of Holocene fan characteristics, see Haner, 1971, Table 5). In the Brushy Canyon Formation, sandstone beds are restricted to channel floors; these beds taper abruptly at channel margins, are flat-topped and do not extend up the channel margin, show no lateral fining in texture, and are not bounded by levees. All of these characteristics indicate that sand was transported by traction mechanisms close to the channel floors. If the sand had been transported as part of a turbid flow, the finer part of the dispersed sediment might in some places extend up the channel margins for a distance equivalent to the maximum thickness of the passing turbid water mass, or it might build levees as the channels filled. The middle and lower parts of modern deep-sea fans formed by turbidity currents have substantial levees separating channel and interchannel areas. Systematic textural gradients related to levee position have been observed or implied in several studies of modern fans. Siltstone beds of the Brushy Canyon mantle channel floors, margins, and interchannel areas without appreciable changes in thickness or texture. If the silt was moved as bottom-hugging turbid flows, a greater thickness of silt presumably would be deposited on channel floors because the column of turbid water would be thicker over such areas. Because this is not the case, silts must have been transported by currents that were unaffected by bottom topography. Sullwold (1961, Fig. 2) presented a diagram of turbidites similar in some respects to Figure 2 of this paper. However, important differences are evident; in his diagram, sandstone beds are graded, some natural levees develop, and mantling layers are lutite rather than coarser silt.

5. No proximal and distal facies relations have been established for the Delaware Group on a local or regional scale. Studies of modern and ancient turbidity current deposits suggest that gradients in texture, bed thickness, and stratification sequence commonly exist (Walker, 1967; Haner, 1971, Fig. 15). Brushy Canyon sedimentary rocks exposed along the west face of the Guadalupe Mountains show no recognizable gradients of these kinds. Core samples of the Bell Canyon and Cherry Canyon Formations taken in the Delaware basin 50 to 80 km from the basin margin closely resemble outcropping sediments in texture, bed thickness, and type of sedimentary structures. The currents carrying sediment into the Delaware basin did not change in transport capacity or regime over large distances.

Considering these five points, I believe that density currents flowed into the Delaware basin primarily because of higher salinity or lower temperature, and not because of suspended fine sediment. These evaporation-concentrated or seasonally chilled water masses must have developed on the northwestern shelf while the middle and upper parts of the San Andres Limestone and the Artesia Group were being deposited. Once set in motion, entrained sediment would add to the effective density of the water. I picture the bottom-hugging

TABLE 1. DENSITY AND VISCOSITY OF NaCl SOLUTIONS FOR VARIOUS CONCENTRATIONS AND TEMPERATURES (INTERPOLATED FROM INTERNATIONAL CRITICAL TABLES)

Salinity wt % NaCl		0°C	10°C	20°C	30°C	40°C
0	ρ*	1.000	0.999	0.998	0.996	0.992
	μ†	1.79	1.31	1.00	0.80	0.66
1.5	ρ	1.011	1.010	1.009	1.006	1.003
	μ	1.81	1.33	1.02	0.82	0.68
3	ρ	1.022	1.021	1.019	1.016	1.013
	μ	1.83	1.35	1.04	0.84	0.70
6	ρ	1.061	1.059	1.056	1.052	1.048
	μ	1.87	1.40	1.08	0.88	0.73
10	ρ	1.077	1.074	1.071	1.067	1.062
	μ	2.05	1.54	1.19	0.97	0.81
15	ρ	1.116	1.113	1.108	1.104	1.099
	μ	2.29	1.72	1.33	1.08	0.90
22	ρ	1.173	1.169	1.164	1.159	1.154
	μ	2.97	2.22	1.70	1.37	1.13

* ρ = *density in g/cm³.*
† μ = *viscosity in centipoise.*

currents moving like a river, flowing from the shelf into the basin, cutting channels, and filling them with sand. These currents flowed under an "atmosphere" of basin waters, whereas the silt-depositing intrastratal flows moved over the basin like a high-altitude dust storm.

Is it plausible to suggest that saline, cold currents could move into a basin with sufficient velocity to erode or transport sand-size sediment, especially when stratification indicates that upper flow regime was commonly attained? I believe the suggestion is plausible, but our lack of knowledge of many important variables prevents an unconditional affirmation. The density and viscosity of sodium chloride solutions over a range of salinities and temperatures are listed in Table 1. Temperature influences the density of these solutions slightly between 0° and 40°C, but viscosity varies by a factor of about 2.5. Salinity changes density to a greater degree than temperature over a range of likely concentrations and has a lesser effect on viscosity. Based on the summary by Middleton (1966a, 1966b) of his experiments with saline density currents, among others, it appears that the head of a density current can move faster than 0.5 m/sec when density contrast is 0.05 g/cm^3 and the head is more than 1 m thick (Middleton, 1966a, Fig. 17). The velocity of uniform flow behind the head, a more important factor in evaluating my interpretation of the Delaware Mountain Group sediment, is more difficult to estimate because of the uncertainty about slope, hydraulic radius, density contrast, and resistance coefficient (Middleton, 1966b, Eq. 4). However, velocities of uniform flows would commonly equal or exceed the velocities attained by head surges (Middleton, 1966a, Fig. 15). Therefore, it seems possible that thin density flows could move at velocities exceeding 0.5 m/sec or more if density contrasts reached a few hundredths of a gram per cubic centimeter. Combinations of salinity and temperature in Table 1 can be selected to obtain density contrasts of this magnitude that still remain within environmentally reasonable limits. Larger viscosities, caused by lower temperatures and higher salinities, can additionally shift transport to upper flow regime mechanisms (Harms and Fahnestock, 1965, p. 87).

ACKNOWLEDGMENTS

R. L. Brenner, M. J. Brady, and R. A. Windecker provided able field assistance; Brenner and D. M. Poole worked on samples in the laboratory. D. B. MacKenzie, F. G. Knight, and R. G. Walker read the manuscript and offered suggestions for improving it. I must single out L. C. Pray for special thanks for introducing me to the geology of this area.

REFERENCES CITED

Adams, J. E., and Frenzel, H. N., 1950, Capitan barrier reef, Texas and New Mexico: Jour. Geology, v. 58, p. 289–312.

Anderson, R. Y., Dean, W. E., Kirkland, D. W., and Snider, H. I., 1972, Permian Castile varved evaporite sequence, west Texas and New Mexico: Geol. Soc. America Bull., v. 83, p. 59–86.

Bagnold, R. A., 1941, The physics of blown sand and desert dunes: London, Methuen & Co., 265 p.

——1954, Experiments on gravity-free dispersion of large solid spheres in a Newtonian fluid under shear: Royal Soc. London Proc., v. 225, ser. A, p. 49–63.

Bouma, A. H., 1962, Sedimentology of some flysch deposits: Amsterdam, Elsevier Pub. Co., 168 p.

Boyd, D. W., 1958, Permian sedimentary facies, central Guadalupe Mountains, New Mexico: New Mexico Bur. Mines and Mineral Resources Bull. 49, 100 p.

Chester, R., and Johnson, L. R., 1971, Atmospheric dust collected off the west African coast: Nature, v. 229, p. 105–107.

Dunham, R. J., 1965, Vadose pisolite in the Capitan reef [abs.]: Am. Assoc. Petroleum Geologists Bull., v. 49, p. 338.

——1969, Vadose pisolite in the Capitan Reef (Permian), New Mexico and Texas, *in* Depositional environments in carbonate rocks: Soc. Econ. Paleontologists and Mineralogists Spec. Pub. 14, p. 182–191.

——1972, Capitan reef, New Mexico and Texas: Facts and questions to aid interpretation and group discussion: Soc. Econ. Paleontologists and Mineralogists (Permian Basin Sec.), Pub. 72–14, 270 p.

Haner, B. E., 1971, Morphology and sediments of Redondo submarine fan, southern California: Geol. Soc. America Bull., v. 82, p. 2413–2432.

Harms, J. C., 1968, Permian deep-water sedimentation by nonturbid currents, Guadalupe Mountains, Texas: Geol. Soc. America, Abs. for 1968, Spec. Paper 121, p. 127.

——1969, Hydraulic significance of some sand ripples: Geol. Soc. America Bull., v. 80, p. 363–396.

Harms, J. C., and Fahnestock, R. K., 1965, Stratification, bed forms, and flow phenomena (with an example from the Rio Grande): Soc. Econ. Paleontologists and Mineralogists Spec. Pub. 12, p. 84–115.

Hayes, P. T., 1964, Geology of the Guadalupe Mountains, New Mexico: U.S. Geol. Survey Prof. Paper 446, 69 p.

Hull, J.P.D., Jr., 1957, Petrogenesis of Permian Delaware Mountain sandstone, Texas and New Mexico: Am. Assoc. Petroleum Geologists Bull., v. 41, p. 278–307.

Jacka, A. D., Beck, R. H., St. Germain, L. C., and Harrison, S. C., 1968, Permian deep-sea fans of the Delaware Mountain Group (Guadalupian), Delaware basin, *in* Guadalupian facies, Apache Mountains area, west Texas: Soc. Econ. Paleontologists and Mineralogists (Permian Basin Sec.), Pub. 68–11, p. 49–90.

Johnson, A. M., 1970, Physical processes in geology: San Francisco, Freeman, Cooper, and Co., 577 p.

Kerr, S. D., and Thomson, A., 1963, Origin of nodular and bedded anhydrite in Permian shelf sediments, Texas and New Mexico: Am. Assoc. Petroleum Geologists Bull., v. 47, p. 1726–1732.

King, P. B., 1942, Permian of west Texas and southeastern New Mexico: Am. Assoc. Petroleum Geologists Bull., v. 26, p. 535–763.

——1948, Geology of the southern Guadalupe Mountains, Texas: U.S. Geol. Survey Prof. Paper 215, 183 p.

——1965, Geology of the Sierra Diablo region, Texas: U.S. Geol. Survey Prof. Paper 480, 185 p.

——1967, Reefs and associated deposits in the Permian of west Texas, *in* Paleotectonic maps of the Permian System: U.S. Geol. Survey Misc. Geol. Inv. Map I–450, p. 36–44.

McDaniel, P. N., and Pray, L. C., 1967, Bank to basin transition in Permian (Leonardian) carbonates, Guadalupe Mountains, Texas [abs.]: Am. Assoc. Petroleum Geologists Bull., v. 51, p. 474.

McKee, E. D., and Oriel, S. S., 1967, Paleotectonic maps of the Permian System: U.S. Geol. Survey Misc. Geol. Inv. Map I–450, 164 p.

Meissner, F. F., 1969, Cyclical sedimentation in Middle Permian strata of the Permian basin, west Texas and New Mexico [abs.], *in* Cyclical sedimentation in the Permian basin: West Texas Geol. Soc. Symposium, 1967, p. 135.

——1972, Cyclic sedimentation in Middle Permian strata of the Permian basin (2d ed.): West Texas Geol. Soc. Pub. 72–60, p. 203–232.

Middleton, G. V., 1966a, Experiments on density and turbidity currents, I. Motion of the head: Canadian Jour. Earth Sci., v. 3, p. 523–546.

——1966b, Experiments on density and turbidity currents, II. Uniform flow of density currents: Canadian Jour. Earth Sci., v. 3, p. 627–637.

Motts, W. S., 1972, Geology and paleoenvironments of the northern segment, Capitan shelf, New Mexico and west Texas: Geol. Soc. America Bull., v. 83, p. 701–722.

Newell, N. D., Rigby, J. K., Fischer, A. G., Whiteman, A. J., Hickox, J. E., and Bradley, J. S., 1953, The Permian reef complex of the Guadalupe Mountains region, Texas and New Mexico — A study in paleoecology: San Francisco, W. H. Freeman & Co., 236 p.

Nottingham, M. W., 1960, Recent Bell Canyon exploration in the north Delaware basin: Southwestern Fed. Geol. Soc. Trans., v. 1, p. 139–153.

Oriel, S. S., Myers, D. A., and Crosby, E. J., 1967, West Texas Permian basin region, *in* Paleotectonic investigations of the Permian System in the United States: U.S. Geol. Survey Prof. Paper 515C, p. C17–C60.

Pray, L. C., 1971, Submarine slope erosion along Permian bank margin, west Texas [abs.]: Am. Assoc. Petroleum Geologists Bull., v. 55, p. 358.
Pray, L. C., and Stehli, F. G., 1962, Allochthonous origin, Bone Springs "patch reefs," west Texas: Geol. Soc. America, Abs. for 1962, Spec. Paper 73, p. 118A–119A.
Silver, B. A., and Todd, R. G., 1969, Permian cyclic strata, northern Midland and Delaware basins, west Texas and southeastern New Mexico: Am. Assoc. Petroleum Geologists Bull., v. 53, p. 2223–2251.
Simons, D. B., Richardson, E. V., and Nordin, C. F., Jr., 1965, Forms generated by flow in alluvial channels: Soc. Econ. Paleontologists and Mineralogists Spec. Pub. 12, p. 34–52.
Southard, J. B., and Harms, J. C., 1972, Sequence of bedform and stratification in silts, based on flume experiments [abs.]: Am. Assoc. Petroleum Geologists Bull., v. 56, p. 654–655.
Sullwold, H. H., Jr., 1961, Turbidites in oil exploration, *in* Geometry of sandstone bodies: Tulsa, Okla., Am. Assoc. Petroleum Geologists, p. 63–81.
Thomas, C., 1968, Vadose pisolites in the Guadalupe and Apache Mountains, west Texas, *in* Guadalupian facies, Apache Mountains area, west Texas: Soc. Econ. Paleontologists and Mineralogists (Permian Basin Sec.), Pub. 68–11, p. 32–35.
Vertrees, C. D., and others, 1964, Cross section through Delaware and Val Verde basins from Lea County, New Mexico, to Edwards County, Texas: West Texas Geol. Soc. Pub. 64–49.
Walker, R. G., 1967, Turbidite sedimentary structures and their relationship to proximal and distal environments: Jour. Sed. Petrology, v. 37, p. 25–43.

Manuscript Received by the Society August 27, 1973
Revised Manuscript Received April 8, 1974

5) Bone Springs Formation

Amanda Calle, Rattanaporn Fongngern, and Valentina Rossi

STRATIGRAPHY OF THE BONE SPRING FORMATION

The Bone Spring Fm:

- Age: Leonardian (284.8 – 270.6 Ma);
- Heterolithic sequence up to 1,060 m thick;
- It comprises slope-to-basin carbonate and siliciclastic sedimentary rocks;
- It represents the downdip equivalent to thick shelf and shelf-margin carbonates (Abo, Yeso Fms) that rimmed the Delaware basin during deposition of Leonardian strata.
- It conformably overlies limestones dated as lower Leonardian.
- It is overlain by the Cutoff Fm (uppermost Leonardian?), which in turn underlies the thick **Delaware Mountain Group: Brushy Canyon, Cherry Canyon, and Bell Canyon Fms**.

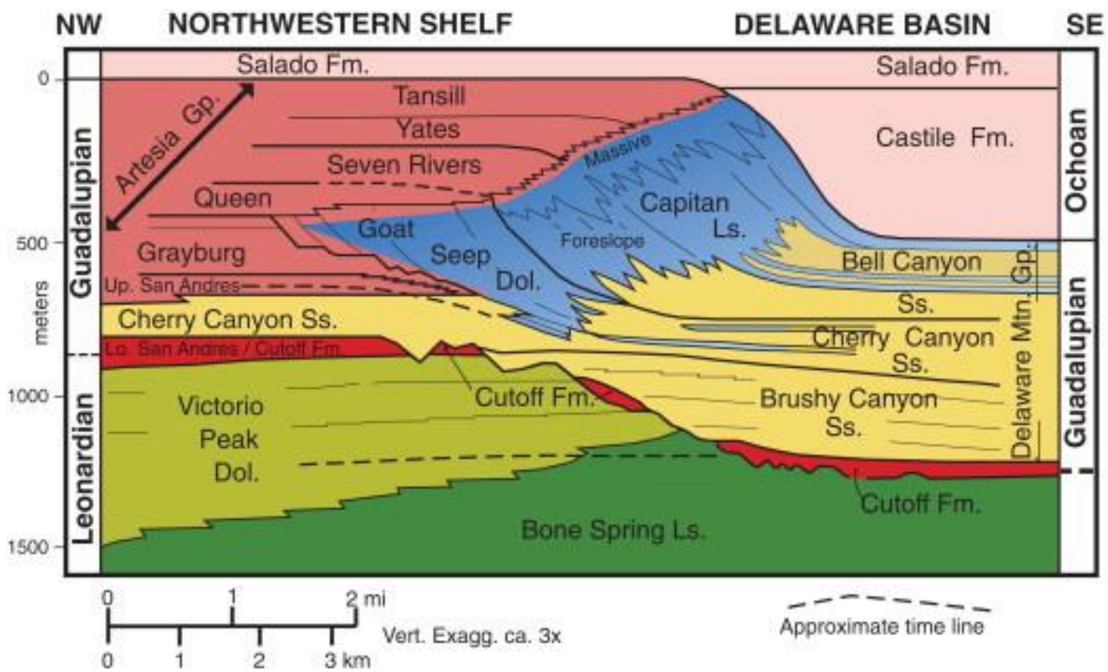

Miall, 2008

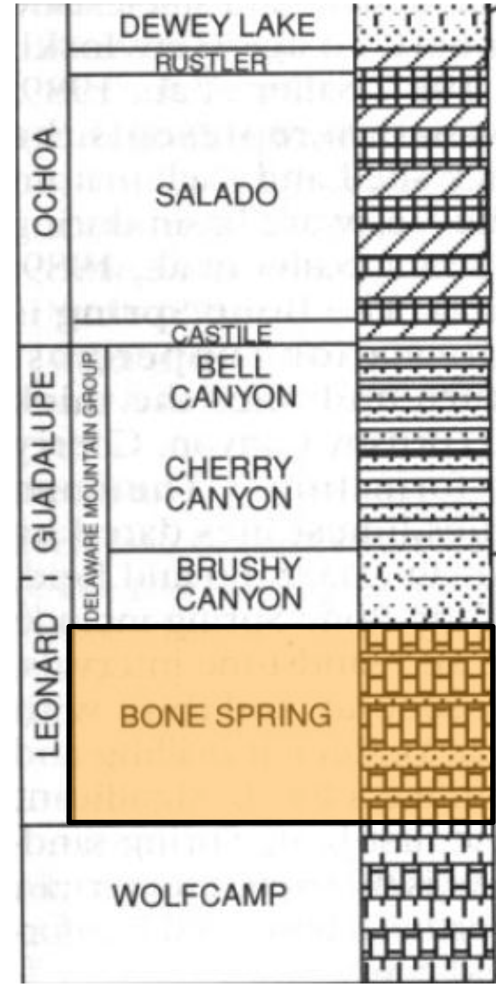

Montgomery, 1997

Internal divisions of the Bone Spring Fm:

- 3 alternating carbonate and sandstone intervals: first, second, and third (with increasing depth);
- Recent drilling has identified a fourth significant sandstone interval above the first Bone Spring sandstone. This fourth sandstone is restricted to certain portions of the slope and northern basin and is informally named the Avalon sandstone.

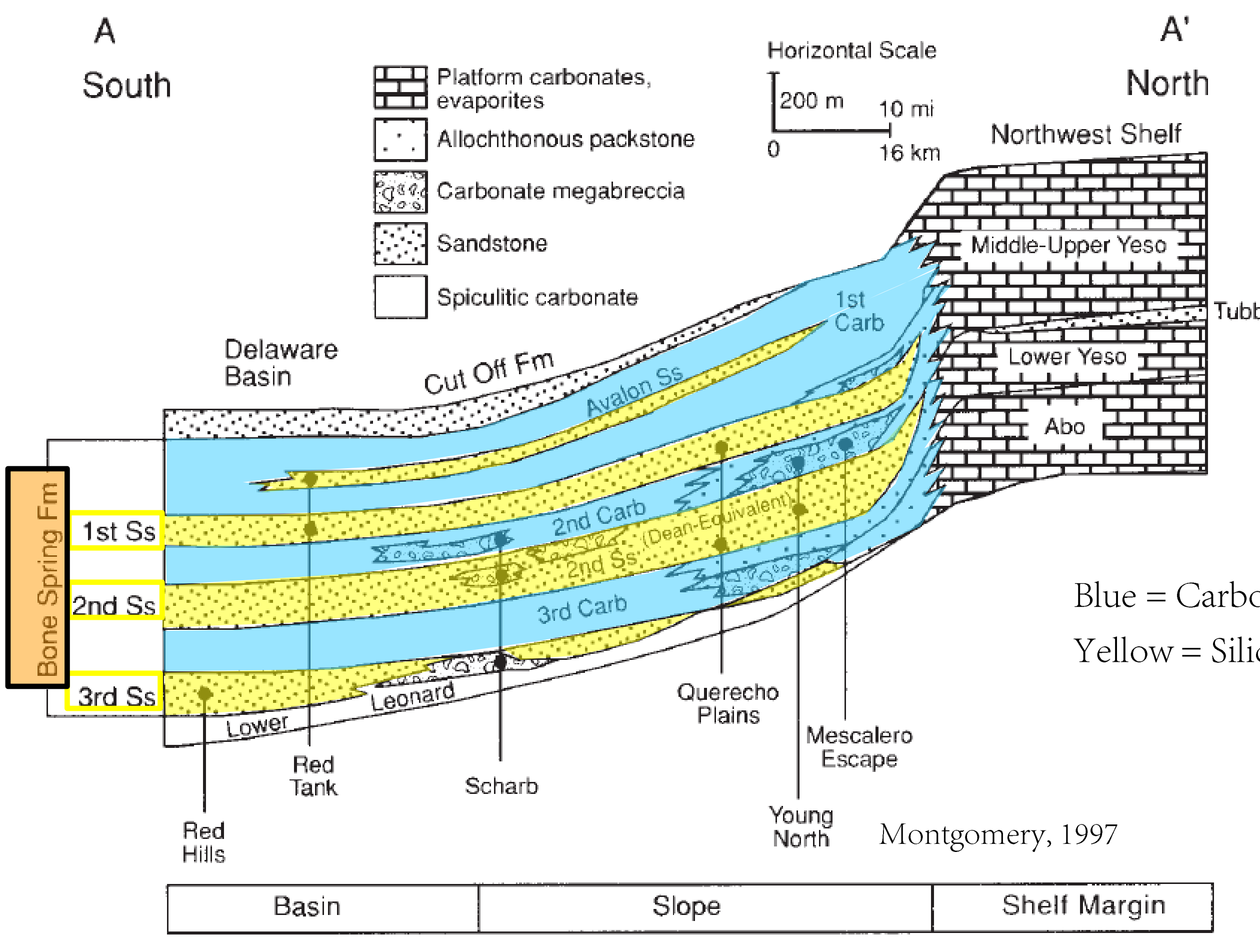

Figure 2—Schematic north-south regional cross section, northern Delaware basin, illustrating general shelf-to-basin relationships in Leonard deposits and productive Bone Spring zones for various fields. Modified from Gawloski (1987), Saller et al. (1989), and Mazzullo (1991).

Blue = Carbonate sediments

Yellow = Siliciclastic sediments

Montgomery, 1997

LITHOFACIES OF THE BONE SPRING FORMATION

Lithofacies 1: Spiculitic Limestone Facies

- Dark, dense, carbonaceous wackestone and mudstone with sponge spicules
- Facies present in:

  first Bone Spring carbonate

  Basinal facies of the second and third carbonate intervals
- Source rock within the basin proper

Lithofacies 2: Pelagic shales and siltstones

- Thinly bedded, calcareous shales and siltstones
- Interbedded in sandstones facies, in the shelf and basin
- Important seal capacity to submarine-fan sandstones

Nance, 2011

Lithofacies 3: Laminated mudstone facies

- Black, laminated dolomitic mudstone that grades downdip to spiculitic limestones
- 75-90% microcrystalline dolomite
- Rarely intercalacated with thin beds of bioclastic chert
- TOC 4.3%
- Probable oil source rocks

Nance, 2011

Lithofacies 4: Dolomitized breccia

- Coarse, angular detritus
- Wackestone-packestone matrix
- Dark brown-gray, fine-medium crystalline dolomite
- Clasts composition: laminated siltstone, cross-bedded peloidal packstones and grainstones, bryozoan-algal boundstones and coral-bearing skeletal debris (crinoids, brachiopods , pelecypods)
- Lighter colored shelf derived material and darker colored slope-derived material
- Angular and brittle shelf-derived clasts, probably lithified prior to transport
- Upper and lower, abrupt and erosive contacts
- Variable thickness: 0.05-24 m
- Submarine debris flows deposits

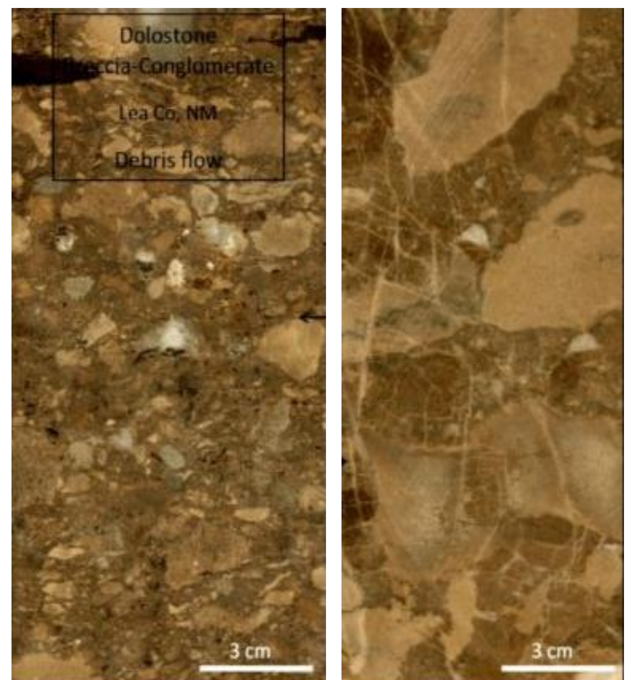

Lithofacies 5: Dolomitized bioclast packstone

- Associated with dolomitized megabreccia facies
- Bioclast-pelloid packstones
- Minor wackestone and grainstone
- Grains: skeletal debris derived from crinoids, bivalves, sponges, etc.
- Some areas affected by fracture-enhancing reservoir quality
- Present in the 1st and 3rd carbonate intervals

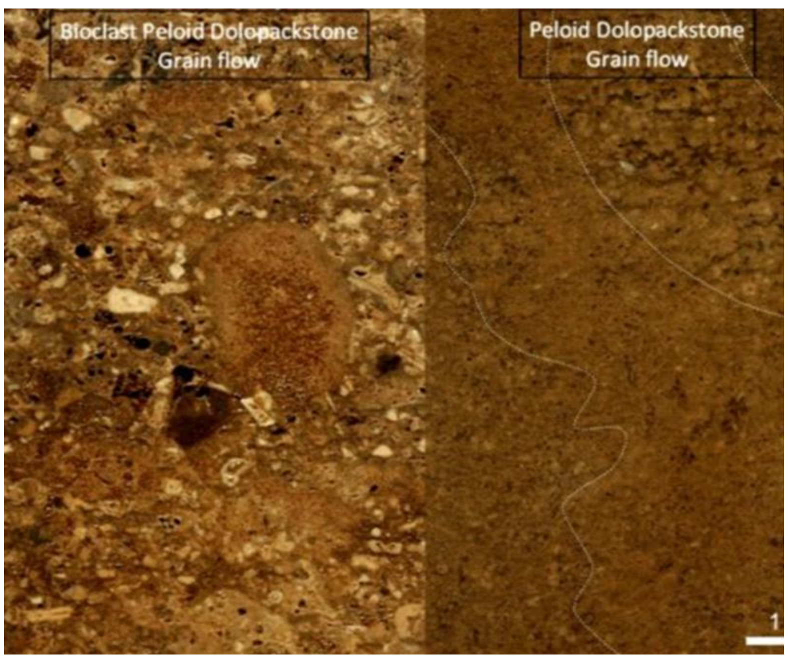

Nance, 2011

Lithofacies 6: Fine-grained sandstone

- Light gray, very fine to fine grained quartzose sandstone and siltstones
- Well sorted to poorly sorted
- Angular-subangular quartz grains, minor feldspars
- Authigenic dolomite cement (up to 30%)
- Interlayered dark organic rich layers
- Sedimentary structures: horizontal and inclined lamination, ripple cross-lamination, trace fossils, convolute bedding, flame structures, bioturbation, rip-up clasts
- Abrupt upper and lower boundaries

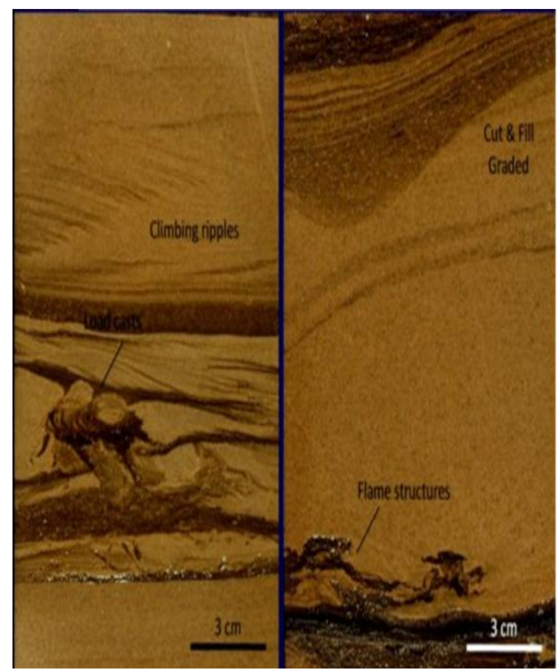

Nance, 2011

DEPOSITIONAL ENVIRONMENTS OF THE BONE SPRING FORMATION

= Turbidite deposits in submarine channel/canyon, slope fans

Characteristics:

- Reciprocal and cyclic sedimentation (sea-level control)
- Depositional styles influenced by syndepositional relief
- Localized deposition (variation of sedimentation along slope causes complex lateral continuity)
- **Lowstand**: siliciclastic slope and basin floor fans

Processes: density current& mass wasting (sediments transported through local submarine canyon, channel, debris flow, and slump)

- **Transgression and Highstand**: slope carbonate, detrital carbonate, mega breccia

Processes: density current and mass wasting

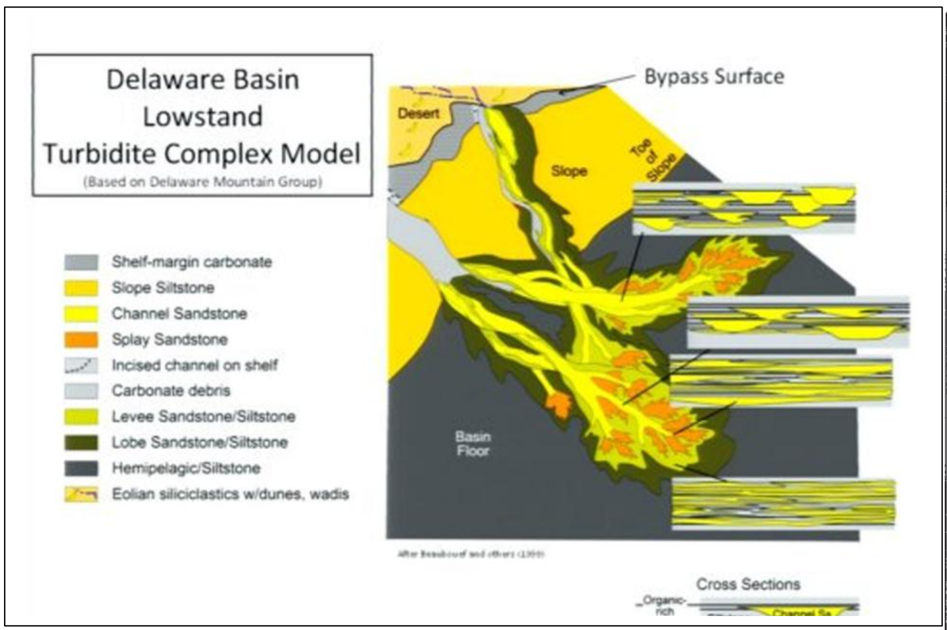

Nance, 2011

Depositional model of the Bone Spring Fm. (Montgomery, 1997)

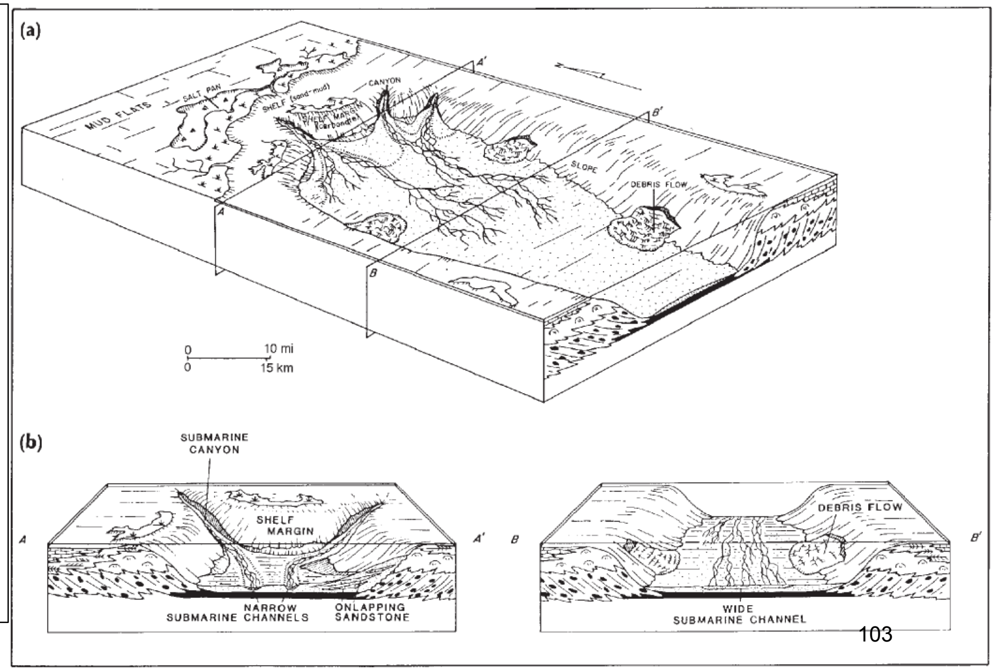

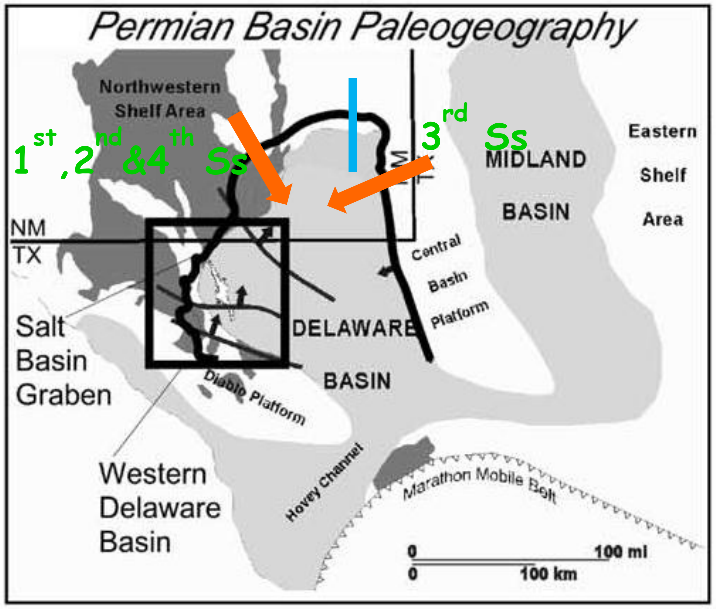

Gardner et al. (2003)

In the northern Delaware basin, Central Basin platform (CBP) supplied sediment for the third Bone Spring sandstone while the first and second Bone Spring sandstones derived sediments from the Northwestern shelf.

During lowstand of sea level the carbonate factory was shut down and siliciclastic sediments bypassed shelf to the slope and basin floor (turbidite deposits). Carbonate platform was reactivated during sea level transgression and highstand and built up the platform margin which periodically collapsed and produced debris flows or tubidity currents that deposited on the slope and basin floor such as megabreccia.

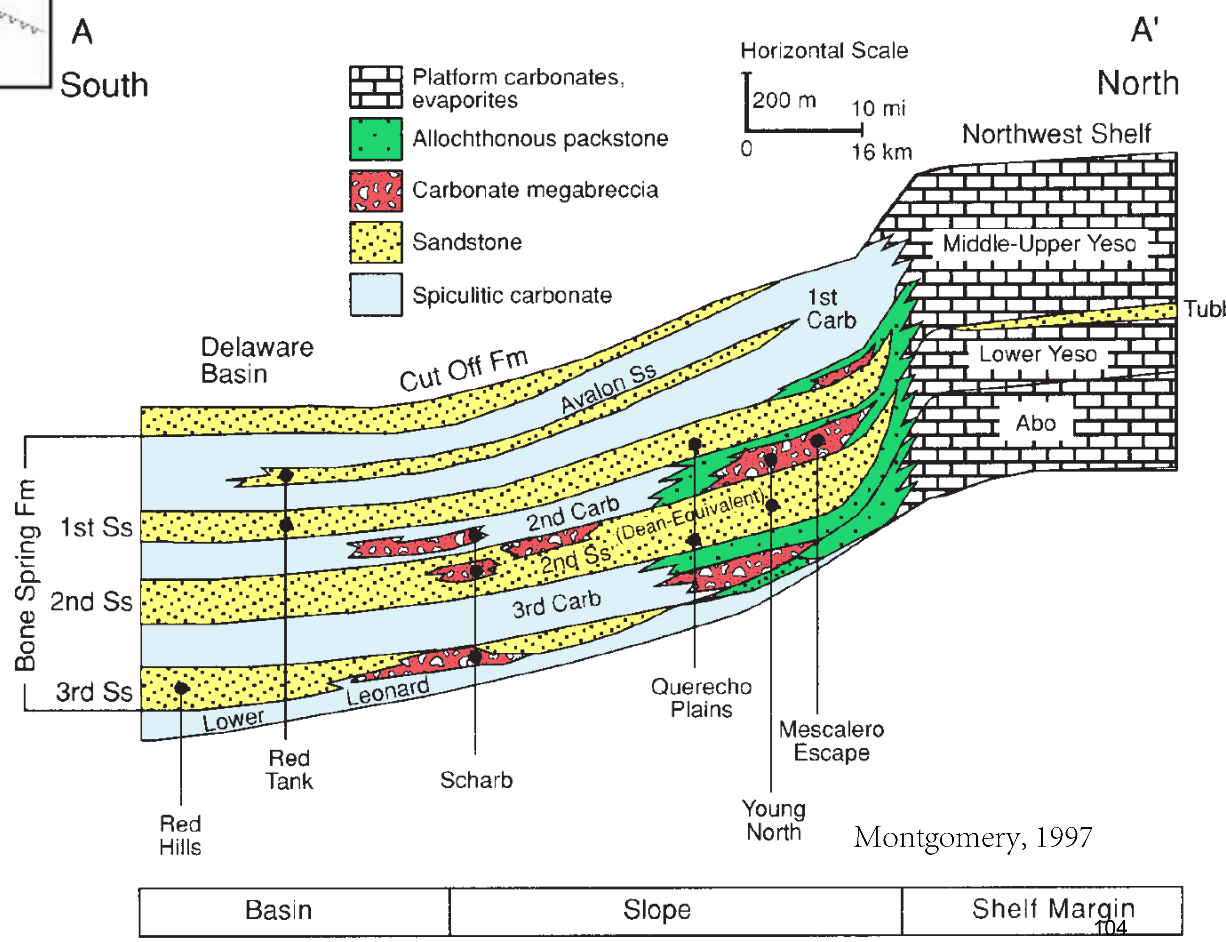

Montgomery, 1997

Key papers

Gawloski, T. F., 1987, Nature, distribution, and petroleum potential of Bone Spring detrital sediments along the northwest shelf of the Delaware Basin, *in* Cromwell, D., and Mazzullo, L. J., eds., The Leonardian facies in W. Texas and S.E. New Mexico and guidebook to the Glass Mountains, West Texas: Society of Economic Paleontologists and Mineralogists Permian Basin Section Publication 87-27, p. 85-105.

Montgomery, S. L., 1997, Permian Bone Spring Formation; sandstone play in the Delaware Basin; Part I, slope:American Association of Petroleum Geologists Bulletin, v. 81, no. 8, p. 1239-1258.

<u>Additional material: Presentation available on BEG website</u>,

Nance, S., 2011, Bone Spring Formation Deep-Water Succession of the Delaware Basin, Texas and New Mexico: Facies, Rock-Body Geometries, Depositional Model, and Developing Investigation of Mudrock, BEG seminar (Oct 7, 2011)

E & P Notes

Permian Bone Spring Formation: Sandstone Play in the Delaware Basin Part I—Slope

Scott L. Montgomery[1]

ABSTRACT

New exploration in the Permian (Leonardian) Bone Spring formation has indicated regional potential in several sandstone sections across portions of the northern Delaware basin. Significant production has been established in the first, second, and third Bone Spring sandstones, as well as in a new reservoir interval, the Avalon sandstone, above the first Bone Spring sandstone. These sandstones were deposited as submarine-fan systems within the northern Delaware basin during periods of lowered sea level. The Bone Spring as a whole consists of alternating carbonate and siliciclastic intervals representing the downdip equivalents to thick Abo-Yeso/Wichita-Clear Fork carbonate buildups along the Leonardian shelf margin. Hydrocarbon exploration in the Bone Spring has traditionally focused on debris-flow carbonate deposits restricted to the paleoslope. Submarine-fan systems, in contrast, extend a considerable distance basinward of these deposits and have been recently proven productive as much as 40–48 km south of the carbonate trend.

INTRODUCTION

Recent exploration in the Delaware basin of southeastern New Mexico and west Texas has significantly expanded oil and gas production from the Permian Bone Spring formation (Figure 1). The Bone Spring is a heterolithic sequence up to 1060 m thick comprising slope-to-basin carbonate and siliciclastic sedimentary rocks of Leonardian age (Gawloski, 1987; Mazzullo and Reid, 1987; Saller et al., 1989; Mazzullo, 1991). The formation represents the downdip equivalent to thick shelf and shelf-margin carbonates that rimmed the Delaware basin during deposition of Leonardian strata (Saller et al., 1989; Mazzullo, 1991) (Figure 2). The Bone Spring is overlain by the Cutoff formation (uppermost Leonardian?), which in turn underlies the thick Delaware Mountain Group (Brushy Canyon, Cherry Canyon, and Bell Canyon formations). The Bone Spring conformably overlies limestones dated by fusulinids as lower Leonardian (Mazzullo and Reid, 1987). Internal divisions of the Bone Spring include three alternating carbonate and sandstone intervals, labeled, respectively, first, second, and third with increasing depth (Figures 2, 3). Recent drilling and field reevaluation have identified a fourth significant sandstone interval above the first Bone Spring sandstone. This fourth sandstone is restricted to certain portions of the slope and northern basin and is informally named the Avalon sandstone.

These rocks can be broadly divided into slope and basin assemblages, with significant overlap between the two. Slope deposits consist mainly of highstand basinal carbonates and lowstand detrital carbonates and submarine-fan siliciclastics (Gawloski, 1987; Mazzullo and Reid, 1987; Saller et al., 1989). In the basin assemblage, detrital carbonates are rare, and the Bone Spring formation is comprised of alternating

[1]Petroleum Consultant, 1511 18th Avenue East, Seattle, Washington 98112.
Gratitude is expressed to the following individuals and companies: Larry Brooks, Parker and Parsley, who contributed data and considerable expertise; Frank Messa, Harvey E. Yates Company; Mike Hays, Yates Petroleum; S. J. Mazzullo, Wichita State University; Tom Tiny, Santa Fe Energy; and Ralph Worthington, Consultant.
Send reprint requests to AAPG Publications Manager, P.O. Box 979, Tulsa, Oklahoma 74101-0979.
Gcf = billion cubic feet; Mcf = million cubic feet; kcf = thousand cubic feet.

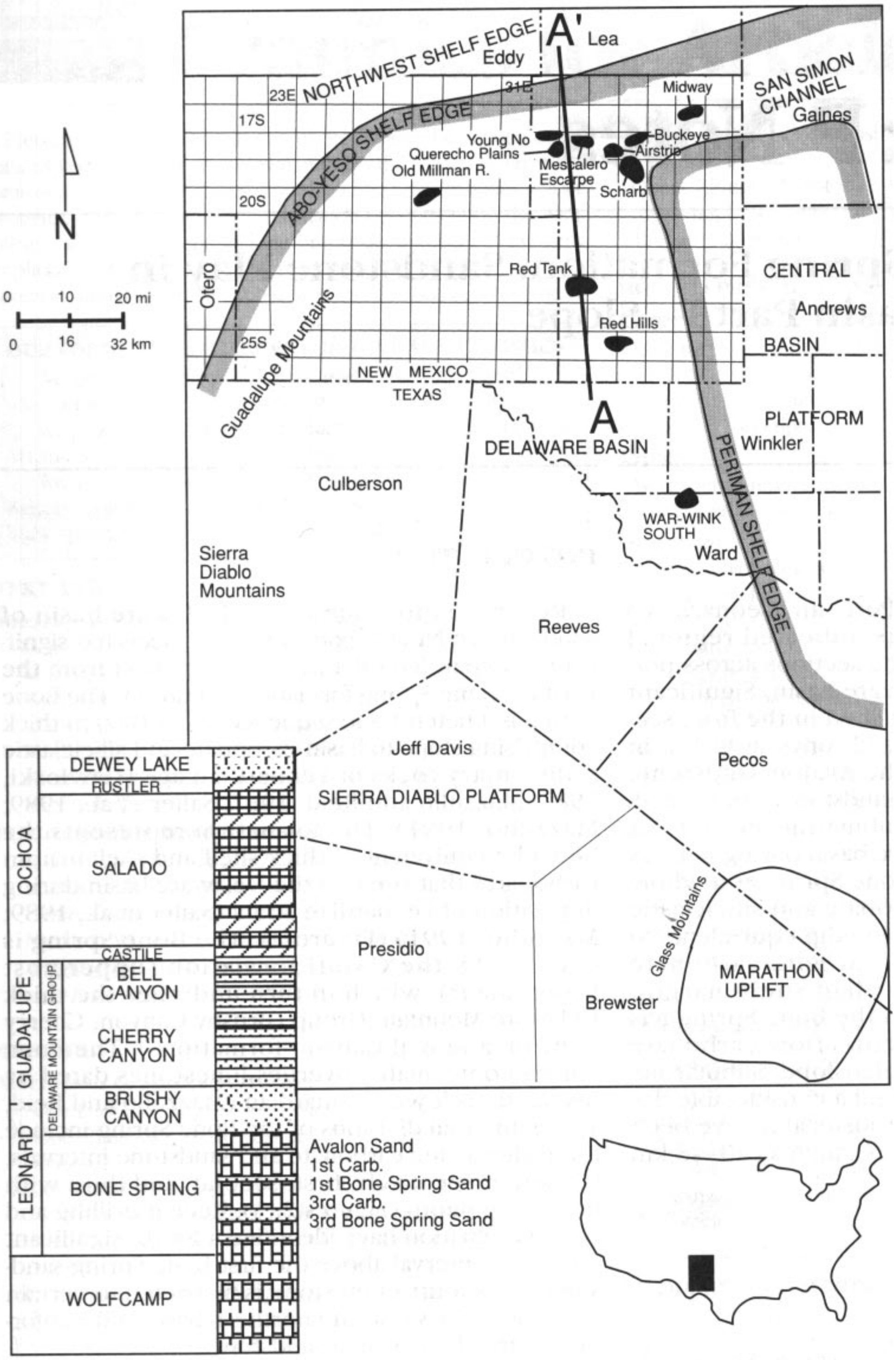

Figure 1—Regional map and Permian stratigraphic column, Delaware basin. Map shows location of Bone Spring production relative to major tectonic elements. Cross section line refers to Figure 2.

spiculitic limestone, pelagic shales, and submarine-fan deposits.

Reservoirs in slope assemblage rocks occur in three lithologies: (1) dolomitized carbonate megabreccias, (2) dolomitized bioclastic and peloidal packstones, and (3) very fine to fine grained turbiditic sandstones. Basin assemblage reservoirs are exclusively in the last reservoir type, corresponding to submarine-fan sandstones. Allochthonous carbonates were deposited as submarine debris flows, with material derived mainly from the shelf and deposited along the lower portions of the slope.

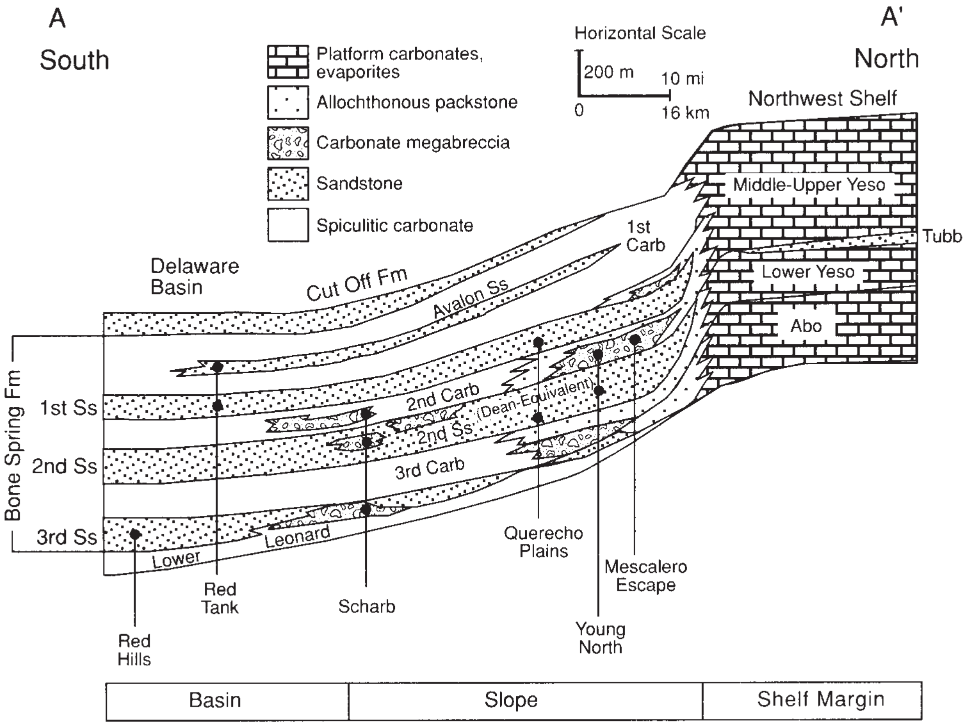

Figure 2—Schematic north-south regional cross section, northern Delaware basin, illustrating general shelf-to-basin relationships in Leonard deposits and productive Bone Spring zones for various fields. Modified from Gawloski (1987), Saller et al. (1989), and Mazzullo (1991).

These deposits thus have a restricted occurrence; however, reservoir sandstones, representing mainly submarine channel and levee deposits, extend into the basin proper and thus define more regional exploratory targets. This more regional distribution has been recently confirmed by discoveries in southern Lea County (New Mexico), including Red Hills field, located approximately 64 km south of the main slope productive trend (Figure 1). Equally significant are Bone Spring sandstone discoveries in western Ward County (Texas) along the margin of the Central Basin platform (CBP). Drilled in late 1996 and early 1997, these Texas discoveries effectively open up large new areas for Bone Spring exploration both in the deeper basin and along the CBP margin.

To date, drilling on the slope has established production in the second and third carbonate intervals, as well as in the Avalon, first Bone Spring, and second Bone Spring sandstones. Not all these reservoirs produce in any single location. South of the main slope trend in Lea County (New Mexico), between T20S and T24S, the Avalon, first Bone Spring, and second Bone Spring sandstones have proven productive. Still farther south, in T25S, R33-34E (Red Hills field), and along the western margin of the CBP in Ward County (Texas), the third Bone Spring sandstone forms the dominant reservoir zone.

Early exploration in the Bone Spring formation focused on sandstone intervals because these represent regional equivalents to the highly productive Dean and lower Spraberry intervals of the Midland basin. In addition, early scattered production in the eastern part of the basin, near the margin of the CBP, was established in what were called upper Wolfcampian sandstone reservoirs, now known to compose the third Bone Spring sandstone. During the 1970s and 1980s, interest shifted to oil potential in the second Bone Spring and third Bone Spring carbonate intervals (Gawloski, 1987). This resulted in a number of significant fields, such as Mescalero Escarpe, Scharb, Airstrip, Young North, and Buckeye (see Figure 1). Moderate-to-good reservoir quality and high production rates in these carbonates contrasted with low-permeability, and often low-productivity, Bone Spring sandstones. Subsequent activity during the early 1990s focused new interest on these sandstones in light of serendipitous and targeted discovery in fields such as Old Millman Ranch and Young North. Success in these areas in the first and second Bone Spring sandstones encouraged reevaluation of the third Bone Spring sandstone interval to the south, resulting in discovery at Red Hills field in 1995 and at War-wink West in 1996.

Recent drilling has had several important consequences, including (1) extending the existing Bone Spring sandstone productive trend as much as 48 km to the southwest, (2) locating reserves in new portions of the basin, (3) discovering a new productive reservoir zone (Avalon sandstone), and (4) delineating areas and patterns of productivity for different sandstone intervals in the Bone Spring. The overall result is that there now exist three overlapping sandstone play areas for Bone Spring drilling in the Delaware basin. These areas consist of two basin margin plays—the first along the northern slope and the second along the margin of the CBP to the east—and a downdip basinal play concentrated in the northern one-half of the basin. A fourth potential play, not discussed here, exists in detrital carbonates along the CBP margin.

This paper is divided into two parts, both focusing on sandstone reservoirs. Part one provides regional background and specific data on first and second Bone Spring sandstone production along the northern slope. Part two examines downdip areas, concentrating on the Red Hills field area. Previous work on the petroleum geology and potential of the Bone Spring formation can be found in Silver and Todd (1969), Wiggins and Harris (1985), Gawloski (1987), Mazzullo and Reid (1987), Saller et al. (1989), Mazzullo (1991), Hayes (1995), and Hart (1997). In addition, in this paper, I summarize and update such work, presenting new data from Old Millman Ranch, Young North, Red Tank, and Red Hills fields.

REGIONAL SETTING

The Delaware basin represents the westernmost portion of the Permian basin geologic province and is bounded on three sides by major basement uplift features (see Figure 1): the Marathon fold belt to the south, the Diablo platform to the west, and the CBP on the east. The northern boundary of the Delaware basin is the Northwest shelf. Between this boundary and the CBP, a narrow passage known as the San Simon channel connected the Delaware basin with the Midland basin during Leonardian deposition.

The Delaware basin as a whole is divided into southern and northern portions by the east-west–trending Mid-Basin fault, a major strike-slip fault zone that continues eastward into the CBP and is related to late Paleozoic structural evolution of this uplift (Shumaker, 1992). North of this fault zone, structures include local reverse faulting and graben development along the border of the CBP, and minor anticlinal features along the Leonardian slope in southeastern New Mexico. Published seismic and structural data for the western margin of the CBP reveal large-scale faulting with considerable diversity in structural style and up to 666 m or more of offset at the base of the Wolfcampian (Hills, 1984; Frenzel et al., 1988; Kosters et al., 1989; Shumaker, 1992; Yang and Dorobek, 1995) (Figure 3). Proprietary isopach and structure data suggest that movement continued locally through deposition of the lowermost Leonardian and third Bone Spring sandstone. An apparent southeastern regional tilt was imposed during the Late Cretaceous–early Tertiary as a result of Laramide transpression in the Trans-Pecos region to the west (Dickerson, 1985).

BONE SPRING LITHOFACIES

The Bone Spring formation consists of three main carbonate intervals and three or four sandstone zones (Figure 4). Six major lithofacies have been identified.

Spiculitic Limestone Facies

The spiculitic limestone facies consists of dark, dense, carbonaceous wackestone and mudstone containing varying amounts of sponge spicules. Such basinal material composes the major portion of the first (or upper) Bone Spring carbonate and the downdip, basinal portions of the second and third Bone Spring carbonate intervals. This lithofacies may constitute an important source rock within the basin proper.

Pelagic Shales and Siltstone Facies

The pelagic shales and siltstone basinal facies consist of dark, thinly bedded, calcareous shales and siltstones that occur within Bone Spring sandstone intervals, both along the slope and in the basin. Pelagic facies rocks act as important seals to productive submarine-fan sandstones.

Laminated Mudstone Facies

Black, laminated dolomitic mudstone exists mainly along the slope, grading downdip into spiculitic limestones. The laminated mudstones consist of 75–90% microcrystalline dolomite and contain up to 4.3 wt. % total organic carbon. These facies have been identified geochemically as probable source rocks for oil in Bone Spring reservoirs along the slope (Saller et al., 1989). In places, the mudstones are intercalated with thin beds of bioclastic chert (e.g., at Scharb field) (see Bradshaw, 1989).

Dolomitized Breccia Facies

Coarse, angular detritus in a packstone-wackestone matrix comprises the dolomitized breccia facies.

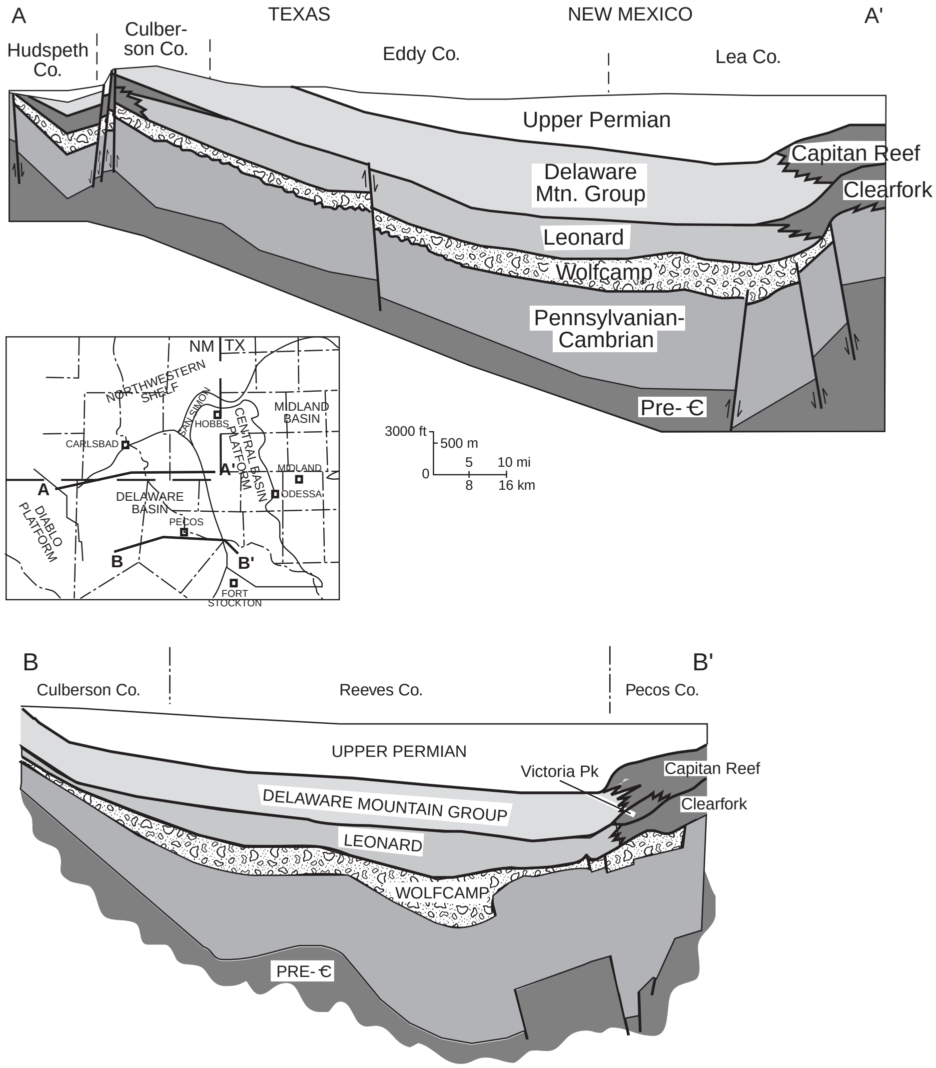

Figure 3—East-west regional cross sections showing generalized structure in the northern and central Delaware basin and western margin of the Central Basin platform. Modified from Hills (1984).

Individual clasts display a range of compositions, including laminated siltstone, cross-bedded peloidal packstones and grainstones, bryozoan-algal boundstones, and coral-bearing skeletal debris (Wiggins and Harris, 1985; Gawloski, 1987; Saller et al., 1989). Such variety is interpreted to indicate derivation from the shelf and upper slope. Deposition is inferred to have taken place by submarine debris flows, possibly during periods of sea level lowstand (Wiggins and Harris, 1985; Mazzullo and Reid, 1987). This facies comprises an important reservoir within the second and third Bone Spring carbonates of the slope productive trend.

Dolomitized Bioclast Packstone Facies

The dolomitized bioclast packstone facies is associated with the dolomitized megabreccia facies and consists of bioclast-pelloid packstones with lesser amounts of wackestone and grainstone. Grains are mainly skeletal debris derived from crinoids, bivalves, sponges, and other genera. Fractures are abundant in certain portions of this facies, producing in-situ breccias and greatly enhancing reservoir quality. At Mescalero Escarpe field, bioclast-peloid dolomites comprise the lower, thicker portion of the second Bone Spring carbonate. Elsewhere, this facies has been proposed for parts of the first and third carbonate intervals as well (Mazzullo, 1991).

Fine-Grained Sandstone Facies

The fine-grained sandstone facies is generalized to include all four sandstone intervals in the Bone Spring formation (Avalon, first, second, third Bone Spring sandstones). (Individual sandstone facies types will be discussed in following sections.)

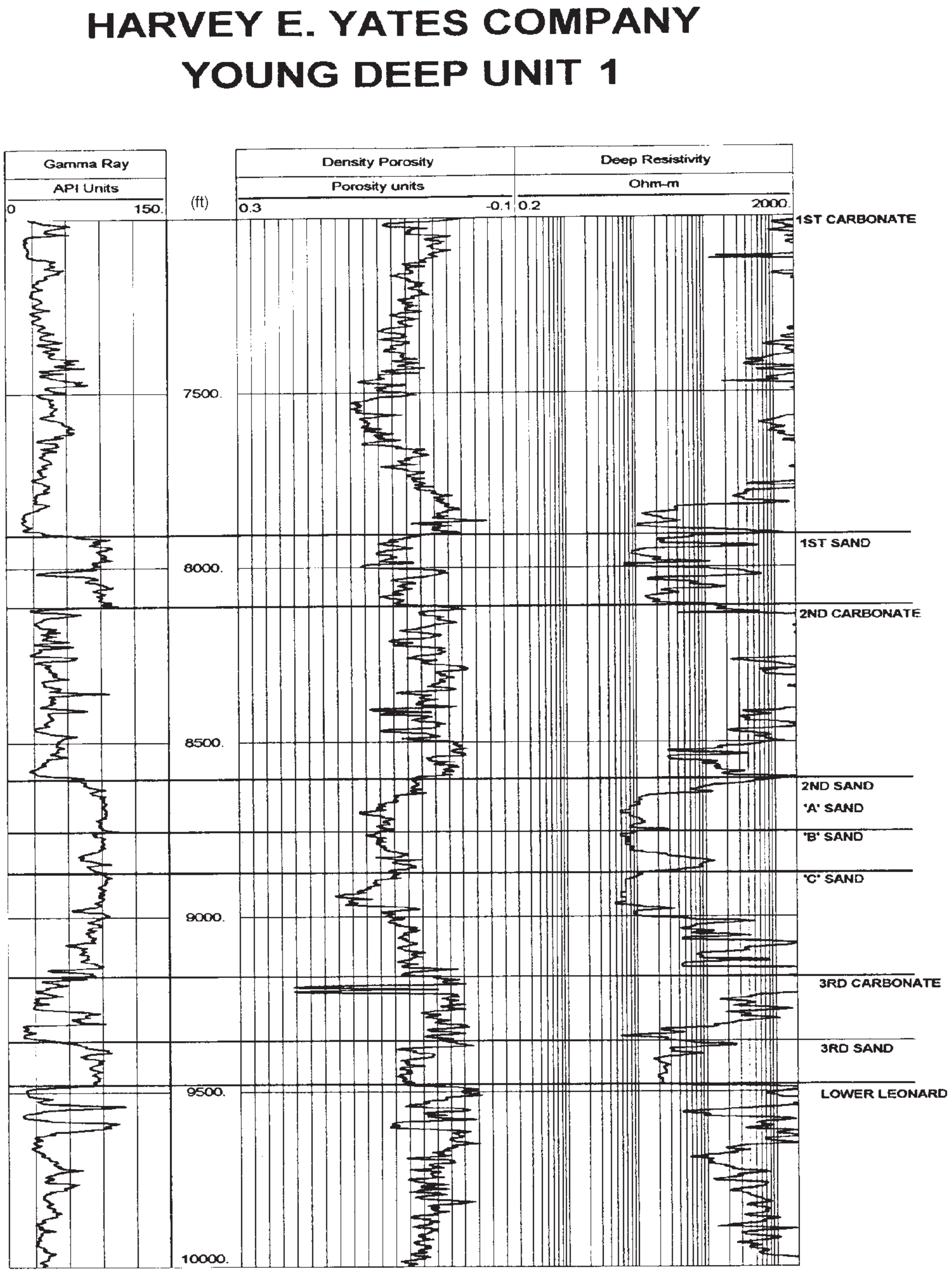

Figure 4—Type log, Bone Spring formation, Young North field, Lea County, New Mexico. Courtesy Harvey E. Yates Company.

These strata consist of very fine to fine grained quartzose sandstones and siltstones with 6–12% clay (by volume) and significant authigenic dolomite cement (up to 30%). Sand grains consist of angular to subangular quartz (45–75%) and lesser feldspar (4–22%), with textures ranging from well sorted to very poorly sorted. The sandstones are commonly interlaminated with dark organic-rich layers. Sedimentary structures include horizontal and inclined lamination, ripple cross-lamination, trace fossils, convoluted bedding, flame structures, and bioturbation. The high clay content of these sandstones generally produces a low-resistivity, high gamma-ray log signature.

Slope assemblage strata include all six lithofacies types. Basin assemblage rocks consist of spiculitic limestones, pelagic shales and siltstones, and sandstone lithofacies. Depending upon the location, individual Bone Spring sandstone zones consist of varying proportions of channel, levee/overbank, and fan-lobe subfacies with occasional interbeds of basinal limestone and pelagic shale. Clay content and dolomite cement are lowest (both <10%) and reservoir quality is highest in channel sandstones.

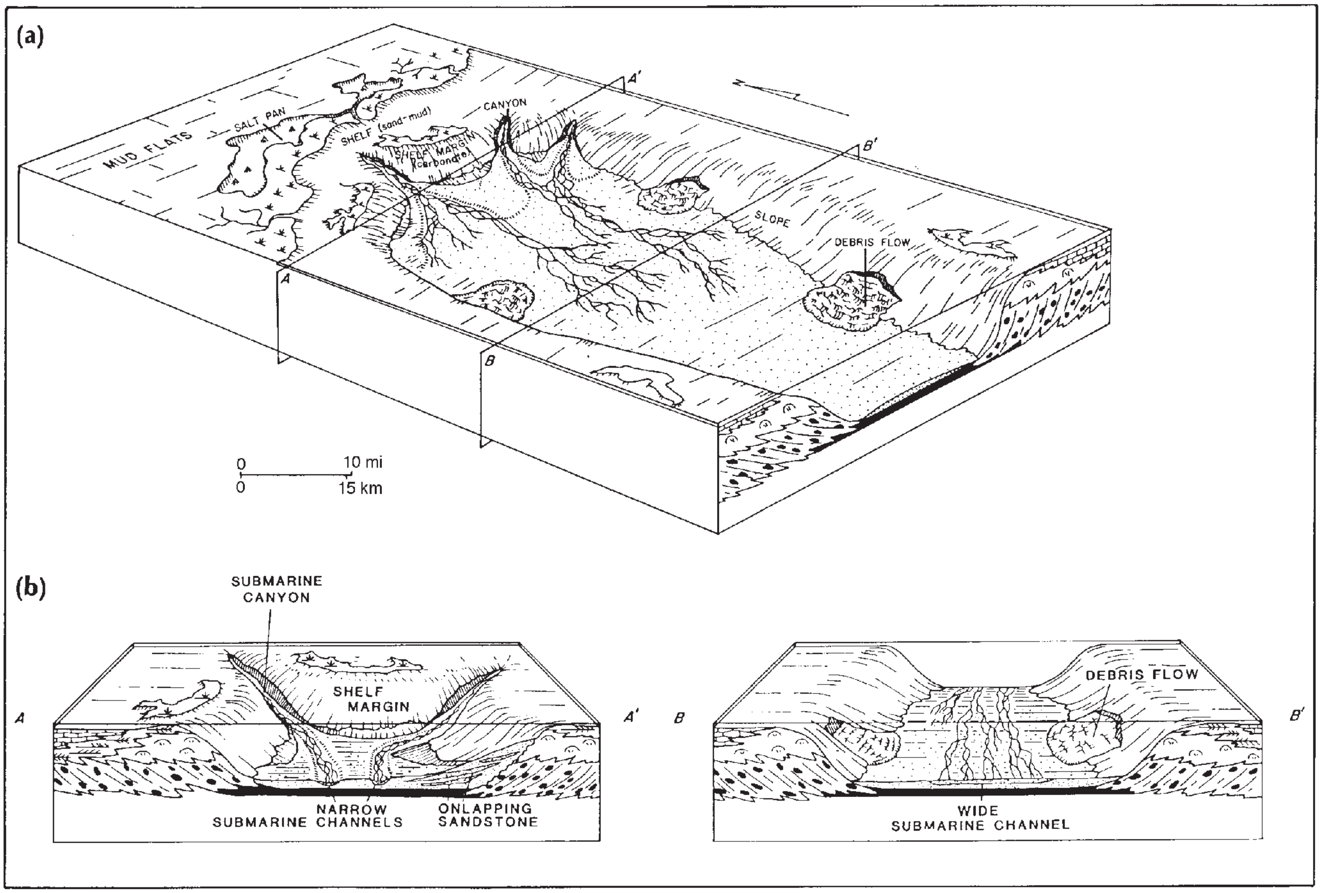

Figure 5—Block diagram illustrating depositional environments inferred for the Spraberry and Dean sandstones of the Midland basin. Similar environments may have existed for the equivalent Bone Spring sandstones of the Delaware basin. From Handford (1981).

SANDSTONE DISTRIBUTION

The specific distribution of sandstone development in the Bone Spring is an important consideration in recent Bone Spring exploration. Regional isopach data indicate the basin had a north-northwest axis, with sediment delivered to the slope by means of local submarine canyons and channels, as well as slump and debris flows. In the northern one-half of the Delaware basin, sediment source areas included both the Northwestern shelf (first and second Bone Spring sandstones) and CBP (third Bone Spring sandstone). Comparison of isopach maps for individual sandstone intervals suggests that sediment supply was somewhat localized along the slope, producing complex lateral relationships between individual submarine-fan systems with sheet-type sands downdip. Sea level drop caused fan systems to prograde into the basin proper, producing coarsening-upward vertical successions in some areas.

The first and second Bone Spring sandstones are widespread throughout the northern Delaware basin (New Mexico portion), but display maximum development along the northern slope. Along the margin of the CBP, they are silty and clay rich and thus appear to represent distal deposits. On the slope, the first Bone Spring sandstone is slightly coarser grained on average than the second Bone Spring sandstone, suggesting more proximal sediment input. The Avalon sandstone exists only along the central portion of the slope and in areas immediately downdip, with maximum development south of the slope productive trend (for example, in southeastern Eddy County, New Mexico). The Avalon, first Bone Spring sandstone, and second Bone Spring sandstone were derived from the north, as indicated by dipmeter data, isopach patterns, fan morphology, and channel orientation.

In contrast, the third Bone Spring sandstone is thin to absent along much of the northern slope, instead displaying maximum development in the

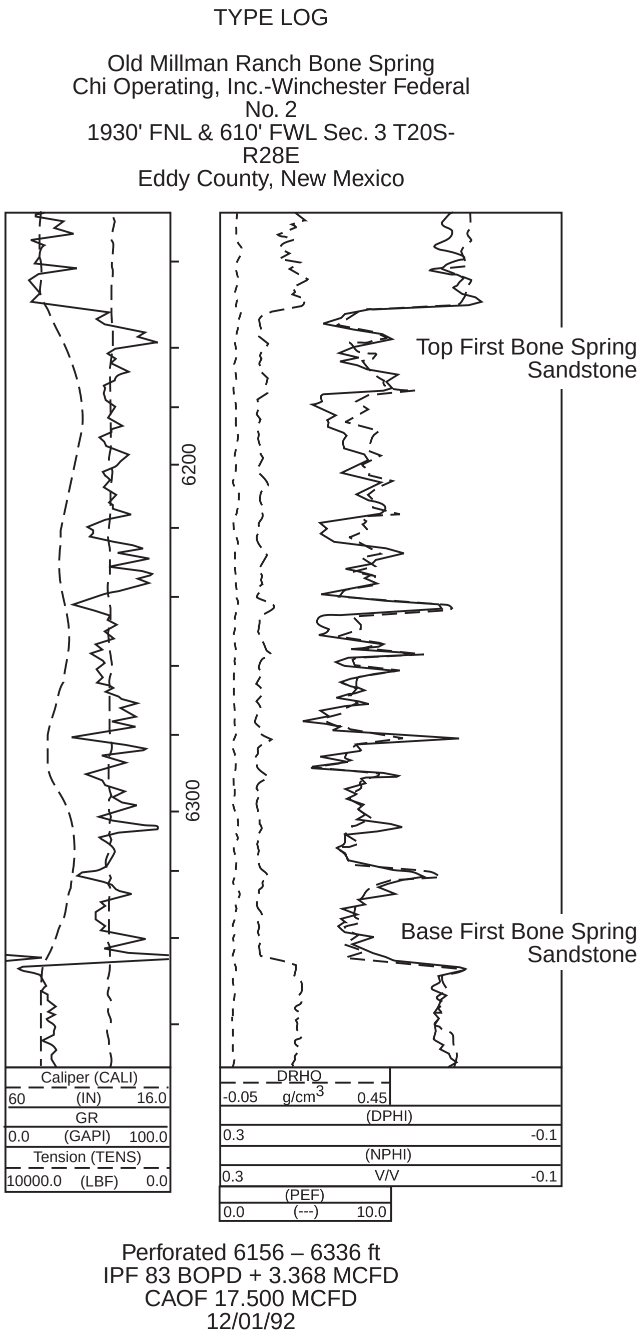

Figure 6—Type log through the productive first Bone Spring sandstone, Old Millman Ranch field, Eddy County, New Mexico. Modified from Hayes (1995).

northeastern basin and along the margin of the CBP. Regional cross sections between western Ward County (Texas) and southernmost Lea County (New Mexico) show the third Bone Spring sandstone to be consistently 90 m or more thick. In contrast, it is less than 33 m thick at Young North field and absent in Mescalero Escarpe field. Dipmeter data from wells at Red Hills field suggest a source area to the northeast (L. Brooks, 1997, personal communication). Published isopach, structural, and facies distribution data at Scharb field, Lea County (New Mexico), located 19 km south of the Abo-Yeso shelf edge, indicate a similar northeastern source for multiple carbonate debris-flow units (Mazzullo and Reid, 1987). This source has been explained as the result of local channeling; however, proximity to the CBP margin (8 km) may argue for more detailed study.

DEPOSITIONAL HISTORY

The Bone Spring formation was deposited as the slope and basinal equivalent to thick carbonate sequences that rimmed the Delaware basin (Saller et al., 1989). These carbonate sequences are variously referred to as the Abo and Yeso intervals along the Northwest shelf and the Clear Fork and Wichita intervals along the Central Basin platform (see Figures 2, 3). The thick, laterally confined shelf margin buildups in these sequences indicate a dominance of vertical growth during this time, with only slight basinward progradation. Sedimentation was controlled by a combination of basinal subsidence and cyclic sea level fluctuations (Saller et al., 1989). Subsidence appears to have been fairly rapid, because up to 365–455 m of depositional relief exists between the northern shelf margin and toe of the slope (Wiggins and Harris, 1985; Gawloski, 1987; Saller et al., 1989), with even greater relief along the CBP (Hills, 1984).

Interpretations of Bone Spring depositional history have proposed cyclic sedimentation, with major lithofacies tracts associated with sea level changes (Saller et al., 1989; Mazzullo, 1991). During periods of rapid sea level rise, carbonate production and vertical growth along the shelf margin were presumably at a maximum, with resedimented carbonates dominant on the slope and in the basin. At maximum highstand, the shelf margin built to near sea level, and a combination of physical (e.g., wave related) and biological erosion produced significant amounts of accumulating detritus that periodically collapsed into debris flows that reached the slope and slightly beyond. Deposition was fairly localized and produced numerous individual lenses of megabreccia with complex lateral relationships. Saller et al. (1989) indicated that paleoslope angles of at least 10–15° may have been required for breccia deposition. In central and southwestern Eddy County (New Mexico), paleoslope angles averaged about 6° and progradation of the shelf margin took place. Strong currents within the San Simon Channel dispersed most or all debris-flow material that may have been produced.

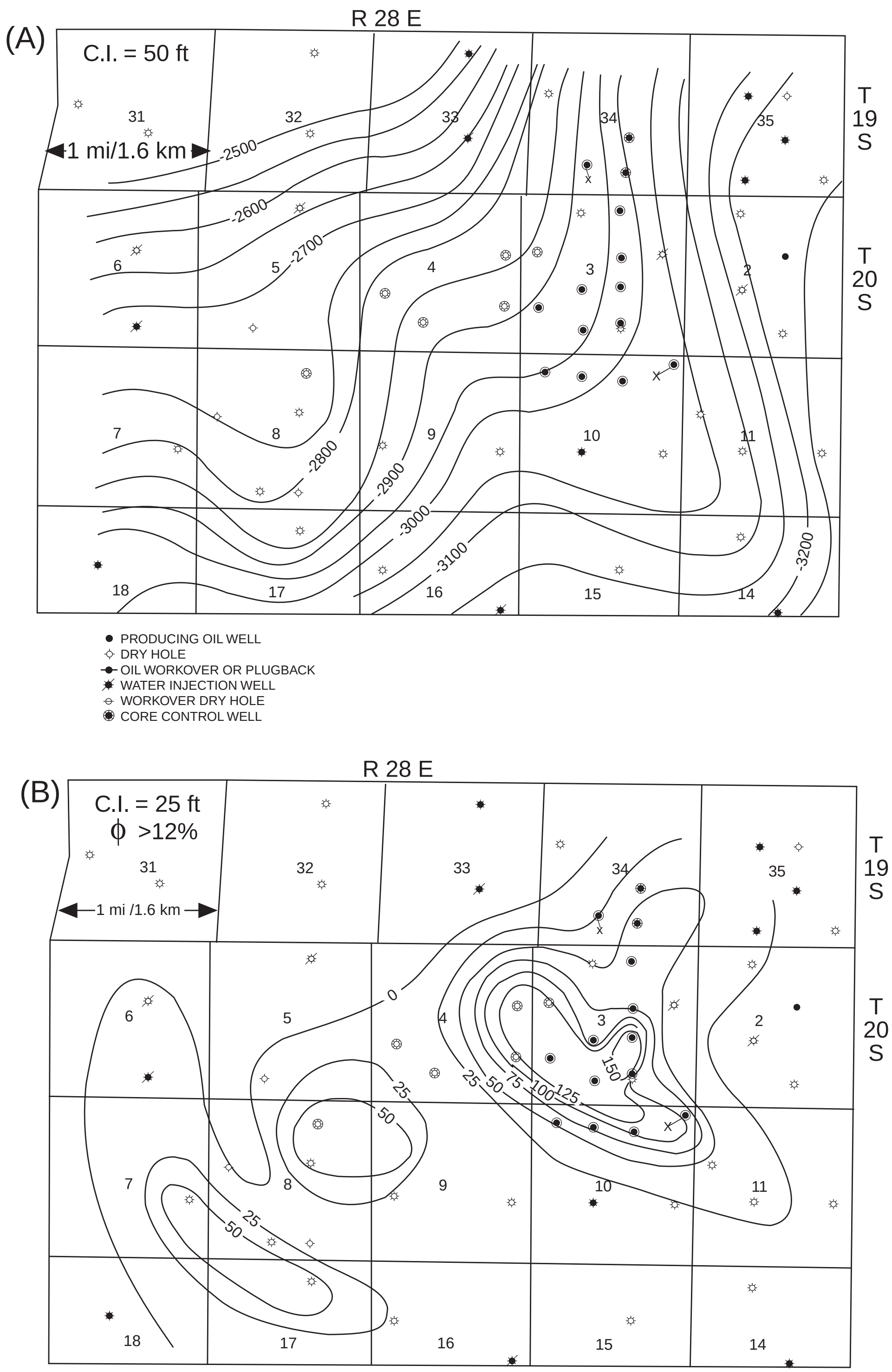

Figure 7—(A) Structure map, top of first Bone Spring sandstone, and (B) isopach map of net first Bone Spring sandstone pay, Old Millman Ranch field, Eddy County, New Mexico. Modified from Hayes (1995).

An important question concerns the possibility of Leonardian carbonate debris-flow deposits along the western margin of the CBP. Similar deposits, traditionally assigned to the Wolfcampian but possibly Leonardian in part, are well known at Coyanosa field (northern Pecos County, Texas), along the southern margin of the CBP.

Episodes of sea level fall and lowstand allowed sand to be carried across the shelf and to bypass the shelf margin. On the basis of paleoclimatic

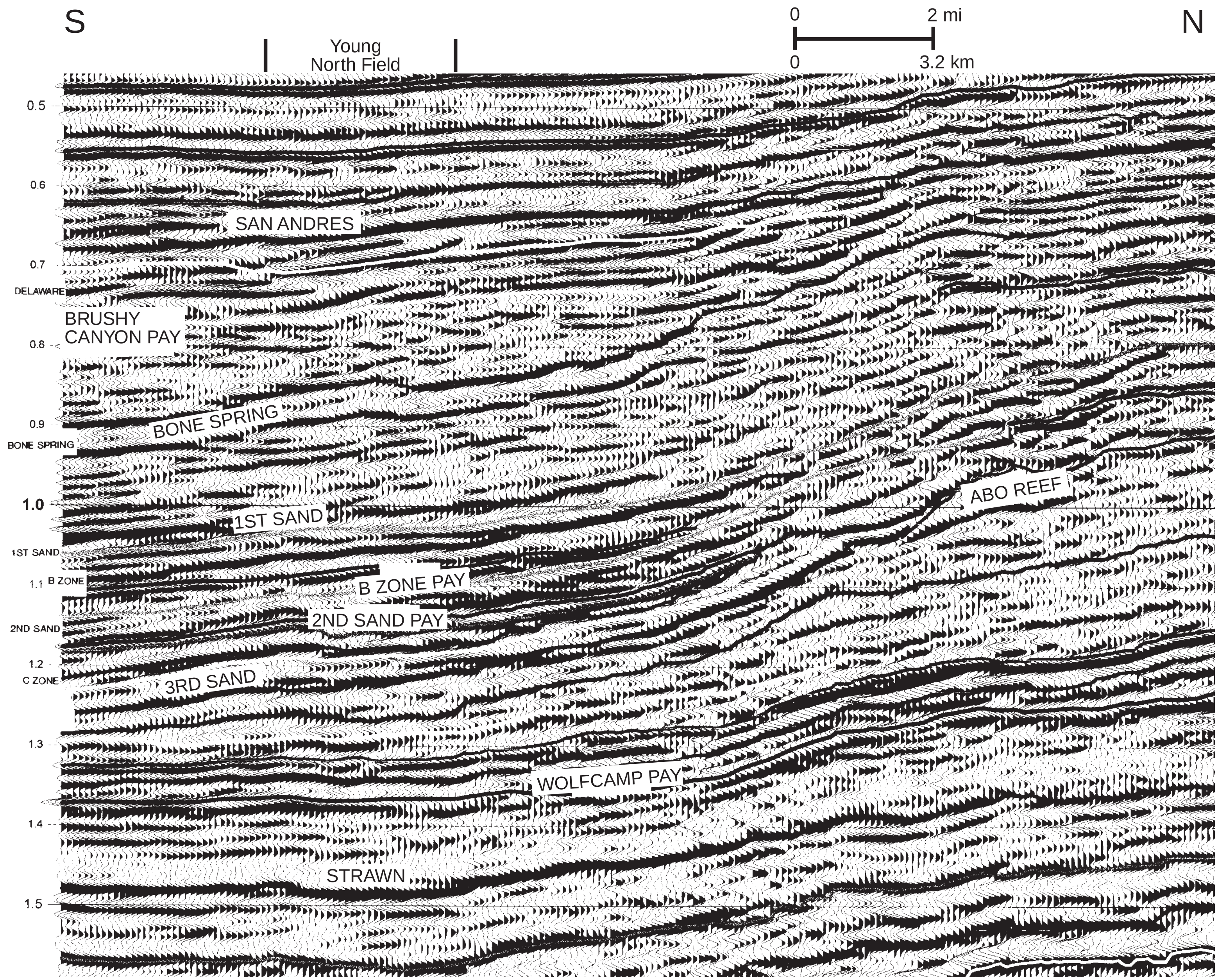

Figure 8—Three-dimensional seismic line showing location of Young North field relative to shelf margin, slope, and upper basin settings, northeastern Lea County, New Mexico. Data courtesy Harvey E. Yates Company. Time is two-way traveltime in seconds.

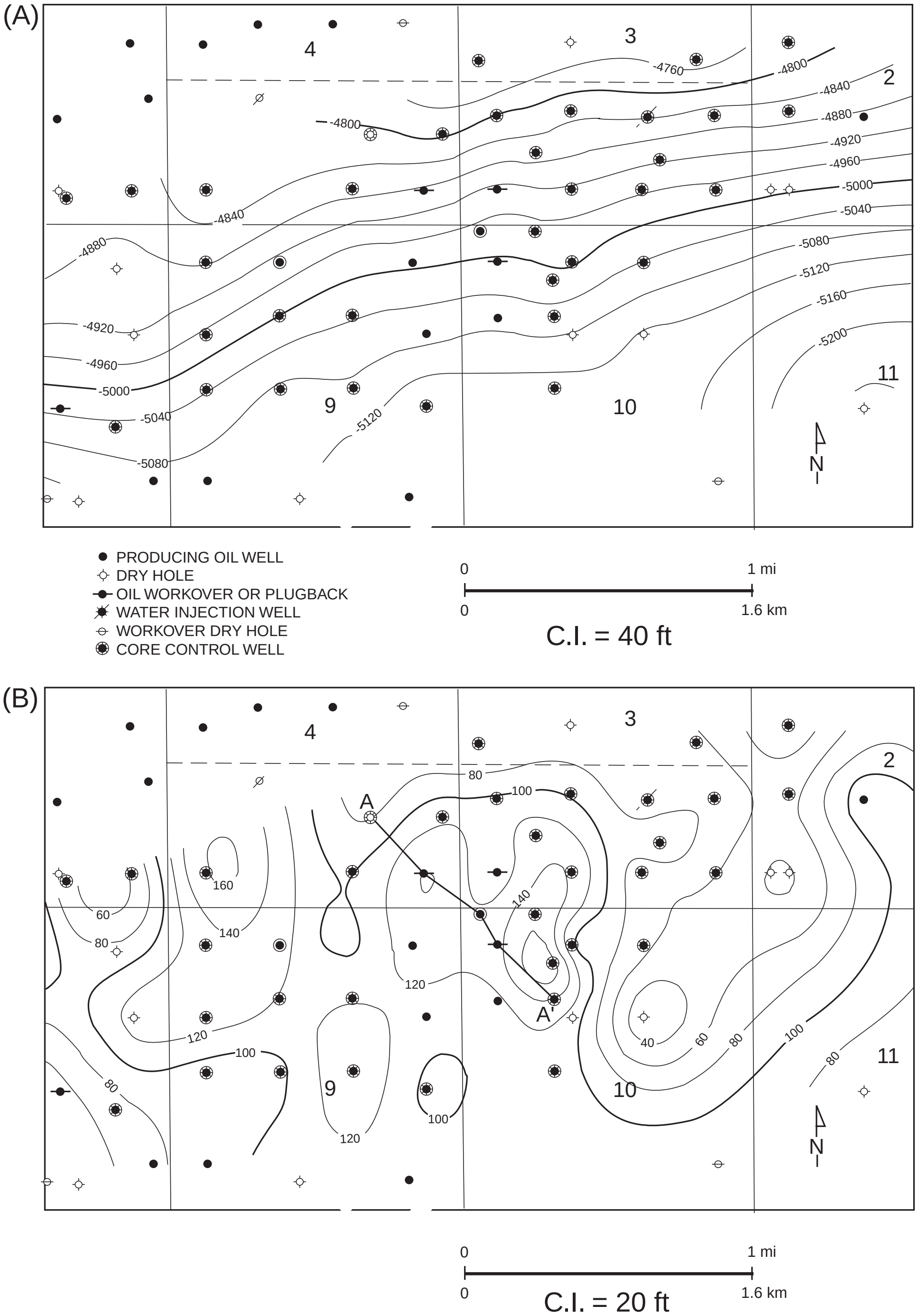

Figure 9—(A) Structure and (B) isopach maps, productive C zone, second Bone Spring sandstone, Young North field. Logs for AA′ shown on Figure 11. Data courtesy Harvey E. Yates Company.

interpretations, some workers have proposed that much sand was supplied to the shelf margin by eolian processes (Saller et al., 1989). From there, it was conveyed to the slope and basin floor mainly by means of gravity flow processes, such as submarine slump, debris flow, and canyon-incised valley transport, similar to those processes proposed for the correlative Spraberry and Dean submarine-fan systems of the Midland basin (Figure 5) (see, for example, Handford, 1981). Specific patterns of submarine-fan development were influenced by slope morphology, including bathymetric changes introduced by underlying carbonate debris-flow deposits. Fan systems that developed relatively early during periods of sea level fall were prone to subsequent basinward progradation, producing downlapping

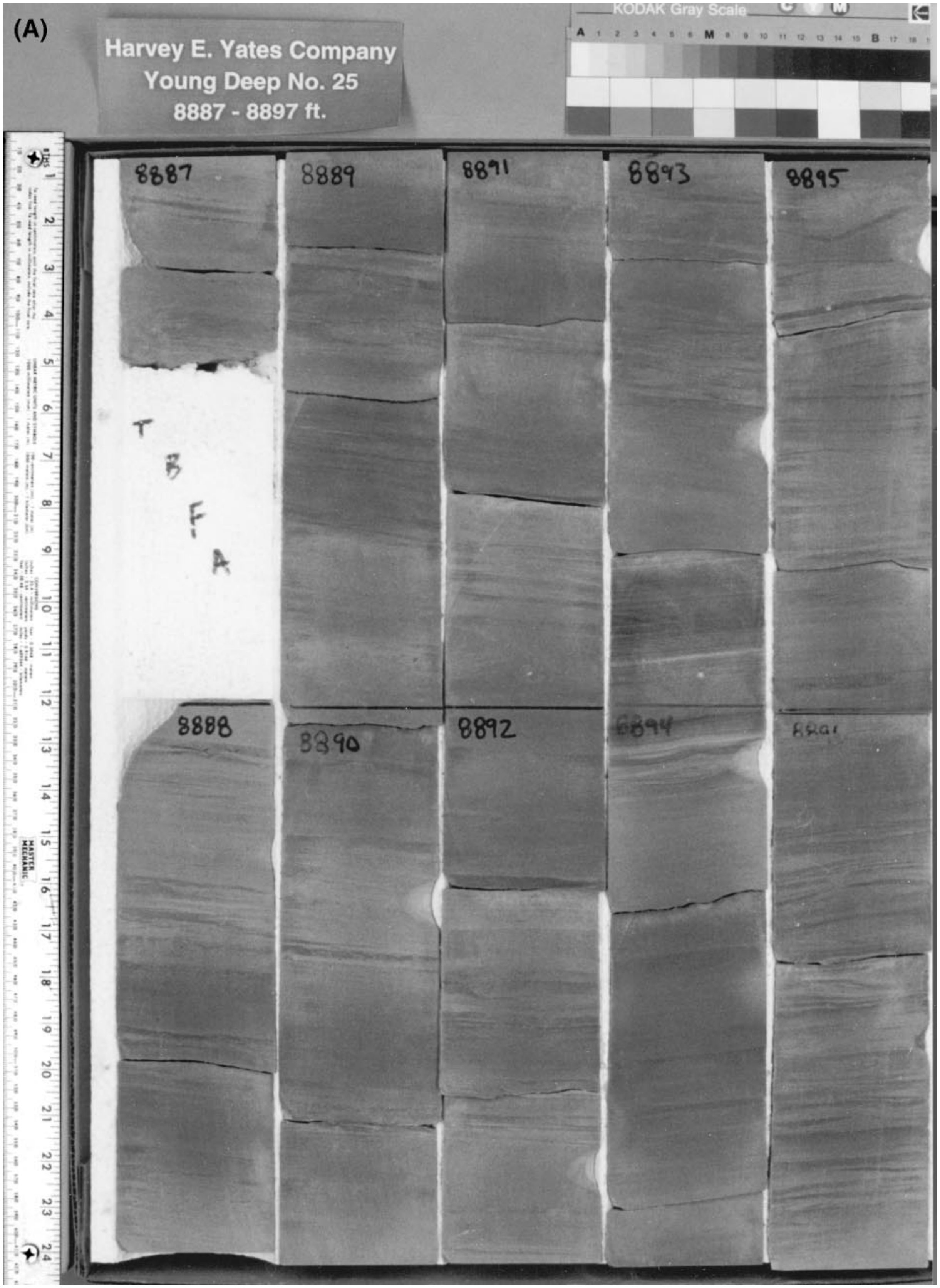

Figure 10—Core photographs from the Young Deep 25 well (Sec. 10, T18S, R32E) showing three major facies types associated with the productive C zone, Young North field. (A) Ripple cross-bedded channel facies; (B) levee/overbank facies; (C) pelagic facies. Data courtesy Harvey E. Yates Company.

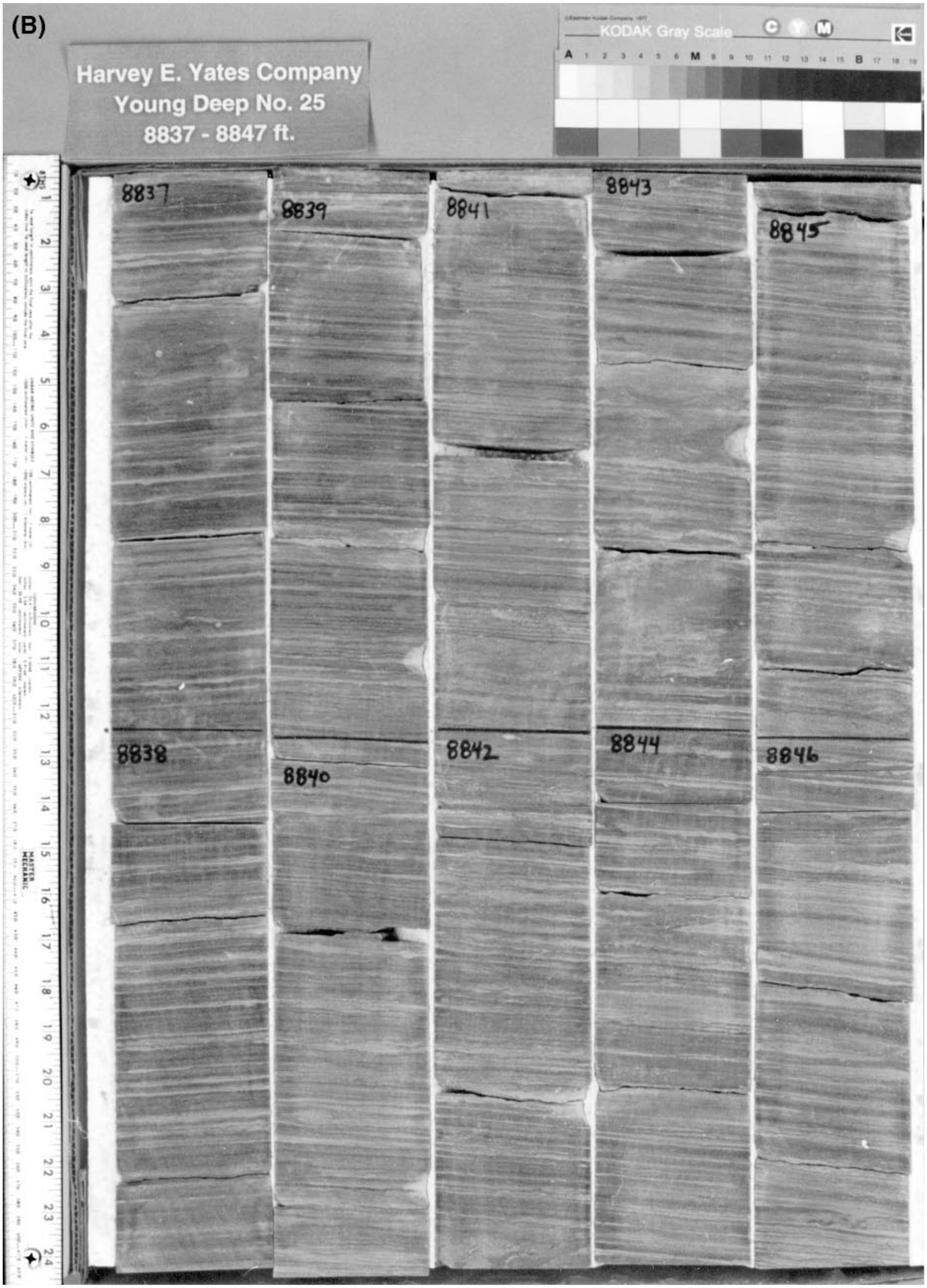

Figure 10—Continued.

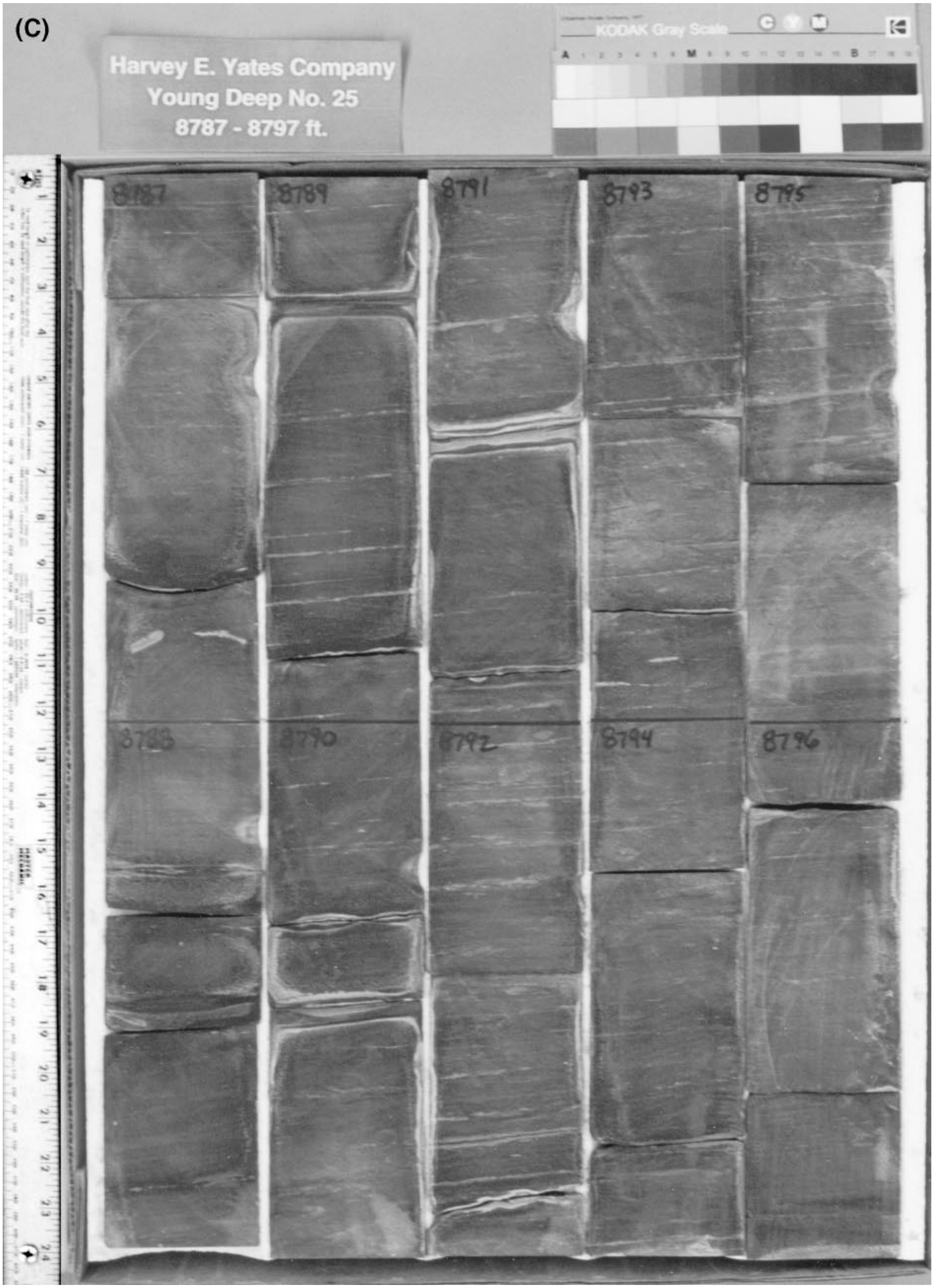

Figure 10—Continued.

relationships between channel-levee facies and underlying distal fan-lobe facies. Lobe abandonment and lower energy regimes associated with sea level rise resulted in deposition of pelagic facies.

BONE SPRING SANDSTONE RESERVOIRS: THE SLOPE

New drilling in the Bone Spring formation along the northern slope has targeted three intervals in particular: the first Bone Spring, the second Bone Spring, and the Avalon sandstones. Of these, the first and second Bone Spring sandstone intervals displayed better reservoir quality and higher per-well reserves. Core and log analyses have related reservoir properties to specific subfacies of each submarine-fan system. Lateral pinch-out of reservoir sandstones and low-relief closures comprise the major traps. The Avalon zone appears to show maximum productivity downdip from the slope; for example, in Red Tank field (T23S, R32E).

Old Millman Ranch: First Bone Spring Sandstone

Old Millman Ranch field is located in central Eddy County (T20S, R28E), approximately 32 km west-southwest of the main slope productive trend (see Figure 1). The field is associated with a structural nose and produces from multiple zones, including the Pennsylvanian Strawn and Morrow and Permian "Wolfcamp" and Delaware Mountain Group (Hayes, 1995). Initial production from the first Bone Spring sandstone was established in 1991; by 1995, over 20 producers had been drilled, with cumulative production of 383,571 bbl oil and 10.5 Gcf gas.

A hydrocarbon column of at least 182 m is present in the field, with net pay in the first Bone Spring sandstone ranging up to 56 m. Reservoir sandstones are described as very fine grained, with porosities of 10–16.5%, permeabilities of 0.1–6.3 md, and an average water saturation of 60% (high due to clay-bound water). The first Bone Spring sandstone produces sweet, 40° API oil and high-BTU gas (1180 BTU/kcf). A type log through the entire reservoir interval is given in Figure 6. The first Bone Spring sandstone is 55–61 m thick, with up to 90% of this comprising the net pay section.

Figure 7 provides structure and net pay isopach data for the field and shows the presence of a southeast-trending anticlinal feature and a submarine-fan system fed from the northeast. The data suggest structurally controlled ponding of sediment, with maximum pay thickness in channel sandstones along the northeastern flank of the anticline. Log data indicate southwestward progradation of the relevant fan system due to spillage of sediment across the structure.

Young North: Second Bone Spring Sandstone

Young North field (T18S, R32E) is located in western Lea County (New Mexico), approximately 35 km northeast from Old Millman Ranch. Among the more western pools within the Bone Spring detrital carbonate trend, the field also produces from Pennsylvanian (Morrow, Strawn) and Permian (Bone Spring, Delaware Mountain) reservoirs. The second Bone Spring sandstone was developed as an oil reservoir in the field during the early 1990s. As of mid-1996, a total of 25 wells had been completed in the second sandstone, with cumulative production of approximately 575,000 bbl. Volumetric calculations indicate 22 million bbl of original oil in place, of which 14% (2.5 million bbl) are considered recoverable.

The regional structural position of the field is indicated on the three-dimensional seismic profile of Figure 8. Young North lies near the base of the slope, where major sandstone intervals, both within the Bone Spring and the overlying Delaware Mountain Group, undergo rapid updip thinning with accompanying pinch-out of individual sandstone zones. Three units are identified in the second Bone Spring sandstone at Young North field, informally designated the A, B, and C zones, with nearly all production from the C zone. Figure 9 shows structure (top of the C zone) and isopach data for the C reservoir, suggesting the presence of several fan systems developed over a gentle slope dipping 4° south-southeast. No structures are apparent at this location.

Detailed core study of the C zone has identified three main facies: (1) ripple cross-bedded channel facies, (2) levee/overbank facies, and (3) pelagic facies (Figures 10, 11). An underlying silty shale and shaly sandstone section is interpreted to represent lowstand basin floor deposits subsequently downlapped by higher energy submarine-fan material of the C zone. Channel sandstone facies of the C zone are up to 12 m thick and display good continuity in the east-west direction, although with significant lateral thinning (Figure 11). Channel sandstones comprise the major reservoir lithology and display porosities of 8–17% and permeabilities of 0.10–5.75 md (Figure 11). Average pay thickness for the field as a whole is 11 m, using a cutoff of 12–13% log cross-plot porosity. Testing has indicated that intervals with lower than 10% sandstone porosity will not be economic even after fracture stimulation.

Laminated portions of the levee/overbank facies are also productive, with somewhat lower reservoir quality (maximum porosity of 13% and

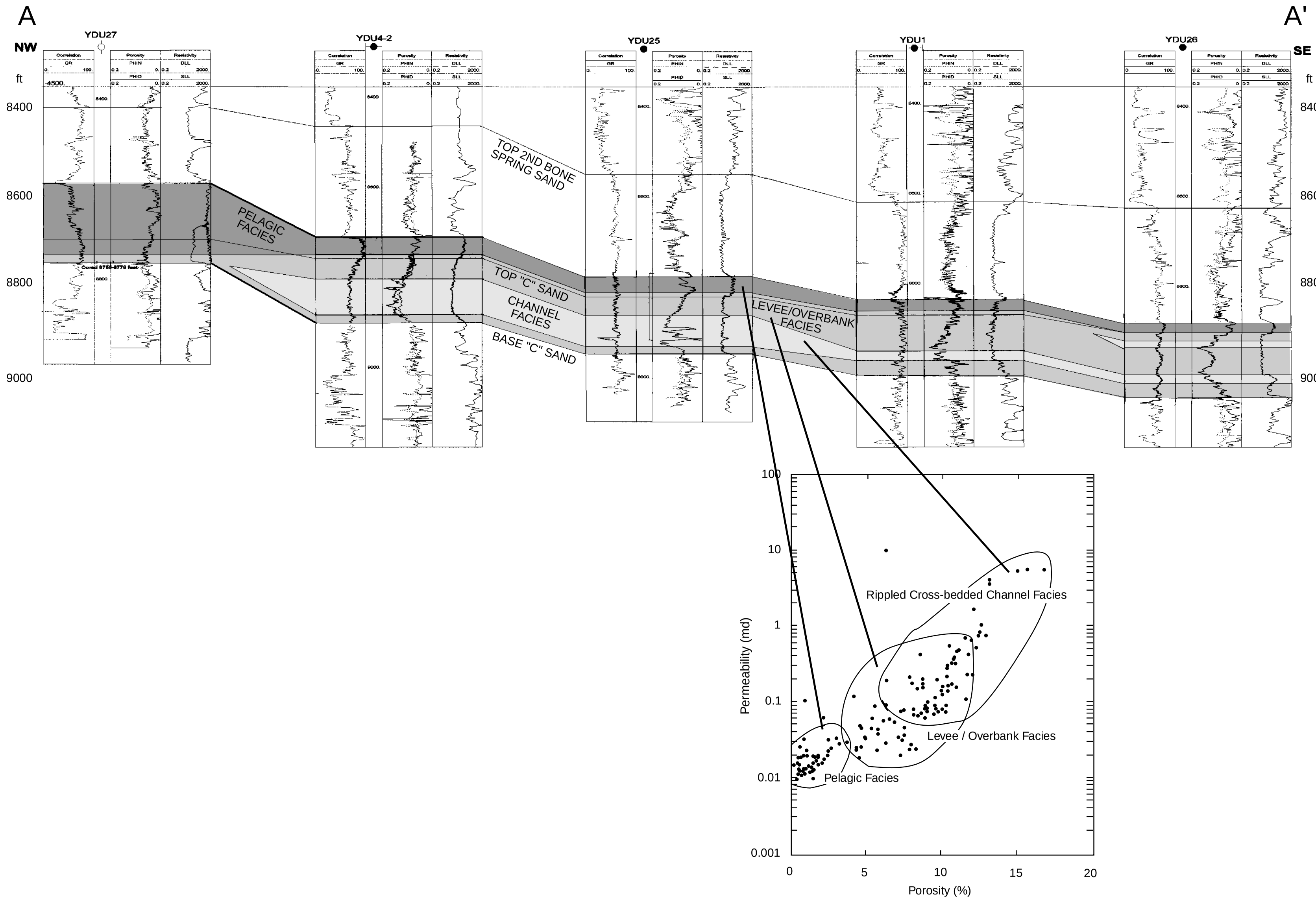

Figure 11—Log cross section illustrating interpreted facies in the lower, productive portion of the second Bone Spring sandstone, Young North field. Inset shows porosity vs. permeability data for identified facies domains, Young Deep 25 well. Cross section location shown in Figure 9. Data courtesy Harvey E. Yates Company.

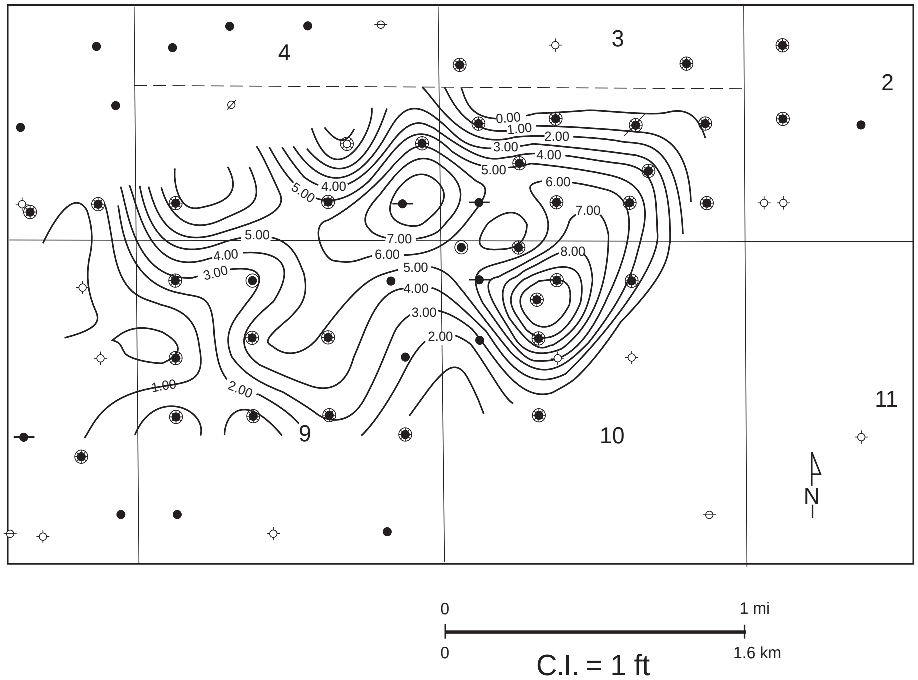

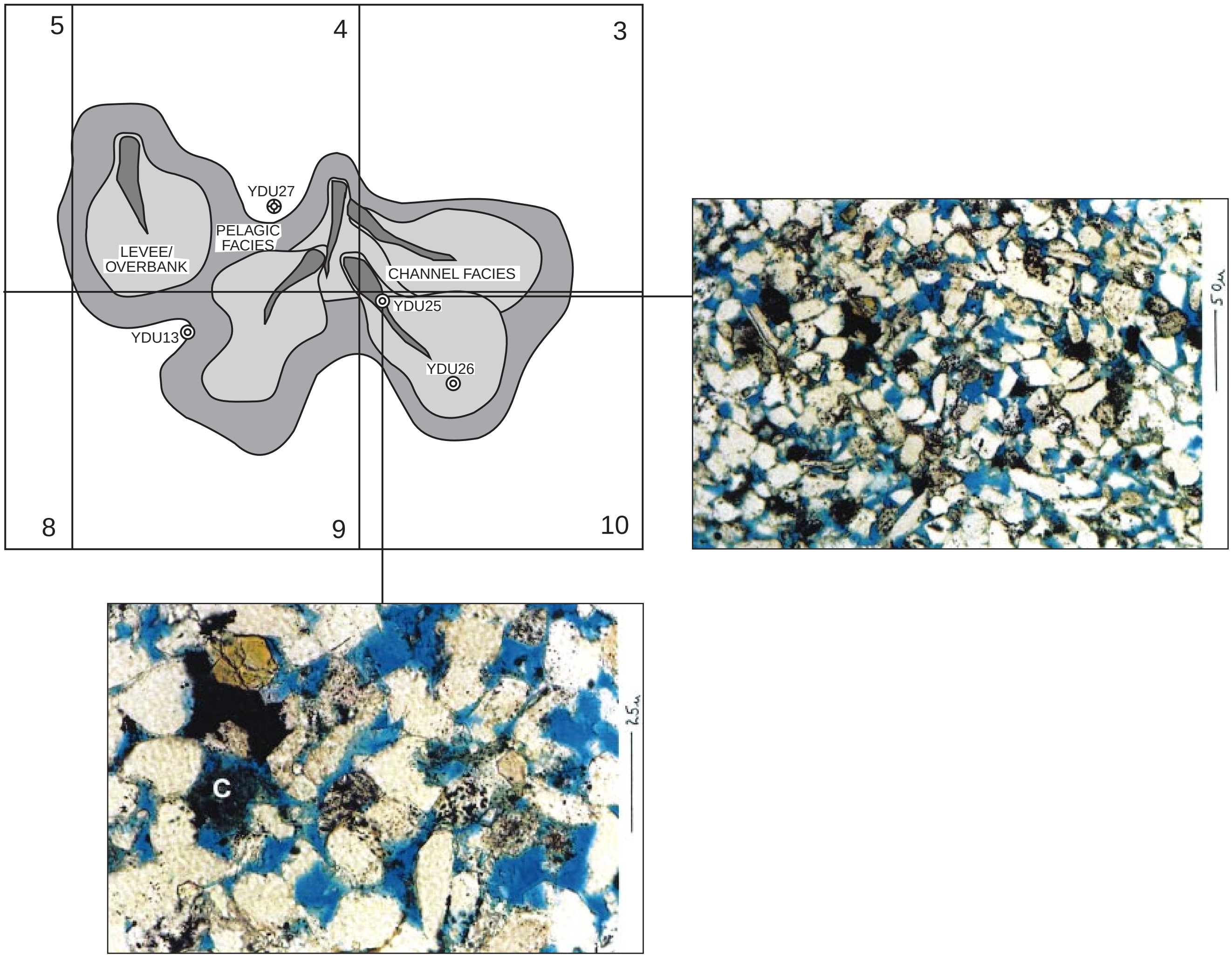

Figure 12—Net porosity-thickness map ($\phi \geq 10\%$) for C zone, Young North field, and interpreted facies model showing location of channel and levee/overbank development. Photomicrographs illustrate sandstone texture development in productive rippled cross-bedded channel facies, Young Deep 25 well, Young North field. Data courtesy Harvey E. Yates Company.

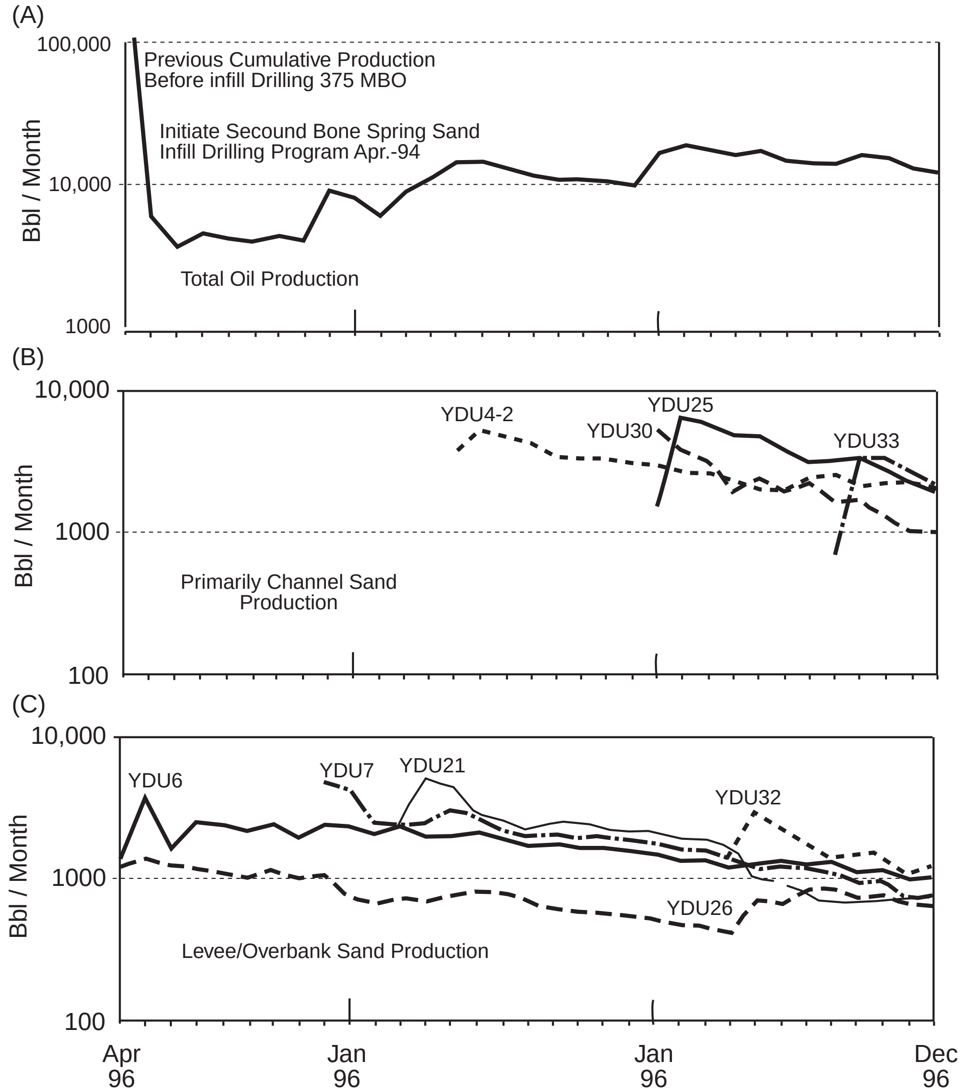

Figure 13—Production data, Young North field, showing total field oil production and selected well production, divided by reservoir facies. Data courtesy Harvey E. Yates Company.

permeability of 1 md). Pelagic facies rocks act as top and lateral seals. Thin sections of samples from channel sandstones reveal an abundance of angular quartz grains, moderate to well-sorted texture, and a well-developed pore system with only minor dolomite cement present (Figure 12). Low permeability results from a combination of restricted pore throats and lack of interconnectivity.

Net porosity-thickness (ϕ-h) data for the C zone reservoir at Young North delineate several maxima that, when combined with mapped facies distributions, suggest the depositional model depicted in Figure 12. This model shows four separate, overlapping fan systems. Note that the highest porosity-thickness maxima, located in the vicinity of the Young Deep 26 well, is associated with two thin channel sandstones and a thickened levee/overbank facies (see Figure 10).

PRODUCTION

Well productivity and reserves are different for the first and second Bone Spring sandstone reservoirs. The first Bone Spring sandstone typically produces by pressure depletion at rates of 50–100 bbl oil and 0.75-2.5 Mcf gas per day and has per-well estimated ultimate recoveries of 100,000–175,000 bbl oil and 1–3 Gcf gas. The reservoir in Old Millman Ranch field has a significant gas cap. Good wells in the field have yielded 60,000–100,000 bbl oil and 1.5–2.0 Gcf gas within a 5-yr period. Limited entry, two-stage stimulation techniques have resulted in wells able to flow oil and gas for up to 12 months before being put on pump. Estimates of original oil in place are in the range of 15–20 million bbl, with 10–15% of this amount recoverable.

At Young North, wells in the second Bone Spring sandstone commonly produce in the range of

50–200 bbl per day and have estimated ultimate reserves of 150,000–200,000 bbl oil and 0.3–0.5 Gcf gas. Production data for Young North field are shown in Figure 13. As indicated, per-well productivity is higher in channel sandstone facies (150–200 bbl/day on completion) compared to levee/overbank facies (50–150 bbl/day). Both facies display similar patterns of linear decline (25–35% per year). A good second Bone Spring sandstone well in Young North is the Young Deep 26, which yielded 118,537 bbl oil and 209.7 Mcf gas over a 5-yr period, with an average 25% annual decline. Due to the purely stratigraphic nature of the accumulation, established correlations between porosity and permeability (see Figure 11), and the presence of a solution gas drive in the reservoir, perforations are selected on the basis of porosity maxima alone. Estimated total oil in place is 22 million bbl, of which 14% (2.5 million bbl) is considered recoverable.

OUTLOOK

Exploration in first and second Bone Spring sandstones will continue to expand significantly. Reasons for future activity include (1) proven reserves of up to 200,000 bbl oil and 0.5-3.0 Gcf gas per well, (2) improved understanding of sandstone facies and their relationship to productivity, (3) adequate well control to support first-order predictions of sandstone fairways along the slope and, possibly, the northern basin as well, and (4) recent confirmation of first and second Bone Spring sandstone productivity in downdip areas. Success in the first and second Bone Spring sandstones at Old Millman Ranch and Young North fields suggests that, at the least, these intervals might be reevaluated in other existing fields along the slope and within the basin proper.

REFERENCES CITED

Bradshaw, W. A., 1989, Carbonate petrology and diagenesis of the Bone Spring formation dolostones, Scharb field, Lea County, New Mexico: M.S. thesis, West Texas State University, Canyon, Texas, 95 p.

Dickerson, P. W., 1985, Evidence for Late Cretaceous–early Tertiary transpression in Trans-Pecos Texas and adjacent Mexico, *in* P. W. Dickerson and W. R. Muehlberger, eds., Structure and tectonics of Trans-Pecos Texas: West Texas Geological Society Publication 85-81, p. 185–194.

Frenzel, H. N., et al., 1988, The Permian basin region, *in* L. L. Sloss, ed., Sedimentary cover of North America, The Geology of North America: Geological Society of America, v. D-2, p. 261–306.

Gawloski, T. F., 1987, Nature, distribution, and petroleum potential of Bone Spring detrital sediments along the Northwest shelf of the Delaware basin, *in* D. Cromwell and L. J. Mazzullo, eds., The Leonardian facies in west Texas and southeast New Mexico and Guidebook to the Glass Mountains, west Texas: Permian Basin Section SEPM, Publication 87-27, p. 85–105.

Handford, C. R., 1981, Sedimentology and genetic stratigraphy of Dean and Spraberry formations (Permian), Midland basin, Texas: AAPG Bulletin, v. 65, no. 9, p. 1602–1616.

Hart, B. S., 1997, Slope to basin transition: Bone Spring formation reservoirs, Delaware basin, New Mexico (abs.): AAPG Annual Meeting Program with Abstracts, p. A48.

Hayes, M. D., 1995, Old Millman Ranch Bone Spring, a symposium of the oil and gas fields of southeastern New Mexico (supplement): Roswell Geological Society, p. 302–305.

Hills, J. M., 1984, Sedimentation, tectonism, and hydrocarbon generation in Delaware basin, west Texas and southeastern New Mexico: AAPG Bulletin, v. 68, no. 3, p. 250–267.

Kosters, E. C., et al., 1989, Atlas of major Texas gas reservoirs: Gas Research Institute and Bureau of Economic Geology, University of Texas at Austin, 161 p.

Mazzullo, L. J., and A. M. Reid, Jr., 1987, Stratigraphy of the Bone Spring formation (Leonardian) and depositional setting in the Scharb field, Lea County, New Mexico, *in* D. Cromwell and L. J. Mazzullo, eds., The Leonardian facies in west Texas and southeast New Mexico and Guidebook to the Glass Mountains, west Texas: Permian Basin Section SEPM, Publication 87-27, p. 107–111.

Mazzullo, S. J., 1991, Permian stratigraphy and facies, Permian basin (Texas–New Mexico) and adjoining areas in the midcontinent United States, *in* P. A. Scholle, T. M. Peryt, and D. S. Ulmer-Scholle, eds., The Permian of northern Pangea, v. 2: Berlin, Springer-Verlag, p. 41–60.

Saller, A. H., J. W. Barton, and R. E. Barton, 1989, Slope sedimentation associated with a vertically building shelf, Bone Spring formation, Mescalero Escarpe field, southeastern New Mexico, *in* D. Cromwell and L. J. Mazzullo, eds., The Leonardian facies in west Texas and southeast New Mexico and Guidebook to the Glass Mountains, west Texas: Permian Basin Section SEPM, Publication 87-27, p. 275–288.

Shumaker, R. C., 1992, Paleozoic structure of the Central Basin uplift and adjacent Delaware basin, west Texas: AAPG Bulletin, v. 76, no. 11, p. 1804–1824.

Silver, B. A., and R. G. Todd, 1969, Permian cyclic strata, northern Midland and Delaware basins, west Texas and southeastern New Mexico: AAPG Bulletin, v. 53, p. 2223–2251.

Wiggins, W. D., and P. M. Harris, 1985, Burial diagenetic sequence in deep-water allochthonous dolomites, Permian Bone Spring formation, southeast New Mexico, *in* P. D. Cromwell and P. M. Harris, eds., Deep water carbonates: buildups, turbidites, debris flows and chalks: SEPM Core Workshop 6, p. 140–173.

Yang, K.-M., and S. L. Dorobek, 1995, The Permian basin of west Texas and New Mexico: tectonic history of a composite foreland basin and its effects on stratigraphic development, *in* S. L. Dorobek and G. M. Ross, eds., Stratigraphic evolution of foreland basins: SEPM Special Publication 52, p. 149–174.

ABOUT THE AUTHOR

Scott L. Montgomery

Scott L. Montgomery is a geologist, author, and translator residing in Seattle, Washington. He received his B.A. degree in English from Knox College in 1973 and his M.S. degree in geological sciences from Cornell University in 1978. He is the author of the quarterly monograph series *Petroleum Frontiers*, published by Petroleum Information Corporation, and of books and articles on the history of science. His current research interests include frontier plays and technologies and various topics in the history of geology and astronomy.

6) Victorio Peak Formation

Meredith Bush and Mariya Levina

VICTORIO PEAK FORMATION

Compiled By Mariya Levina and Meredith Bush

- **uppermost Leonardian (early Permian)— 280Ma-270.6Ma**
- **thickness: 800 – 1600 ft**
- **underlies major sequence boundary between *Leonardian Bonespring, Victorio Peak, Yeso*, etc and *Guadalupian Brushy Canyon, Cherry Canyon, Bell Canyon, etc.***
- **light gray, calcic to dolomitic, fossiliferous limestone**
- **deeper water equivalent of Yeso Formation, a near-shore patch reef deposit that grades into the carbonate bank deposits of the Victorio Peak**

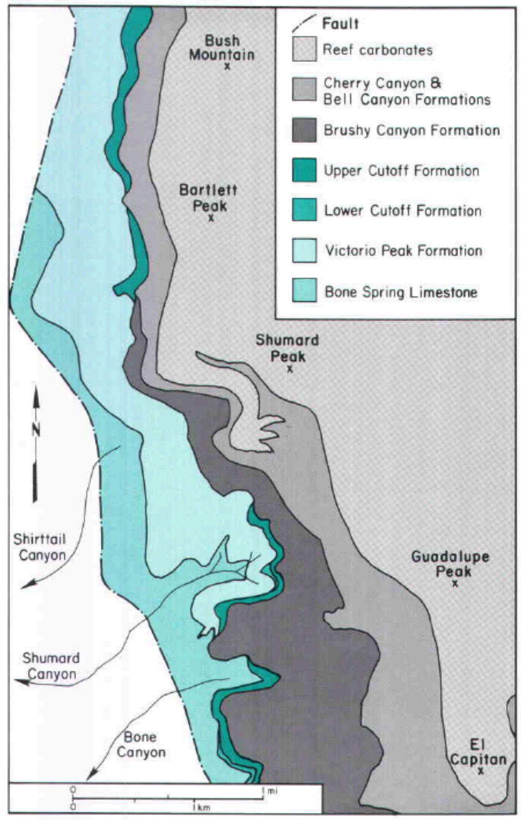

FIGURE 4—Geologic map of the shelf margin area.

Figure 1: Geological map of the western Guadalupe Mountains. From Harris 1989.

From USGS Professional Paper 446: Geology of the Guadalupe Mountains, New Mexico

The Bone Spring Limestone of the Delaware basin grades laterally northwestward into the Victorio Peak Limestone which was originally named the Victorio Peak Massive Member of the Bone Spring Limestone by P. B. King and R. E. King (1929, p. 921) for exposures in the Sierra Diablo. Because it is a distinct mappable unit, the Victorio Peak is now classified as a separate formation (King, P. B., 1964). Relations between the Victorio Peak and Bone Spring of the Delaware basin cannot be observed in the report area, but exposures in the Texas part of the Guadalupe Mountains were described by P. B. King (1948, p. 26-27), who wrote:

> During the last half of Leonard [Bone Spring] time, the gray Victorio Peak was spread out on the shelf area, extending as far southeastward as the edge of the Delaware Basin, where it apparently intergraded with black limestone. During the first half of Leonard time, black limestones extended for several miles farther northwestward toward the shelf, underneath the gray Victorio Peak beds. In the Guadalupe Mountains, exposures of the black limestone do not extend deeply enough to indicate their relations to the shelf area.

Subsurface data indicate that the black limestone beds of the Bone Spring do not extend as far northwest as the Union White 1 well (sec. 17, T. 24 S., R. 22 E.). Instead, they apparently grade northwestward into the light-gray dolomite beds of the basal part of the Victorio Peak Limestone and, possibly, into the uppermost part of the Hueco Limestone, assuming the upper part of the Hueco of the Hueco Mountains is Leonard in age, as has been suggested (King, P. B., King, R. E., and Knight, J. B., 1945; Bachman and Hayes, 1958, fig. 5).

P. B. King (1948, p. 17-18, 164) recognized three informal divisions of the Victorio Peak in its exposures on the west side of Cutoff Mountain south of the New Mexico-Texas State line. The incompletely exposed lower division consists of gray fine-grained somewhat dolomitic limestone in 1- to 6-foot beds. It contains rare small chert concretions. The middle division, 117 feet thick, consists (p. 18) "of slope-making, thin-bedded, light-gray or white limestone, with much buff, fine-grained, calcareous sandstone interbedded." The upper division consists of gray fine-grained limestone in beds as much as 7 feet thick in its basal 217 feet and of thin-bedded limestone in the top 25 feet.

The lower and middle divisions of the Victorio Peak Limestone presumably grade northwestward into the Yeso Formation, whereas the upper division of the Victorio Peak probably grades into the basal part of the San Andres Limestone (pl. 3). The southeasternmost occurrence of gypsum in the Yeso Formation is arbitrarily used as the dividing line between shelf and basin-margin terminology.

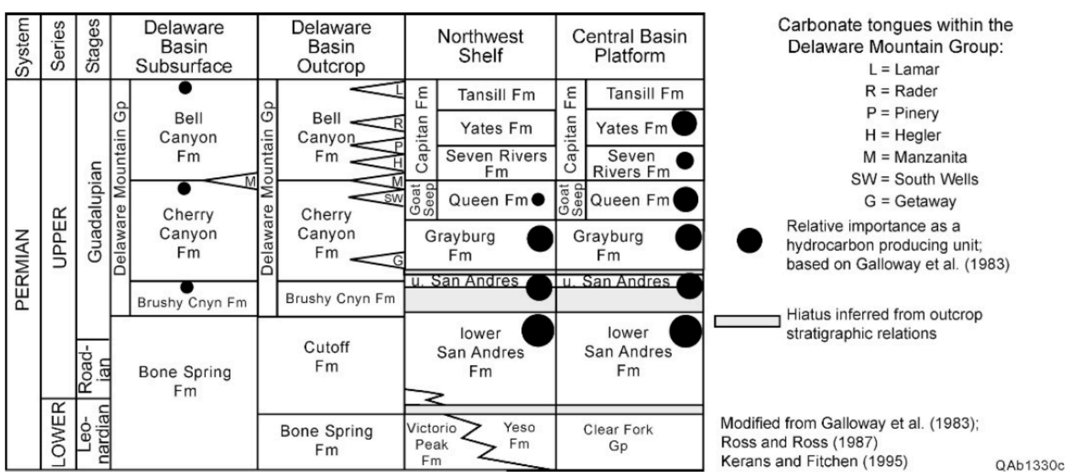

Figure 2: Permian Stratigraphy of the Delaware Basin. From Barnaby et al. 2007.

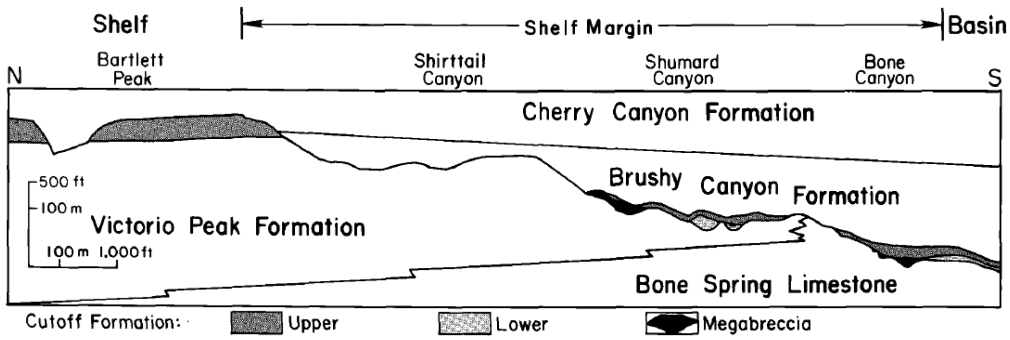

FIGURE 3—Detailed cross section of the Cutoff shelf-to-basin transition area. Section is oriented north–south through the study area (Fig. 1). Vertical exaggeration = 2×.

Figure 3: Cross section of Guadalupe Mountains Cutoff shelf-to-basin transition. From Harris 1989.

References

Ashworth, J.B., 1995, Ground-water resources of the Bone Spring-Victorio Peak Aquifer in the Dell Valley Area, Texas:.

Barnaby, R.J., and Ward, W.B., 2007, Outcrop Analog for Mixed Siliciclastic-Carbonate Ramp Reservoirs--Stratigraphic Hierarchy, Facies Architecture, and Geologic Heterogeneity: Grayburg Formation, Permian Basin, U.S.A.: Journal of Sedimentary Research, v. 77, no. 1, p. 34-58, doi: 10.2110/jsr.2007.007.

Behnken, F.H., 1975, Leonardian and Guadalupian (Permian) Conodont Biostratigraphy in Western and Southwestern United States: Journal of Paleontology, v. 49, no. 2, p. 284-315.

Harms, J., 1974, Brushy Canyon Formation, Texas: A Deep-Water Density Current Deposit: Geological Society of America Bulletin, v. 86, no. 11, p. 1763-1784, doi: 10.1130/0016-7606(1974)85<1763.

Harris, M.T., 1987, Sedimentology ol the Cutotf Formation (Permian), western Guadalupe Mountains, west Texas: New Mexico Geology, , no. November, p. 74-79.

Sarg, J.F., 1984, Middle-Late Permian depositional sequences, Permian Basin, West Texas and New Mexico, *in* Bally, A.W. ed., Atlas of Seismic Stratigraphy, AAPG Studies in Geology no. 27, Am Assoc Petrol Geol, p. 140-155.

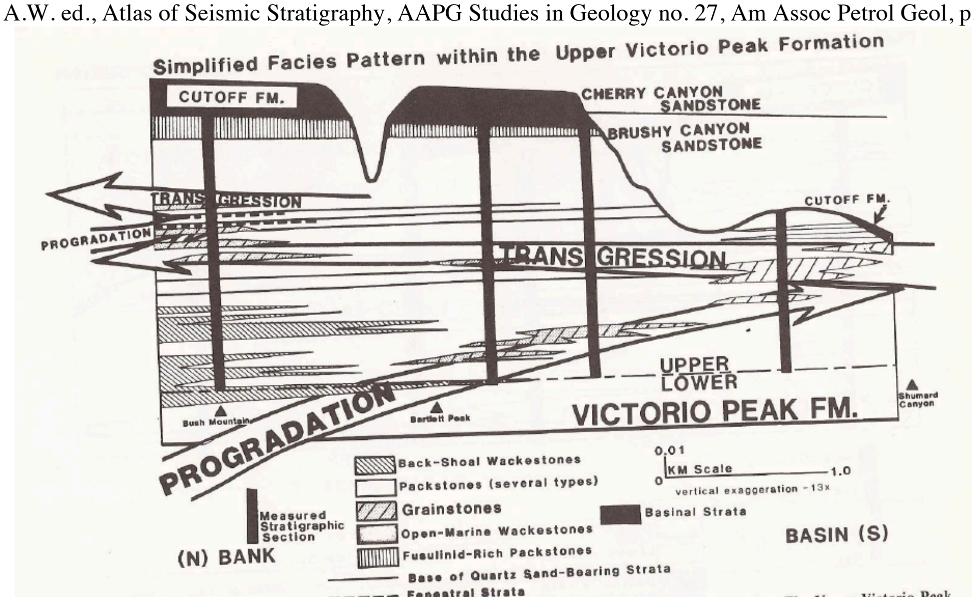

Figure 2. Transgressive and progradational patterns within the Upper Bone Spring Victorio Peak Formation. The Upper Victorio Peak strata are interpreted as bank-top deposits whose contemporaneous bank margin and basin strata were largely removed by bank margin erosion. Patterns of progradation and transgression of the Upper Victorio Peak shown in diagram are based mostly on position of grainstones considered as open marine shoals. The lower third of the Upper Victorio Peak shows a continuation of the progradation of the underlying Lower Victorio Peak-Bone Spring strata, the upper two-thirds of the Upper Victorio Peak strata suggest a major transgression, except for a minor progradational interruption. Thus the youngest Victorio Peak strata appear to reflect the start of the major regional transgression culminated by shelf-top and bank margin submarine erosion (see text) and subsequent deposition of basin facies (Cutoff, Brushy Canyon and Cherry Canyon Formations) across the shelf, the truncated bank margin, and into the basin.

Figure 4: Facies Patterns for upper Victorio Peak Formation. From Kirkby 1988.

7) Lidar 1: Williams Ranch
Sheila Wilkins and Anine Pedersen
Class Presentation

Guadalupe Mountains - Overview

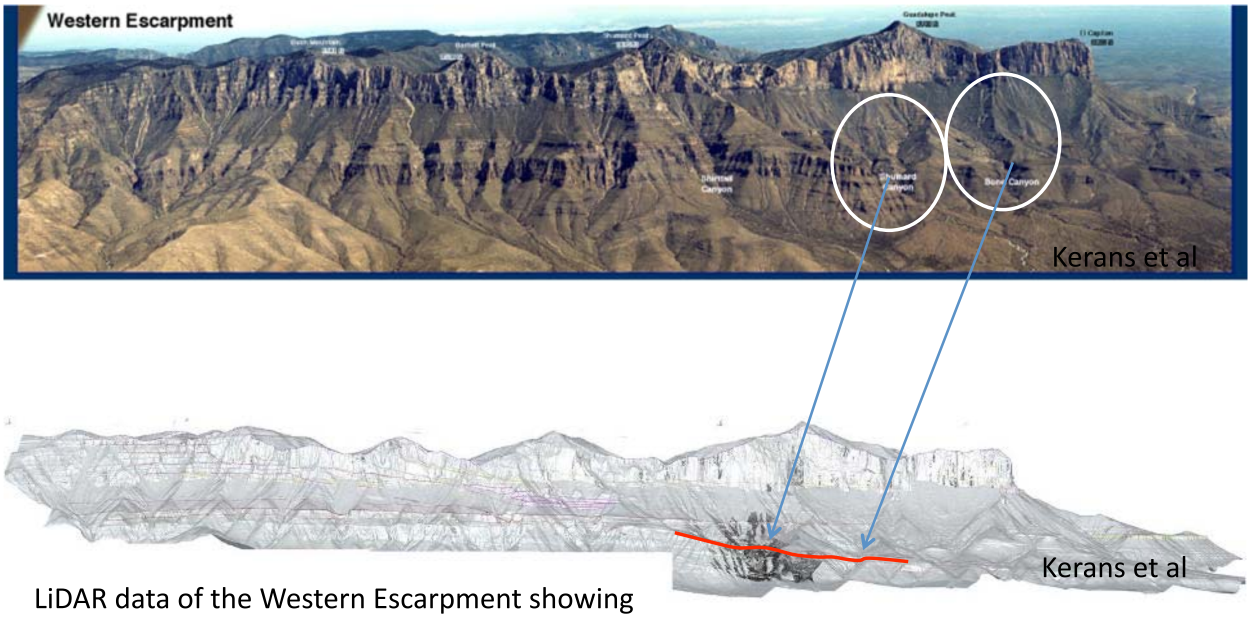

LiDAR data of the Western Escarpment showing various surface/boundary correlations- The red line is the interpreted major unconformity through Shumard and Bone Canyons

Major Unconformity

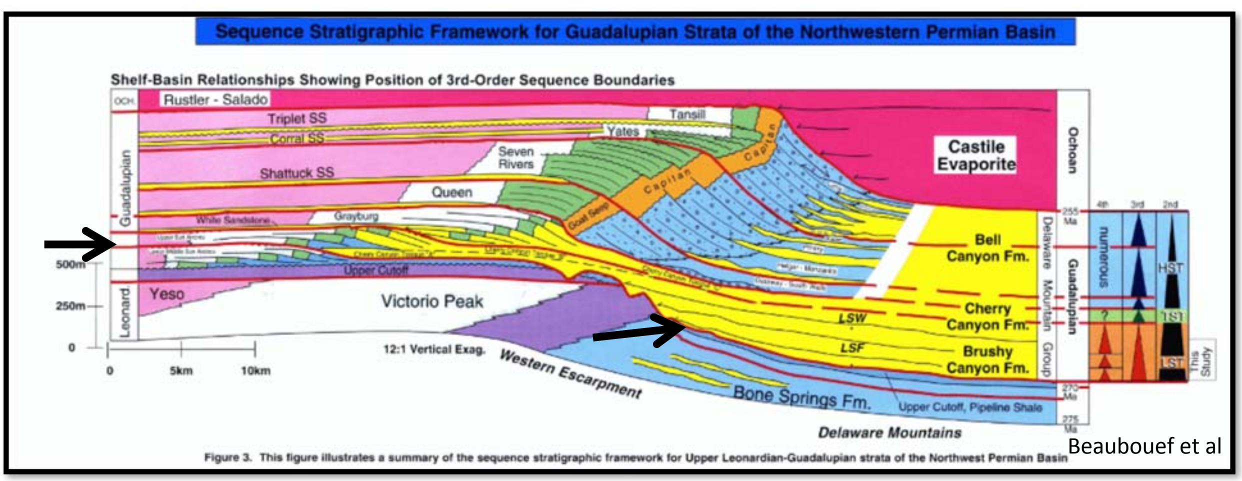

Figure 3. This figure illustrates a summary of the sequence stratigraphic framework for Upper Leonardian-Guadalupian strata of the Northwest Permian Basin

-A major unconformity marks the boundary between the lower Bone Springs Formation and the upper Brushy Canyon Formation.

-This unconformity is thought to be due to submarine erosion.

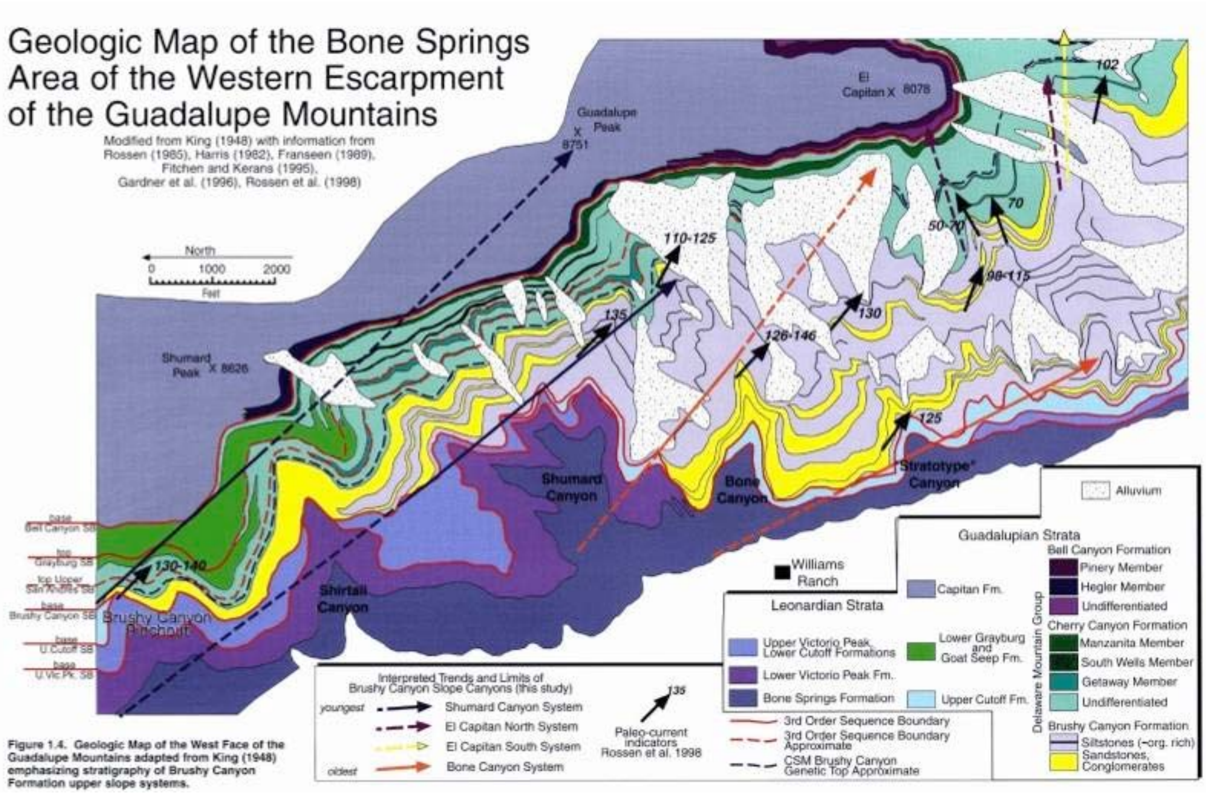

Figure 1.4. Geologic Map of the West Face of the Guadalupe Mountains adapted from King (1948) emphasizing stratigraphy of Brushy Canyon Formation upper slope systems.

Beaubouef et al

LiDAR

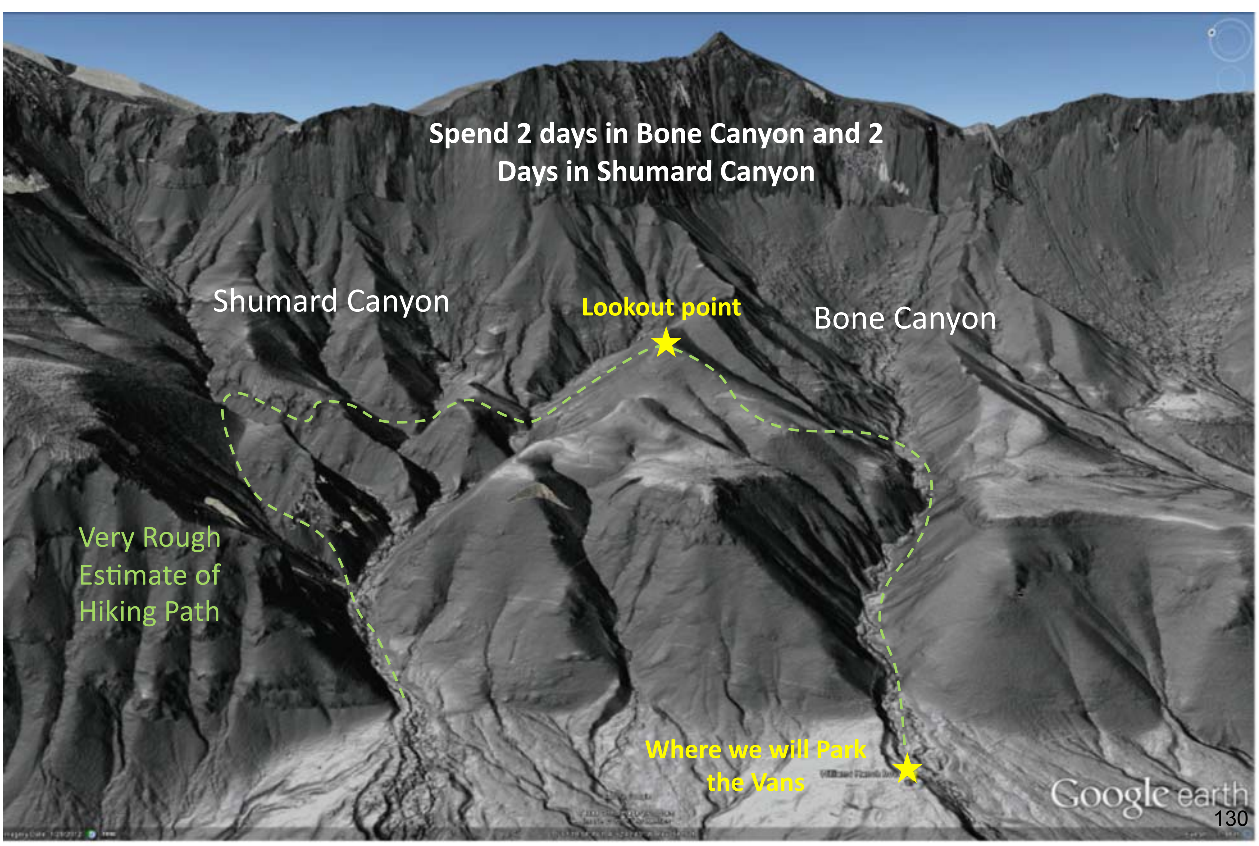

Bone Canyon - LiDAR

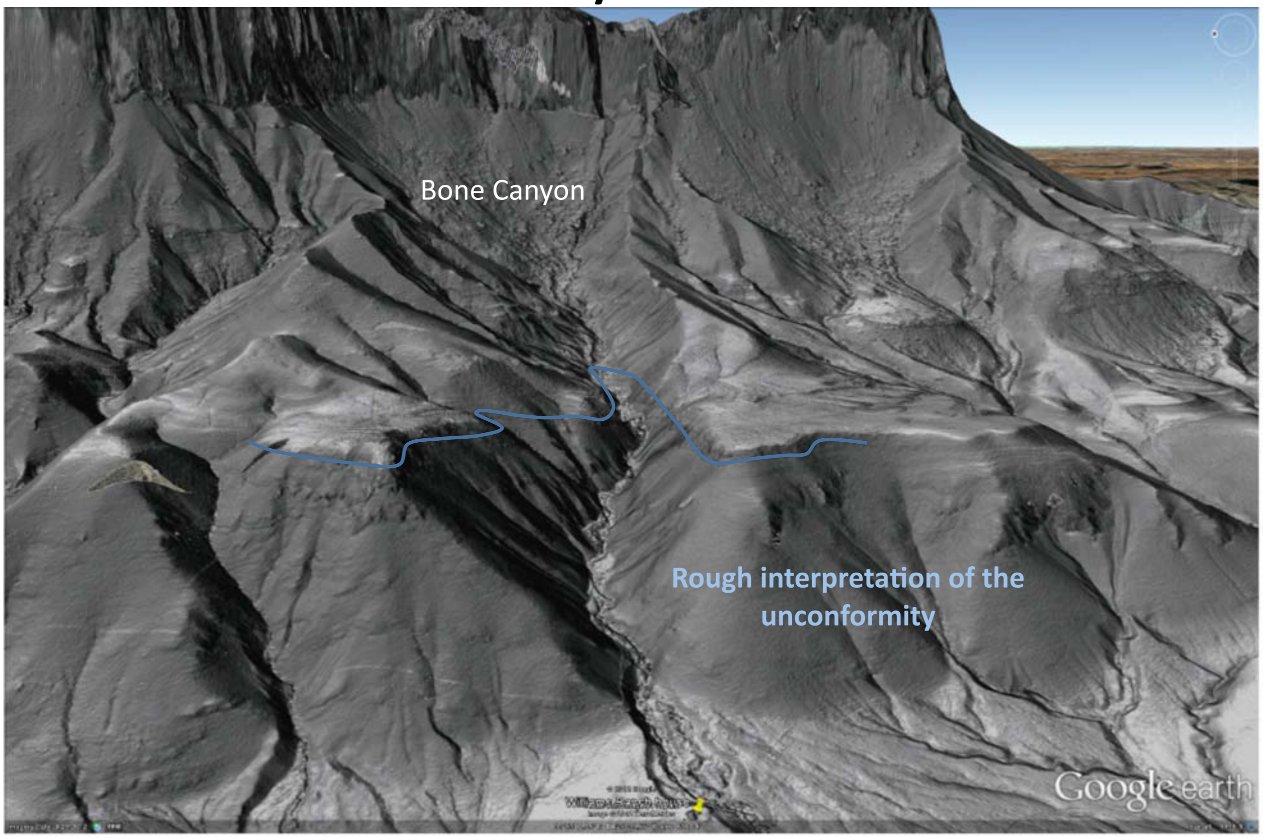

Bone Canyon Stratigraphy

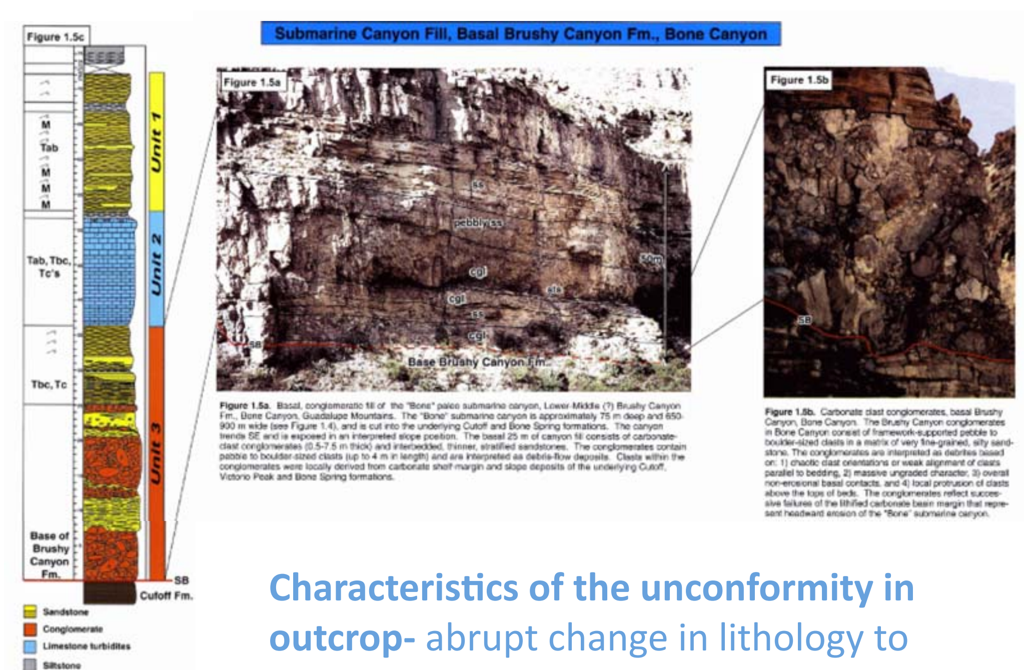

Characteristics of the unconformity in outcrop- abrupt change in lithology to thick packages of conglomerates and sandstones.

Beaubouef et al

Shumard Canyon - LiDAR

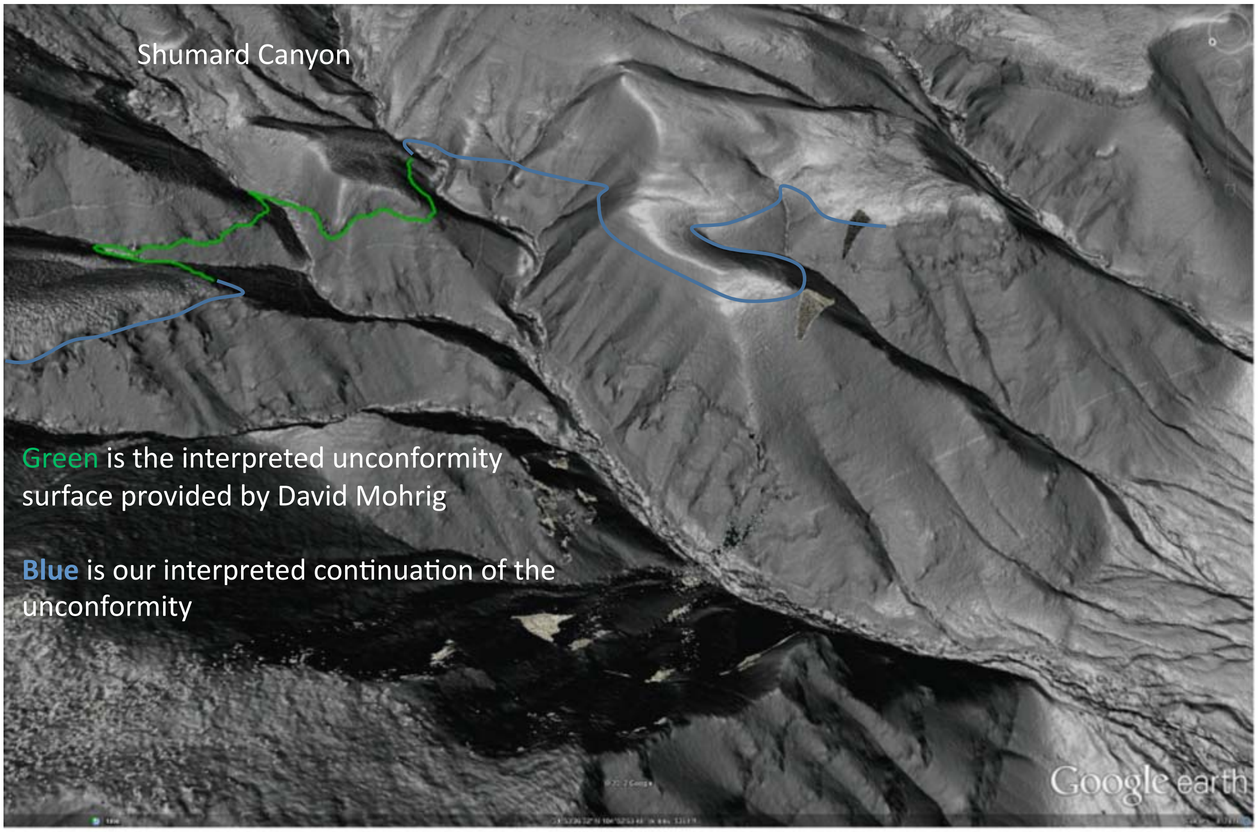

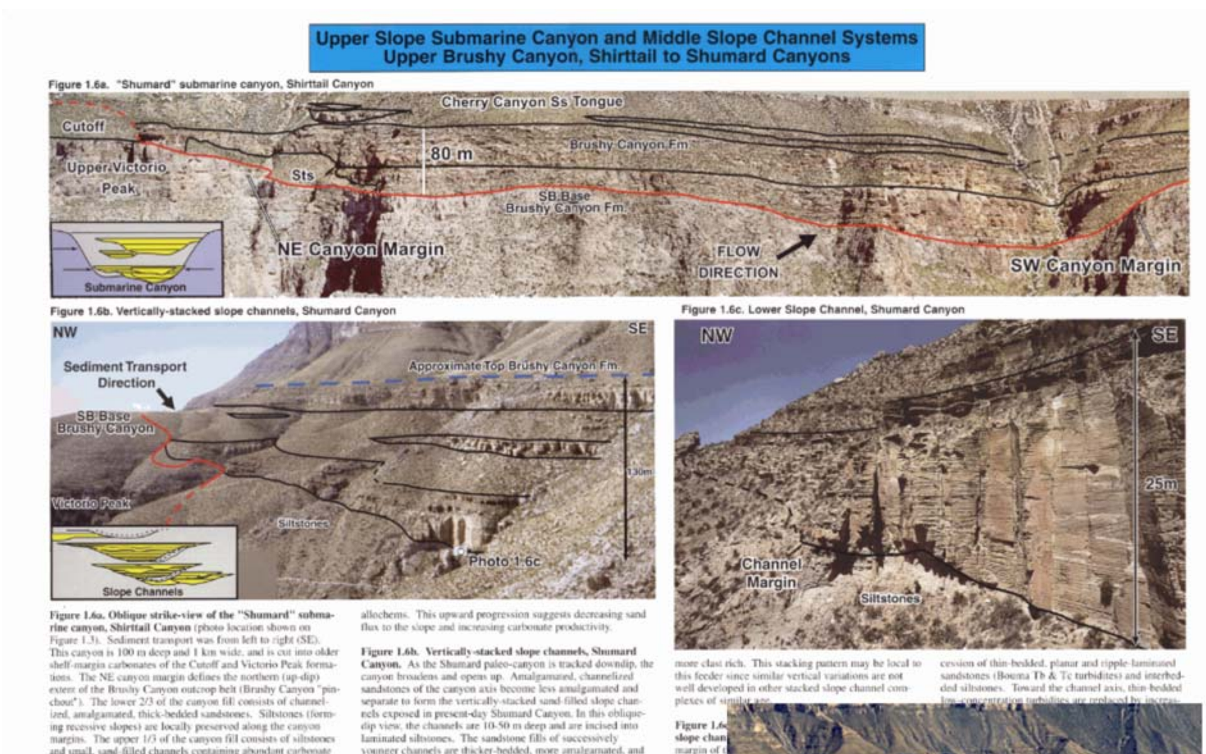

Upper Slope Submarine Canyon and Middle Slope Channel Systems
Upper Brushy Canyon, Shirttail to Shumard Canyons

Figure 1.6a. Oblique strike-view of the "Shumard" submarine canyon, Shirttail Canyon (photo location shown on Figure 1.3). Sediment transport was from left to right (SE). This canyon is 100 m deep and 1 km wide, and is cut into older shelf-margin carbonates of the Cutoff and Victorio Peak formations. The NE canyon margin defines the northern (up-dip) extent of the Brushy Canyon outcrop belt (Brushy Canyon "pinchout"). The lower 2/3 of the canyon fill consists of channelized, amalgamated, thick-bedded sandstones. Siltstones (forming recessive slopes) are locally preserved along the canyon margins. The upper 1/3 of the canyon fill consists of siltstones and small, sand-filled channels containing abundant carbonate allochems. This upward progression suggests decreasing sand flux to the slope and increasing carbonate productivity.

Figure 1.6b. Vertically-stacked slope channels, Shumard Canyon. As the Shumard paleo-canyon is tracked downdip, the canyon broadens and opens up. Amalgamated, channelized sandstones of the canyon axis become less amalgamated and separate to form the vertically-stacked sand-filled slope channels exposed in present-day Shumard Canyon. In this oblique-dip view, the channels are 10-50 m deep and are incised into laminated siltstones. The sandstone fills of successively younger channels are thicker-bedded, more amalgamated, and more clast rich. This stacking pattern may be local to this feeder since similar vertical variations are not well developed in other stacked slope channel complexes of similar age.

Figure 1.6c. ... slope chan... margin of t...

... cession of thin-bedded, planar and ripple-laminated sandstones (Bouma Tb & Tc turbidites) and interbedded siltstones. Toward the channel axis, thin-bedded low-concentration turbidites are replaced by increas-

1.8

Beaubouef et al

Shirttail Canyon is N/NW of Shumard Canyon

Sources:

•Beaubouef, R.T., Rossen C., Zelt F.B., Sullivan, M.D., Mohrig, D.C., Jennette G. Field Guide For AAPG Hedberg Field Research Conference - April 15-20, 1999: *Deep-Water Sandstones, Brushy Canyon Formation, West Texas*

•Kerans, C., Zahm, C., Azzi, J, Harman, C., and Jones, N. *Towards a High-Resolution 3D Stratigraphic Framework for the Guadalupe Mts. (PowerPoint Presentation)*

TRAIL GUIDE FOR DAY 1: SHUMARD TO BONE CANYON TRAVERSE

C. ROSSEN
P. J. LEHMANN
J. F. SARG
Exxon Production Research Co.

INTRODUCTION TO THE FIELD TRAVERSE

Geologic Setting

The locale of this field traverse is the western escarpment of the Guadalupe Mountains where the autochthonous and allochthonous facies of the shelf-edge and basin margin are exposed along the major western boundary-fault escarpment. Details of the regional setting for this trip to selected localities on the Late Leonard-Early Guadalupian basin margin are well known. The major pertinent reference is that of King (1948).

The stratigraphic units of concern on this day trip are the Bone Spring, Victorio Peak, Cutoff, and Brushy Canyon formations (see Fig. 3 of introduction to guidebook). The geologic setting of these formations is that of the rim of a broad carbonate shelf province to the north and northwest (Northwest Shelf) and a deeper intracratonic basin (Delaware Basin) on the southeast and east. The strata of principal concern for today are marine carbonates of the basin margin and siliciclastic wedges of the toe-of-slope and basin. The structural history during late Leonard-early Guadalupian deposition was that of regional subsidence at rates that (1) permitted the shelf to remain shallow, and (2) permitted the development of low angle (5 degrees or less) shelf-to-basin bank margins.

Purpose and Scope

This field traverse and the accompanying locality guide do not attempt comprehensive coverage of the Permian strata such as that of King. Nor do we here attempt an overall topical coverage. Our purpose is to concentrate on two major interpretive problems of the Late Leonard-Early Guadalupian shelf and basin margin: (1) the genesis of the depositional geometries and accompanying facies of the Bone Spring to Brushy Canyon strata; and (2) the correlation of the basin margin strata further to the north. Examination of the shelf strata is recommended as subsequent Days 2 and 3 to this Day 1. Road logs and locality guides for these days are found in Sarg and Lehmann, 1986 (Permian Basin Section-SEPM pub. 86-25). Application of depositional sequence concepts has, we think, provided new interpretational leverage in understanding the genesis of the late Permian rocks of the Delaware Basin. Application of sequence stratigraphy includes both correlation of major physical surfaces (i.e., sequence boundaries, downlap surfaces) and biostratigraphic time markers. The fusulinid biostratigraphy has been provided by Garner L. Wilde (see articles in PBS-SEPM pub. 86-25). Details of the depositional environments and their paleobathymetry, and of the degree to which sea-level fluctuation exposed the shelf and basin-margin strata and controlled deposition are the subjects of intense continuing discussion. Some of these are dealt with on this field trip.

Acknowledgments

We gratefully acknowledge the support of Exxon Production Research Company for the past and continuing program in the Guadalupe Mountains. We also thank Exxon Production Research Company for permission to publish this work. We thank the staff of the Guadalupe Mountain National Park for their support and cooperation in making the field work for this report a success.

STRATIGRAPHIC FRAMEWORK OF THE BONE SPRING TO BRUSHY CANYON STRATA

To provide a stratigraphic framework for the interpretations presented on this field trip, it is helpful to recognize several specific depositional systems tracts (Brown and Fisher, 1977) (i.e., a linkage of contemporaneous depositional facies—such as shelf, slope, and basin) bounded by sequence boundaries[1] and/or downlap surfaces[2]. The chronostratigraphic significance of an unconformity or sequence boundary is that all the rocks below the unconformity are older than the rocks above it. The ages of strata immediately above and below the unconformity differ geographically according to the areal extent of erosion or nondeposition. The duration of the hiatus associated with an unconformity differs correspondingly, but the unconformity itself is a chronostratigraphic boundary because it separates rocks of different ages, and no chronostratigraphic surfaces cross it.

Although several chronostratigraphic surfaces may merge along an unconformity, none actually cross the unconformity. For these reasons, unconformities are not diachronous but are time boundaries that may be assigned a specific geologic age dated in those areas where the hiatus is least and/or where the rocks above and below become conformable. By careful identification of unconformities and their correlative conformities, a sedimentary section can be divided into genetic depositional sequences bounded by these unconformities (Vail et al., 1984).

The Permian strata of the Delaware and Midland basins comprise a number of depositional sequences. Each sequence is composed of three parts or systems tracts: (1) a wedge restricted to the basin and slope areas that is interpeted to have been deposited during a relative fall and lowstand of sea level; and (2) a transgressive depositional systems tract deposited during a regional landward shift in the shoreline intepreted to have been deposited during a relative sea level rise; and (3) a capping progradational or regressive depositional systems tract interpreted to have been deposited during a relative highstand in sea level.

[1]Sequence boundary: Unconformity and its correlative conformity. Unconformity is defined as a surface representing a significant time gap with erosional truncation (subaerial or subaqueous) and/or subaerial exposure. Erosional truncation is commonly evident at the basin margin. The sequence boundary surface commonly becomes conformable over much of both the shelf and basin areas. Marine surfaces with significant hiatuses, but without evidence of erosion, are not unconformities according to this usage (Vail et al., 1984).

[2]Downlap surface: Submarine surface that is characterized seismically by a downlap over a concordant pattern and is commonly associated with a marine hiatus. Downlap surfaces associated with marine condensed sections mark the change from the end of transgression to the start of regression (Vail et al., 1984).

The western escarpment of the Guadalupe Mountians exposes the slope to basin transition of six Permian sequence boundaries which range in age from Late Leonardian to Late Guadalupian. These sequence boundaries subdivide the strata into five genetic depositional sequences (see summary sequence diagram in front of guidebook). The portions of the two sequence boundaries that we will observe today in a slope and toe-of-slope position are highly erosional and appear to be submarine in origin. These boundaries are: (1) top of the Victorio Peak/Bone Spring formations, and (2) the top of the Cutoff Formation/base of the Brushy Canyon Formation. High above our traverse in the rocks exposed along the escarpment are the sequence boundaries, or correlative basinward conformities that correspond to (3) the top of the San Andres Formation, (4) the top of the Grayburg Formation, (5) the top of the Goat Seep Formation/base Manzanita Member, and (6) the top of the Hegler Member of the Capitan Reef Complex. Days 2 and 3 of this trip will examine the shelfward expression of the two sequence boundaries we will examine today and the sequence boundary at the top of the San Andres Formation, and their enclosed strata. The first sequence boundary we will encounter today, the top of the Victorio Peak/Bone Spring, correlates shelfward to the base of the Glorieta Member of the Yeso Formation of the northern Guadalupe Mountains and forms the base of the sequence which includes the lower and middle parts of the San Andres Formation of Hayes (1964). The second major sequence boundary we will examine, the base of the Brushy Canyon, correlates shelfward to the top of the middle San Andres of Sarg and Lehmann (1986) and forms the basal boundary of a sequence which includes the upper San Andres. The upper San Andres carbonate bank is capped by the sequence boundary that forms the base of the Grayburg Formation. In the basin margin position, this boundary is overlain by Grayburg Formation quartz sandstones and dolomites interpreted to be of shallow-water to tidal origin (Sarg and Lehamnn, 1986). In addition to the sequence boundaries, we want to emphasize three major features we will see today: (1) debris flow breccias deposited on top of the sequence boundaries in slope to toe-of-slope positions which are intepreted, by us, to be the result of erosion of the bank margins during falls and lowstands in sea level; (2) two basinally restricted wedges consisting of (a) limestone strata of the lower Cutoff Formation intepreted to have been deposited during rising sea level, and (b) siliciclastics of the Brushy Canyon Formation interpreted to be the result of shelf bypass during a lowstand in sea level; and (3) the slope to basin transition of two carbonate banks deposited during highstands in sea level, the upper Victorio Peak/Bone Spring formations and the upper Cutoff Formation.

STOP 1—BASIN/SLOPE TO BANK TRANSITION, BONE SPRING LIMESTONE AND VICTORIO PEAK FORMATIONS

Starting from William's Ranch, we will follow the Guadalupe Mountain National Park trail up into Shumard Canyon (Fig. 1-I-1). In Shumard Canyon, we will observe the lithofacies, sedimentary structures, and geometries associated with a classic vertical facies transition from a lower slope to basin environment to a carbonate bank environment. This transition encompasses the Leonardian-age, coeval, Bone Spring Limestone (slope/basin) and Victorio Peak Formation (bank). These formations have been mapped and studied by King (1948), Newell and others (1953), McDaniel and Pray (1967), and Kirkby (Upper Victorio Peak, 1982, 1984).

The Bone Spring Limestone is interpreted as a euxinic, slope to basin deposit (King, 1948, Newell and others, 1953, and McDaniel and Pray, 1967). It consists of dark gray, cherty, thin-bedded, internally laminated lime mudstones that are organic-rich and sparsely- to non-fossiliferous. In contrast, the Victorio Peak Formation consists of medium to light gray, fossiliferous, thick-bedded, predominantly massive dolomites and minor limestones that are interpreted as carbonate bank deposits. The Victorio Peak can be further subdivided into a bank facies (lime grainstones and dolopackstones) and a bank margin facies (dolowackestones and mudstones)(see Fig. 1-I-3 and enclosed abstract of McDaniel and Pray, 1967). In a shelfward direction (approximately 15-20 miles northwest of Shumard Canyon), normal-marine, fossiliferous carbonates of the Victorio Peak Formation change facies into sparsely fossiliferous, interbedded dolomites, siltstones and gypsum of the Yeso Formation (Boyd, 1958).

In the Guadalupe Mountains, an incomplete Bone Spring-Victorio Peak section (maximum thickness 520 m, 1700 ft) is exposed (King, 1948). Distribution of the Bone Spring and Victorio Peak formations in the area of today's traverse is shown on King's (1948) map of the Bone Canyon area (Figure 1-I-2, in pocket). Figures 1-I-4 and 1-I-5 from McDaniel and Pray (1967) show the distribution of lithologies and facies within the Victorio Peak and Bone Spring formations. The Victorio Peak-Bone Spring bank complex prograded 3-5 km (2-3 miles) during the accumulation of 460 m (1500 ft) of Leonardian carbonates (McDaniel and Pray, 1967).

As we will see on our traverse today through Shumard and Bone Canyons, the Bone Spring-Victorio Peak section thins dramatically in a southeast (basinward) direction. Basinward thinning of the Victorio Peak-Bone Spring section results in part from depositional downlap, but is primarily due to post-depositional erosion associated with the sequence boundary that forms the base of the overlying Cutoff Formation (Fig. 1-I-6). This sequence boundary truncates 250 m (780 ft) of strata over a distance of 3 km (1.8 miles) (Pray et al., 1980).

Stop 1a — Bone Spring Lithofacies

Examples of characteristic Bone Spring (slope to basin environment) lithofacies (Fig. 1-I-7) can be seen in outcrops on the south side of the trail at the mouth of Shumard Canyon (Stop 1a, Fig.1-I-1). The Bone Spring typically consists of thin-bedded, dark gray, organic-rich, lime mudstones (actually fine silt-sized packstones, Pray, pers. comm. and Fig. 1-I-8). Chert is abundant and commonly forms lenses parallel to bedding. Beds are internally laminated, and display both planar and irregular laminations. The irregularity of some laminations is due to soft sediment deformation and the formation of small-scale ripples. According to Pray irregular laminations are more common in proximity to the basin margin. Evidence of autochthonous organic activity in the Bone Spring Limestone is sparse and consists of silicious sponge spicules and uncommon trace fossils on bedding planes.

Stop 1b — Intraformational Bone Spring Erosion Surfaces

Proceeding up the canyon from Stop 1a, numerous intraformational erosion surfaces, marked by discordances in bedding orientation, are evident within the Bone Spring Limestone. These surfaces are spectacularly exposed on the north wall of Shumard Canyon and are diagrammed on cross section B-B' of King's map (Fig. 1-I-2, in pocket). The erosion surfaces have up to 30 m (100 ft) or more of relief and are dipping, planar to curved,

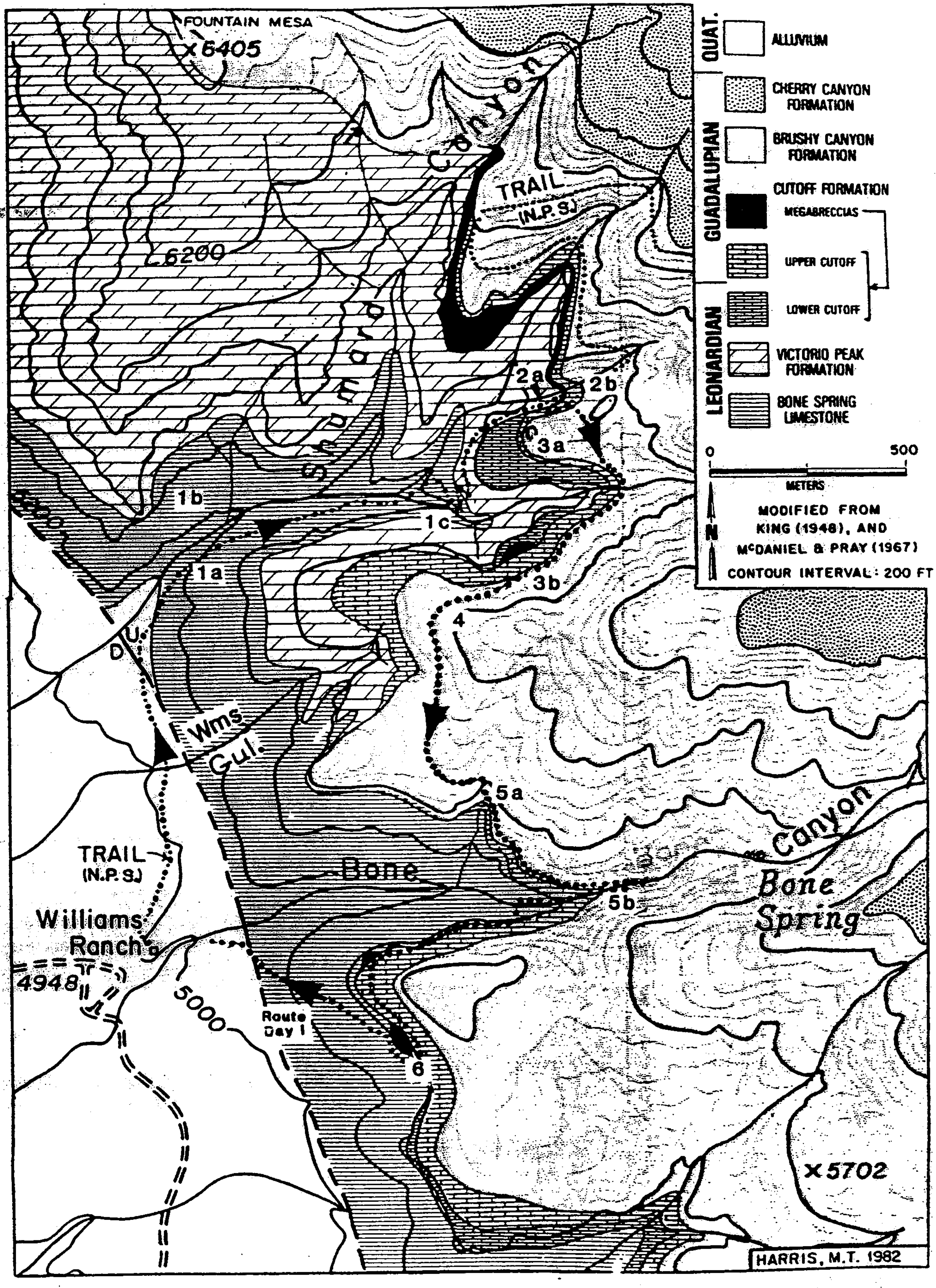

Figure 1-I-1. Geologic map of Shumard Canyon/Bone Canyon area showing traverse and stop locations for Fieldtrip Day 1: "Western Escarpment of the Guadalupe Mountains."

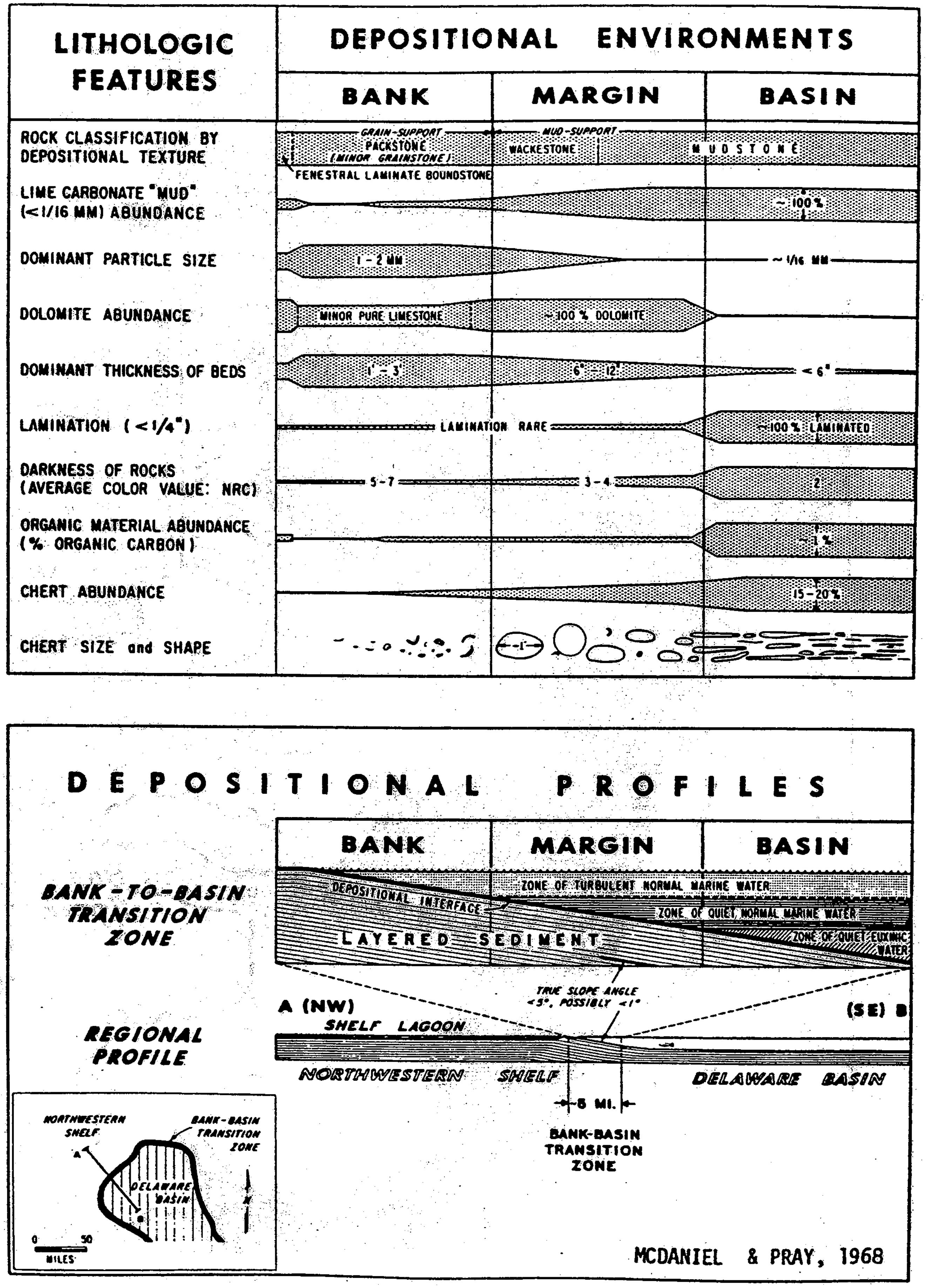

Figure 1-1-3. Lithologic features of bank, bank margin and basin facies, Victorio Peak and Bone Spring Limestone formations.

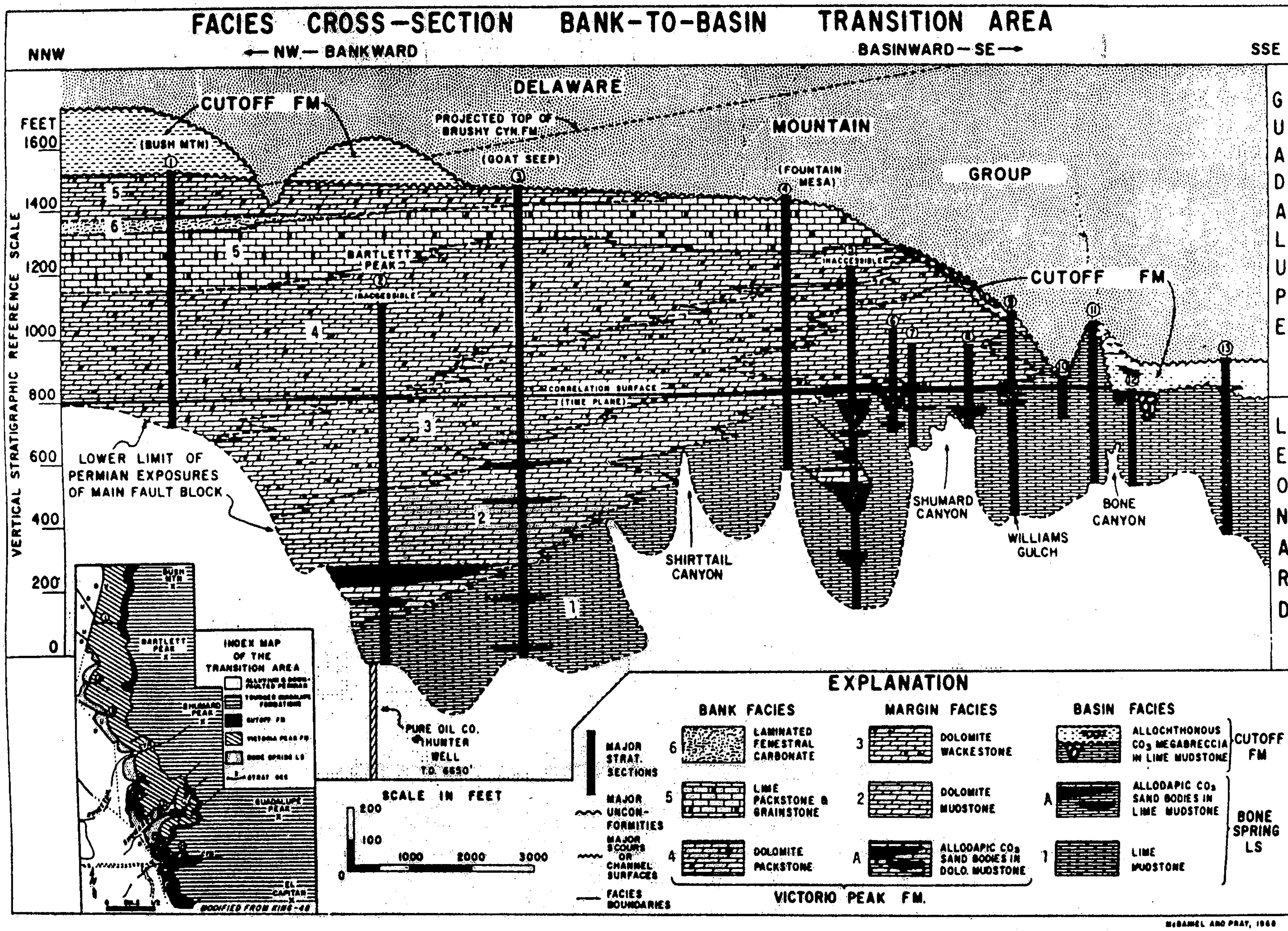

Figure 1-1-4. Facies cross-section of bank to basin transition area, Victorio Peak and Bone Spring Limestone formations, from McDaniel and Pray (1967).

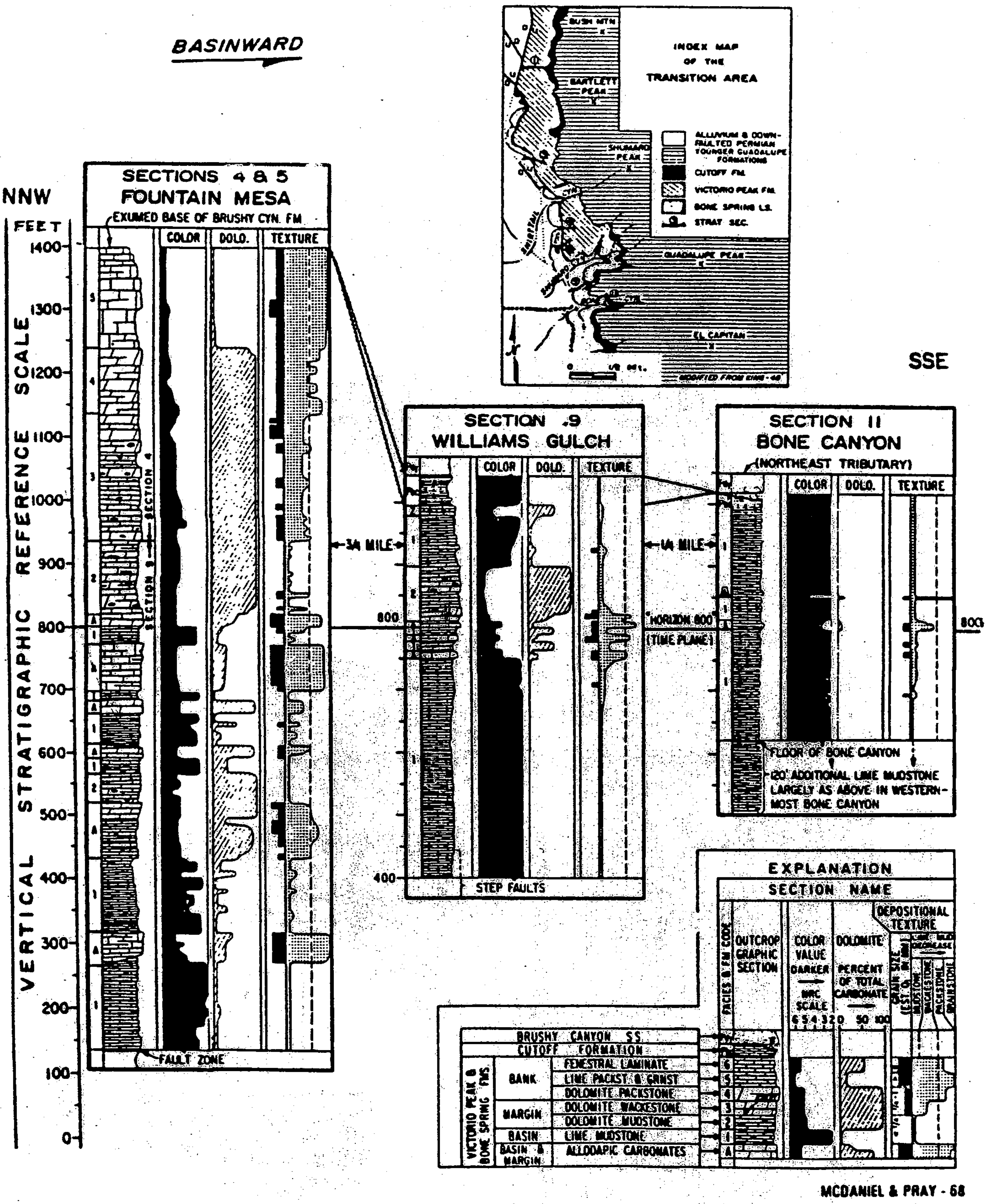

Figure 1-I-5. Stratigraphic sections of the bank to basin transition area, Victorio Peak and Bone Spring Limestone formations, from McDaniel and Pray (1968).

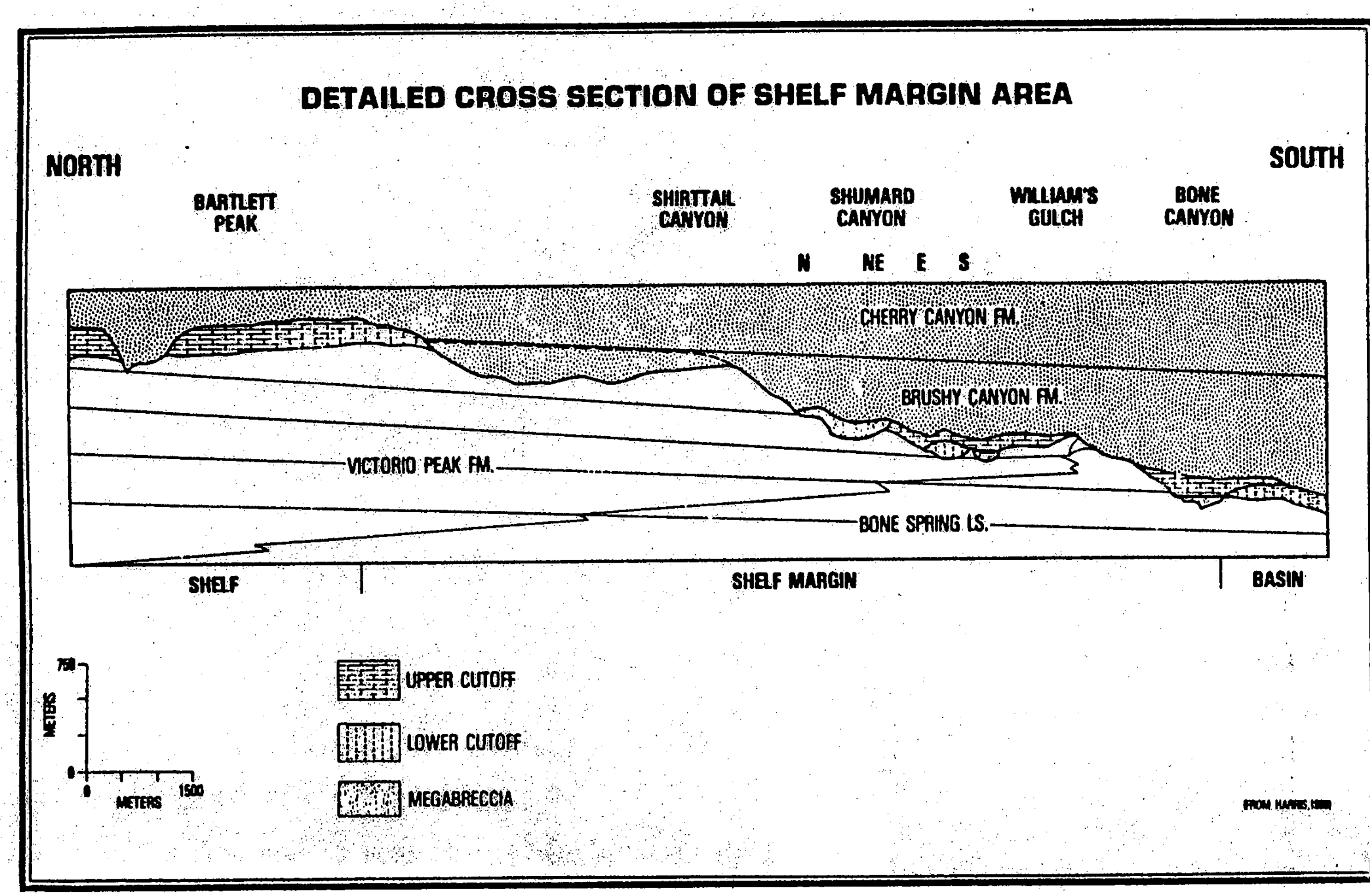

Figure 1-1-6. Cross-section of shelf margin area, Bone Spring, Victorio Peak, Cutoff and Brushy Canyon formations, from Harris (1982).

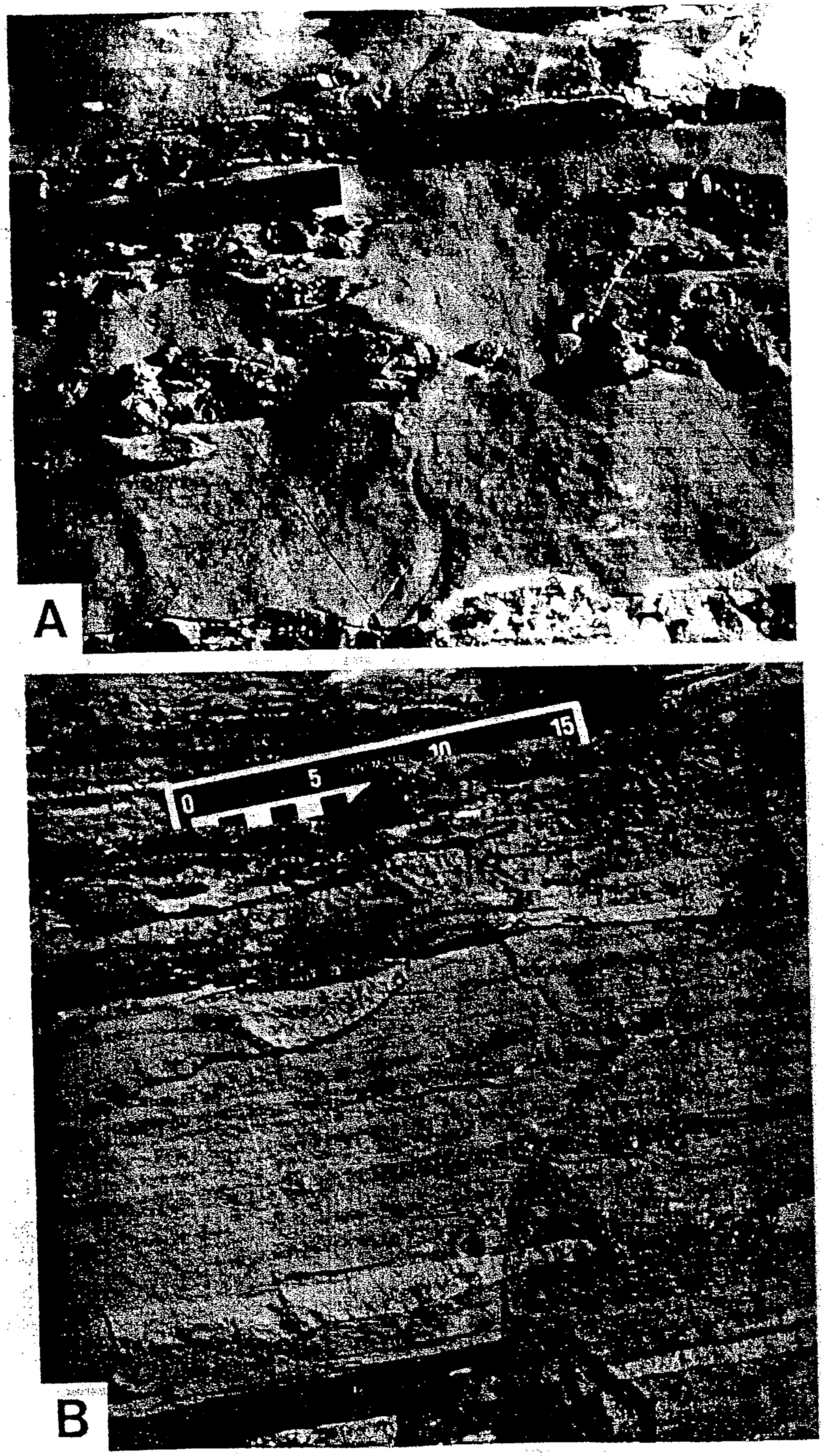

Figure I-I-7. Characteristic lithofacies of Bone Spring Limestone (slope/basin facies). Stop Ia. Shumard Canyon. ***A. Example of planar laminated*** *lithofacies with resistent chert lenses. B. Example of irregularly laminated lithofacies.* ***Irregular laminae show evidence of small-scale*** *current ripples and soft sediment deformation.*

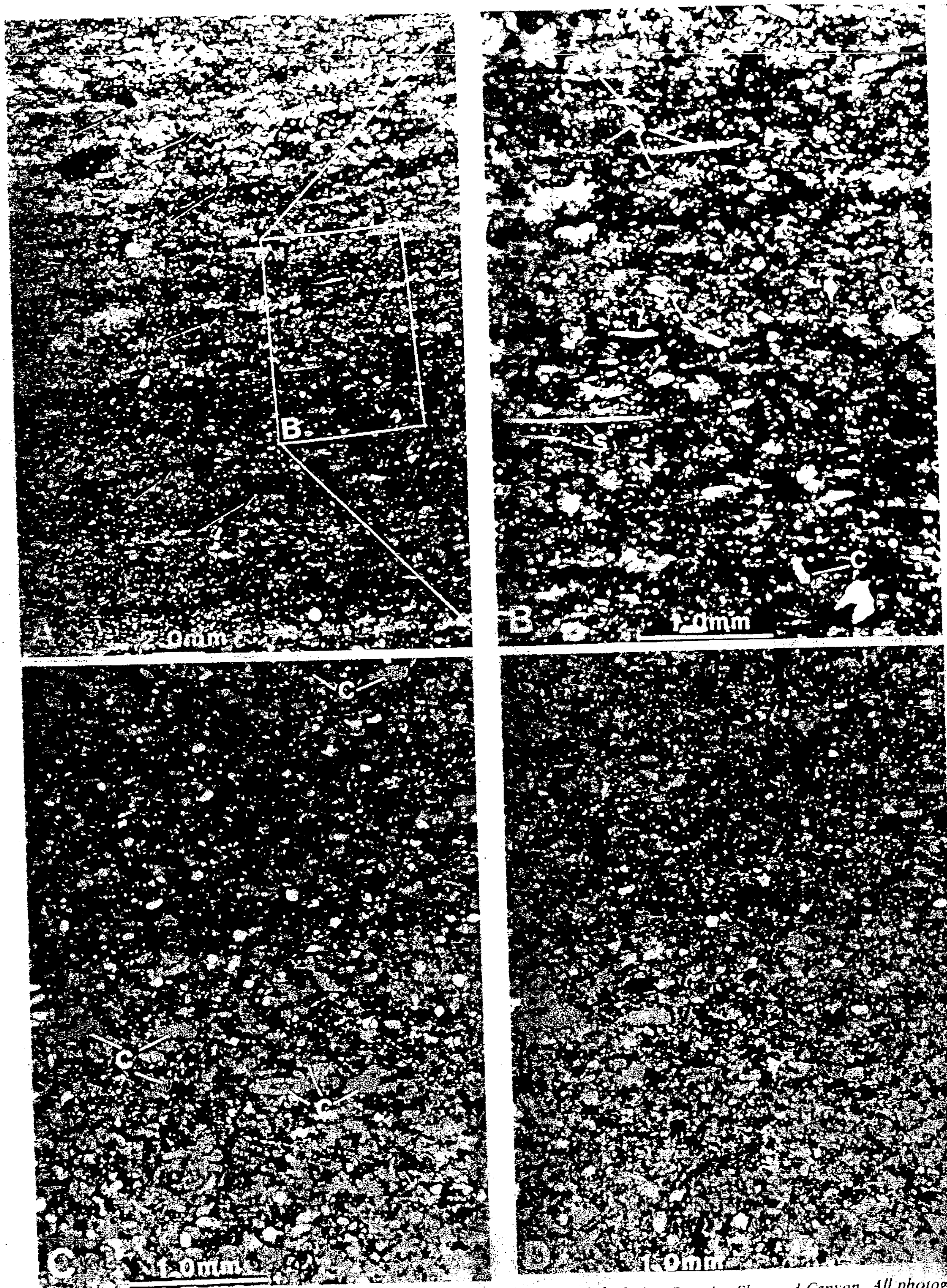

Figure 1-1-8. Thin section photomicrographs of the Bone Spring ***Limestone*** *lithofacies. Stop 1a, Shumard Canyon. All* ***photographs*** ***are oriented*** *with present stratigraphic up at the top of* ***photograph.*** *A&B. Thin section photomicrographs, plane* ***polarized*** ***light of*** ***the sample*** *shown in outcrop in Fig. 1-1-7. Spicules (S),* ***echinoderm (crinoid)*** *debris (C) and quartz silt are* ***conspicuous in this fine*** ***grained*** *skeletal packstone/wackestone. Note the inclined* ***laminations*** *interpreted as current ripples (arrows). C&D. Thin* ***section*** ***photomicrographs.*** *C-plane polarized light and D-cross* ***polarized light.*** *Quartz silt and echinoderm fragments (C)* ***are common in this*** ***fine grained packstone/wackestone.*** *This sample shows* ***alternation of coarser*** *(lower half of photo) and finer grained laminations.*

concave-up in geometry. At the mouth of the canyon, eastward-dipping surfaces are prominent. Farther up canyon, erosion surfaces dipping to the west can be observed. As was first described by King (1948), beds below the erosion surfaces are cleanly truncated and show no evidence of deformation or brecciation. Beds above the erosion surface typically parallel or drape the underlying erosional surface and are similar in lithofacies to beds below the erosion surfaces.

Origin of the intraformational erosion surfaces has been attributed to: 1) development of basinward-trending channels on the slope, 2) detachment surfaces related to slumping, and 3) faulting. The intraformational erosion surfaces are limited in distribution to an area extending from Shumard Canyon to a point about 1 mile south of Bone Canyon (King, 1948). This distribution suggests that the erosion surfaces were formed by processes active in a slope environment. Many of the large-scale erosional features in Shumard Canyon do not show onlap fill by material coarser than the underlying lime mud, but show drape by lime mud onto lime mud. Further south, in the Delaware Mountains, large-scale sediment deformation features (King, 1948, p. 15-16 and Plate 11B) are abundant in the upper Bone Spring limestones. The lack of coarse fill material and the downdip slump features suggests that these surfaces originated as detachment surfaces. Some of the erosional surfaces are, however, overlain by coarser-grained deposits favoring an erosional channel origin for these surfaces. Erosion surfaces, interpreted as channel structures (King, 1948, and Kirkby, 1982) do occur in Shumard Canyon in the lower part (basin margin facies) of the overlying Victorio Peak Formation.

Stop 1c — Allocthonous Carbonate Sand Sheet (Allodapic Sand)

Thick allochthonous channel-fill and sheet deposits composed of skeletal grainstones, packstones, and wackestones are common to basin margin facies of the lower Victorio Peak Formation and slope to basin facies of the Bone Spring Limestone (McDaniel and Pray, 1967). These allochthonous deposits were shed from the bank and bank margin areas of the Victorio Peak bank complex and are allodapic carbonate sands and sandy muds.

A thick allodapic skeletal grainstone unit is well exposed on the south wall of Shumard Canyon where the National Park trail crosses a gully (Figs. 1-I-1, 1-I-9). The base of this 10 m (33 ft) thick unit is poorly exposed below the park trail in the gully. Generally, however, these units exhibit sharp erosional bases. The lower half of the unit consists of medium to thick beds, with thick to very thick beds in the upper half. Internal channelling and trough cross-bedding are present (Fig. 1-I-10). Flow directions obtained from these features are roughly east-southeast in a basinward direction. The top of the unit is clearly marked by a change in bedding style from thick-bedded grainstones with trough cross-bedding to thin to medium-bedded mudstones and wackestones with lenticular chert lenses that are characteristic of the Bone Spring Limestone. Skeletal grains in these grainstones include: brachiopods, crinoids and echinoderm spines, fusulinids and other benthonic foraminifers, bryozoans, gastropods, calcareous algae and other finer skeletal debris (Fig. 1-I-10). The brachiopod fauna is diverse. Skeletal grains with micrite envelopes are common suggesting a shoal water source for these allochthonous deposits.

Figure 1-1-9. Unit of allochthonous skeletal grainstone to packstone within Bone Spring Limestone Formation along National Park trail, Stop 1c, Shumard Canyon.

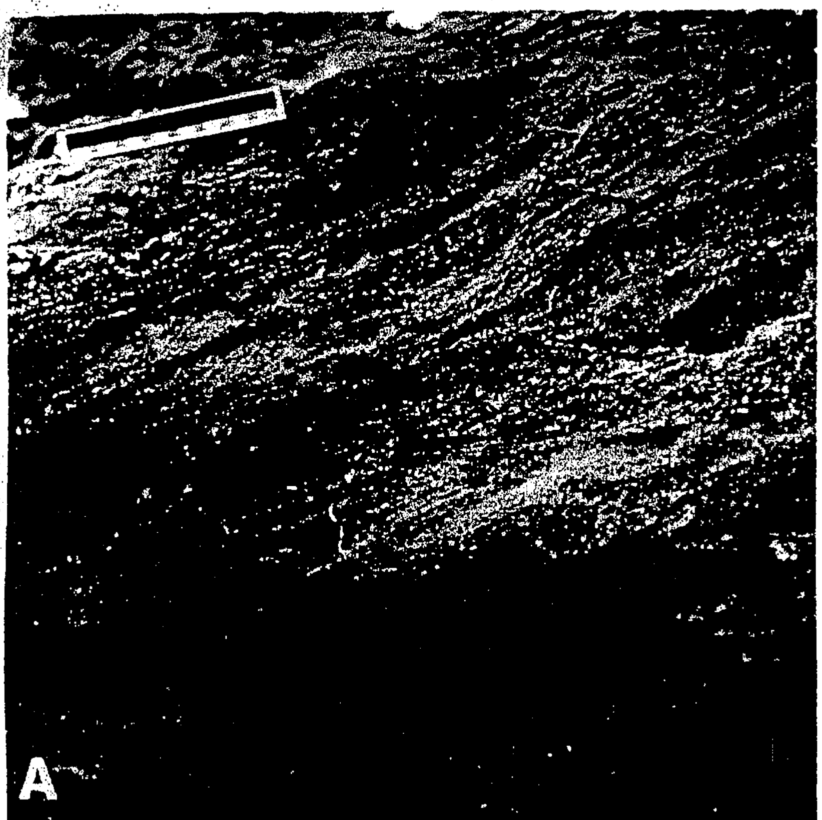

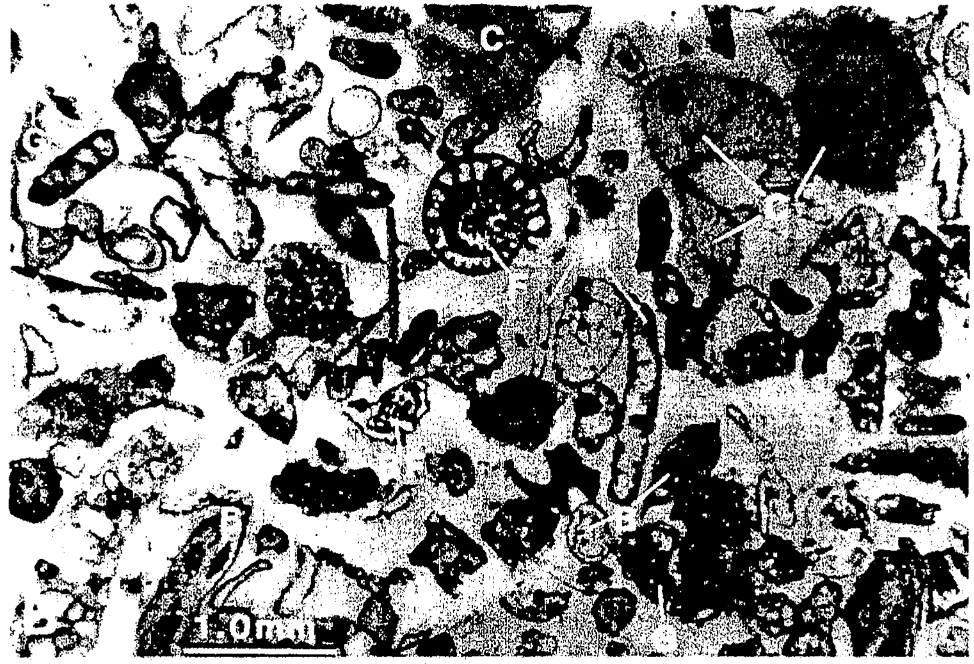

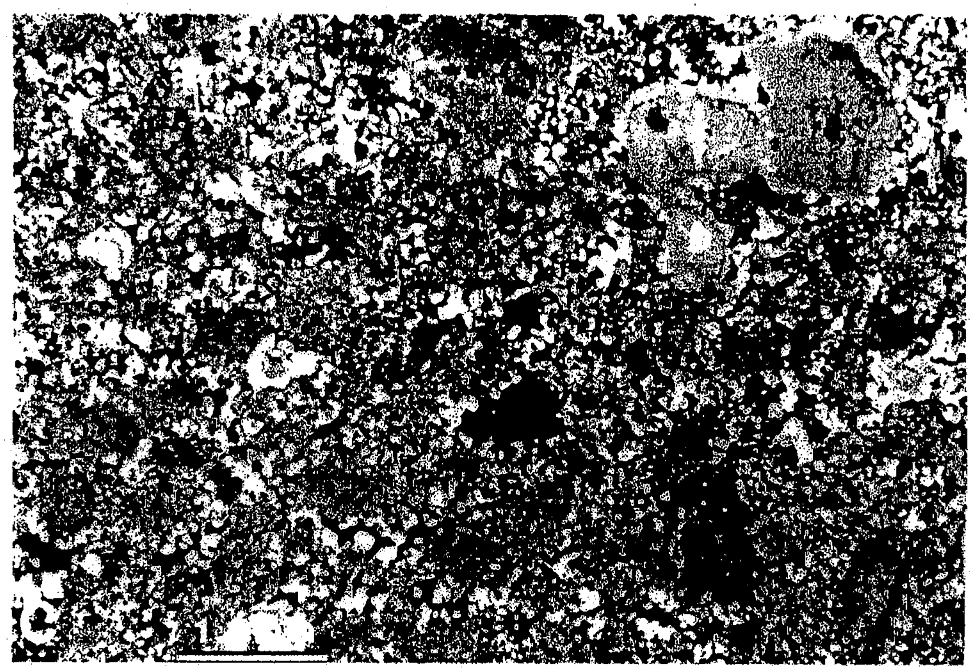

Figure 1-I-10. Outcrop and thin section photographs of the allodapic skeletal grainstone pictured in Fig. 1-I-9, Stop 1c, from Shumard Canyon. All photographs are oriented with present stratigraphic up at the top of the photograph. A. Outcrop photograph of trough cross-bedded grainstone located just above the geologist's head in Fig. 1-I-9. Scale is 15cm. B. Thin section photomicrograph, plane polarized light of the allodapic, skeletal dolomite grainstone shown in A. Grains consist largely of skeletal fragments including: echinoderm (crinoid) fragments (C), bryozoans (B), molluscan fragments preserved as micrite envelopes, (M), fusulinids (F), other benthonic foraminifers (BF), gastropods (G), and other unidentifiable skeletal debris. C. Thin section photomicrograph, cross polarized light of sample shown in B. Porosity in this grainstone has been completely occluded by megaquartz and chert.

STOP 5 — BONE CANYON

Stop 5a — Overview of south wall, Bone Canyon

Bone Canyon is situated at the "toe of slope" of the basinward-sloping sequence boundaries that mark the base of the Cutoff and of the Brushy Canyon formations (Fig. 1-I-6). The sequence boundaries and the lithofacies deposited on them are well exposed on the south wall of Bone Canyon (Fig. 1-V-1 and Fig. 1-V-2). The Bone Spring Limestone comprises the resistant, thin-bedded, dark-colored strata that form the lower visible part of the canyon wall. The recessive, grayish, vegetated slopes make up the Cutoff Formation, and the overlying resistant, tannish cliff consists of basal strata of the Brushy Canyon.

Fig. 1-V-2 shows the detailed geometry of the basal Cutoff and Brushy Canyon sequence boundaries along this wall, and lithofacies and intraformational erosion surfaces of the Cutoff Formation. Key features exposed here are listed below.

1) *The sequence boundary at the base of the Cutoff Formation.* Along much of the canyon wall, the basal Cutoff sequence boundary truncates underlying Bone Spring strata at a low angle. The boundary is overlain by lime mudstones and silicious shales of the upper Cutoff (Harris, 1982). At the west end of the canyon wall, two steep-sided, channel-shaped erosional surfaces filled with resistant, gray, massive-weathering megabreccia carbonates are developed on the sequence boundary (Fig. 1-V-2, 1-V-3A). These masses were first interpreted as patch reefs by King (1948), and Newell and others (1953) largely due to their internal massive character and abundance of fossils. They were subsequently reinterpreted as allochthonous megabreccias by Pray and Stehli (1962, see enclosed abstract) and Harris (1982), based on the following characteristics: 1) common erosional basal contacts, 2) presence within the masses of clasts of basinal to shallow-marine origin, and 3) chaotic orientation of geopetal fabrics from clast to clast. We will examine the contacts and internal fabric of a similar megabreccia located 0.25 km (0.15 mi) south of Bone Canyon during the final stop of the day (Stop 6).

2) *Intraformational erosion surfaces within the Cutoff.* These surfaces are broad, shallow, channel-like features up to 10 m (32 ft) deep, and 100-200 m (330-650 ft) wide (Harris, 1982). The scours are filled with coarse-grained material (intraclast rudstone) or with fine-grained material (lime mudstone and siliceous shale).

3) *Sequence boundary at the base of the Brushy Canyon Formation.* On the south wall of Bone Canyon, this boundary is a predominantly planar, eastward-dipping surface (strike N10E, dip 13° E). Brushy Canyon strata deposited on this surface comprise a coarse-grained package (unit BC of Fig. I-II-5), up to 75 m (240 ft) thick, which consists of megaconglomerate, planar-stratified sandstone, and allochthonous, fossiliferous lime grainstone (the gray, blocky weathering unit at the top, west end of the canyon wall). On both the south and north walls of the canyon, basal Brushy Canyon strata thin and pinchout to the west by onlap onto the eastward-sloping sequence boundary (Fig. 1-V-3B). These basal Brushy Canyon strata also pinch out by onlap to the north such that the 75 m thick package of sandstone, megaconglomerate and limestone is absent in Shumard Canyon, 1 km to the north.

Stop 5b — Traverse from north wall to floor of Bone Canyon

The traverse from the rim of the north wall of Bone Canyon to the canyon floor provides an opportunity to examine: 1) the sequence boundary separating the Cutoff and Brushy Canyon formations, and 2) the lithofacies and sedimentary structures present at the base of the Brushy Canyon in this "toe of slope" position.

Fig.1-V-4 is a section of the basal 75 m of the Brushy Canyon Formation in Bone Canyon. Representative lithofacies of this coarse-grained section are well exposed in the prominent draw located at the center of the north wall of Bone Canyon (Fig. 1-I-1). These units are, from top to bottom:

1) *Gray-weathering, allochthonous carbonates*, 32 m (66 ft) thick, consisting of sandy, dolomitic, skeletal-peloidal grainstones. Beds are internally massive, or exhibit Tabc, Tab, and Tbc Bouma sequences (Fig. 1-V-5A). Skeletal grains consist of fusulinids, crinoids, brachiopods, and rugose corals; nonskeletal grains consist of peloids, ooids and sand-sized intraclasts (1-V-8C, D). These grains are believed to have been derived from a contemporaneous shallow, normal-marine environment.

2) *Fine-grained sandstones*, 10 m (33 ft) thick, are parallel-laminated, current-rippled or display broad, shallow, trough cross-stratification. Lenses of pebble to cobble-sized carbonate clasts indicate high-energy flow conditions.

3) *Carbonate-clast megaconglomerate*, 2.5 m (8.2 ft) thick, forms the base of the Brushy Canyon at this locality (Fig. 1-V-6). This megaconglomerate is similar to other megaconglomerates that occur with interbedded parallel-stratified sandstones in the basal 25 m (78 ft) of the Brushy Canyon in Bone Canyon. Common characteristics of the megaconglomerates (Fig. 1-V-5B, 1-V-7A) are: 1) clast-support texture, 2) matrix of very fine sandstone, 3) clast sizes ranging from pebbles to boulders up to 5 m (16 ft) in longest dimension, and 4) internally massive, ungraded character. In a few megaconglomerates, large clasts protrude above the tops of beds as if they had been rafted (1-V-7B). The megaconglomerates are interpreted as debris flow deposits (Harms, 1974, Rossen, 1985). Megaconglomerate clast types include: (1) dark gray lime mudstones, (2) light gray skeletal wackestones, packstones and grainstones of limestone and dolomite composition, (3) lesser amounts of fenestral limestone and dolomite (Fig.1-V-7A and Fig. 1-V-8 A, B), and (4) very fine-grained quartz sandstone. With the exception of the fenestral dolomite and limestone, these clast types are similar to lithologies found in the Cutoff, Victorio Peak and Bone Spring formations beneath the basal Brushy Canyon sequence boundary. Fenestral dolomite clasts may have been eroded from bank top Victorio Peak strata that are now preserved to the north at Cutoff Mountain in the lower part of the Upper Victorio Peak, or from uppermost Victorio Peak strata that were completely eroded during formation of the basal Brushy Canyon sequence boundary.

Strata of the Cutoff Formation, consisting of gently eastward-dipping, thin-bedded, dark gray, lime mudstones, crop out directly beneath the Brushy Canyon megaconglomerate on the east side of the draw (Fig. 1-V-6). The subhorizontal lime mudstone beds truncated below the Cutoff beds are strata of the Bone Spring Limestone. The Cutoff Formation thins to the west by truncation beneath the basal Brushy Canyon sequence boundary, and pinches out completely some 10 m (30 ft) west of the draw (Harris, 1982). This truncation marks the shelfward pinchout of the basin segment of the Cutoff (Fig. 1-I-6). The Cutoff reappears beneath the basal Brushy Canyon sequence boundary approximately 0.25 km (0.15 mi) north of Bone Canyon.

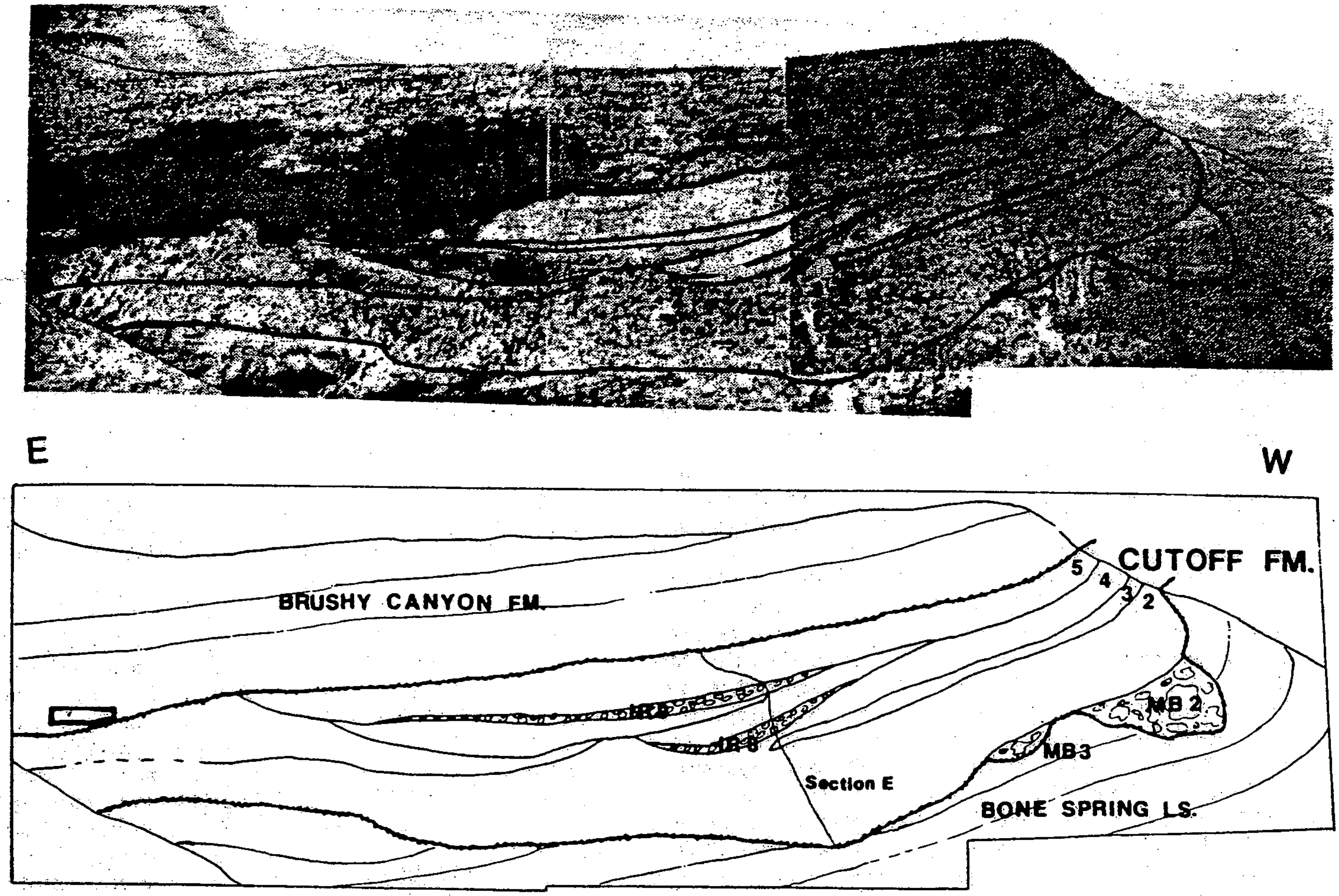

Figure 1-V-2. Sketch of south wall, Bone Canyon, from Harris (1982), showing geometry of basal Cutoff and basal Brushy Canyon sequence boundaries. Note channel-filling carbonate megabreccias at base of Cutoff (MB2 and MB3), and numerous Cutoff intraformational, channelized surfaces filled with intraclast rudstone (IR) or mudstone.

Stop 5c — Floor of Bone Canyon at the Juniper Tree

At this locality, the interbedded megaconglomerates and sandstones which form the basal 10 m (33 ft) of the Brushy Canyon Formation (Fig. 1-V-7B) can be examined.

Traverse along south wall of Bone Canyon to Cutoff megabreccia of Stop 6.

As you walk along the south wall of Bone Canyon, the following features can be noted on the north wall of Bone Canyon:

1) East end of canyon wall; westward thinning and pinchout of basal Brushy Canyon megaconglomerates and sandstones by onlap onto the smooth, eastward-dipping, basal Brushy Canyon sequence boundary (Fig. 1-V-3B).

2) West and central parts of canyon wall; irregular, undulating morphology of basal Brushy Canyon sequence boundary on underlying thin-bedded strata of the Bone Spring Limestone.

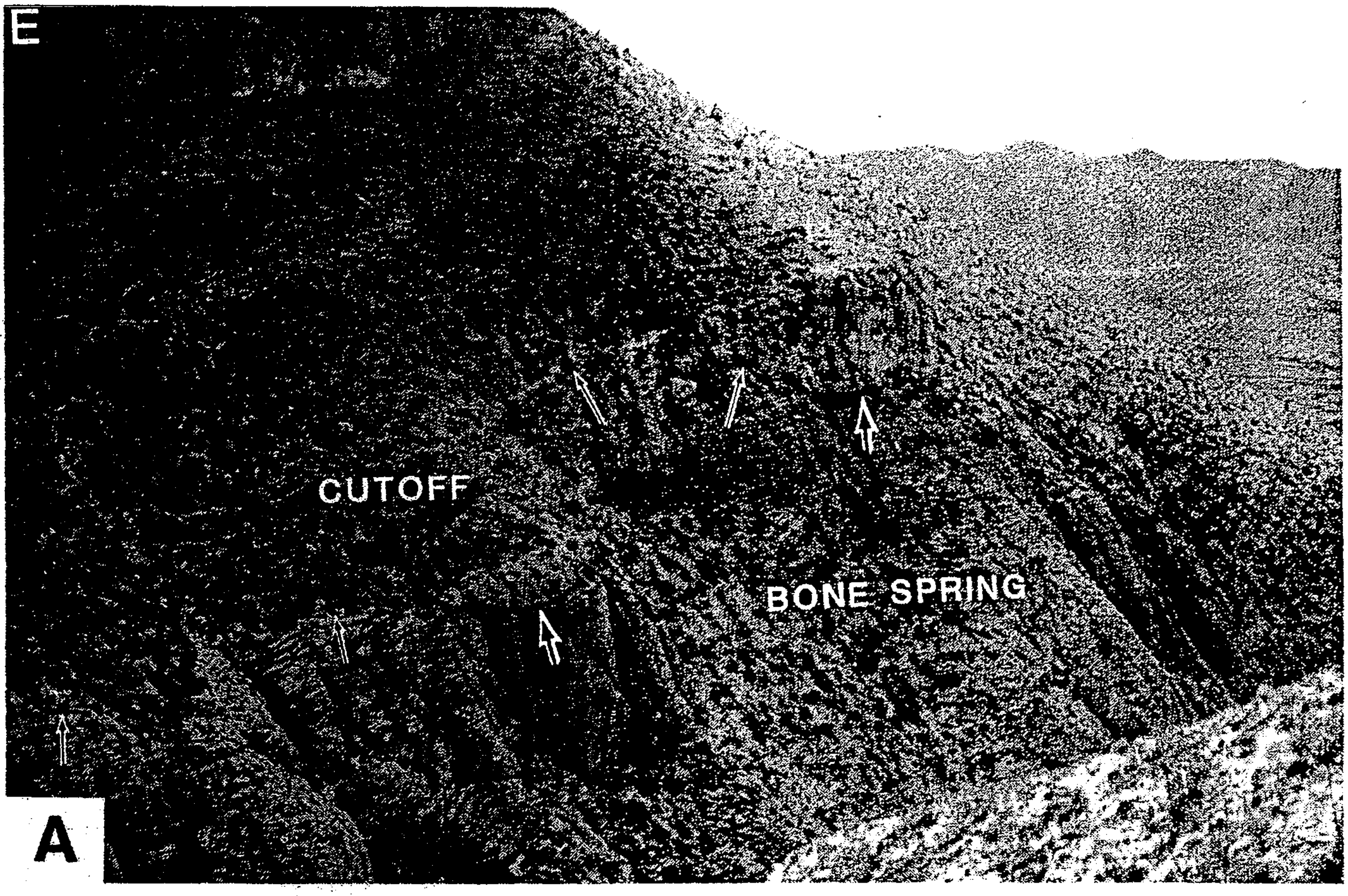

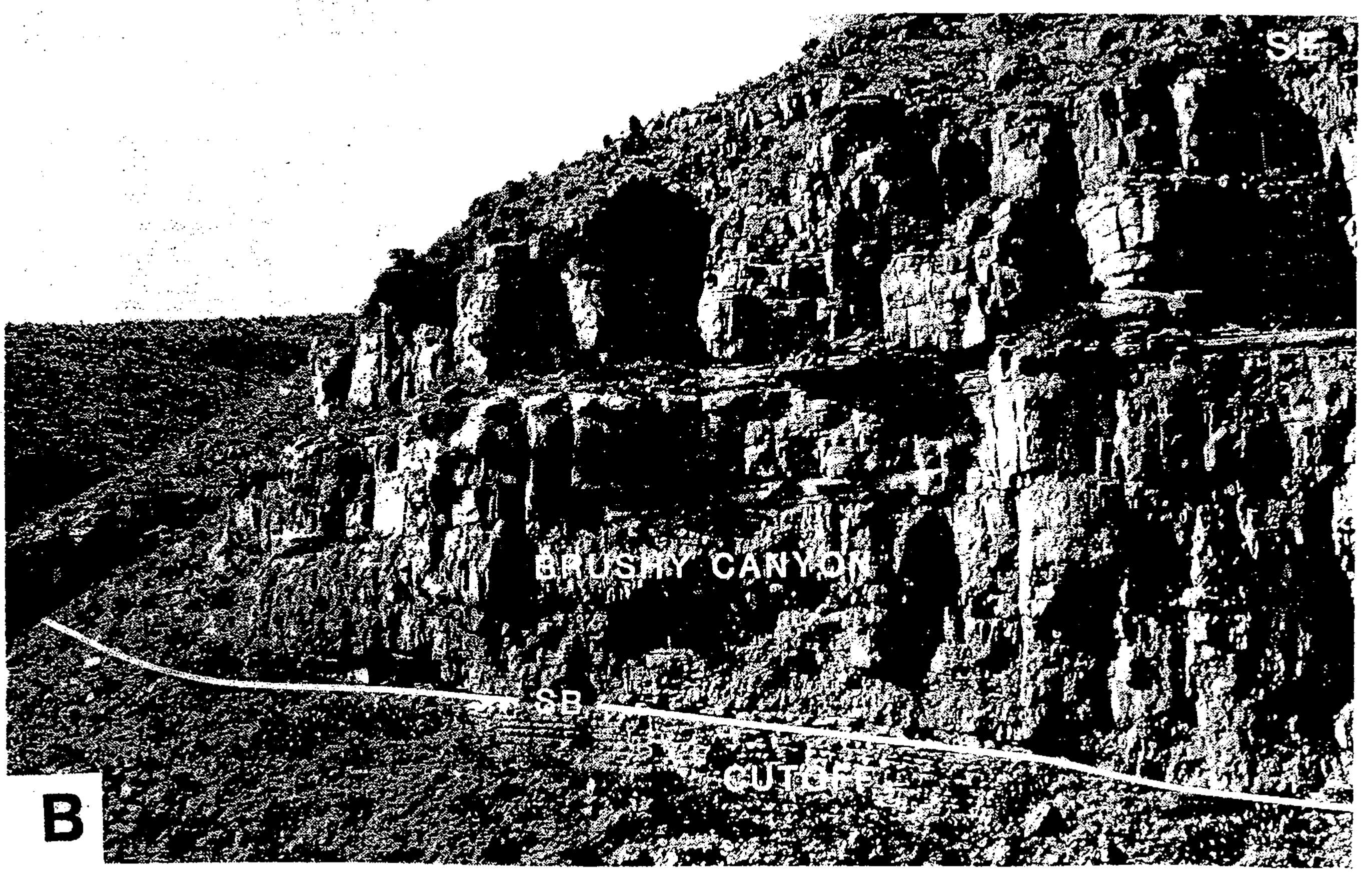

Figure 1-V-3. A. Close-up of Cutoff carbonate megabreccias (large arrows), MB2 and MB3 of Fig. 1-V-2, at base of Cutoff Formation, west end of south wall, Bone Canyon. Megabreccias fill spoon-shaped scours developed on basal Cutoff sequence boundary (small arrows) that are incised into underlying strata of the Bone Spring Limestone. B. View of Cutoff Formation and interbedded sandstones and conglomerates of basal 25 m (80 ft) of Brushy Canyon Formation, north wall Bone Canyon. Basal Brushy Canyon strata thin to the west (left) by onlap onto the eastward-dipping basal Brushy Canyon sequence boundary (SB).

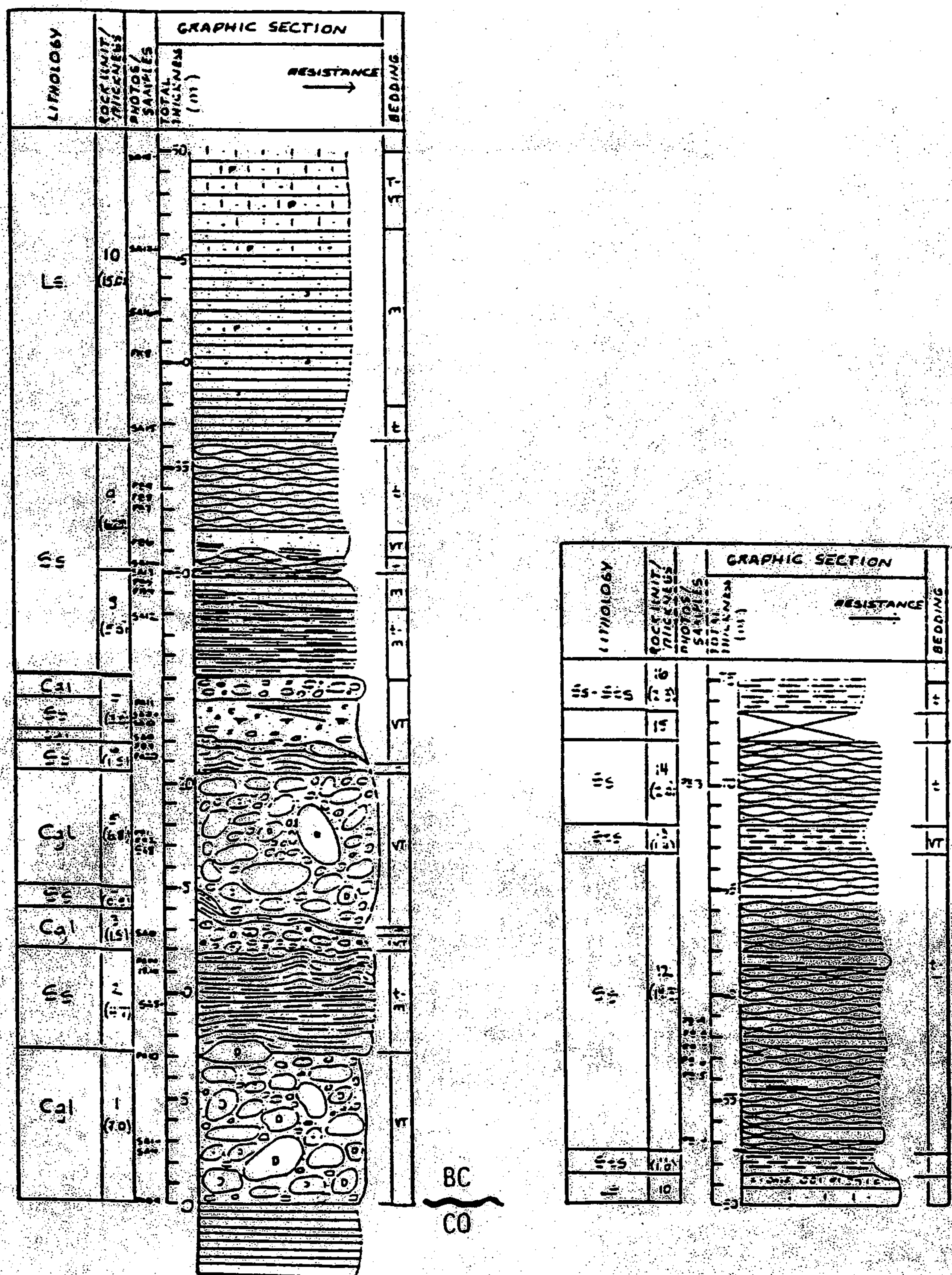

Figure 1-V-4. Stratigraphic section of basal 75 m (250 ft) of Brushy Canyon Formation in Bone Canyon, as measured along canyon floor, from Rossen (1985). BC = Brushy Canyon Fm., CO = Cutoff Fm.

LEGEND FOR GRAPHIC SECTIONS

MAJOR LITHOLOGIES:

Siltstone

- light-colored, coarse silt
- organic-rich (dk gray) medium-coarse silt
- organic-rich (gray) medium-coarse silt

Sandstone

- medium
- very fine-fine

MINOR LITHOLOGIES:

Conglomerate

- clast support
- matrix support

Clast types:

- sandstone
- limestone
- dolomite
- chert
- unidentified

Limestone

- • sandy
- M mudstone
- W wackestone
- P packstone
- G grainstone

SEDIMENTARY STRUCTURES:

- thin laminations
- thick laminations
- ripples
- cross-bedding
- massive
- contorted layer

For example:

- interbedded ripples and thin laminations

FOSSILS:

- F fusulinid
- forams (undifferentiated)
- brachiopod
- ★ crinoid
- mollusc
- Q gastropod
- T trace fossil
- unidentified

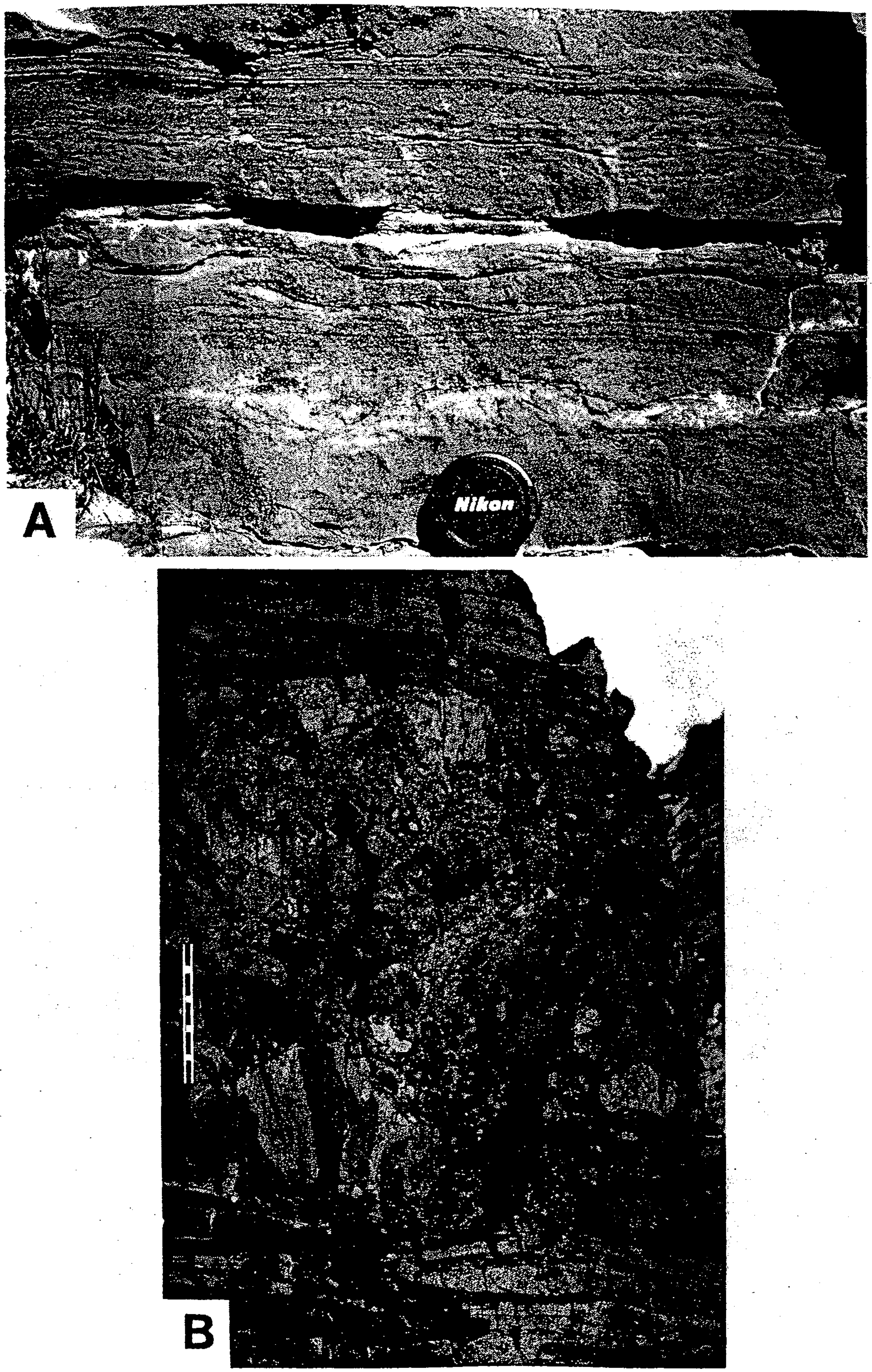

Figure I-V-5. A. Allochthonous sandy carbonate grainstone unit, north wall Bone Canyon, showing this Bouma Tab, Tabc, and Tbc sequences. Lens cap is 6 cm (2.4 inches) in diameter. B. Megaconglomerate at base of Brushy Canyon Formation, north wall Bone Canyon, showing internally massive, poorly-sorted, clast-supported character. Thin beds beneath megaconglomerate are Cutoff strata. Scale bar =0.5 m (1.6 ft).

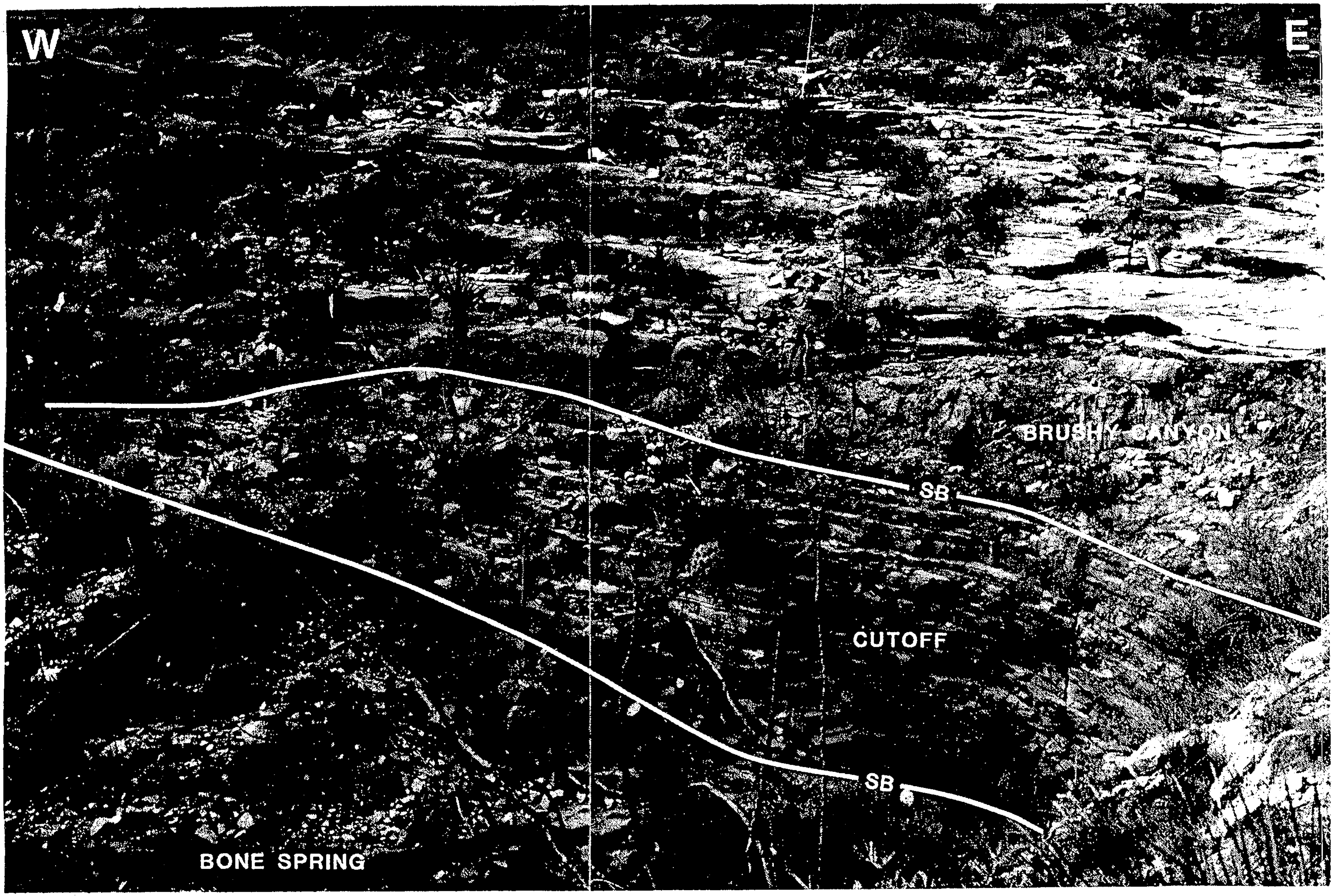

Figure 1-V-6. Basal Cutoff and basal Brushy Canyon sequence boundaries (SB) exposed in prominent draw located at center of north wall, Bone Canyon. Gently eastward-dipping strata of Cutoff Formation overlie truncated, subhorizontal beds of Bone Spring Limestone. The Cutoff Formation thins to pinchout towards the west as the result of truncation by the overlying basal Brushy Canyon sequence boundary. Megaconglomerate at base of Brushy Canyon Formation thins to west by onlap onto eastward-dipping basal Brushy Canyon sequence boundary.

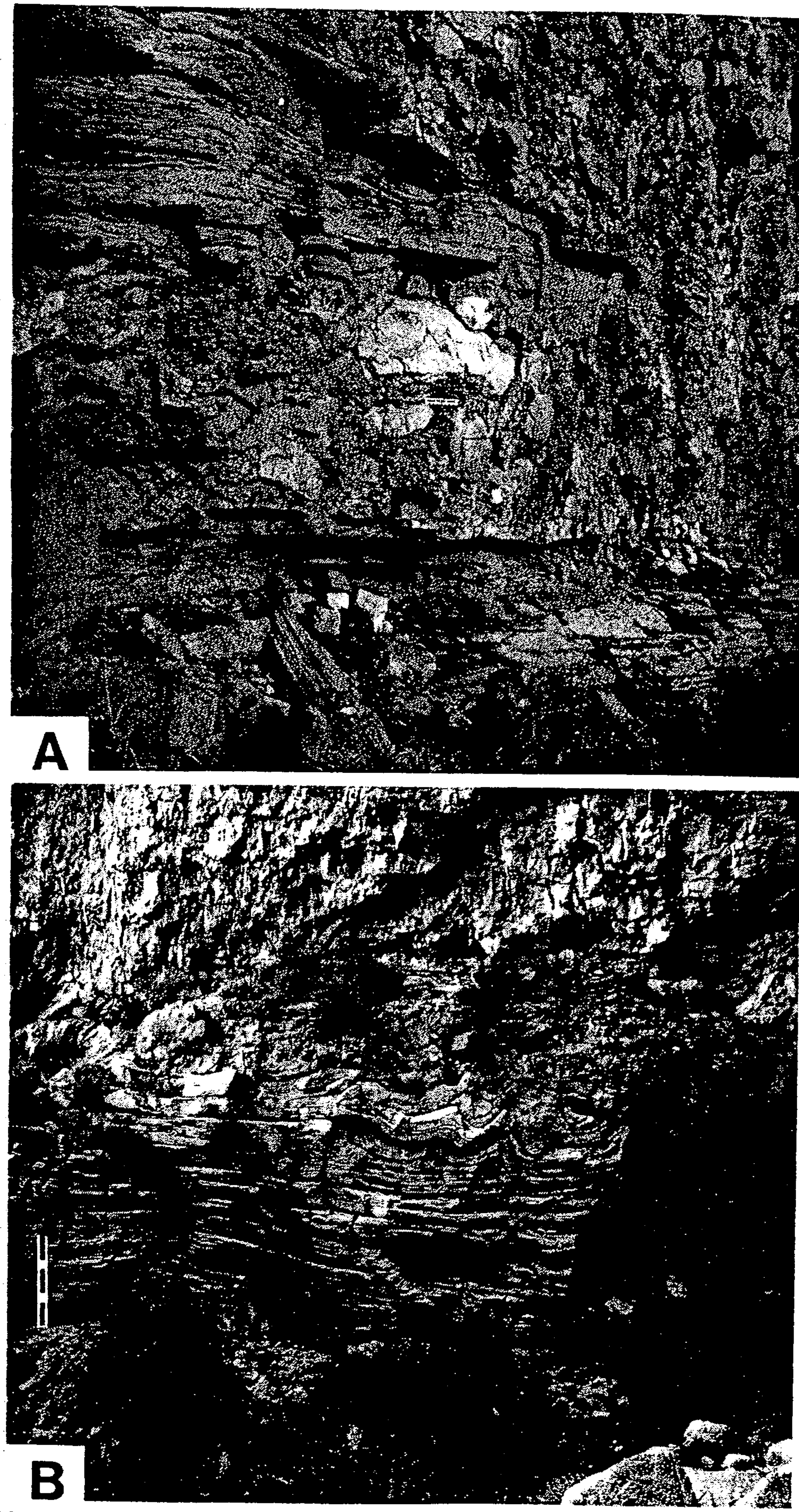

Figure 1-V-7. A. Megaconglomerates and interbedded parallel-laminated sandstone of basal Brushy Canyon **Formation, north wall Bone Canyon. Cutoff** *Formation comprises thin beds below recessive in lower 1/3 of photo. Scale is 15 cm.* **Prominent white clast above scale consists** *of fenestral lime grainstone (see Fig. 1-V-8A,B). B. Parallel-laminated sandstone* **unit interbedded with megaconglomerates in** *basal 15 m of Brushy Canyon Formation, canyon floor near Juniper tree, Bone Canyon.* **At base of sandstone unit, note drape of sandstone** *laminae over boulder (0.5 m relief) protruding from top of underlying* **megaconglomerate. Sandstone is deformed into fold and** *flame structures beneath overlying megaconglomerate. Scale bar = 1.0 m (3.28 ft).*

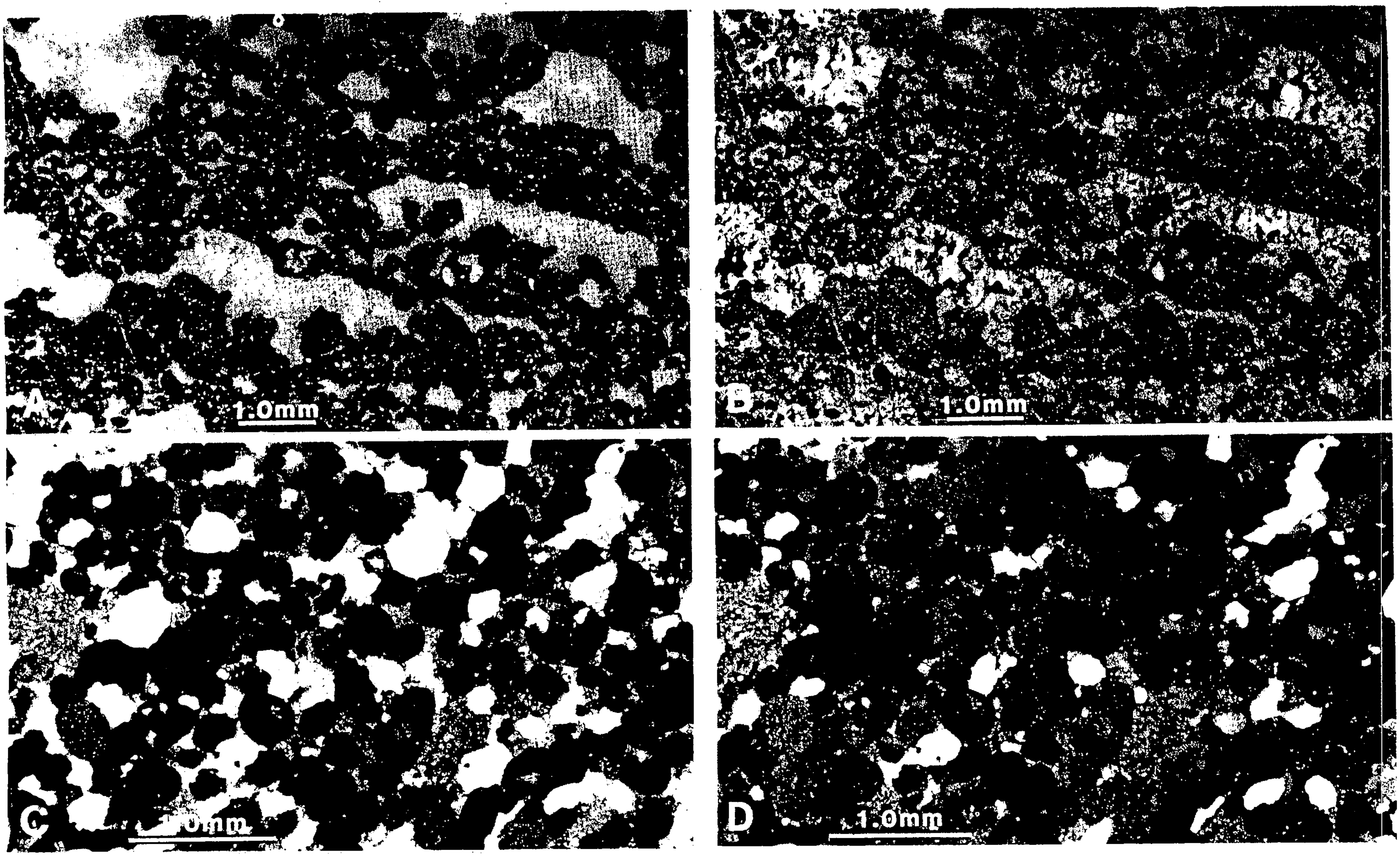

Figure 1-V-8. Thin section photomicrographs from the lower Brushy Canyon Formation, north wall Bone Canyon. All photographs are oriented with present stratigraphic up to the top of photograph. A&B. Thin section photomicrographs, A-plane polarized light and B-cross polarized light of a sample taken from the light colored boulder in the center of the photo in Fig. 1-V-7. The fenestrae are overturned as collected in the field. This meter-sized boulder is composed of a peloid, intraclast, lime grainstone. Two generations of cement fill the large fenestrae: 1) a fibrous to bladed isopachous cement of probable marine origin and 2) a coarse equant calcite spar of probable meteoric origin. These cements are interpreted to have been precipitated in a shelf setting before being redeposited in the slope setting where they are preserved today. C&D. Thin section photomicrographs, C-plane polarized light and D-cross polarized light, from a parallel-laminated dolomite sample taken from the allochthonous carbonate unit of lower Brushy Canyon. This grainstone is composed of rounded dolomite and siliciclastic grains. The dolomite grains include: intraclasts (including ooid grainstones), peloids (some of which are likely former ooids or skeletal grains), and ooids. The siliciclastic grains include: quartz, chert, and K-feldspar.

8) Lidar 2
Emily Finkelman and David Brown

McKittrick Canyon and Salt Bench Field Sites

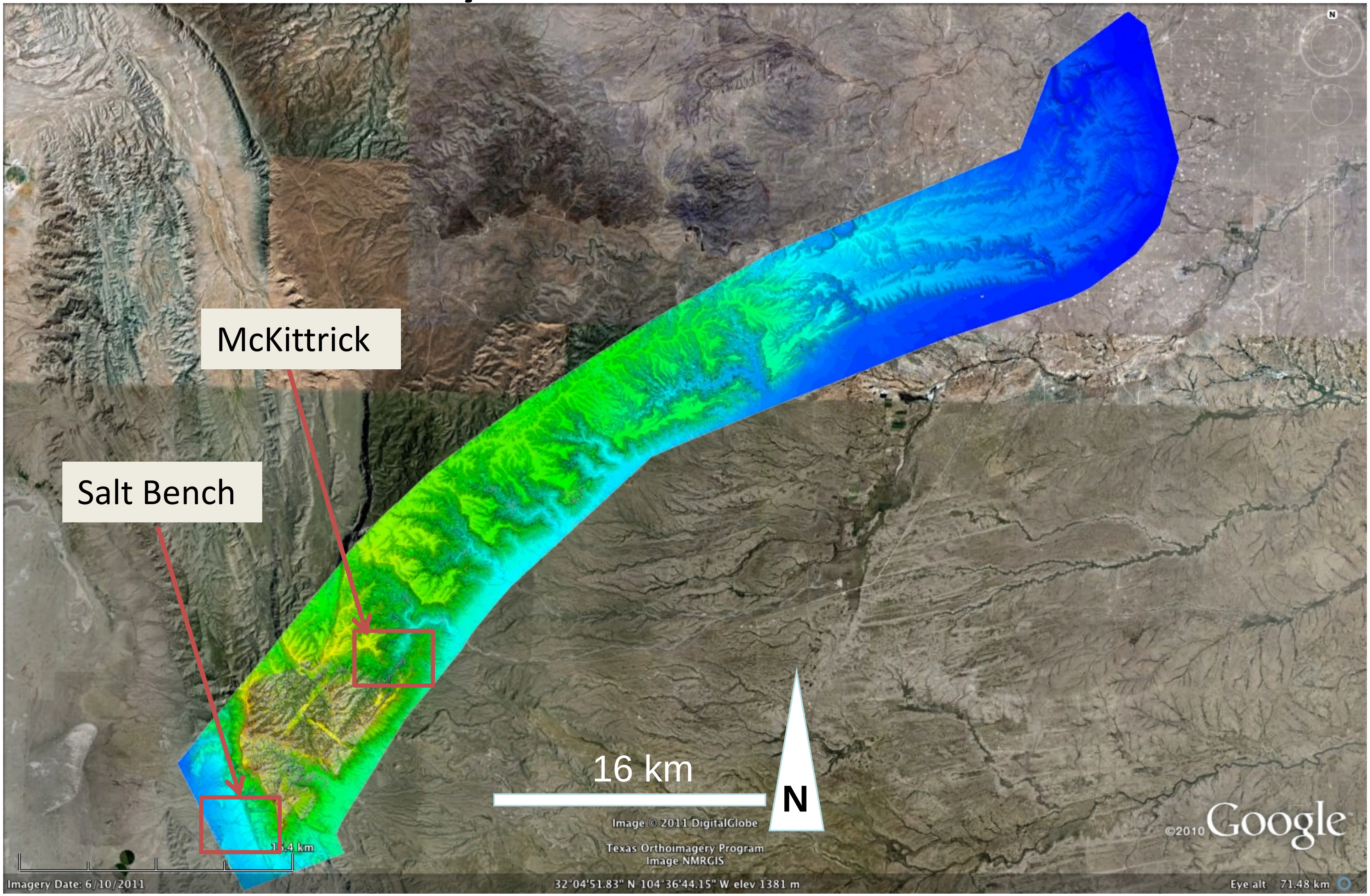

North Western Wall of McKittrick Canyon

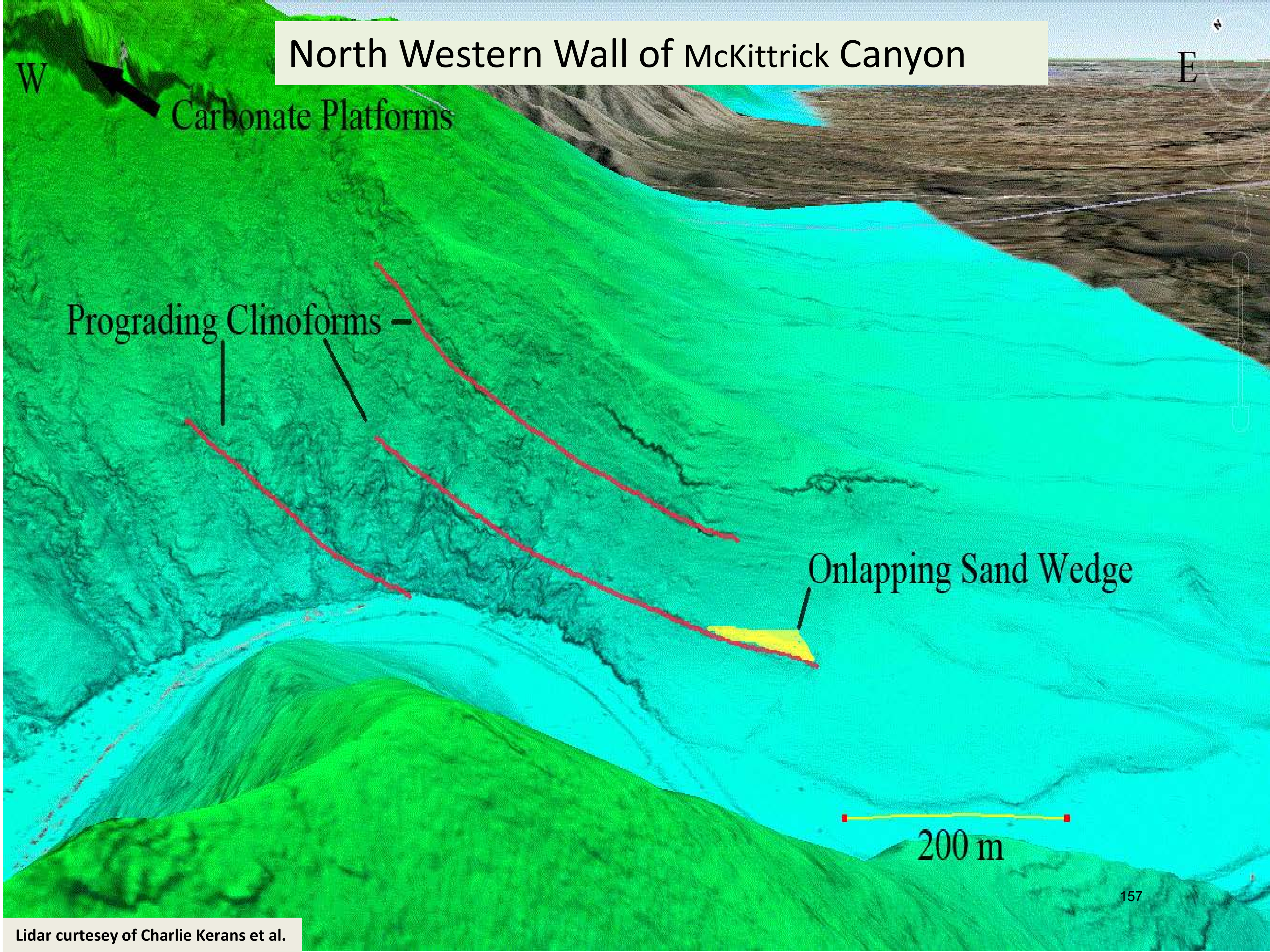

Lidar curtesey of Charlie Kerans et al.

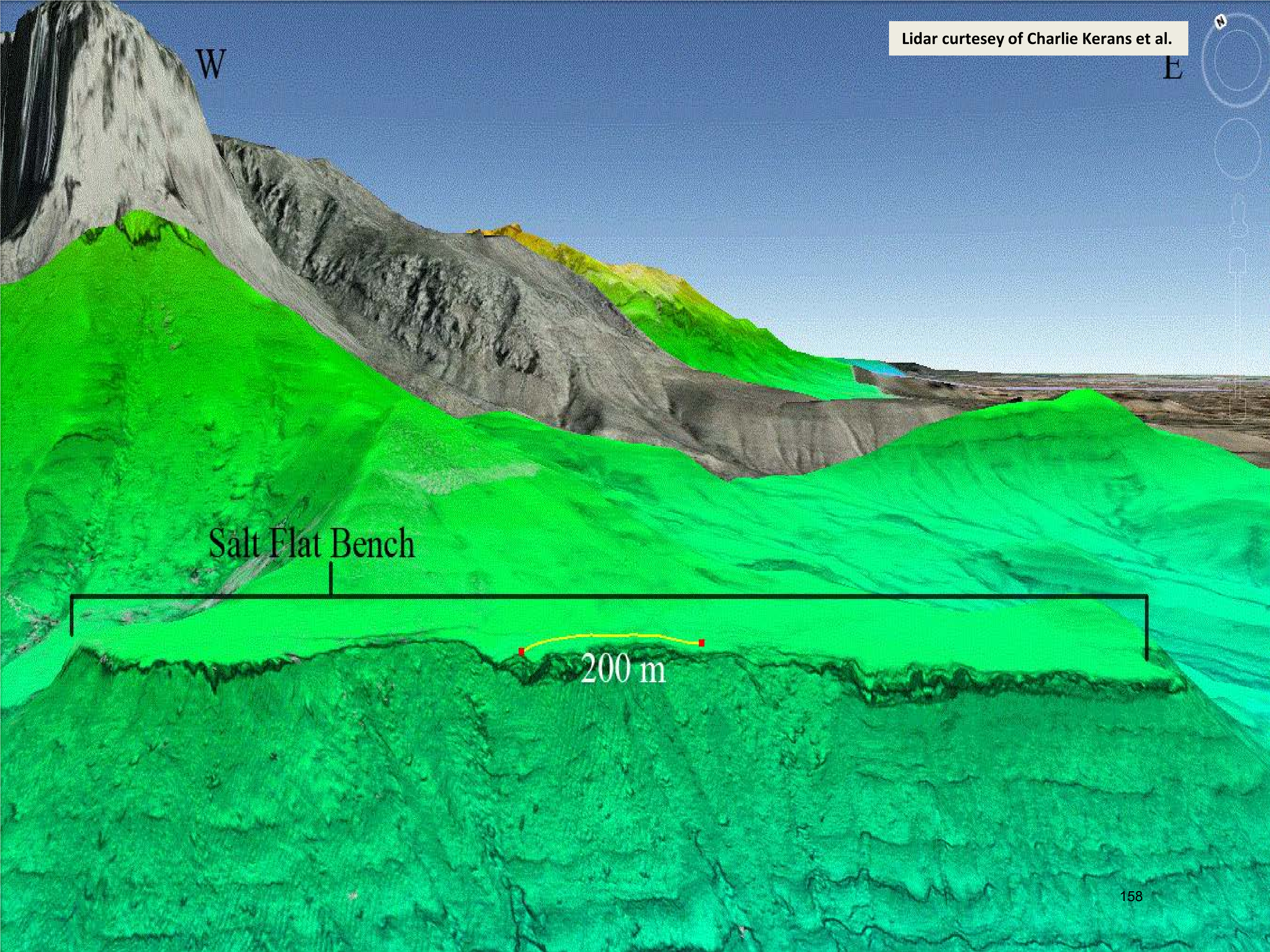
Lidar curtesey of Charlie Kerans et al.
W
E
Salt Flat Bench
200 m

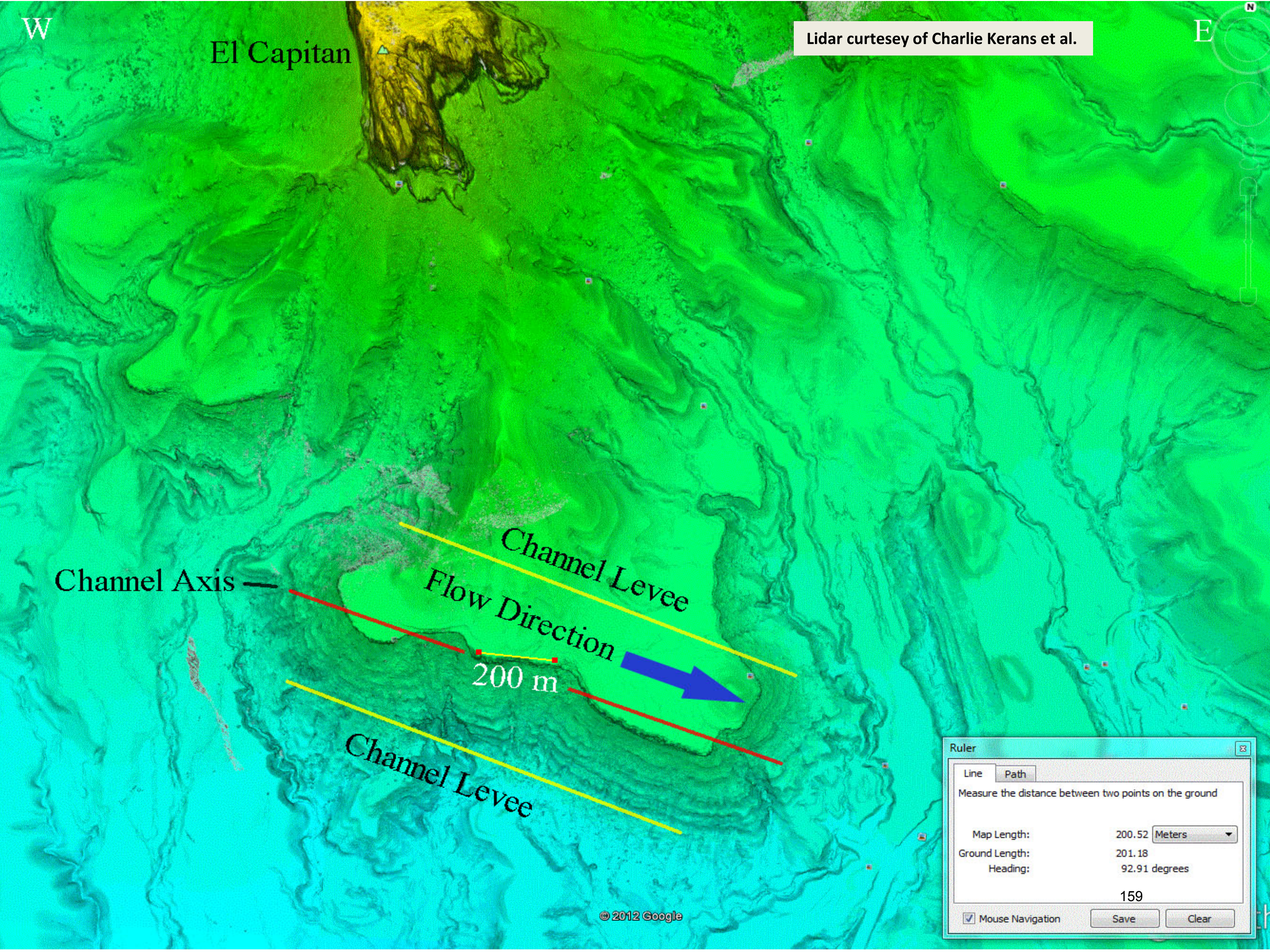
W
El Capitan
Lidar curtesey of Charlie Kerans et al.
E
Channel Levee
Channel Axis
Flow Direction
200 m
Channel Levee
© 2012 Google
Ruler
Line
Path
Measure the distance between two points on the ground
Map Length: 200.52 Meters
Ground Length: 201.18
Heading: 92.91 degrees
Mouse Navigation
Save
Clear

3. Salt Flat Bench

A view from Highway 62, looking up at El Capitan and Salt Flat Bench

Salt Flat Bench is a 40m thick sand body, which extends laterally for more than a kilometer.

Erosional truncations at the base of the sand body have been interpreted as slump scars. The sand-body is believed to be housed within a 'spoon-shaped' master confinement created by repreated slump scars.

Multiple truncation surfaces within the deposit have been attributed to repeated episodes of cut-and-fill.

The proportion of sand decreases laterally, interpreted as the gradation into overbank deposition.

This deposit is a large isolated sand-body encased in siltstones, interpreted as characteristic channelized deposit found in upper slope settings

The abundant siltstones are believed to be the result of deposition away from the main sand fairways. Two siltstone lithofacies have been described by previous workers.

1. Light grey laminated siltstones with milli-meter scale graded laminations are interpreted as deposits of dilute, fine-grained turbidity currents

2. Dark grey organic rich siltstones which contain organic content derived from marine algae. These are believed to represent hemipelagic sedimentation, characteristic of condensed intervals. These are excellent marker horizons.

The siltstone interval above the SFB gets steadily more organically rich and has been interpreted by Gardner & Borer (2000) as the

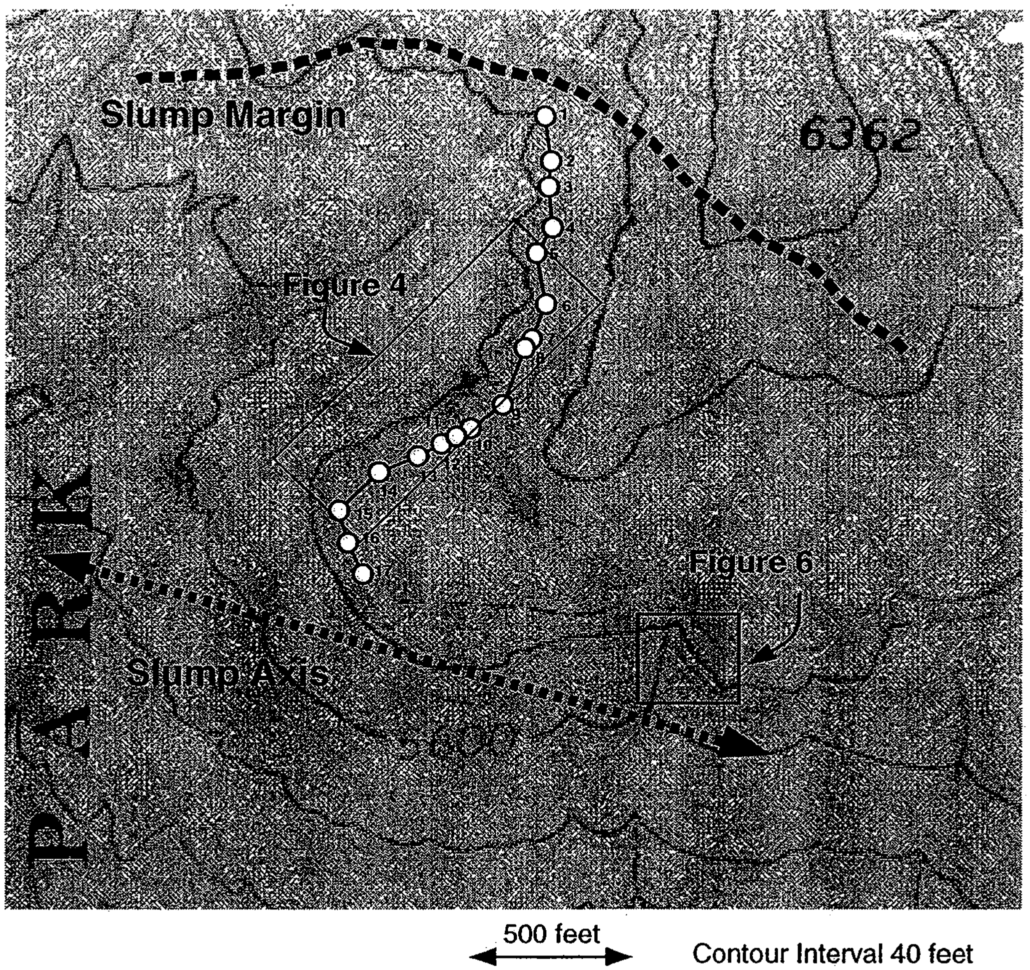

Figure 3.14. Inferred slump orientation in map view, as interpreted from measured sections. Axis of slump is unknown because bench is eroded to south, but orientation is interpreted to parallel dominant flow orientation measured from massive sands in facies D_L. For reference, locations of Figures 3.4 and 3.6 (photos of southward-thickening sandstones are outlined.

Gardener, M. H. and J. M. Borer, 2000, Submarine channel architecture along a slope to basin profile, Brushy Canyon Formation, west Texas, *in* A. H. Bouma and C. G. Stone, eds., Fine-grained turbidite systems, AAPG Memoir 72/SEPM Special Publication 68, p. 195–214.

Chapter 19

Submarine Channel Architecture Along a Slope to Basin Profile, Brushy Canyon Formation, West Texas

Michael H. Gardner
James M. Borer
Department of Geology and Geological Engineering, Colorado School of Mines
Golden, Colorado, U.S.A.

ABSTRACT

Slope and basin-floor channel sand bodies in the Permian Brushy Canyon Formation comprise a depositional profile, along which changes in the facies architecture of a fourfold channelform hierarchy are compared. Channel complexes form sand bodies with serrated margins consisting of stacked channels that increase in offset basinward. Channels and complexes record "cut," "fill," and "spill" phases of bypass and deposition, with channel and overbank deposition offset in time.

Upper slope siltstones encase the largest channelform sand bodies confined to intraslope depressions. Sediment bypass gives way to deposition downprofile, producing multistory, multilateral, and eventually distributary channel patterns. As complexes widen, "build" phase deposits that precede channelization, and spill-phase overbank deposits, thicken downprofile to equilibrate sandstone volumes inside and outside channels.

INTRODUCTION

Submarine channels are the principal sediment pathway linking the shelf to the basin. Their sediment-fill and bounding surfaces provide insight into fan growth and gravity-flow processes that produce channel form sediment bodies. Despite their prominent role in submarine fan depositional processes, the architecture of submarine channels is poorly understood. Important issues include the (1) controls on channel size and shape, (2) scalar hierarchy of channel sand bodies (Figures 1, 2), and (3) sedimentological criteria that distinguish depositional processes and predict position along a slope to basin profile.

Build-Cut-Fill-Spill Model

The "cut-fill-and-spill" model relates facies patterns in submarine channel and overbank deposits to their position on a slope to basin profile (Gardner et al., 1998). An important premise is that submarine channels generally backfill. Therefore, a fixed point on the depositional profile will record a transition from erosion and bypass, to confined aggradation, to focused, unconfined deposition. These cut, fill, and spill stages of deposition occur at multiple temporal and spatial scales.

The "build-cut-fill-spill" model incorporates the important phase of deposition that may precede channelization. In the upper slope, the "build

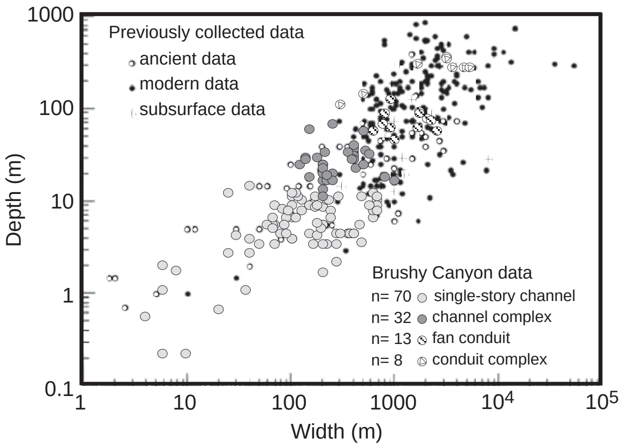

Figure 1—Aspect ratios (width:depth) of Brushy Canyon Formation channelform sand bodies compared with modern and other ancient submarine channels. Note that the larger channels are primarily from modern data reflecting a resolution bias, with outcrops of ancient channels typically not large enough to resolve channelform features remotely imaged using modern data. Modified from Clark and Pickering (1997). The Brushy Canyon channelform hierarchy is shown as patterned dots.

phase" is recorded as an erosional surface of sediment bypass. Erosion and sediment bypass transition to pure bypass and ultimately deposition basinward. As channels extend farther basinward, the physical and temporal separation between the channel fill and the underlying strata decreases.

The preservation of build-cut-fill-spill phases of deposition varies according to position on the depositional profile and/or position in a depositional cycle that records migration of the profile. The percentage of build and spill phase deposits increase downprofile to increase the sandstone percentage within basin-floor successions. Slope and upper-basin floor settings have steep gradients that promote sediment bypass. This produces cut-fill-spill motifs with little or no build-phase deposits. Sandstone percentage is low overall, but locally is high in intraslope depressions confining composite channelform sand bodies. Spill-phase deposits are poorly developed because the topographic depressions are large and difficult to completely backfill. The temporal phases of channel deposition change basinward along the basin-floor profile from complex build-cut-fill-spill, to build-fill-spill, to simple build-spill patterns.

The build-cut-fill-spill model for submarine channel development has important implications for sand bypass and facies prediction. Each depositional phase records different sedimentologic processes and energy trends that directly control the type, distribution, and correlation length of architectural elements and facies.

This paper uses four detailed outcrop architecture studies to document proximal-to-distal changes in submarine channel architecture related to variable preservation of the build-cut-fill-spill phases of deposition. Four important attributes of submarine channels are examined: (1) the effect topographic confinement has on channel architecture, (2) the hierarchy of channelform sand bodies, (3) the mechanisms promoting flow confinement, and (4) the timing of channel and overbank deposition.

GEOLOGIC SETTING

Outcrops of the Brushy Canyon Formation in the Guadalupe and Delaware mountains are exposed by Tertiary displacement along basin-and-range faults that define the uplifted western margin of the Delaware Basin, the western subbasin of the Permian basin (King, 1948; Goetz, 1985; Hill, 1995; Figure 3). During middle Permian time, west Texas was the site of a bowl-shaped, epicontinental sea with a restricted southern opening to the ocean through a relict foredeep (the Hovey Channel) (King, 1942; Ross, 1986; Yang and Dorobek, 1995; Hill, 1995; Figure 3). Permian carbonate platforms nucleated on basement highs rim the basin margin and further built shelf-to-basin relief.

The distally steepened carbonate ramp (600 m relief and up to 10° dip) underlying the Brushy Canyon Formation formed a physiographic break that controlled subsequent clastic slope and basin depositional patterns (King, 1948; Pray, 1988; Rossen and Sarg, 1988; Kerans et al., 1992; Kerans and Fitchen, 1994; Zelt and Rossen, 1995). Along the western Delaware Basin margin, this southwest-to-northeast–trending ramp formed an embayment encircling the Brushy Canyon outcrop belt. This ramp margin provides a common reference point for positioning channel complexes located from 7 to 32 km basinward of its terminus. The "outcrop fan complex" is one of three fan complexes that form a bajada-like submarine apron around the northern Delaware Basin (Figure 3).

The Brushy Canyon outcrop is oriented obliquely to Permian sediment transport, with paleoflow indicators shifting from 120° to 85° southward across the outcrop belt (345° trend). Consequently, proximal-to-distal channel morphologies are a composite reconstruction from eight submarine conduits that obliquely intersect the outcrop belt. Change in channel complex architecture is assumed to primarily record depositional processes related to position on a slope and basin depositional profile (Figure 4).

STRATIGRAPHIC FRAMEWORK

The Brushy Canyon Formation in outcrop is part of a submarine fan complex that corresponds with one third-order composite sequence of about 2 m.y.

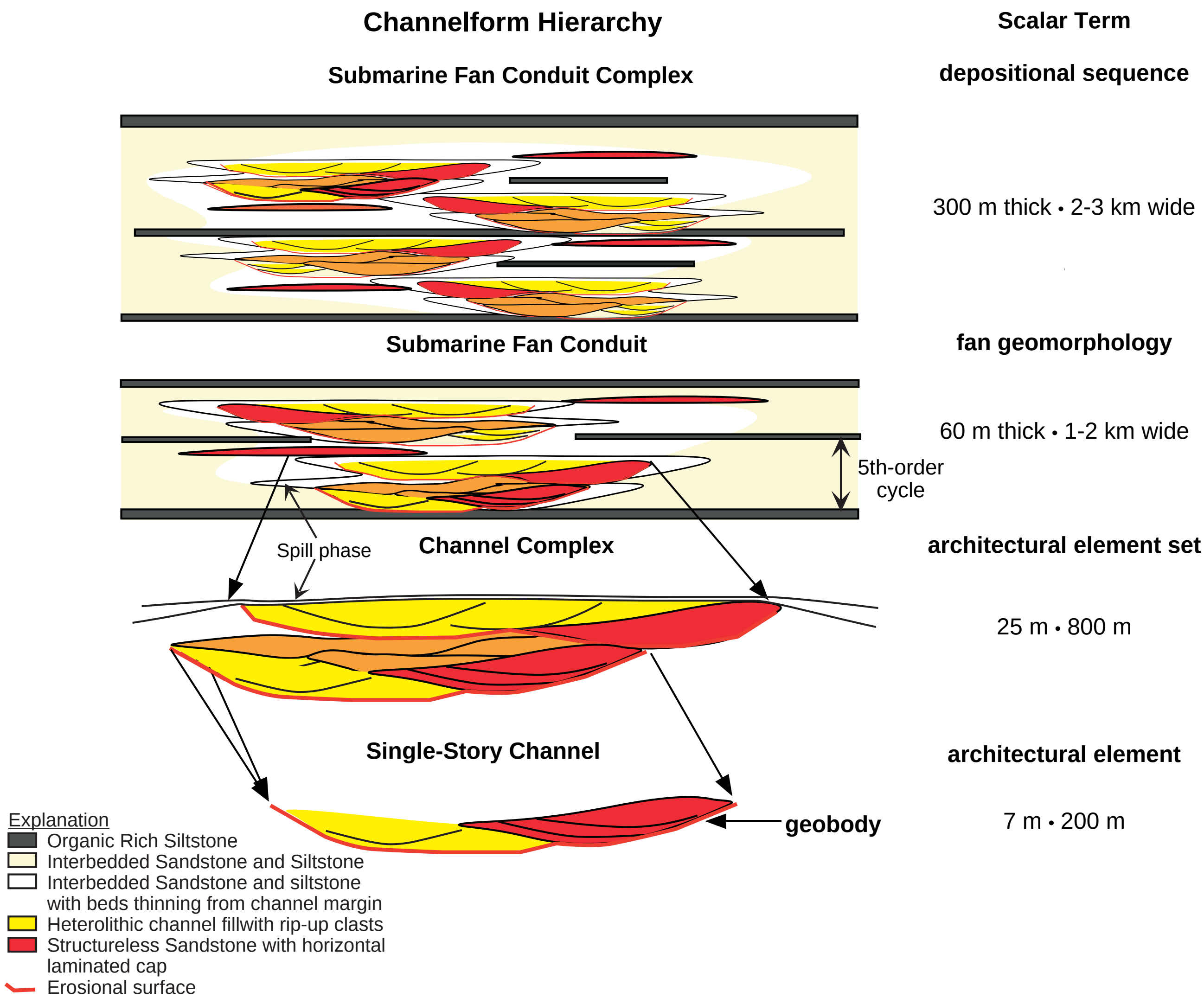

Figure 2—Hierarchy of submarine channelform sediment bodies recognized in the Brushy Canyon Formation in outcrop. In order of decreasing scale: (A) conduit complexes represent fan conduits that remained active through deposition of the fan complex; (B) fan conduits contain more than one channel complex and form kilometer-wide sandstone fairways hundreds of meters thick within a fan; (C) channel complexes are up to 1-km-wide and 40-m-thick multistory and multilateral sandstone bodies with serrated margins; (D) discrete channel fills are up to 7 m thick and hundreds of meters wide and may contain multiple erosive-based sediment bodies.

duration (Vail et al., 1977; Kerans et al., 1992; Figure 5). This fan complex includes the lower part of the Cherry Canyon Formation and is exposed as a 400-m-thick succession bracketed by correlatable siltstone intervals. Each of the eight siltstone-bounded slope and basin cycles up to 90 m thick contain deposits that can be correlated across conduits and show systematic facies changes that correspond to slope and basin positions along a fan profile. Fans are offset across the siltstone intervals that form fourth-order cycle boundaries. These fourth-order cycles in turn contain up to four fifth-order cycles, which can occur as shingled clinoform packages (20 km long and 60 m thick). The thickest part, or clinothem, of a fifth-order cycle is the depocenter along that segment of the fan profile.

This stratigraphic framework permits a comparison of architectural changes in upper and lower slope, base of slope, and basin-floor channel complexes. Architectural element analysis establishes a hierarchy of sediment bodies and bounding surfaces comprising these channelform sand bodies (Figure 2).

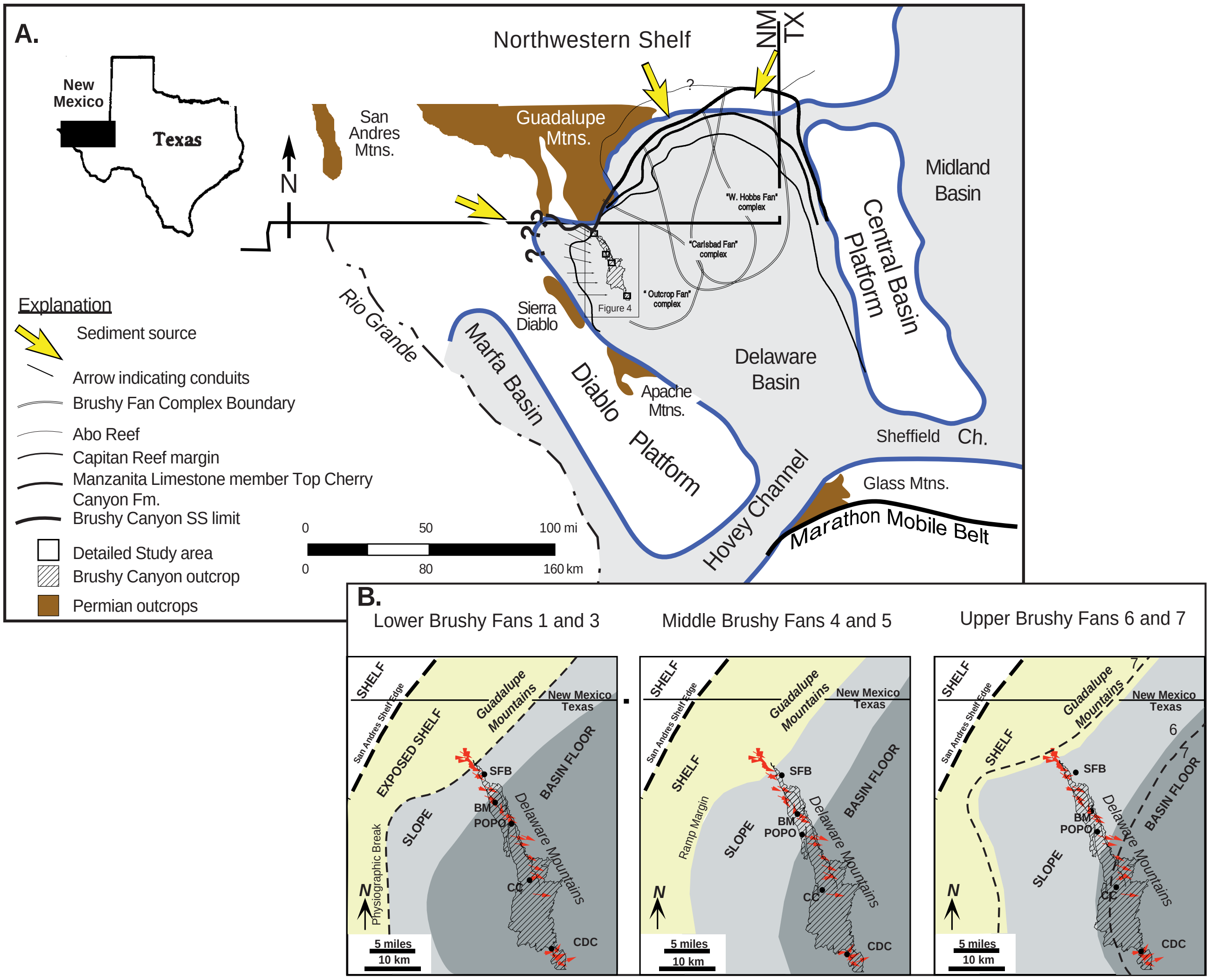

Figure 3—(A) Regional paleogeography of Delaware Basin area (after King, 1948, and Oriel et al., 1967), showing Abo and terminal Capitan shelf-margin trends. Late Leonardian shelf-margin trends (pre-Brushy) probably show similar, although muted, tectonic influence as Abo trend. Mega-embayments in Leonardian carbonate margins are believed to control sand input points, feeding three submarine fan complexes. Small arrows outline Brushy Canyon fan conduits that trend S60°E-trending along Guadalupe Mountains but shift eastward across the outcrop belt. (B) Paleogeographic reconstructions of Brushy Canyon slope and basin facies tracts. Fans 1–3 represent older basin-floor dominated sediment thicks, Fans 4 and 5 represent channelized basin-floor fans, and Fans 6 and 7 occur above the 40-ft siltstone marker and record slope expansion, producing a slope-centered thickness pattern in outcrop. Dark pattern is outcrop belt in Delaware and Guadalupe mountains, with arrows showing position of fan conduits.

A fourfold hierarchy in order of increasing size includes (1) single-story channel fills forming architectural elements, (2) multistory and multilateral channel complexes consisting of two to 26 channels, (3) fan conduits consisting of more than one channel complex, and (4) conduit complexes representing sediment pathways active during fan complex deposition (Figure 2). We have documented a sedimentological hierarchy of structures, sediment bodies, and cross-cutting relationships among bounding surfaces from the four channel complexes, discussed below in a proximal-to-distal order.

UPPER SLOPE CHANNEL COMPLEX, SOUTHERN GUADALUPE MOUNTAINS

A prominent sandstone mesa known as the Salt Flat Bench (SFB) caps the Brushy Canyon Formation at the southern end of the Guadalupe Mountains (Figure 4).

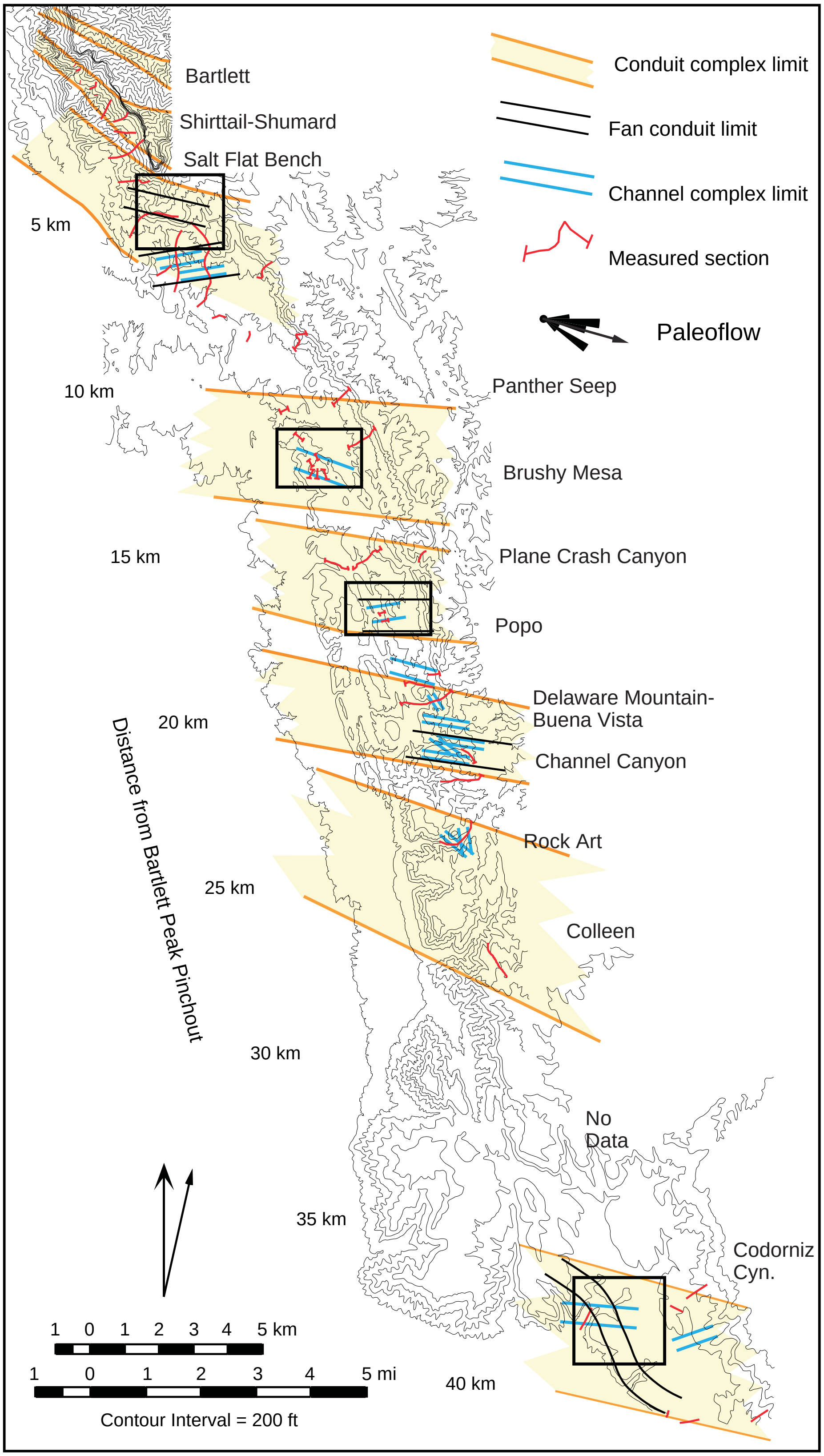

Figure 4—Topographic map of Brushy Canyon Formation outcrop belt in Guadalupe and Delaware mountains showing locality of the four deepwater channel complexes studied. Shaded areas show the position, limits, and orientation of inferred fan conduit complexes (averaged for all fans) that record along-strike variations in sediment supply along the oblique depositional dip outcrop belt; black lines show channel complexes.

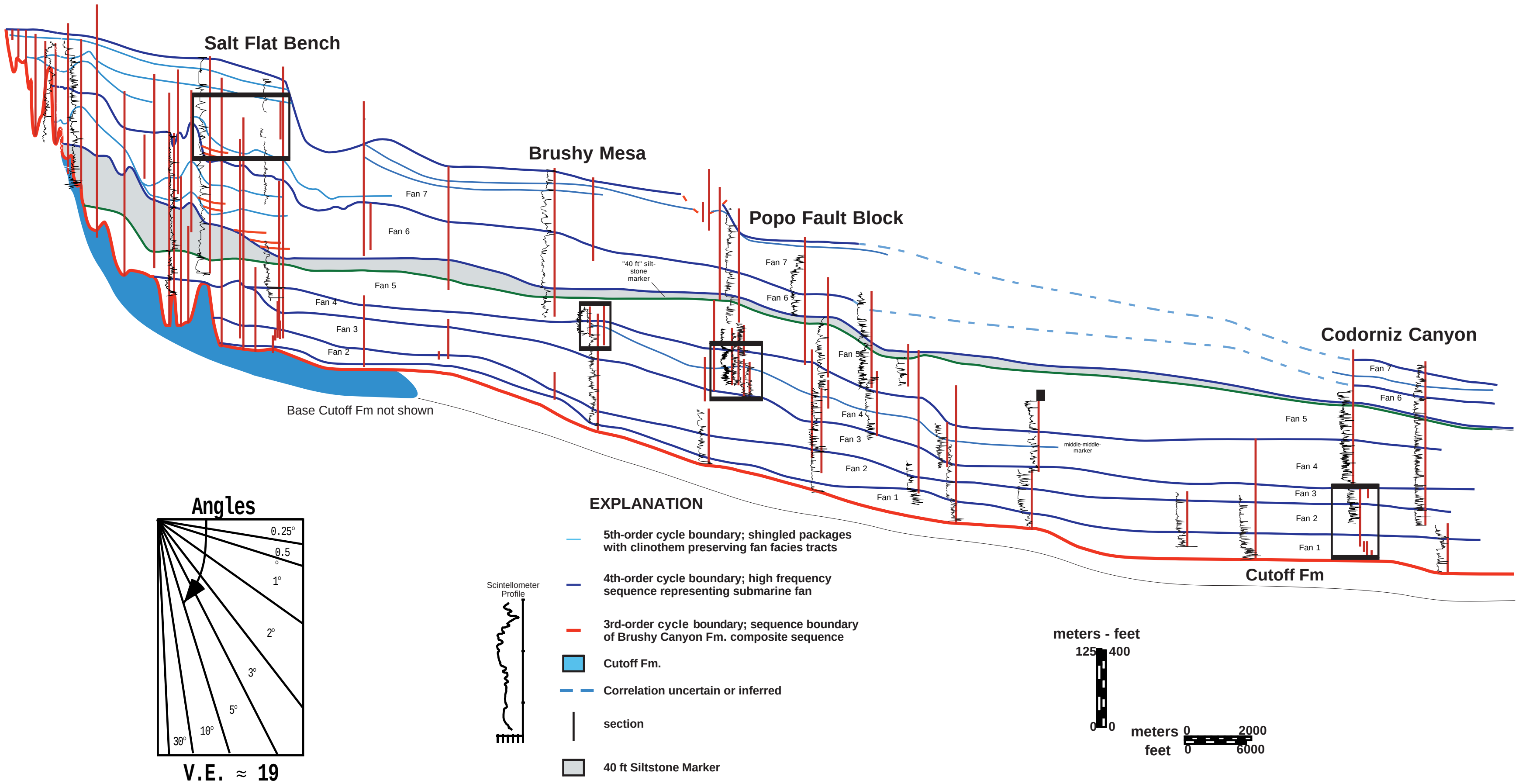

Figure 5—Oblique depositional-dip section of the Brushy Canyon Formation along the Guadalupe and Delaware mountains, west Texas. These basin-restricted deposits of a third-order composite sequence include the basal Pipeline Shale Member and the genetic top siltstone marker within the lower part of the Cherry Canyon Formation. The seven submarine fan cycles are shown by fourth-order cycle boundaries. The 40-ft siltstone marker is shown as a grayed area and records a change in thickness pattern within the fan complex from older basin-centered to younger slope-centered thicks. The right margin of the cross section corresponds with Delaware Mountain outcrops south of Bitterwell Mountain. Inset blocks show study areas of channel complexes discussed in the text.

The SFB occurs in the most basinward of three regularly spaced fan conduits that trend S60°E along the Western Escarpment of the Guadalupe Mountains. Fans 6 and 7 form the majority of the fan complex in this area (Figure 6). The SFB was deposited during the initial transgression of Fan 7. Siltstones below the SFB are organic-poor, contain numerous stratal discordances, and correlate down-profile to large sand-filled channel complexes. Siltstones above the SFB are laterally continuous and progressively increase in organic richness to the "genetic-top" siltstone marker (Sageman et al., 1998). The siltstone-dominated interval above the SFB correlates upprofile to shelfward-stepping, deep-water sandstones that record the final abandonment of the Brushy Canyon fan complex.

The upper slope setting is characterized by large isolated sandstone bodies encased in thick siltstone-rich successions, such as the 40-m-thick and kilometer-scale SFB sand body (Figure 7; Batzle and Gardner, this volume). The SFB is interpreted as an intraslope sand body positioned on the margin of a fan conduit and ponded within an isolated spoon-shaped depression. The SFB outcrop is U-shaped in plan view and represents only about one-half of the depositional sand body geometry. Its outcrops can be divided into proximal and distal strike and dip walls (Gardner and Sonnenfeld, 1996). No single facies is laterally continuous along the entire 2.7-km outcrop length. Wavy-lenticular silty sandstone is the most common facies vertically separating the sandstone beds. It is also the only facies that shows a correlation between bed length and thickness (Johnson, 1998). The sand body contains seven truncated architectural element sets consisting of 26 smaller channelform, wedge-shaped overbank, lobeform, and tabular siltstone architectural elements.

Sandstone content across the outcrop is about 89% (Johnson, 1998; Table 1) but dramatically decreases laterally along strike, where finer-grained turbidite overbank deposits dominate. The high proportions of turbidites in the proximal (western) strike outcrop (610 m long) produce a bimodal sandstone bed thickness distribution, reflecting channelform and overbank elements. Turbidite bed lengths are 28% longer and sandstone conglomerate proportions are the highest (29% vs. 2%) along the distal (eastern) strike outcrop (>1 km long), yet their overall abundance decreases. There is no observed correlation between bed length and facies.

The basal surface of the SFB sand body consists of a series of erosional discordances that form a master surface interpreted to represent coalesced slump scars (Figure 6). In the shallowest part of the depression, this surface is concordant and draped by organic-rich siltstone. Intraslope depressions restrict channel migration, promoting multiple cut-and-fills and confined depositional patterns. The proximal strike outcrop illustrates confined deposition by the channel and overbank deposits that terminate against the basal surface (Figure 7). The distal strike wall illustrates how multiple episodes of erosion and deposition, within a confinement, controls facies architecture (Figure 7). Younger sandstones that thicken toward the depression axis truncate older clast-rich sandstones forming the sandbody base along the eastern distal outcrop. These stratigraphically higher, but older, "perched" deposits are preserved remnants eroded by multiple cut-and-fills in the depression axis. These cut-and-fill surfaces represent an additional surface type that only occurs in association with stratigraphic confinements (Gardner et al., 1995).

Architectural elements that are younger in the proximal strike outcrop than in the distal strike outcrop suggest depositional backfilling of the depression. Additionally, a systematic upward increase in sandstone bed length reflects increased preservation of younger architectural elements within the broader upper part of the (master) confinement. Bed patterns in overbank deposits are also consistent with depositional backfilling of the depression. Turbidite bed lengths are greater in the distal strike outcrop, but their proportion is higher in the proximal outcrop. These observations suggest that deposits recording unconfined flow at distal sites correlate with deposits showing increased aggradation at proximal sites.

LOWER SLOPE CHANNEL COMPLEX, NORTHERN DELAWARE MOUNTAINS

Lower slope deposits in the lower and middle Brushy Canyon Formation record a significant increase in sandstone percentage at Brushy Mesa (BM) relative to more proximal outcrops. Fan 4 dominates BM outcrops, which are fed by a different conduit than the SFB. This conduit's intersection is 13 km basinward from its coeval ramp margin. This setting is basinward relative to the SFB. At BM, Fan 4 forms a 40-m-thick succession, exposing two sand bodies that represent southeast-trending multistory channel complexes (Figure 8). In contrast to the confined architecture at SFB, these isolated siltstone-encased channel complexes show steep serrated margins (Figure 9). One 30-m-thick and 200-m-wide sand body margin shows siltstone interfingering with seven vertically stacked channel sandstone margins that step up and shift laterally along the sand body base. Siltstones are compactionally deformed with bedding rotated at the channel margins and dipping into the channel axis. In these discrete sandstone channels (1–3 m thick), bed length and thickness progressively increase upward as discrete beds amalgamate to form thicker bed sets (Figure 9). Discrete meter-thick sandstone bed sets in the lower half record the amalgamation of multiple high-density gravity flows. Sandstone bed sets show evidence of amalgamation as well as fluidized tractive structures and soft-sediment deformation. Some channel axis deposits have coarse-grained sandstone bases containing centimeter-size siltstone ripup clasts and horizontal laminations with siltstone interbeds (Table 1). Sediment bypass is interpreted from these "left-behind" deposits because they indicate a condensed chronology of many depositional events.

Fine-grained deposits flanking the channelform sand body appear to record active deposition within a lower

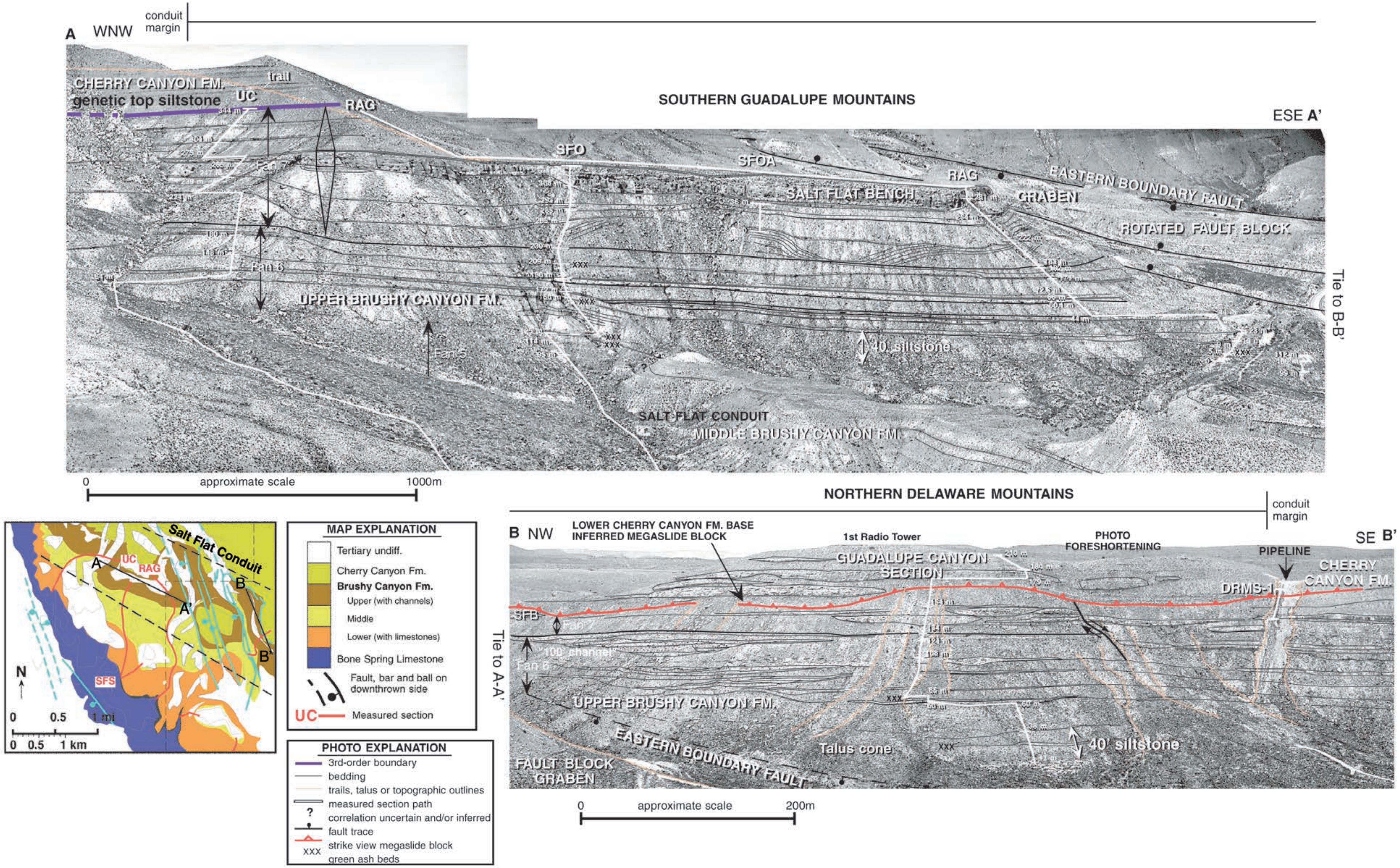

Figure 6—Reconstruction of faulted upper Brushy Canyon Formation stratigraphy showing the (A) southern outcrop (along depositional dip) of the Salt Flat Bench (SFB) sand body below El Capitan, Guadalupe Mountains, and (B) the west face of Guadalupe Canyon in the northern Delaware Mountains. Together these photos illustrate the scale of a Brushy Canyon fan conduit. The siltstone-rich Fan 7 succession below the SFB is dissected by numerous stratal discordances interpreted to represent slump scars and slump deposits. This contrasts with the laterally continuous siltstone beds that form the thick siltstone succession overlying the SFB to the "genetic top" siltstone marker. Forming the eastern boundary of the graben that offsets the SFB to the west, Guadalupe Canyon exposes the eastern margin of the SFB sand body and deposits in the conduit axis. Note the numerous stratal discordances and sandstone channel fills that correlate with the interval below the SFB on the conduit margin.

Table 1. Summary of Aspect Ratios for Four Brushy Canyon Formation Channel Complexes.

Locality (Facies Tract)	Sand Body Aspect Ratio (W/D measured in meters)		Channel Complex Aspect Ratio (W/D measured in meters)			Channel Stories Aspect Ratio (W/D measured in meters)			Net-to-Gross Sandstone Ratio Outside channel Inside channel
Salt Flat Bench	2000 m × 40 m	50	7.5	††1100 × 69	13	7.6.0	1970 × 9.8	201	89%
(Upper Slope)			7.4	900 × 44.8	38	7.5.5	980 × 13	75	(slump
			7.4	1970 × 52.4	20	7.5.4	980 × 16	61	confined
			7.2	2200 × 168	16	7.5.3	1100 × 13	85	facies)
						7.5.2	1000 × 20	50	
						7.5.1	1000 × 7	143	
						7.4.3	900 × 22	41	
						7.4.2	900 × 9.8	95	
						7.4.1	900 × 13	69	
						7.3.2	1970 × 16.4	120	
						7.3.1	1970 × 36	55	
						7.2.6	780 × 30	26	
						7.2.5	980 × 30	33	
						7.2.4	1400 × 30	47	
						7.2.3	2200 × 26	85	
						7.2.2	2200 × 22	100	
						7.2.1	1570 × 30	52	
						7.1.3	1470 × 16.4	90	
						7.1.2	1200 × 13.2	91	
						7.1.1	656 × 9.8	67	
						7.0.5	1244 × 2.13	584	
Brushy Mesa			4.3?	168 × 22	8	4.3.8	†400 × 7.4	54	43%
(Lower Slope)						4.3.7	†168 × 5	34	83%
						4.3.6	†152 × 4.5	34	
						4.3.5	†146 × 4.1	36	
						4.3.4	†150 × 2.5	60	
						4.3.3	†114 × 4.8	24	
						4.3.2	†100 × 4.2	24	
						4.3.1	†30 × 2.4	13	
Popo Fault Block	600 m × 35 m =	17	4.4	430 × 11.8	30	4.4.2	360 × 8	45	61%
(Base of Slope)			4.3	388 × 22.5	17	4.4.1	380 × 5.7	67	90%
			4.2	375 × 12.4	36	4.3.7	143 × 5.8	25	
						4.3.6	120 × 6.5	18	
						4.3.5	55 × 6.8	8	
						4.3.4	84 × 5.8	14	
						4.3.3	160 × 6.8	8	
						4.3.2	287 × 10.2	28	
						4.3.1	320 × 6	53	
						4.2.2	130 × 7.3	18	
						4.2.1	200 × 2.7	74	
Codorniz Canyon			2.2	137 × 20	7	2.2.4	†16 × 2	8	88%
(Basin Floor)			2.1	134 × 13	10	2.2.3	†40 × 3	13	99%
						2.2.2	†22 × 2.5	9	
						2.2.1	†29 × 4.5	3	
						2.1.5	†85 × 5	16	
						2.1.4	†10 × 1	10	
						2.1.3	†110 × 7	16	
						2.1.2	†75 × 2	38	
						2.1.1	†40 × 3	13	

† Half measurement of channel dimension extrapolated for aspect measurement.
†† At Salt Flat Bench channel complex = architectural element set.
††† At Salt Flat Bench channel stories = architectural elements.

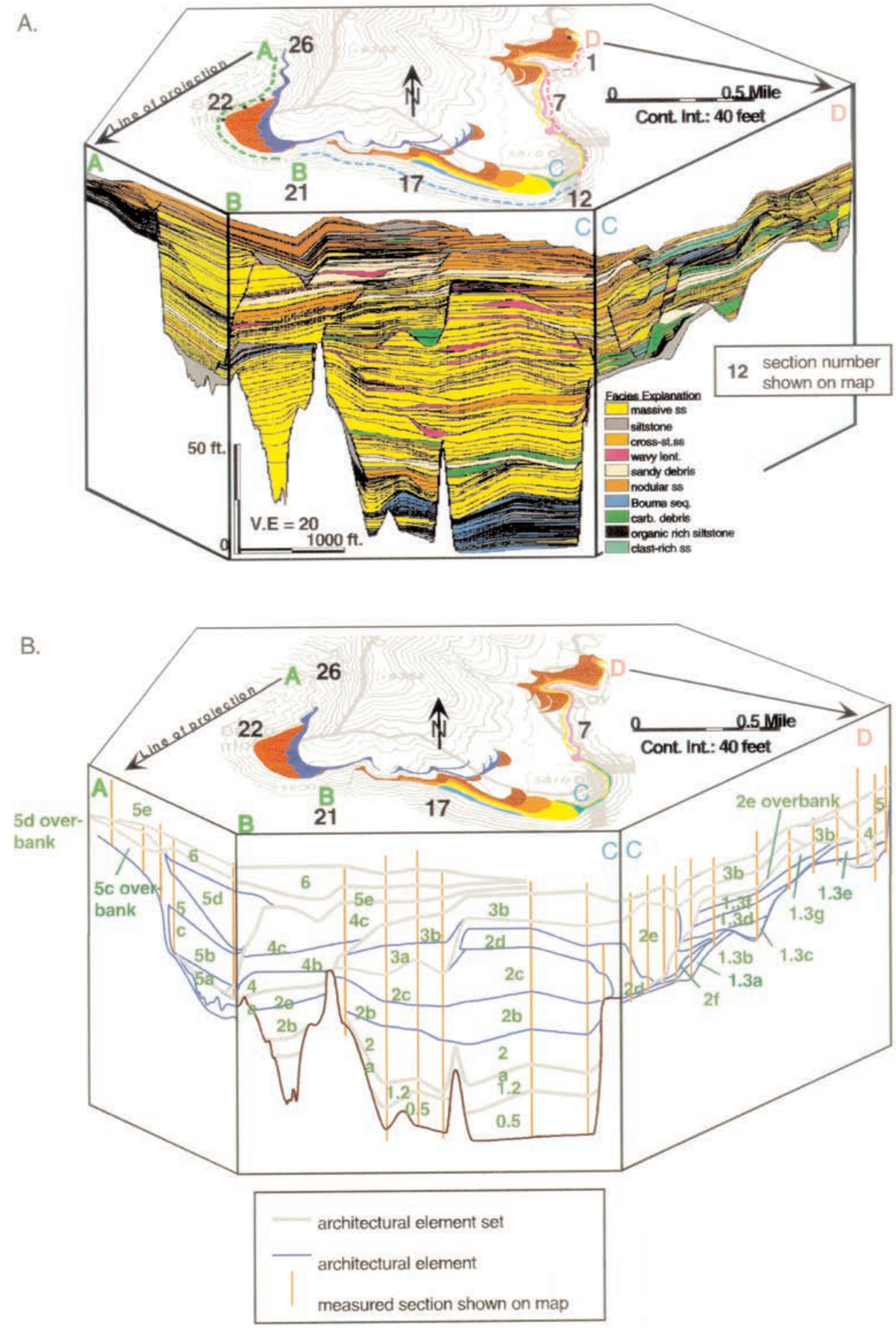

Figure 7—(A) Fence diagram showing facies of upper Brushy Canyon Formation at the Salt Flat Bench. The base of each diagram is the master bounding surface forming a topographic confinement. Note the irregular nature of the basal surface interpreted to represent coalesced slump scars. The panels show the facies architecture along proximal (western) and distal (eastern) strike walls, and the southern dip wall of the sandstone body. No sandstone bed extends across the sandstone body, with the bed length controlled by position within architectural elements shown in B. (B) Fence diagram showing architectural elements and architectural element sets representing truncated channel complexes. Note the truncated deposits forming the sandstone body base along the eastern strike wall. These deposits provide evidence of multiple episodes of cut-and-fill within this topographic depression. The base map shows progressively younger architectural elements toward the north-reflecting depositional backfilling within the topographic confinement.

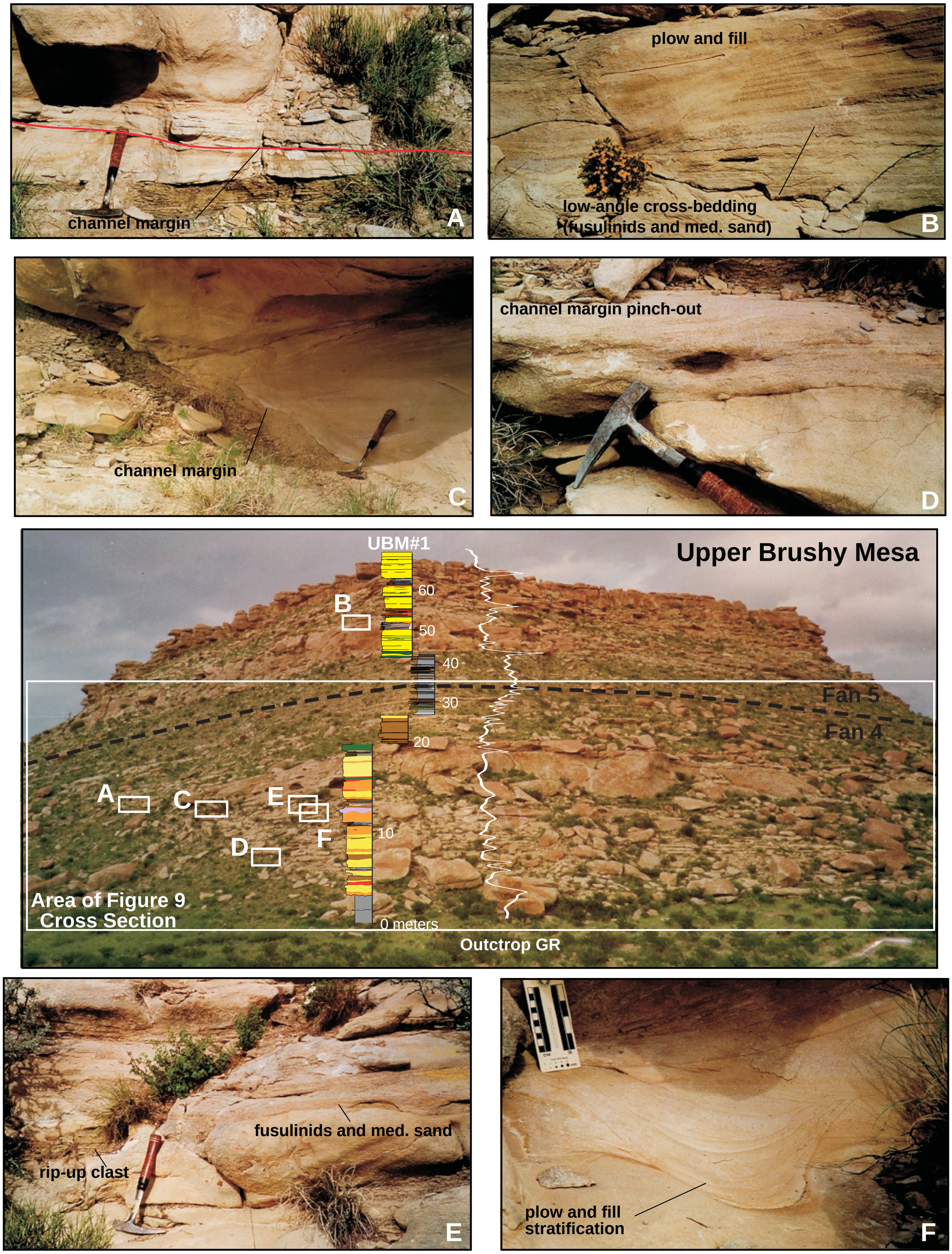

Figure 8—Views of Fan 4 submarine channel complex and facies exposed at Brushy Mesa. Note the serrated margin that results from stacking of multiple meter-scale channel fills to form the 200-m-wide, 30-m-thick channel complex. Outcrop scintillometer profiles shown.

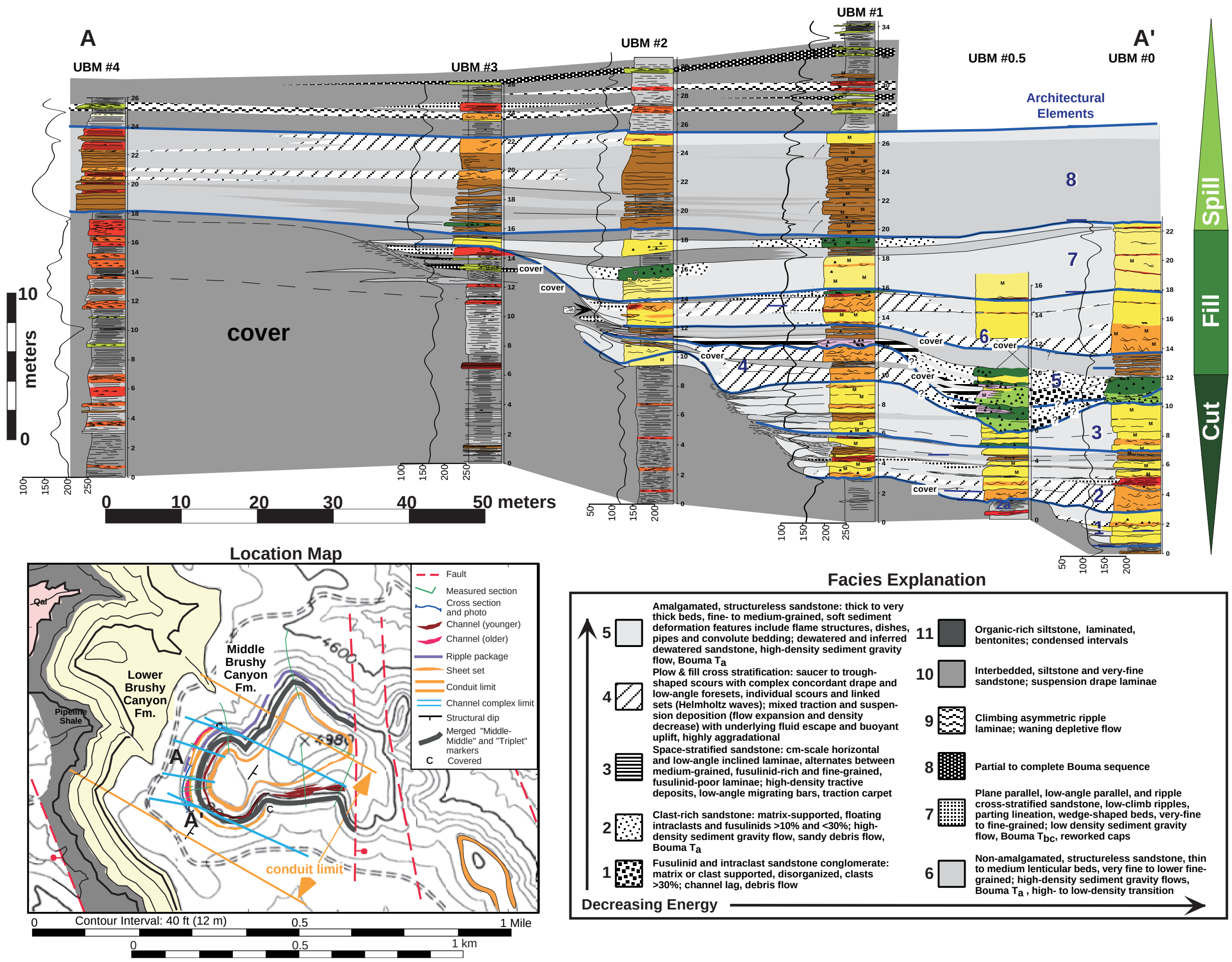

Figure 9—Facies cross section of a Fan 4 channel complex at upper Brushy Mesa (middle Brushy Canyon). Note the high degree of lateral facies change within the channel complex, which is typical of Fan 4 channel fills. Facies correlation length increases and facies diversity decreases upsection through the cut, fill, and spill phases. The channel is multistoried, with a highly serrated margin consisting of many identifiable 1- to 3-m cuts.

slope fan conduit. Interlaminated siltstone and sandstone with rippled sandstone interbeds are common Brushy Canyon slope facies, regardless of proximity to channels. The rippled sandstone interbeds, however, extend from the top and record spillover of discrete channel fills forming the complex (Figure 9). The serrated sand-body margin and coeval ripples in flanking deposits demonstrate the absence of a master surface. In the absence of a master confining surface, a high degree of lateral offset might be expected from one channel to the next. The BM (Brushy Mesa) complex is multistory, not multilateral; therefore, the limited channel offsets must reflect the focusing of sediment from an upper slope confinement. This upprofile confinement repeatedly directed high-density gravity flows that created small channels. The sand-poor overbanks helped confine the subsequent channel fills, which ultimately stacked to form this multistory body.

The sandstone beds capping this channelform sand body show a larger-scale version of this cut-fill-spill depositional pattern. These wedge-shaped bodies consist of amalgamated to nonamalgamated, lenticular and sheetlike sandstones that extend laterally away from the sand body axis to give the complex an overall funnel-shaped geometry. These medium-bedded sandstones thin laterally to interbedded, 1- to 2-m-thick, upward bed-thinning packages of climbing ripple cosets and formsets that decrease upward in frequency and thickness.

BASE-OF-SLOPE CHANNEL COMPLEX, CENTRAL DELAWARE MOUNTAINS

The Popo fault block occurs in yet another fan conduit, 1.5 km wide, intersecting a more basinal position than BM. It lies 5.2 km south of BM, and 25 km from its coeval ramp margin (Figure 10). The base-of-slope to proximal basin-floor deposits of Fan 4 (50 m thick) show an increased sandstone volume (avg. 76%

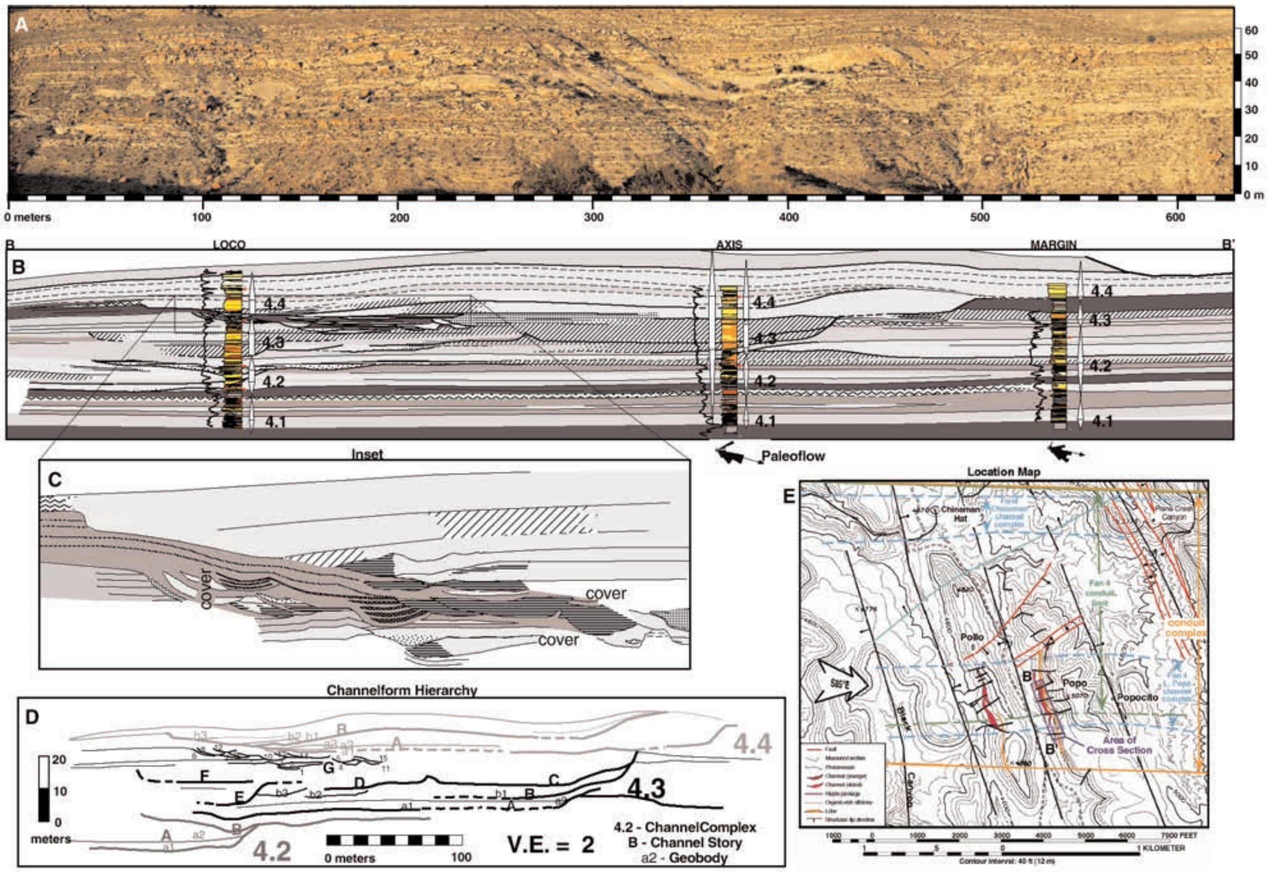

Figure 10—Strike-oriented photomosaic (A) and line-sketch interpretation (B) of Fan 4 submarine channels exposed along the Popo fault block. Outcrop scintillometer profiles shown next to measured sections (see Figure 8 for facies explanation). The outcrop is 25 km basinward of the inferred physiographic margin and exhibits nested offset channel architecture at the base-of-slope to proximal basin floor. The middle Brushy Canyon is the most channelized interval in outcrop. The Popo–Plane Crash area was major sediment conduit where channels repeatedly reinitiated after fan abandonment to form a conduit complex. Inset (C) shows evidence for continued channelization and sediment bypass across the fifth-order abandonment phase. During Fan 4 deposition, the conduit contained two main areas of nested channel complexes, the 600-m-wide Popo sand body and a smaller (lower Chinaman Hat) sand body north of the photo. The Popo area has four fifth-order cycles, three nested channel complexes, and at least 12 single-story channels that stack to form a distinct serrated or stepped southern margin and a less distinct northern margin (D). There is an upward trend from amalgamated high-frequency cuts with abundant sediment-bypass indicators (4.2 and early 4.3), to vertically-stacked (multi-story) cuts (late 4.3), to large offset-stacked, but still highly interconnected, multi-lateral channel stories (4.4). A well-developed, fourth-order spill-phase occurs at the top of cycle 4.4 and bridges the Chinamans Hat and lower Popo complexes. Base map (E) shows Popo area dataset and location of B-B'.

sandstone) relative to BM and the SFB. Progradation internal to Fan 4 is inferred from four offlapping fifth-order cycles. The lower three cycles contain multistory and multilateral channel complexes. These complexes stack vertically, but are also offset 300 m laterally. They collectively form a 35-m-thick and 600-m-wide sand body encased by thin- to medium-bedded sandstone and siltstone. Sand content is 90% within and 61% outside the sand body. The offset stacking of the three channel complexes forms a serrated or stepped sand body margin that erodes siltstone intervals of fifth-order cycle boundaries (Figure 10).

Each channel complex changes upward from highly truncated multistory fills, to heterolithic multilateral fills, to vertically offset multistory sand bodies that show serrated margins. Channel fills comprising complexes shift in both directions across the conduit but generally stack to form only one well-defined margin. The basal multistory and multilateral fills contain frequent erosional surfaces alternating with interbedded siltstone, sandstone with horizontal to inclined laminations and centimeter-thick fusulinid bands, and lag deposits with siltstone ripup clasts. The vertically stacked parts of each complex are the most sandstone-rich. These fills change upward from amalgamated sandstone with Helmholtz waves and aggradational "plow-and-fill" stratification to dewatered structureless sandstone (Figure 8). Where not dewatered this succession is capped by horizontal stratification.

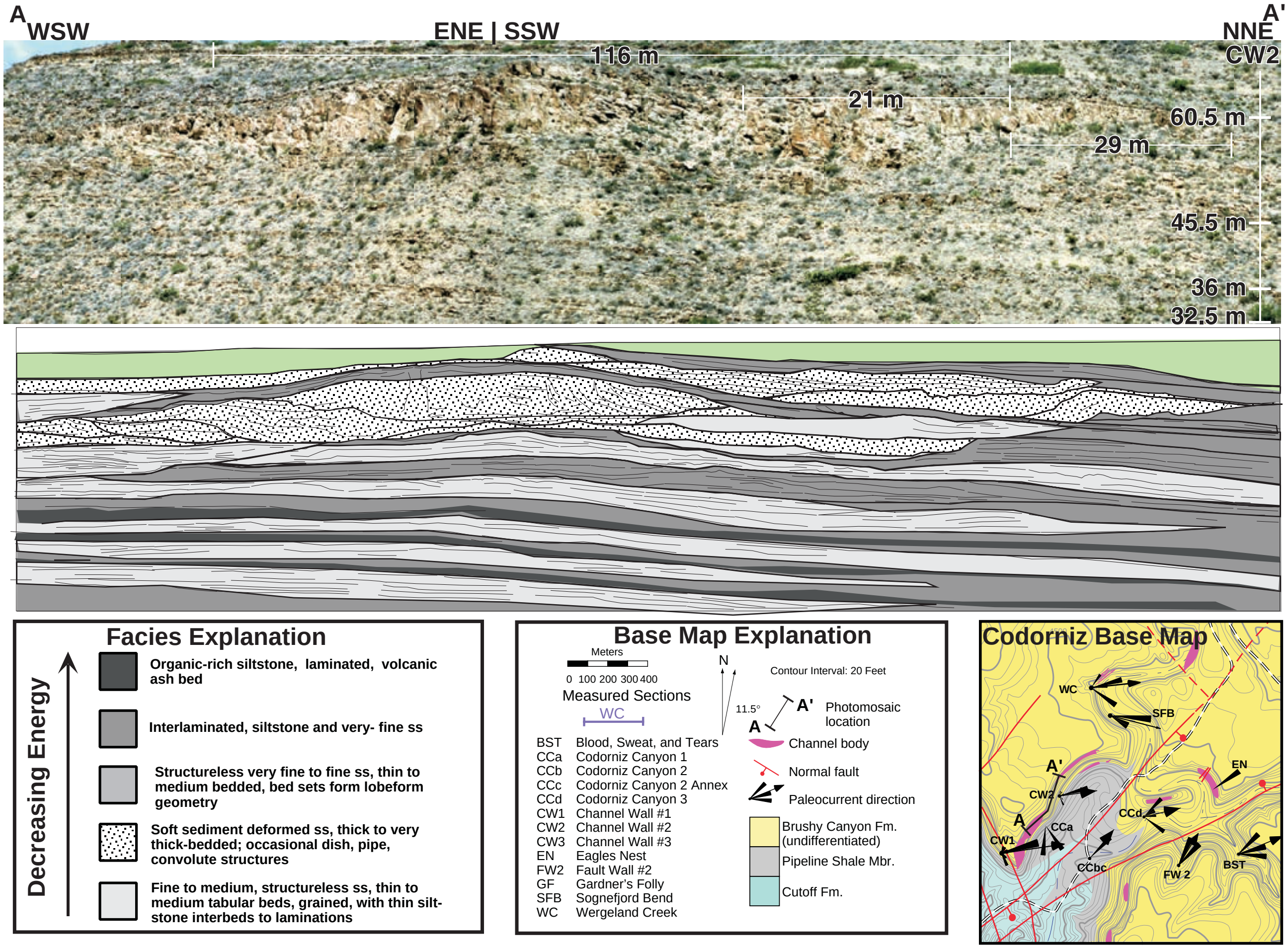

Figure 11—Strike-oriented photomosaic (A) and line-sketch interpretation (B) of Fan 2 submarine channels exposed along Channel Wall, Codorniz Canyon. This wall exposes closely spaced channel complexes encased within a thick succession of tabular sandstone sheets. Channel fills consist of dewatered and soft sediment deformed sandstone forming bi-convex sandbodies that stacked to form a topographic high flanked by younger compensating channelform sandbodies. Thick and sandy build and spill-phase deposits equilibrate the sandstone proportion inside and outside channels.

Channel-flanking deposits consist of interbedded sandstone and siltstone organized as upward-thickening sandstones capped by more continuous siltstone intervals of fifth-order cycles. The sandstones are laterally continuous and locally amalgamated, but generally are interbedded with thin, organic-poor siltstones. Internally, they are structureless, show cryptic stratification, or form thin 300-m-long beds composed of climbing ripples. The sandstone-rich intervals in channel-flanking successions occur near the top of adjacent channel complexes. These intervals contain rippled beds that thin laterally away from the channel and show sediment transport both parallel and transverse to the channel. These spill-phase deposits are eroded by channel rejuvenation during the next fifth-order cycle. Like BM, the multiple episodes of channelization reflect flows persistently directed to this conduit from a confined site upprofile that remained active through deposition of the fan complex.

BASIN-FLOOR CHANNEL COMPLEXES, SOUTHERN DELAWARE MOUNTAINS

Codorniz Canyon provides three-dimensional exposures of channel complexes positioned about 32 km basinward of the ramp margin in the most southerly fan conduit (Figure 4). Although Brushy Canyon sediment transport indicators show a more easterly trend (84°), this area is interpreted to occupy the position farthest from the sediment source along the outcrop belt. Depositional patterns that indicate distal basin-floor position include (1) the thickness and high sand content (65%) of Fan 1 deposits (43 m), reflecting the culmination of a basinward-thickening depositional pattern that is best developed here; (2) the thin Fan 3 interval is a continuation of a basinward-thinning depositional pattern; (3) low conglomerate proportion is consistent with textural sorting trends; and (4) relative to Fan 2 deposits at Colleen

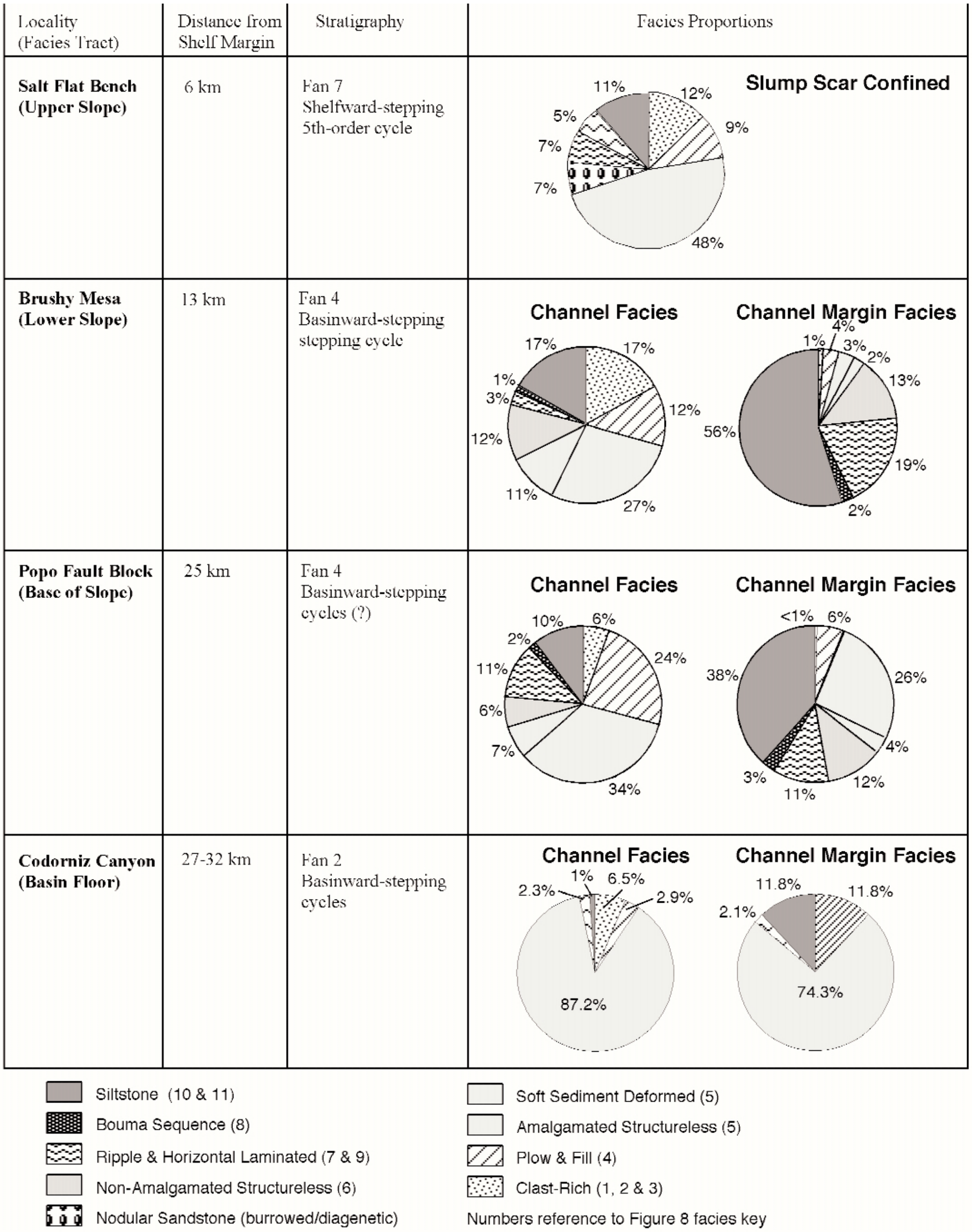

Figure 12—Summary of architecture of four Brushy Canyon Formation channel complexes.

Figure 13—Diagram summarizing changes in Brushy Canyon submarine channel architecture along a composite slope to basin profile. Along this composite reconstruction, there is a 68% increase in sandstone deposited outside and an 18% increase inside channelform bodies. This increase in sandstone volume outside channel complexes corresponds with a downprofile decrease in channel size. Channel complexes and fan conduits, however, widen downprofile, reflecting increasing offset of both channels and channel complexes, until bed topography from older build-phase deposits begin to control channel pattern and channel complex size decreases.

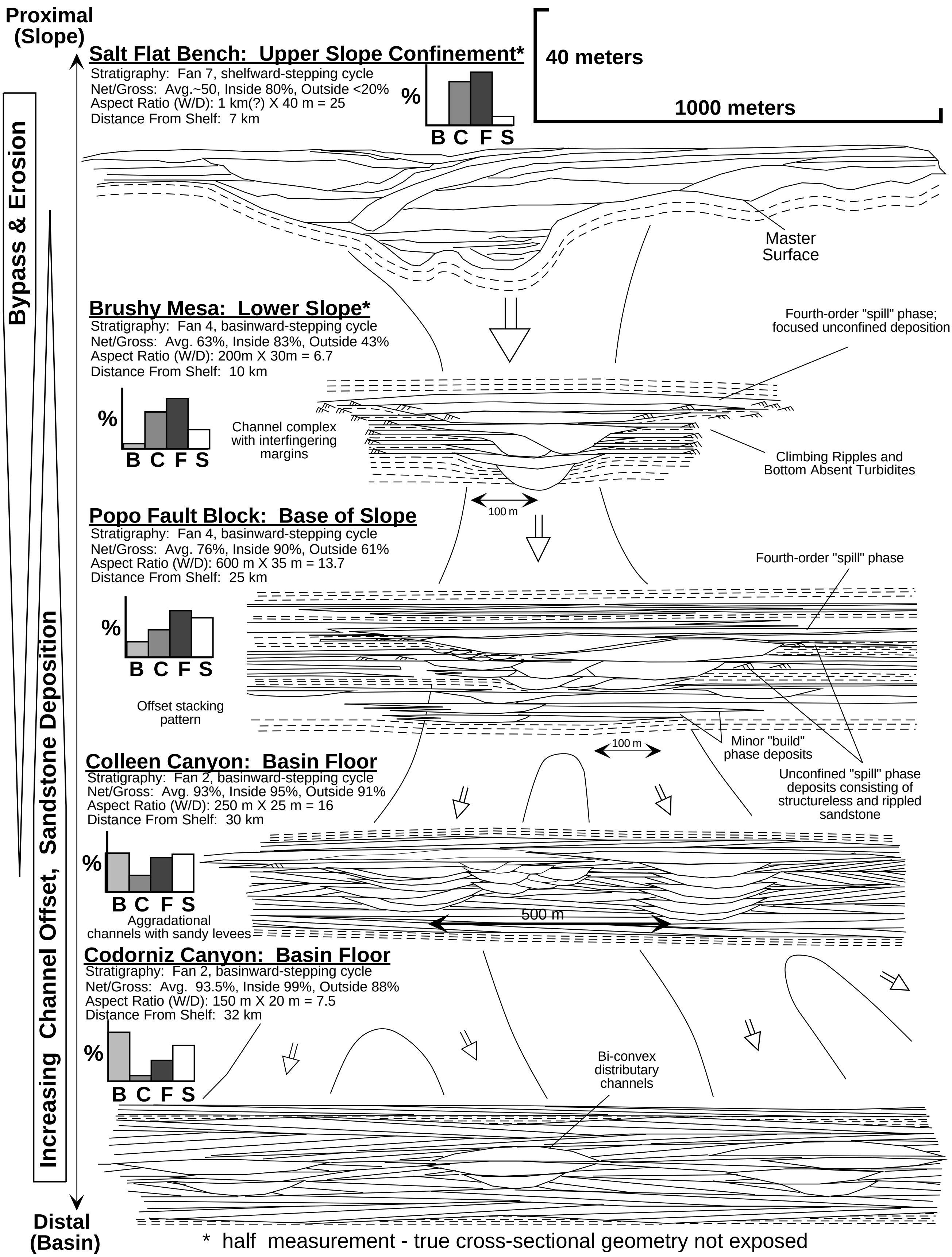

Proximal (Slope)
Salt Flat Bench: Upper Slope Confinement*
Stratigraphy: Fan 7, shelfward-stepping cycle
Net/Gross: Avg.~50, Inside 80%, Outside <20%
Aspect Ratio (W/D): 1 km(?) X 40 m = 25
Distance From Shelf: 7 km
%
B C F S
40 meters
1000 meters
Master Surface
Bypass & Erosion
Brushy Mesa: Lower Slope*
Stratigraphy: Fan 4, basinward-stepping cycle
Net/Gross: Avg. 63%, Inside 83%, Outside 43%
Aspect Ratio (W/D): 200m X 30m = 6.7
Distance From Shelf: 10 km
Fourth-order "spill" phase; focused unconfined deposition
Channel complex with interfingering margins
Climbing Ripples and Bottom Absent Turbidites
100 m
Popo Fault Block: Base of Slope
Stratigraphy: Fan 4, basinward-stepping cycle
Net/Gross: Avg. 76%, Inside 90%, Outside 61%
Aspect Ratio (W/D): 600 m X 35 m = 13.7
Distance From Shelf: 25 km
Fourth-order "spill" phase
Offset stacking pattern
Minor "build" phase deposits
Unconfined "spill" phase deposits consisting of structureless and rippled sandstone
Colleen Canyon: Basin Floor
Stratigraphy: Fan 2, basinward-stepping cycle
Net/Gross: Avg. 93%, Inside 95%, Outside 91%
Aspect Ratio (W/D): 250 m X 25 m = 16
Distance From Shelf: 30 km
Aggradational channels with sandy levees
500 m
Codorniz Canyon: Basin Floor
Stratigraphy: Fan 2, basinward-stepping cycle
Net/Gross: Avg. 93.5%, Inside 99%, Outside 88%
Aspect Ratio (W/D): 150 m X 20 m = 7.5
Distance From Shelf: 32 km
Bi-convex distributary channels
Increasing Channel Offset, Sandstone Deposition
Distal (Basin)
* half measurement - true cross-sectional geometry not exposed

Caption

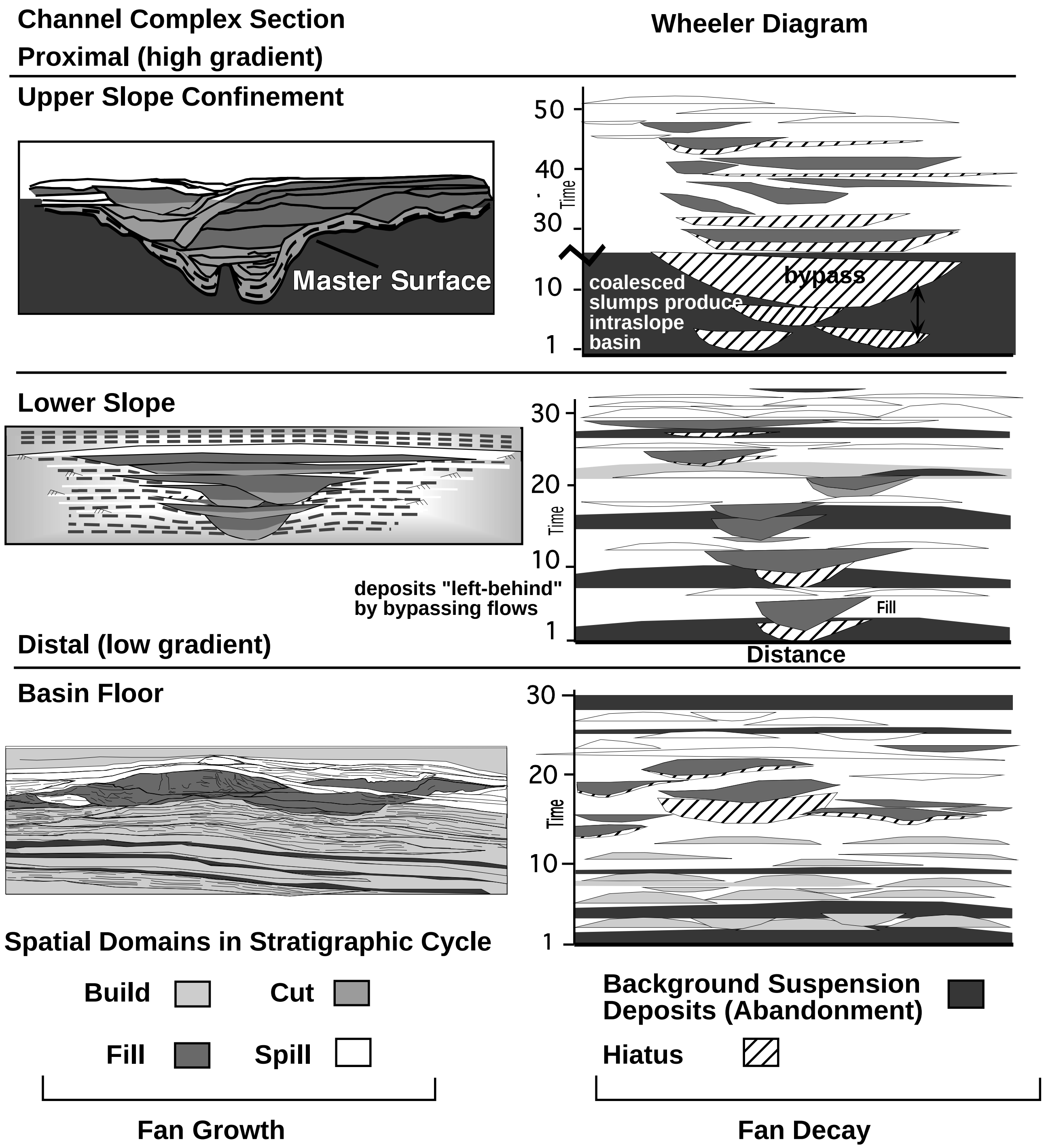

Figure 14—Facies architecture and companion Wheeler diagram summarizing temporal and spatial build-cut-fill-spill phases of submarine channel development along a slope to basin profile. (A) Upper slope channel complex showing the significant time gap between formation of a master bounding surface and depositional filling of the topographic confinement. (B) Lower slope channel architecture and companion Wheeler diagram emphasizes the multiple cut-fill-spill events that stack to form a channel complex. (C) Basin-floor channel architecture showing the high proportion of build-phase deposits that encase small compensating channel complexes.

Canyon, the channel complexes are smaller but show thicker sandstone bedding and slightly increased sand content, demonstrating that the smaller complex size at Codorniz Canyon is not related to decreased sediment supply (Carr and Gardner, this volume). Siltstone intervals that bound fans are laterally continuous across the area, but siltstones that bound fifth-order cycles internal to fans may be eroded.

The lower three fans of the Brushy Canyon fan complex form a 95-m-thick succession with an average sand content of 80% across the 1.7 km^2 area (Figure 11). Fan 2 deposits are the thickest (47 m) and have the highest sand content (94%). Fan 2 consists of four fifth-order cycles containing thick-bedded tabular sandstone bedsets encasing channelform sand bodies (Table 1). Sandstone content is 99% inside and 88% outside channel complexes. Each sand body contains two to 10 channel stories that stack vertically, collectively forming nested complexes 20 m thick and 200 m wide (Figure 11). These multistory complexes are characterized by: (1) close spacing, (2) a high proportion of bi-convex channelform sand bodies, (3) little facies variation in channel fills, and (4) amalgamated bed sets in channel axes that become nonamalgamated beds at interfingering channel margins. The dominant facies include ungraded, structureless sandstone with floating siltstone clasts and local soft-sediment deformation and dewatering features. Channel bases show only minor erosion and in many cases appear to drape underlying bed topography. Load amalgamation is more common than amalgamation due to erosive truncation.

Fan 2 channel complexes at Codorniz Canyon are encased by laterally continuous, thick-bedded sandstones interbedded with thin siltstones that form tabular bedsets (Figure 11). The geometry of a nonamalgamated sandstone bed is lobate or lobeform. These lobeform bodies are interpreted to record compensating deposition by low-gradient, unconfined, high-density gravity flows deposited on the basin floor. Significantly, bed topography of preceding lobeform deposits created preferred gravity-flow pathways that controlled sites of channelization and produced a closely spaced distributary pattern. These comparatively small channel complexes are equivalent in size to base-of-slope channel fills, hence "build" phase deposits contribute significantly to the observed distal increase in Fan 2 sandstone volume. Build-phase bed topography exerts a strong control on channel complex size and shape. Channel-flanking successions in between bracketing "build" and "spill" phase deposits are thicker bedded, contain frequent yet small-scale erosional cuts, complex soft-sediment deformation features, and rippled sandstones (Figure 12).

DISCUSSION

Recognizing the sediment body hierarchy for submarine channelform sand bodies provides insight into architectural changes that occur along a slope and basin profile. The wide scatter in compiled submarine channel aspect-ratios highlights the limited utility of quantitative measurements, unless they are collected within a stratigraphic framework that reflects a hierarchy of architectural elements. For example, a prevailing view holds that the aspect ratio of channelform bodies increases down a fan (Barnes and Normark, 1983/84; Clark and Pickering, 1997; Figure 1). Brushy Canyon data also show a downprofile decrease in channel width, but channel complexes and fan conduits increase in size to the point where channel complexes become distributary and then decrease in size. (Figure 12; Figure 13). These channelforms get bigger for several reasons, despite the decreased size of individual channels. First, the restriction of stratigraphic confinements to upper slope settings produces a systematic downprofile increase in the offset of channel bodies forming channel complexes and channel complexes in fan conduits. Second, upprofile confinement focuses gravity flows to the same site to generate build-cut-fill-spill patterns that construct the hierarchy of channels and channel complexes. These cluster to create fan conduits of enhanced sandstone volume. Third, there is a downprofile increase in sandstone content (build-and-spill phase) of overbank deposits, which promotes lateral offset and widening of the erosional channel complex. Fourth, the lithology contrast between deposits inside and outside channel complexes decreases down the profile. This reflects the increased proportions of build and spill-phase deposits flanking and encasing channel complexes. This depositional pattern reduces the ability to resolve smaller-scale channel bodies, making larger-scale fan conduits the only resolvable channelform sand body.

Master bounding surfaces that cluster, amalgamate, and confine channel fills to construct large channelform bodies most likely occur in proximal slope and canyon settings. Here, a long history of slope adjustment, combined with sediment bypass and erosion, helps develop compound erosional surfaces. Recognizing master bounding surfaces in slope systems is aided by applying stratigraphic criteria also used to distinguish nonmarine valley fills from their fluvial counterparts. Although not analogous in process to the formation of nonmarine valleys, intraslope depressions share a common stratigraphy, reflecting the significant period of time required to develop a master bounding surface and the resulting confined deposition. In the Brushy Canyon, slope confinements are produced by lateral coalesced slump scars (Gardner and Sonnenfeld, 1996). Master bounding surfaces define topographic depressions and "containers" that also direct and focus gravity flows basinward. Furthermore, preexisting degradational topography affects subsequent gravity flows by conserving energy that would otherwise be lost through erosion, but is instead translated downslope to support and maintain basinward-directed flows. This upprofile focusing mechanism has a direct impact on the pattern of channel and flanking overbank deposition.

Submarine channel deposits show a complex internal stratigraphy expressed by repeated episodes of erosion and deposition (Piper, 1970; Walker, 1975; Mutti and Normark, 1987; Clark and Pickering, 1997). This pattern is expressed in Brushy Canyon channel-overbank deposits as an organized record of build-cut-fill-spill deposition that occurs at multiple scales and stacks to form a hierarchy of channelform bodies (Figure 14). In general, a build-cut-fill-spill cycle is initiated by focusing gravity flows through a topographic low. The proportion of deposits that precede channelization increases down the profile to form bed topography during the "build" phase of deposition, which has an increasing influence on channelization basinward. Maintenance and/or erosional expansion of the channel in the "cut" phase occurs during bypass and limited deposition of remnant deposits. The amount of time separating cut-and-fill phases systematically decreases downprofile. Temporal discontinuities are greatest in upprofile positions where master bounding surfaces separate wholly younger strata above from older strata below. Amalgamated vertical sandstone bed successions record depositional backfilling and lateral offset of beds in the "fill" phase of channel deposition.

Deposits that record aggradation and passive backfilling dominate Brushy Canyon channel fills. This contrasts with both the "classic" upward-fining profile of an active channel fill and with the fine-grained passive fill of channels abandoned through updip avulsion. Continued deposition of unconfined gravity flows at the filled channel site produces a "spill" phase of deposition and is a precursor to shifting subsequent flows to a new site. These build-cut-fill-spill phases represent spatial and temporal domains in submarine channel development. They do not represent a particular sediment body type, although skewing of sediment body and facies proportions occurs within these temporal phases. They occur at multiple scales and explain depositional patterns in a hierarchy of channels, complexes, and fan conduits. The stacking of multiple cut-fill-spill channels yields thick successions of channel-overbank successions, but channel and overbank deposition are offset in time.

Although unique and site-specific depositional processes help define the position of a submarine channel on a slope-to-basin profile, the preservation is controlled by stratigraphic position. For example, a proximal slope position for the SFB sand body is indicated by the high proportion of siltstone, conglomerate and slump deposits, slide blocks, and slump scars. This facies architecture occurs only on the upper slope segment of the Brushy Canyon profile, where slope confinements restrict lateral movement of channels. Although older fans contain slope deposits, the fact that these confined slope sand bodies are best developed in younger slope deposits of Fan 7 reflects changing from net bypass to net deposition during the stratigraphic evolution of the fan complex. The repeated rejuvenation of channelization along the basin-floor profile to maintain a fan conduit emphasizes the important control of upper slope and canyon confinements on directing gravity flows basinward. This requires that these proximal confinements remain underfilled until the latest stages of fan complex evolution.

CONCLUSIONS

Sediment gravity flows produce a hierarchy of submarine channel deposits. If data on channel shape and size are going to be used to predict trends and patterns in submarine channel development, and/or for quantitative reservoir modeling, then the hierarchy of bodies that compose a channelform body must be resolved. Architectural element analysis of the Brushy Canyon Formation reveals a fourfold hierarchy of channelform sand bodies. Brushy Canyon channel complexes change downprofile. Large upper slope channelform sand bodies have multiple cut-and-fills, where both channel and overbank deposits are contained within a stratigraphic confinement. Channel complexes widen downprofile because of increasing offset of component channel bodies, and they are encased within higher proportions of overbank deposits that contribute to channel offset and increase the fan sandstone volume.

Stratigraphic changes in facies architecture reflect the "build," "cut," "fill," "spill," spatial, and temporal domains of submarine channel development. Facies and lithology proportion, sediment-body type, and the connectivity and clustering of sediment bodies change within these spatial domains based on the channel complex position along the slope-to-basin profile.

ACKNOWLEDGMENTS

Financial support for this research was provided by members of the Slope and Basin Consortium administered by Michael H. Gardner. Consortium sponsors include ARCO Exploration & Production Technology, Amoco Production Company, British Petroleum, Conoco Inc., Elf Exploration Production, Exxon Production Research Company, Marathon Oil Company, Mobil Exploration and Producing Technical Center, ORYX Energy Company, Phillips Petroleum Company, Shell Offshore Inc., Statoil, Texaco Exploration and Production, Inc., and Unocal Corporation.

Bente Blikeng, Marieke Dechesne, Edith Fugelli, Frode Hadler-Jacobsen, Brian Horn, John Law, Laird Little, Jesse Melick, Jeremy Merrill, Ted Playton, Mark Sonnenfeld, Roger Wagerle, and Conrad Woodland helped collect field data. Mary Carr contributed as project manager. Shell Offshore Inc. supported Kyle Johnson's DEPSIM SFB model. Linda Martin, Leann Wagerle, and Ted Playton helped draft figures. Fred Armstrong, resource manager, Guadalupe Mountains National Park, Tony Kunitz and Mike and Anne Capron, Six Bar Ranch, and Dr. Fred Speck and Jim Dackus, Sibley Ranch, provided access and logistics support. We thank Arnold Bouma, Roger Slatt, Charles Stone, and Mark Sonnenfeld for careful review of an early version of this manuscript.

REFERENCES CITED

Barnes, N. E., and W. R. Normark, 1983/84, Diagnostic parameters for comparing modern submarine fans and ancient turbidite systems, COMFAN: Geo-Marine Letters, v. 3, p. 2–4.

Clark, J. D., and K. T. Pickering, 1997, Submarine channels, processes and architecture: London, Vallis Press, 231 p.

Gardner, M. H., B. J. Willis, and W. Dharmasamadhi, 1995, Outcrop-based characterization of low accommodation/sediment supply fluvial-deltaic sandbodies, *in* The 3d JNOC-TRC International Symposium: reservoir characterization: integration of geology, geophysics and reservoir engineering: Special Publication of the Technology Research Center, JNOC, No. 5, p. 17–54.

Gardner, M. H., and M. D. Sonnenfeld, 1996, Stratigraphic changes in facies architecture of the Permian Brushy Canyon Formation in Guadalupe Mountains National Park, west Texas: Permian Basin Section—SEPM publication 96-38, p. 17–40.

Gardner, M. H., J. M. Borer, and M. Dechesne, 1998, Cut, fill and spill: a new look at the overbank paradigm for sandy deep water systems (abs.): AAPG National Convention Program, Salt Lake City, Utah.

Goetz, L. K., 1985, Salt Basin Graben: a basin and range right-lateral transtensional fault zone—some speculations, *in* W. Dickerson and W. Muhlberger, eds., Structure and tectonics of Trans-Pecos Texas: West Texas Geological Society, Field Conference Publication 85-81, p. 165–167.

Hill, C. A., 1995, Geology of the Delaware Basin, Guadalupe, Apache, and Glass mountains, New Mexico and west Texas: Permian Basin Section-SEPM publication 96–39, 480 p.

Johnson, K. R., 1998, Outcrop and reservoir characterization of the Brushy Mountain Formation, Guadalupe Mountains National Park, West Texas, and Cabin Lake field, Eddy County, New Mexico: Unpublished M.S. thesis, Colorado School of Mines, 256 p.

Kerans, C., W. M. Fitchen, M. H. Gardner, M. D. Sonnenfeld, S. W. Tinker, and B. R. Wardlaw, 1992, Styles of sequence development within uppermost Leonardian through Guadalupian strata of the Guadalupe Mountains, Texas and New Mexico, *in* D. H. Murk and B. C. Curran, eds., Permian Basin exploration and production strategies—Applications of sequence stratigraphic and reservoir characterization concepts: West Texas Geological Society Symposium, Publication 92-91, p. 117.

Kerans, C., and W. M. Fitchen, 1994, Sequence hierarchy and facies architecture of a carbonate-ramp system: San Andres Formation of Algerita Escarpment and Western Guadalupe Mountains, West Texas and New Mexico: Bureau of Economic Geology, Report of Investigations No. 235, 86 p.

King, P. B., 1942, Permian of west Texas and southeast New Mexico: AAPG Bulletin, v. 26, p. 535–763.

King, P. B., 1948, Geology of the southern Guadalupe Mountains, Texas: U.S. Geological Survey Professional Paper P-215, 183 p.

Mutti, E., and W. R. Normark, 1987, Comparing examples of modern and ancient turbidite systems: problems and concepts, *in* J. K. Leggett and G. G. Zuffa, eds., Marine clastic sedimentology: concepts and case studies: London, Graham & Trotman, p. 1–38.

Oriel, S. S., D. A. Myers, and E. J. Crosby, 1967, West Texas Permian Basin region, *in* Paleotectonic investigations of the Permian System in the United States: U.S. Geological Survey Professional Paper P-515C, p. C17–C60.

Piper, D. J. W., 1970, A Silurian deep sea fan deposit in western Ireland and its bearing on the nature of turbidity currents: Journal of Geology, v. 78, p. 509–522.

Pray, L. C., 1988, Trail Guide: day one, Bone and Shumard Canyon area, *in* S. T. Reid et al., eds., Guadalupe Mountains revisited, West Texas Geological Society Publication, 88-84, p. 41–60.

Ross, C., 1986, Paleozoic evolution of southern margin of Permian Basin: Geological Society of America Bulletin, v. 97, p. 536-554.

Rossen, C., and J. F. Sarg, 1988, Sedimentology and regional correlation of a basinally restricted deep-water siliciclastic wedge, Brushy Canyon Formation, Cherry Canyon Tongue (Lower Guadalupian), *in* S. T. Reid et al., eds., Guadalupe Mountains revisited: West Texas Geological Society Publication, 88-84, p. 127–132.

Sageman, B. B., M. H. Gardner, J. M. Armentrout, and A. E. Murphy, 1998, Stratigraphic hierarchy of organic-rich siltstones in deepwater facies, Brushy Canyon Formation (Guadalupian), Delaware Basin, west Texas: Geology, v. 26, p. 451–454.

Vail, P. R., R. M. Mitchum, Jr., and S. Thompson III, 1977, Seismic stratigraphy and global changes in sea level: relative changes of sea level from coastal onlap, *in* C. E. Payton, ed., Seismic stratigraphy—Applications to hydrocarbon exploration: AAPG Memoir 26, p. 83–97.

Yang, K. M., and S. L. Dorobek, 1995, The Permian Basin of west Texas and New Mexico: flexural modeling and evidence for lithospheric heterogeneity across the Marathon Foreland, *in* S. Dorobek and J. Ross, eds., Stratigraphic evolution of foreland basins: SEPM Special Publication 52, p. 37–53.

Walker, R. G., 1975, Nested submarine-fan channels in the Capistrano Formation, San Clemente, California: Geological Society of America Bulletin, v. 86, 915–924.

Zelt, F. B., and C. Rossen, 1995, Geometry and continuity of deep-water sandstones and siltstones, Brushy Canyon Formation (Permian) Delaware Mountains, Texas, *in* K. T. Pickering, R. N. Hiscott, N. H. Kenyon, F. Ricci Luchi, and R. D. A. Smith, eds., Atlas of deep water environments—architectural style in turbidite systems: London, Chapman & Hill, p. 167–183.

9) Permian Reef Trail

Nataleigh Vann and Erin Miller

Nataleigh Vann and Erin Miller

Map (location)
Topography
Ages
Stratigraphy

-Capitan reef separates shallow water deposits NW from deepwater to the SE (pg 2)

-Permian (upper Guadalupian), [270.6 ± 0.7 - 260.4 ± 0.7 Mya

-topography approximates that of the Capitan Reef along the edge of the Deleware Basin (pg 1), erosional profile, shelf to basin(tinker)

-CARBONATE FACIES

-controversial depositional environments assigned to some of the facies

Capitan Formation" to refer to all massive carbonates separating Artesia Group shelf deposits from sandstones of the Bell Canyon Formation (fig. 4).

Lamar Limestone Member of the Bell Canyon Formation exposed on the lower third of the trail (fig. 7).

High-frequency cycles (referred herein as cycles; Fig. 4) are the fundamental stratigraphic building blocks in this study, and refer to the smallest set of genetically related lithofacies (facies) deposited during a single baselevel cycle (James 1979; Grotzinger 1986; Koerschner and Read 1989; Goldhammer et al. 1990; Borer and Harris 1991; Crevello 1991).

Seven Rivers HFS and Yates HFS

Therefore, it is useful to group facies into facies tracts. A facies tract is a genetically linked association of facies and facies successions that records a discrete energy–water depth–sediment supply setting

c-shelf crest and outer shelf

Notes for Field Stratigraphy

Bone Spring Formation

-carbonate, siliciclastic sequence
-6 lithofacies
1)source rock in the basin
2)pelagic shale siltstone, basin seal
3)laminated mudstone facies, source rock, dolomitized, bioclastic chert interbedded. TOC 4.3
4)dolomitized Breccia, light-shelf,dark-slope, reservoir in 2nd and 3rd carbonates
5) dolomitize bioclast packstone, skeletal grains, 1st and 3rd carbonates
6)fine grained ss, illlite, dolomite cement, interlayered organics, lots of sed structures

depositional environment
1)reciprocal and cyclic sedimentation-controlled by sl
2)depositional style influence by topography
3)Aeolian bypass ???
4)ss deposit lowstand, highstand carbonates,

-margin fails by steepness, boundstone forming in place,

pelagic-sed. Settling through the water column→some beds tremendous organic content, slow accumulation, no dilution

swaley cut offs-impressive

-Bone Springs world class carbonate turbidites, unconventional reservoirs popping up in W TX

Victorio Peak

Carb bank
Laterally grades into Bone Springs and Brushy canyon
Progradation followed by transgression (worldwide major transgression)

Brushy Canyon Formation

Depositional Setting-deepwater slope, silt and ss, located between two platfroms, early guad, 400-600m water, SE directed paleocurrent

Sequence Strat-3rd order sequence-lower middle upper separated by thin siltstones—basin has less silt than slope,
Upper-large incised channels
Middle-laterally extensive, channels,
Lower-sheet like tabular

Cm thick volcanic ash

90% turbidites, bedload, suspension, sandy turb, silty turb

5% Debrites-gravels with ss fill in pore space, rip ups

5% Hemipelagites Mudstones, High TOC

Reservoir Quality-analog for deepwater reservoirs

Sand provenance-upper Paleozoic unconf of central W US…details of provenance not well resolved, argue for White Horse Group-aeolian sands….longshore drift as a source for the sand

LIDAR

Katherine Goepfert
April 30, 2008

McKittrick Canyon (Permian Reef Trail)

Overview/ Introduction:

McKittrick Canyon is located on the eastern side of the Guadalupe Mountains near El Capitan. The mouth of McKittrick Canyon shows great exposures of the shelf crest, outer shelf, reef, slope, and toe of slope leading out onto the Delaware basin.

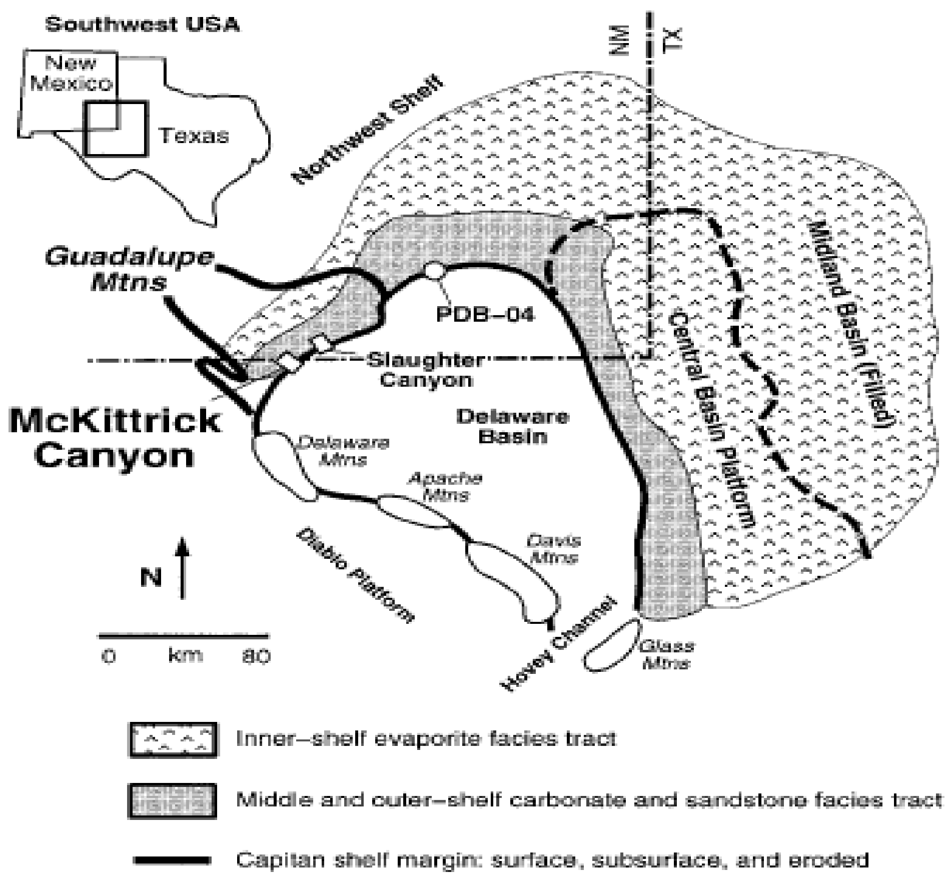

Figure 1: Regional location of McKittrick Canyon during the Permian. (Tinker, 1998)

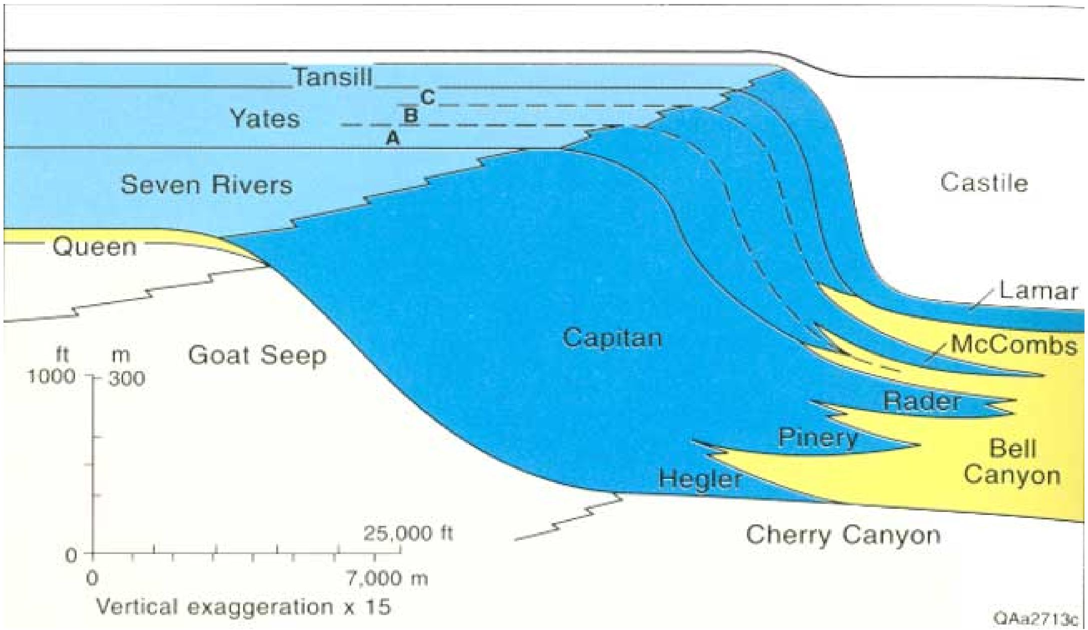

Figure 2: Cross section showing shelf-to-basin correlations of the Capitan Formation and equivalents. Modified from Garber and others (1989).

Only the younger units, the Lamar Member of the Bell Canyon Formation, the Yates Formation, and the Tansil Formation can be seen along the trail. This is a great example of a reef-rimmed platform which occurred during the Guadalupian 16-28 High Frequency Sequences.

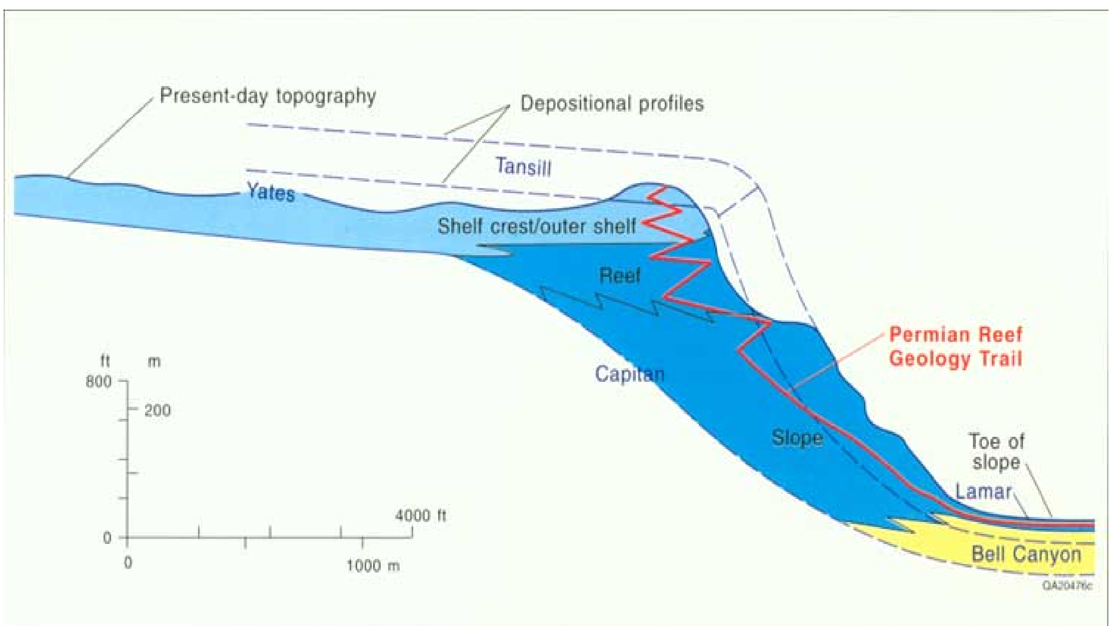

Figure 3: Shows location of Permian Reef Trail on the erosional cross-section of the North Wall of McKittrick Canyon. (Bebout et al., 1993)

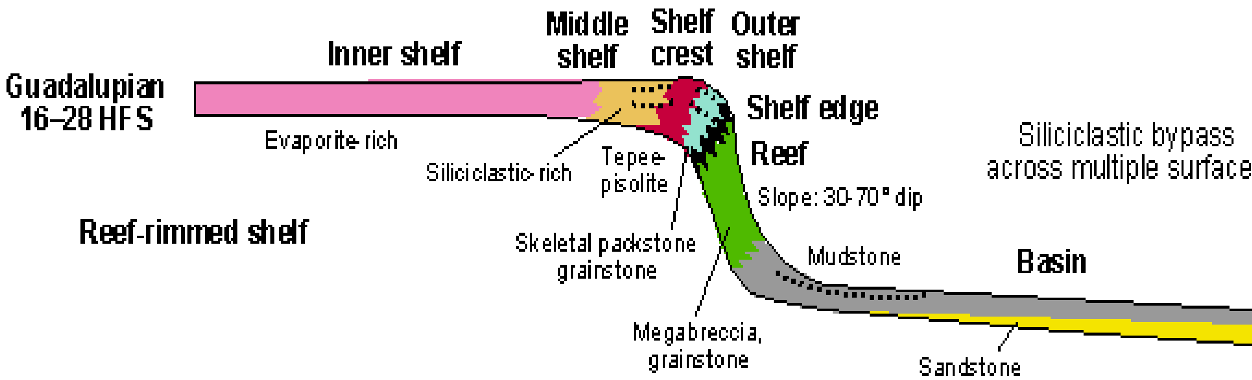

Figure 4: Simplified Facies of the Reef-Rimmed Shelf from the Guadaulupian 16-28 High Frequency Sequences. (Kerans and Kempter, 2000)

Toe of Slope:
The toe of slope lies in the Lamar Member which is the upper unit of the Bell Canyon Formation. It is dominantly laminated to thinly bedded skeletal wackestone with less prevalent thin layers of skeletal packstone. The amount of skeletal packstone increases with increasing dip and unit layer thickness (closer to the slope). These units were mostly created by turbidity currents and debris flows from the slope and shelf margin. Common fossils in these units are foraminifera, sponge spicules, ostracodes, brachiopods, and bryozoans. Most of these fossils are not in-situ, but carried by the gravity flows or sediment settling out of suspension to the toe of slope.

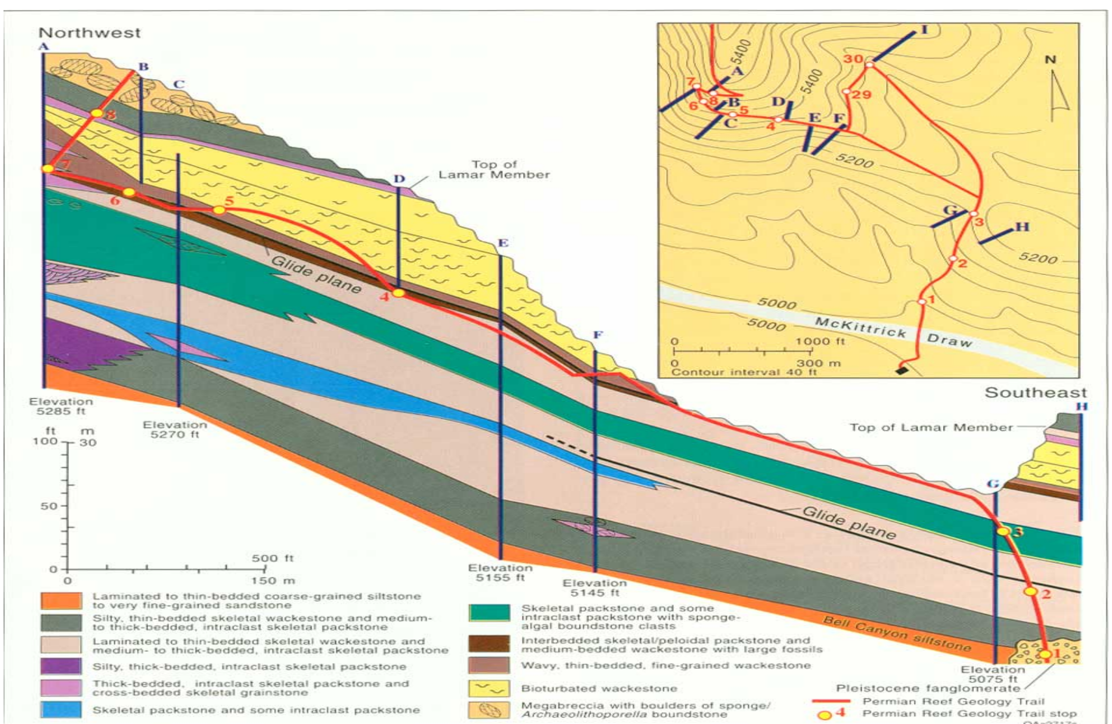

Figure 5: Diagram showing the facies present in the toe of slope and the path the Permian Reef Trail takes through it. (Bebout et al., 1993)

Slope:
The slope is part of the Capitan Formation and the Yates-equivalent and Tansil-equivalent sections are exposed in McKittrick Canyon. As you walk up the lower and middle slope, you will be in the Tansil-equivalent part of the formation. This unit has facies ranging from skeletal wackestones to grainstones, as well as megabreccias. The upper slope will be Yates-equivalent and has skeletal wackestones to grainstones, siliclastics, and reef talus. The siliclastics are believed to have been deposited during a lowstand. The reef talus near the top of the slope has large blocks of sponge-algal boundstones from the overlying reef. The slope has beds that were mostly deposited from gravity flows and have dips ranging from 10-70^{o}. The closer to the reef, the steeper the beds dip. The fossils found are sponges, bryozoans, brachiopods, crinoids, fusulinids, gastropods, and encrusting Archaeolithporella (algae). Most of these fossils can be found in the reef itself. The fusulinid grainstone at the top of the slope might be evidence for a channel going through the reef because these fusulinids are very common behind the reef in the outer shelf.

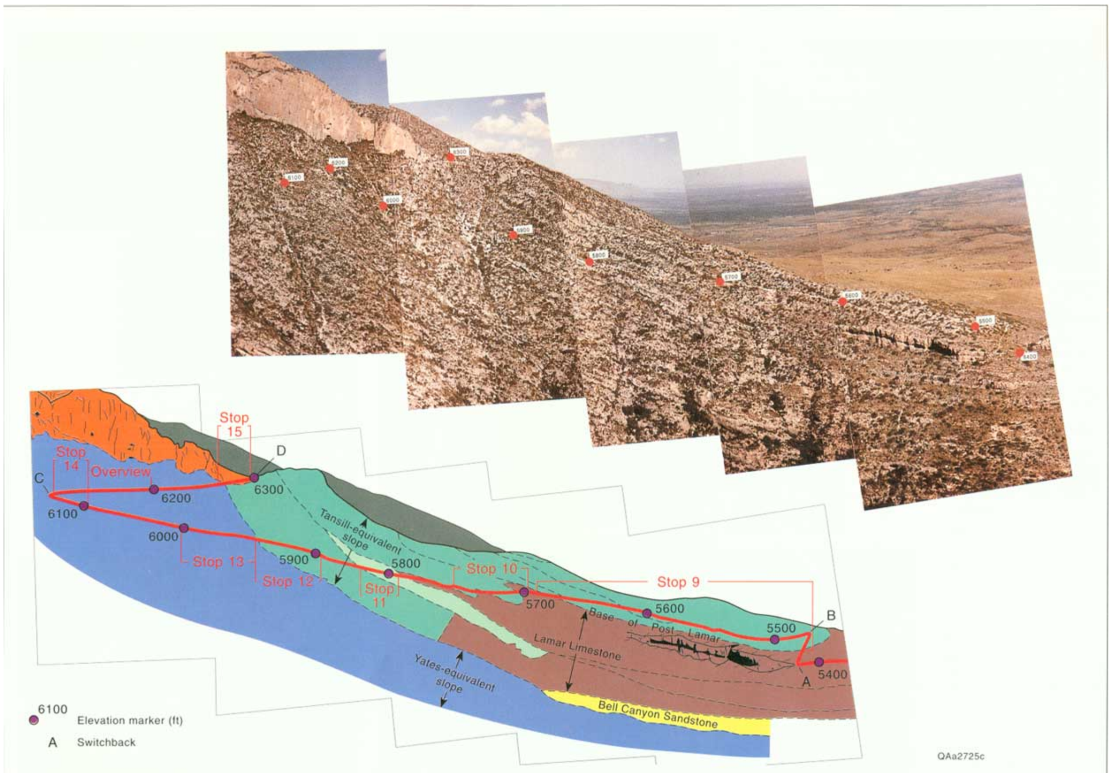

Figure 6: Diagram and Photomosaic of slope on north wall of McKittrick Canyon. Shows path of the Permian Reef Trail and the formations is crosses. (Bebout et al., 1993)

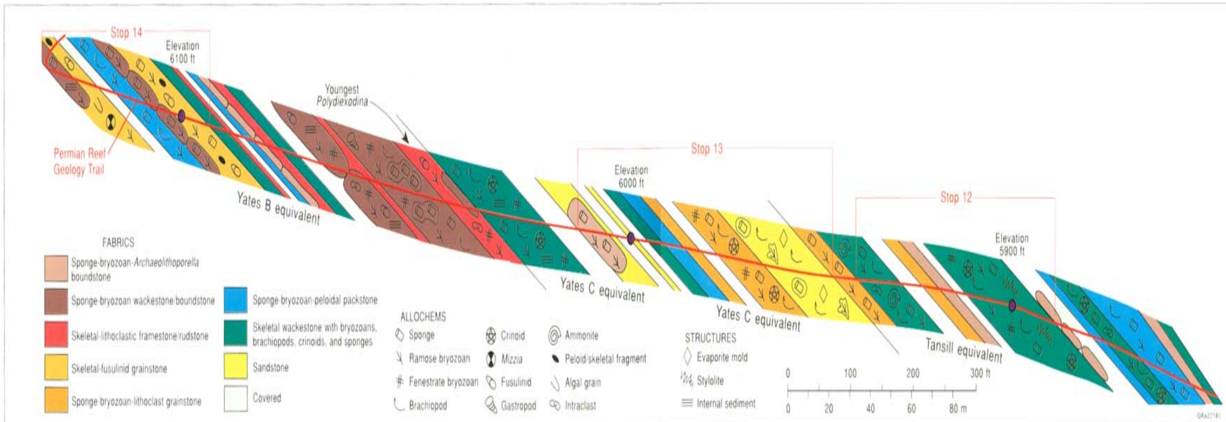

Figure 7: Diagram showing facies and dominant fossils for the transition between the Tansil-equivalent part of the slope and the Yates-equivalent portion. (Bebout et al., 1993)

Reef:

The reef is a steeply dipping (near vertical) part of the Capitan Formation. Tansil-equivalent portion of the reef has been eroded in the McKittrick Canyon locality so you are only seeing the Yates-equivalent part of the reef. For this reef-rimmed platform, the reef is not the topographic high. It is down-dip form the higher shelf crest in estimated water depths of 30-43 meters. The reef would prograde outwards, become unstable and create the gravity flows which are deposited on the slope and toe of slope. The dominant reef-builders are a variety of sponges, bryozoans, Tubiphytes, and *Archaeolithoporella*, with minor crinoids, fusulinids, and *Collenella* (a type of algae). The presence of the *Collenella* at the top of the reef might indicate that the reef was in shallower waters at the termination of the Yates Formation. There are several types of cement present in the reef. There is the botryoidal cement, the isopachous fibrous cement, the inclusion-rich prismatic cement, dolomite, and three types of calcite spar. The botryoidal cement is found around botryoidal fans and fills in framework voids. The isopachous fibrous cement tends to line framework voids while the inclusion-rich prismatic cement tends to fill the rest of the void in.

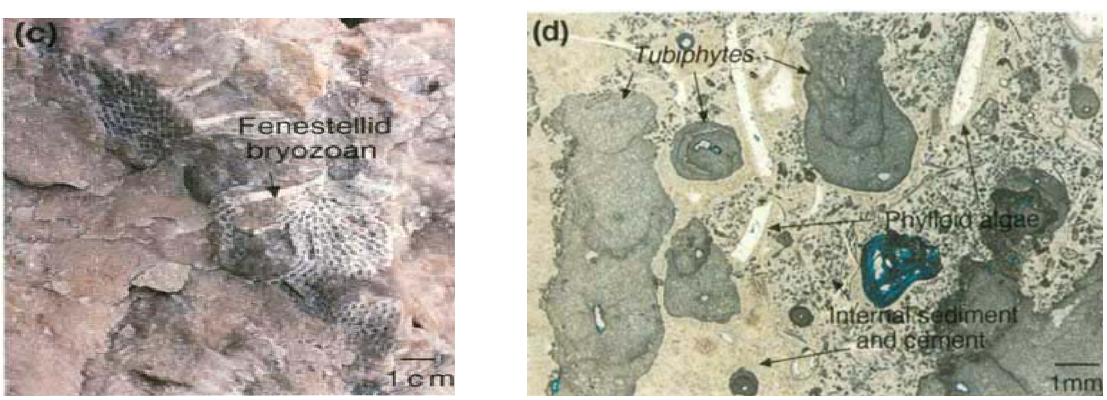

Figure 8: Pictures of fenestellid bryozoans, Tubiphytes, and phylloid algae in outcrop and thin section taken from Permian Reef Trail in McKittrick Canyon. (Bebout et al., 1993)

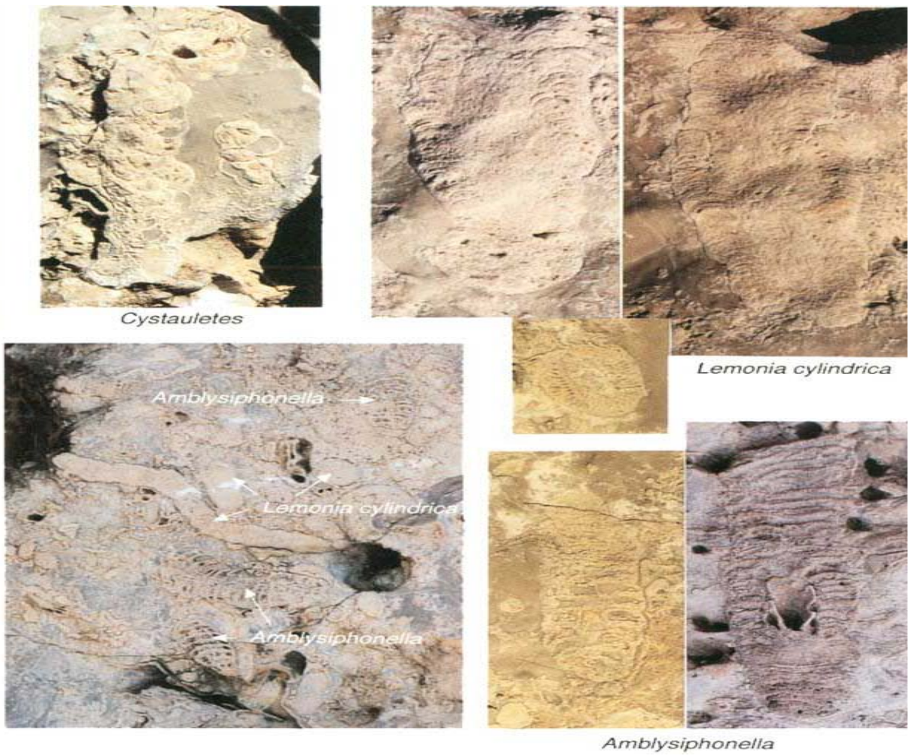

Figure 9: Pictures of a variety of sponges in outcrop along the Permian Reef Trail. (Bebout et al., 1993)

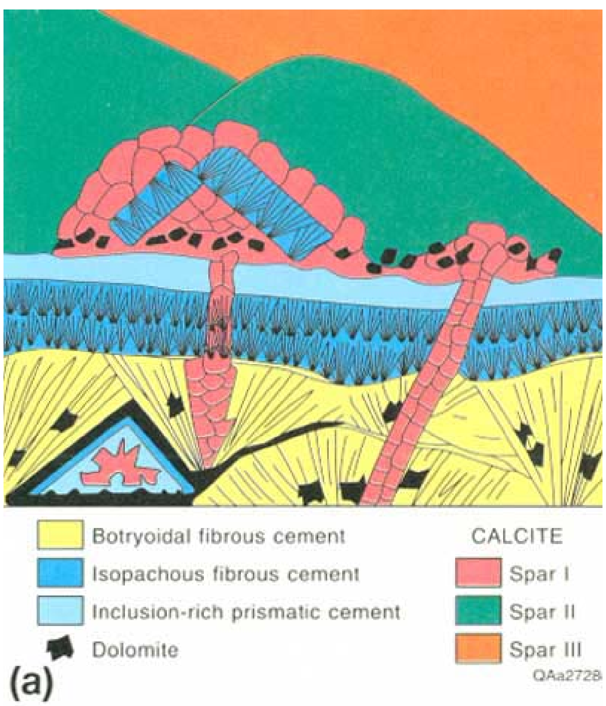

Figure 10: Diagram of the different cements found in the reef and in other parts of the margin in McKittrick Canyon. (Bebout et al., 1993)

Outer Shelf/ Shelf Crest:
The beds dip down in the outer shelf going from the shelf crest to the reef. The fossils that make up these units are fusulinids, crinoids, bivalves, gastropods, pisolites, ooids, and algae. The algae are seen in the forms of Stromatolites and fenestral laminites.

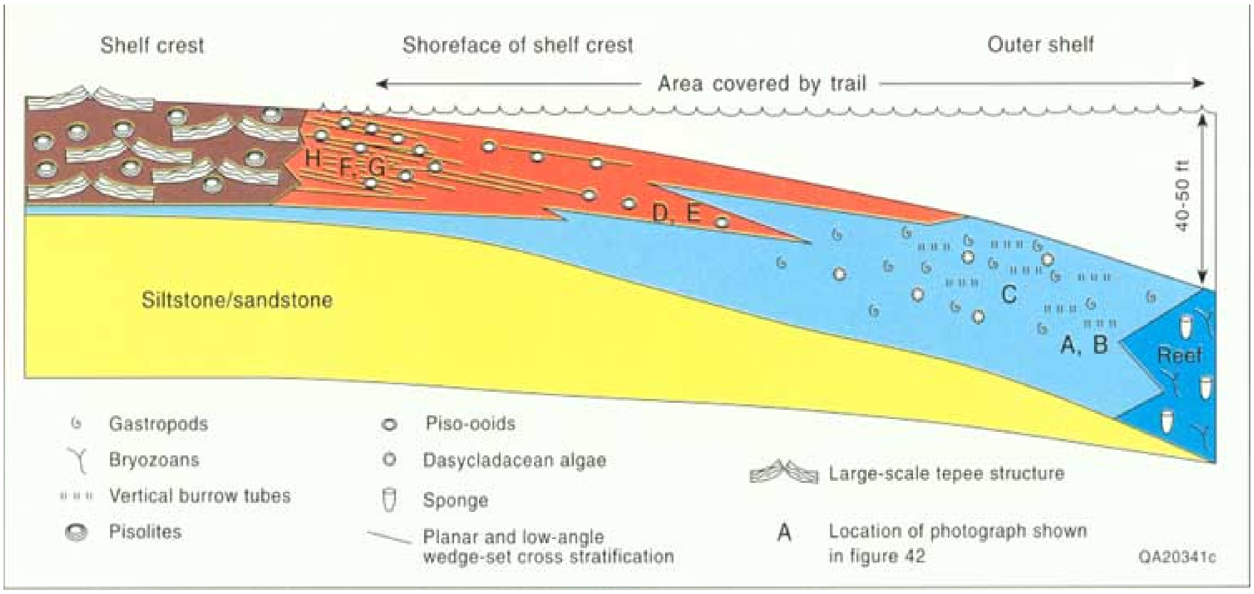

Figure 11: Diagram showing the transition from reef to shelf crest. (Bebout et al., 1993)

The outer shelf of the Yates Formation shows a transition from open-marine facies (fusulinid skeletal packstone) to subaerial exposure (evidence in algal laminites) to middle shelf facies (siliclastics).

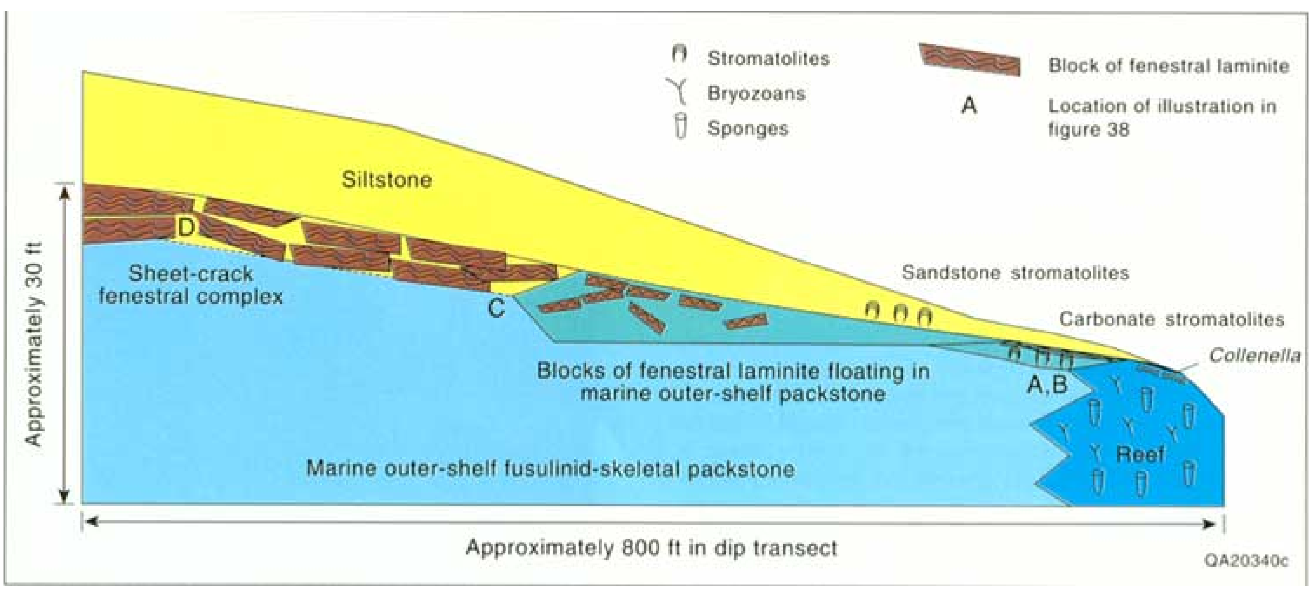

Figure 12: Diagram showing changes in facies as you move up section in the outer shelf of the Yates Formation. (Bebout et al., 1993)

In the outer shelf Tansil Formation there are strong upward-coarsening cycles. These cycles go from a subtidal wackestone/packstone up to tidal flats. There are also tepee structures found near the top of the Tansil. This indicates that increasing subaerial exposure as the relative sea-level drops throughout the deposition of the Tansil in this area.

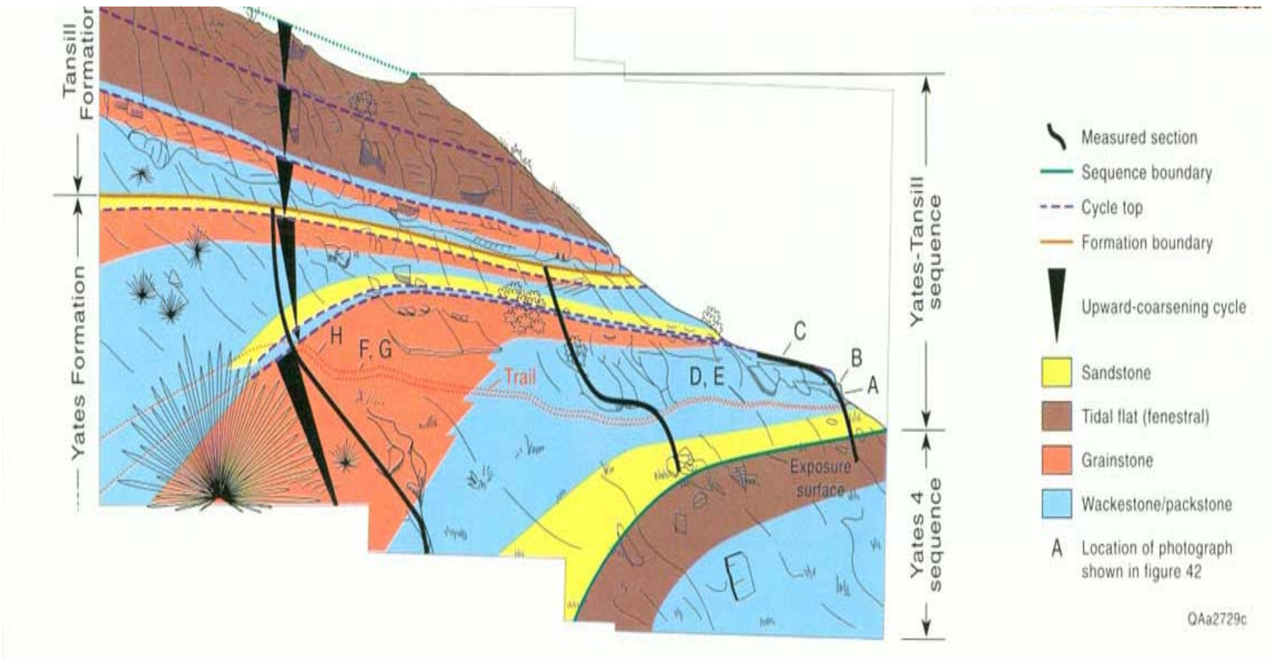

. *Figure 13: Diagram showing changing facies as you go from the Yates Formation to the Tansil Formation of the outer shelf along the Permian Reef Trail. (Bebout et al., 1993)*

WEST TEXAS GEOLOGICAL SOCIETY 1988 FIELD SEMINAR TO GUADALUPE MOUNTAINS

ROAD LOG: SECOND DAY McKITTRICK CANYON

Compiled by the Road Log Committee
with contributions by Alton Brown and Bob Loucks

ROADLOG STARTS FROM INTERSECTION OF HIGHWAY 62/182 WITH THE McKITTRICK CANYON ROAD

MILES

Cum	Int.	
0.0	**0.0**	Intersection of U.S. 62/180 with McKittrick Canyon Road.
0.3	**0.3**	Lamar Limestone capping hills on right at 2 o'clock. Upper Bell Canyon Sandstone forms the slopes below and small knob at 3 o'clock.
0.5	**0.2**	Water well and tank on left at 9 o'clock. Well is 400 ft deep.
0.8	**0.3**	Bell Canyon Sandstone in hill at 9 o'clock.
1.1	**0.3**	Bell Canyon Sandstone to right, Bear Creek on left. One of Mr. Pratt's water wells in Bear Canyon encountered more than 100 ft of Quaternary alluvium before reaching bedrock. Thick alluvial sediments are typical of the side canyons originating on the high escarpments of this region.
1.7	**0.6**	Wooden guard rails.
1.9	**0.2**	Stock pens at right.
2.0	**0.1**	**JUNCTION (OPTIONAL STOP).** Detour to the left on a private road (locked gate) leading to "The Ship in the Desert", Mr. Pratt's former home. Continuing on McKittrick Canyon paved road, Capitan reef ahead. Note the steep dip of the reef talus beds on the lower slope at 10 o'clock. Road crosses outcrop which has been correlated with the McCombs member of the Bell Canyon Group, but is about 150 ft out of place to be so designated. This limestone is a "stray" and is unnamed. It pinches out a short distance from this outcrop. This point is very close to the divide separating Black River and Delaware Draw drainage.
2.2	**0.2**	Water reservoir to right.
3.3	**1.1**	Road curves left. Lamar limestone in scarp ahead and across McKittrick Draw. To the right of the massive cliff is an anticline which is subparallel to the reef front. The Lamar at the crest of the anticline, forming the low hill at 2 o'clock, has been eroded but is present in the creek bank at 3 o'clock. Note how much more massive and thicker this unit is than in the scarp along the highway. Note also how rapidly the dip of the Lamar increases toward the mountain front where it forms a dip slope and merges with the cliff near the crest of the ridge.
3.7	**0.4**	Windmill. Now crossing the axis of a northwest-southeast syncline.
3.8	**0.1**	Cliff on the left is Lamar limestone containing mound-shaped structures. These structures were called bioherms by earlier workers, but they fail to fulfill the requirements for any variety of true organic reef deposits. Newell et al., 1953, estimated that the depth of water in the Delaware basin two miles from the rim was 1700 ft during Lamar time. This would make any reef interpretation of these structures questionable. The structures here are quite different from the primary slump structures, seen later in McKittrick Canyon, which are obviously the result of reef and reef talus debris sliding down the front, picking up more material as it moves, and contorting semiconsolidated beds before it. As would be expected such slump bodies are composed of broken skeletal material (of all sorts of organisms) in a lime mud matrix, and seldom display any sort of symmetry. The structures here, are very symmetrical with no contortion of sediment either beneath or on either side. The lateral slopes of the mounds are filled in with thin-bedded material to where flat beds again can be seen covering the structures. This gives the appearance of bioherms, but the textural fabric of the mounds precludes such a possibility. They are composed of micro-crystalline lime mud with no discernable skeletal remains. Chert, in the form of small nodules is present but extremely rare. It has been suggested that these structures are lime mud "banks" or "ridges" and that these outcrops are cross sections of linear deposits that parallel the reef front.
4.2	**0.4**	Cattleguard.
4.3	**0.1**	**STOP 2-3, PHOTOS A, B.** National Park Service Information Station and McKittrick Draw. The park information station stands approximately at the same stratigraphic horizon as the Rader limestone, 400 ft below the top of the Bell Canyon, while equivalent parts of the reef section in the north wall of the canyon rise some 2000 ft due to greater thicknesses as it goes from basinal to reef facies. McKittrick Canyon has incised a cross sectional cut of the Capitan reef complex

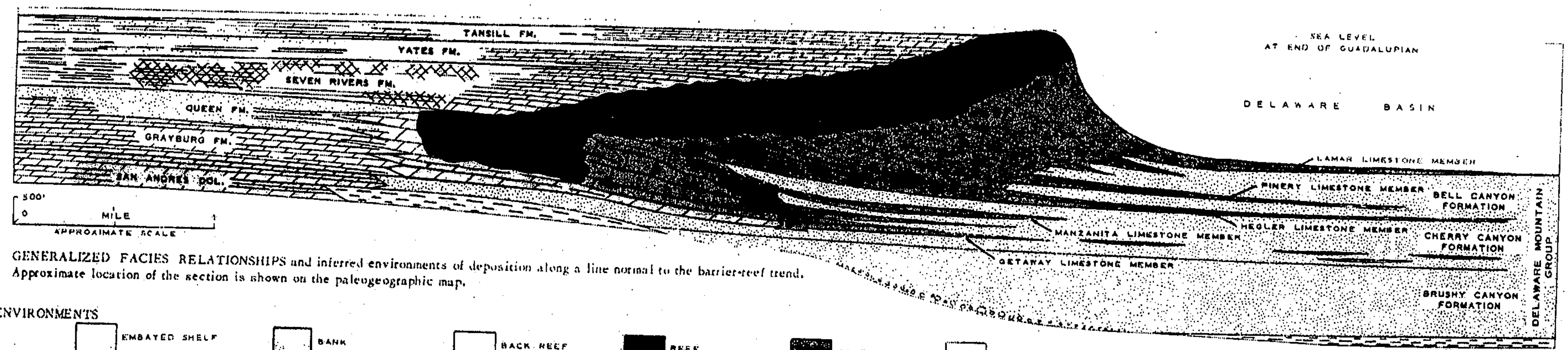

GENERALIZED FACIES RELATIONSHIPS and inferred environments of deposition along a line normal to the barrier-reef trend. Approximate location of the section is shown on the paleogeographic map.

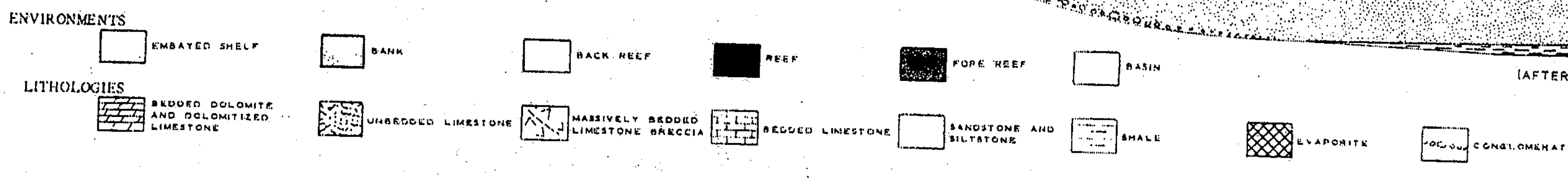

(AFTER DUNBAR ET AL., 1960.)

Courtesy of Exxon Production Research Co.

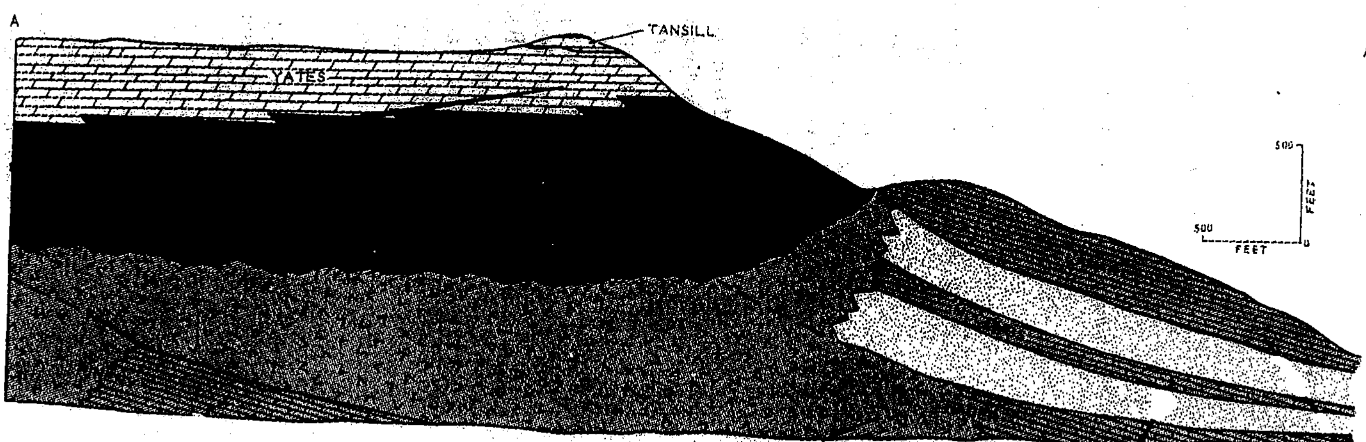

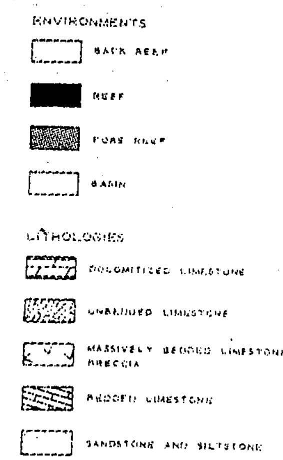

(AFTER NEWELL ET AL., 1953.)

FACIES RELATIONSHIPS and inferred environments of deposition of the reef complex and basin forming the north wall of McKittrick Canyon. Location of cross section is shown on index map. Arrows point to the approximate interpreted positions of the illustrated textures.

Courtesy of Exxon Production Research Co.

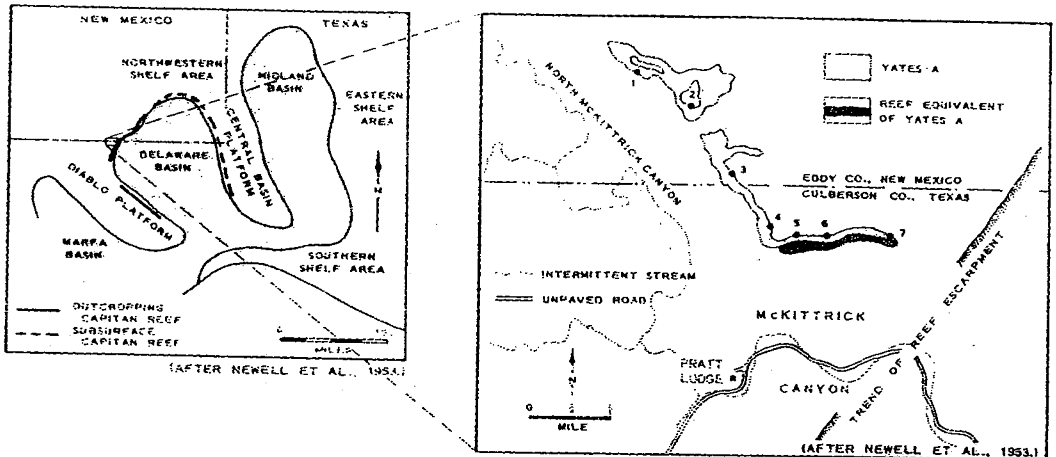

LOCATION OF THE MEASURED SECTIONS below and surface distribution of Yates A and of reef portion equivalent to Yates A.

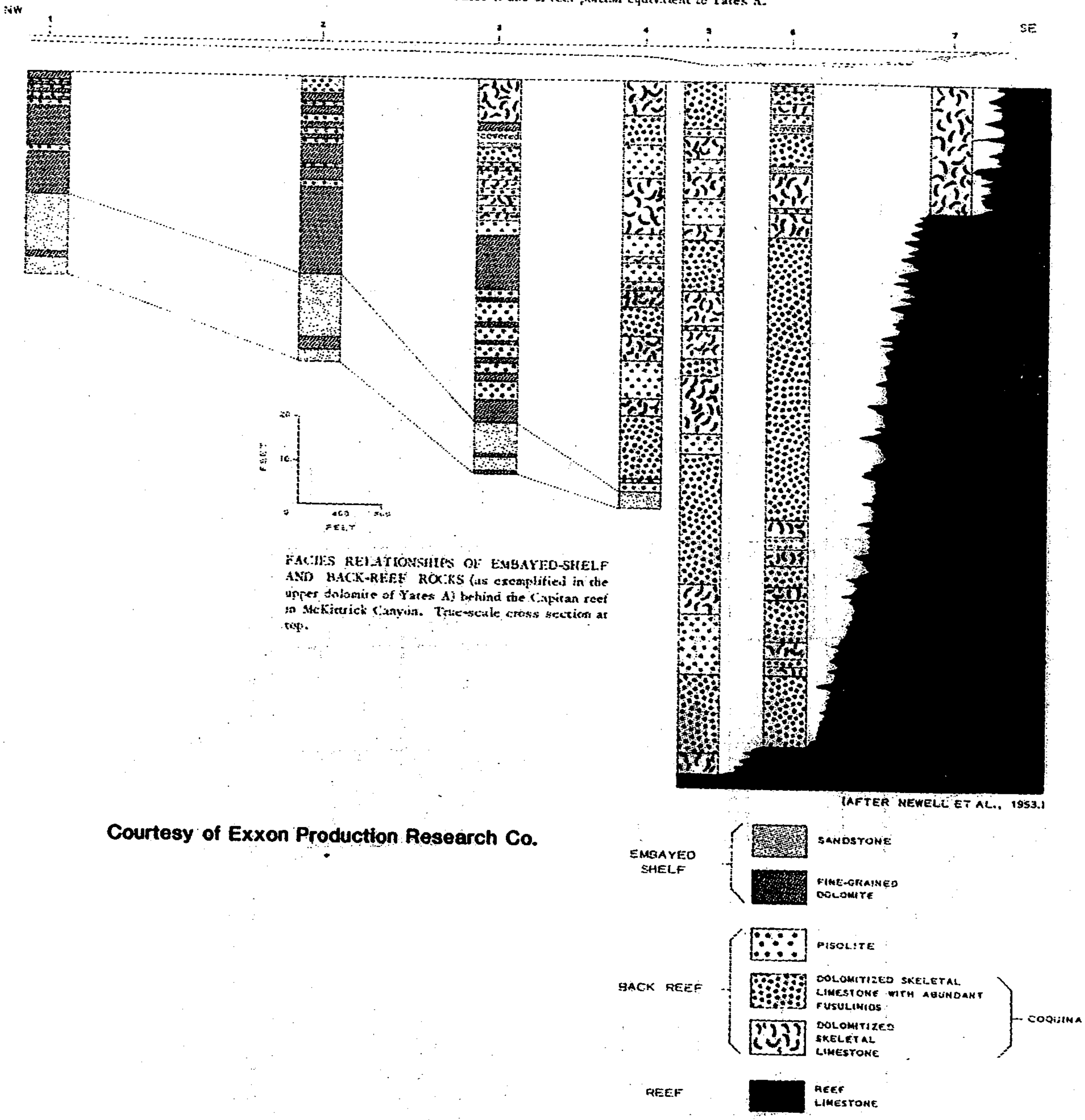

FACIES RELATIONSHIPS OF EMBAYED-SHELF AND BACK-REEF ROCKS (as exemplified in the upper dolomite of Yates A) behind the Capitan reef in McKittrick Canyon. True-scale cross section at top.

Courtesy of Exxon Production Research Co.

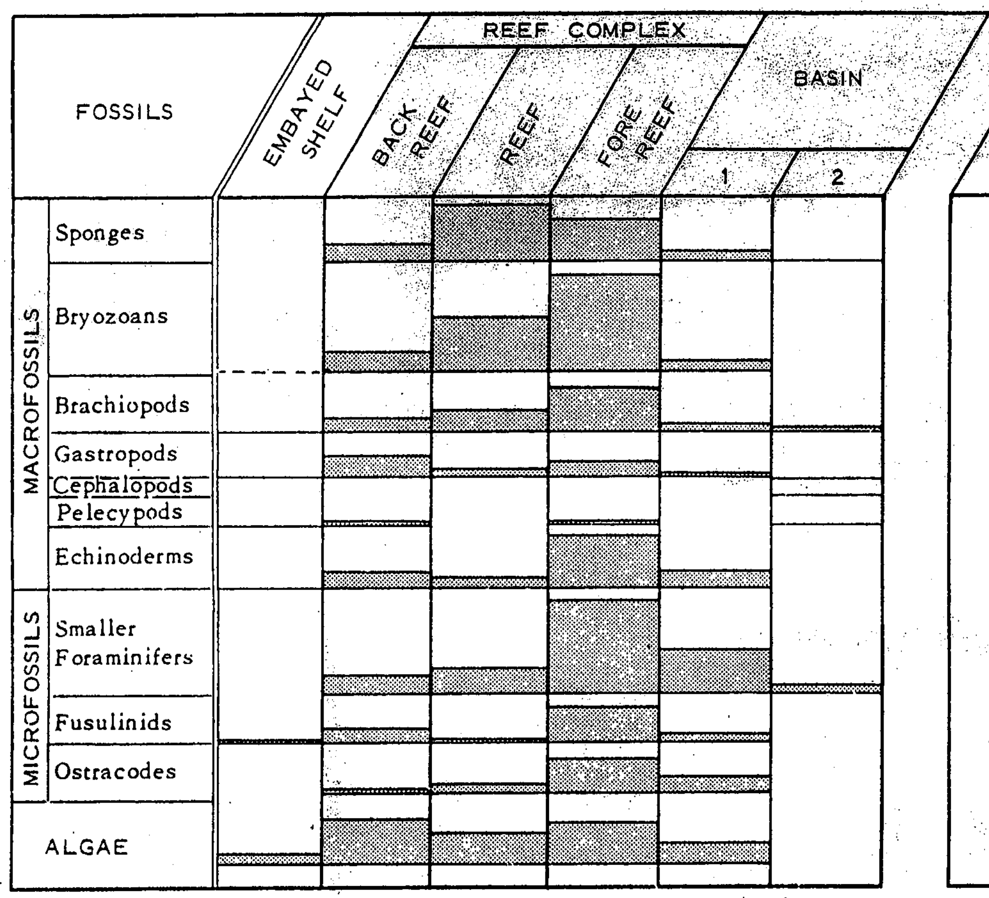

1 *Dark-colored limestones made up of submarine-slide material and other limestones containing abundant transported debris.*

2 *Dark-colored, thin-bedded, laminated limestone, massive sandstone, and thin-bedded, laminated, fine-grained sandstone and siltstone.*

RELATIVE ABUNDANCES of major fossil groups of the embayed-shelf, reef-complex, and basin rocks as determined from examination of polished surfaces, peels, thin sections, and the literature.

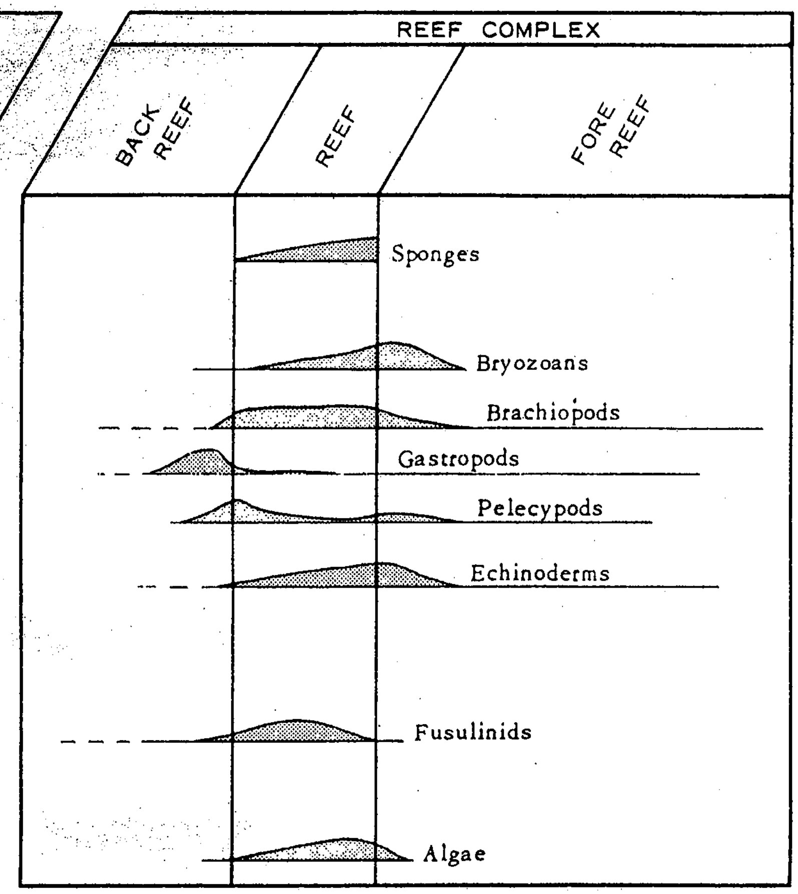

PROBABLE LIFE DISTRIBUTION of major fossil groups in the Capitan reef and associated environments as reported by Newell et al., 1953.

Courtesy of Exxon Production Research Co.

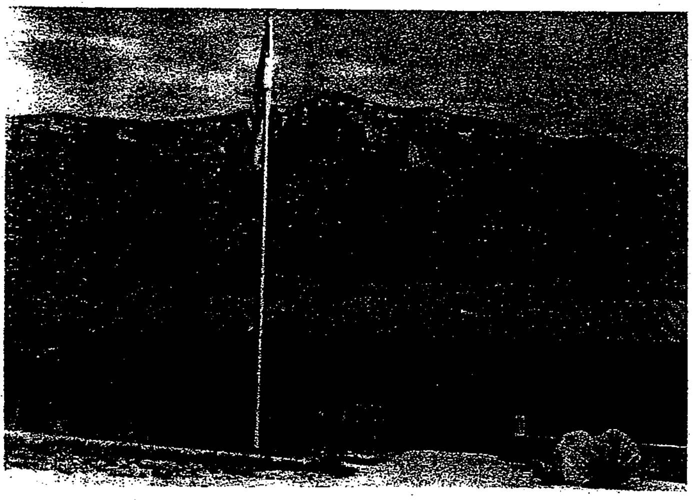

Photo A. McKittrick Canyon Visitor Center (Stop 2-3).

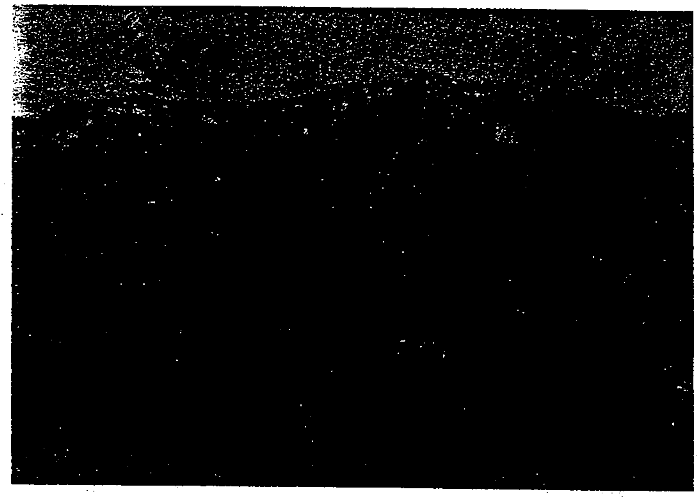

Photo B. North wall of McKittrick Canyon (Stop 2-3).

that includes fore-reef, reef wall and backreef facies. For about the last mile coming up the stream bed, the road traversed the fore-reef facies, with its large amount of debris shed off the reef into the Delaware basin.

Most of the rock in the walls of the canyon at this point is bedded fore-reef material, but on the north wall, the cliff forming Capitan reef wall stands out prominently. It is age equivalent to the Lamar. The reef grew laterally in a basinal direction, with the older fore-reef talus forming the substrate for continued reef growth. The Lamar member can be traced along the north side of the canyon from its basin-floor position, through its fore-reef equivalent and then merging into the reef-wall facies. The back-reef facies immediately overlies the reef-wall facies and represents a more basinal extension of the reef that is no longer present due to erosion.

Northwestward up the canyon, the base of the back-reef facies drops lower in the section with less and less of the reef and fore-reef facies present. After several miles, the canyon walls, nearly 2000 ft high, are composed of backreef facies only.

The volume of true reef wall seen in the Capitan reef complex is much smaller than the volume of either fore-reef or back-reef material preserved in the section. A living reef is a complex balance between the processes of construction and destruction. It is never a static feature. The process of reef destruction carries the once living reef material elsewhere for preservation. Only a small portion of the reef itself survives the processes of destruction to be preserved in the geologic column.

King's map of the southern Guadalupes shows a northeasterly plunging syncline marking the edge of the Delaware basin here, roughly parallel and in front of the fore-reef facies. Basinward of this syncline is a roughly parallel anticline. The limb common to both of these structural features has northerly dips, and shallow waterwells in the Bell Canyon on this feature have unusual shows of oil in them.

Newell et al., 1953, studied the Rader limestones and concluded they were slides of reef debris (some of this debris is very large) into the basin. Before his efforts these occurrences of reef material, four miles out in the basin in waters some 1500 ft deep, were considered to be patch reefs, even though their position in the basin posed distinct problems.

Fore-reef, Reef and Back-reef Facies

The Bell Canyon Fm is interbedded fore-reef limestones and basinal sandstones. The limestones are light gray proximal to the reef and become dark basinward. They are comprised primarily of reef derived material including bryozoans, sponges, brachiopods, foraminifera, crinoids and algae, and grade completely from coarse, unsorted talus near the reef to finer grained, sorted and laminated calcarenite basinward. Primary dips near the reef are 20 to 35 degrees. Diagenesis has resulted in permeability reduction due to recrystallization and secondary cementation, and there is patchy dolomitization. Basinal sandstone between the limestone units is light gray to buff and ranges from massive to laminated and, toward the reef, wedge out into the reef talus.

The Capitan Limestone, the reef unit, is an unstratified, fine-grained, light-colored limestone with a varied fossil fauna. The calcareous framework was provided by calcareous sponges, calcareous algae, bryozoans and hydrocorallines(?). Other members of the reef community include solitary corals, fusulinids and brachiopods. This facies is vuggy, with the vugs commonly infilled with sediment generated within the reef itself.

The back-reef Yates Fm. is a dolomitized limestone with abundant pisolites and a highly varied and abundant fauna of dasycladacean algae, foraminifera, brachiopods, gastropods, sponges, and bryozoans. Fossil material from the reef itself is carried into the back-reef and preserved there. Near the reef, the back-reef beds are thick to massive limestones with indistinct and erratic bedding, but landward the time-equivalent units become interbedded sandstones and fine-grained dolomites.

McKITTRICK CANYON

by Alton Brown and Bob Loucks

McKittrick Canyon is a world-famous location illustrating the translation from shallow-to deep-water carbonate sedimentation across a platform margin. We will examine the lower-slope limestones and sandstones exposed here and observe stratigraphic relationships exposed on the south canyon wall.

Upon leaving the visitor center, proceed down the trail marked "Pratt's Lodge." The trail crosses unlithified alluvium from the Lamar and Capitan Formations for about the first 250 yards. The first bedrock outcrop begins as the trail drops into the creek crossing. From here, we will leave the trail and follow the creek bed up the canyon. The units exposed in the first long outcrop are the McComb Limestone and underlying Bell Canyon Sandstones. Scattered exposures along the creek from here to the next trailcrossing of the creek are more exposures of Bell Canyon sandstones and the upper part of the Rader Limestone. After examining these units, continue up the creek past the second trail crossing. Most of the cemented, round-boulder conglomerates with porous matrix are Quaternary stream deposits. The best Radar Limestone exposure lies about 200 yards upstream from where the second trail crosses the creek.

The McComb Limestone consists of silty, medium to-thin-bedded, lime grainstone. Several beds of relatively pure, fine to very-fine grained sandstones are intercalcated into the unit along with coarse-grained carbonate turbidites. This member of the Bell Canyon Fm is not traceable far into the basin.

The underlying Bell Canyon Sandstone is a fine to very-fine grained, well sorted sandstone. This outcrop consists of broad channeling and laminated bedding with scattered low-relief hydrodynamic sedimentary structures typical of Bell Canyon sandstones. The long exposure also contains boulders of dolomitized Capitan in the Bell Canyon Sandstone. At this stratigraphic level, boulders become more abundant up depositional slope, until the sandstone interfingers with carbonate debris flows and breccias.

The uppermost Rader Limestone Mbr of the Bell Canyon Fm is exposed in scattered outcrops southeast of the second trail crossing. The upper part of the Rader Limestone generally consists of carbonate turbidite grainstones. Debris flows and transported boulders occur lower in the formation, as exposed in the low cliff on the north side of the creek beyond the trail crossing. The largest boulder, over 8 ft high and 20 ft wide, shows well-developed sponge-algal fabric characteristic of the upper part of the Capitan Fm. Finer-grained units below the boulder are silty, platey limestones.

The Lamar Limestone and Capitan Fm can be examined on the Geology trail, if time permits. This trail also provides an overview of slope facies relationships. Most of the lower part of the trail follows a dip slope in the middle part of the Lamar Mbr. Typical lithologies are thin-bedded, platey mudstones to wackestones. A thin, burrowed wackestone occurs near the top of the cliff section. Silicified fossils are common along some beds. These fossils are characteristic of the upper slope facies and contain few species found in the lower deposits of the Capitan Fm. Lamar debris flow beds are exposed in small isolated outcrops about 20 to 40 ft below the trail level near the cliff.

The cliff area has a good, shaded overview of the stratigraphic relationships exposed on the south wall of the canyon. Dipping units of the McComb Limestone, Bell Canyon Sandstone and Rader Limestone can be traced from the creek outcrops up the canyon wall. The sandstone units thin up slope and carbonate units thicken. Most sand-rich units have an intermediate facies with abundant carbonate boulders just downdip of merging with the Capitan Fm. The percentage of boulder beds in the carbonates generally increases up slope. Individual beds are difficult to trace. The more massive, thick-bedded limestones are characteristic of the Capitan Fm.

After the second switchback farther up the trail, good sponge-algal fabrics in the upper part of the Capitan facies are exposed on weathered surfaces and the low blasted cuts along the trail. The trail leads on to other exposures of Capitan Fm. Even farther up the trail, the Tansill Fm is exposed. these outcrops are too far up the trail to visit today.

SHELF-TO-BASIN FACIES DISTRIBUTIONS AND SEQUENCE STRATIGRAPHY OF A STEEP-RIMMED CARBONATE MARGIN: CAPITAN DEPOSITIONAL SYSTEM, McKITTRICK CANYON, NEW MEXICO AND TEXAS

SCOTT W. TINKER

Marathon Oil Company, Petroleum Technology Center, Littleton, Colorado, U.S.A. and Department of Geological Sciences, University of Colorado, Boulder, Colorado, U.S.A.; Mailing Address, 5895 East Kettle Place, Englewood, Colorado 80112, U.S.A.

ABSTRACT: **Shelf-to-basin outcrop studies in steep-rimmed, shelf-margin settings are uncommon because continuous shelf-to-basin transects are rarely exposed in a single outcrop. Discontinuous or absent stratigraphic marker beds across the shelf margin further complicate outcrop studies in the shelf-margin setting. This paper discusses the results of a high-resolution investigation of the shelf-to-basin profile along the north wall of North McKittrick Canyon, New Mexico and Texas. In McKittrick Canyon, carbonate-dominated sedimentary rocks associated with the steep-rimmed, Upper Permian Capitan depositional system are exposed along a continuous 5-km outcrop face. Measured sections, lateral transects, scintillometer readings, and geochemical data were synthesized into a digital database and interpreted in conjunction with a digital photomosaic of the entire canyon wall.**

Results of this work include a shelf-to-basin facies map and sedimentologic interpretation of the north wall of North McKittrick Canyon, and indicate that the dominant bathymetric profile during Capitan deposition was a marginal mound. In this model, the Capitan reef facies was deposited at the shelf–slope break in water depths ranging from 15 to 75 m, but always downdip from the topographically higher shelf crest. This model is supported by the following observations and interpretations: (1) a facies progression from the shelf crest to the shelf margin interpreted to represent a shallow-to-deeper-water succession; (2) proportional expansion of beds in a downdip direction; (3) presence of oriented (transported) fusulinid grainstones downdip from *in situ* fusulinid wackestones and packstones updip; (4) siltstones that thin and pinch out towards the shelf margin; (5) a decrease in dolomite from the shelf crest to the shelf margin; and (6) the absence of true toplap stratal geometries.

In reality, a static paleobathymetric model cannot characterize the depositional system, because the facies distributions, facies proportions, stratal geometries, and quantified depositional parameters vary systematically from the Seven Rivers through the Tansill. In order to understand the observed variations, emphasis was placed on *quantifying* key depositional parameters such as progradation, aggradation, offlap angle, outer-shelf dip, water depth, distance to the shelf margin and toe of slope, and facies-tract width. The systematic variations in these parameters, in conjunction with the facies distribution map and stratal geometries, helped to define the sequence-stratigraphic framework, and allowed for comparative evaluation of such things as sediment accumulation rates and sites, and stratigraphic evolution.

The Capitan depositional system is represented by three composite sequences, each containing four high-frequency sequences. Two and one half of these composite sequences are exposed in McKittrick Canyon. The overall depositional system is interpreted to have evolved predictably from a deeper-water margin in the Seven Rivers composite sequence, to a shallow-water margin in the Tansill composite sequence. The subtidal outer-shelf and shelf-margin facies tracts were sites of major sediment production. Accumulation rates across the shelf margin indicate a relatively continuous growth history, with periods of nondeposition or erosion limited to the terminal phase of each composite sequence. As a result, the preserved sedimentary record of high-frequency and composite sequences in the outer-shelf to upper-slope position is equally proportioned between transgressive and highstand systems tracts. This symmetric outer-shelf to upper-slope record of carbonate accumulation is significantly different from the asymmetric, highstand-dominated middle-shelf accumulation record reported previously for this and many other carbonate shelves.

INTRODUCTION AND OBJECTIVE

Carbonate shelf strata have been studied in detail in recent years (e.g., Read 1989; Koerschner and Read 1989; Goldhammer et al. 1990; Borer and Harris 1991; Crevello 1991; Osleger and Read 1991; Drummond and Wilkinson 1993; Goldhammer et al. 1993; Montañez and Osleger 1993). Less attention has been given to the more complex, shelf-to-basin stratigraphic setting because continuous shelf-to-basin transects are not commonly exposed in a single outcrop (e.g., Playford et al. 1989; Legarreta 1991; García-Mondéjar and Fernández-Mendiola 1993; Pomar 1993; Sonnenfeld and Cross 1993; Fitchen et al. 1995). Even when exposures are continuous, physical correlation across steeply dipping shelf margins is difficult, because lateral facies changes occur in short distances, and lithostratigraphic markers in shelf-margin and slope facies are rare (Wilson 1975). Because correlation across a steep-rimmed margin is difficult, data regarding stratal geometry, progradation, aggradation, and stratigraphic cyclicity are rarely synthesized.

The objective of this study is to map the stratal geometries and facies distributions along the continuous, shelf-to-basin outcrop exposures of the steep-rimmed carbonate margin associated with the upper Permian Capitan Formation. The following goals were implicit within the overall objective: (1) a more complete, high-frequency sequence-stratigraphic interpretation; (2) an updated shelf-to-basin stratigraphic correlation for the Capitan depositional system; (3) a critical evaluation of the long-standing controversy regarding the nature of the Capitan paleobathymetric profile and depositional model; and (4) collection of data regarding spatial and temporal variability in cyclicity, facies distribution, stratal geometry, and sediment accumulation rates and sites in a steep-rimmed setting.

GEOLOGIC BACKGROUND

The Permian reef complex, located on the northwest margin of the Delaware Basin, is partially exhumed in the Guadalupe Mountains. By the late Guadalupian, the Midland basin east of the Central Basin Platform was filled, and the Capitan reef and age-equivalent strata were deposited around the rim of the Delaware basin (Fig. 1). The Guadalupe Mountains, which dip gently as a block to the northeast, are bounded on the west by ''basin-and-range'' normal faults (King 1948). The present-day topography along the east side of the Guadalupe Mountains is an erosional profile along the Capitan reef margin (Fig. 2).

The Guadalupe Mountains provide spectacular, shelf-to-basin outcrop exposures of carbonate–siliciclastic sequences. The north wall of North McKittrick Canyon, located in New Mexico and Texas, represents a complete shelf-to-basin exposure across the upper Permian (upper Guadalupian) Capitan shelf margin (Figs. 2, 3). North McKittrick Canyon trends WNW, nearly perpendicular to the Capitan reef margin, is approximately five kilometers long, and has from 350 to 550 m of relief from the valley floor to the rim. The Permian Reef Geology Trail, one of the world's classic

JOURNAL OF SEDIMENTARY RESEARCH, VOL. 68, NO. 6, NOVEMBER, 1998, P. 1146–1174
 1073-130X/98/068-1146/$03.00

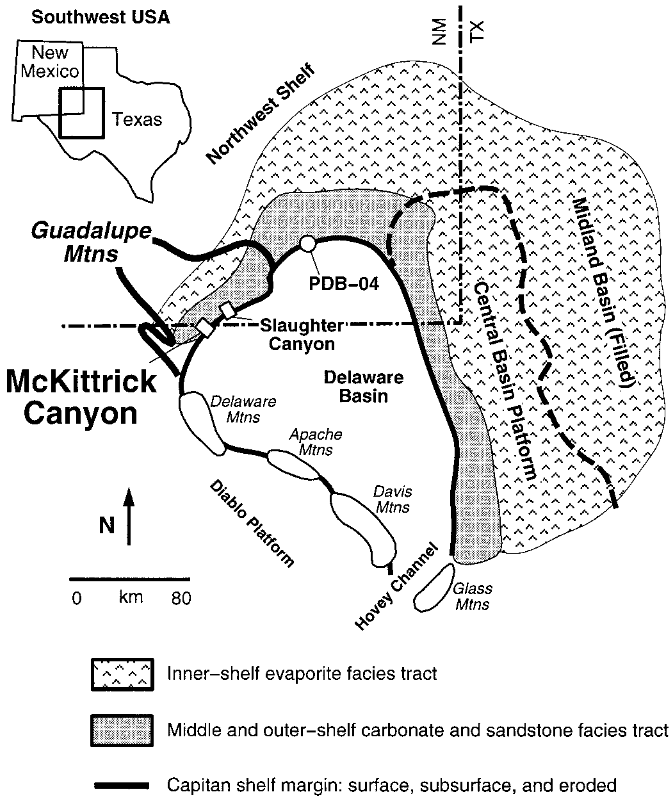

FIG. 1.—Simplified map of late Guadalupian facies in the Permian basin, west Texas and southeast New Mexico (modified from Ward et al. 1986). Note location of McKittrick Canyon, Slaughter Canyon, and the Gulf PDB-04 well.

carbonate field-trip locations (Bebout and Kerans 1993), is situated at the mouth of McKittrick Canyon.

The Guadalupe Mountains have received as much attention in the geologic literature as any ancient carbonate province in the world. Correlative strata in the Delaware and Midland basins are some of the most prolific hydrocarbon-producing reservoirs in the United States (Ward et al. 1986). King (1948), Newell et al. (1953), Hayes (1964), and Dunham (1972) did important regional studies of the general geology of the Guadalupe Mountains. Models for shelf deposition and cyclicity of late Guadalupian rocks in the Permian basin include publications by Silver and Todd (1969), Meissner (1972), Dunham (1972), Hurley (1978), Garber et al. (1989), and Borer and Harris (1991). Detailed studies of the Capitan Reef complex include those by Adams and Frenzel (1950), Achauer (1969), Babcock (1977), Yurewicz (1976, 1977), and Melim (1991). Recent studies have helped to put the Permian of the Guadalupe Mountains and Delaware Basin into a sequence-stratigraphic context (Sarg and Lehmann 1986; Kerans and Nance 1991; Kerans et al. 1992; Kerans et al. 1994; Sonnenfeld and Cross 1993; Kerans and Fitchen 1995; Gardner and Sonnenfeld 1996).

TERMINOLOGY

High-frequency cycles (referred herein as cycles; Fig. 4) are the fundamental stratigraphic building blocks in this study, and refer to the smallest set of genetically related lithofacies (facies) deposited during a single base-level cycle (James 1979; Grotzinger 1986; Koerschner and Read 1989; Goldhammer et al. 1990; Borer and Harris 1991; Crevello 1991). Cycles are analogous to the siliciclastic parasequence (Van Wagoner et al. 1988) but can contain a deepening and shallowing component. Allogenic cycles (vs. autogenic) are composed of vertical facies successions that can be mapped across multiple facies tracts. In McKittrick Canyon, cycles are easily recognizable in the intertidal to supratidal setting of the middle shelf and shelf crest, but are more difficult to document in the subtidal setting of the outer shelf, where thick vertical successions of similar facies dominate. Cycles are analogous in scale to fifth-order cycles (Goldhammer et al. 1990).

Several cycles make up a cycle set (Fig. 4), defined as a set of cycles bounded by marine flooding surfaces (Harris et al. 1993; Kerans et al. 1994) whose component cycles typically show a consistent progradational, aggradational, or retrogradational trend (Kerans and Tinker 1997). The lateral distribution, proportions, and geometry of facies within a cycle set commonly vary predictably as a function of position within the overall sequence-stratigraphic hierarchy.

Cycles and cycle sets make up high-frequency sequences (HFSs; Fig. 4).

FIG. 2.—Oblique air photograph of the southern end of the Guadalupe Mountains (photo courtesy of C. Kerans). The erosional Capitan reef margin trends from southwest (lower left) to northeast (upper right). Regional structural dip is to the ENE. Basin-and-range-related normal faults define the western limit of the Guadalupe Mountains as seen along the Algerita Escarpment and Shattuck Valley wall (upper left).

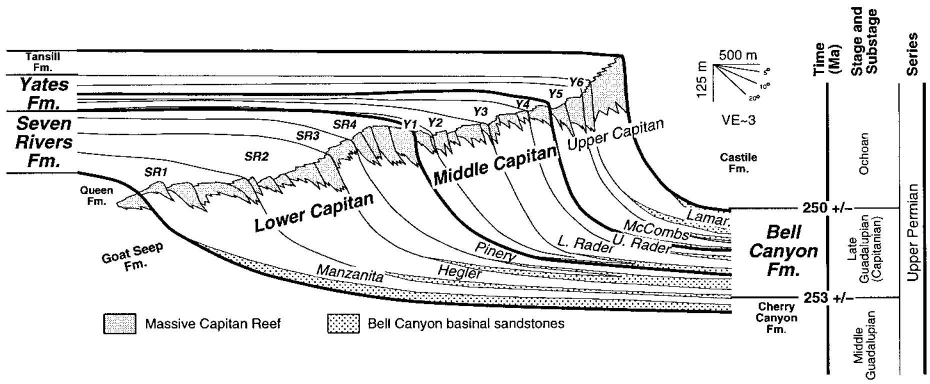

FIG. 3.—Simplified cross section of McKittrick Canyon. Heavy lines are CS boundaries. SR1 through SR4 make up the Seven Rivers CS. Y1 through Y4 make up the Yates CS. Y5 and Y6 are part of the genetic CS following the Yates CS. Thin lines are high-frequency sequence (HFS) boundaries. Formations included in this study are the Seven Rivers and Yates on the shelf, the lower and middle Capitan at the shelf margin, and the Bell Canyon in the basin. Time estimates are from Ross and Ross (1987).

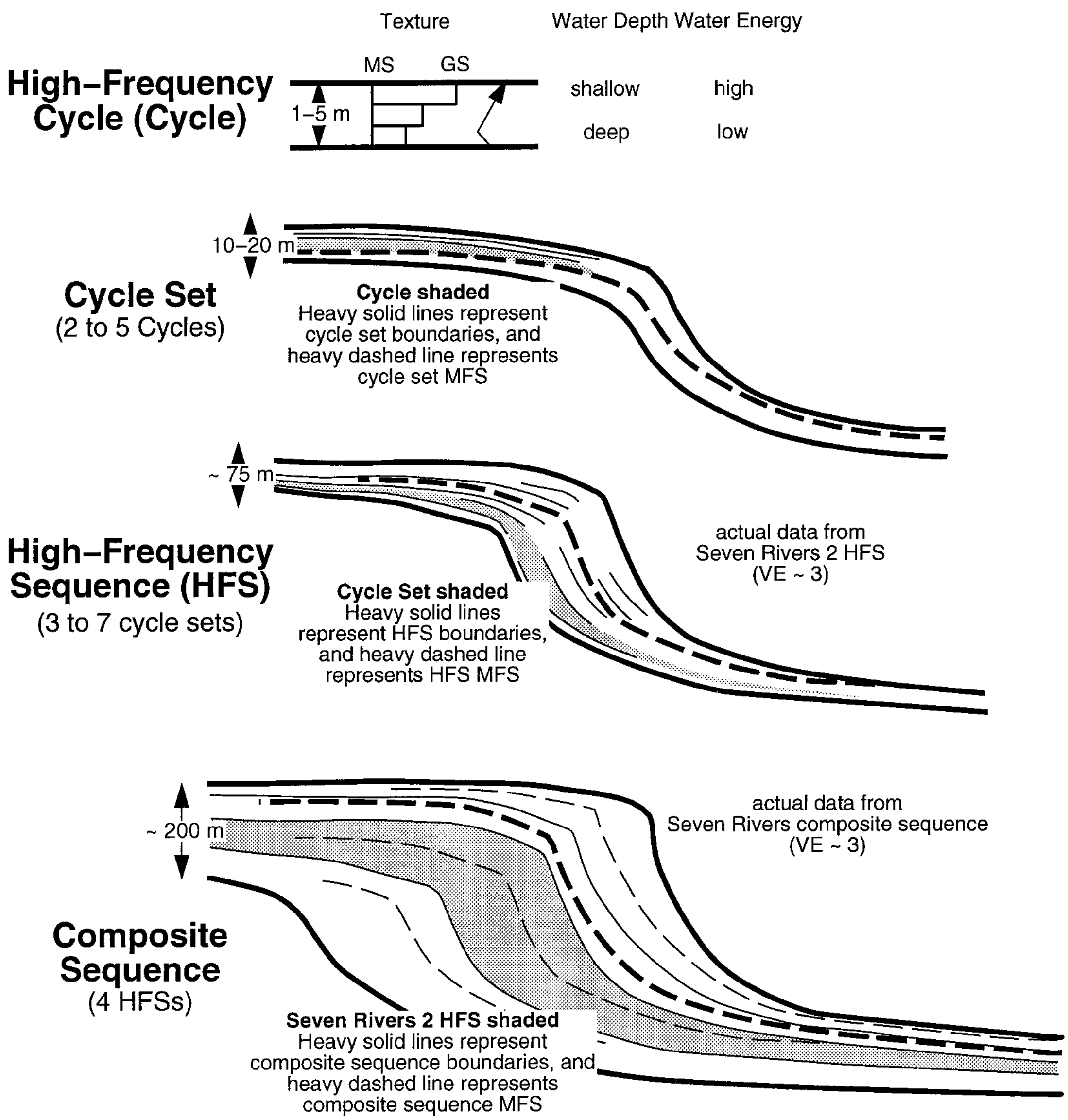

FIG. 4.—Hierarchy of cyclicity. Each stratigraphic element is a component of the subsequent lower-order element. Specific interpretations from McKitt rick Canyon were used to construct the figures, as noted.

HFSs are intermediate-order cycles bounded locally by unconformities (Mitchum and Van Wagoner 1991), and are composed of lowstand, transgressive, and highstand systems tracts (LST, TST, and HST). The TST is separated from the HST by a maximum flooding surface (MFS). In McKittrick Canyon, the MFSs are commonly represented by the maximum landward position of outer-shelf facies, a more highly aggrading shelf margin, and a condensed zone overlain by progradational downlap geometry in the basin. HFSs are estimated to represent time periods of 100–400 ky, and are analogous in scale to fourth-order cycles (Goldhammer et al. 1990).

Composite sequences (CSs; Fig. 4; Mitchum and Van Wagoner 1991) are the lowest order of cyclicity discussed in this study, and are analogous in scale to depositional sequences (Mitchum et al. 1977; Vail et al. 1977; Vail 1987; Van Wagoner et al. 1988) and third-order cycles (Goldhammer et al. 1990). Composite sequences, estimated to represent average time periods of 1–3 my, are composed of multiple, unconformity-bounded HFSs, and therefore differ subtly from depositional sequences, which are defined as a single unconformity-bounded rock succession.

In McKittrick Canyon, two complete CSs were recognized, and named ''Seven Rivers'' and ''Yates'' to remain consistent with the formation names on the shelf established by Hayes (1964). However, each CS incorporates part of the Capitan Formation across the shelf margin and Bell Canyon Formation in the basin. Four HFSs in the Seven Rivers CS (SR1 to SR4; Fig. 3), and four HFSs in the Yates CS (Y1 to Y4; Fig. 3) were identified. These HFSs are equivalent to Guadalupian 20 through 26 of Kerans et al. (1992). In addition, two HFSs were recognized in the CS deposited after the Yates CS, but were named Y5 and Y6 to remain consistent with the shelf formation names of Hayes (1964).

METHODS

Data in the study come from 36 vertical measured sections (1900 m), six published sections (330 m; Hurley 1978; Kerans and Harris 1993), several miles of lateral transects (Fig. 5), approximately 500 thin sections, scintillometer measurements (780 m), a digital photomosaic, and wireline logs from the Pratt #1 well drilled at the mouth of McKittrick canyon, the Guadalupe Ridge #1 well drilled on Wilderness Ridge, and the PDB-04 well (Fig. 1). Many of the data used in the interpretation were collected from shelf deposits, because slope deposits are commonly covered in talus and vegetation, and have crude to chaotic bedding with disorganized spatial textural variations. The slope and basin interpretations in this study are based on one vertical measured section, two basin-to-margin transects, correlation with the Pratt #1 well, data from exposures along the geology trail at the mouth of the canyon, bed tracing from helicopter and low-angle photographs taken from the south wall of the canyon, and use of data from other studies of the slope (Garber et al. 1989; Brown and Loucks 1993; Mruk and Bebout 1993; Melim and Scholle 1995).

Eighteen color photographs taken during a helicopter flight down the axis of the canyon were used to create a 2-D digital photomosaic. Reference points were marked on the photographs in the field every 5–20 m, and tied to vertical measured sections. Beds were traced laterally in the field, and marked on the photographs to document stratal geometries and facies variations. Graphical facies data were scaled vertically to fit between each photo-reference point marked in the field, and the resulting combination of measured sections, lateral transects, and the digital photomosaic were used to construct a stratigraphic and structural line interpretation on ''photo thickness'' (Fig. 6).

The photomosaic distorts the 3-D topography of the north McKittrick Canyon wall onto a 2-D projection. For example, 50 vertical meters at the base of the canyon wall, which was closer to the helicopter, appears much thicker than 50 vertical meters at the top of the canyon wall, which was farther from the helicopter. This is a common problem when interpreting photographic data in most field studies. Because the photomosaic line interpretation is on ''photo thickness'', it had to be converted to true vertical thickness (TVT) in order to quantify the depositional parameters determined from the sequence-stratigraphic interpretation (Fig. 7).

Texture, lithology, porosity, grain components, sedimentary structures, and cycles were described in the field for all measured sections on a per-foot basis. A hand-held scintillometer was used to measure the natural radioactivity of 780 m of section for comparison to subsurface gamma-ray logs. All of the quantified measured section data were entered into a digital SAS™ (Statistical Analysis Systems) dataset (1.52 million cells) on a SGI™ (Silicon Graphics) workstation for analysis and output.

Nearly 500 hand samples were slabbed and polished. A vacuum-impregnated thin section and/or acetate peel was made from each hand sample, and 50% of each section was stained with Alizarin red S. Petrography included systematic visual estimates of lithology (%), calcite cement (%), and present-day porosity (%), as well as description of grain types, texture, and dolomite crystal size. The descriptions and estimates of lithology, porosity, and texture made in the field were checked by petrographic analysis, and field estimates vary less than 10% from petrographic data (Tinker 1996b).

In addition to petrographic work, stable isotopes ($\delta^{18}O$ and $\delta^{13}C$) were examined from two densely sampled reef to back-reef vertical transects. Acetate peels of each sample were made to determine the best locations to sample for isotopic analysis. Eighty samples were analyzed by the University of Michigan Stable Isotope Laboratory with a reported precision (standard deviation) of $< 0.05‰$.

APPROACH

The data collection and interpretation phase of this study proceeded as follows: description of vertical sections; identification of cycles; walking of stratigraphic contacts; documentation of strata geometries; interpretation of photomosaics; mapping of lateral facies distributions; description of thin sections; construction of depositional models; and interpretation of the sequence-stratigraphic framework (cycle sets, HFSs, and CSs). Many of the collection and interpretation steps overlapped, and several iterations were made over a period of five years and four field seasons.

The remaining sections of this paper are presented in the general order of interpretation, with descriptions of facies and facies tracts first, followed by an interpretation of the static depositional models based on facies and sedimentologic data, and then a sequence-stratigraphic interpretation made with the initial depositional models in mind. The interpretations are followed by discussions regarding the dynamic stratigraphic and sedimentologic variations, the paleobathymetric model, and the sites and rates of sediment accumulation.

FACIES AND FACIES TRACTS

Eighteen distinct facies were recognized and described in McKittrick Canyon, defined using a combination of lithology, texture, grain composition, and sedimentary structures. Most of these facies have been described previously by other workers examining upper Guadalupian strata in the Guadalupe Mountains (e.g., Dunham 1972; Babcock 1977; Yurewicz 1976; Hurley 1978). Detailed facies descriptions for rocks in McKittrick Canyon can be found in Tinker (1996b). Therefore, the detailed measured section data, petrographic data, scintillometer data, well data, and lateral transect data for each facies are presented here in summary form only (Table 1). The tabular summary of the facies data is not intended to diminish their significance. To the contrary, the sedimentologic understanding that resulted from the descriptive work was critical to the interpretation of the initial depositional models and the subsequent sequence-stratigraphic interpretation; it is impossible to separate sedimentology and sequence stratigraphy.

A ''map'' of true vertical thickness (TVT) facies distribution and stratal geometry was constructed for the entire north wall of McKittrick Canyon

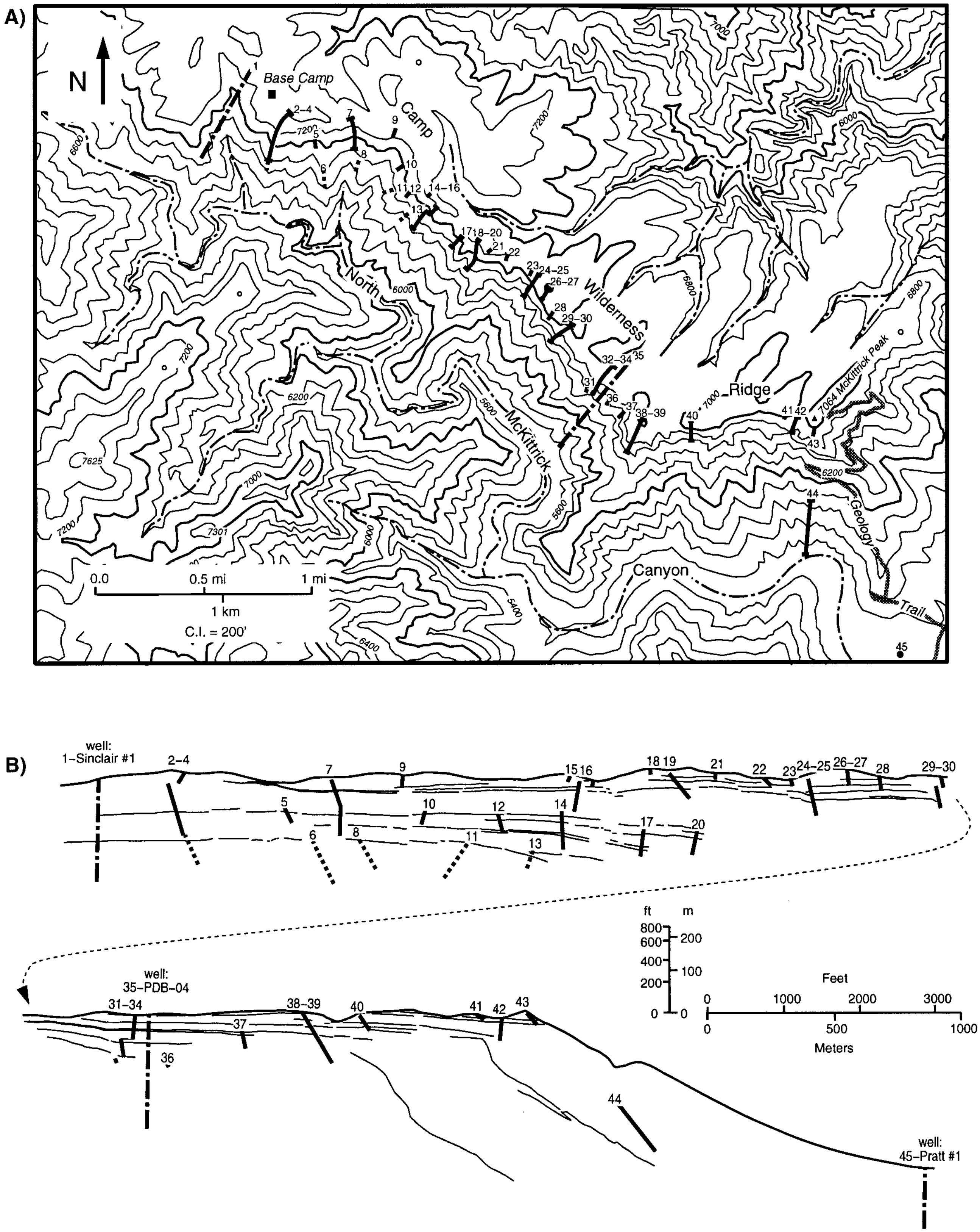

FIG. 5.—Topographic base map of McKittrick Canyon showing the location of measured sections (A, B) and lateral transects (thin horizontal lines) made in the field (B). Short-dashed lines (4, 6, 8, 11, 13) represent sections measured by Hurley (1978). Variable dashed lines are wells. See text for explanation of the variable vertical scale.

WNW
ESE
SR1
SR2
SR3
SR4
Y1
Y2
Y3
Y4
Y5
Tansill Fm.
Shattuck Sandstone
Queen Fm.
Measured Sections
* Color indicates facies
* Width of bar indicates texture
* Black bars on right are cycles picked in field
* Black bars on left are photo reference points
* All sections scaled vertically to fit "photo depth"
MS RS
Middle Shelf/Shelf Crest Facies
SC8 – Pisoid RS
SC7 – Composite grain RS
SC5 – Cryptalgal laminite BS
SC6 – Ooid, coated grain GDPS/GS
SC4 – Peloid, bioclast, intraclast PS/GS
SC3 – Peloid, bioclast MS/WS
SC2 – Silty dolomite
SC1 – Dolomitic siltstone
Outer Shelf/Shelf Margin Facies
OS9 – Ooid, coated grain, foram GS
OS8 – Oncoid RS
OS7a – Fusulinid, ooid GS
OS7 – Peloid, bioclast, fusulinid, GDPS/GS
OS6 – Peloid, bioclast, fusulinid, WS/PS
OS5 – Foram, mizzia, bioclast PS/GS
OS4 – Crinoid, peloid, foram WS/PS
OS3 – Peloid, bioclast MS/WS
OS2 – Silty dolomite
OS1 – Dolomitic siltstone
OS0 – Sponge, algal, ALP, cement FS/BS
Slope/Basin Facies
S5 – Bioclast, lithoclast RS/GS/BR/CG
S4 – Bioclast, lithoclast RS/WS/PS/CG
S3 – Burrowed, lithoclast MS/WS
S2 – Silty dolomite
S1 – Very–fine to medium sandstone, dolomitic siltstone
Abbreviations
MS Mudstone
WS Wackestone
PS Packstone
GDPS Grain–dominated packstone
GS Grainstone
BS Boundstone
RS Rudstone
FS Framestone
BR Breccia
CG Conglomerate
ALP *Archaeolithoporella*
SR1 – Seven Rivers 1 High–Frequency Sequence
Y1 – Yates 1 High–Frequency Sequence
Symbols and Patterns
Composite Sequence Boundary
High–Frequency Sequence Boundary
Cycle Set or Cycle Boundary
Outcrop of Shelf Margin Massive Reef
Covered Area
Fault
Drainage
Ridge or Outcrop Limit

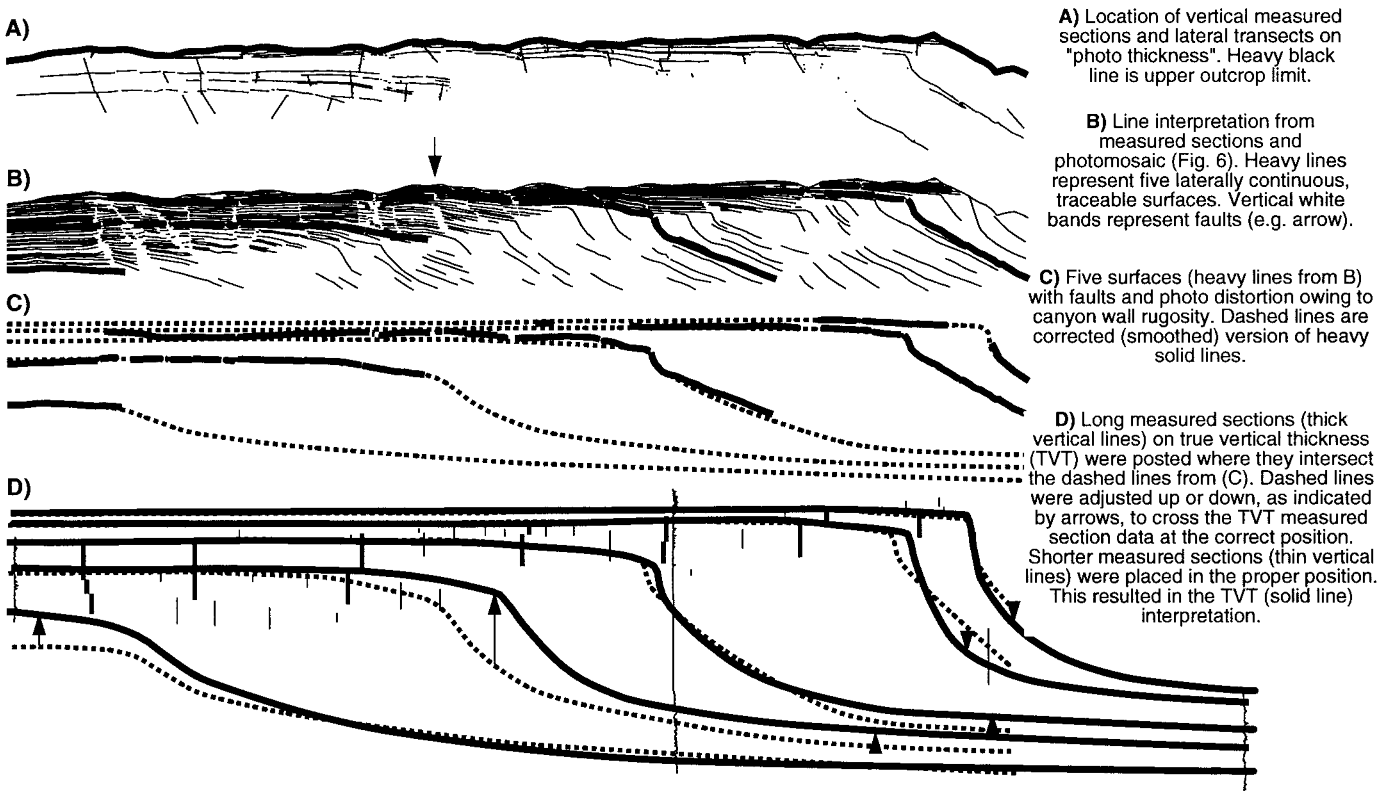

FIG. 7.—Steps to convert the photomosaic from ''photo thickness'' to true vertical thickness (TVT).

(Fig. 8) using the measured section data, lateral transect data, and the photomosaic. The TVT map represents the spatial distribution of all eighteen facies described in each measured section; no vertical averaging was done.

Owing to autocyclic processes, depositional topography, and position in the long-term eustatic hierarchy, individual facies are not always laterally continuous. Therefore, it is useful to group facies into facies tracts. A facies tract is a genetically linked association of facies and facies successions that records a discrete energy–water depth–sediment supply setting (*sensu* Kerans and Fitchen 1995, and analogous to a facies belt of Wilson 1975). Eight facies tracts were defined in McKittrick Canyon (Fig. 9), ranging along a depositional dip profile from the shelf-crest supratidal to the basinal. A generalized map of the facies tracts for the entire north wall of North McKittrick Canyon (Fig. 10) illustrates the complex yet systematic variation in proportion, width, thickness, and geometry of facies tracts.

Most carbonate depositional systems have key ''indicator'' facies or facies tracts, defined on the basis of lithology, grain components, and sedimentary structures. These indicator facies represent interpreted depth/energy positions such as shoreline, fair-weather wave base, and storm wave base (Kerans and Tinker 1997), and are therefore very useful for sequence-stratigraphic interpretation. In McKittrick Canyon the shelf-crest supratidal, outer-shelf subtidal, and shelf-margin facies tracts are such ''indicators''.

The *shelf-crest supratidal facies tract* is composed of cryptalgal laminite boundstone, composite-grain rudstone, and pisoid rudstone, with rare to common small (a few centimeters tall) to large (several meters tall) teepee complexes (see also Esteban and Pray 1983). This facies tract is a shoreline indicator. The *outer-shelf subtidal facies tract* has a low- to moderate-energy component composed principally of silty, peloid, bioclast, foram dolowackestones and dolopackstones, and a moderate- to high-energy component composed principally of foram, *Mizzia*, bioclast, peloid, fusulinid packstones and grainstones. The low- to moderate-energy component is interpreted to indicate a position from well below fair-weather wave base to below storm wave base, and represents the flooding events on the shelf. The moderate- to high-energy component is interpreted to indicate a position just below fair-weather wave base. The *shelf-margin facies tract*, commonly called the Capitan reef, is composed of marine-cemented, sponge, algal, bryozoan, *Archaeolithoporella* (ALP), *Tubiphytes* framestones and boundstones (see also Kirkland et al. 1993; Wood et al. 1994). This facies represents a similar fair-weather to sub-storm-wave-base position as the low- to moderate-energy component of the outer-shelf subtidal facies tract.

In addition, there is a siltstone and very-fine grained sandstone facies (referred to collectively as siltstones) that cuts across most facies tracts (S1, OS1, SC1 in Figure 8; Table 1). The siltstones are composed of quartz, potassium feldspar, kaolinite, and illite, have dolomite and calcite cements, are remarkably devoid of diagnostic sedimentary structures (see also Candelaria 1982), and are more naturally radioactive than the associated carbonates. The siltstones are a very useful indicator of stratal geometry, because their position can be followed in outcrop with a high degree of confidence.

DEPOSITIONAL MODELS

By definition, a depositional model is a generalization, because the depositional setting and associated facies arrangements are not static, but are instead strongly related to the position in the overall composite sea-level curve. For example, the depositional model for a TST in the SR1 HFS is quite different from the depositional model for the HST in the SR1 HFS. The same variation is observed at the CS scale.

Stratigraphic and sedimentologic data in McKittrick Canyon uphold the model of reciprocal sedimentation. The concept of ''reciprocal sedimentation'' (Wilson 1967) was first applied to Permian strata in the Delaware basin by Silver and Todd (1969), Jacka et al. (1972), and Meissner (1972). The model involves clastic progradation and bypass across the shelf into the basin during relative sea-level lowstand, and carbonate growth on the


WNW
ESE
Estimated base of Salado evaporite
1) Sinclair Guadalupe Ridge #1
Projected 2100 m from NNE
35) Gulf PDB–04
Projected 90 km from NE
McKittrick Peak
Elev. 7064 ft
Tansill Fm.
Yates Fm.
Seven Rivers Fm.
Queen Fm.
Shattuck Sandstone
7000'
6000' Present Elevation
(with ~3 degrees of SE dip removed)
5000'
300 m
150 m
1°
5°
10°
20°
30°
VE ~ 1.7
Composite Sequence Boundary
MFS
High-Frequency Sequence Boundary
MFS
High-Frequency Sequence Boundary
HST
TST
Cycle Set
SR1
SR2
SR3
SR4
Y1
Y2
Y3
Y4
Yates A
Y5
Yates B
Y6
Yates C
Approximate Upper Outcrop Limit
Geology Trail
Upper occurrence of
Polydiexodina
Lamar
McCombs
U. Rader
lower Rader
Pinery
Hegler
Manzanita
Approximate Basal Outcrop Limit
45) Humble Pratt #1
K.B. 4889'
McCombs
U. Rader
L. Rader
Pinery
Hegler
Manzanita
Bell Canyon Fm.
Cherry Canyon Fm.
207
Middle Shelf/Shelf Crest
Pisoid RS, composite grain RS
with Tepee
Cryptalgal laminite BS
Ooid, coated grain GDPS/GS
Peloid, bioclast, intraclast PS/GS
Peloid, bioclast MS/WS
Silty dolomite
Dolomitic silt
Outer Shelf/Shelf Margin
Oncoid RS
Fusulinid GS
Peloid, bioclast, fusulinid, GDPS/GS
Peloid, bioclast, fusulinid, WS/PS
Foram, Mizzia, bioclast PS/GS
Crinoid, peloid, foram WS/PS
Peloid, bioclast MS/WS
Silty dolomite
Dolomitic silt, very-fine sandstone
Sponge, algal, ALP, cement FS/BS (reef)
Measured Section Location
Gamma Ray (API) or
Scintillometer (cps)
Slope/Basin
Bioclast, lithoclast RS/GS/BR/CG
Bioclast, lithoclast RS/WS/PS/CG
Burrowed, peloid MS/WS
Silty dolomite
Very-fine to medium sandstone, dolomitic silt
Abbreviations
MS Mudstone
WS Wackestone
PS Packstone
GDPS Grain-dominated packstone
GS Grainstone
BS Boundstone
RS Rudstone
FS Framestone
BR Breccia
CG Conglomerate
ALP Archaeolithoporella
SR1 Seven Rivers 1 HFS

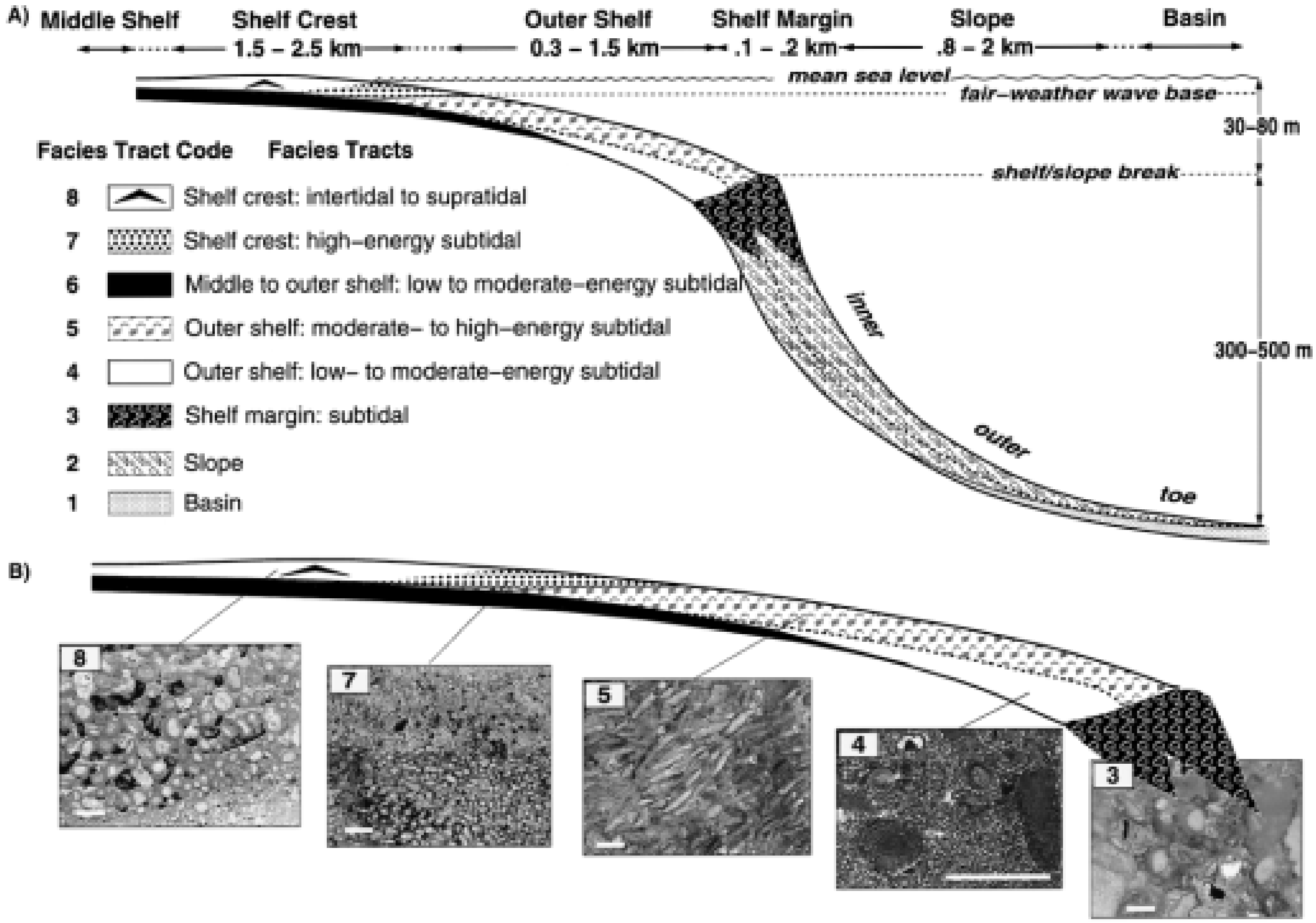

FIG. 9.—**A)** Generalized 2-D cycle showing vertical and lateral position and width ranges of major facies tracts related to paleobathymetric profile. **B)** Expanded shelf part of the cycle with photographs of key facies showing a general decrease in interpreted depositional energy downdip. Scale bar is 1 cm for all photographs. Numbers correspond to facies-tract legend.

shelf during relative sea-level rise and highstand. Detailed petrography and facies mapping on the shelf in McKittrick Canyon documents a higher-frequency timing of siliciclastic sediment delivery, similar to that proposed by Borer and Harris (1989, 1991) for the Yates Formation, Gardner (1992) for the Bell Canyon Formation, Brown and Loucks (1993) for the Tansill-equivalent toe-of-slope, and Melim and Scholle (1995) for the Capitan slope.

In the continuous outcrops of McKittrick Canyon, sedimentology, petrography, stratal geometry, and vertical and lateral facies associations were all used to develop the initial depositional models. Closely spaced vertical measured sections and lateral transects within the Y3 HFS were used to construct a detailed 2-D cross section (Fig. 11) and a series of 3-D block diagrams (LST, TST, HST; Fig. 12) that represent the depositional history of a typical HFS. Unless otherwise cited, the interpretations that follow are based on this work (see also Tinker 1996b).

Lowstand Systems Tract

Siltstones were transported tens to hundreds of kilometers across the shelf into the basin by eolian (Mazzullo et al. 1985) and shallow-water marine-coastal processes (Candelaria 1982; Figure 12), where they were deposited by suspension in deep water. At maximum relative sea-level lowstand, the entire *shelf crest* and much of the *middle shelf* were subaerially exposed, and underwent either erosion or silt deposition by eolian and sabkha processes. Individual siltstone deposits thin towards the shelf margin owing to increased depositional slope in the outer shelf and slope, and silt transport across the margin by storm-related, marine processes. *The outer shelf* and *shelf margin* remained submerged, the outer-shelf facies tract was narrow (500 m), the shelf margin was narrow (20 m) and relatively shallow (~ 15 m), and a minimal volume of carbonate sediment was transported into the *basin.*

Transgressive Systems Tract

During marine transgression the shoreline receded, and shelf siltstones were partially to completely reworked and buried by low-energy carbonate deposits. *Shelf-crest* deposits backstepped and aggraded (Figs. 11, 12).

Outer-shelf rates of carbonate-sediment production were at a maximum, which is common for the TST in most HFSs in McKittrick Canyon (see outer-shelf thickness in Figures 8, 10, 11). There was a systematic, landward increase in current reworking, resulting in higher-energy, grainier facies updip from lower-energy, muddier facies (Figs. 9, 11, 12). Fusulinid grainstones are an exception, and can be found downdip from the lower-energy facies in close proximity to the shelf margin. Fusulinid tests in these grainstones are commonly oriented parallel to depositional dip, indicating mobilization and downslope transport of fusulinids.

Fusulinids are important indicators of paleoenvironment. The large (1–3 cm) Guadalupian fusulinids found in outer-shelf facies of the Seven Riv-

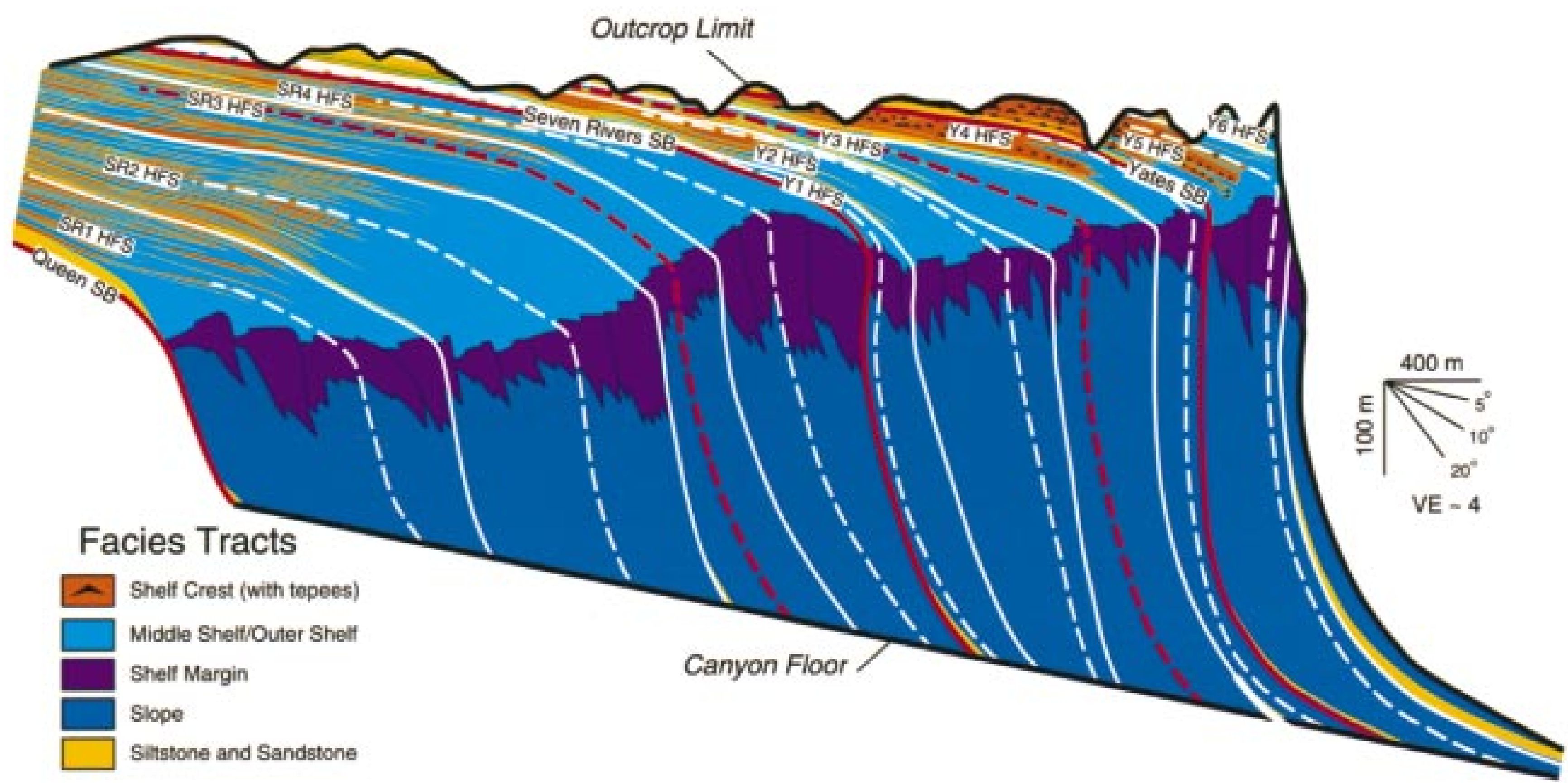

FIG. 10.—Facies-tract distribution, simplified from Figure 8, illustrating the organization in McKittrick Canyon. Figure is shown with present-day, t ectonically enhanced basinward dip (to the right) to illustrate the potential pitfall of misinterpreting the amalgamated shelf-crest facies (Y2 to Y5) as a single lithostratigraphic unit (similar to the Yates Formation definition by Hayes 1964). Solid red lines are CS boundaries, dashed red lines are CS MFSs, solid white lines are HFS boundaries, and dashed white lines are HFS MFSs.

TABLE 1.—*Lithofacies data*

Facies					
Code	Major Grain(s)	Texture[1]	Minor grain(s)	Facies Tract: Energy Modifier	Depositional Environment (water–depth range in parentheses)
SC8	Pisoid	RS	Composite grain, eploid	Shelf crest: intertidal to supratidal	Intertidal to supratidal; subaerial island
SC7	Composite grain	RS	Pisolite, peolid, ooid, mollusc	Shelf crest: intertidal to supratidal	Intertidal to supratidal; rare subaerial exposure
SC5	Cryptalgal, peloid	WS/BS	Foram, ostracod	Shelf crest: intertidal to supratidal	Intertidal to supratidal tidal flat
SC6	Ooid, coated grain	GDPS/GS	Foram, peloid, pisoid	Shelf crest: high-energy subtidal	Lower foreshore and shoreface (3–10 m)
SC4	Peloid, bioclast, intraclast	PS/GS	Foram, mollusc	Middle shelf: low to moderate-energy subtidal	Shallow subtidal shoals (5–10 m)
SC3	Peloid, bioclast	MS/WS	Foram, mollusc	Middle shelf: low to moderate-energy subtidal	Subtidal (10–25 m)
SC2	Silty dolomite	MS/WS	Peloid, bioclast	Middle shelf: low to moderate-energy subtidal	Erg transport, transgressive reworking and subtidal preservation
SC1	Siltstone (dolomitic)		Peliod	Middle shelf: low to moderate-energy subtidal	Erg transport, transgressive reworking and subtidal preservation
OS9	Ooid, coated-grain, foram	GS	Foram, peliod, pisoid	Outer shelf: moderate to high-energy subtidal	Shoals (5–10 m)
OS8	Oncolite	RS	Ooid, peloid, composite grain, foram	Outer shelf: moderate to high-energy subtidal	Shoal and intershoal; transported deposits (5–30 m)
OS7A	Fusulinid, ooid	GS	Peloid	Outer shelf: moderate to high-energy subtidal	Shoal and intershoal; transported deposits (5–40 m)
OS7	Peloid, bioclast, fusulinid	GDPS/GS	Foram, mollusc	Outer shelf: moderate to high-energy subtidal	Shoal and intershoal (5–50 m)
OS6	Peloid, bioclast, fusulinid	WS/PS	Foram, mollusc	Outer shelf: moderate to high-energy subtidal	Intershoal (10–80 m)
OS5	Foram, mizzia, bioclast	PS/GS	Peloid	Outer shelf: moderate to high-energy subtidal	Moderately protected back reef (5–50 m)
OS4	Crinoid, foram, peloid	WS/PS	Mizzia, Bioclast	Outer shelf: low- to moderate-energy subtidal	Immediate back reef (20–80 m)
OS3	Peloid, bioclast	MS/WS	Foram, mollusc	Outer shelf: low- to moderate-energy subtidal	Quiet-water outer shelf (10–80 m)
OS2	Silty dolomite	MS/WS	Peloid, bioclast	Outer shelf: lowstand transport, transagressive reworking	Erg transport, transgressive reworking and subtidal preservation
OS1	Siltstone (dolomitic)		Peloid	Outer shelf: lowstand transport, transagressive reworking	Erg transport, transgressive reworking and subtidal preservation
OS0	Sponge, ALP, cement	FS/BS	Sediment, bryozoan, cephalopod, tubiphytes, foram	Shelf margin reef	Organic, cement reef, dominantly quiet water (10–80 m)
S5	Bioclast, lithoclast	RS/GS/BR/CG	Spectrum of shelf and shelf margin derived grains	Slope (inner)	Upper and middle slope, rock fall, grain flow, debris flow
S4	Bioclast, lithoclast	RS/WS/PS/CG	Spectrum of shelf and shelf margin derived grains	Slope (inner to outer)	Lower slope, debris flow, high-density turbidite
S3	Peloid, foram	MS/WS	Spectrum of shelf and shelf margin derived grains	Slope (outer) and basin	Toe of slope, low-density turbidity current
S2	Silty dolomite	MS/WS	Peloid, bioclast	Slope (outer) and basin	Distal slope and basin, low-density turbidity current
S1	Siltstone (dolomitic)		Peloid	Basin	Distal slope and basin, low-density turbidity current
S0	Vf–md sand			Basin	Distal slope and basin, low-density turbidity current

[1] After Embry and Klovan's (1971) modification of Dunham's (1962) classification. GDPS is grain-dominated packstone after Lucia (1995).

TABLE 1.—*Continued.*

Code	Sedimentary Structures	Lithology (Average %)[2] ST/SD	DM	LM	Calcite	Oth	∅	Pore Type(s)[3]	Radioactivity (cps)/# Measurements[4]	Measured Feet (#)/Thin Sections (#)[5]
SC8	Tepee, sheet crack, breccia	0	64	14	15	1	6	BP, WP, BR, SH	63/359	886/29
SC7	Tepee, sheet crack, breccia	1	68	15	10	0	6	BP, WP, BR, SH	67/94	252/51
SC5	Fenestral to wavy laminated, stromatolite	1	73	11	9	0	6	FE, BC, FR, MO	68/168	322/39
SC6	Planar and cross stratified	1	55	30	8	0	6	BP, BC, MO	62/123	211/24
SC4	Planar laminated	1	59	27	8	1	4	BP, BC, MO	70/356	822/89
SC3	Laminated to massive, vertical burrow	2	79	13	4	0	2	mBC, BC, BP	65/23	289/16
SC2	Planar laminated, graded beds	24	71	0	1	1	3	mBC	101/55	160/15
SC1	Planar laminated, graded beds	67	22	0	2	0	9		134/47	371/8
OS9	Planar and cross stratified	0	64	16	10	0	10	BP, BC, MO, WP	63/61	180/21
OS8	Planar laminated	0	53	28	13	0	6	BP, WP	58/10	344/6
OS7A	Planar and minor cross stratified	0	62	15	13	0	10	BP, BC, MO	66/82	258/6
OS7	Planar laminated	2	53	29	8	0	8	BP, BC, MO	63/510	1074/30
OS6	Planar laminated	0	60	23	11	0	6	BP, BC, MO	68/241	781/33
OS5	Planar laminated	0	59	24	12	0	5	BP, BC, MO	64/19	138/9
OS4	Planar laminated	0	43	41	12	0	4	BP, BC, MO	58/13	73/8
OS3	Laminated to massive, vertical burrow	2	92	0	2	0	4	mBC, BC, BP	83/15	24/5
OS2	Planar laminated, graded beds	29	59	0	7	0	5	mBC	89/16	59/5
OS1	Planar laminated, graded beds	53	15	0	20	2	10		112/22	55/3
OS0	Massive	0	30	50	18	0	2	VG, FR, MO, BP	53/21	187/50
S5	Steep dipping, medium to chaotic bedded	0	51	26	18	0	5	BP, MO, VG, FR	48/77	138/7
S4	Planar and cross stratified, inverse graded	0	50	40	7	0	3	BP, MO, VG, FR	48/202	383/7
S3	Fine laminated to thick bedded, graded beds							BP, WP FR		
S2	Planar laminated, bioturbated, graded beds							mBC		1/1
S1	Planar laminated, bioturbated, graded beds									1/1
S0	Laminated to thin bedded	70	10	0	5	5	10		63/2	2/1

[2] Average of all samples based on visual estimates in the field, calibrated by thin section petrography: ST/SD = siltstone/sandstone; DM = dolomite; LM = limestone; Oth = other, ∅ = porosity.
[3] After Choquette and Pray (1970).
[4] From hand-held Scintillometer.
[5] Includes samples from lateral transects.

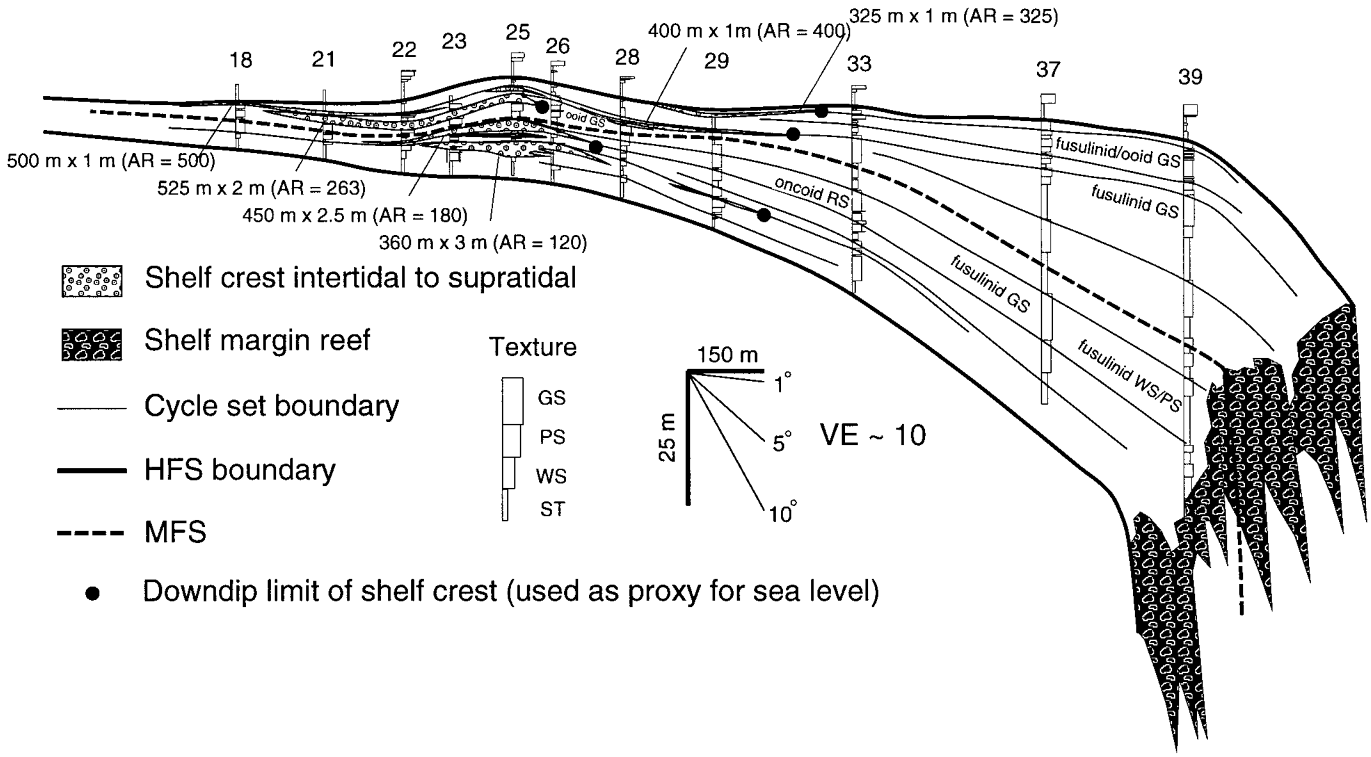

FIG. 11.—Detailed cross section of the Y3 HFS. Note: (1) the proportional expansion in thickness of cycle sets, and the systematic progression from high- energy shelf-crest facies (PS/GS) to lower-energy, outer-shelf facies (WS/PS) from the shelf crest downdip to the shelf margin; (2) the downdip limit of the shelf-crest facies tract (black circles) backsteps to just above the maximum flooding surface (MFS), and progrades above the MFS; (3) the aspect ratios (AR) of the shelf crest bodies increase upwards toward the MFS and decrease away from the MFS. MS, Mudstone; WS, Wackestone; PS, Packstone; GS, Grainstone; ST, Siltstone. Measured section numbers correspond to Figures 5, 6, and 8.

ers through the middle Yates are *Polydiexodina.* Considerably smaller fusulinids, *Yabeina* and *Codonofusiella,* first occur in the lower Tansill Formation, and the still smaller *Reichelina* first occurs in the middle Tansill (Tyrrell 1969; Wilde 1975). Although these Paleozoic fusulinids are extinct, *Alveolinella quoyi* is considered a modern counterpart (Severin and Lipps 1988). Fusulinids and alveolines (Miliolida) belong to different suborders because of variations in test structure, yet their similar morphology, taphonomy, associated rock types, and latitudinal ranges argue that the development of individuals, and the community in which they lived, must have been comparable (Haynes 1981). On Papua New Guinea, *A. quoyi* is most abundant ($750/m^{2)}$ on stable sand and coral rubble slopes in water depths from 12 to 30 m. Alveolinids are most abundant between 25 and 35 m in the Gulf of Aqaba and in the Maldives. In addition, the deeper-water modern alveolinids have greater length-to-thickness ratios than the shallower forms (Haynes 1981).

The *shelf-margin* facies tract was dominantly aggradational (Fig. 12). This aggradational mode was common for the shelf-margin facies tract during the marine transgressive phase of most HFSs in McKittrick Canyon, and is also observed at the CS scale (Figs. 8, 10).

Whereas shelf-derived *slope* deposits were a mix of siltstones and carbonates during the early TST, they were dominantly carbonate during the late TST, and were probably deposited as downlapping strata onto toe-of-slope and basinal carbonates and siltstones (documented for the Tansill-equivalent Lamar member by Brown and Loucks 1993).

Highstand Systems Tract

With progressive infill of shelf accommodation, the *shelf-crest* and *outer-shelf* facies tract deposits were forced to prograde basinward (Fig. 11, 12). The decrease in accommodation is documented by the changing aspect ratio of the shelf-crest supratidal facies tract, which increased from 100 to 200 (350 to 450 m width and 2 to 3 m thickness) in the TST, to 200 to 500 (300 to 500 m width and 1 to 2 m thickness) in the HST (Fig. 11). Kerans and Fitchen (1995) have documented a similar relationship for the shelf-crest facies in San Andres and Grayburg ramp deposits.

Facies diversity and the net volume of grain-dominated sediments increased in the higher-energy, *outer-shelf* facies tract of the HST relative to the lower-energy, outer-shelf facies tract of the TST (Fig. 12). The *shelf-margin* reef was progradational, and shelf-derived *slope* deposits were grain-dominated (documented for the Tansill-equivalent Lamar member by Brown and Loucks 1993).

SEQUENCE STRATIGRAPHIC INTERPRETATION

Carbonate strata commonly show an ordered stratigraphic hierarchy that repeats at many scales (Cross et al. 1993; Goldhammer et al. 1993; Montañez and Osleger 1993). Many workers in the Permian of West Texas and New Mexico have recognized this type of ordered stratigraphic hierarchy (Borer and Harris 1991; Sonnenfeld 1991; Kerans et al. 1992; Kerans et al. 1994; Kerans and Fitchen 1995). It is possible to challenge the statistical significance, or even the existence, of an ordered stratigraphic hierarchy, by isolating only 1-D data (Wilkinson et al. 1997). However, the challenge weakens considerably when 2-D data are considered, because facies proportions, cycle thickness, and stratal geometries commonly vary along depositional dip in most carbonate settings (see Figures 8, 9, 10). Therefore, even in ordered stratigraphic systems the 1-D succession of facies will vary as certain facies substitute laterally for other facies. In McKittrick Canyon, analysis of the 2-D facies distribution data indicates a remarkably well organized stratigraphic hierarchy, emphasizing the need to examine all of the data using as many analytical ''tools'' as possible.

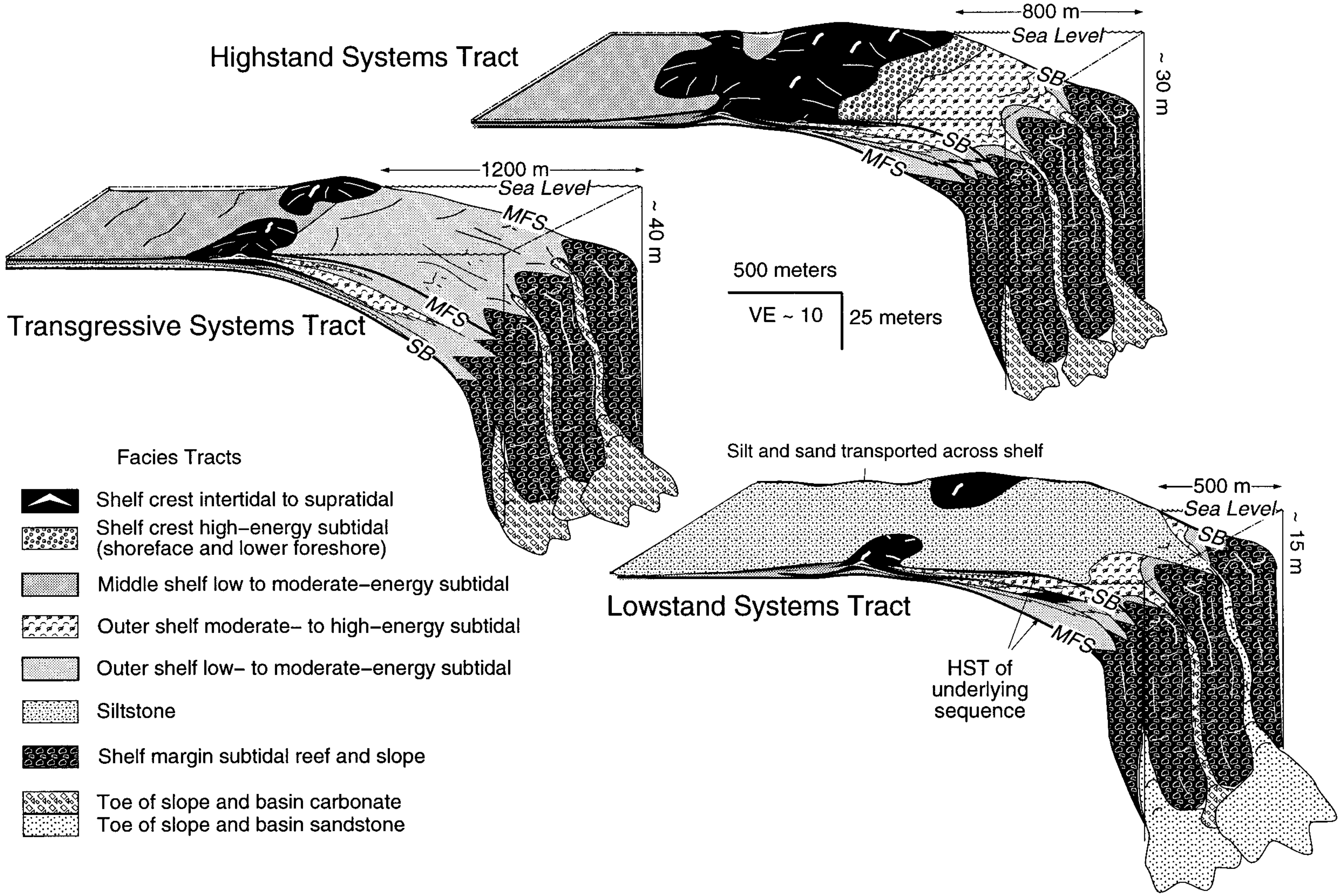

FIG. 12.—Three-dimensional facies distribution based on the Y3 HFS depositional model in Figure 11. Note: (1) increasing interpreted depth to the top of the shelf-margin reef from the LST to the TST; (2) greater distance from the shelf-crest shoreline to the shelf margin in the TST versus HST; and (3) greater shelf-crest width and outer-shelf facies diversity in the HST versus the TST. SB, sequence boundary. MFS, maximum flooding surface. This systematic variation in facies is observed in most of the Seven Rivers and Yates HFSs and CSs (Figs. 8, 10).

TABLE 2.—*Sequential Facies Data*

Lithofacies Below \ Lithofacies Above	SC8	SC7	SC5	SC6	SC4	SC3	SC2	SC1	OS9	OS8	OS7a	OS7	OS6	OS5	OS4	OS3	OS2	OS1	OS0
SC8		*20%*	*22%*	*17%*	*25%*	*16%*	***30%***	***42%***	*3%*	*6%*	*2%*	*1%*	*6%*			*9%*		*8%*	
SC7	**25%**		9%	5%	6%	14%	8%	4%	8%	12%	4%	1%	2%						
SC5	29%	**29%**		24%	15%	9%	8%	13%		5%		2%	2%	5%					
SC6	11%	11%	**14%**		8%	3%	11%	7%		4%									
SC4	9%	13%	34%	**44%**		16%	9%	11%		18%		2%							
SC3	4%	10%	4%	1%	**19%**			3%		14%									
SC2	6%	3%	8%	4%	**12%**	8%		**17%**	2%			1%							
SC1	8%		2%	1%	5%	7%	**32%**			1%				16%					
OS9	*3%*	*3%*	*1%*		*1%*	*3%*	*1%*			*11%*	*13%*	*13%*	*3%*	*5%*			***16%***	***17%***	
OS8	3%	8%	2%	2%	7%	**22%**		1%	**15%**		5%	8%	2%	11%			3%	8%	
OS7a	0%	1%			1%				**18%**	5%		11%	11%				22%	8%	
OS7	2%	2%	2%	2%	2%			3%	36%	16%	**66%**		38%	11%	14%	27%	31%	33%	
OS6									8%	4%	5%	**49%**		16%		18%	19%	8%	
OS5			2%				1%		2%	1%	4%		**11%**		14%				
OS4													4%	**32%**					
OS3									2%			1%	9%						
OS2			1%						6%	4%	2%	7%	9%			**36%**		17%	
OS1	1%		1%						2%			4%	2%			9%	**9%**		
OS0					1%	3%								5%	71%				
Total Count	216	126	178	96	183	76	76	72	66	83	56	150	95	19	7	11	32	12	0

Notes: The table is read as follows: 49% of the time facies OS7 is preceded by facies OS6 (light gray boxes). Although there is a broad range in the vertical succession, the bold numbers represent the largest percentage, and dictate the sequential placement. Percentages calculated for lithofacies with a Total Count <30 (OS0-OS5) are less reliable. When a facies is followed by itself, it is dropped from the calculation (vertical striped shading). Two ''ideal'' cycles are represented by the vertical successions of lithofacies, the Outer Shelf (OS0-OS9) and the Shelf Crest (SC1-SC8). Facies OS9 (italics) represents the uppermost facies in the OS cycle, and is most commonly followed by OS1 and OS2 to begin a new cycle. Facie SC8 (italics) represents the uppermost facies in the SC cycle, and is most commonly followed by SC1 and SC2 to begin a new cycle.

Several analytical tools or techniques were used to examine the 2-D stacking patterns in McKittrick Canyon. *Lithologic analysis* and *facies proportion analysis* examine the changing percentage of a given lithology or facies preserved in each cycle, respectively. It can also be useful to examine the preservation of facies in transgressive (base-level rise) and regressive (base-level fall) hemicycles (Gardner 1993; Tinker 1996b, Kerans and Tinker 1997). *Facies offset analysis* examines changes in facies that interrupt the anticipated vertical (''Waltherian'') facies succession (e.g., a fusulinid packstone lying sharply above a pisolite rudstone represents a significant, non-Waltherian increase in depositional water depth). *Scintillometer* measurements provide data regarding the spatial variation in natural radioactivity. *Geochemical stratigraphy* looks at changes in a chemical signature (e.g., carbon isotopes) that can be indicative of stratigraphic and/or diagenetic processes. *Cycle thickness analysis* examines the spatial variation in thickness of each cycle. *Stratal geometry* provides information about depositional topography along dip, and when combined with other information, is an indicator of varying accommodation conditions through time.

A subsurface interpretation would proceed in much the same fashion as on the outcrop, using 1-D sedimentologic and facies data from logs and cores, and 2-D and 3-D data from seismic, interwell production tests, and predictive Walther's Law models. Multivariate (e.g., lithology, facies proportions, facies offsets, cycle thickness) stacking-pattern analysis performed on several wells provides a powerful tool for prediction of stratal geometry and facies distributions in 2-D and 3-D (Tinker 1996a; Kerans and Tinker 1997). Because the resolution of the 2-D and 3-D data in the subsurface is significantly lower than from continuous outcrops, the confidence in the subsurface interpretation is also lower. Tinker (1996a) provides examples of stratigraphic interpretation problems in the subsurface, and the subsequent impact on 3-D reservoir characterization.

The interpretation criteria, analytical ''tools'' used, and specific observations are discussed below for each of the stratigraphic elements in McKittrick Canyon.

Cycles

Field observations of facies (texture, grain composition and sedimentary structures), lithology, porosity, radioactivity, and the nature of the bounding contacts indicate crudely ordered (nonrandom) vertical successions. For example, OS8 commonly follows OS7; OS7 commonly follows OS6, and so on. These ordered successions were described as cycles in the field.

Statistical analysis of the facies database supports the field observations of facies successions (Table 2). Because facies were described every foot, successive feet commonly have repeating facies. For example, one foot of OS7 is most commonly preceded by another foot of OS7. However, when OS7 is not preceded by OS7, 49% of the time it is preceded by OS6. Using this kind of analysis, all of the facies were arranged in their most commonly observed vertical succession (Table 2, Fig. 13). When average lithology, porosity, radioactivity and texture are compared in the most common vertical facies succession, two stacking patterns are apparent (Tables 1, 2; Fig. 13), one for the shelf crest (SC) and one for the outer shelf (OS).

From the base up, the stacking pattern in the shelf crest (SC) setting consists of: (1) a sharp basal contact overlain by siltstones (9% porosity; SC1); (2) decreased siltstones and increased, thick-bedded, low-energy subtidal dolomudstones and dolowackestones (2–3% porosity; SC2, SC3); (3) planar-laminated to cross-laminated, moderate to high energy, subtidal lime to dolopackstones (4–6% porosity; SC4, SC6); (4) fenestral-laminated, peritidal dolowackestones (6% porosity; SC5); and (5) sheet-cracked, teepee, peritidal to supratidal dolorudstones (6% porosity; SC8). This pattern describes an initial increase and then dominant decrease in accommodation upward (Fig. 13).

In contrast to the shelf crest, the outer shelf (OS) has a greater proportion of subtidal facies. From the base up, the stacking pattern in the outer shelf (OS) setting consists of: (1) low- to moderate-energy dolomudstones to dolopackstones (4% porosity; OS3, OS4); (2) moderate- to high-energy subtidal dolopackstones and dolograinstones (5–10% porosity; OS5 through OS9); and (3) rare peritidal to supratidal dolowackestones capping

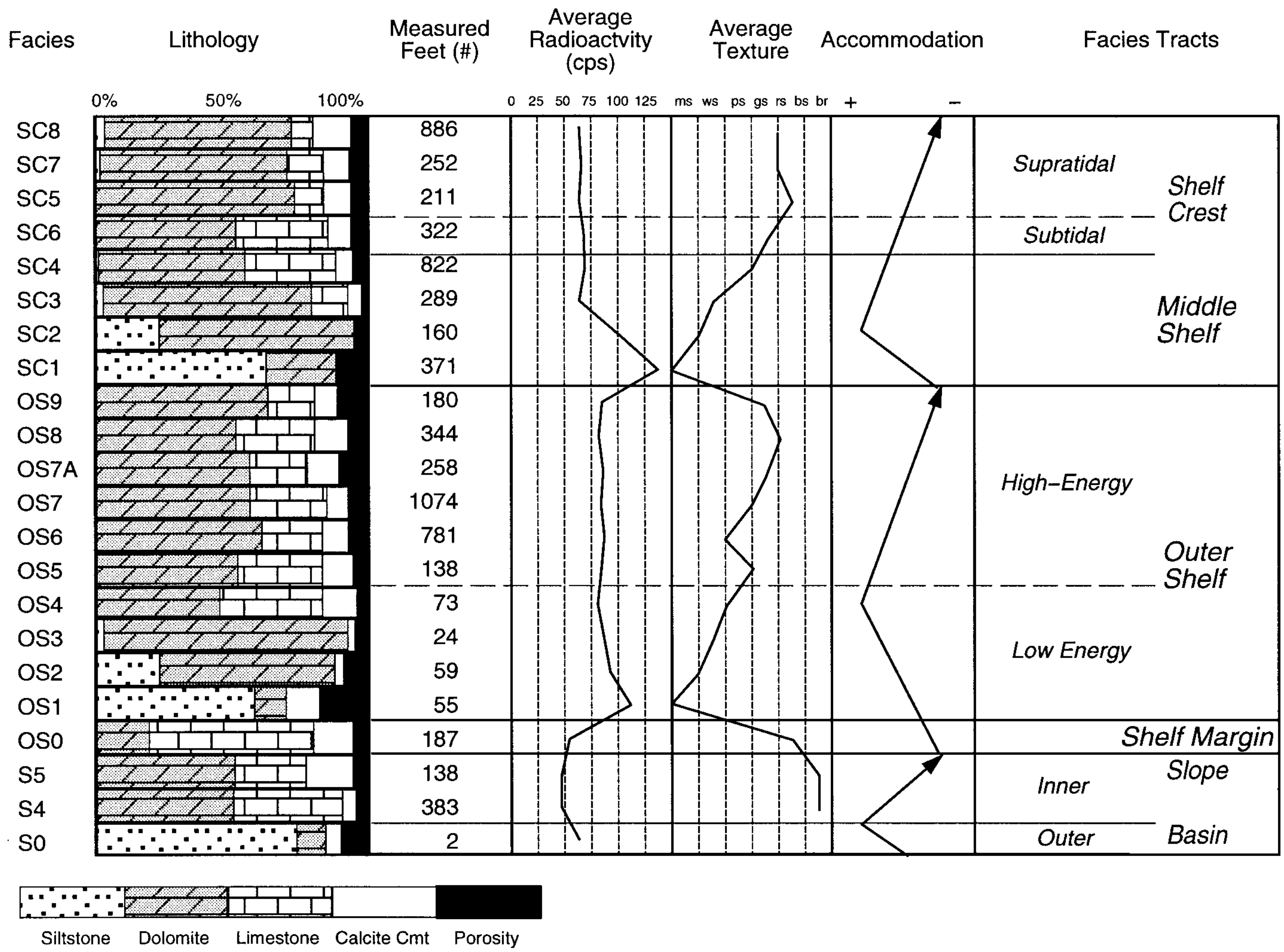

FIG. 13.—Stacking patterns as determined from lithology, porosity, radioactivity, and texture averages of the complete measured section database. Fa cies are arranged in terms of the most common vertical succession of facies (Table 2). Solid and dashed horizontal lines separate the facies into facies tracts. Lithology, porosity, radioactivity, and texture trends were used to help derive the accommodation interpretation.

the succession (Fig. 13). Like the shelf crest, the stacking pattern in the outer-shelf setting indicates an initial increase and then decrease in accommodation upward (Fig. 13). However, the increase in the proportion of subtidal facies in the outer shelf relative to the middle shelf supports a deeper-water interpretation for the outer shelf.

Cycle Sets

Cycle sets are defined by variations in facies, lithology, porosity, and thickness of component cycles. Whereas individual cycles may not be laterally continuous, cycle sets commonly can be traced across the dip width of the entire canyon wall. An initial deepening and then overall shallowing-upward succession of component facies, and a crude thinning-upward succession of component cycles characterize cycle sets. Cycle sets thicken towards the outer shelf, and have a thicker proportion of subtidal facies in their lower portions (Figs 8, 10, 11). Cycle sets can be defined using 1-D data alone, but 2-D data are valuable in order to document the basinward expansion and changing facies proportions.

Cycle sets in the Seven Rivers CS (Fig. 14) typically begin with a cycle dominated by siltstone or lime mudstone at the base, followed by a relatively thick succession of subtidal carbonate wackestone or packstone cycles, capped by thin shelf-crest supratidal rudstone and fenestral laminated cycles. The upper contact is commonly sharp, and is frequently overlain by a cycle dominated by siltstone or lime mudstone at the base of the subsequent cycle set.

Cycle sets in the Yates CS (Fig. 15) are considerably more amalgamated, and are either dominated by stacked subtidal cycles (Y2, Y3) or stacked intertidal to supratidal cycles (Y4, Y5). Cycle set boundaries in the amalgamated supratidal setting are interpreted where very thin mudstone or siltstone overlies erosionally truncated tepees.

HFSs and CSs

HFSs were defined using a combination of vertical variation in component cycle sets, facies, lithology, porosity, thickness, geochemical signature, and stratal geometry interpreted from the photomosaic and from lateral tracing of contacts in the field. CSs were defined using the same criteria, as well as variations in component HFSs.

1-D Data

HFS stacking patterns are defined on the shelf by an overall thickening and deepening (subtidal-dominated) succession of component cycle sets upward, interpreted to represent the TST, followed by an overall thinning

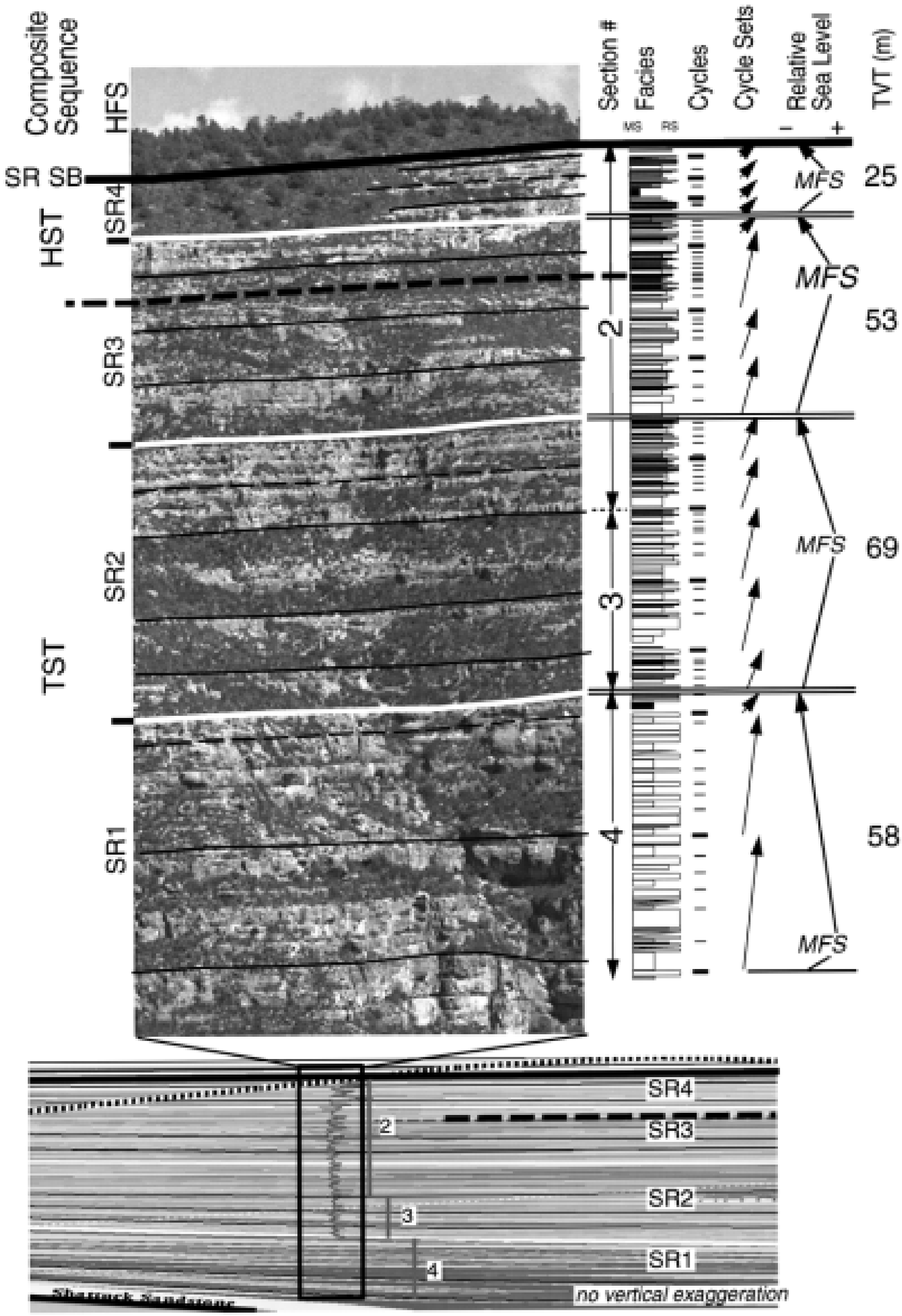

FIG. 14.—Stacking patterns illustrated using outcrop photograph and measured sections in the Seven Rivers CS. Location of measured sections 2, 3, and 4 o n the sequence-stratigraphic interpretation (Fig. 8) is shown in the window at the bottom of figure, which represents 600 m from left to right. True vertical thickness (TVT, in meters) illustrates the outcrop distortion from bottom to top.

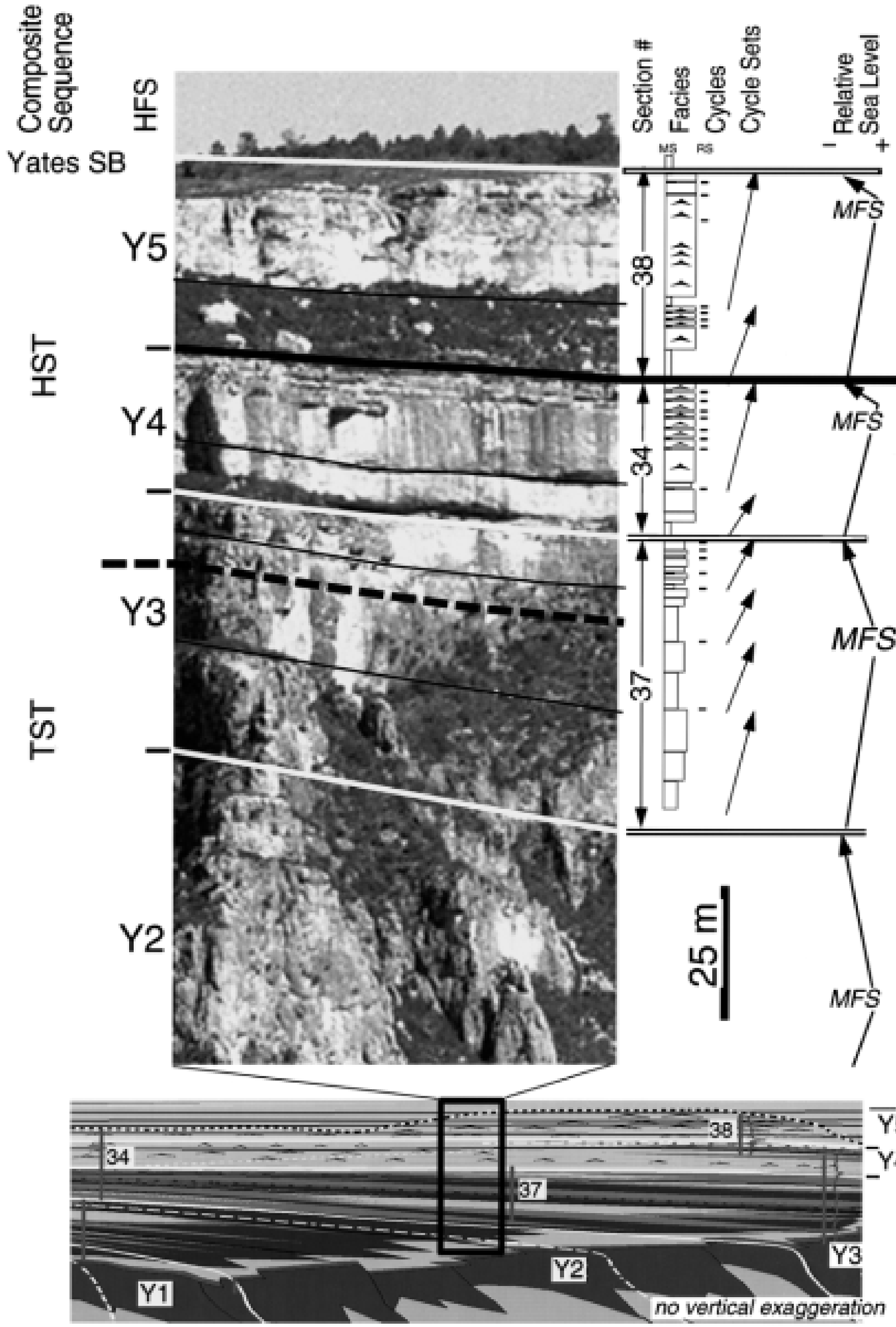

FIG. 15.—Stacking patterns in the Yates CS. Window at the bottom of figure represents 650 m from left to right. Measured sections 34, 37, and 38 are projected onto a single vertical section.

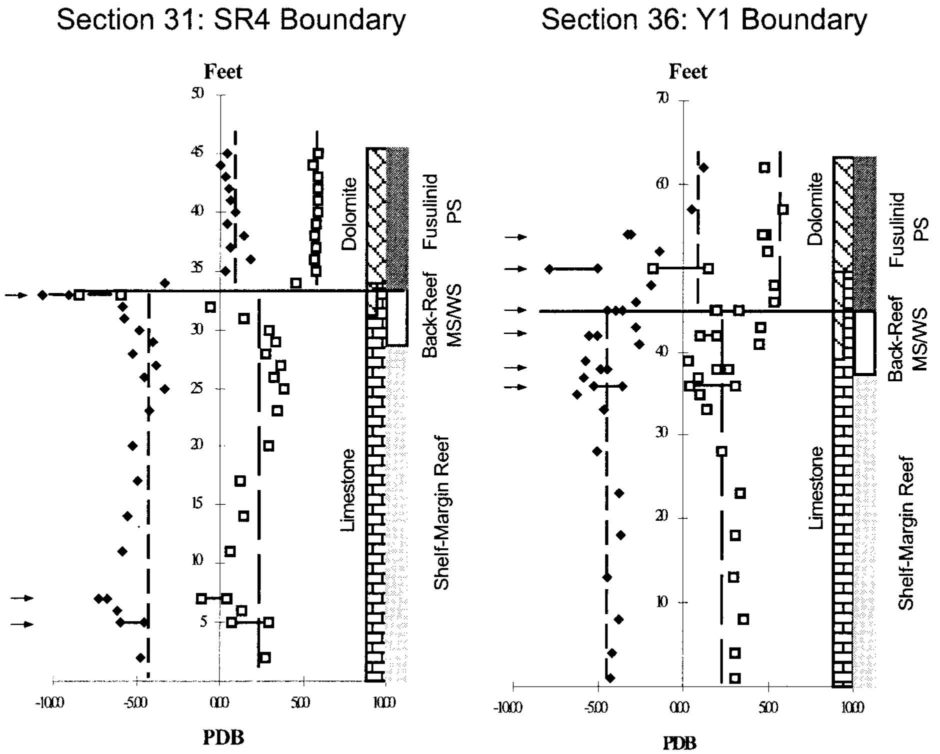

FIG. 16.—Geochemical stratigraphy. Vertical distribution of $\delta^{18}O$ (diamonds) and $\delta^{13}C$ (squares) in two reef transects, with dominant lithology and facies illustrated for each. Some hand samples were analyzed twice (indicated by arrows to left of each plot), using powder from two different areas of the sample. Vertical short-dashed lines indicate the approximate mean oxygen values (base line), and vertical long-dashed lines indicate the approximate mean carbon values (base line) for limestone and dolomite. Note the sharp boundary near the top of the limestone reef (33 feet; 10.1 m) in SR4 as compared to a more gradual transition (32 to 50 feet; 9.8–15.2 m) in Y1.

and shallowing (shelf-crest-dominated) succession of component cycle sets upward, interpreted to represent the HST (Figs. 14, 15). Comparison of 1-D sections shows that the proportion of TST versus HST tends to increase downdip within a HFS (Figs. 8, 10).

CS stacking patterns are characterized on the shelf by an overall thickening- and deepening-upward (subtidal dominated) succession of component HFSs (SR1 to SR2; Y1 to Y3; Figs. 8, 10, 14), followed by an overall thinning- and shallowing-upward (shelf-crest dominated) succession of component HFSs (SR2 to SR4; Y3 to Y4; Figs. 8, 10, 15). Using the 1-D data shown in Figure 14 alone, the CS MFS could be picked erroneously within SR2 instead of SR3, emphasizing the importance of analyzing multiple 1-D sections, and the added value of 2-D data.

Stable isotopes provide another important kind of 1-D data for identifying HFS and CS boundaries. Two vertical sample transects were made, one across the interpreted SR4 HFS boundary (Section 31; Figs. 6, 8), and one across the Y1 HFS boundary (Section 36; Figs. 6, 8). Microsamples (~ 3 mm diameter sample area) of the Capitan massive limestone and immediate back-reef dolostones were collected for stable-isotope analysis from the ''micritic'' part of each sample on the assumption that they were the most likely to preserve depositional and early diagenetic signatures (Given and Lohmann 1986).

The results for SR4 indicate a sharp, negative isotopic shift in $\delta^{18}O$ relative to an average base line near the top of the limestone reef, followed by an abrupt positive shift (~ 10‰) associated with passage into the dolomitized back-reef facies (Fig. 16). These $\delta^{18}O$ shifts relative to a base line exceed those reasonably expected from simple limestone-to-dolomite lithologic change (3–6‰; Land 1992). The pronounced negative shift at the top of the back reef, overlain by a positive shift across the SR4 (Seven Rivers CS) boundary, supports the possibility of subaerial exposure and depletion of the reef limestone by meteoric water prior to deposition and dolomitization of the overlying back reef sediment (*sensu* Allen and Matthews 1982). The results for Y1 show lower positive shifts in $\delta^{18}O$ (~ 7‰), and more gradual transitions (ranging over an 18-foot (5.5 m) interval), indicating little, if any, subaerial exposure at the shelf margin across this boundary.

The $\delta^{13}C$ response in SR4 shows a similar negative isotopic shift relative to an average base line near the top of the limestone reef, followed by an abrupt positive shift (~12‰) associated with passage into the dolomitized back reef facies (Fig. 16). This depleted response at the top of the reef could reflect the influence of a non-rock carbon source such as a biogenic soil zone, supporting the possibility of a subaerial exposure surface across the SR4 boundary. Additional work testing this hypothesis across other HFS boundaries is needed before definitive conclusions are drawn.

2-D Data

The 2-D distribution of four ''indicator'' facies, introduced in the Facies and Facies Tracts Section and described in the Depositional Model section, is critical for defining HFS and CS boundaries, maximum flooding surfaces (MFSs), and internal sequence architecture.

Siltstones.—Silts were delivered across the shelf during times of relative sea-level lowstand. Therefore, the 2-D position and spatial thickness variation of siltstones provide important criteria for sequence-stratigraphic interpretation. Thick siltstones with the greatest basinward extent help to define HFS and CS boundaries, because greater exposure time likely allowed for silt delivery farther across the shelf. Thin or absent siltstone helps to define HFS and CS maximum flooding, because the shoreline was pushed landward.

The base of the Seven Rivers CS boundary is marked by a thick (up to 10 m) siltstone, present across the complete outer shelf (Fig. 17). A thin (up to 3 m) siltstone that persists nearly to the shelf margin helps to define the upper SR1 HFS boundary (Fig. 17).

Two-dimensional stacking-pattern analysis of siltstones was used to help define the TST, MFS, and TST within each CS. Within the TST of the Seven Rivers CS, individual siltstones thin upward, the vertical distance between siltstones generally increases upward, and the downdip limit of siltstone preservation steps landward. Within the HST of the Seven Rivers

FIG. 17.—Distribution of siltstone and very fine sandstone in McKittrick Canyon. **A)** Y1–Y5 HFSs. **B)** Seven Rivers CS. Note the thickness increase of siltstones at HFS and CS boundaries, and the backstepping and thinning toward the MFS.

CS, individual siltstones thicken, the vertical distance between siltstones decreases, and the downdip limit of siltstone preservation steps basinward (Fig. 17). There is a 500-m basinward shift in siltstone position across the upper SR3 HFS boundary. Above the Seven Rivers CS boundary, a thick (up to 5 m) siltstone reaches to within 400 m of the shelf margin (Fig. 17).

Relative to the Seven Rivers, the Yates CS shows an overall increase in percentage of siltstone, thickness of individual siltstone bodies, and maximum basinward position of siltstone deposits (Fig. 17). In the Yates CS, siltstones are strongly aggradational in the HST (Y1, Y2, Y3) and strongly progradational in the HST (Y4).

The same general stacking pattern observed at the CS scale is repeated at the HFS scale in both the Seven Rivers and Yates CSs, whereby siltstones aggrade or step slightly landward toward the MFS, and step strongly seaward at HFS boundaries (Fig. 17). Two-dimensional stacking-pattern analysis is less reliable when applied to higher-frequency stratigraphic elements, because the effects of inherited topography and autocyclic processes can have a greater influence on deposition over the shorter time duration.

Shelf Crest.—Shelf-crest supratidal facies-tract deposits tended to fill the available accommodation. Therefore, the basinward edge of the shelf-crest facies tract can be used as a shoreline proxy to track movements of sea level (*sensu* Pomar 1993), and steps landward overall in the TST and seaward in the HST, at both the CS and HFS scales. The proportion of shelf-crest facies, the abundance and size of tepees, and the thickness of individual shelf-crest bodies are used as interpretation criteria as follows: abundance should decrease in the TST and increase in the HST at the CS scale; thick, amalgamated, aggradational shelf-crest deposits should represent HFS-scale TSTs deposited during early CS-scale transgression or late highstand; and the aspect ratio of shelf-crest sediment bodies should be lower (narrower and thicker deposits) in the TST compared to the HST of a HFS or CS.

At the CS scale, shelf-crest facies tracts aggrade during relative sea-level rise (TST) and prograde strongly during relative sea-level fall (HST). For example, in the Yates TST, the downdip position of the shelf-crest facies tract below the MFS (Y1 and Y2) is virtually the same (Fig. 18). Above the MFS, as accommodation decreased (Y3 and Y4), the shelf crest prograded significantly. By contrast, Y5 is shifted only 500 m basinward of Y4, has an aggradational stacking pattern of component cycles, and thus records the first HFS of the subsequent CS. This pattern is repeated at the HFS scale, whereby shelf-crest deposits aggrade or step slightly landward systematically in each TST (circles to squares in Figure 18), whereas they are strongly seaward stepping in each HST (squares to circles in Figure 18).

Outer Shelf.—Because the deepest-water shelf deposits are found in the outer shelf, the maximum landward position of this facies tract is used as an important criterion for defining CS and HFS-scale MFSs.

An interesting phenomenon occurs at the HFS and CS scale, whereby in the TST the shelf crest retrogrades at the same time the shelf margin progrades, causing the dip width of the intervening outer-shelf facies tract to expand bidirectionally (squares in Figure 18). In addition, there is a general decrease in outer-shelf width upward through the Seven Rivers, and again through the Yates CS, to a point where the shelf-crest facies tract is nearly coincident with the shelf margin by SR4 and Y5 time (Fig. 18).

Paleoecology provides additional data for sequence-stratigraphic interpretation. Using the analogy between the Permian fusulinids and the modern alveolines, it is reasonable to infer that the peloid–fusulinid WS/PS in the outer-shelf facies tract represents water depths in the range of 12 to 35 m. The water-depth interpretation indicates that the stratal geometries observed in the outer shelf are dominantly depositional in origin.

In addition, by analogy with the modern alveolinid morphology, the stratigraphic change from the large *Polydiexodina* (greater length-to-thickness ratios) in the Seven Rivers and Yates Formations to the smaller *Yabeina, Codonofusiella,* and *Reichelina* (lower length-to-thickness ratios) in the lower Tansill Formation indicates a progressive shallowing of water in the outer-shelf high-energy facies tract through time. The overall upward increase in abundance of *Mizzia*, a dasycladacean alga common in higher-energy, back-reef deposits (Kirkland and Moore 1990), from the Seven Rivers through the Yates CS also supports a shallowing profile through time.

Shelf Margin.—The paleoecology of the shelf-margin reef facies has been studied by several workers (Adams and Frenzel 1950; Achauer 1969; Babcock 1977; Yurewicz 1976, 1977; Kirkland and Moore 1990; Melim 1991; Kirkland et al. 1993; Wood et al. 1994; Kirkland 1995). Although the sedimentology and paleoecology cannot be used to determine specific water depths for the reef, documented faunal changes from the lower to the upper Capitan are interpreted to represent a shallowing of the reef through time (Babcock and Yurewicz 1989). The paleoecologic data are consistent with the water-depth interpretations from on the sequence-stratigraphic framework (see also Kerans and Tinker 1998).

The shelf-margin facies tract was used in conjunction with other shelf data to help define the TST, HST, and MFS at both the HFS and CS scales. The shelf margin prograded when accommodation was limited, and when there was an underlying slope foundation over which to prograde. Such conditions existed in the TST and late HST of the CS (Fig. 18). The shelf margin aggraded during times of maximum transgression, when the margin was trying to keep up with the accommodation being created during relative sea-level rise. Such conditions existed in the late TST and early HST of the CS (Fig. 18). These progradation/aggradation data, and several other stratigraphic parameters that emphasize the dynamic, yet systematic nature of the Capitan system, are quantified and discussed below.

DISCUSSION

Dynamic Stratigraphic and Sedimentologic Variations

The stratigraphic evolution of the Capitan depositional system can be examined by quantifying (Table 3) and visualizing (Figs. 19–21) several key depositional parameters. The shelf-crest (sea level), shelf-margin (shelf/slope break), and outer-slope facies tracts were used as bathymetric ‘‘tie points’’ (*sensu* Pomar 1993; Franseen et al. 1993) to calculate the following key depositional parameters: progradation and aggradation (and associated offlap angle) of the shelf-crest and shelf-margin facies tract; distance from the shelf crest to reef; reef depth; outer-shelf dip angle; and lateral distance and depth from the shelf crest to the toe of slope. Definitions for each of these parameters are contained in the footnotes of Table 3.

The more important variations in these depositional parameters are summarized for the shelf crest and shelf margin in Figures 19–21. These variations emphasize the dynamic nature of the Capitan system, and indicate that depositional styles were not random but varied systematically in time and space as a function of the HFS position within the longer-term CS (Table 3; Figs. 8, 10, 17–21). This type of dynamic system has been observed by other workers in a variety of carbonate and siliciclastic sediment environments (e.g., Wilkinson 1975; Galloway 1986; Grotzinger 1986; Cross et al. 1993; Gardner 1993; Sonnenfeld and Cross 1993; Kerans et al. 1994; Kerans and Fitchen 1995).

In a general sense, during marine transgression at the CS scale, shelf-crest deposits were thinner and retrogradational, outer-shelf deposits expanded in width, and shelf-margin deposits aggraded and prograded to ‘‘keep up’’ with a rising sea level. Commonly there was simultaneous retrogradation of the shelf crest and progradation of the shelf margin (Fig. 19). During highstand at the CS scale, shelf-crest deposits amalgamated and prograded as they filled available space, outer-shelf deposits narrowed in width, and shelf-margin deposits prograded. This same general pattern is observed at the HFS scale but varies as a function of position within the CS.

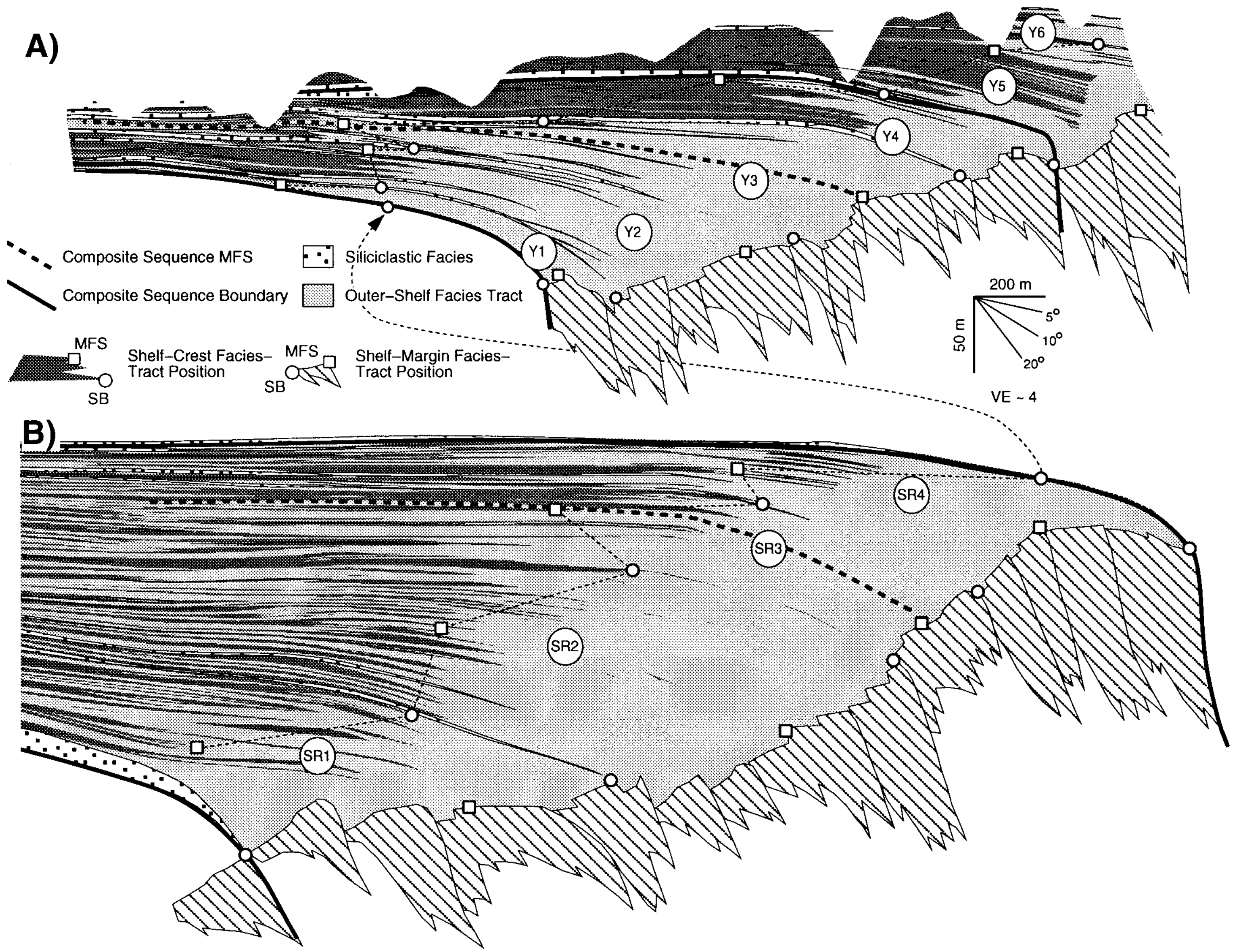

FIG. 18.—Generalized facies-tract distribution on the shelf in McKittrick Canyon. **A)** Y1–Y5 HFSs. **B)** Seven Rivers CS. The maximum basinward position of the shelf-crest facies and maximum landward position of the shelf-margin facies are marked for each HFS boundary (circles) and MFS (squares). Note the systematic backstepping of the shelf crest, broadening of the outer shelf, and aggradation of the shelf margin in the TST of each HFS (from circles to squares) and CS. The pattern is reversed in the HSTs (squares to circles). Note also the overall aggradational nature of the CS TST, and prodradational nature of the CS HST.

TABLE 3.—*Quantified Stratigraphic Data*

	Shelf Crest[1] Prograd. (meters)	Aggrad. (meters)	Pro/Agg	Offlap Angle[3] (degrees)	(vector)	Accum. Rate[4] HFS	(Bubnoffs)	Shelf Margin[2] Prograd. (meters)	Aggrad. (meters)	Pro/Agg	Offlap Angle (degrees)	(vector)	Accum. Rate[5] HFS	(Bubnoffs)	Shelf Crest to Reef (meters)	Depth of Reef (meters)	Outer Shelf Dip[6] (degrees)	Shelf Crest to Basin[7] (meters)	Depth to Basin[8] (meters)	Composite Sequence
Y5-HST	285	4	71	0.8		Y4	80	80	30	3	20.6		Y4	806	195	14	4.1	1387	618	
Y5-TST	288	28	10	5.6				235	38	6	9.2				405	41	5.8			SB
Y4-HST	432	-10	-43	-1.3		Y3	45	100	-9	-11	-5.1		Y3	650	446	44	5.6	1551	596	
Y4-TST	480	28	17	3.3				160	16	10	5.7				820	51	3.6			
Y3-HST	555	4	139	0.4		Y2	50	255	14	18	3.1		Y2	1142	1140	39	2.0	2280	593	MFS
Y3-TST	-255	16	-16	-3.6				200	28	7	8.0				1430	50	2.0			
Y2-HST	195	1	195	0.3		Y1	65	120	18	7	8.5		Y1	1206	1035	60	3.3	2139	601	
Y2-TST	-35	25	-1	-35.6				360	31	12	4.9				1045	70	3.8			
Y1-HST	275	-1	-275	-0.2		Y0	35	155	-15	-10	-5.5		Y0	476	645	76	6.7	1998	576	
Y1-TST	-285	15	-19	-3.0				35	6	6	9.7				765	63	4.7			SB
SR4-HST	855	-6	-143	-0.4		SR4	48	420	-15	-28	-2.0		SR4	1439	420	49	6.7	1889	576	
SR4-TST	-75	25	-3	-18.4				155	45	3	16.2				855	41	2.7			
SR3-HST	585	4	146	0.4		SR3	118	160	23	7	8.2		SR3	637	605	63	5.9	2350	568	MFS
SR3-TST	-220	43	-5	-11.1				90	26	3	16.1				1035	81	4.5			
SR2-HST	590	40	15	3.9		SR2	253	300	50	6	9.5		SR2	1999	730	64	5.0	2374	534	
SR2-TST	85	61	1	35.7				495	34	15	3.9				975	73	4.3			
SR1-HST	605	23	26	2.2		SR1-HFS	58	395	19	21	2.8		SR1-HFS	2566	560	45	4.6	2350	459	
SR1-TST								630	34	19	3.1				765	43	3.2			

(1) **Shelf Crest** (sea level proxy) is defined as the downdip limit of the shelf crest facies tract.
(2) **Shelf Margin** is defined as the updip limit of the shelf margin facies tract.
(3) **Offlap Angle** is illustrated in Figure 19, and is positive during times of prograding stratigraphic rise, and negative during times of prograding stratigraphic fall or retrograding stratigraphic rise.
(4) **Accumulation Rate** is the rate of sediment accumulation (Bubnoffs; meters/1000 years) calculated assuming a 400 k.y. HFS duration. Shelf Crest accumulation assumes horizontal time lines and vertical growth (sum of the aggradation component; Fig. 23).
(5) **Accumulation Rate** calculation for the shelf margin assumes dipping time lines and lateral growth (accounts for both the aggradation and progradation component; Fig. 23).
(6) **Outer Shelf Dip** is the primary stratigraphic dip angle of the outer shelf, measured along a vector from the shelf crest to the shelf margin (see Fig. 21).
(7) **Shelf Crest to Basin** is the horizontal distance from the shelf crest to the toe of slope (a point where where the basinward dip is less than ~5°).
(8) **Depth to Basin** is the vertical distance from the shelf crest to the toe of slope.

Summary by Composite Sequence

	Shelf Crest Pro (m)	Agg (m)	Pro/Agg	Pro (%)	Agg (%)	Shelf Margin Pro (m)	Agg (m)	Pro/Agg	Pro (%)	Agg (%)
Yates HST	1467	22	66.7	108%	28%	515	21	24.5	37%	24%
Yates TST	-105	56	-1.9	-8%	72%	870	68	12.8	63%	76%
7R HST	1365	23	59.3	56%	12%	735	53	13.9	28%	25%
7R TST	1060	167	6.3	44%	88%	1910	163	11.7	72%	75%

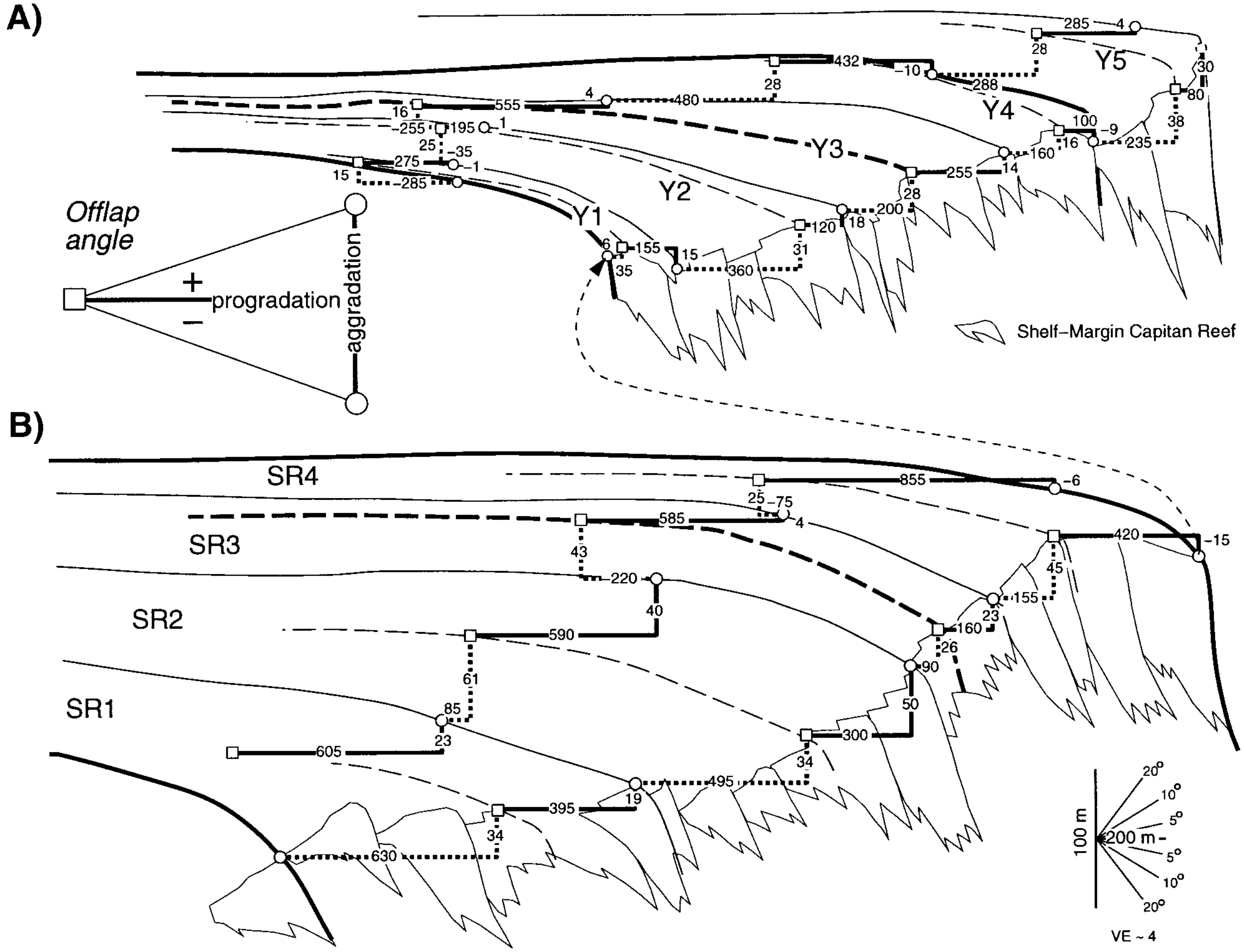

Shelf Crest

For each HFS, offlap angle and aggradation are greater in the TST than the HST.

In the TSTs of SR3, SR4, Y1, Y2, and Y3, the dip width of the outer shelf expands bidirectionally.

Shelf Margin

For every HFS except SR2, offlap angle and aggradation are greater in the TST than in the HST.

The P/A ratio of each HFS decreases toward the composite–sequence MFS, and then increases toward the upper composite–sequence boundary; concurrently the offlap angle increases and then decreases.

FIG. 19.—Method for determining progradation and aggradation distances of the shelf crest and shelf margin. Circles and squares are from Figure 18. Posi tive numbers represent basinward shifts or positive aggradation; negative numbers represent landward shifts or negative aggradation. Offlap angle is the angle between a horizontal line and the vector connecting a circle and square (see Table 3). Systematic changes are noted to the right of figure.

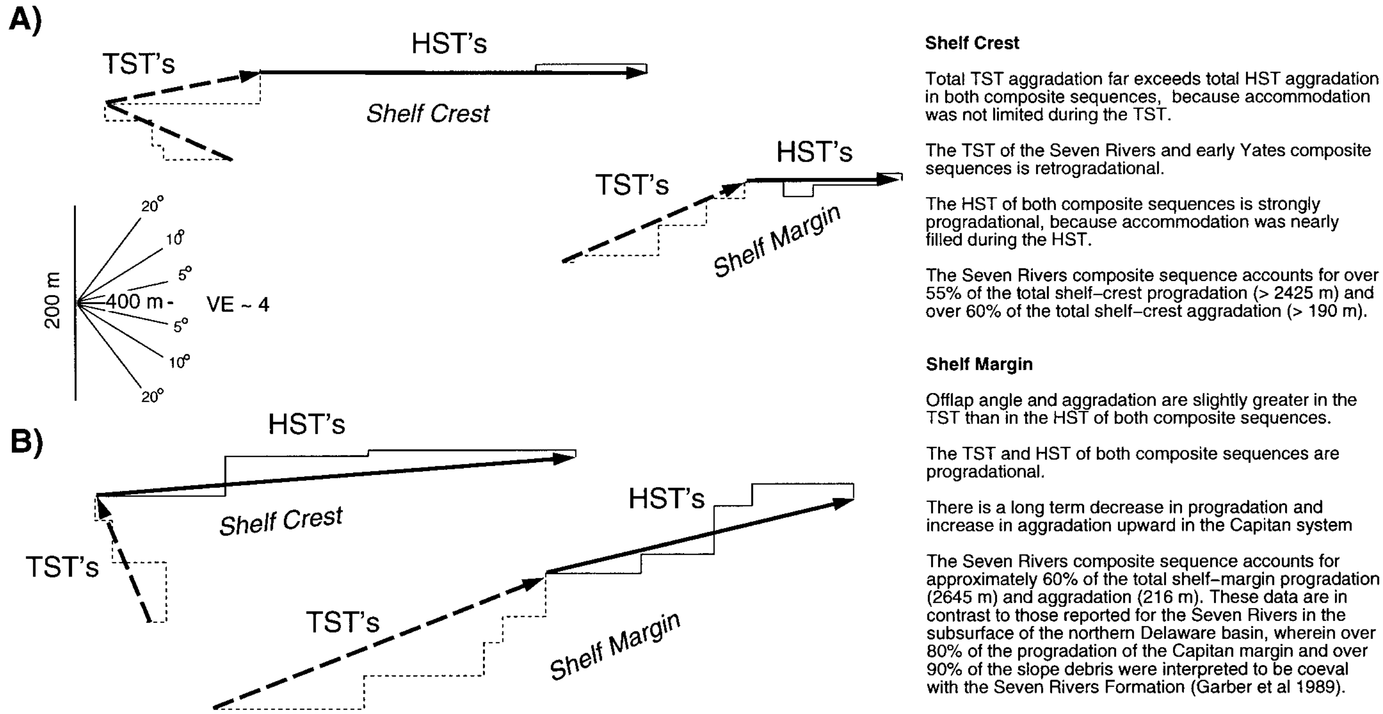

FIG. 20.—The dashed (TST) and solid (HST) lines from Figure 19 have been consecutively stacked to illustrate the cumulative TST and HST components for each CS. Note the simultaneous retrogradation/aggradation of the shelf crest and progradation/aggradation of the shelf margin during marine transgression (TST). Systematic changes are noted to the right of figure.

In addition to the variations highlighted by the depositional parameters (Figs. 19–21), several other systematic variations warrant mention.

(1) Low-energy facies dominate the HFS TST, whereas higher-energy facies dominate the HFS HST. This is interpreted to be the result of higher-energy wave and tidal currents in the shallow-water deposits of the HST.

(2) Individual cycles are easier to define in the Seven Rivers CS (Fig. 14) because accommodation conditions favored high-frequency subtidal–supratidal facies alternations. By contrast, in the Yates CS (Fig. 15) accommodation conditions favored amalgamation of fusulinid facies in the subtidal setting (Y2, Y3), and of pisolite facies in the supratidal setting (Y4, Y5).

(3) Shelf-crest facies-tract deposits amalgamated and aggraded (up to 30 m) when the TST of a HFS was in phase with the HST of a CS (TST of SR4, Y4) because HFS-scale transgression created the necessary accommodation for aggradation (Fig. 18; see also Kerans and Harris 1992). By contrast, when the HST of a HFS was in phase with the HST of a CS (HST of SR4, Y4), accommodation was limited, and shelf-crest deposits were thinner and prograded basinward. Regardless of position within the HFS, shelf-crest facies-tract deposits are commonly thin and discrete, and often backstep in the TST of a CS (SR1, SR2, SR3, Y1, Y2, and Y3), owing to conditions of high accommodation. The exception is Y5, which contains a significant thickness of aggradational shelf-crest facies deposited in the first HFS of the Tansill composite sequence.

(4) When the HSTs of a HFS and composite sequence were in phase (SR4 and Y5), the dip width of the outer-shelf facies tract was compressed, outer-shelf facies diversity was great, much of the outer shelf accommodation was filled, and the likelihood of protracted subaerial exposure of the shelf crest was maximized (Figs. 8, 10).

(5) During HFS transgression, facies in the outermost shelf were dominantly aggradational or backstepping, and shelf-margin facies were aggradational, as sediment production tried to keep pace with increasing accommodation created by rising relative sea level. During HFS highstand, sediment production rates exceeded available accommodation, and facies in the outer-shelf and shelf margin were dominantly progradational, as indicated by the progradation:aggradation ratios (Table 3; Figs. 8, 19).

(6) The negative progradation:aggradation ratios recorded in the HST of SR4 represent a time of downstepping or stratigraphic fall (Table 3; Fig. 19). This stratigraphic signature can be indicative of extremely limited accommodation caused by relative sea-level fall (see also Sonnenfeld and Cross 1993). When combined with other stratigraphic and facies data, this geometry supports the interpretation of the upper Seven Rivers composite-sequence boundary.

(7) The Y1 HFS can be interpreted either as the last HFS of the Seven Rivers CS, deposited as a shelf-margin systems tract (*sensu* Van Wagoner et al. 1988) during relative sea-level fall, or as the first HFS of the Yates CS, deposited during the initial Yates transgression, which was not of sufficient magnitude to completely flood the shelf (Fig. 8). Although the depositional environment would be similar in either interpretation, the major Yates CS boundary would be above Y1 in the first interpretation and below Y1 in the second interpretation. Geochemical stratigraphy (Fig. 16) supports the second interpretation.

(8) Although mud- and silt-dominated rocks (OS1-OS3) represent only a minimal volume of the outer-shelf facies tract (Fig. 13), they are significant because 60–80% of the time they are preserved within the TST of a HFS (Fig. 8).

(9) The Seven Rivers CS contains a greater volume of subtidal deposits than does the Yates CS, because outer-shelf accommodation was greater (Fig. 8).

These variations illustrate that care must be taken when applying interpretations from a limited geographic window to a basin-wide scale. Similarly, using the detailed facies architecture interpretations as an analog for interpretation of older or younger stratigraphic units must be done with care.

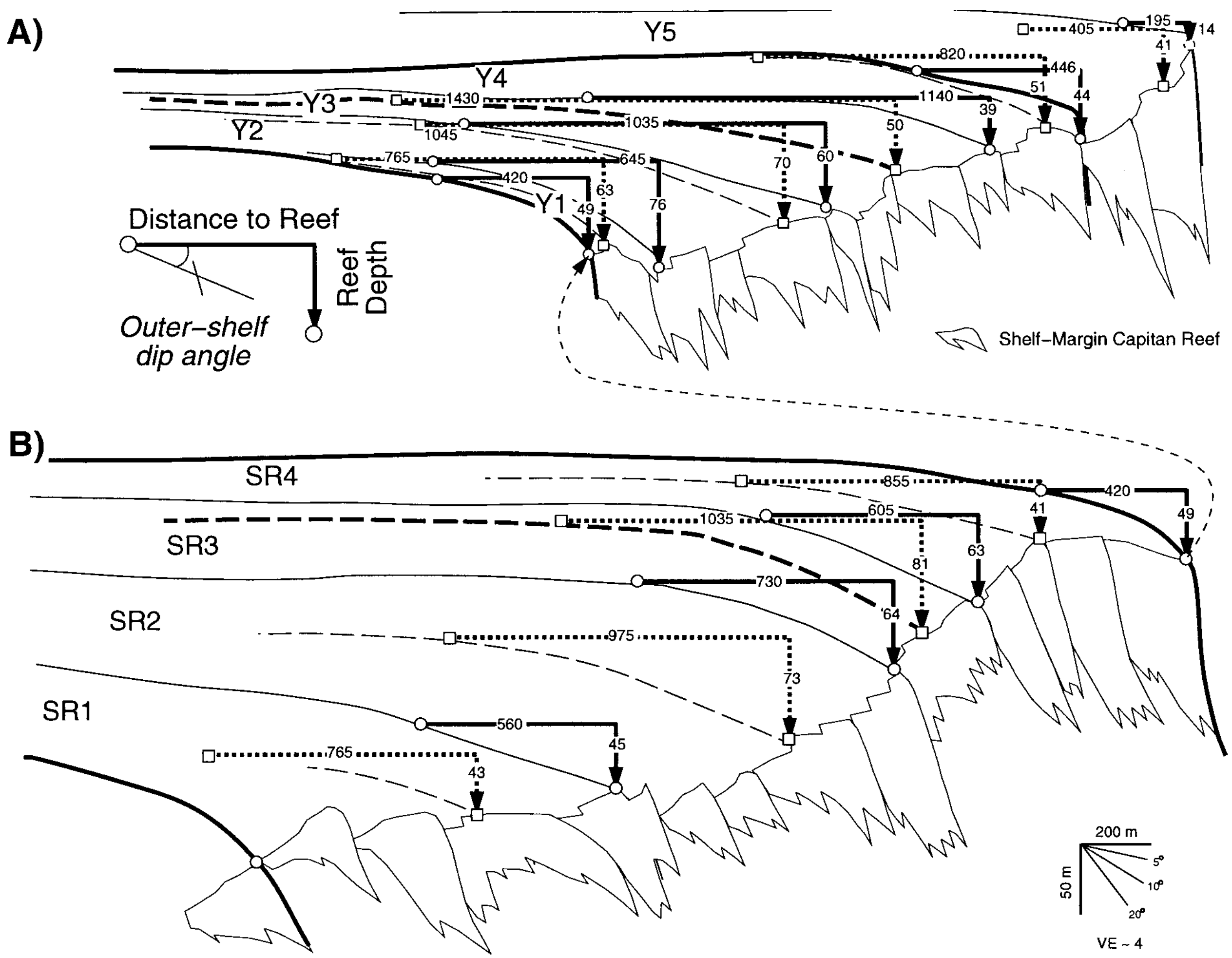

The distance from shelf crest to reef is greater at the MFS than the sequence boundary of every HFS.

The depth to reef increases in the TST and decreases in the HST of the Seven Rivers and Yates composite sequences.

The outer–shelf dip angle ranges from 2 to 7 degrees, and tends to decrease at the MFS and increase at the sequence boundary of a composite sequence.

There is an overall decrease in reef depth, distance to outer shelf from SR1 through Y4, and outer shelf dip angle.

FIG. 21.—Method for determining distances from the shelf crest to the shelf margin, and reef depths. Circles and squares are from Figure 18. These numbers are represented in Table 3. Systematic changes are noted to the right of figure.

Paleobathymetric Models

Although the Capitan depositional system has been studied extensively, the interpretation of its paleobathymetric profile remains somewhat controversial. There are two viable end-member models, the marginal mound and the barrier reef. Early investigators converged on a barrier-reef hypothesis (Crandall 1929; Lloyd 1929), and later studies supported this model (Newell et al. 1953; Hayes 1957, 1964; Boyd 1958). Dunham (1972) argued for a marginal-mound hypothesis, for which he gave credit to Lang (1937). In this model, shallow-subtidal carbonate grainstones were deposited downdip from topographically high, intertidal to supratidal, shelf-crest deposits. Subsequent workers in the 1970s and 1980s tended to support the marginal-mound hypothesis (Babcock 1977; Pray 1977; Yurewicz 1977; Hurley 1978, 1979, 1989). However, Kirkland and Moore (1990) and Kirkland (1995) resurrected a modified version of the barrier-reef model on the basis of studies of the upper Yates and Tansill-equivalent reef and outer shelf. Saller (1996) argued in support of this revision. Hunt et al. (1995) proposed a flat-topped platform created prior to ''differential compaction-induced subsidence'', resulting in toplap geometries.

The critical issue regarding paleobathymetry is whether the present-day outer-shelf dip is primary or secondary. If the paleobathymetric profile was a marginal mound and the outer-shelf basinward dips are primary, then the facies and stratigraphic architecture of the outer shelf should indicate a progressive deepening towards the margin. If the paleobathymetric profile was a barrier reef (flat-topped platform), and the outer-shelf dip was caused by syndepositional or postdepositional tilting of once flat-lying outer-shelf beds (Smith 1973) or early differential compaction of the underlying slope (Hunt et al. 1995, Saller 1996), then the opposite relationships should be found.

Data from McKittrick Canyon indicate that the Capitan paleobathymetric profile was a marginal mound. However, the depth to the top of the shelf margin and associated outer-shelf dips increased and then decreased substantially within each CS, and decreased overall from the Seven Rivers through the Tansill, such that by Tansill time the shelf-margin reef was deposited in relatively shallow water. Key observations and interpretations include: (1) the progression from high-energy, supratidal-capped cycles in the shelf crest to lower-energy, subtidal-capped, fusulinid-rich cycles in the outer shelf (Figs. 8, 9), which would not exist in a flat-topped model; (2) an expansion of cycle-set thickness downdip across the outer shelf (Figs. 9, 11, 12), which could not exist in a flat-topped model; (3) *systematic* changes in progradation and aggradation, offlap angles, shelf crest to reef distance, reef depth, and outer-shelf dip angle at both the HFS and CS scale that can be correlated around the basin (Osleger 1998; Osleger and Tinker in press), resulting in a stratigraphic organization that would be very difficult to produce with postdepositional tilting or differential compaction; (4) outer-shelf water depths in the range of 12 to 35 m on the basis of analogy with the modern alveolinids, and reef water depths ranging from 14 to 81 m; (5) oriented fusulinid grainstones near the shelf margin, indicating mobilization and probable sediment-gravity-flow transport of fusulinids into water depths greater than 12–35 m; (6) the abundance of the shallow reef indicator *Mizzia* in the upper Yates and Tansill CSs relative to the Seven Rivers CS, indicating progressive shallowing of the Capitan system; (7) the decrease in percent dolomite from the shelf crest to the shelf margin (also see Melim 1991); and (8) the absence of true toplap stratal geometries. Differential compaction or postdepositional tilting of an original flat-topped shelf-margin barrier reef system cannot explain this combination of facies and stratigraphic data.

Testing An Alternative Model.—If the differential compaction model were viable, then the late Yates HFSs, which were deposited above slope clinoforms with nearly 400 m of total relief, should have compacted more than the early Seven Rivers HFSs, which were deposited above clinoforms with less than 150 m of relief, resulting in greater outer-shelf dips in the upper Yates. The opposite is observed (Table 3; Fig. 21).

To test the postdepositional compaction hypothesis, the mechanics of differential compaction were examined graphically with data from a 50–100-m thick interval in the SR2 HFS. This type of analysis requires translation of photo thickness to true vertical thickness. Present-day stratal geometries illustrate the outer-shelf dip and proportional bed-thickness expansion from the shelf crest to the shelf margin (Fig. 22A, B). The same cycle thickness is illustrated for a ''barrier reef'' model (Fig. 22C). The vertical compaction vectors necessary to change the lower, pre-compaction boundary in the barrier-reef model (L2) to the observed geometry (L1) are illustrated in Figure 22D. The same compaction history, even if it was very early, must also have acted on the upper surface (U2) of the barrier-reef model. However, when the vertical differential compaction vectors determined for the lower barrier-reef boundary are applied to its upper surface (U2), the result (U?, Fig. 22E) looks nothing like the observed bedding clinoforms (U1, Fig. 22B). This simple data-driven graphic illustrates the untenable nature of the compaction hypothesis when applied to the Seven Rivers and Yates CSs in McKittrick Canyon.

Sediment Accumulation Rates, Sites, and Variation

Sediment accumulation volumes are controlled by the ratio of accommodation to sediment supply (e.g., Swift and Thorne 1991; Cross et al. 1993). In a simple system, as the ratio of accommodation to sediment supply decreases, the volume of sediment that can be accumulated at a given geographic/bathymetric location decreases, because more sediment is available than space. This commonly results in progradation. By contrast, when the accommodation:sediment supply ratio increases, the volume of sediments that can accumulated at a given geographic/bathymetric location increases. This can result in aggradation or backstepping.

In terms of direct comparative value, sedimentation-rate calculations are limited, because they require an estimate of the depositional duration for each stratigraphic interval of interest. Assuming that the late Guadalupian represents approximately 2 to 3 my (Ross and Ross 1987), each of the eight Seven Rivers and Yates HFSs represent from 250 to 375 ky. Accumulation rates, uncorrected for compaction or missing rock, were calculated in McKittrick Canyon along a vector perpendicular to growth direction in all locations (Fig. 23). To be conservative, values were calculated using a 400 ky duration for each HFS.

Results indicate that Seven Rivers accumulation rates are generally greater than Yates accumulation rates (Fig. 23). This can be explained, in part, by the fact that Yates HFSs contain significantly more accommodation-limited shelf-crest supratidal facies than do the Seven Rivers HFSs, resulting in considerably greater periods of slow deposition, nondeposition, or erosion. Particularly noteworthy is that the shelf-margin accumulation rates are at least one order of magnitude greater than those calculated for the outer shelf (Fig. 23).

The sediment accumulation data from McKittrick Canyon are significant for two reasons. First, the high accumulation rates in the outer shelf and especially the shelf margin (20–80 m water depth), relative to the middle shelf and shelf crest ($<$ 10 m water depth), are significantly different from commonly accepted models that report the greatest sedimentation rates in the warm, shallow waters of the inner to middle shelf (e.g., Tucker and Wright 1990; Enos 1991). It is important to emphasize that most of the sediment accumulated in the outer shelf was locally sourced, and not transported to the outer shelf from the middle or inner shelf. Second, sediment accumulation rates in dominantly subtidal settings, such as the outer shelf in McKittrick Canyon, were high in both the TST and the HST, which contrasts with many reports of HST-dominated production for other carbonate shelf models (e.g., Coogan 1969; Wilson 1975; James 1979, 1984; Wilkinson 1982; Sarg 1995).

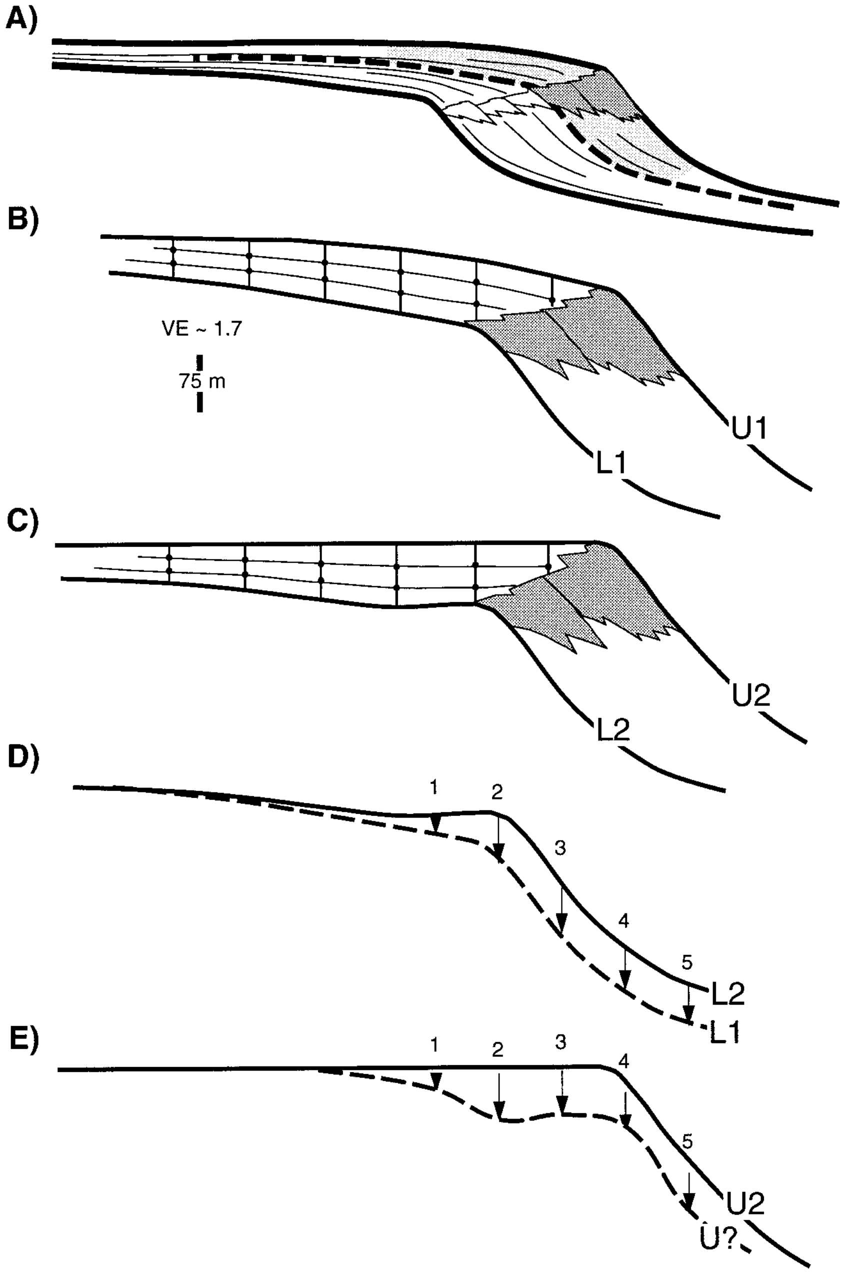

FIG. 22.—Illustration of the inability of differential compaction to explain outer-shelf dip geometries. **A)** SR2 HFS with HST detail area shown in (B) shaded light gray and shelf margin shaded dark gray. **B)** Detail area from (A) showing observed stratal geometries and bed thickness relationships. L1 is lower bounding surface and U1 is upper bounding surface. Three cycle sets are illustrated. **C)** Reinterpretation of (B) using same thickness but with a pre-compaction, ''barrier-reef'' geometry. L2 and U2 are the pre-compaction lower and upper bounding surfaces for this model. **D)** Vertical differential compaction vectors necessary to change L2 pre-compaction geometry to L1 observed geometry. **E)** Vertical differential compaction vectors from (D) applied to U2 result in U?, which does not resemble the U1 observed geometry at all, but should if the compaction model were valid.

CONCLUSIONS

The sequence-stratigraphic interpretation presented in this work documents a high degree of stratigraphic order in the Capitan depositional system, reflected by systematic changes in facies distributions, facies proportions, stratal geometries, and progradation:aggradation ratios. These parameters were quantified using a 2-D facies distribution and stratal geometry ''map'' of the 5-km continuous outcrop wall in North McKittrick Canyon, and would be difficult to work out from a more limited stratigraphic or geographic window. The sequence-stratigraphic interpretation resulted in a revised outer shelf and shelf-to-basin correlation (see Tinker 1996b for a detailed description of shelf-to-basin stratigraphic correlations; compare Figure 3 to the frequently referenced cross sections of King 1948 and Garber et. al. 1989).

The systematic evolution documented in McKittrick Canyon is hierarchical (repeated at several scales). Within a high-frequency sequence (HFS), the dip width of the shelf-crest facies tract decreases upward to the maximum flooding surface (MFS) and increases upward to the HFS boundary, whereas the dip width of the outer-shelf facies tract and the angle of outer-shelf basinward dip increase upward to the MFS and decrease upward to the upper sequence boundary. This pattern is repeated at the CS scale. The aspect ratios of shelf-crest sediment bodies tend to be lower (narrower and thicker deposits) in the transgressive systems tract (TST) than in the highstand systems tract (HST) of HFSs and CSs. The progradation/aggradation ratio decreases toward the MFS and then increases toward the upper sequence boundary at both the HFS and CS scales. The distance from shelf crest to reef and the interpreted water depth to the reef is greater in the TST than the HST of HFSs and CSs.

The sequence-stratigraphic interpretation in McKittrick Canyon provides several important results. First, all of the data, including facies associations, cyclicity, stratal geometry, and paleoecology, support a marginal-mound

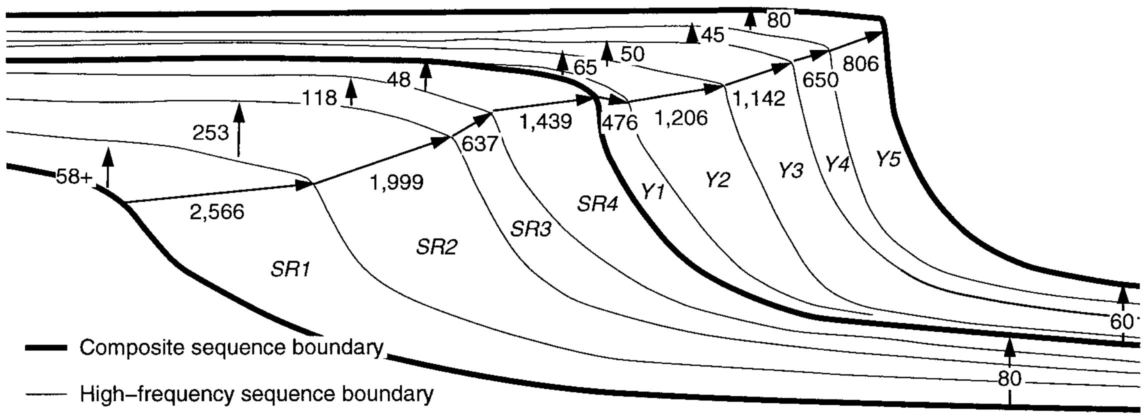

FIG. 23.—Accumulation rates, uncorrected for compaction or missing rock, calculated along a vector perpendicular to interpreted growth direction. Va lues are based on an estimated 400 ky HFS duration, and reported in Bubnoffs (μm/yr; mm/1000 yr).

depositional model in which the shelf-margin reef is located downdip from the shelf-crest facies tract. However, there was an initial increase and then decrease in water depth at the shelf margin within each composite sequence, and an overall decrease in water depth from Seven Rivers through Tansill time. Second, predictable variations in the quantified depositional parameters such as progradation, aggradation, offlap angle, outer-shelf dip, water depth, and distance between facies tracts emphasize the dynamic yet systematic nature of the Capitan system. A stratigraphic hierarchy similar to that from McKittrick Canyon has been documented along strike (Osleger and Tinker in press), which strengthens the overall interpretation and helps document the basinwide evolution of the Capitan system. Third, the most active sediment production and accumulation sites were located in the subtidal, outermost-shelf and shelf-margin facies tracts of both the TST and HST. This is significantly different from commonly accepted models that report the greatest sedimentation rates in the warm, shallow ($<$ 10 m) waters of the inner and middle shelf (e.g., Tucker and Wright 1990; Enos 1991). Fourth, the high accumulation rates support the possibility of a relatively complete shelf-margin sedimentation and accumulation record, which results in a comparatively equal (''symmetrical'') TST and HST sediment-preservation record on the shelf and across the shelf margin. This record is different from many asymmetric, HST-dominated shoaling-upward carbonate sedimentation models (e.g., Coogan 1969; Wilson 1975; James 1979, 1984; Wilkinson 1982; Sarg 1995). Finally, the 2-D cycle hierarchy, facies distributions, and general timing of siliciclastic sediment bypass into the basin can be worked out from vertical 1-D data. However, in contrast to flat or low-angle ramps and shelves, the 2-D prediction of facies and stratal geometries in a shelf-margin setting requires a depositional model that includes information regarding the paleobathymetric profile.

ACKNOWLEDGMENTS

I would like to thank Marathon Oil Company for permission to publish this work, and for financial support for the color figures, fieldwork, and laboratory work. Sincere thanks to the following: the staff at Guadalupe National Park, especially Fred Anderson, and the staff at the Lincoln National Forest, for permission to conduct field work in McKittrick Canyon; David Budd, Charlie Kerans, Mark Sonnenfeld, Neil Hurley, Emily Stoudt, Julie Kupecz, Laura Zahm, and John Southard for thoughtful reviews and excellent suggestions for improvement of the manuscript; Jerry Lucia and Charlie Kerans at the Texas Bureau of Economic Geology for providing the original helicopter photographs; D. Henry at Digital Video Productions for the final mosaic created in PHOTOSHOP™; Charlie Kerans and Lisë Brinton for lively discussions in the field; field assistants Mark Tinker, Chris Stephenson, Allyson Tinker, and Clint Cowan; David Budd and Scott Raymond for support during crunch time; and Allyson, Nathan, Derek, and Tyler, too.

REFERENCES

ACHAUER, C.W., 1969, Origin of Capitan Formation, Guadalupe Mountains, New Mexico and Texas: American Association of Petroleum Geologists, Bulletin, v. 53, p. 2314–2323.

ADAMS, J.E., AND FRENZEL, H.N., 1950, Capitan barrier reef, Texas and New Mexico: Journal of Geology, v. 58, p. 289–312.

ALLEN, J.R., AND MATTHEWS, R.K., 1982, Isotope signatures associated with early meteoric diagenesis: Sedimentology, v. 29, p. 797–817.

BABCOCK, J.A., 1977, Calcareous algae, organic boundstones, and the genesis of the Upper Capitan Limestone (Permian, Guadalupian), Guadalupe Mountains, West Texas and New Mexico, *in* Hileman, M.E., and Mazzullo, S.J., eds., Upper Guadalupian Facies, Permian Reef Complex, Guadalupe Mountains, New Mexico and West Texas: 1977 Field Conference Guidebook, v. 1, Permian Basin Section SEPM, Publication 77–16, p. 3–44.

BABCOCK, J.A., AND YUREWICZ, D.A., 1989, The massive facies of the Capitan Limestone, Guadalupe Mountains, Texas and New Mexico, *in* Harris, P.M., and Grover, G.A., eds., Subsurface and Outcrop Examination of the Capitan Shelf Margin, Northern Delaware Basin: SEPM, Core Workshop 13, p. 365–372.

BEBOUT, D.G., AND KERANS, C., eds., 1993, Guide to the Permian Reef Geology Trail, McKittrick Canyon, Guadalupe Mountains National Park, West Texas: Texas Bureau of Economic Geology, Guidebook 26, 48 p.

BORER, J.M., AND HARRIS, P.M., 1989, Depositional facies and cycles in Yates Formation outcrops, Guadalupe Mountains, New Mexico, *in* Harris, P.M., and Grover, G.A., eds., Subsurface and Outcrop Examination of the Capitan Shelf Margin, Northern Delaware Basin: SEPM, Core Workshop 13, p. 305–317.

BORER, J.M., AND HARRIS, P.M., 1991, Facies and cyclicity of the Yates Formation, Permian Basin: Implications for reservoir heterogeneity: American Association of Petroleum Geologists, Bulletin, v. 75, p. 726–779.

BOYD, D.W., 1958, Permian sedimentary facies, central Guadalupe Mountains, New Mexico: New Mexico Bureau of Mines and Mineral Resources, Bulletin 49, 100 p.

BROWN, A.A., AND LOUCKS, R.G., 1993, Influence of sediment type and depositional processes on stratal patterns in the Permian basin-margin Lamar limestone, McKittrick Canyon, Texas, *in* Loucks, R.G., and Sarg, J.F., eds., Carbonate Sequence Stratigraphy: Recent Developments and Applications: American Association of Petroleum Geologists, Memoir 57, p. 435–474.

CANDELARIA, M.P., 1982, Sedimentology and depositional environment of Upper Yates Formation siliciclastics (Permian, Guadalupian), Guadalupe Mountains, southeast New Mexico [unpublished M.S. thesis]: University of Wisconsin, Madison, Wisconsin, 267 p.

CHOQUETTE, P.W., AND PRAY, L.C., 1970, Geologic nomenclature and classification of porosity in sedimentary carbonates: American Association of Petroleum Geologists, Bulletin, v. 54, p. 207–250.

COOGAN, A.H., 1969, Recent and ancient carbonate cyclic sequences, *in* Cyclic Sedimentation in the Permian Basin, 1st Edition: Midland, Texas, West Texas Geological Society, p. 5–27.

CRANDALL, K.H., 1929, Permian stratigraphy of southeastern New Mexico and adjacent parts of western Texas: American Association of Petroleum Geologists, Bulletin, v. 13, p. 927–944.

CREVELLO, P.D., 1991, High-frequency carbonate cycles and stacking patterns: interplay of orbital forcing and subsidence on Lower Jurassic rift platforms, High Atlas, Morocco, *in* Franseen, E.K., Watney, W.L., Kendall, C.G.St.C., and Ross, W., eds., Sedimentary Modeling: Computer Simulations and Methods for Improved Parameter Definition: Kansas Geological Survey, Bulletin 233, p. 207–230.

CROSS, T.A., BAKER, M.R., CHAPIN, M.A., CLARK, M.S., GARDNER, M.H., HANSON, M.S., LESSENGER, M.A., LITTLE, L.D., MCDONOUGH, K.J., SONNENFELD, M.D., VALASEK, D.W., WILLIAMS, M.R., AND WITTER, D.N., 1993, Applications of high-resolution sequence stratigraphy to reservoir analysis, *in* Eschard, R., and Doligez, B., eds., Subsurface Reservoir Characterization from Outcrop Observations: 7th Institute of French Petroleum Exploration and Production Conference, Proceedings, p. 11–33.

Drummond, C.N., and Wilkinson, B.H, 1993; Carbonate cycle stacking patterns and hierarchies of orbitally forced eustatic sea level change: Journal of Sedimentary Petrology, v. 63, p. 369–377.

Dunham, R.J., 1962, A classification of carbonate rock types according to depositional texture, *in* Ham, W.E., ed., Classification of Carbonate Rocks: American Association of Petroleum Geologists, Memoir 1, p. 108–122.

Dunham, R.J., 1972, Capitan Reef, New Mexico and Texas: facts and questions to aid interpretation and group discussion: Society of Economic Paleontologists and Mineralogists, Permian Basin Section, Publication 72–14, 291 p.

Embry, A.F., and Klovan, J.E., 1971, A late Devonian reef tract on northeastern Banks Island, N.W.T.: Bulletin of Canadian Petroleum Geology, v. 19, p. 730–781.

Enos, P., 1991, Sedimentary parameters for computer modeling, *in* Franseen, E.K., Watney, W.L., Kendall, C.G.St.C., and Ross, W., eds., Sedimentary Modeling: Computer Simulations and Methods for Improved Parameter Definition: Kansas Geological Survey, Bulletin 233, p. 63–99.

Esteban, M., and Pray, L.C., 1983, Pisoids and pisolite facies (Permian), Guadalupe Mountains, New Mexico and West Texas, *in* Peryt, T.M., ed., Coated Grains: New York, Springer-Verlag, p. 503–537.

Fitchen, W.M., Starcher, M.A., Buffler, R.T., and Wilde, G.L., 1995, Sequence stratigraphic framework of lower Permian carbonate platform margins, Sierra Diablo, west Texas, *in* Garber, R.A., and Lindsay, R.F., eds., Wolfcampian–Leonardian Shelf Margin Facies of the Sierra Diablo—Seismic Scale Models for Subsurface Exploration: West Texas Geological Society, Publication 95–97, p. 23–66.

Franseen, E.K., Goldstein, R.H., and Whitesell, T.E., 1993, Sequence stratigraphy of Miocene carbonate complexes, Las Negras area, southeastern Spain: implications for quantification of changes in relative sea level, *in* Loucks, R.G., and Sarg, J.F., eds., Carbonate Sequence Stratigraphy: Recent Developments and Applications: American Association of Petroleum Geologists, Memoir 57, p. 409–434.

Galloway, W.E., 1986, Reservoir facies architecture of microtidal barrier systems: American Association of Petroleum Geologists, Bulletin, v. 70, p. 787–808.

Garber, R.A., Grover, G.A., and Harris, P.M., 1989, Geology of the Capitan shelf margin—subsurface data from the northern Delaware basin, *in* Harris, P.M., and Grover, G.A., eds., Subsurface and Outcrop Examination of the Capitan Shelf Margin, Northern Delaware Basin: SEPM, Core Workshop 13, p. 3.

Garćia-Mondéjar, J., and Fernández-Mendiola, A., 1993, Sequence stratigraphy and systems tracts of a mixed carbonate and siliciclastic platform-basin setting: the Albian of Lunada and Soba, northern Spain: American Association of Petroleum Geologists Bulletin, v. 77, p. 245–275.

Gardner, M.H., 1992, Sequence stratigraphy of eolian-derived turbidites: deep water sedimentation patterns along an arid carbonate platform and their impact on hydrocarbon recovery in Delaware Mountain Group reservoirs, West Texas, *in* Mruk, D.H., and Curran, B.C., eds., Permian Basin Exploration and Production Strategies: Applications of Sequence Stratigraphic and Reservoir Characterization Concepts: West Texas Geological Society, Symposium 92–91, p. 7–11.

Gardner, M.H., 1993, Sequence stratigraphy of upper Ferron sandstone member of the Mancos shale, east central Utah [unpublished Ph.D. thesis]: Colorado School of Mines, Golden Colorado, 528 p.

Gardner, M.H., and Sonnenfeld, M.D., 1996, Stratigraphic changes in facies architecture of the Permian Brushy Canyon Formation in Guadalupe Mountains National Park, west Texas *in* DeMis, W.D., and Cole, A.G., eds., The Brushy Canyon Play in Outcrop and Subsurface: Concepts and Examples: SEPM Permian Basin Section, Publication 96-38, p. 17–40.

Given, R.K., and Lohmann, K.C, 1986, Isotopic evidence for the early meteoric diagenesis of the reef facies, Permian Reef Complex of West Texas and New Mexico: Journal of Sedimentary Petrology, v. 56, p. 183–193.

Goldhammer, R.K., Dunn, P.A., and Hardie, L.A., 1990, Depositional cycles, composite sea-level changes, cycle stacking patterns, and the hierarchy of stratigraphic forcing: Examples from Alpine Triassic platform carbonates: Geological Society America, Bulletin, v. 102, p. 535–562.

Goldhammer, R.K., Lehmann, P.J., and Dunn, P.A., 1993, The origin of high-frequency platform carbonate cycles and third-order sequences (Lower Ordovician El Paso Gp, west Texas): constraints from outcrop data and stratigraphic modeling: Journal of Sedimentary Petrology, v. 63, p. 318–359.

Grotzinger, J.P., 1986, Cyclicity and paleoenvironmental dynamics, Rocknest platform, northwest Canada: Geological Society of America, Bulletin, v. 97, p. 1208–1231.

Harris, P.M., Kerans, C., and Bebout, D.G., 1993, Ancient outcrop and modern examples of platform carbonate cycles—implications for subsurface correlation and understanding reservoir heterogeneity, *in* Loucks, R.G., and Sarg, J.F., eds., Carbonate Sequence Stratigraphy: Recent Developments and Applications: American Association of Petroleum Geologists, Memoir 57, p. 475–492.

Hayes, P.T., 1957, Geology of the Carlsbad Caverns east quadrangle, New Mexico: U.S. Geological Survey, Geologic Quadrangle Map GQ-98.

Hayes, P.T., 1964, Geology of the Guadalupe Mountains, New Mexico: U.S. Geological Survey, Professional Paper 446, 69 p.

Haynes, J., 1981, Foraminifera: New York, Wiley, 433 p.

Hunt, D., Allsop, T., and Swarbrick, R., 1995, Compaction as a primary control on the architecture and development of depositional sequences: conceptual framework, applications and implications, *in* Howell, J., and Aitken, J.F., eds., High Resolution Sequence Stratigraphy: Innovations and Applications: Geological Society of London, Special Publication 104, p. 321–345.

Hurley, N.F., 1978, Facies mosaic of the Lower Seven Rivers Formation (Permian), North McKittrick Canyon, Guadalupe Mountains, New Mexico [unpublished M.S. thesis]: University of Wisconsin, Madison, Wisconsin, 198 p.

Hurley, N.F., 1979, Seaward primary dip of fall-in beds, lower Seven Rivers Formation, Permian, Guadalupe Mountains, New Mexico (abstract): American Association of Petroleum Geologists, Bulletin, v. 63, p. 471.

Hurley, N.F., 1989, Facies Mosaic of the Lower Seven Rivers Formation, McKittrick Canyon, New Mexico, *in* Harris, P.M., and Grover, G.A., eds., Subsurface and Outcrop Examination of the Capitan Shelf Margin, Northern Delaware Basin: SEPM, Core Workshop 13, p. 325–346.

Jacka, A.D., Thomas, C.M., Beck, R.H., Williams, K.W., and Harrison, S.C., 1972, Guadalupian depositional cycles of the Delaware Basin and Northwest Shelf, *in* Elam, J.G., and Chuber, S., eds., Cyclic Sedimentation in the Permian Basin, 2nd Edition: West Texas Geological Society, Publication 69-56, p. 152–196.

James, N.P., 1979, Shallowing-upward sequences in carbonates, *in* Walker, R.G., ed., Facies Models: Geoscience Canada, Reprint Series 1, p. 109–119.

James, N.P., 1984, Shallowing-upward sequences in carbonates, *in* Walker, R.G., ed., Facies Models, 2nd Edition: Geoscience Canada, Reprint Series 1, p. 213–228.

Kerans, C., and Fitchen, W.M., 1995, Sequence hierarchy and facies architecture of a carbonate-ramp system: San Andres Formation of the Algerita escarpment and western Guadalupe mountains, West Texas and New Mexico: Texas Bureau of Economic Geology, Report of Investigations 235, 86 p.

Kerans, C., and Harris, P.M., 1992, Relative sea level record of Yates and Tansill Formation shelf facies, Permian reef geology trail: implications for platform development (abstract): American Association of Petroleum Geologists, Annual Convention, Book of Abstracts, v. 1, p. 65.

Kerans, C., and Harris, P.M., 1993, Outer shelf and shelf crest, *in* Bebout, D.G., and Kerans, C., eds., Guide to the Permian Reef Geology Trail, McKittrick Canyon, Guadalupe Mountains National Park, West Texas: Texas Bureau of Economic Geology, Guidebook 26, p. 32–42.

Kerans, C., and Nance, H.S., 1991, High frequency cyclicity and regional depositional patterns of the Grayburg Formation, Guadalupe Mountains, New Mexico, *in* Meader-Roberts, S., Candelaria, M.P., and Moore, G.E., eds., Sequence Stratigraphy, Facies, and Reservoir Geometries of the San Andres, Grayburg, and Queen Formations, Guadalupe Mountains, New Mexico and Texas: SEPM, Permian Basin Section, Publication 91–32, p. 53–69.

Kerans, C., and Tinker, S.W., 1997, Sequence Stratigraphy and Characterization of Carbonate Reservoirs: SEPM, Short Course Notes 40, 130 p.

Kerans, C., and Tinker, S.W., in press, Extrinsic stratigraphic controls on development of the Capitan reef complex, *in* Saller, A.H., Harris, P.M., Kirkland-George, B., and Mazzullo, S.J., eds., Geologic Framework of the Capitan Reef: SEPM, Concepts in Sedimentology and Paleontology.

Kerans, C., Fitchen, W.M., Gardner, M.H., Sonnenfeld, M.D., Tinker, S.W., and Wardlaw, B.R., 1992, Styles of sequence development within uppermost Leonardian through Guadalupian strata of the Guadalupe Mountains, Texas and New Mexico, *in* Mruk, D.H., and Curran, B.C., eds., Permian Basin Exploration and Production Strategies: Applications of Sequence Stratigraphic and Reservoir Characterization Concepts: West Texas Geological Society, Symposium 92–91, p. 1–7.

Kerans, C., Lucia, F.J., and Senger, R.K., 1994, Integrated characterization of carbonate ramp reservoirs using Permian San Andres Formation outcrop analogs: American Association of Petroleum Geologists, Bulletin, v. 78, p. 181–216.

King, P.B., 1948, Geology of the southern Guadalupe Mountains, Texas: U.S. Geological Survey, Professional Paper 215, 183 p.

Kirkland, B.L., 1995, More evidence for a barrier reef: microfacies analysis of the Tansill outer shelf, Permian Capitan reef complex (abstract): American Association of Petroleum Geologists, Annual Convention, Book of Abstracts, v. 4, p. 50A.

Kirkland, B.L., and Moore, C.H., Jr., 1990, New evidence for the barrier reef model, Permian Capitan Reef Complex, New Mexico (abstract): American Association of Petroleum Geologists, Bulletin, v. 74, p. 696.

Kirkland, B.L., Longacre, S.A., and Stoudt, E.L., 1993, Reef, *in* Bebout, D.G., and Kerans, C., eds., Guide to the Permian Reef Geology Trail, McKittrick Canyon, Guadalupe Mountains National Park, West Texas: Texas Bureau of Economic Geology, Guidebook 26, p. 23–31.

Koerschner, W.F., and Read, J.F., 1989, Field and modeling studies of Cambrian carbonate cycles, Virginia Appalachians: Journal of Sedimentary Petrology, v. 59, p. 654–687.

Land, L.S., 1992, The dolomite problem: stable and radiogenic isotope clues, *in* Clauer, N. and Chaudhuri, S., eds., Isotopic Signatures and Sedimentary Records: Berlin, Springer-Verlag, Lecture Notes in Earth Science 43, p. 49–68.

Lang, W.B., 1937, The Permian formations of the Pecos Valley of New Mexico and Texas: American Association of Petroleum Geologists, Bulletin, v. 21, p. 833–898.

Legarreta, L., 1991, Evolution of a Callovian–Oxfordian carbonate margin in the Neuquen basin of west-central Argentina: facies, architecture, depositional sequences and global sea level changes: Sedimentary Geology, v. 70, p. 209–240.

Lloyd, E.R., 1929, Capitan Limestone and associated formations of New Mexico and Texas: American Association of Petroleum Geologists, Bulletin, v. 13, p. 645–658.

Lucia, F.J., 1995, Rock-fabric/petrophysical classification of carbonate pore space for reservoir characterization: American Association of Petroleum Geologists, Bulletin, v. 79, p. 1275–1300.

Mazzullo, S.J., Mazzullo, J., and Harris, P.M., 1985, Eolian origin of quartzose sheet sands in Permian shelf facies, Guadalupe Mountains (abstract), *in* Cunningham, B.K., and Hedrick, C.L., eds., Permian Carbonate/Clastic Sedimentology, Guadalupe Mountains: Analogs for Shelf and Basin Reservoirs: SEPM, Permian Basin Section, Publication 85-24, p. 71.

Meissner, F.F., 1972, Cyclic sedimentation in Middle Permian strata of the Permian Basin, *in*

Elam, J.G., and Chuber, S., eds., Cyclic Sedimentation in the Permian Basin, 2nd Edition: West Texas Geological Society, Publication 72-60, p. 203–232.

Melim, L.A., 1991, The origin of dolomite in the Permian (Guadalupian) Capitan Formation, Delaware Basin, west Texas and New Mexico: Implications for dolomitization models [unpublished Ph.D. thesis]: Southern Methodist University, Dallas, Texas, 200 p.

Melim, L.A., and Scholle, P.A., 1995, The forereef facies of the Permian Capitan Formation: the role of sediment supply versus sea-level changes: Journal of Sedimentary Research, v. B65, p. 107–118.

Mitchum, R.M., and Van Wagoner, J.C., 1991, High-frequency sequences and their stacking patterns: sequence stratigraphic correlation evidence of high-frequency eustatic cycles: Sedimentary Geology, v. 70, p. 131–160.

Mitchum, R.M., Vail, P.R., and Thompson, S., III, 1977, Seismic stratigraphy and global changes in sea level, Part 2: The depositional sequence as a basic unit for stratigraphic analysis, *in* Payton, C.E., ed., Seismic Stratigraphy—Applications to Hydrocarbon Exploration: American Association of Petroleum Geologists, Memoir 26, p. 63–81.

Montañez, I.P., and Osleger, D.A., 1993, Parasequence stacking patterns, third-order accommodation events, and sequence stratigraphy of middle to upper Cambrian platform carbonates, Bonanza King Formation, southern Great Basin, *in* Loucks, R.G., and Sarg, J.F., eds., Carbonate Sequence Stratigraphy: Recent Developments and Applications: American Association of Petroleum Geologists, Memoir 57, p. 305–326.

Mruk, D.H., and Bebout, D.G., 1993, Slope, *in* Bebout, D.G., and Kerans, C., eds., Guide to the Permian Reef Geology Trail, McKittrick Canyon, Guadalupe Mountains National Park, West Texas: Texas Bureau of Economic Geology, Guidebook 26, p. 14–22.

Newell, N.D., Rigby, J.K., Fischer, A.G., Whiteman, A.J., Hickox, J.E., and Bradley, J.S., 1953, The Permian Reef Complex of the Guadalupe Mountains region, Texas and New Mexico: San Francisco, W.H. Freeman, 236 p.

Osleger, D.A., 1998, Sequence architecture and sea level dynamics of late Permian shelfal facies, Guadalupe Mountains, southern New Mexico: Journal of Sedimentary Research, v. 68, p. 327–346.

Osleger, D.A., and Read, J.F., 1991, Relation of eustacy to stacking patterns of meter-scale carbonate cycles, Late Cambrian, U.S.A.: Journal of Sedimentary Petrology, v. 61, p. 1225–1252.

Osleger, D.A., and Tinker, S.W., in press, Three-dimensional architecture of upper Permian high-frequency sequences, Yates–Capitan shelf margin, Permian basin, USA, *in* Harris, P.M., Saller, A.H., Simo, T., and Handford, R., eds., Advances in Carbonate Sequence Stratigraphy—Application to Reservoirs, Outcrops, and Models: SEPM, Special Publication.

Playford, P.E., Hurley, N.H., Kerans, C., and Middleton, M.F., 1989, Reefal development, Devonian of the Canning Basin, western Australia, *in* Crevello, P., Wilson, J.L., Sarg, J.F., and Read, J.F., eds., Controls on Carbonate Platform and Basin Development: SEPM, Special Publication 44, p. 187–202.

Pomar, L., 1993, High-resolution sequence stratigraphy in prograding Miocene carbonates: application to seismic interpretation, *in* Loucks, R.G., and Sarg, J.F., eds., Carbonate Sequence Stratigraphy: Recent Developments and Applications: American Association of Petroleum Geologists, Memoir 57, p. 389–408.

Pray, L.C., 1977, The shelf-edge Capitan-massive and the outer-shelf facies, *in* Pray, L.C., and Esteban, M., eds., Upper Guadalupian Facies, Permian Reef Complex, Guadalupe Mountains, New Mexico and West Texas, Vol. 2, Road Logs and Locality Guides: SEPM, Permian Basin Section, Publication 77-16, p. G-5 to G-16 and G-79 to G-81.

Read, J.F., 1989, Controls on evolution of Cambrian–Ordovician passive margin, U.S. Appalachians, *in* Crevello, P., Wilson, J.L., Sarg, J.F., and Read, J.F., eds., Controls on Carbonate Platform and Basin Development: SEPM, Special Publication 44, p. 147–165.

Ross, C.A., and Ross, J.R.P., 1987, Late Paleozoic sea levels and depositional sequences, *in* Ross, C.A., and Haman, D., eds., Timing and Depositional History of Eustatic Sequences, Constraints on Seismic Stratigraphy: Cushman Foundation for Foraminiferal Research, Special Publication 24, p. 137–149.

Saller, A., 1996, Differential compaction and basinward tilting of the prograding Capitan reef complex, Permian, west Texas and southeast New Mexico, USA: Sedimentary Geology, v. 101, p. 21–30.

Sarg, J.F., 1995, Carbonate sequence architecture and sea-level records (abstract), *in* First SEPM Congress on Sedimentary Geology, Program and Abstracts Volume 1.

Sarg, J.F., and Lehmann, P.J., 1986, Lower–middle Guadalupian facies and stratigraphy, San Andres/Grayburg formations, Permian Basin, Guadalupe Mountains, New Mexico, *in* Moore, G.E., and Wilde, G.L., eds., Lower and Middle Guadalupian Facies, Stratigraphy, and Reservoir Geometries, San Andres/Grayburg Formations, Guadalupe Mountains, New Mexico and Texas: SEPM, Permian Basin Section, Publication 86-25, p. 1–8.

Severin, K.P., and Lipps, J.H., 1988, Comparative taphonomy of large fusiform foraminifera: test destruction by biotic agents during deposition (abstract): Geological Society of America, Annual Meeting, Abstracts with Programs, p. A370.

Silver, B.A., and Todd, R.G., 1969, Permian cyclic strata, northern Midland and Delaware basins, West Texas and southeastern New Mexico: American Association of Petroleum Geologists, Bulletin, v. 53, p. 2223–2251.

Smith, D.B., 1973, Geometry and correlation along Permian Capitan escarp ment, New Mexico and Texas: discussion: American Association of Petroleum Geologists, Bulletin, v. 57, p. 940–945.

Sonnenfeld, M.D., 1991, High-frequency cyclicity within shelf-margin and slope strata of the upper San Andres sequence, Last Chance Canyon, *in* Meader-Roberts, S., Candelaria, M.P., and Moore, G.E., eds., Sequence Stratigraphy, Facies, and Reservoir Geometries of the San Andres, Grayburg, and Queen Formations, Guadalupe Mountains, New Mexico and Texas: SEPM, Permian Basin Section, Publication 91-32, p. 11–51.

Sonnenfeld, M.D., and Cross, T.A., 1993, Volumetric partitioning and facies differentiation within the Permian Upper San Andres Formation of Last Chance Canyon, Guadalupe Mountains, New Mexico, *in* Loucks, R.G., and Sarg, J.F., eds., Carbonate Sequence Stratigraphy: Recent Developments and Applications: American Association of Petroleum Geologists, Memoir 57, p. 435–474.

Swift, D.J.P., and Thorne, J.A., 1991, Sedimentation on continental margins, I: A general model for shelf sedimentation, *in* Swift, D.J.P., Oertel, G.F., Tillman, R.W., and Thorne, J.A., eds., Shelf and Sandstone Bodies—Geometry, Facies, and Sequence Stratigraphy: International Association of Sedimentologists, Special Publication 14, p. 3–31.

Tinker, S.W., 1996a, Building the 3-D jigsaw puzzle: applications of sequence stratigraphy to 3-D reservoir characterization, Permian basin: American Association of Petroleum Geologists, Bulletin, v. 80, p. 460–485.

Tinker, S.W., 1996b, Reservoir-scale sequence stratigraphy: McKittrick Canyon and three-dimensional subsurface examples, west Texas and New Mexico [unpublished Ph.D. thesis]: Boulder, Colorado, The University of Colorado, 245 p.

Tucker, M.E., and Wright, V.P., 1990, Carbonate Sedimentology: London, Blackwell, 482 p.

Tyrrell, W.W., Jr., 1969, Criteria useful in interpreting environments of unlike but time-equivalent carbonate units (Tansill–Capitan–Lamar), Capitan Reef Complex, West Texas and New Mexico, *in* Friedman, G.M., ed., Depositional Environments in Carbonate Rocks: Society of Economic Paleontologists and Mineralogists, Special Publication 14, p. 80–97.

Vail, P.R., 1987, Seismic stratigraphy interpretation procedure, *in* Bally, A.W., ed., Atlas of Seismic Stratigraphy: American Association of Petroleum Geologists, Studies in Geology, v. 1, p. 1–10.

Vail, P.R., Mitchum, R.M., Jr., and Thompson, S., III, 1977, Seismic stratigraphy and global changes of sea level, Part 4: global cycles of relative changes of sea level, *in* Payton, C.E., ed., Seismic Stratigraphy—Applications to Hydrocarbon Exploration: American Association of Petroleum Geologists, Memoir 26, p. 83–97.

Van Wagoner, J.C., Posamentier, H.W., Mitchum, R.M., Vail, P.R., Sarg, J.F., Loutit, T.S., and Hardenbol, J., 1988, An overview of the fundamentals of sequence stratigraphy and key definitions, *in* Wilgus, C.K., Hastings, B.S., Kendall, C.G.St.C., Posamentier, H.W., Ross, C.A., and Van Wagoner, J.C., eds., Sea-Level Changes: An Integrated Approach: SEPM, Special Publication 42, p. 39–45.

Ward, R.F., Kendall, C.G.St.C., and Harris, P.M., 1986, Upper Permian (Guadalupian) facies and their association with hydrocarbons—Permian Basin, West Texas and New Mexico: American Association of Petroleum Geologists, Bulletin, v. 70, p. 239–262.

Wilde, G.L., 1975, Fusulinid-defined Permian stages, *in* Cys, J.M., and Toomey, D.F., eds., Permian Exploration, Boundaries, and Stratigraphy: West Texas Geological Society, Publication 75-65, p. 67–83.

Wilkinson, B.H., 1975, Matagorda Island, Texas: the evolution of a Gulf Coast barrier complex: Geological Society of America, Bulletin, v. 86, p. 959–967.

Wilkinson, B.H., 1982, Cyclic cratonic carbonates and Phanerozoic calcite seas: Journal of Geological Education, v. 30, p. 189–203.

Wilkinson, B.H., Drummond, C.N., Rothman, E.D., and Diedrich, N.W., 1997, Stratal order in peritidal carbonate sequences: Journal of Sedimentary Petrology, v. 67, p. 1068–1082.

Wilson, J.L., 1967, Cyclic and reciprocal sedimentation in Virgilian strata of southern New Mexico: Geological Society of America, Bulletin, v. 78, p. 805–818.

Wilson, J.L., 1975, Carbonate Facies in Geologic History: New York, Springer-Verlag, 471 p.

Wood, R., Dickson, J.A.D., and Kirkland-George, B., 1994, Turning the Capitan reef upside down: a new appraisal of the ecology of the Permian Capitan reef, Guadalupe Mountains, Texas and New Mexico: PALAIOS, v. 9. p. 422–427.

Yurewicz, D.A., 1976, Sedimentology, paleoecology, and diagenesis of the massive facies of the Lower and Middle Capitan Limestone (Permian), Guadalupe Mountains, New Mexico and West Texas [unpublished Ph.D. thesis]: University of Wisconsin, Madison, Wisconsin, 278 p.

Yurewicz, D.A., 1977, The origin of the massive facies of the Lower and Middle Capitan Limestone (Permian), Guadalupe Mountains, New Mexico and West Texas, *in* Hileman, M.E., and Mazzullo, S.J., eds., Upper Guadalupian Facies, Permian Reef Complex, Guadalupe Mountains, New Mexico and West Texas: 1977 Field Conference Guidebook, Vol. 1: SEPM, Permian Basin Section, Publication 77-16, p. 45–92.

Received 25 August 1997; accepted 16 June 1998.